Characterization of UmamiTs in *Arabidopsis*: amino acid transporters involved in amino acid cycling, phloem unloading and the supply of symplasmically isolated sink tissues

Doktorarbeit

Benedikt Müller

Supervisor: PD Dr. Ulrich Hammes

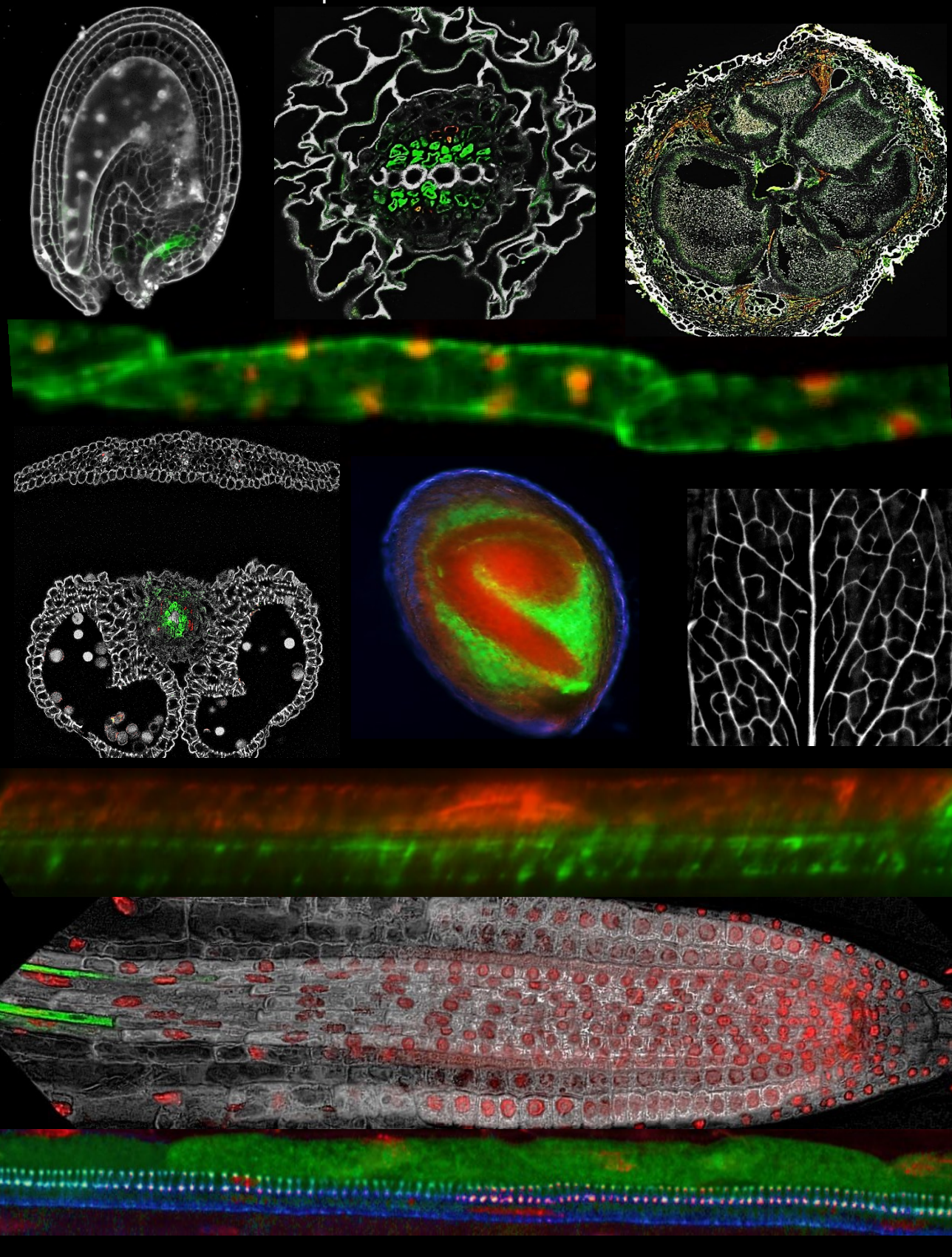

Characterization of UmamiTs in *Arabidopsis*: amino acid transporters involved in amino acid cycling, phloem unloading and the supply of symplasmically isolated sink tissues

Dissertation

zur Erlangung des Doktorgrades der Naturwissenschaften (Dr. rer. nat.)

der Fakultät für Biologie und Vorklinische Medizin

Universität Regensburg

Vorgelegt von Benedikt Müller

aus Tiefenbach

im April 2016

PhD Supervisor: PD Dr. Ulrich Hammes

1st Mentor: Prof. Dr. Thomas Dresselhaus

2nd Mentor: Prof. Dr. Ralph Hückelhoven

Das Promotionsgesuch wurde eingereicht am:

Die Arbeit wurde angeleitet von: PD Dr. Ulrich Hammes

Unterschrift: _____

(Benedikt Müller)

contents

1. ZUSAMMENFASSUNG 10

2. SUMMARY 12

3. INTRODUCTION 14

3.1. Human nutrition: a challenge for the future 14

3.2. Seeds: an evolutionary hallmark for plants and human civilization 15

3.3. Transport processes in higher plants 17

3.3.1. Transport between cells 17

3.3.2. Transport between organs 18

3.3.2.1. Long distance transport in the phloem 19

3.3.2.2. Long distance transport by the xylem 21

3.4. From nitrogen to amino acids…. a journey with breakpoints 22

3.5. Amino acid transporters in plants 24

3.5.1. APC- transporter family 25

3.5.2. AAP- transporter family 25

3.5.3. Amino acid transporters from other gene families 25

3.6. Transport processes at symplasmically isolated sink tissues 26

3.6.1. The seed: an endogenously induced symplasmically isolated sink tissue 27

3.6.2. The root-knot: an exogenously induced symplasmically isolated sink tissue 30

3.7. The identification of UmamiTs 33

4. AIM OF THE PROJECT 36

5. RESULTS 37

5.1. Vascular anatomy in the seed 37

5.2. The seed: a symplasmically isolated domain 40

5.3. Distribution of secondary plasmodesmata during seed development 42

5.4. Hormonal regulation of the reproductive tissue: dynamics during seed development 46

5.4.1. Cytokinin response in the reproductive tissue 46

5.4.2. Auxin response in the reproductive tissue 49

5.4.3. Auxin dynamics in the reproductive tissue 54

5.4.4. PIN3 localization during seed development 59

5.4.5. D6 protein kinase localization during seed development 70

5.5. Expression of *SCR* during ovule and seed development 72

5.6. B-type cyclin expression in ovule and seed development 74

5.6.1. CYCB1.2 74

5.6.2. CYCB1.3 77

5.7. *UmamiTs* are plasma membrane localized and expressed in various tissues 78

5.7.1. Subcellular localization of *UmamiTs* 78

5.7.2. *UmamiT* expression in different tissues: focus on the RNA level and promoter activity .81

5.8. *UmamiT* promoter activity and protein localization in *planta* 83

5.8.1. Leaves 83

5.8.2. Stem 87

5.8.3. Inflorescence 89

5.8.4. Anthers 92

5.8.5. Replum, transmitting tract and funiculus 95

5.8.6. SAM 98

5.8.7. Hypocotyl 102

5.8.8. Germination 104

5.8.9. Seed 106

5.8.9.1. UmamiT14 localization in the seed 107

5.8.9.2. UmamiT11 localization in the seed 111

5.8.9.3. UmamiT29 localization in the seed 112

5.8.9.4. UmamiT28 localization in the seed 117

5.8.9.5. UmamiT37 localization in the seed 119

5.9. Characterization of the unloading zone 120

5.9.1. UmamiT localization in functional transfer cells 120

5.9.2. Differentiation of UmamiT-positive cells is not regulated by APL 122

5.9.3. UmamiT postive cells are connected with companion cells 124

5.9.4. UmamiT-positive cells are connected with sieve elements 126
5.9.5. Whole mount immunolocalization of the unloading zone: sieve elements are nucleated and physically connected to UmamiT-positive cells 129
5.9.6. UmamiT-positive cells at the unloading zone show colocalization with PIN3..... 131
5.9.7. Auxin response in UmamiT14-positive cells during seed development 133

5.10. Root..... 135
5.10.1.1. Introduction of the marker lines in roots used in this thesis..... 135
5.10.1.2. Promoter activity of *UmamiTs* in the root..... 139
5.10.1.3. Tissue specific localization of UmamiTs in the root..... 145
5.10.1.4. Polar distribution of UmamiT14 in the root..... 150
5.10.1.5. UmamiTs and the protophloem paradoxon 152
5.10.1.6. Analysis of UmamiT-GFP overexpression in the root 154
5.10.1.7. UmamiTs in the root: interplay with auxin 156
5.10.1.8. Immunolocalization of different marker lines in roots 159
5.10.1.9. Characterization of UmamiT-positive cells in the root by immunolocalization..... 162
5.10.1.10. Validation of the sieve element identitiy of UmamiT positive cells by ..... marker lines 167
1.1.1.3.1. UmamiT14 colocalized in cells with SE-ENOD promoter activity 168
1.1.1.3.2. UmamiT14 colocalized with APL in differentiating sieve elements 169
1.1.1.3.3. UmamiT14 colocalized with PD1 in sieve elements..... 170

5.11. Analysis of the root-knot nematode feeding site by different marker lines: focus on giant cell associated tissue 172

5.12. Expression of *UmamiTs* during root knot nematode infestation..... 178
5.12.1. Characterization of UmamiT-positive cells in the root-knot by immunolocalization... 186

5.13. Characterization of knock-out plants 194
5.13.1. Analysis of the level of free amino acids 197
5.13.2. Phenotypical characterization of roots in *umamit* mutants 200
5.13.2.1. Root length in single knock-out background..... 200
5.13.2.2. Cripple plants in the double knock-out background..... 201
5.13.2.3. Lugol staining of roots from *umamit* mutants 205
5.13.2.4. mPS-PI staining of roots from umamit mutants 206
5.13.2.5. Whole-mount *in situ* RNA hybridization in the mutant background of *UmamiTs* 209

5.14. UmamiTs: filling the gaps..... 213

5.14.1. Localization of UmamiT41 in the seed and silique 215
5.14.2. Localization of UmamiT15 in the seed 216
5.14.3. Localization of UmamiT2 in the seed 217
5.14.4. Localization of UmamiT25 in the seed 218
5.14.5. Localization of UmamiT21 in the seed and siliques 219
5.14.6. Localization of UmamiT10 in the seed 220
5.14.7. Localization of UmamiT34 in the seed 221
5.14.8. Localization of UmamiT23 in the seed and embryo 222
5.14.9. Localization of UmamiT1 in the seed and embryo 224

6. DISCUSSION 226

6.1. The seed: nutrients on a complex route. 226

6.2. Hormonal dynamics during seed development 229

6.3. UmamiTs: the missing link in the amino acid supply of symplasmically isolated sink tissues and nitrogen cycling between xylem and phloem 232

6.3.1. Candidate UmamiTs are plasma membrane localized and broadly expressed in the vasculature of the above ground vegetative tissue 232
6.3.2. UmamiTs are spatio-temporally distinct expressed in the seed and impact amino acid composition and yield 235
6.3.3. Integrating UmamiTs with hormonal dynamics and assimilate routes during seed development 241
6.3.4. UmamiTs in the physiological gap of symplasmically isolated sink tissues 243
6.3.5. UmamiTs during interaction with root-knot nematodes: supply of symplasmically isolated giant cells. 245
6.3.6. UmamiTs in the root: a role in amino acid cycling 249
6.3.7. UmamiTs in the root: phloem-dependent impact on stem cells 252

6.4. UmamiTs as key transporters for amino acid cycling and the supply of symplasmically isolated sink tissues: a comprehensive summary 257

7. FUTURE ASPECTS 260

8. MATERIAL AND METHODS 262

8.1. Plants 262
8.1.1. Arabidopsis thaliana 262

8.1.1.1. Growth on soil 262
8.1.1.2. Growth on plates 262
8.1.2. *Lysopersicum esculentum* (tomato) 263
8.1.2.1. Isolation of eggs from infected roots 263
8.1.2.2. Isolation of second-stage juveniles 263
8.1.2.3. Infection of *Arabidopsis* with *Meloidogyne incognita* 264

8.2. GUS staining 265

8.3. Sectioning of plant tissues 265

8.4. Immunohistochemistry 265
8.4.1. Embedding of plant tissue in methacrylate and sectioning 265
8.4.2. Immunolocalization on sections 266
8.4.3. Whole mount immunolocalization 266

8.5. Propidium iodid staining of plant tissues 266

8.6. Whole-mount in situ RNA hybridization 267

8.7. mPS-PI staining 267

8.8. Seed measurement 267

8.9. Amino acid analytic 267

8.10. Statistical data processing 268

8.11. Microscopy 268

8.12. Molecular work 268

9. LITERATURE 269

9.1. References 269

9.2. Publications 278

10. APPENDIX 279

10.1. Colocalization study 279

10.2. Amino acid analytics..... 280

11. DANKSAGUNG..... 281

ERKLÄRUNG..... 283

1. Zusammenfassung

Eine der großen Herausforderungen der nahen Zukunft wird die Ernährung der voraussichtlich 10 Billionen Menschen darstellen. Dieses Ziel wird nur dann erreichbar werden, wenn eine immense Steigerung der Erträge von Nutzpflanzen, sowie eine Reduktion der Verluste durch Pathogene einhergehen. Hinsichtlich Ernährung sind Aminosäuren von besonderer Bedeutung, insbesondere wegen der so genannten essentiellen Aminosäuren, die nur über die Nahrung zugeführt werden können. Pflanzliche Nahrungsmittel setzen sich zum Großteil aus Früchten und Speichergeweben zusammen. Diese werden auch als „sink"-Gewebe bezeichnet, da sie von der Versorgung mit Assimilaten aus den grünen Geweben, den so genannten „source"-Geweben, abhängen. In Pflanzen stellt der sich entwickelnde Embryo eine Sonderform des endogenen sink-Gewebes dar. Auch biotrophe Pathogene können sich von Pflanzen mittels der Induzierung eines sink-Gewebes ernähren. Die Versorgung von symplasmisch isoliertem sink-Gewebe mit Zuckern und Aminosäuren wird über eine Reihe von Transportern sicher gestellt.

In der vorliegenden Arbeit wurden Plasmamembran lokalisierte Transporter (UmamiTs) bezüglich der zellbiologischen Charakteristika detailliert untersucht. Hierbei wurde herausgefunden, dass diese Transporter im vegetativen Gewebe sehr spezifisch mit der Vaskulatur assoziiert sind und hierbei besonders im Gefäßparenchym anzutreffen sind. Des Weiteren zeigte sich ein hoher Grad an Kolokalisierung in Siebelementen, weswegen ihre Funktion im Langstreckentransport von Aminosäuren und dem Aminosäurecycling zwischen Phloem und Xylem diskutiert wurde. Im Same zeigten UmamiTs eine zeitlich und räumliche sehr fein regulierte Expression in verschiedenen symplasmisch isolierten Domänen wie der Entladungszone, dem äußeren und inneren Integument, sowie dem Endosperm. Physiologisch betrachtet sind UmamiTs strategisch genau an den Stellen gefunden worden, an denen ein Export von Aminosäuren aufgrund der symplasmischen Isolierung notwendig ist, um die Aminosäuren in tiefer liegende Zellschichten zu transportieren. Funktionsverlustmutanten charakterisierten sich über erhöhte Level von freien Aminosäuren in der Schote, sowie einer Reduktion der Samengröße. All diese Resultate unterstreichen deutlich, dass die Funktion der UmamiTs direkt mit dem Ertrag verknüpft ist, weswegen diese Gene im Zuge einer zukünftigen Ertragssteigerung von Nutzpflanzen von besonderem Interesse sind.

In Wurzeln zeigte sich ebenfalls eine starke Assoziierung der UmamiTs mit dem Leitgewebe. Phänotypische Untersuchungen von Mutanten offenbarten, dass diese im Sämlingsstadium kürzere Wurzeln aufwiesen, sowie eine veränderte Organisation des Wurzelmeristems. Dies hatte zur Folge, dass sich Columella Stammzellen ungewöhnlich weit differenzierten bzw. eine zusätzliche Zellschicht undifferenzierter Zellen ausbildeten. In der meristematischen Zone der

Wurzel wurde zusätzlich eine Reduzierung der Anzahl an sich teilender Zellen dokumentiert. Doppelmutanten von clade I UmamiTs zeigten einen starken Phänotyp, der sich in der Ausprägung von extrem Wachstumsgestörten Keimlingen äußerte, die nicht überlebensfähig waren. Mutationen von *UmamiT14* und *UmamiT29* führten zu einer Reduktion des RNA Levels von PLT1 in Stammzellen der Wurzel. Überexprimierer deckten eine polare Verteilung der Transporter in antikliner Orientierung der Zellen des differenzierenden Protophloem auf, sowie eine Expression in Stammzellen, wodurch sich ein starker Zusammenhang zwischen der Rolle von UmamiTs im Langstreckentransport von Aminosäuren und der Versorgung der Stammzellen mit diesen ergibt.

Während der Infektion mit Wurzelknotennematoden wurden UmamiTs induziert. Die Transporter lokalisierten sehr speziell am induzierten Ernährungsgewebe in juvenilen Phloemzellen, welche direkt den symplasmisch isolierten Riesenzellen anliegend waren. Die Charakterisierung dieser UmamiT-positiven juvenilen Phloemzellen erfolgte über den Nachweis von Kernen, der Kolokalisierung mit dem Siebelement Epitop RS6, sowie der besonderen Präsenz der Transkriptionsfaktoren APL und SCR, was die Sonderstellung dieser Phloemzellen sehr deutlich betont. Infektionsanalyen in Verlustmutanten zeigten weiterhin, dass ein knock-out von UmamiTs signifikant die Besiedlung mit Wurzelknotennematoden und im Falle einer Infektion die Größe des Wurzelknotens reduzierte.

Die Ergebnisse dieser Arbeit zeigen welche Sonderstellung UmamiT-positive Zellen in der Entladungszone des Same, sowie im Ernährungsgewebe von Wurzelknotennematoden haben und charakterisieren sie als funktionale Transferzellen, um symplasmisch isolierte Gewebe mit Aminosäuren zu versorgen.

2. Summary

In the near future 10 billion people will live on our planet. To support the world's population yield has to increase dramatically. This goal can only be achieved by an enhancement in productivity and minimization of yield loss by pathogens. Amino acids are of special interest for human nutrition, because essential amino acids cannot be synthesized *de novo* by animals. Roots and fruits often represent the edible part of plants. These tissues depend on the supply from the green parts of the plant and therefore represent sink tissues. An example for an endogenous sink tissue is the developing seed including the embryo. Furthermore, also biotrophic pathogens force the plant to establish sink tissues. The supply of sink tissues is facilitated by a range of transporters.

In this work the plasma membrane-localized UmamiT amino acid facilitators were characterized in detail. They showed overlapping expression in the vascular tissue of roots, hypocotyl, leaves and stems, where they colocalized with phloem sieve elements. According to their position in the vascular parenchyma they are discussed to play a role in the amino acid cycling and in long distance transport. In the seed, UmamiTs displayed a spatio-temporally distinct expression pattern in symplasmically isolated tissues: the unloading zone, the outer and inner integument and the endosperm. From a physiological point of view, *UmamiTs* are located in strategically important domains for the transfer of amino acids within the sink tissue. It could be shown that a loss of function of *UmamiTs* resulted in elevated levels of free amino acids in seeds and a reduction of seed size. These findings indicate that the function of UmamiTs is directly linked with yield, which makes them interesting in the case of enhancement of productivity of crop plants in agriculture in the future.

In roots, *UmamiTs* were found to be differentially expressed in the xylem parenchyma and phloem. Also here, a colocalization with sieve elements was observed. Phenotypical analysis of mutants showed a reduction of root length in young seedlings and an altered organization of the root meristem, resulting in a unusual differentiation of columella stem cells or an additional layer of undifferentiated columella cells. Additionally, it was found that the cell cycle was also affected and the number of dividing cells in the root tip was significantly reduced. Higher order mutants of clade I *UmamiTs* investigated here showed a strong phenotype due to a complete loss of the root meristem. Double mutation of *UmamiT14* and *UmamiT29* led to a reduction of the mRNA of PLT1 in the stem cells. Overexpression of *UmamiTs* revealed a polar distribution of the fusion protein in anticlinal direction and an expression in stem cells and in differentiating protophloem, which suggests a role of UmamiTs in the directed long distance transport of amino acids along the vasculature and the supply of the root stem cells with amino acids.

During pathogen interaction with root knot nematodes, *UmamiTs* were specifically expressed in the feeding site, which is a tumor like sink tissue. Expression was detected in small parenchyma cells located close to the symplasmically isolated giant cells. UmamiT-positive cells were characterized as juvenile phloem: they were nucleated and APL-positive, colocalized with the sieve element specific epitope RS6 and showed a remarkable expression of *SCR*.

The findings presented in this thesis suggest that UmamiT-positive cells in the unloading zone of the seed and the feeding site of root knot nematodes function as unique cells with transfer function to supply symplasmically isolated sink tissues in plants.

3. Introduction

3.1. Human nutrition: a challenge for the future

In the year 2015 the human population increased up to more than 7 billion people (countrymeters.info.de), which means an increase of more than 0.8 billion people in the last year, about 230000 humans per day. Most of these people live in developing countries (ourworldindata.org). This huge number of people living on the planet must be fed, especially taking into account, that the world´s per capita milk and meat consumption is also growing (world resources institute, www.wri.org). This obvious food gap is especially apparent in Africa, where more than a quarter of the people are undernourished. The food gap is not a simple distribution problem. Even if it would be possible to distribute all produced food amongst the planet equally, still about 1000 calories per person more are need in the future (Alexandratos and Bruinsma 2012). Taking this scenario into consideration, we have to face the coming challenge to increase productivity of agriculture and to minimize the loss of food by pests and pathogens. Besides political issues that have to be overcome, the effort in agriculture will be the main obstacle to reach the increase of about 69% more calories than today to nourish the predicted 9.6 billion people in 2050 (world resources institute, www.wri.org). The agricultural area is limited and cannot increase further without destroying natural habitats needed for stabilizing the climate change. This means that the only way to get the postulated increase of the yield is to enhance the productivity in the same agricultural area (Maurino and Weber 2013).

Plant science plays a central role in this field. Understanding the mechanisms of yield production in crop plants and application of the results in the field will be the big future topic for breeders, plant physiologists and cell biologists.

No matter how we will achieve the increment of yield, in the end it will be always be the same where the basis of our diet comes from: the seed of a plant.

3.2. Seeds: an evolutionary hallmark for plants and human civilization

Plants became the rulers of the planet by the subsequent accumulation of certain key innovations during evolutionary time (Donoghue 2005). Two of them, the evolution of the vasculature and the seed, were those with the highest impact on the success of land plants (Fig.1). Seeds represent a fascinating plant structure that combines two purposes: to harbor storage compounds for the embryo and to protect the next plant generation. In principle the diaspora, the distributive unit, of a plant, represents the unit that is able to ensure widespread directed dispersal. This became necessary as plants conquered the land where the movement of the plant is strictly dictated by gravity and where the light intensity is present at a much higher level than in underwater habitats (Linkies et al. 2010). The development of seeds yielded not only a structure to shield the embryo from solar radiation, but even more a possibility to provide expanded horizontal migration by using accessory structures around the seed for air, water or animal long distance dispersal (Nathan et al. 2008). Long distance dispersal was a requirement to react to climate changes and sustain the gene pool between populations, which defines the wingspread of genetic variance and the capacity to response to natural dynamics of abiotic and biotic factors (Imbert and Lefévre 2003, Sork 2015).

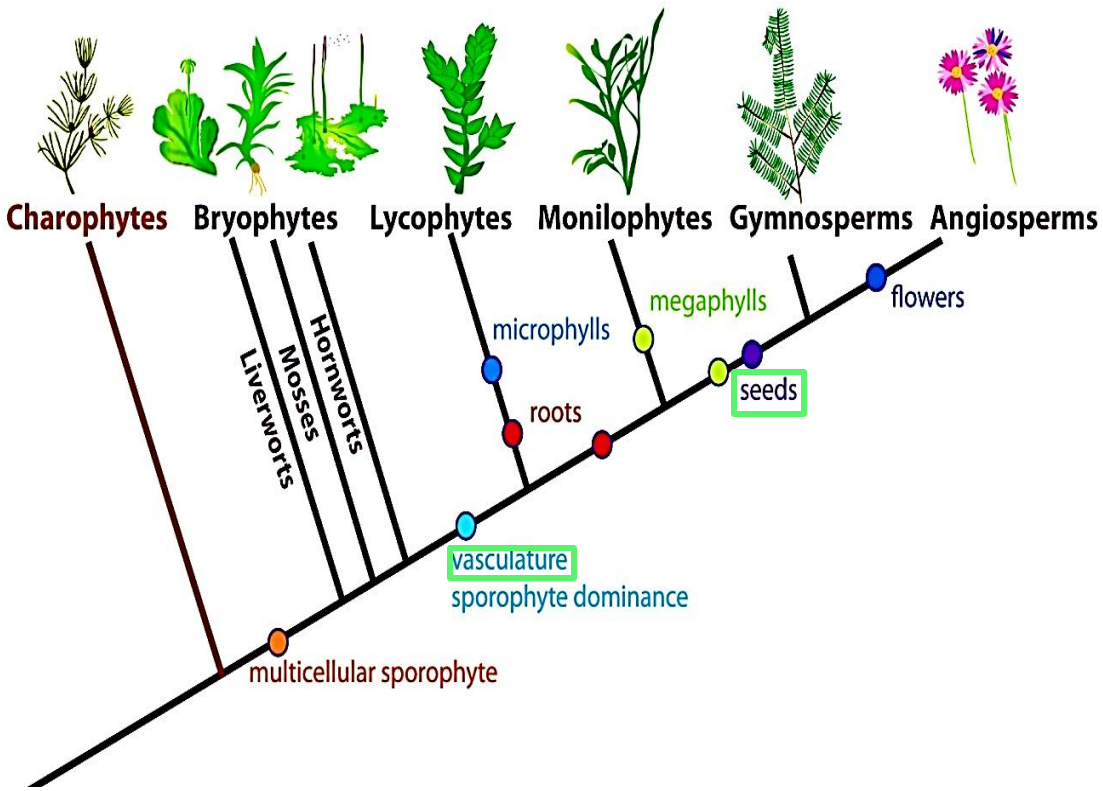

Figure 1. Cladogram of the evolution of plants. Key innovations are marked by filled circles. Hallmarks of evolution are marked in a green box. Modified from the Langdale lab (langdalelab.com 2015).

The first seeds have already appeared before the appearance of gymnosperms about 350 million years ago (Linkies et al. 2010). Later on a further invention was adopted in the lineage of the angiosperms by the invention of a triploid endosperm, which led to a massive incorporation of nutrient storage material like starch, proteins or oil in the seed (Baroux et al. 2002), which made them even more attractive for nutrition of animals. This enabled seeds to sustain centuries and to be vital after that time (Sallon et al. 2008). Especially the evolution of the human clade benefited from the use of seeds of grasses for nutrition as they became sessile (Diamond 2002). The origin of domestication of plants took place in southwest Asia's Fertile Crescent, where the wild ancestors were selected for farming. Humans started to change the hunter–gatherer lifestyle as they began to use seeds of annual plants for nutrition (Smith 2001). They became sessile and developed agriculture in order to provide food, which lead to the broad-spectrum revolution (Flannery 1969). During this time, humans learned to increase the spectrum of edible plants and enhance the bioavailability of nutrients in seeds by using food preparations like grinding or soaking.

Also today, after thousands of years of civilization, seeds of crops represent the base of our daily diet. This is a result of a massive change of the seed phenotype and an increase in yield by successful breeding activity of humans. Crop plant seeds became bigger and accumulated in number per plant by agricultural selection (Gepts 2004).

For future aspects it will not be sufficient to focus on the “more and bigger” issue on seeds. The quality aspects of the storage tissue, meaning the bioavailability of the compounds that are used for nutrition must be taken into account. Although animal physiology is able to produce most of the metabolites needed to maintain homeostasis itself, it still needs minerals and amino acids that are present in plants in limited number and define the quality of the diet (Young 1994).

Amino acids are of special interest, because only plants serve as resource for the so called essential amino acids, that animals cannot synthesize *de novo*.

Also the plant embryo needs those amino acids and hence they accumulate in the seeds of certain plants, e.g. legumes to a much higher degree than in any other plant tissue, where they are metabolized to proteins (Galili et al. 2014). This depends strictly on transport processes that occur between the mother plant and the seed tissues including the embryo.

3.3. Transport processes in higher plants

3.3.1. Transport between cells

Higher plants are multicellular organisms. To supply every cell of the plant body with assimilates and to ensure communication to each other, transport processes are essential. In contrast to animals, plant cells are enclosed by a massive cell wall. But besides that, plant cells have connections in between, the so-called plasmodesmata that allow ions and small metabolites with small molecular weight (~ 800 Da) to diffuse between cells (Tucker and Tucker 1993). This diffusion can be regulated by the size exclusion limit (SEL) regulated by actin, callose and other so far undiscovered proteins. The SEL defines the maximum molecular weight of compounds which can be diffuse through plasmodesmata.

Another possibility to enable transport into a cell is by plasma membrane-localized transporters, which are proteins that allow the selective uptake or efflux of metabolites and ions. Trans-membrane transport does not only occur between cells, but also within a cell in different compartments. Plasmodesmata connect plant cells (Fig. 2) and enable every single cell to get access to the symplast (Kim et al. 2002, Ruiz-Medrano et al. 2004). During some developmental events, like in the stomatal differentiation, the seed maturation or the embryo development, the symplasmic continuity between tissues is interrupted by the closure of plasmodesmata with callose (Simpson et al. 2009). This leads to the formation of symplasmically isolated domains, which depend exclusively on apoplasmic transport processes across the plasma membrane.

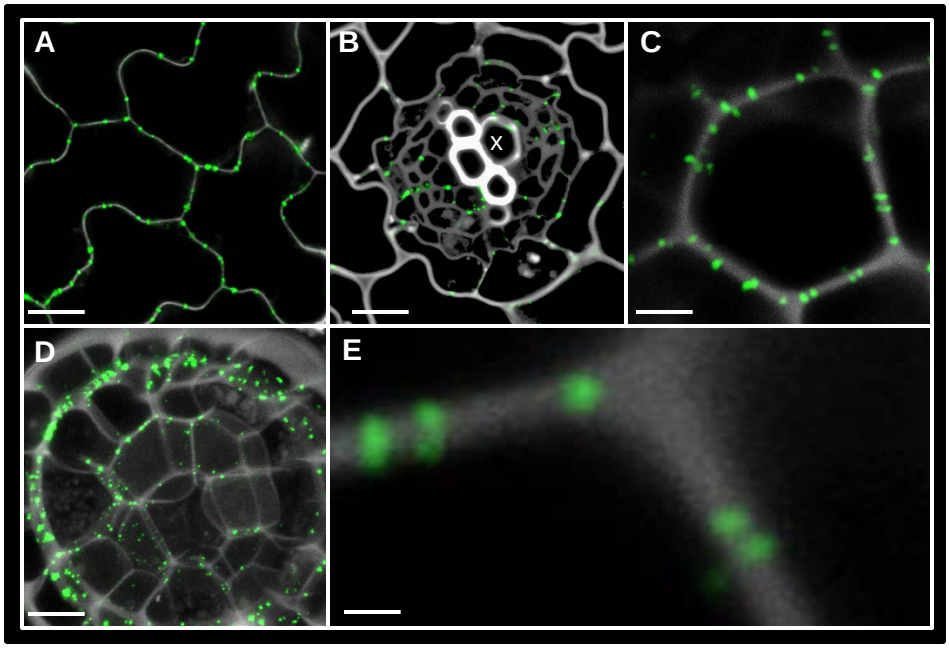

Figure 2. Plasmodesmata in different plant tissues. Plasmodesmata are labeled in green using the reporter line *P35S: MP17-GFP*. (A) Leaf epidermis cells, scale bar: 12µm. (B) Cross section through a root, scale bar: 8µm. (C) Single columella cell, plasmodesmata facing in direction of each neighboring cell, scale bar: 3µm. (D) Maximum projection of root tip with focus on columella cells, root tip tissue connected by plasmodesmata, scale bar: 8µm. (E) Plasmodesmata show tunnel like structure, scale bar: 800nm.

3.3.2. Transport between organs

The transport between different tissues and organs is achieved by conduction tissues for long distance transport. Specialized cells form the vasculature connect every organ of the plant body. As mentioned before, the vasculature was one of the most important key innovations of plants that accelerated the evolution from mosses to flowering plants (Bowman et al. 2007). The vasculature forms a cylinder, called stele. Herein tissues specialized for assimilate transport, the phloem, and tissues specialized for water and mineral transport, the xylem, are present. The two major cell types of the phloem are the sieve elements and companion cells. Xylem and phloem are embedded in a population of ground tissue, the vascular parenchyma (Fig. 3). The organization of the vascular tissue in *Arabidopsis* shows that xylem and phloem display a diarch symmetry of the stele (Esau 1977) as a result of xylem differentiation in the adaxial pole and phloem differentiation in two abaxial poles (Fig. 3 C, E). Xylem and phloem locate in collateral position to each other in the root (Fig. 3 A, C, E, F) and in the aboveground tissues like leaves (Fig. 3 D). During secondary growth the phloem gets organized circularly around the xylem vessels by proliferation and differentiation processes of the vessel parenchyma (Dolan et al. 1993).

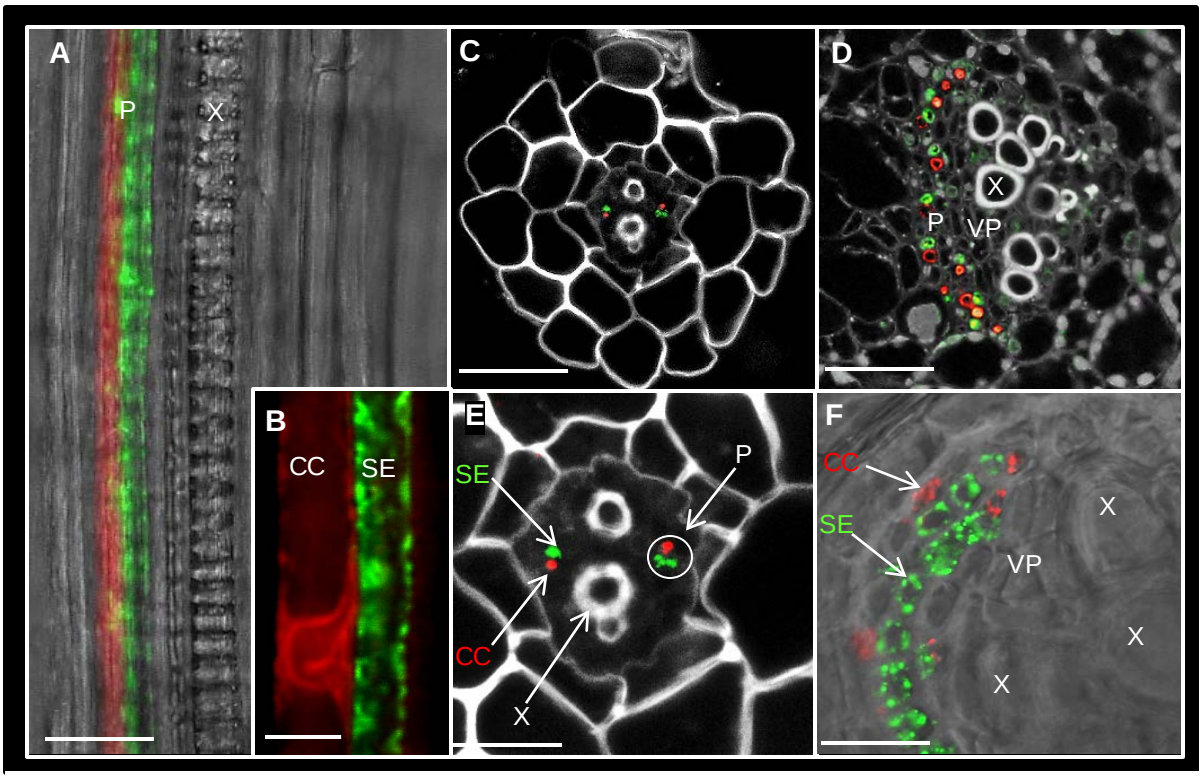

Figure 3. Organization of the vascular tissue in *Arabidopsis*. (A-C, E, F) *P_{PD1}: ER-GFP x P_{SUC2}: mCherry* reporter line (Müller et al. 2015): green cells: sieve elements, red cells: companion cells. (D) Immunolocalization of a *P_{suc2}: SUC2-HA* plant with α-HA and α-RS6: green cells: companion cells, red cells: sieve elements. (A) Maximum projection of phloem and xylem in the root, scale bar: 18µm. (B) The two major cell types of phloem, red: companion cell, green: sieve element, scale bar: 4.5µm. (C) Overview of a primary root cross section, scale bar: 30µm. (D) Leaf cross section, scale bar: 25µm. (E) Magnification of the stele of (C), scale bar: 12µm. (F) Cross section of a root that has undergone secondary thickening, scale bar: 20µm. X (xylem), p (phloem), vp (vascular parenchyma), se (sieve element), cc (companion cell).

3.3.2.1. Long distance transport in the phloem

The phloem consists of the long-stretched, bone-shaped cells, the so called sieve elements and the companion cells, which accompany the sieve elements. Both are embedded in a population of undifferentiated parenchymatic cells (Fig. 4). Sieve elements and companion cells are tightly connected by branched plasmodesmata, which enable them to function as a symplasmic unit, called sieve element-companion cell complex (Esau, 1969; Knoblauch and Van Bel, 1998; Van Bel, 2003). Sieve elements represent zombie-like cells, half alive and half dead. They lose most of their organelles and show degenerated nuclei during the differentiation process, which means they function as tube for the flow of assimilates, whereas metabolic functions were taken over by the companion cells.

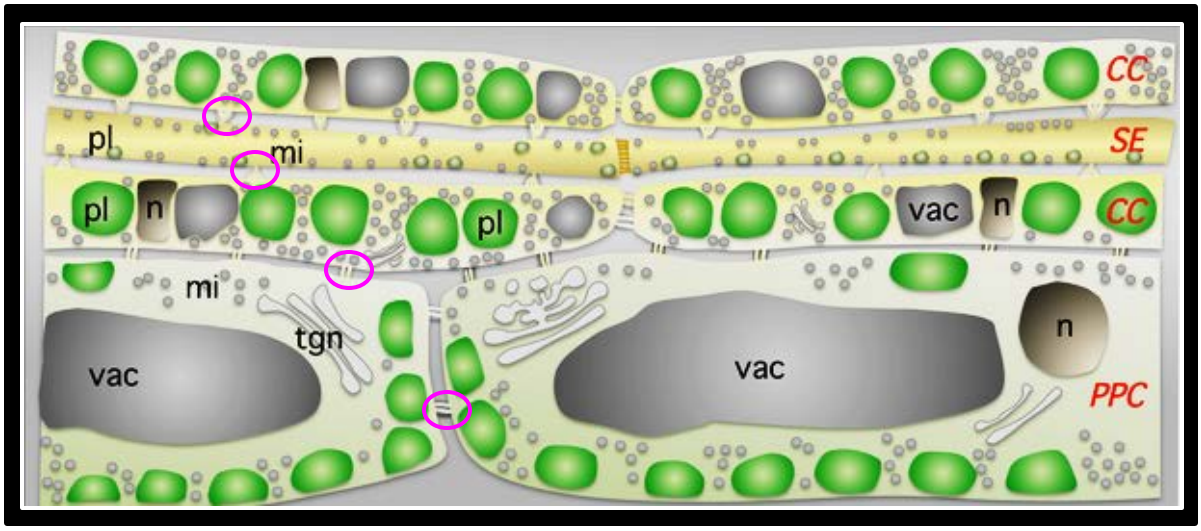

Figure 4. The three main cell types of the phloem. PPC (Phloem, parenchyma cell), CC (companion cell), SE (sieve element), vac (vacuole), n (nucleus), tgn (trans-golgi network), pl (pastids), mi (mitochondria). All cell types are interconnected by plasmodesmata (circle). Degenerated nucleus of SE not shown. Modified from Cayla et al. 2015.

A characteristic feature that becomes visible after differentiation is the sieve plate; this callose structure at the apical cell edges has pores that connect the sieve elements to each other and contributes to the symplasmic unit of sieve elements (Turgeon et al. 2001, Mullendore et al. 2010).

The transport direction of the phloem is dictated by the concentration of the main osmolyte, generally sucrose, which accumulates in photosynthetically active parts of a plant (green parts, Fig. 5). These tissues represent the so-called source tissues, which function as net exporters for assimilates. The assimilates form an osmotic gradient, which leads to a pressure directed to heterotrophic organs, called sink tissues, which function as net importers of assimilates (Van Bel 1996, Sauer and Stadler 1993; Truernit et al. 1996). The loading of sucrose from mesophyll

cells into the phloem can occur simply by plasmodesmata or via the apoplastic way. The latter includes the efflux of assimilates into the apoplast and their reuptake by transporters in the plasma membrane of companion cells (Sauer, 2007). In the case of sucrose this path is well studied: SWEET (Sugars Will Eventually be Exported Transporters) proteins function as sucrose exporters in the mesophyll while SUC2 (Sucrose Carrier 2) in the companion cells imports it again from the apoplast (Stadler and Sauer 1996, Chen et al. 2012).

After loading of the phloem the transport direction goes specifically along the concentration gradient into the sink tissues. The high concentration of sugar in the transport phloem drives the osmotic influx of water from the xylem and leads to an osmotic pressure gradient towards the sink tissues (Münch 1930). Phloem unloading can occur again symplasmically by plasmodesmata or apoplastically via transporters from the phloem into the parenchymatic tissues (Turgeon and Wolf, 2009). According to the unloading at the sink tissue, the sucrose driven osmotic pressure in the phloem gets reduced and the water potential decreases. As a consequence the sieve elements loose water again, which can flow to the xylem via the apoplast.

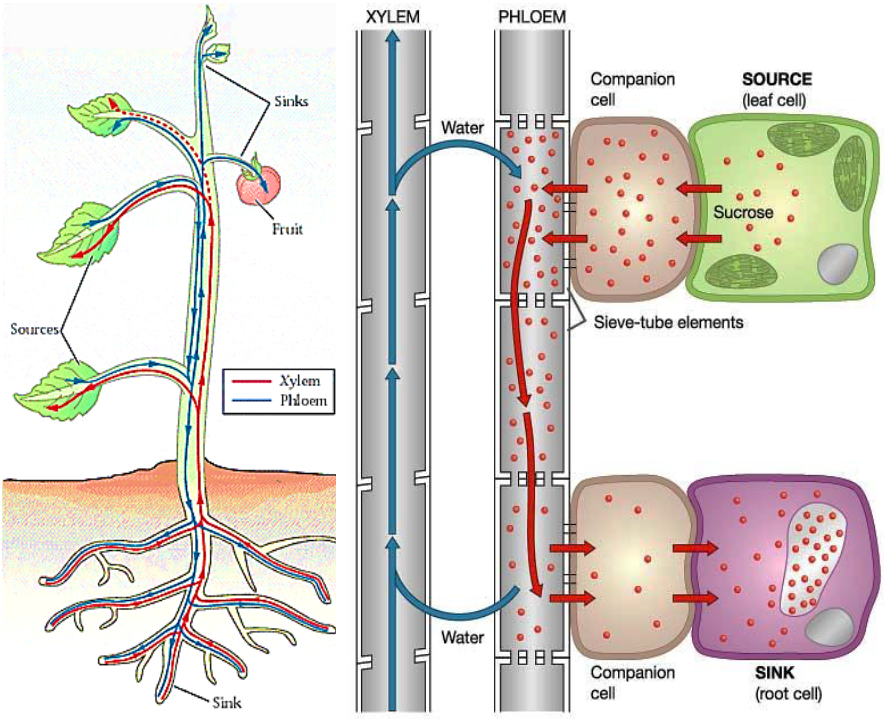

Figure 5. Long distance transport in a plant. Xylem shows unidirectional flow, phloem-mediated transport is bidirectional driven by sink-source relations. Osmotic influx of water in the phloem leads to a pressure gradient towards sink tissue. Modified from BIOS 100 lecture material (http://bio100.class.uic.edu/indexf04am.htm).

For amino acids moving in the phloem sap together with sucrose in much lower concentrations (Lalonde et al. 2003), no efflux and import mechanism was described so far. This means that the supply of sink tissues with amino acids that is contributed by efflux transporters is at the moment not understood.

3.3.2.2. Long distance transport by the xylem

The xylem consists of vessels with the tracheary elements and the xylem parenchyma. Two vessel types can be distinguished by their position and lignification (Esau 1977): protoxylem and metaxylem. The protoxylem is the first differentiated vessel type appearing in the stele and can easily be determined by the annual and spiral wall thickenings (Kobayashi et al. 2002, Baum et al. 2002; Demura and Fukuda 2007). The metaxylem, starts its differentiation during elongation and matures afterwards (Esau 1977). This vessel type builds pitted wall thickenings. Proto- and metaxylem are within a population of uniformly shaped cells, the so called xylem parenchyma tissue (Fig. 6).

The vessels fulfill their function after degradation of the nucleus and loss of all organelles, meaning they are dead at maturity. Xylem elements are responsible for structural stability of the plant body (fibers) and the long distance transport of water, minerals and amino acids (Lalonde et al. 2004). The flow direction is a consequence of the root pressure in combination with the negative water potential of the aerial parts of the plant. This leads to bulk flow of xylem sap directed upward.

Water, minerals and nitrogen or nitrogenous compounds are taken up by root hair cells (Fischer et al. 2002). Their lateral movement to the endodermis can occur via the apoplast or symplasm. Endodermal cells have a water-impermeable suberin layer. As a consequence, all flow of water and minerals proceeds through the symplasm. This enables the root tissue to be highly selective towards minerals and nitrogenous compounds, which can subsequently be concentrated in the xylem sap. To achieve selectivity in the root a transport process must be

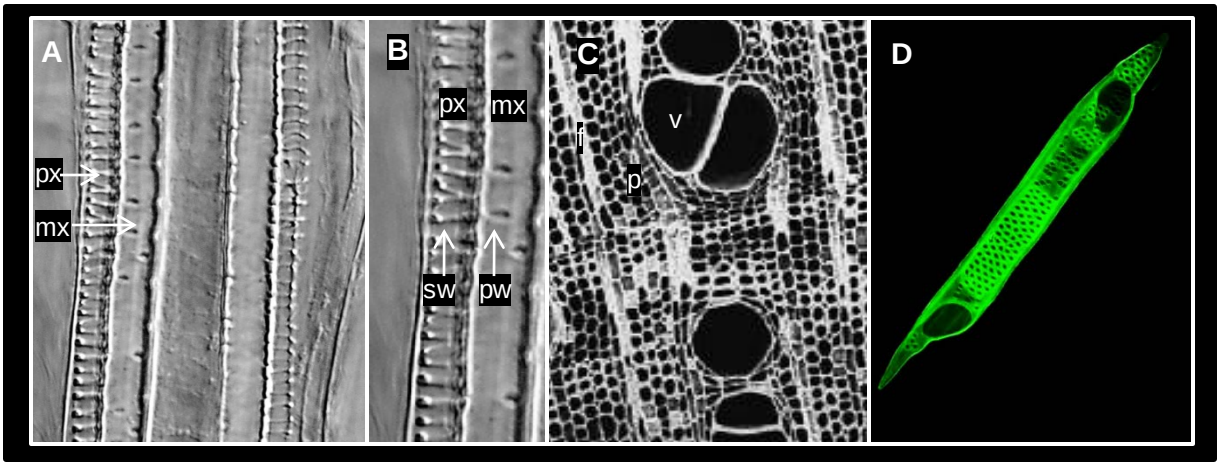

Figure 6. Organization of the xylem. (A) *Arabidopsis* root, protoxylem elements (px) and metaxylem (mx) in focus; scale bar: 25µm. (B) Magnification of (A) showing the specific cell wall modifications, spiral wall thickenings (sw) in the prtoxylem, pitted walls in the metaxylem, scale bar: 8µm (C) Scanning electron micrograph (SEM) of a transverse section form the xylem of a tree; large xylem vessels (water transport) are embedded in fibers (function in structural support) and small parenchmya cells, modified from Plants In Action (http://plantsinaction.science.uq.edu.au), v(vessel), f(fiber), p (parenchyma). (D) Isolated vessel that contributes for water transport, modified from the Regan lab: http://http-server.carleton.ca/~sregan/.

present in the plasma membrane of endodermal cells as well as in the parenchymatic tissue around the xylem.

Water flux into the xylem vessels is supported by aquaporins located in the membranes of the xylem parenchyma tissue (Postaire et al. 2010). Aquaporins are channels belonging to the MIP (Major Intrinsic Protein) family (Agre et al.1998). They are expressed in root cells and facilitate the passive movement of water into the xylem (Javot and Maurel 2002). Soluble compounds like ions, nitrogen and amino acids are enriched in the xylem by the selective translocation barrier in the endodermis, where membrane localized transporters concentrate these compounds. This check point causes the osmotic pressure in the xylem vessels, which leads to bulk flow in the upward direction (Steudle and Peterson 1998). From there, unloading of the xylem sap can occur by selective removal.

In the case of nitrogen compounds the selective removal of nitrate happens by nitrate transporters of the nitrate transporter gene family in the xylem parenchmya cells (Li JY et al.2010). This is an important step for amino acid biosynthesis concerning the reduction of nitrogen to ammonia and the assimilation into amino acids. These can be either built to proteins or translocated over long distance by the vasculature.

Although amino acids are found in considerable amounts in the xylem sap (50 mM, Schobert and Komor 1990), no mechanism explaining their efflux into the xylem in the root and their reuptake into the aerial tissues has been reported so far.

3.4. From nitrogen to amino acids…. a journey with breakpoints

Whereas carbon is available for plants in nearly unlimited amounts, the nitrogen nutrition is very limited. Nitrogen is the nutrient required by plants in the largest amount and often a growth-limiting factor. The main reason for this is that plants cannot deal with non-reduced, inorganic nitrogen or atmospheric N_2 which represents approximately 80% part of the air. Biodegradant destruents from the organic layer in the soil continuously produce oxidized versions of nitrogen (nitrate and ammonia) by the degradation of proteins which serve plants as resource for nitrogen (Andrews 1986). Additionally, some plants harbor symbionts that are able to fix atmospheric nitrogen which serves as nitrogen source for these plants, too (Crawford, 1995). The uptake of nitrate or ammonia from the interstitial water occurs by exchange with protons or carboxyl. In the case of nitrate it was shown that NRT1 (Nitrate Transporter 1) and NRT2 are membrane localized transporters in the cortex and apex of the root and responsible for the uptake of nitrate (Tsay et al. 1993, Tsay et al. 2007).

Ammonium can be directly incorporated into amino acids, whereas nitrate must be reduced prior to assimilation (Crawford, 1995) (Fig.7). In the chloroplasts the nitrate is reduced by nitrate reductase to ammonia, which is incorporated into glutamate to produce glutamine. This

primary product together with the further products asparagine and aspartate form the major pool of soluble amino acids that are highly abundant in higher concentration in green tissues (Xu et al. 2012, Pratelli and Pilot 2014).

Of course, nitrate is in respect to soil pH the predominant form of nitrogen used by plants, other nitrogenic compounds are also present in numbers they could be considered to contribute directly to plant nutrition. Peptides and free amino acids are not that uncommon in soil and especially in extreme habitats, where nitrification is hindered due to climatic constraints (too dry, too cold), those compounds are in much higher concentration available than in the temperate areas. It has been reported that plants show a significant capacity of amino acid uptake from the soil (Schobert et al. 1988, Näsholm et al. 1998, Svennerstam et al. 2011).

Amino acids are transported in the xylem and phloem (Lalonde et al. 2004). Whereas the xylem flux is always directed from basal to apical tissues, the direction of phloem flow is determined strictly by source to sink gradients. The composition of free amino acids found in both tissues is similar, but the concentration differs significantly (Lohaus et al. 1998). In the phloem it varies from 60 to 300mM and in xylem from 3 to 50mM (Rosnick-Shimmel 1985, Lohaus et al. 1994, Schobert and Komor 1990).

Several crosslinks of amino acid distribution in a plant are possible due to the vicinity of the phloem and xylem that leads to a cycling of amino acids, thus an exchange of amino acids between both conduction tissues can occur (Cooper et al. 1986, Cooper and Clarkson 1989, Imsande and Touraine 1994). This mechanism can contribute to an enhancement of the filling of sink tissues like roots and seeds, with amino acids.

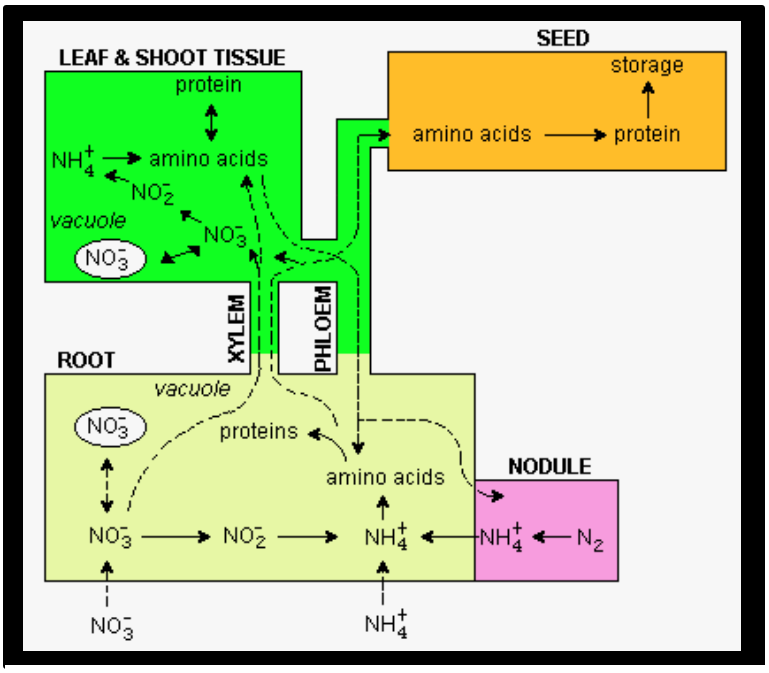

Figure 7. Pathways of nitrogen compounds through the plant. Allocation of amino acids to the sinks (seed, root) is managed by the xylem and phloem, modified from David Hildebrand (2013), http://www.uky.edu/~dhild/biochem.

3.5. Amino acid transporters in plants

Amino acid transporters are broadly distributed across all eukaryotic kingdoms of life. Altogether they can be classified into five different superfamilies (Table 1) according to their tissue specificity, transport mechanism and substrate spectrum (Wipf et al. 2002).

Table 1. Amino acid transporters in fungi, plants and animals.

Overview of the five superfamilies of amino acid transporters in the eukaryotic kingdom.

abbreviation	full name	found in	function
SDS	sodium-dicarboxylate symporter transporter superfamily	animals	glutamate and aspartate uptake in cotransport with Na^+ and with countertransport of K^+
NTS	neurotransmitter superfamiliy	animals	amino acid uptake by cotransport of Na^+ or Cl^-
APC	amino acid-polyamine-choline transporter superfamily	fungi animals plants	uptake of a wide spectrum of amino acids by Na^+ or H^+ coupled transport
ATF1	amino acid transporter superfamily 1	fungi animals plants	uptake and export of amino acids by Na^+ or H^+ coupled transport
MFS	major facilitator superfamily	fungi animals plants	transport a wide spectrum of compounds unrelated to amino acids by different transport mechanisms (Na^+ or H^+ coupled uniport or cotransport)

Two of them, the SDS (Sodium-Dicarboxylate Symporter transporter superfamily) and the NTS (Neurotransmitter Superfamiliy) superfamily are exclusively found in animals. They work as Na^+-coupled transporters. In contrast, plants use proton gradients to translocate amino acids. This gradient is achieved by proton ATP-ases that are the driving force for secondary active transport (Mitchell 1962). The direction of transport is along the electrochemical gradient. Secondary active transport is also referred to ion-coupled transport.

According to the recent collection at the plant membrane protein database homepage (Schwacke et al. 2003, http://aramemnon.uni-koeln.de/), more than 70 amino acid transporters are described in *Arabidopsis*. All of them function as secondary active transporters and are responsible for the import of amino acids into the cytosol. Their transport characteristic differs and they have different affinities for certain amino acids. Additional differences occur due to their distinct expression pattern within the plant and their subcellular localization.

3.5.1. APC- transporter family

In plants two distinct taxa of APC-transporters (Amino Acid –Polyamine-Choline Transporter Superfamily) are known so far. The one build the clade of the CATs (Cationic Amino Acid Transporters); these proteins are specialized for cationic amino acids (Frommer et al. 1995) as well as for neutral amino acids and lysine (Hammes et al. 2006).The other members are grouped in the clade of the LATs (L-Type Amino Acid Transporters), which is so far only poorly investigated.

3.5.2. AAP- transporter family

This group consists of six plant protein subfamilies: AAPs (Amino Acid Permeases), LHTs (Lysine, Histidine Transporters), ProTs (Proline Transporters), ANTs (Aromatic and Neutral Amino Acid Transporters), AUX (Auxin- Resistant-Transporter) and GATs (g-Aminobutyric Acid Transporters). The AAPs represent the biggest and best investigated group. They act as proton coupled symporters and transport preferentially neutral amino acids and glutamate with different affinities into the cytosol (Boorer et al. 1996, Fischer et al. 2002, Okumoto et al. 2002). LHTs play a role in the uptake of amino acids in the root (AtLHT1) as well as in the supply of mesophyll cells with amino acids, coming from the xylem sap (Hirner et al. 2006). The other members are less well studied so far with exception of AtAUX1 and LAX3 from the AUX subfamily, which acts as a high affinity auxin influx transporter (Yang et al. 2006, Swarup et al. 2008).

3.5.3. Amino acid transporters from other gene families

Also in other not related families amino acid transporters with a broad substrate specificity are described. Single proteins with the capacity to mediate amino acid transport are known from the following gene families: MFS (Major Facilitator Superfamiliy, Law et al. 2008), MCF (Mitochondrial Carrier Familiy), OEP16 (Plastid Outer Envelope Porin of 16kDa) (Rentsch et al. 2007). Until now the knowledge about their transport properties is limited and nothing is known concerning the amino acid transporters at the inner envelope which would be important to translocate amino acids to the outer envelope.

3.6. Transport processes at symplasmically isolated sink tissues

Every organ of the plant body is linked to each other by the vasculature. The conductive tissue is like a network with big highways and small roads spanning through the complete plant body. Xylem and phloem supply each organ with nutrients and information molecules. Most cells within a plant body have access to the symplast. This facilitates the communication between cells as well as the nutrition of cells located in the periphery of the tissue, which means that transport processes via the symplast contribute to the short distance transport (Ruiz-Medrano et al. 2004). But besides that, the plant still needs transport processes to enhance the directed translocation of compounds also between tissues where the connectivity of plasmodesmata is very tight. Translocation of compounds along the whole plant is achieved by the long distance transport using the conduction tissues phloem and xylem (Lalonde et al. 2003). Transport processes become more obvious in areas of a plant that are only poorly connected by plasmodesmata with the surrounding tissues.

Such situations can be found during differentiation processes like stomata development, where guard cells are symplasmically isolated from other epidermal cells (Wille and Lucas 1984, Ding et al. 1997). The need for transporters becomes most obvious in the seed.

3.6.1. The seed: an endogenously induced symplasmically isolated sink tissue

The seed of *Arabidopsis* consists of five different integument layers (Fig. 8 A, H). The outer integument is assembled by two layers and the inner integument by three layers (Schneitz et al.1995). Both integument types are symplasmically isolated from each other (Werner et al. 2011, Stadler et al. 2005). This indicates that transport processes along the plasma membrane must occur between the outer and the inner integument.

The vasculature ends in the reproductive sink tissues, where unloading occurs. Across the unloading phloem a distribution of the assimilates can be facilitated by the symplasmic connectivity (Fisher and Oparka 1996; Patrick 1997; Hoth et al. 2005; Stadler et al. 2005). But at some points this route is interrupted by an apoplasmic step as a consequence of the lack of functional plasmodesmata (Zhang et al. 2004). This occurs, when genome interfaces must be overcome like in the seed, where the maternal and filial generations are separated, as well as in the host/parasite relationship, like giant cells and juvenile phloem tissue (→ chapter 3.6.2).

A look at the vascular anatomy in the seed makes it obvious, that from the mother plant the vasculature stretches from the septum through the funiculus into the chalazal pole of the seed (Fig.8 A, D, E). Dagmar Werner (2011) and Ruth Stadler (2005) could already show that before fertilization the ovule forms a symplasmically isolated unit and after fertilization new plasmodesmata in the sieve elements of the seed are built (Fig. 8 E, F). This enormous increase in the frequency of plasmodesmata in the sieve elements of the chalazal region contributes to the restoring of the symplasmically unloading unit.

In young ovules of closed flowers the sieve elements get deeper into the chalazal region than the companion cells. Here the phloem extends into an unloading area that enhances the surface of the release phloem. Even after fertilization the companion cells are only poorly branched, whereas sieve elements show a visible increase of branching to two major cell files with some cells forming branch points of second order (Müller et al. 2015). Although this morphological change of the vascularization in the seed could be explained by the higher amount of nutrients that must be delivered from the mother plant into this enormous developing sink tissue, it appears really small compared to the size of the seed.

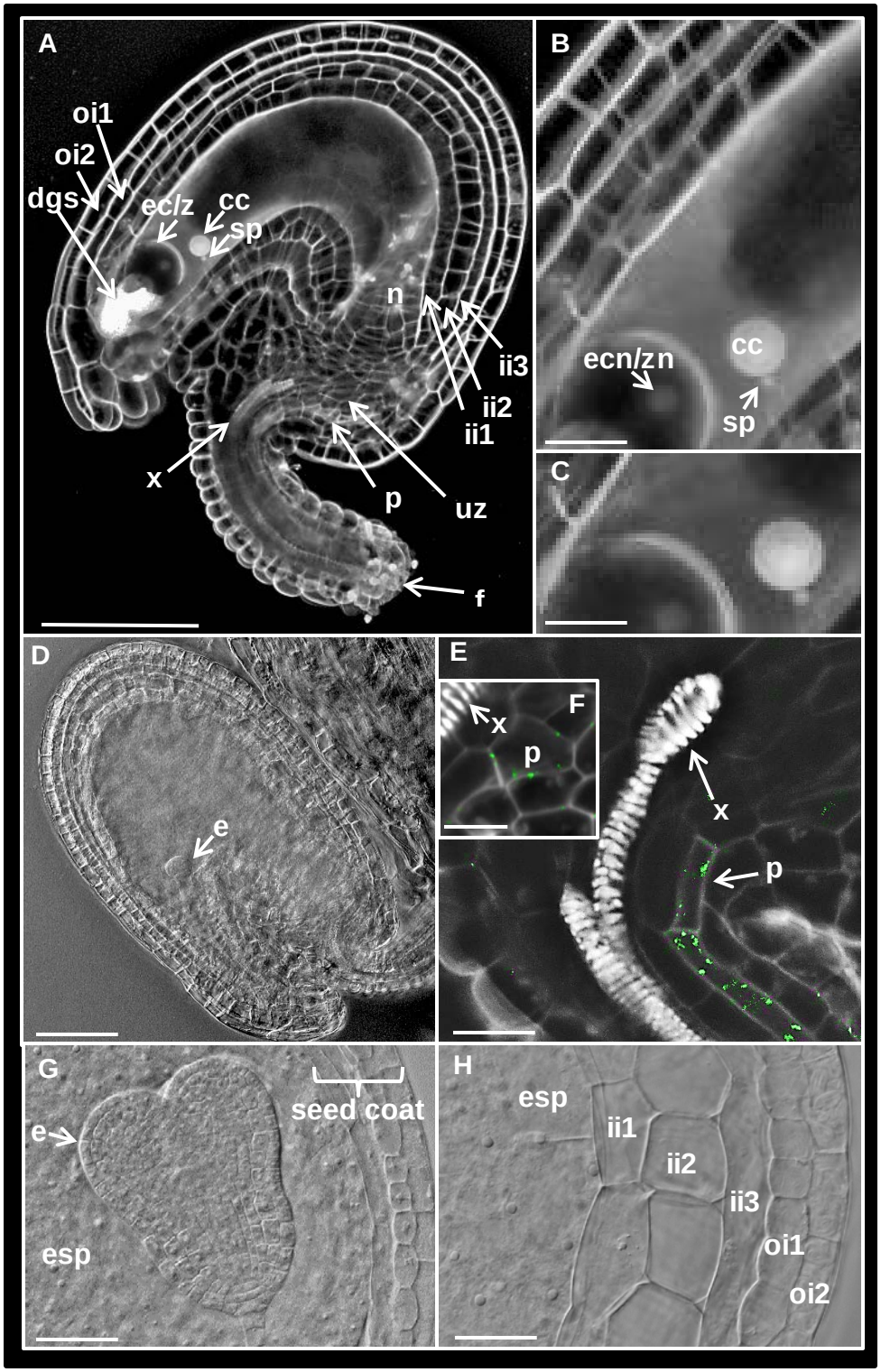

Figure 8. Seed anatomy of *A. thaliana*. (A-C) Maximum projections. (A) Overview of an ovule after fertilization, scale bar: 70µm. (B, C) Magnifications of the micropylar pole showing in detail egg cell/zygote, central cell and one sperm cell nucleus, scale bars: (B) 15µm, (C) 10µm . (D) Seed with embryo, scale bar: 70µm. (E, F) Unloading zone after fertilization, branched plasmodesmata in the phloem are marked by MP17-GFP. (E) Unloading zone with ending xylem and phloem, scale bar: 10µm. (F) Focus on sieve element decorated with MP17-GFP, scale bar: 10µm. (G) Seed with heart stage embryo in the endosperm, enclosed by the seed coat, scale bar: 40µm. (H) Magnification of the seed coat layers from a cleared seed, scale bar. 22µm. F (funiculus), p (phloem), x (xylem), uz (unloading zone), ii (inner integument), oi (outer integument), dgs (degenerated synergid cell), ec (egg cell), ccn (central cell nucleus), spn (sperm cell nucleus), ecn (egg cell nucleus), z (zygote), zn (zygote nucleus), n (nucellus),e (embryo), esp (endosperm).

Although the embryo increases in size and the need for a higher exchange area becomes obvious, the structure of the vascularization remains the same, which immediately suggests that the increasing demand is covered by increasing transport(er) activity.

Based on the observation that following the unloading zone of the phloem the layers of the outer and inner integument form symplasmically isolated layers (Stadler et al. 2005), it becomes necessary that transport processes occur between the unloading zone and the integuments as well as between the integuments, the endosperm and the embryo. Recently the group of Wolf Frommer identified several candidates of the *SWEET* transporter gene family (*SWEET11, 12, 15*), that are expressed in the seed coat and efflux sucrose into the apoplast (Chen et al. 2015).

The supply of the developing seed with amino acids still remains unclear. Several members of the AAP family are indeed expressed in the seed coat (Okumoto et al. 2002), as well as the importer CAT6 (Hammes et al. 2006). But the open question still is: how do the amino acids get into the apoplast to be taken up by these importers. The bottleneck of all processes that will occur in the integuments is the unloading zone, the structure in the seed at the chalazal pole where phloem and xylem end. In contrast to the published results of Stadler (2005), it will be shown later on that also between this unloading zone and the integuments transport across plasmodesmata is limited. These new findings underline the need of export transporters in the unloading zone to translocate assimilates into the integuments.

All import activities in the integuments are depending on selective export processes into the apoplast occurring at the unloading zone.

Although the importance of the cells there is obvious no investigations have been done so far explaining how the filling of the seed with amino acids takes place.

3.6.2. The root-knot: an exogenously induced symplasmically isolated sink tissue

Sink tissues are not only attractive for humans as a source for nutrition. Also some pathogens use sink tissues for feeding and development. A very special case of symplasmically isolated sink tissues is given by the feeding site of sedentary root knot nematodes. Parasitic nematodes are responsible for a yield loss of more than 100 MRD (Sasser and Freckman, 1987) and therefore an important target of pest control. There are two major types of soil borne parasitic nematodes: root-knot nematodes and cyst nematodes. Both nematode types start their life cycle by hatching from eggs. After reaching the second juvenile stage the juveniles start to migrate through the soil to find an appropriate host plant. This is the only free living stage in their life-cycle (Fig. 9). The entrance point into the host root is commonly between the elongation and differentiation zone of the root.

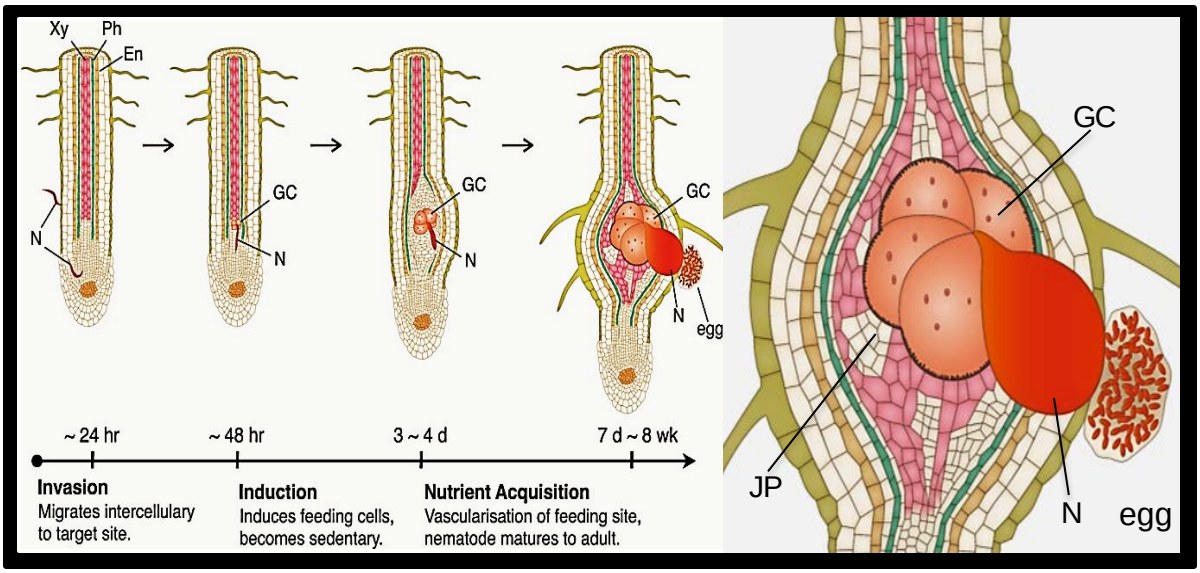

Figure 9. Schematic representation of the root-knot nematode infestation life-cycle. Modified from Bartlem et al. 2013. Xy (xylem), Ph (phloem), En (Endodermis), N (nematode), GC (giant cell), JP (juvenile phloem).

In the root they move to the stele and choose one procambial initial cell (cyst nematodes) or several initial cells (root-knot nematodes), in which they inject secretions from the subpharingeal glands (Davis et al. 2000).

At this point the establishment of the feeding site between the two types of pathogens differs significantly: infection with cyst nematodes induces a syncytium in the stele by the breakdown of cell walls and the subsequent fusion of up to 200 surrounding cells (Jones and Northcote 1972, Golinowski et al. 1997). Infection with root-knot nematodes causes the formation of several giant cells that reenter mitosis without cytokinesis and cell division. As a result they increase the cell volume and become multinucleated and maintain their single cell identity.

Additionally, also the neighboring tissue starts to proliferate, which leads to the characteristic swelling of the infection area (Bleve-Zacheo and Melillo, 1997). Root-knots become symplasmically isolated from the surrounding tissue, whereas the syncytium becomes highly connected to the surrounding cells by plasmodesmata (Hoth et al. 2008). Nevertheless from a physiological point of view both structures function as sink tissues in the plant. Both, giant cells and syncytia are multinucleated, have a dense cytoplasm and are marked by a high metabolic activity (Jones and Northcote 1972). These feeding sites nourish the nematode and gives all the input for the animal to develop eggs. After maturation of the eggs, the female dies and the eggs are released from the body as a gelatinous package (in root-knot nematodes) or enclosed into the dead body of the mother that becomes the cyst (in cyst nematodes).

The difference between the two nematode-induced sink tissues is the vascularization that is a consequence of the different morphology in those two sinks. Cyst nematode feeding sites are embedded in phloem tissue that contains sieve elements and companion cells in an elevated number (Hoth et al. 2005). This phloem is highly connected with the syncytia by secondary formed plasmodesmata (Hoth et al. 2008). As a consequence the flow of assimilates can be achieved by passive diffusion into the sink tissue where the loading of the syncytia occurs also by the symplast. Transporters seem to play only a limited role in this situation (Puthoff et al.2003) but their role in cyst nematode-induced feeding sites needs further investigation.

The giant cells get also embedded in newly formed phloem cells that share many of the characteristics of a protophloem. These cells show sieve element identity, are nucleated and interconnected by plasmodesmata (Hoth et al. 2008). But in contrast to the phloem of syncytia, the situation is completely different concerning the conductivity between these juvenile phloem cells and the giant cells of root knot nematodes.

In terms of assimilate flow it appears similar to the seed. Giant cells are symplasmically isolated from the surrounding tissues, which means, that transport processes must play an important role there (Hammes et al. 2005, Marella et al. 2013). This can be visualized by driving soluble GFP under the companion cell specific SUC2 promoter (Fig. 10). Similar to the seed there is no influx of GFP into the giant cells. This indicates again that giant cells form a symplasmically isolated unit where the size exclusion limit of the plasmodesmata is different compared to the surrounding tissue and prevents the diffusion of soluble GFP into the giant cells. The situation is similar to the unloading zone and integuments of the seed.

Translocation of assimilates is therefore depending extremely on transport processes: in one step export into the apoplast has to occur at the site of the juvenile phloem cells and the uptake of the released assimilates has to happen at the site of the giant cell. Additional support that transport processes play an important role can be drawn by the cell wall ingrowths of giant cells that is a typical characteristic for transfer cells (Offler et al. 2003).

Although Hammes et al. (2006) have already identified an amino acid importer (CAT6) that is highly expressed in giant cells, candidate genes for the export from the protophloem are still missing.

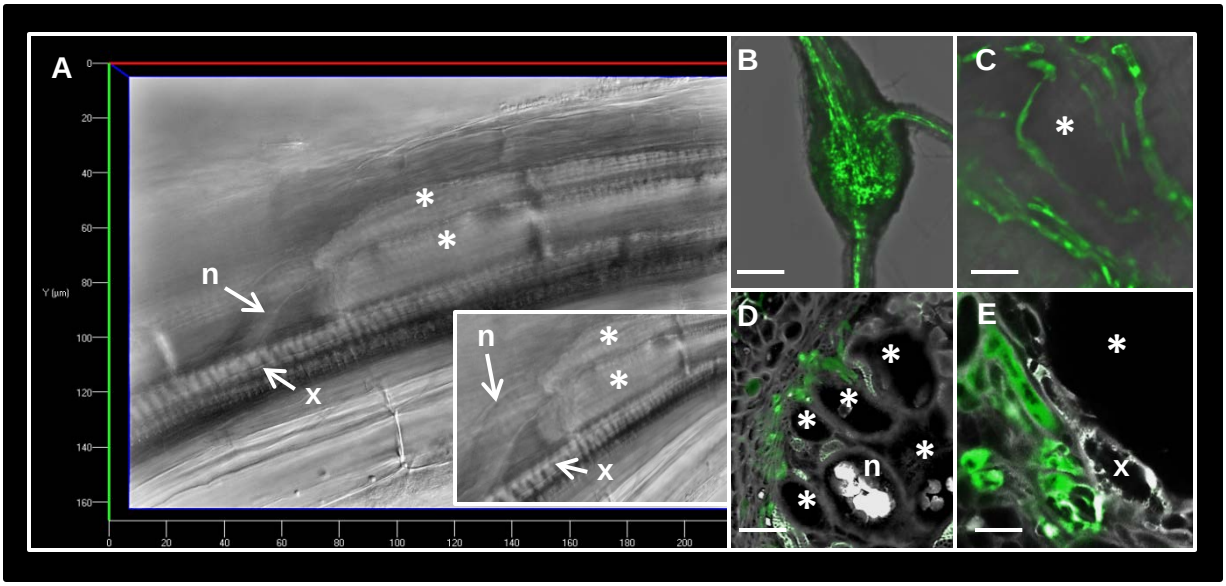

Figure 10. Giant cells are a symplasmically isolated unit. (A) 3D reconstruction of a young root knot showing the nematode in the vascular cylinder with the head directed to the small giant cells, insert shows a magnification of the same picture inverted in y-z direction. (B-D) Root knot of a *P*$_{SUC2}$*: sGFP* plant. (B) Overview of the root with lateral root, scale bar: 200µm. (C) Optical section, giant cell is free from GFP, scale bar: 60µm. (D) Vibratome section, showing several giant cells and the nematode; cells around giant cells show accumulation of soluble GFP, scale bar: 100µm. (E) Soluble GFP does not cross the border to the giant cell, scale bar: 20µm. Asterisks mark giant cells, n (nematode), x (xylem).

3.7. The identification of UmamiTs

The initial aim of this thesis was to identify candidate genes that are involved in the supply of sink tissues with amino acids. At first public microarray data were analyzed from endogenous sink tissue (seed with developing embryo, BAR eFP browser (Toufighi et al. 2005)), exogenous derived sink tissue (root-knots, Hammes et al. 2005). Additionally comparison was done with array data from Christiane Gatz about *Verticillum* infected *Arabidopsis* (personal communication). In all cases the screening was done with focus on induced genes from the MtN21 (*Medicago truncatula* nodulin 21) protein family with a significant fold change bigger than 1.5 as well as their presence in every microarray.

MtN21 was found in *Medicago truncatula* to be induced during the nodulation process (Gamas et al. 1996). This family belongs to the DME (Drug/Metabolite Exporter) superfamily, which consists of 24 phylogenetically distinct families. The first members were described in prokaryotes. It was also reported that members of the prokaryotic Drug/Metabolite Exporter family facilitate the efflux of certain amino acids (Livshits et al. 2003).

Plant specific proteins of the same class are grouped in the clade of the Plant Drug/Metabolite Exporter Family (P-DME). They contain 10 transmembrane domains, which are the result of a duplication event of primordial five transmembrane domains. The widespread distribution of MtN21 homologs among several families of higher non-nodulating plants reveals the ancient function of this protein family (Busov et al. 2004). Their homologs were engineered in gymnosperms and modified in angiosperms, where a specialization occurred for the supply of symplasmically isolated domains like the seed or tissues in symbiotic interactions (Denance et al.2013).

In *Arabidopsis* the nomenclature was still unclear and so the candidates were named as “Broad Specificity Amino Acid Facilitators” (BAFs), according to their putative function in amino acid transport. The first published member of this family was SIAR1 (Siliques Are Red, Ladwig et al. 2012). SIAR1 is a membrane localized amino acid transporter which is expressed in the unloading zone of the seeds and in the pericycle of roots. It turned out that SIAR1 is able to translocate amino acids in both directions: into and out of the cell. The second described member of the MtN21homologs in *Arabidopsis* was WAT1 (WALLS ARE THIN, Ranocha et al. 2013), which is a tonoplast localized auxin transporter.

In agreement with the newest version of TAIR the candidates were renamed to UmamiTs (Usually Multiple Amino Acids Move In And Out Transporters). The name umami is only associated with the taste that is predominantly influenced by the amino acid glutamate, which is one of those amino acids that are present in higher abundance in the phloem and xylem sap. This nomenclature of the transporters is the only association to the animal field that can

be drawn, which means that there is no similarity between plant UmamiTs and umamit receptors from animals.

UmamiTs are already present in basic multicellular land plants like the mosses *Physcomitrella patens* and *Marchantia polymorpha*, but completely absent in unicellular ancestors of the green lineage (Rodriguez-Ezpeleta et al. 2005). Also in fungi and animals no homologs are present. In plants 44 members and three pseudogenes can be found.

According to that we named the identified candidates as followed:

Table 2. Selected candidate UmamiTs characterized in this thesis.

old nomenclature	new nomenclature	AGI identifier
BAF3	UmamiT14	AT2G39510
BAF27	UmamiT11	AT2G40900
BAF11	UmamiT29	AT4G01430
BAF19	UmamiT28	AT1G01070
BAF35	UmamiT37	AT5G40230

A clustering of all core *UmamiT* genes is illustrated in the cladogram of Fig. 11. The only already described members are the vacuolar transporter WAT1 (Ranocha et al. 2013) and the plasma membrane transporter SIAR1 (Ladwig et al. 2012). The chosen candidate genes can be grouped in two major clades. Clade I genes are represented by *UmamiT14* and *UmamiT11* and clade III genes by *UmamiT28* and *UmamiT29*. An outliner is given by *UmamiT37*, which builds a separate cluster according to Ladwig (2012).

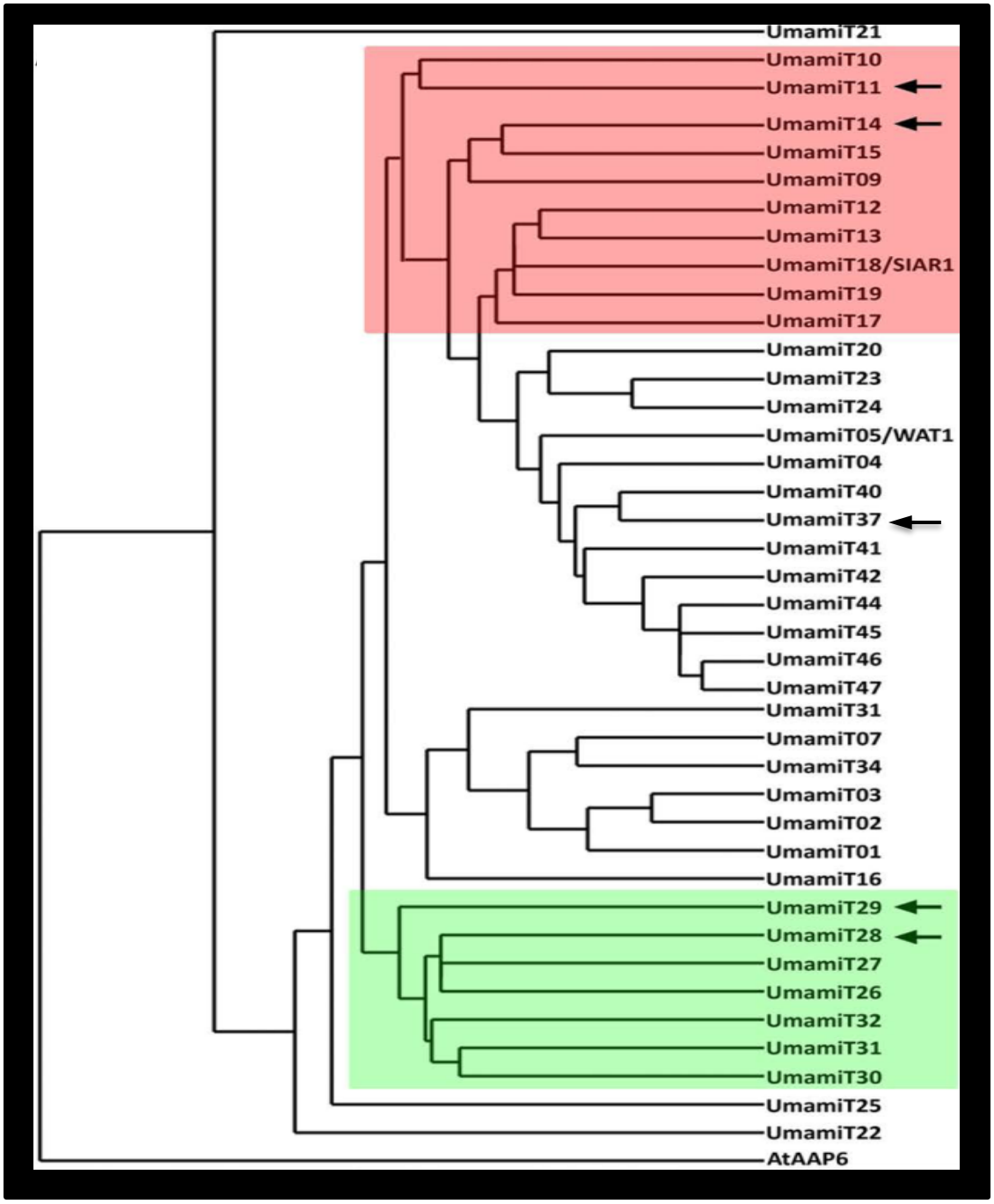

Figure 11. Cladogram of the main UmamiTs without pseudogenes. Phylogeny is based on multiple alignment analysis of the conserved regions of the proteins without variable N and C termini. Outgroup is AtAAP6. Clade I is marked in red, clade III in green. Arrows sign the chosen candidate genes.

4. Aim of the project

The aim of this thesis was to identify and characterize novel amino acid transporters in plants, which have a function in the supply of symplasmically isolated tissues. At first microarray data from developing seeds and root-knots will be screened for possible candidates of the MtN21 transporter families. Q-RT PCR studies on different kind of tissues (roots, leafs, flowers, old and young siliques, root-knot) will furthermore depict the different RNA levels between candidate genes and help to proof the findings on the array data. To validate the predicted plasma membrane localization colocalization studies will be performed. In order to visualize the promoter activity and localization of the protein *in planta*, stable transformed reporter lines for P_{UmamiT}*: GUS* and P_{UmamiT}*: UmamiT-GFP* will be generated and carefully analyzed concerning seed development, the vegetative tissue including roots and the infection with the root-knot nematode *Meloidogyne incognita.* These experiments include tissue preparation by cross sections and the characterization of UmamiT-positive cells by immunohistochemistry. Functional analysis will be carried out by the identification of knock-out plants and the monitoring of seed set, embryo development and the growth phenotype. Furthermore amino acid analytic will be done to estimate the effect of the functional loss of the candidate genes on the amino acid composition in siliques. Different staining methods for roots, as PI, mPS-PI and Lugol, will help to characterize root phenotypes. Finally whole-mount in situ RNA hybridization will be used to characterize effects of the knock-out on the root meristem.

These experiments will help to characterize UmamiTs in planta and to unravel their impact on yield and their functions in seed development and establishment of the nematode feeding site.

5. Results

5.1. Vascular anatomy in the seed

In order to investigate the anatomical properties of the vasculature along the vegetative-reproductive tissues a marker line for sieve elements (shown in green, *P_{PD1}: ER-GFP,* Bauby et al. 2006) and companion cells (shown in red, *P_{SUC2}: ER-mCherry*) was created. The border of the vegetative to the reproductive tissue is an important spot in plants. In the maternal tissue of the silique a highly ordered formation of xylem and phloem elements along the transmitting tract (Fig. 12 A) and funiculus (Fig. 12 B-E) exists. Phloem cells are located in collateral direction to the xylem. Sieve elements and companion cells are physically tightly connected to each other (Fig. 12 C, D).

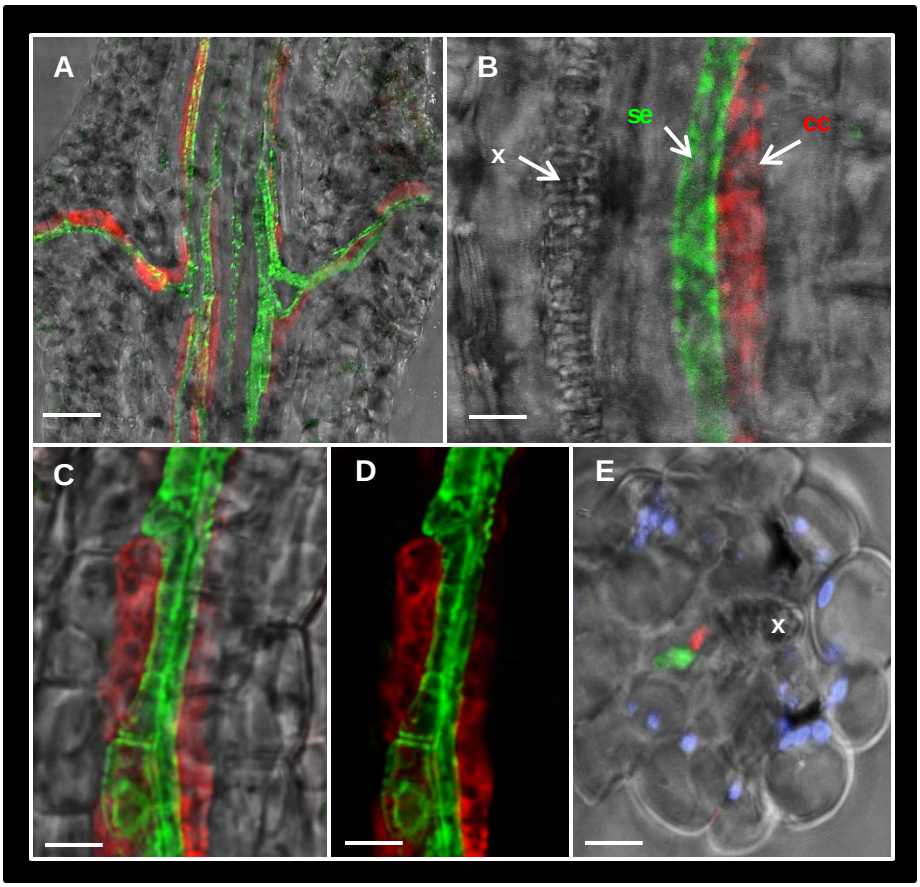

Figure 12. Anatomy of the conducting phloem in the silique.

P_{PD1}: ER-GFP x P_{SUC2}: mCherry reporter line. (A) transmitting tract with diverting strands to the funiculi, scale bar: 18µm. (B) Funiculus, z-stack, showing xylem, a sieve element and a companion cell, scale bar: 8µm. (C, D) maximum projection of the phloem in the funiculus, one sieve element still shows the nuclear envelope, scale bar: 5µm. (E)Cross section of the funiculus, autofluorescence of chloroplasts in purple, scale bar: 7µm. X (xylem), se (sieve element), cc (companion cell).

The vasculature extends through the funiculus into the reproductive sink tissues (Fig. 13 B). Here the morphology of phloem changes with the transition from ovules (= unfertilized stage, Fig. 12 A) to seeds (= fertilized stage, Fig. 13 C).

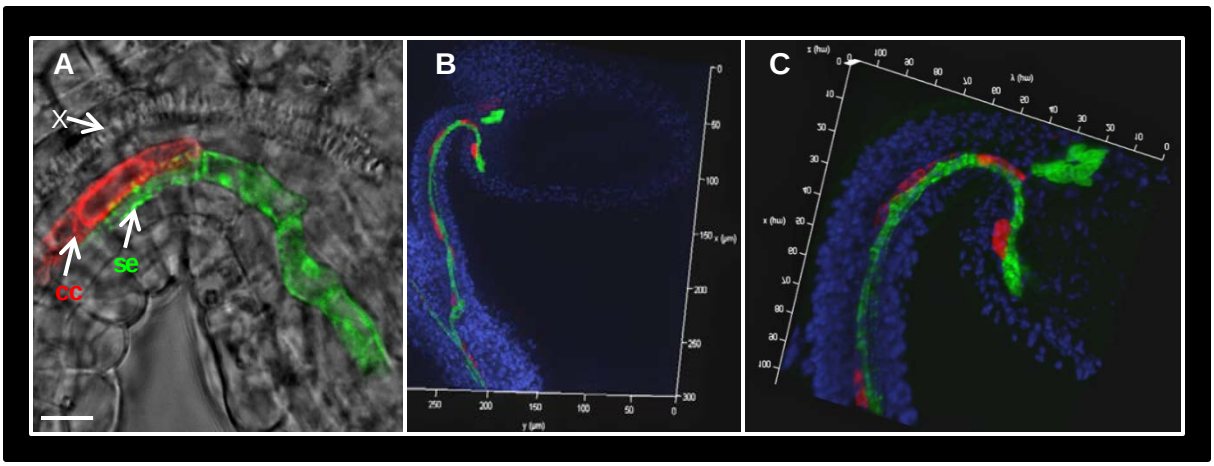

Figure 13. Anatomy of the vasculature at the end of the funiculus. *P_{PD1}: ER-GFP x P_{SUC2}: mCherry* reporter line. (A) Before fertilization: sieve elements are not branching, vasculature is ending with sieve elements, scale bar: 7µm. (B, C) 3D reconstruction of the morphology of sieve elements and companion cells after fertilization; blue color: autofluorescence of the plastids; phloem comes from the replum and moves via funiculus into the chalazal region, where branching occurs. X (xylem), cc (companion cell), se (sieve element).

In the closed flower, phloem and xylem are ending in the chalazal pole of the ovule (Fig. 14 A). Sieve elements and companion cells are closely together and end in the ovule at the same position as the xylem (Fig. 14 B, C). The same is true for companion cells in open flowers, but the sieve elements proliferate and start to extend deeper into the chalaza (Fig. 14 D-F). This process also leads to a branching of sieve elements into two major branching points after fertilization (Fig. 14 G-L). Shortly after fertilization the sieve elements furcate, whereas companion cells end close by without additional branches (Fig. 14 I, L). In early seed stages, (late globular embryo stage) additional branching points of second order appear in the sieve elements, while companion cells remain without intersections (Fig. 13 B, D and Fig. 14 G, H). From this time on, the phloem remains in this morphology state during all phases of embryo development and seed maturation (Fig. 14 J, K). Until the endpoint of seed ripening, no further increase in the exchange area could be observed.

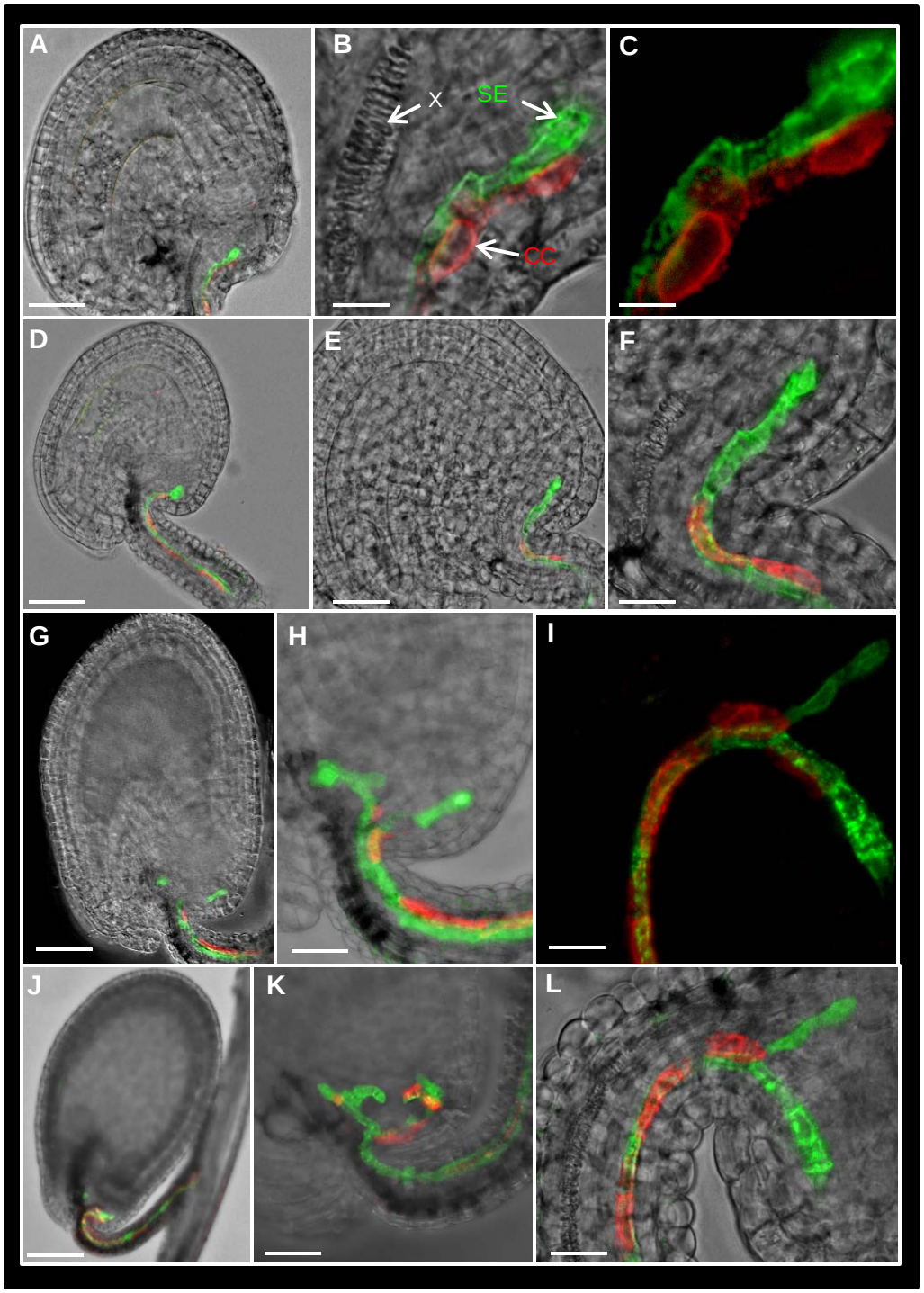

Figure 14. Morphological changes of the phloem during ovule and seed development. *P_{PD1}: ER-GFP x P_{SUC2}: mCherry* reporter line. (A-C) closed flower, (A) overview, scale bar: 30µm, (B) magnification of the endpoint of the vasculature, scale bar: 8µm, (C) magnified fluorescence channel showing ending sieve elements and companion cells close together, scale bar: 4µm. (D-F) ovule from open flower before fertilization, (D) overview, scale bar: 45µm, (E, F) sieve elements stretch deeper into the ovule than companion cells, scale bars: (E) 25µm, (F) 10µm. (G, H) seed at globular embryo stage, (G) overview as single optical section, scale bar: 60µm, (H) z-stack, scale bar: 20µm. (I, L) vasculature right after fertilization, (I) magnified fluorescence channel from (L), scale bar: 8µm, (L) funiculus with xylem and phloem ending in the fertilized ovule, scale bar: 10µm. (J, K) seed at older stage, (J) overview, scale bar: 80µm, (K) z stack, scale bar: 30µm. X (xylem), cc (companion cell), se (sieve element).

5.2. The seed: a symplasmically isolated domain

To investigate the flow of soluble GFP by the symplast through the seed reporter lines expressing soluble GFP under an unloading zone specific promoter and an integument specific promoter were analyzed. In previous studies it was shown that the inner and outer integument of the seed are symplasmically isolated from each other (Werner et al. 2011, Stadler et al. 2005). The outer integument was discussed to be a prolongation of the phloem which is ending in the unloading zone. By expression of cytoslic, soluble GFP under control of the *SUC2* promoter it was suggested that unloading from the unloading zone into the outer integument can occur by the symplasmic route after fertilization. But this is only true using the strong SUC2 promoter. It could be revealed that these results are partially a result of the strong companion cell specific promoter. This means that the already published data concerning the symplasmic flow of GFP from the unloading zone into the outer integuments is conducted by the phloem pressure and does not necessary reflect the situation *in natura*. The experiments performed showed that also the chalazal region, where the vasculature is ending and the unloading happens is isolated from all integuments (Fig. 15). This situation was visualized by driving soluble GFP under the control of an integument specific promoter (Fig. 15 A, B, E, F) and an unloading zone specific promoter (Fig. C, D, G, H).

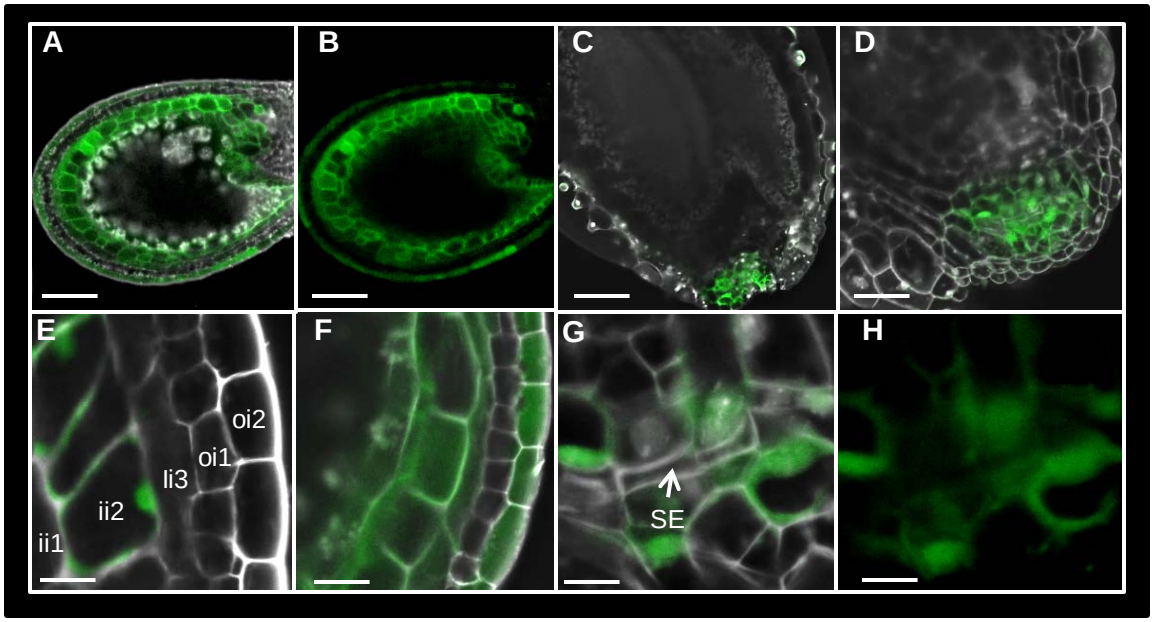

Figure 15. Identification of symplasmically isolated domains in the seed. (A,B, E, F) soluble GFP driven by an integument specifc promoter. (C, D, G, H) Soluble GFP driven by an unloading zone specifc promoter. (A) Overlay of (B) with brightfield image, GFP restricted to the outer integument and inner integument, no GFP in the endosperm and embryo, scale bar: 100µm. (E, F) Magnification of a region from the integuments; (E) GFP restricted to the inner integument layer 2, scale bar: 18µm. (F) No GFP flow visible between inner and outer integument, scale bar: 25µm. (C) Overview of a seed at bending cotyledon stage, showing soluble GFP restricted to the unloading zone, scale bar: 50µm. (D) Z-stack of the unloading zone shows a distinct cell layer around the sieve elements, scale bar: 30µm; (G, H) Magnification of the unloading zone with focus on the sieve elements (marked by wall thickenings), (H) GFP channel; scale bar: 9µm.ii (inner integument), oi (outer integument), SE (sieve element).

Soluble GFP was always restricted to the tissue, where it was produced, meaning no flow was detected form the unloading zone to the integuments, from the outer integument into the inner integument and from the inner integument to the endosperm. This indicates that the plasmodesmata of all this layers have a different size exclusion that prevents the translocation of GFP by the symplasmic route. All presented results underline that several transport processes are necessary to connect this symplasmically isolated domains in the seed. Consequently, there is indeed a need of further investigation on transporters acting in the unloading zone and integuments.

5.3. Distribution of secondary plasmodesmata during seed development

As already described, seeds are a symplasmically isolated sink tissue, which means, that the supply with nutrients by the symplasmic route is interrupted by an apoplastic step. In already differentiated tissues, plasmodesmata can be developed further to branched secondary plasmodesmata or formed *de novo* between cells, also resulting in branched plasmodesmata. To monitor the distribution of those secondary plasmodesmata during seed development the marker MP17 (Kronberg et al. 2007) was analyzed. This marker shows the presence of branched, likely secondary plasmodesmata. In the immature ovules of closed flowers MP17-GFP is found in few cells at the chalazal pole at the basis of the inner integument (Fig. 16 A, B). In open flowers with mature ovules the expression was found at the same position before fertilization (Fig. 16 E) but occurred additionally in the micropylar pole at the membrane of the central cell (Fig. 16 C). No GFP was detected in the unloading zone at the endpoint of the vasculature (Fig. 16 D). Weak signals were also found in the inner integument at the micropylar pole (Fig. 16 F). As shown in Werner et al. (2011) an increase in the frequency of newly formed plasmodesmata happens after fertilization (Fig. 16 G). GFP was monitored especially in the phloem (Fig. 16 G, H). At the unloading zone a much higher number of GFP spots were seen in the phloem than in the surrounding tissues (Fig. 16 I).

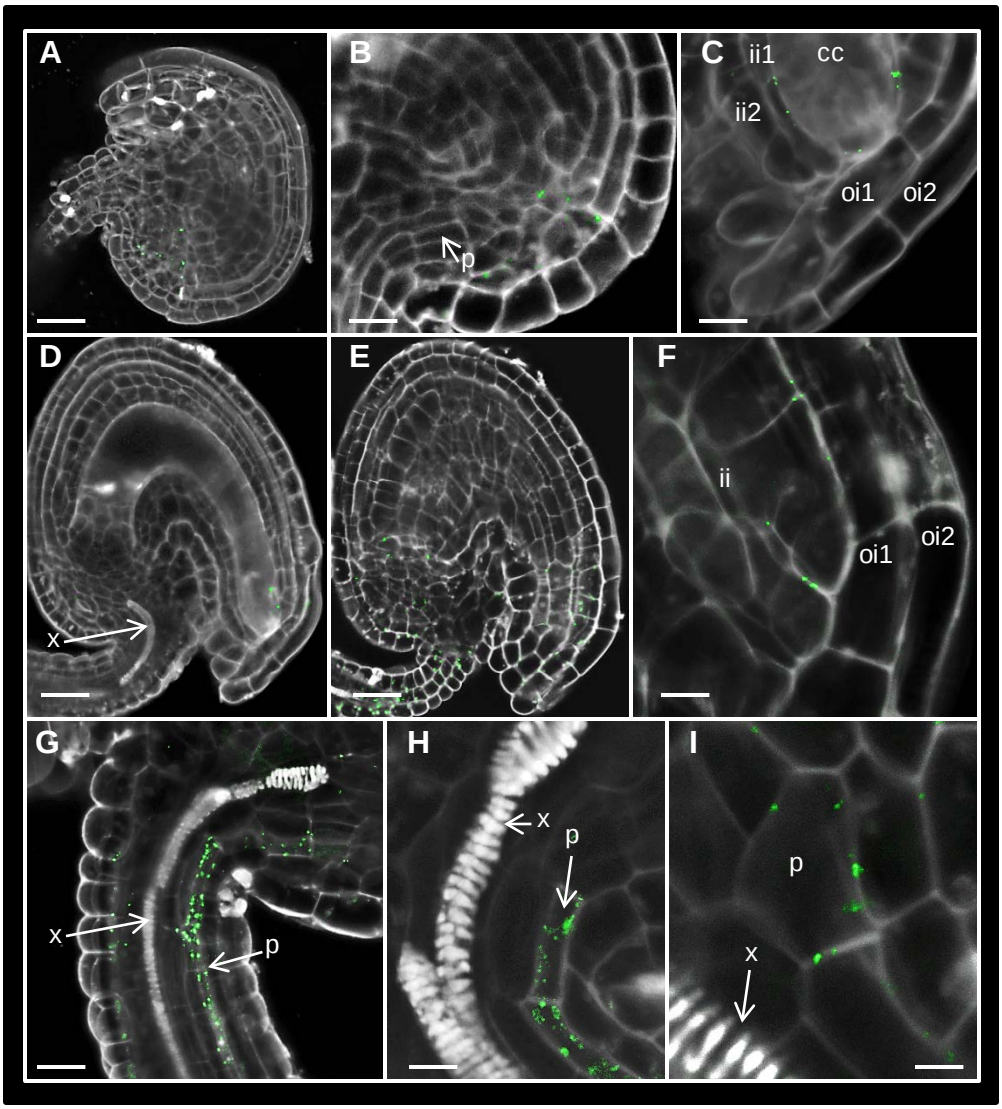

Figure 16. Distribution of plasmodesmata in the ovule before and shortly after fertilization. Plasmodesmata marked by MP17-GFP. (A) Maximum projection of an ovule from a closed flower, scale bar: 22µm. (B) Magnification of the area around the later unloading zone, GFP found in cells of the inner integument at the chalazal region, scale bar: 10µm. (C-F) Ovule taken from an open flower. (C) Magnification of the micropylar region from (D), scale bar: 10µm. (D) Optical section of an ovule, no GFP at the unloading zone, GFP only at the micropylar pole, scale bar: 25µm. (E) Same ovule from (D), GFP in the funiculus, the nucellus and micropylar region, scale bar: 25µm. (F) Optical section shows GFP specifically detected in cells of the inner integument, scale bar: 6µm. (G-I) Distribution of MP17-GFP after fertilization. (G) Funiculus with vascular tissue, huge number of plasmodesmata in the phloem, scale bar: 9µm. (H) Magnification of the unloading zone, scale bar. 5µm. (I) Magnification of phloem, some newly formed plasmodesmata also in neighboring cells, scale bar. 3µm. CC (central cell), x (xylem), p (phloem), ii (inner integument), oi (outer integument).

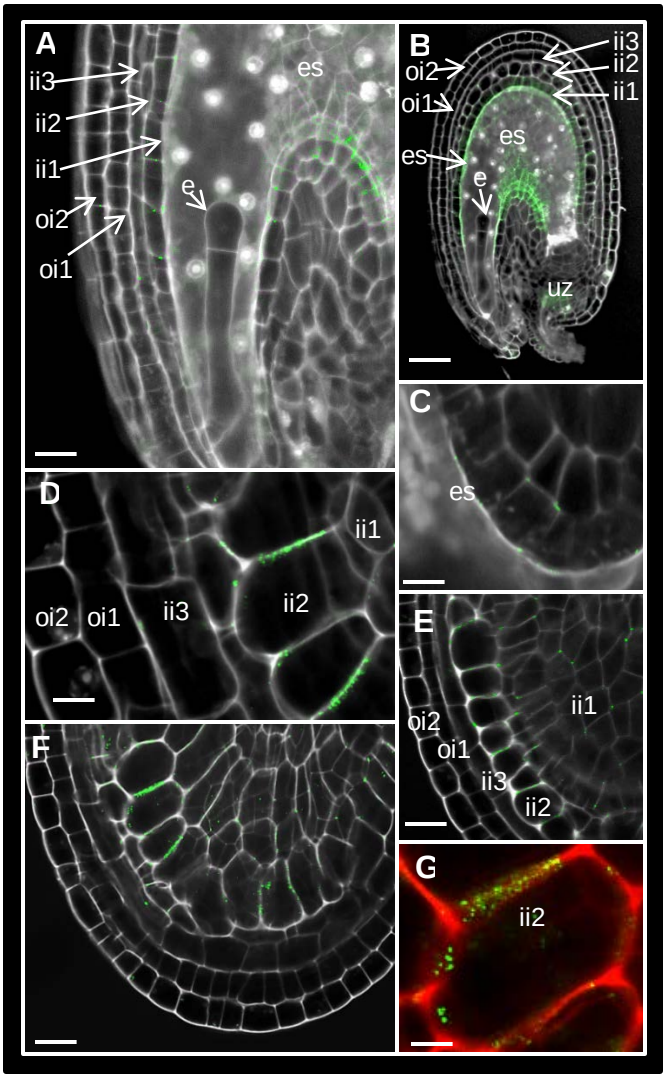

Figure 17. Distribution of plasmodesmata in the young seed. Plasmodesmata marked by MP17-GFP. (A) Seed with embryo in one-cell stage, GFP in the inner integument and embryo sack, scale bar: 17µm. (B) Overview of the seed from (A) showing GFP in the innermost integument layer and the unloading zone, scale bar: 40µm. (C) Magnification of the embryo sack, GFP in the inner integument and embryo sack, scale bar: 7µm. (D) GFP in the inner integument is asymmetrically distributed along the anticlinal position of the cells, scale bar: 6µm. (E) GFP in the inner integument layer 2 and 1, scale bar: 20µm. (F) Overview of the seed coat with focus on inner integument layer 2, signals between cells resulting from GFP in inner integument layer 1, scale bar: 15µm. (G) Magnification of a single cell of the inner integument layer 2, scale bar. 5µm. UZ (unloading

As the zygote develops to an embryo, GFP was still observed in the unloading zone, but much stronger in the embryo sack (Fig. 17 A-C). This was only seen in the beginning of embryo formation till octant or early globular embryo stage. Additionally MP17-GFP was detected at the inner integument layer 1 (Fig. 17 C, E). Strong GFP signals were also monitored in the inner integument layer 2 (Fig. 17 D). Here the decoration with plasmodesmata showed a preference for the anticlinal walls in some cells (Fig. 17 D, G). Simultaneous GFP expression in the two innermost integument layers appeared only in the very young stages of embryo development till the globular stage (Fig. 17 F).

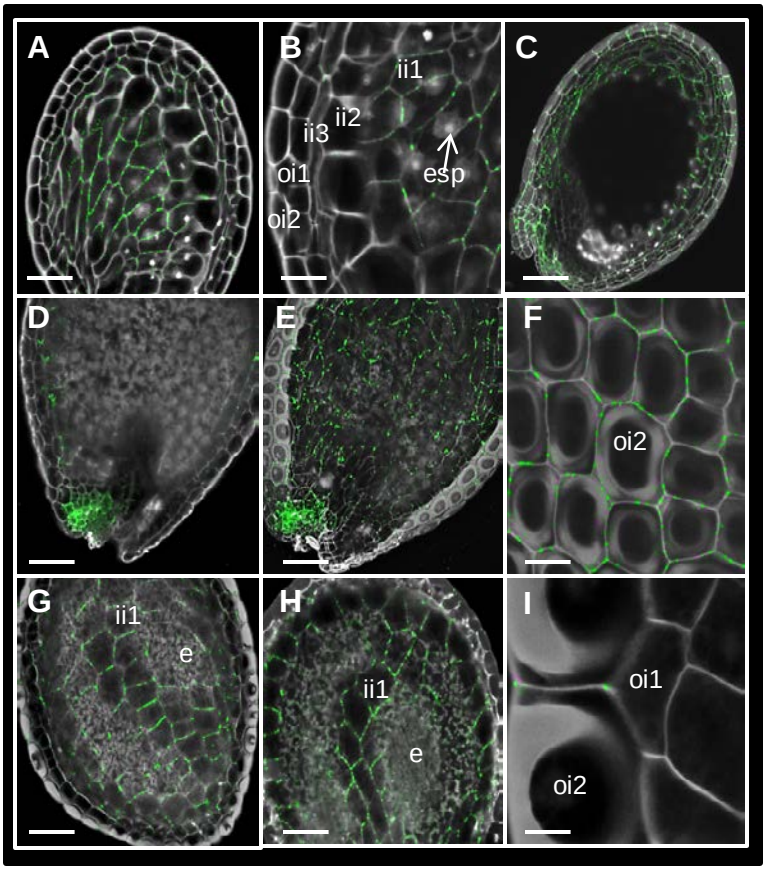

Figure 18. Distribution of plasmodesmata in the older seed. Plasmodesmata marked by MP17-GFP. (A) Overview of seed coat after globular embryo stage, GFP mainly found in the innermost integument layer, scale bar: 55µm. (B) Optical section through the seed coat, scale bar: 35µm. (C) Maximum projection of an older seed, GFP in the innermost integument layer and in the outermost layer, scale bar: 70µm. (D) Seed at early cotyledon bending stage, GFP maxima in the unloading zone and the endothelium, scale bar: 75µm. (E) Maximum projection of (D) shows GFP in the unloading zone, the outermost and innermost integument layer, scale bar: 70µm. (F) Outermost integument layer interconnected by plasmodesmata, scale bar: 23µm. (G) Old seed at late cotyledon bending stage, GFP mainly found in the endothelium, scale bar: 90µm. (H) Almost mature seed, GFP in the innermost integument layer, scale bar: 70µm. (I) Magnification of the two layers of the outer integument showing GFP only in the second layer between two cells of the outer integument layer 2. No GFP in walls facing the outer integument layer 1. Scale bar: 12µm. Ii (inner integument), oi (outer integument), esp (endosperm), e (embryo).

In the further stages of embryo development the strongest GFP signal was detected at the inner integument layer 1 (Fig. 18 A, B). Z-stacks showed that also in the outer integument a huge number of plasmodesmtat were present (Fig. 18 C). This was also observed during early cotyledon bending stage. Signals of MP17-GFP were still found in the unloading zone (Fig. 18 D), the outer integument layer 2 (Fig. 18 E, F) and in the innermost integument layer (endothelium) (Fig.18 E). This expression pattern didn't change during the following stages of seed maturation, the cotyledon bending stage (Fig. 18 G) and the late cotyledon bending stage (Fig. 18 H). In the almost mature seed, the amount of GFP spots in the outer integument decreases compared to the younger stages (compare Fig. 18 C, with Fig. 18 H). GFP marked plasmodesmata in the outer integument layer 2 were always orientated in direction of the next cell of the same layer and were absent in direction of outer integument layer 1 (Fig. 18 I).

5.4. Hormonal regulation of the reproductive tissue: dynamics during seed development

The development of the generative tissue is a tiny regulated processes where phytohormones play a central role in the regulation of gene expression and thus differentiation of tissues. The experiments performed are focusing on cytokinin and auxin response during seed maturation and elucidate the spatial-temporal dynamics of these phytohormones.

5.4.1. Cytokinin response in the reproductive tissue

To understand cytokinin response during seed development the synthetic cytokinin response sensor TCS was monitored, which drives ER-GFP (Zürcher et al. 2013). In the closed flower, before the ovule matures, GFP was detected in the nucellus tissue at the chalazal pole (Fig. 19 A). In the open flower, when the ovule is mature (Fig. 19 D, E), the GFP signal was still found in the nucellus tissue. Very weak signals were reported also in the phloem (Fig. 19 B, C). Directly after fertilization cytokinin response was dected exclusively in the developing endosperm (Fig. 19 F-K), as described in Li et al. (2013). GFP hotspots in the endosperm were around the embryo (Fig. 19 G, J) as well as in the chalazal pole. In the syncytial endosperm GFP was monitored outside of the nuclei (Fig. 19 K). GFP signals in the phloem disappeared almost completely as the endosperm started to develop into a syncytium (Fig. 19 K). Signals in the mature endosperm were still found, when the syncytial phase was almost competed (Fig. 20 A, B, M). Also in the older seed the GFP accumulation in the region around the embryo and the chalazal endosperm was still visible (Fig. 20 C-E). Signal intensity in the chalazal endosperm (Fig. 20 K) and nucellus tissue was strongest in the very early embryo stages (Fig. 20 F). As the embryo was in globular stage (Fig. 19 G) the GFP accumulated strongest in the region around the embryo (Fig. 20 I, J) and disappeared in the chalazal endosperm. Only in very few cases, GFP was detected in cells near the branching phloem (sieve elements) at the endpoint of the funiculus (Fig. 20 L). As the seed was in heart embryo stage, almost all signals in the endosperm were disappeared (Fig. 20 O, P) and solely found in the provascular tissue (Fig. 20 N). This was also seen in later embryo stages (Fig. 20 Q, R) until the seed was completely mature.

In summary cytokinin response was never found in the integuments and was strongest in the developing endosperm before cellularization occurred.

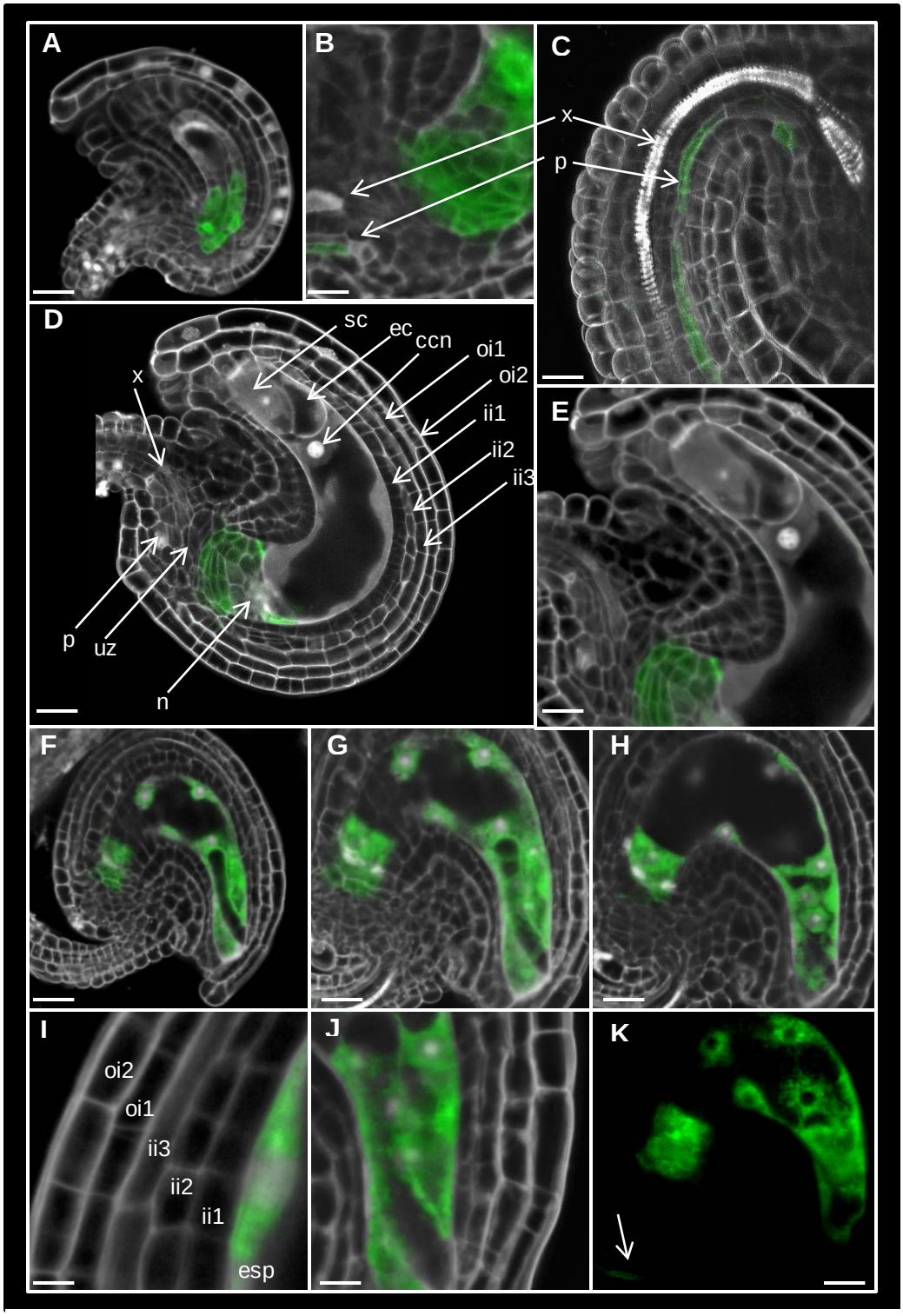

Figure 19. Cytokinin response in the ovule and after fertilization, visualized by P_{TCS}: *ER-GFP*. (A) Ovule of closed flower, GFP signals at nucellus tissue, scale bar: 15µm. (B) Chalazal pole of ovule in an open flower, GFP is present in phloem and nucellus, scale bar: 7µm. (C) Funiculus, weak cytokinin response in the phloem, scale bar: 15µm. (D, E) Ovule before fertilization, GFP restricted to the nucellus tissue, scale bars: (D) 18µm, (E) 12µm. (F-K) Young seed after fertilization, (F) single optical section, scale bar: 50µm. (G) Maximum projection shows endosperm nuclei and chalazal endosperm, scale bar: 30µm. (H) Accumulation of endosperm nuclei at the micropylar and chalazal pole, scale bar: 25µm. (I) Focus on seed coat layers showing GFP restricted to the endosperm, scale bar: 10µm (J) Embryo encircled by endosperm syncytium marked by GFP, scale bar: 12µm. (K) Maximum projection showing GFP signals in developing endosperm, arrow: only very weak GFP in the phloem, scale bar: 35µm. X (xylem), p (phloem), uz (unloading zone), n (nucellus), esp (endosperm), ii (inner integument), oi (outer integument), ccn (central cell nucleus), ec (egg cell), sc (synergid cell).

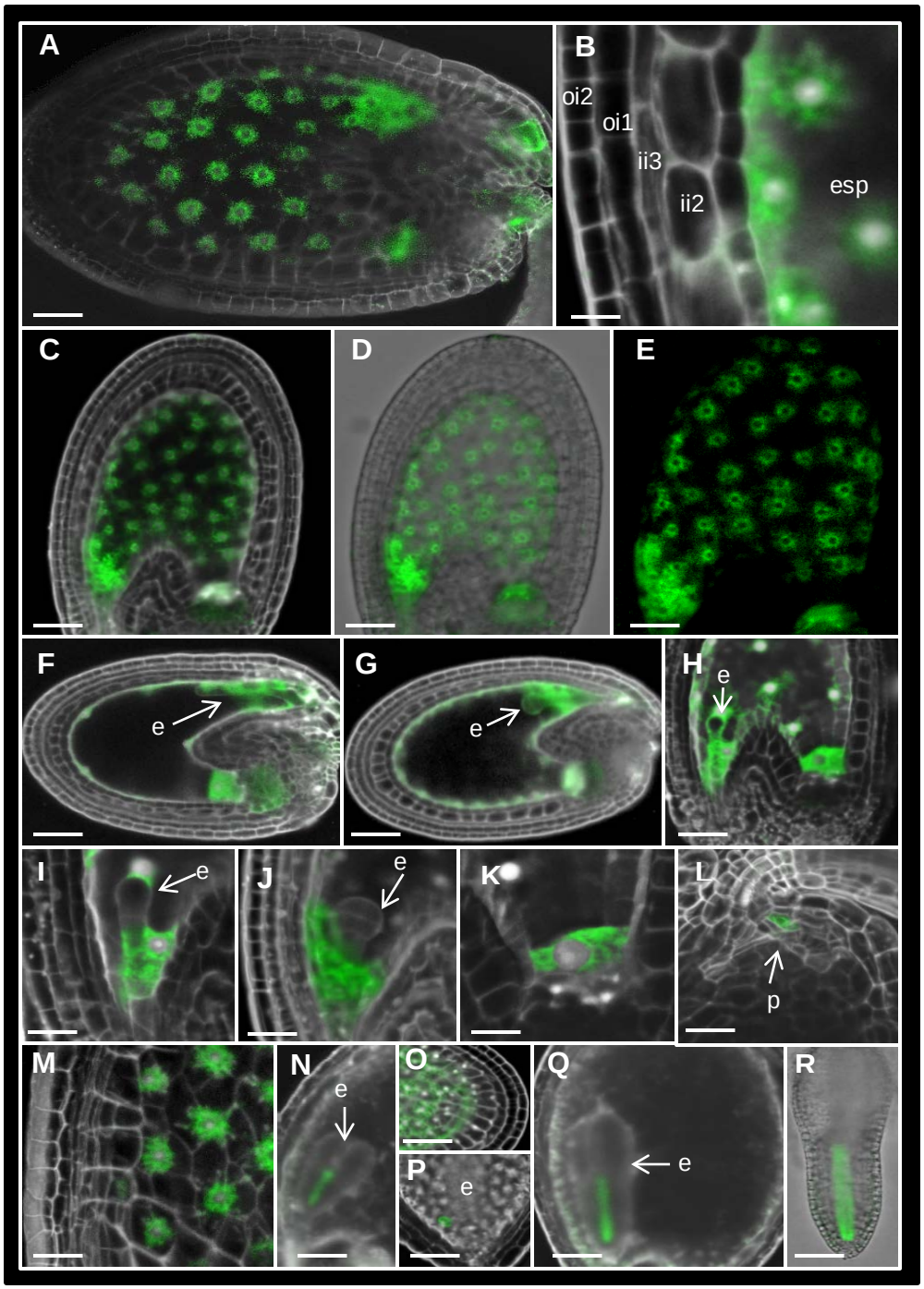

Figure 20. Cytokinin response after fertilization visualized by *PTCS: ER-GFP*. (A) Overview of a seed showing GFP expression in the endosperm and one cell of the outer integument, scale bar: 40µm. (B) Optical section through the seed coat with focus on the endosperm, scale bar: 15µm. (C-D) Maximum projection, GFP expression exclusively found in the endosperm. (D) Overlay with bright field image, scale bar: 40µm. (E) Magnification of the GFP channel, scale bar: 25µm. (F) Seed at two cell embryo stage, scale bar: 35µm. (G) Seed at globular embryo stage, scale bar: 40µm, (H) maximum projection at early globular stage, scale bar: 35µm. (I) Cytokinin response at two cell and (J) globular stage embryo, scale bar: (I) 15µm, (J) 20µm. (K) Magnification of the chalazal endosperm, scale bar: 18µm. (L) Unloading zone with phloem, scale bar: 20µm. (M) Maximum projection of the seed coat, scale bar: 25µm. (N, Q, R) GFP signals after heart stage embryo state of the seed. (O) Cellularized endosperm, GFP starts to disappear, scale bar: 70µm. (N, P) Early torpedo stage, (P) one remaining cell in the endosperm shows GFP, scale bar: (N) 80µm, (O) 65µm. (Q, R) Torpedo stage embryo in the seed (Q) and isolated (R), scale bar: (Q) 75µm, (R) 55µm. Esp (endosperm), e (embryo), ii (inner integument), oi (outer integument), p (phloem).

5.4.2. Auxin response in the reproductive tissue

In order to visualize the dynamics in auxin response during seed development the DR5 reporter was analyzed, driving ER-localized GFP (Ottenschlager et al.2003) in ovules and seeds. Before fertilization takes place GFP was detected in one cell file close to the xylem (Fig. 21 A, B). This single cell file showing GFP originates from the funiculus (Fig. 21 C) and was located in parenchymatic cells next to the xylem in collateral direction to the phloem (Fig. 21 D). From there, it was stretching extending into the ovule (Fig. 21 C, E). Auxin responding cells stopped at the same position the xylem ends in the unloading zone of the ovule (Fig. 21 F). After fertilization, extreme GFP fluorescence was found in the funiculus and the unloading zone (Fig. 22 A, B, D, E). In the seed at globular embryo stage very weak GFP signals were detected in single cells of the inner and outer integument (Fig. 22 A, F). Optical sections showed that GFP was distributed in a patchy pattern along the integument layers (Fig. 22 C, I, L). As the seed matures, more and more cells showed GFP in the integuments (Fig. 22 B, G). In young seeds, auxin response was found to be more present in the outer integuments (Fig. 22 C, D, I, L), whereas older seeds showed signals in the outer integuments and the inner integument (Fig. 22 H). GFP was also strongly observed in cells of the unloading zone directly after fertilization together with two cells of the inner integument, before any signal in the outer integuments was detected (Fig. 22 E). GFP-positive cells were surrounding the phloem (Fig. 22 J) and located in close physical vicinity to sieve elements (Fig. 22 K).

Comparing the state before and after fertilization, auxin response showed a different distribution. Before fertilization it was restricted to one xylem neighboring cell file and ended abruptly with the xylem in the ovule. After fertilization an enormous increase of GFP intensity was found in the funiculus and unloading zone; step-by-step more and more cells of the integuments showed GFP signals. No GFP was detected in the endosperm. In the unloading zone auxin response was found in cells distinct from the phloem but in close proximity to it.

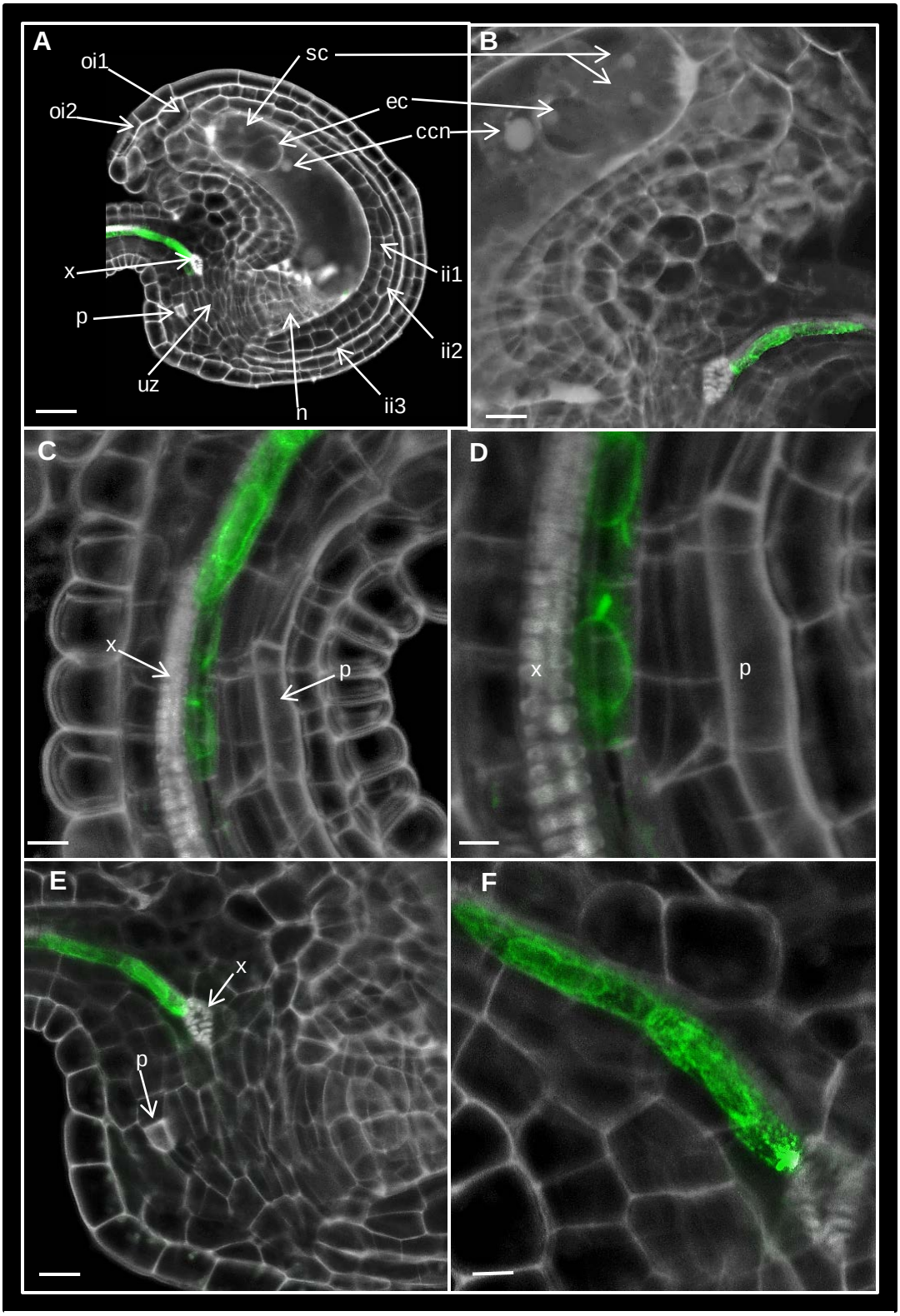

Figure 21. Auxin response before fertilization, visualized by *P_{DR5}: ER-GFP*. (A) Overview of an ovule, scale bar: 25µm. (B) Maximum projection of the micropylar end of the same ovule, two synergid nuclei as well as the nucleus of the egg cell and central cell can be seen, GFP restricted to a cell file next to the xylem, scale bar: 10µm. (C, D) Funiculus, DR5-GFP only present in cells next to the xylem collateral to the phloem, scale bars: (C) 5µm, (D) 3µm. (E, F) Unloading zone, (E) no GFP in phloem or other cells at the chalazal pole, scale bar: 10µm, (F) GFP signal stops together with the endpoint of the xylem, scale bar: 3µm. X (xylem), p (phloem), uz (unloading zone), n (nucellus), ii (inner integument), oi (outer integument), ccn (central cell nucleus), ec (egg cell), sc (synergid cell).

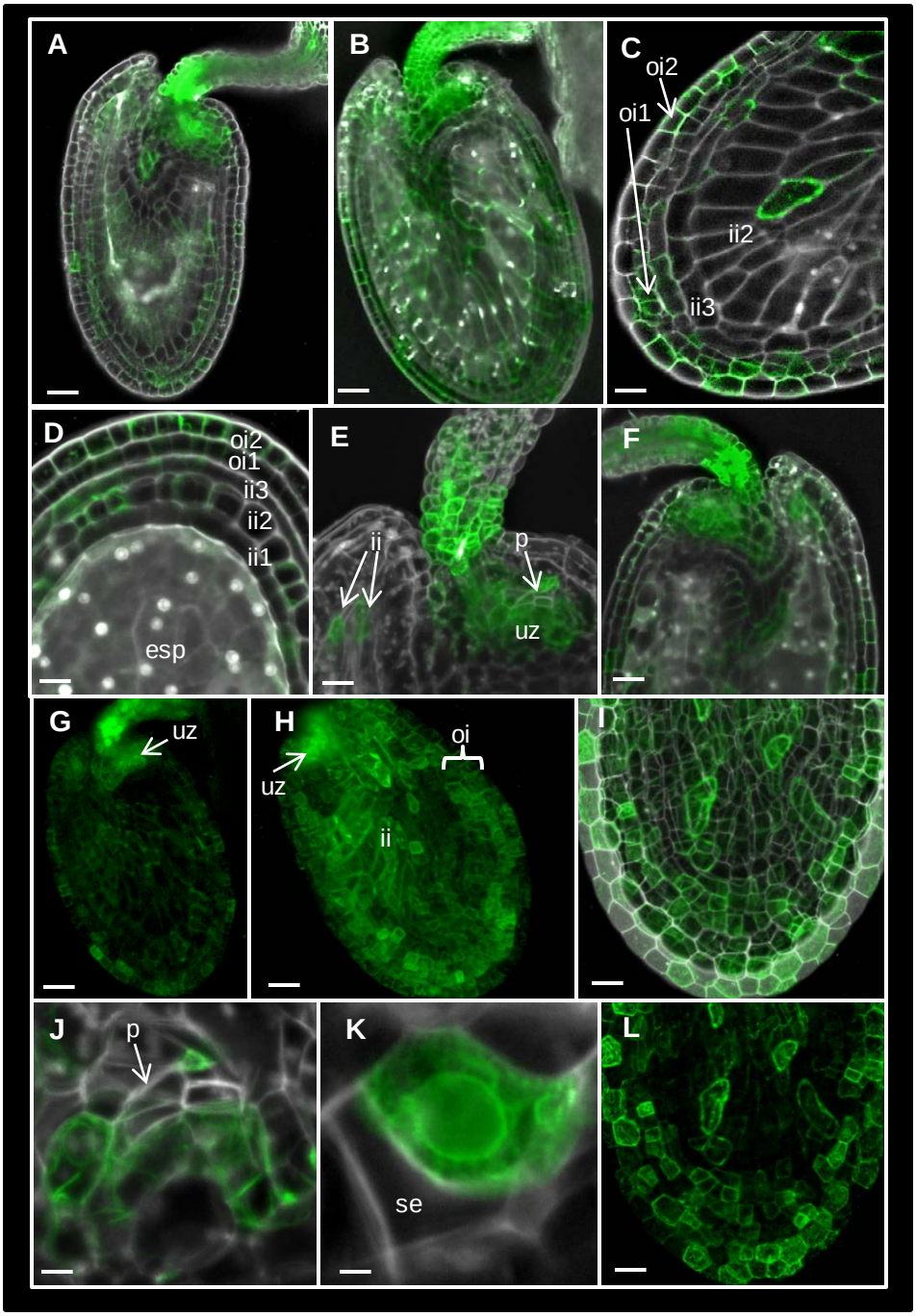

Figure 22. Auxin response after fertilization, visualized by *P_{DR5}: ER-GFP*.
(A) Overview of a young seed, GFP mainly in the funiculus, unloading zone and in single cells of the integuments, scale bar: 30µm. (B) Older seed, more cells of the integuments show GFP expression, scale bar: 50µm. (C) Seed coat with GFP signals in the outer integument and in single cells of the inner integument, scale bar: 25µm. (D) Auxin response is absent from endosperm, scale bar: 15µm. (E) Phloem is surrounded by cells showing auxin response, additional GFP signals detected in two cells of the inner integument, scale bar: 20µm. (F) No GFP was found in the endosperm, scale bar: 40µm. (G) GFP channel of (B) showing patchy pattern of DR5-positive cells, scale bar: 60µm. (H) Maximum projection of a seed before heart stage, GFP found in the unloading zone, the outer and inner integument, scale bar: 50µm. (I, L) Maximum projection through older seed coat, scale bar: (I) 15µm, (L) 18µm. (J) Unloading zone of the seed with phloem surrounded by DR5-positive cells, scale bar: 5µm. (K) Magnification of a sieve element (thicker cell walls) and neighboring DR5-positive cell, scale bar: 1.5µm. Uz (unloading zone), oi (outer integument), ii (inner integument), esp (endosperm), p (phloem), se (sieve element).

The DR5-GFP reporter is suitable to show strong auxin response in the respective tissue but is not sensitive enough to map weak responses. To overcome this limitation additional investigation of auxin response was done using the DR5v2 reporter (Weijers et al. 2015). This reporter is much more sensitive than DR5 due to the high-affinity binding site for ARFs in the promoter and the use of the fast processing mVenus. Fig. 23 summarizes the investigations. In summary the same results as with DR5 were found, but signals in the outer integuments appeared much earlier and stronger in the case of DR5v2 (Fig. 23 A, B, D, G) and were homogeneously distributed along the outer integument (Fig. 23 F), indicating that weak auxin response in the integuments occurred earlier in seed development than reported for DR5-GFP. Signals in the inner integument also appeared in a patchy pattern with the DR5v2 reporter (Fig. 23 C). An accumulation of mVenus was found in the funiculus (Fig. 23 D, H) and in the unloading zone after the endpoint of phloem and xylem (Fig. 23 I, L). Also with the high sensitivity of DR5v2 never any fluorescence in the phloem was monitored (Fig. 23 H, J, K). This result validates the previously shown findings about auxin response during seed development.

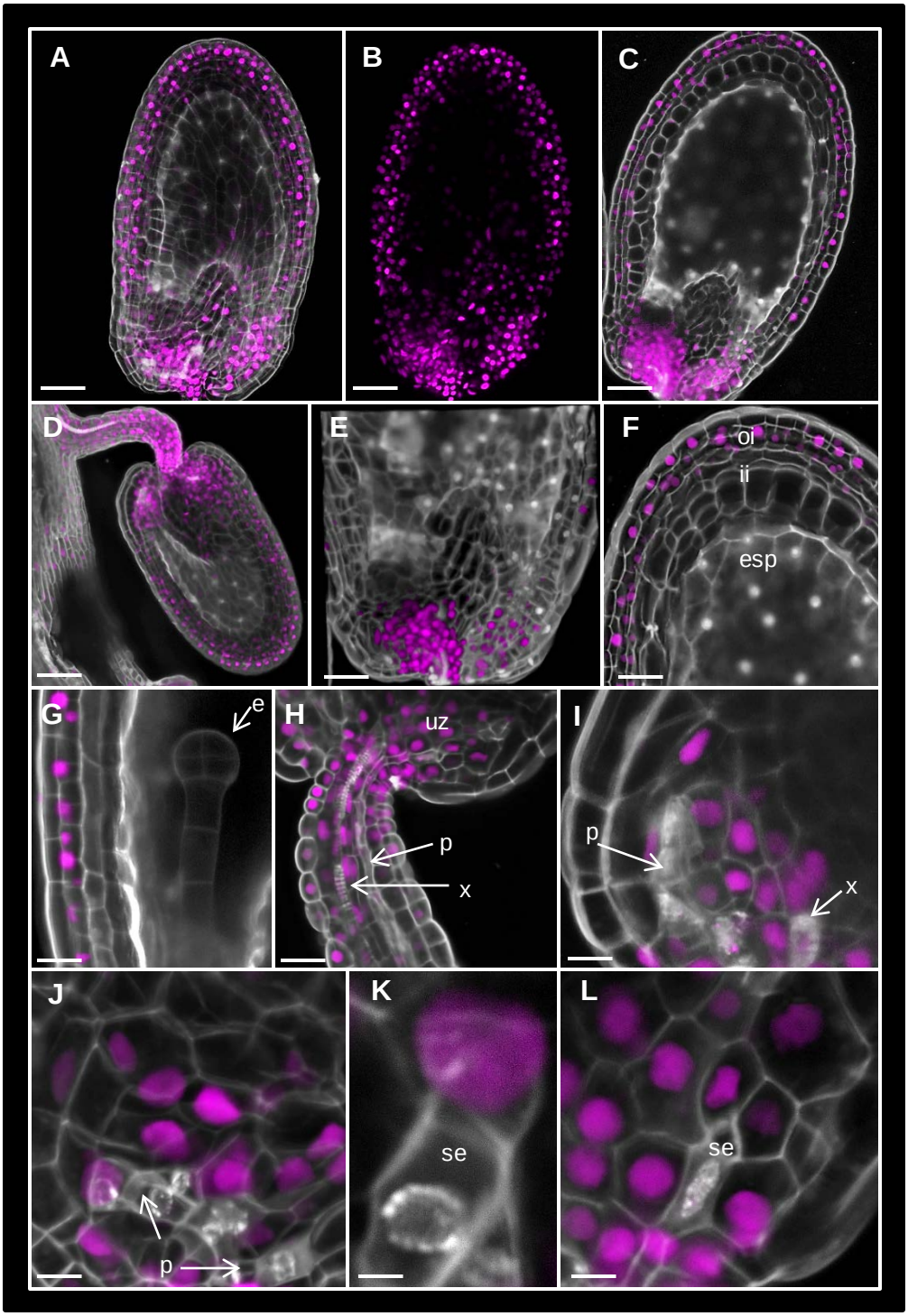

Figure 23. Auxin response after fertilization, visualized by P_{DR5v2}: *NLS-3xVENUS*. (A, B) Maximum projection of a young seed in globular embryo stage, Venus mainly in the unloading zone, the outer integument and in single cells of the inner integument. (B) Venus channel alone, scale bar: 60µm. (C) Single optical section of an older seed, scale bar: 60µm. (D) Strong signals in the funiculus and unloading zone, scale bar: 45µm. (E) 3D reconstruction showing signal maxima in the chalazal region of the seed as well as in the cells of the micropylar pole, single signals present in the posterior outer integument, scale bar: 40µm. (F) Maximum projection of the seed coat, scale bar: 25µm. (G) Strong signals in the two outer layers of the integuments, signals in the embryo were too weak to be visualized through the seed coat, scale bar: 15µm. (G) funiculus with xylem and phloem ending in the unloading zone, scale bar: 20µm. (I) Maximum projection of the unloading zone with endpoint of xylem and phloem, scale bar: 8µm. (J-L) Unloading zone: nucleated phloem cells (sieve elements) are surrounded by cells with high auxin input, scale bar: (J) 8µm, (K) 2µm, (L) 5µm. X (xylem), p (phloem), se (sieve element), oi (outer integument), ii (inner integument), esp (endosperm), e (embryo).

5.4.3. Auxin dynamics in the reproductive tissue

Auxin response is a result of auxin distribution in a tissue, but does not reflect how much auxin is present in the cells showing auxin response. To investigate the distribution of maxima and minima of auxin during development of the ovule and maturation of seeds the R2D2 reporter line was analyzed (Weijers et al. 2015). This line harbors the R2D2 construct (*$P_{RPS5A\text{-}mDII}$: NLS-Tomato/ $P_{RPS5A\text{-}DII}$: NLS-3xVenus)*, which functions as a sensor for auxin. Under the control of a ribosomal promoter the NLS-3xVenus expression occurs constitutively if auxin is absent and is down regulated in the presence of auxin. The DII NLS-Tomato is expressed in cells where high auxin levels are present. This means that green nuclei represent those cells, where an auxin minimum is located and red nuclei indicate a maximum of auxin in the cell. Yellowish color of the nuclei indicates a state between minimum and maximum.

In the beginning of the development of the female gametophyte there is no auxin in the functional megaspore mother cell (FMM. Fig. 24 C). Auxin accumulated in the young outer integuments, whereas cells of the inner integuments and the chalazal region showed less auxin (Fig. 24 A, B). An auxin gradient reaching from no auxin in the megaspore to high auxin levels in the outer integuments was detected. Later on, the gradient gets steeper: very high auxin levels were found in the chalazal pole (Fig. 24 E, H, G, J), no auxin in the female gametophyte and in a cell file stretching from the funiculus into the ovule (Fig. 24 F, I). Auxin levels in the inner integuments were in an intermediate state (Fig. 24 D, K-P). This gradient was also visible in the mature ovule shortly after fertilization, where much auxin was in the chalazal pole as well as in the integuments and much less auxin in the nucellus (Fig. 24 Q, R). After zygote formation this auxin gradient disappeared and a new gradient between the endosperm and the rest of the seed becomes visible (Fig. 24 W). As the embryo entered globular stage the gradient gets weaker (Fig. 24 X) and till heart stage of the embryo the auxin maxima in the integuments disappeared completely (24). At the endpoint of seed maturation, almost no gradient was detected in the integuments (Fig.24 Z). Most signals were present in the embryo tissue and the chalazal region.

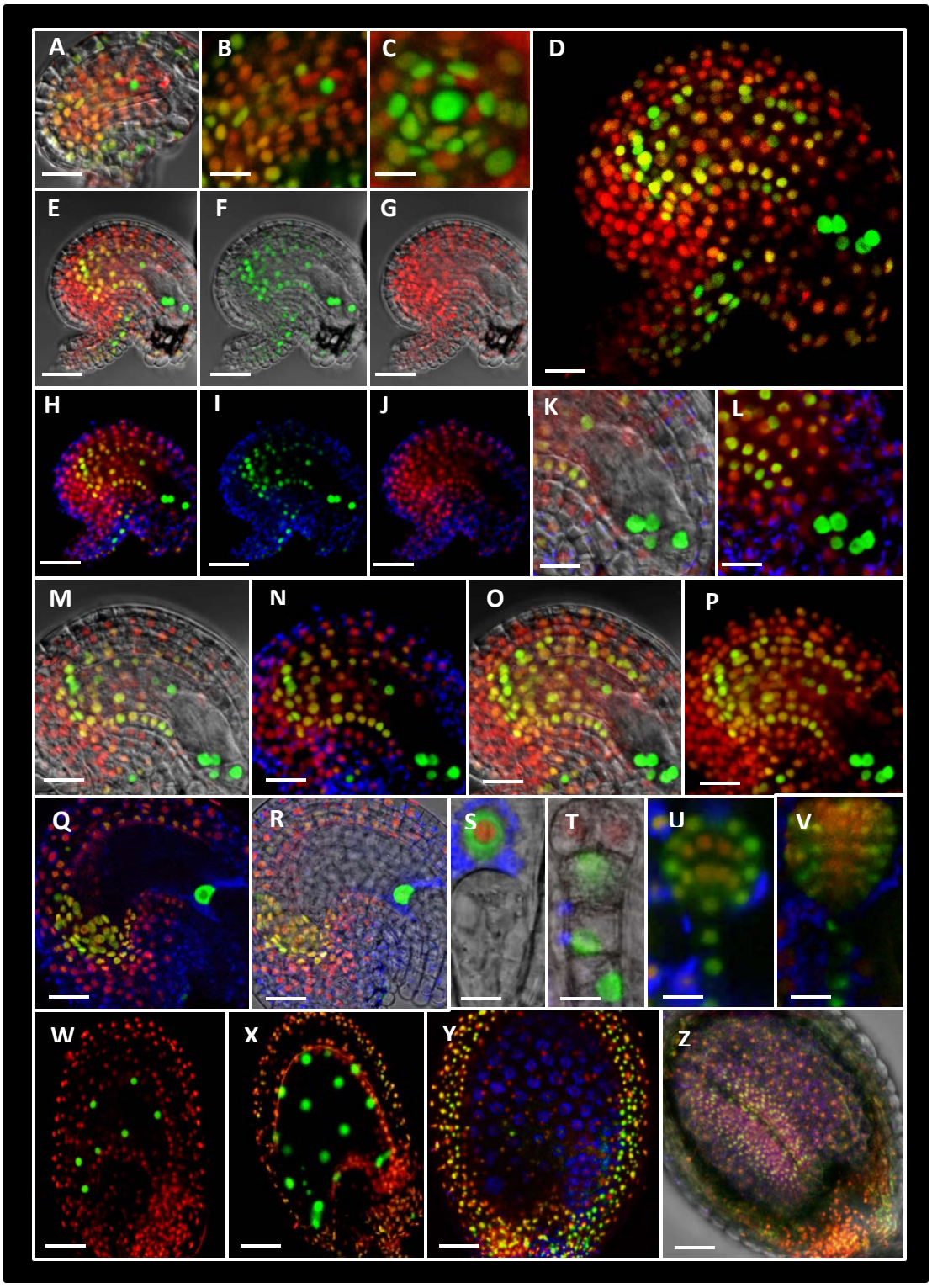

Figure 24. R2D2 expression during ovule and seed development. Red nuclei indicate the presence of auxin, green nuclei show absence of auxin, blue color: autofluorescence. (A-P) Auxin dynamics during development of the female gametophyte, (A-C) FG2-3. (A) Overview, bright field image, scale bar: 30µm, (B) magnification of the fluorescence channel from (A), scale bar: 15µm. (C) Maximum projection with focus on the functional megaspore mother cell, scale bar: 6.5µm. (D-P) ovule at FG5. (D) Maximum projection, scale bar: 25µm, (E-J) same ovule, (E) and (H) represent overlays of (F, G) and (I, J), scale bar: 40µm. (K, L) Magnification of the female gametophyte, scale bar: 18µm. (M-P) Magnification of the chalazal and micropylar end of the ovule showing the different distribution of auxin, scale bar: 22µm. (Q, R) Ovule immediately after fertilization, scale bar: 35µm. (S-V) R2D2 expression in different stages of embryo development, scale bars. (S) 12µm, (T) 10µm, (U) 15µm, (V) 20µm. (W-Z) Auxin dynamics during seed development, two cell embryo stage, scale bar: 40µm, (X) globular stage, scale bar: 50µm, (Y) heart stage, scale bar: 80µm, (Z) late cotyledon bending stage, scale bar: 90µm.

A closer look at the situation right after fertilization showed that only in the beginning of endosperm development a weak gradient of cells with much less auxin was found in the nucellus tissue (Fig. 25 A, B). Later on until the late globular embryo stage an auxin gradient between the syncytial endosperm and the integuments becomes visible (Fig. 25 C, D, E-H). There was no auxin in the endosperm but in contrast, high auxin levels in the two layers of the outer integument and in very few cells of the second layer of the inner integument (Fig. 25 J, K). Cells next to the endosperm also showed a clear auxin maximum. This gradient between endosperm and integuments decreased as the seed became older (Fig. 25 I, J, M). At the moment the embryo was in heart stage (Fig. 25 O, P) there was a change in the integuments concerning the auxin distribution. Cells of the outer integuments showed again higher auxin levels but in contrast to that cells of the inner integuments showed a very low auxin concentration, visualized by the presence of more green nuclei (Fig.25 N). Also in the very end phase of embryo development signals in the chalazal region were present, which indicates that auxin was still there. No further signals in the integuments could be documented in this stage, suggesting that these cells were already fully differentiated and dead.

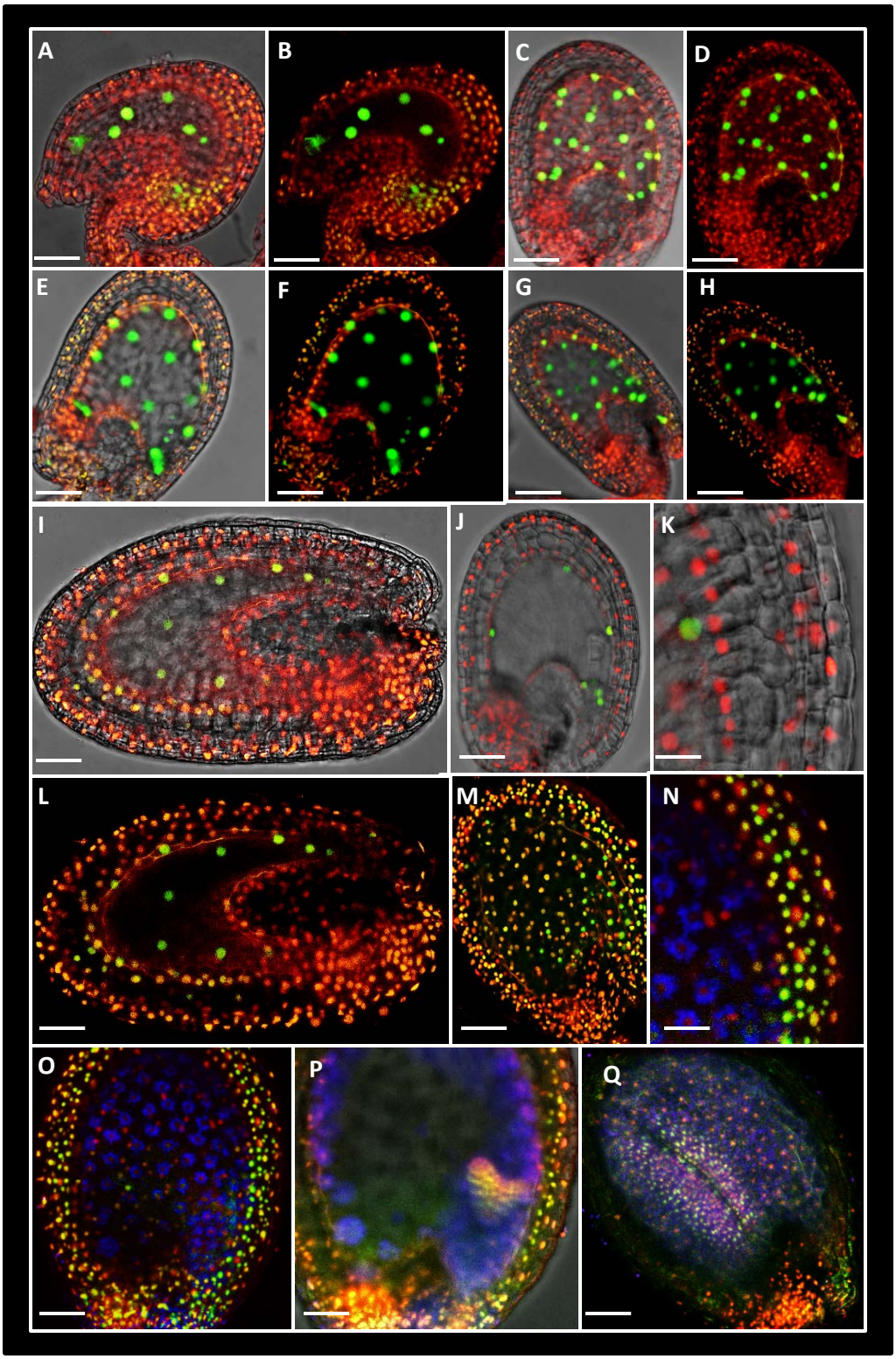

Figure 25. R2D2 expression during seed development. Red nuclei indicate the presence of auxin, green nuclei show absence of auxin, blue color: autofluorescence, seed age increases from top to bottom. (A-I, L) Different stages of early seed development. (B, D, F, H, L) Overlay of green and red channel. (A, C, E, G, I) overlay of fluorescence channels with bright field image, scale bars: (A, B) 30µm, (C, D) 40µm, (E, F) 45µm, (G, H) 60µm, (I, L) 50µm. (J) Optical section of (C), scale bar: 40µm. (K) Maximum projection, focus on seed coat, auxin in the outer integument and the innermost layer next to the endosperm, scale bar: 15µm. (M) Maximum projection of an older seed after cellularization of endosperm, scale bar: 80µm. (N) Seed coat of an older seed, scale bar: 20µm. (O) Auxin distribution in a seed about heart embryo stage, scale bar:80µm. (P) Same seed, with focus on embryo, scale bar: 60µm. (Q) Late cotyledon bending stage, scale bar: 90µm.

To sum up the results of auxin dynamics after fertilization it gets obvious that before the endosperm nuclei started to divide most auxin was in the integuments and in the chalazal pole (Fig. 26 A-C). Only the nucellus tissue and some cells of the inner integument layers at the chalazal end showed lower auxin accumulation (Fig. 26 D). This was also evident as signals resulting from high auxin levels in the seed coat compared to the endosperm (as seen in Fig 25) were gone. The outer integument showed higher auxin levels than the inner integuments (Fig. 26 E, F). In the unloading zone nearby the endpoint of the vasculature more auxin was present than in the periphery shortly after fertilization (Fig. 26 G-I). As the nuclei of the endosperm started to divide it was possible to see the same fluorescence pattern in all cells of the chalazal region and integuments, indicating a massive accumulation of auxin there (shown before in Fig. 25). In summary the auxin dynamics visulaized by R2D2 correlate with the previously shown results of DR5-GFP and DR5v2-mVenus reporters, which occur in those cells, where auxin maxima were found.

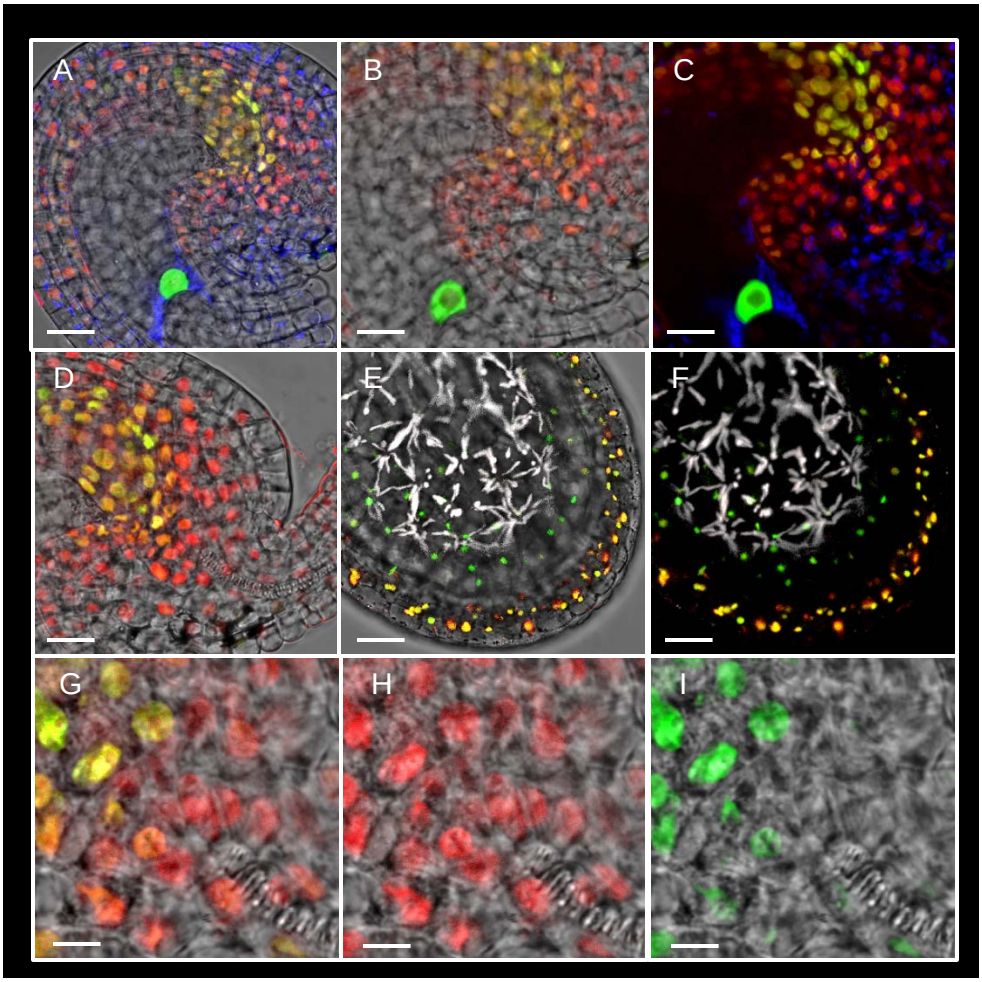

Figure 26. Auxin dynamics at unloading zone and seed coat visualized b R2D2. Red nuclei indicate the presence of auxin, green nuclei show absence of auxin, blue or white color: autofluorescence. (A-D) Ovule after fertilization. (A) Overview, scale bar: 20µm. (B, C) Maximum projection, focus on chalazal pole. (B) Overlay of (C) with bright field image, scale bar: 15µm. (D) Unloading zone before endosperm nuclei start to divide, scale bar: 10µm. (E, F) Maximum projection of a seed after globular embryo stage; mature endosperm in white, auxin maxima in the two outer layers of integuments, scale bar: 25µm. (G-I) Magnification of the unloading zone, auxin maxima in unloading zone. (G) Overlay of (H) and (I). (H) Shows presence of auxin. (I) Shows absence of auxin, scale bar: 8µm.

5.4.4. PIN3 localization during seed development

Based on the findings about the differences in the distribution of cytokinin and auxin response within the seed and the dynamics in the asymmetry of the presence and absence of auxin the question arose how these different auxin levels could be established. The asymmetry of auxin distribution within a tissue is achieved by transporter guided auxin transport. Hence expression of different auxin efflux transport proteins in the seed was analyzed. Marker lines for PIN-GFP under the control of their endogenous promoter were screened for PIN1, 2, 3, 4 and 7. With the exception of PIN3 no candidate was found to be expressed before or after fertilization in any integument or the female gametophyte. PIN3 also showed strong dynamics also in the seed with remarkable differences to the state before fertilization.

In the open and closed flower before fertilization, PIN3-GFP was monitored in the funiculus (Fig. 27 A). Cells next to the xylem showed the highest GFP intensity, which was polarly localized there in the anticlinal walls (Fig. 27 G). GFP was completely absent from the phloem (sieve elements, Fig. 27 G). From the funiculus the PIN3-positive cell file stretches into the ovule (Fig. 27 C, B). PIN3-GFP was limited to the cells near the xylem and ended at the same level the xylem vessel did (Fig. 27 E). Maximum projections showed furthermore that PIN3-GFP was restricted to the endpoint of phloem and xylem and that intensity of PIN3-GFP was strongest in cells close to the ending xylem. The intensity of GFP decreased in distance to the xylem (Fig. 27 D, F). At the chalazal pole of the ovule only very weak signals of GFP could be detected in those cells that were close to the phloem (Fig. 27 F).

Before fertilization PIN3-GFP was found to be associated with the xylem and ended abruptly as the xylem vessel stopped in the unloading zone.

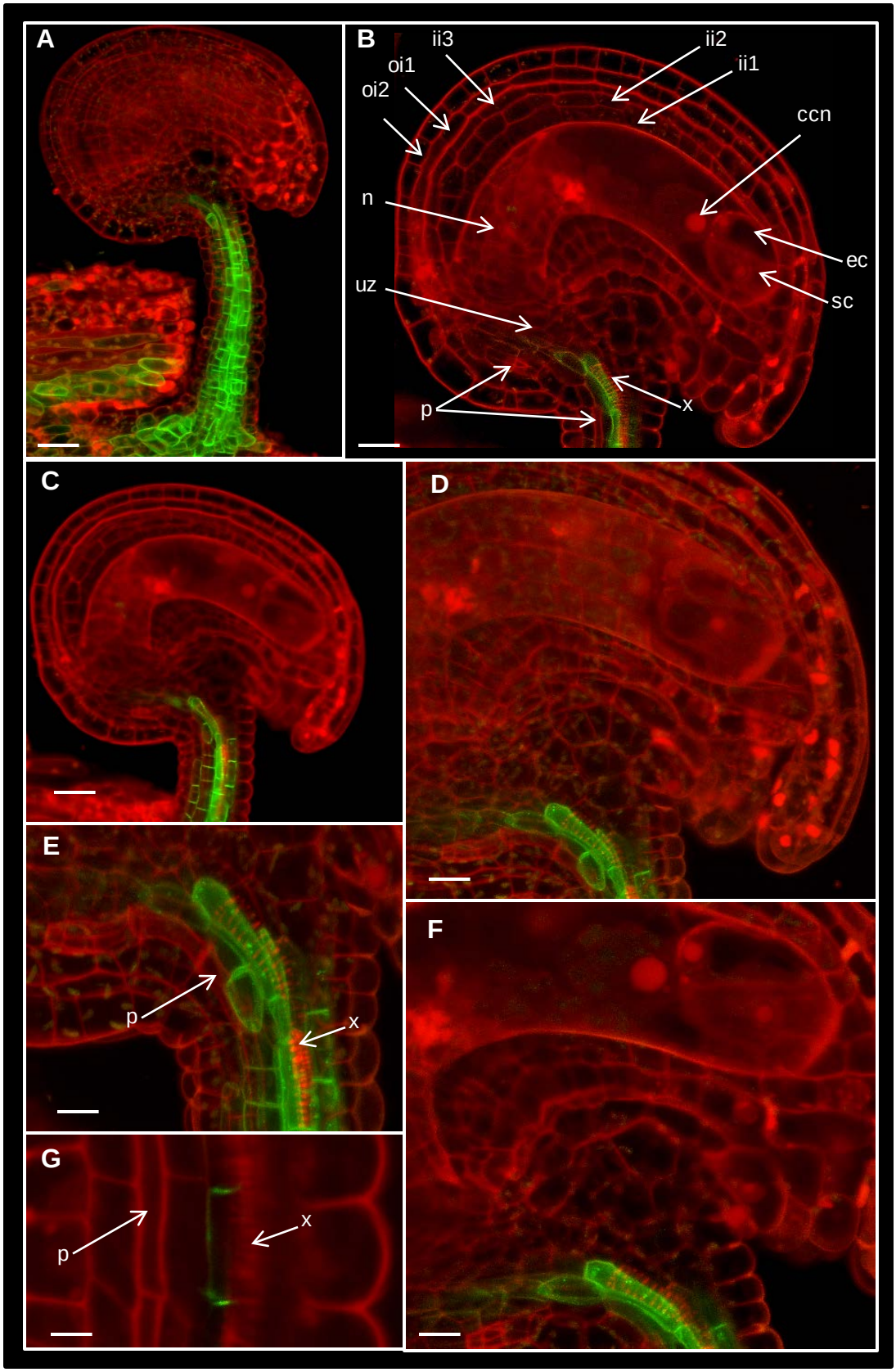

Figure 27. Localization of PIN3 in the ovule. Localization study was done with the *P*$_{PIN3}$*: PIN3-GFP* reporter line**.** (A) Ovule, connected to the funiculus, scale bar: 25µm. (B) Overview of ovule with PIN3-GFP expression at the endpoint of phloem and xylem, scale bar: 12µm. (C) Maximum projection of the same ovule, GFP in several cells from the funiculus, scale bar: 18µm. (D) Maximum projection focusing the endpoint of the vasculature, scale bar: 10µm. (F) Unfertilized ovule, synergid cell is intact, GFP is restricted to the ending vasculature, scale bar. 6µm. (E) Magnification of the ending vasculature with GFP signals ending at the same level, scale bar: 6µm. (G) Funiculus brightest GFP spot was detected in a cell file next to the xylem, scale bar: 4µm. X (xylem), p (phloem), uz (unloading zone), n (nucellus), ii (inner integument), oi (outer integument), ccn (central cell nucleus), ec (egg cell), sc (synergid cell).

Shortly after fertilization the situation changes dramatically. PIN3-GFP was still found in the funiculus, but additional strong signals were detected in the innermost layer of the integument surrounding the central cell and the cells of the unloading zone (Fig. 28 A-D). Looking closer at the endpoint of the funiculus into the young seed revealed additional weak signals in the outer integument (Fig. 28 E, F). The signals there showed a polar distribution towards the anticlinal walls in contrast to the PIN3-GFP signals in the unloading zone. GFP intensity differed also within the seed. The GFP signal found in the inner integument layer 1 was stronger than signals coming from the unloading zone. A single strand of cells in the unloading zone coming from the funiculus showed also much brighter GFP than the surrounding cells (Fig. 28 G). The weakest GFP signals were obtained from the outer integument. A shift of PIN3-GFP signals from the proximal region of the seed close to the funiculus and those parts that were in the distal area far away from the unloading zone was seen: in the distal parts the only GFP signal that could be obtained was from the innermost integument layer, no further GFP in any other layers was visible (Fig. 28 B, H). Single cells of the first layer of the outer integument showed PIN3-GFP in polar distribution at the micropylar pole of the seed, too (Fig. 28 H).

Directly after fertilization PIN3-GFP was spread over the whole unloading zone and appeared very prominent in the innermost integument layer. Polar distribution of PIN3-GFP was seen in cells of the outer integument at the proximal part of the seed at the micropylar and chalazal end. Distal parts of the seed showed GFP restricted to the inner integument layer 1.

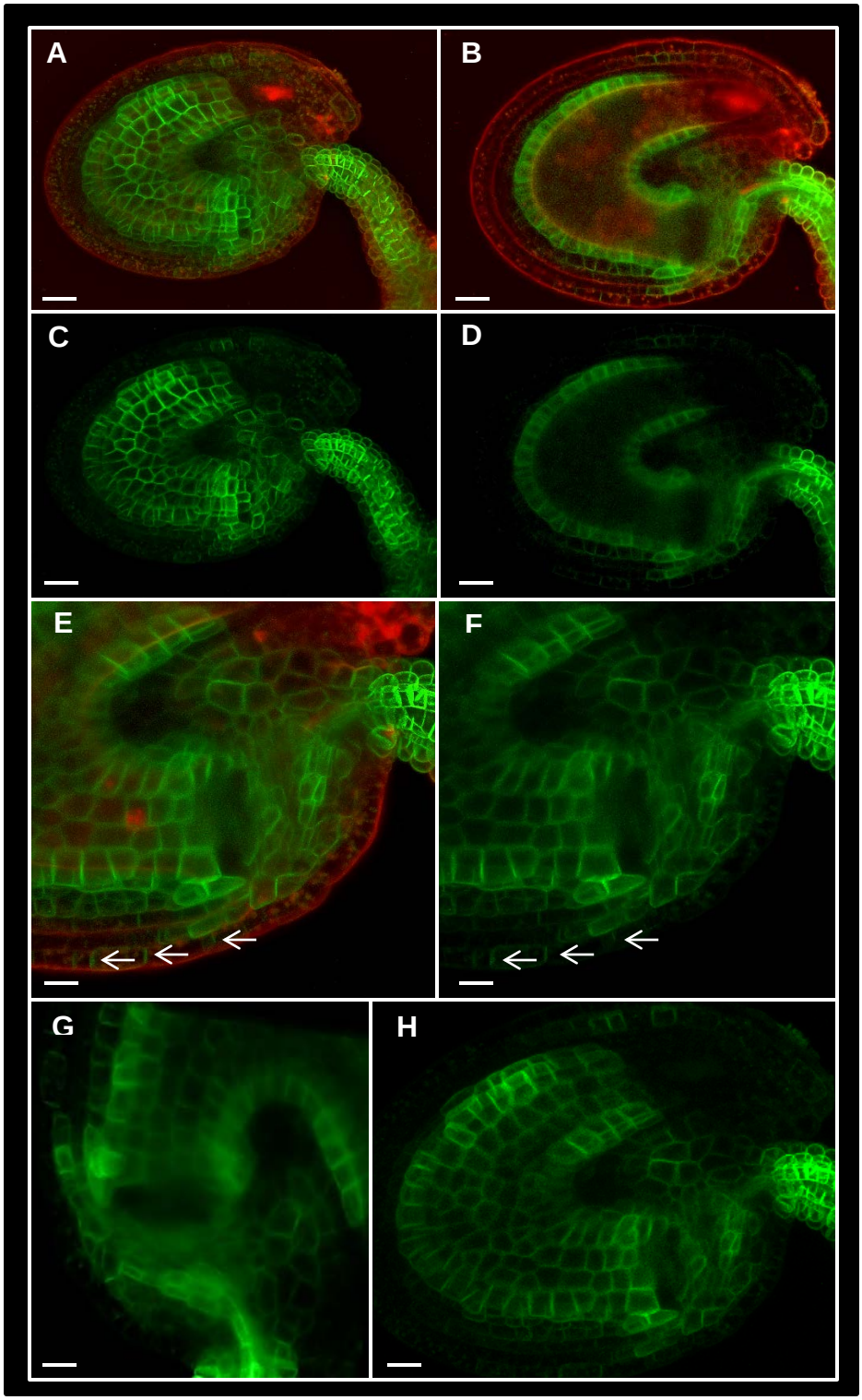

Figure 28. Localization of PIN3 right after fertilization. Localization study was done with the *P*$_{PIN3}$*: PIN3-GFP* reporter line**.** (A, C) Maximum projection in a very young seed before endosperm development started, degenerated synergid visible as bright red spot in the micropylar end. (C) GFP channel, scale bar: 30µm. (B, D) Optical section, PIN3-GFP strongly detected in the funiculus, GFP signals at the unloading zone and in cells of the innermost integument layer, (D) GFP channel, scale bar: 20µm. (E, F) Maximum projection of the unloading zone, GFP in funiculus, unloading zone, inner integument and very weak in the outer integument, arrows mark polar distribution of GFP in the outer integument, (F) GFP channel, scale bar: 12µm. (G) 3D reconstruction of GFP signals found at the unloading zone, GFP is stronger in a cell file coming from the funiculus and in the cells of the inner integument, weak signals in the outer integument, scale bar: 15µm. (H) All cells of the inner integument show PIN3-GFP, signals in the outer integument only in the micropylar and chalazal end, cells in the funiculus show strongest GFP intensity, scale bar: 17µm.

Looking closer at the integuments distal from the funiculus revealed that GFP signals are found exclusively in one cell file close to the embryo sack and that every cell was decorated with PIN3-GFP (Fig. 29 A-C, F). Cells of the inner integument layer 1 showed furthermore a polar distribution of GFP to the anticlinal cell walls (Fig. 29 G, H, K, L). Much weaker signals of PIN3-GFP were seen in the second integument layer which was in proximity to the chalazal pole (Fig. 29 I, J). This signal distribution disappeared in distance to the unloading zone (Fig 29 D, J).

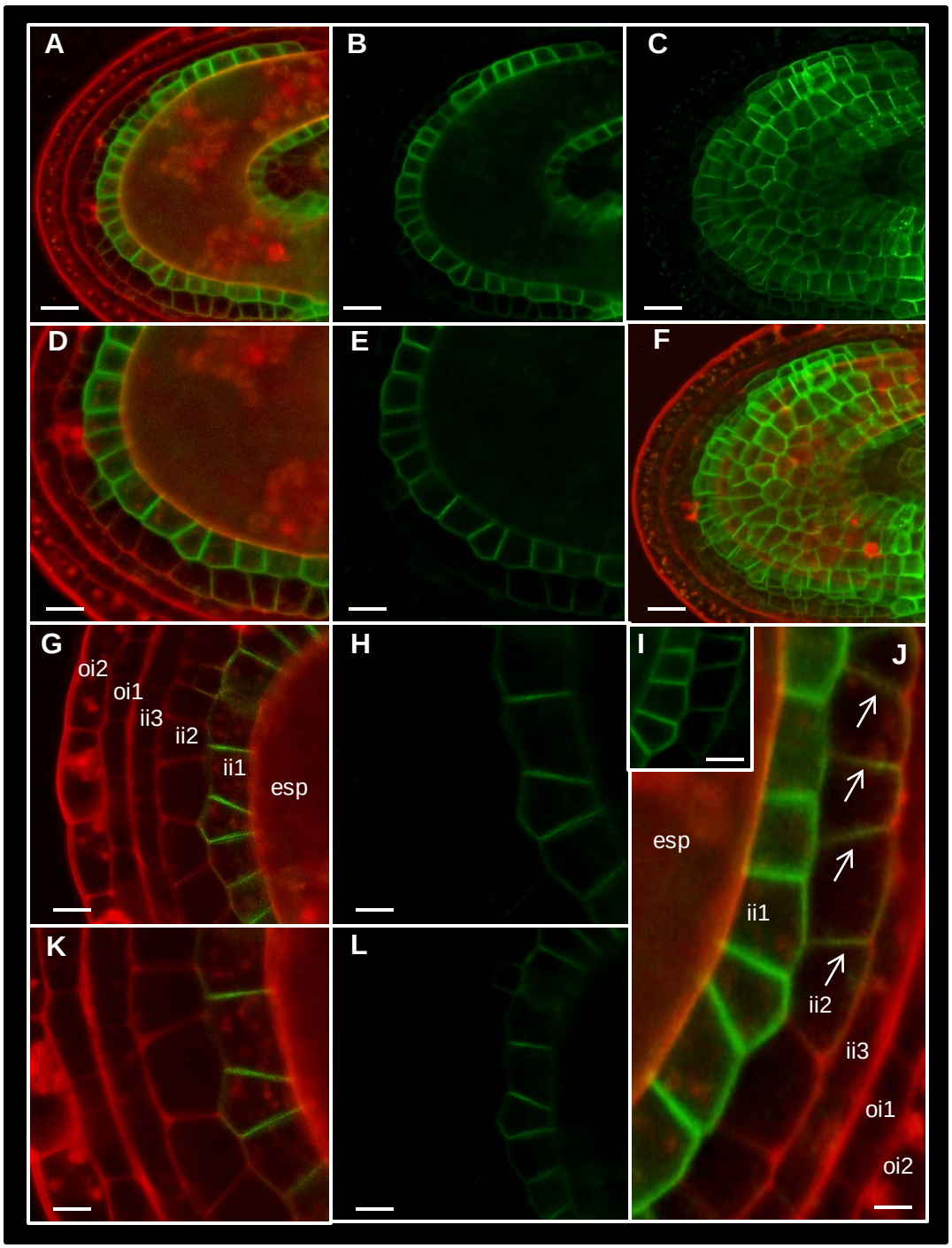

Figure 29. Localization of PIN3 after fertilization in the innermost integument layer. Localization study was done with the *P*$_{PIN3}$*: PIN3-GFP* reporter line**.** (A, D, G, K) Overlay of GFP channel with PI counterstain. (B, E, H, L) GFP channel. (A, B) Overview of the distal end of a young seed, endosperm nucleus migrating towards the chalazal end, scale bar: 17µm. (C, F) Maximum projection of the same area. (C) GFP channel, scale bar: 17µm. (D, E) Magnification of the area near the chalazal pole, weak GFP signals in the inner integument layer 2, scale bar: 10µm. (G, H) Single optical section at the distal end of the seed, GFP exclusively in the innermost integument layer, scale bar: (G) 8µm, (H) 2.5µm. (K) Magnification of the seed coat with polar distribution of PIN3-GFP, scale bar: 5µm. (I, J) Magnification of the integuments coming from the chalazal region (top) and stretching to the distal end (bottom), GFP maxima in the ii1, only very weak GFP intensity in ii2 at the chalazal direction (arrows) indicated by the yellowish color of the cell walls. (I) GFP channel of (J), scale bars: (I) 10µm, (J) 5µm. Esp (endosperm), ii (inner integument), oi (outer integument).

In the older seed, when the embryo reaches the early globular stage PIN3-GFP was found to be broadly distributed at the chalazal zone in the outer integument and inner integument layer 1 and 2 (Fig. 30 B, G). PIN3-GFP in the outer integument was polarly localized at the anticlinal walls (Fig. 30. A, C, D). No polar distribution was seen at the chalazal region in the unloading zone (Fig. 30 E, F). Referring to the signal intensity it was documented, that in the stage shortly after fertilization the inner integument layer 1 had the strongest GFP signal intensity compared to signals detected in the unloading zone. In contrast to the quite weak GFP signals in the outer integument right after fertilization the GFP inensity was much stronger in the later stages of seed development and appeared in polar distribution along the anticlinal walls (Fig. 30 H). Altogether also at the later stages of seed development a gradient of GFP signals between the proximal and distal end of the seed was obvious (Fig. 30 B, G): much more cells of the integuments at the distal part of the seed showed GFP than in the earlier already described stages right after fertilization. Cells of the inner integument layer 3 displayed any GFP signal.

PIN3-GFP in the young seeds showed an increment of signals in the integuments that were in distance from the unloading zone. The expression pattern in the inner integument layer 1 remained as before right after fertilization. Much more cells of the outer integument showed GFP signals in polar distribution, compared to the state shortly after fertilization.

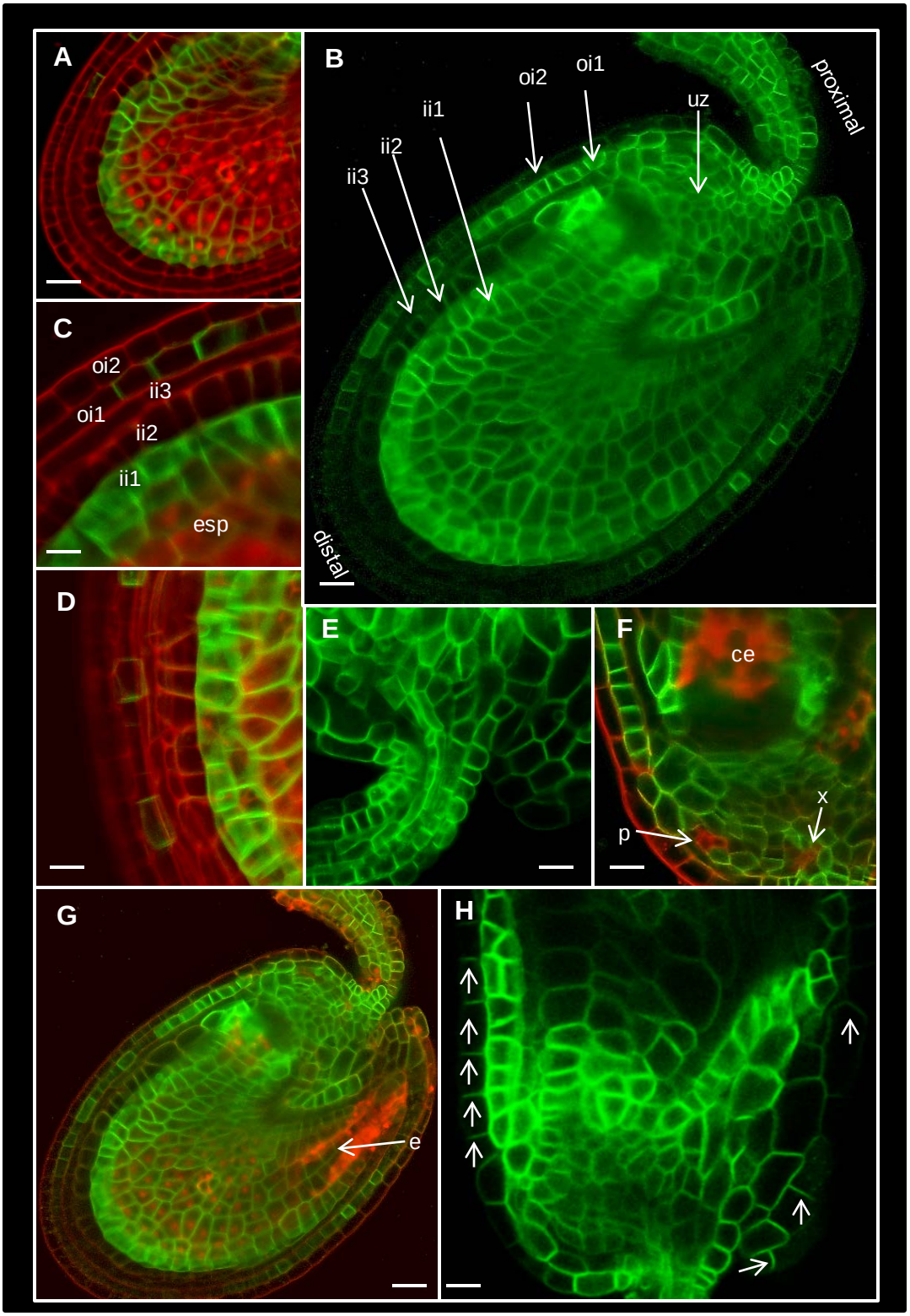

Figure 30. Localization of PIN3 in the young seed. Localization study was done with the *P*$_{PIN3}$*:PIN3-GFP* reporter line**.** (A, C, D) Seed coat at the distal end of the seed, GFP signals mainly in the innermost layer of the inner integument, only few cells of the outer integument show polar GFP distribution. (A) Overview of all integument layers, scale bar: 25µm. (C) Optical section showing single cells of the first layer of outer integument with GFP expression, scale bar: 14µm. (D) Maximum projection, weak PIN3-GFP in the outer integument, scale bar: 14µm. (B, G) PIN3-GFP signals in a seed with globular embryo, tissue close to the funiculus shows stronger fluorescnece as the distal parts of the seed. (B) GFP channel, scale bar: 18µm. (G) Overlay of GFP channel with PI stained seed coat and endosperm, scale bar: 25µm. (E) Funiculus and unloading zone, scale bar: 17µm. (F) Unloading zone with ending phloem, scale bar: 12µm. (H) Polar distribution (arrows) of PIN3-GFP in the second layer of the outer integument, GFP strongest in the inner integument, scale bar: 15µm. X (xylem), p (phloem), uz (unloading zone), ii (inner integument), oi (outer integument), e (embryo), esp (endosperm), ce (chalazal endosperm).

The same was true for the more developed seed (Fig. 31 A, D). GFP was again seen in the innermost integument layer, the second layer of the inner integument and in the outer integument in polar fashion (Fig 31 B, C). GFP signals in the unloading zone also showed no tendency to polarize PIN3 in older stages of the seed (Fig. 31 E, F). In the unloading zone the phloem was completely devoid of PIN3-GFP (Fig. 31 E, F). Signals in the funiculus and near the unloading zone still persist (Fig. 31 G). As the seed developed further to the early heart embryo stage the GFP fluorescence showed a reduction of signal intensity in the inner integument layer1 and an increment in the outer integument layer 1 (Fig. 32 A, F). In this cell layer, signal maxima were observed at the chalzal pole (Fig. 32 A). Almost all cells of the outer integument layer 1 showed PIN3-GFP signals at this developmental stage of the seed (Fig. 31 B, D). Only very few cells of the outer integument layer 2 were PIN3-positive and showed fluorescence in a polar fashion (Fig. 31 C, E). As the seed proceeded further in maturation to the torpedo and cotyledon bending stage the signals in the inner integument layer 1 disappeared completely. Only the outer integument layer 1 showed GFP signals anymore (Fig. 32 G,H) during the maturation phase of the seed coat (Fig. 32 I, J).In the almost mature seed at late bending cotyledon stage the GFP was restricted to the outer integument layer 1 (Fig. 32. G). From there signals stretched into the distal end of the seed. GFP intensity formed again a gradient: strongest GFP fluorescence was fund in those cells of the outer integument near to the chalazal pole and gets weaker the more the cells lay in the distal periphery.

During seed maturation PIN3-GFP showed no differences to the expression pattern seen in the seed at globular embryo stage. The tendency that with increasing age of the seed more cells in the seed coat from the periphery showed GFP signals was continued in the older stages. But also there, cells in the periphery distal to the funiculus showed no GFP fluorescence with exception of the inner integument layer 1. During the later stages of embryo development the signals in the innermost layer of the seed coat disappeared completely. At this moment, all cells of the outer integument layer 1 were PIN3-positive. This expression pattern remained during the final maturation of the seed coat. In the almost mature seed, GFP was restricted to the first layer of the outer integument, where fluorescence intensity was seen as a gradient with high intensity at the chalazal pole to weaker intensity at the distal end of the seed. This correlates well with the analysis of R2D2 and the DR5 reporters, where auxin maxima and the maximum auxin response was found in the chalazal pole of the seed.

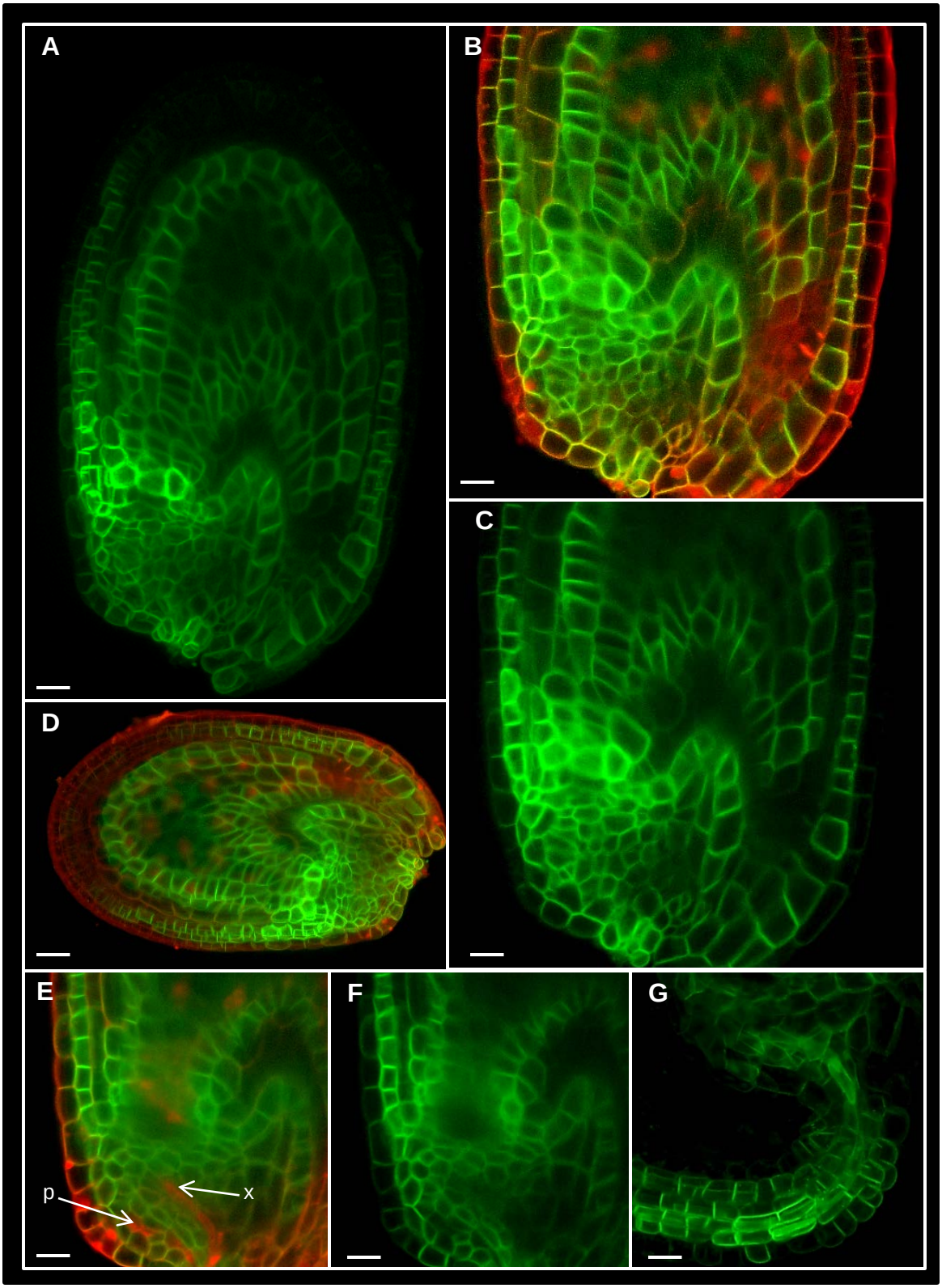

Figure 31. Localization of PIN3 in the older seed. Localization study was done with the *P*$_{PIN3}$*: PIN3-GFP* reporter line**.** (A) Maximum projection of an older seed, GFP maxima in the proximal parts of the seed that are close to the funiculus, scale bar: 25µm. (B, C) Optical section shows polar distribution of PIN3-GFP in the outer integument, cells of the inner integument near the unloading zone show stronger GFP intensity. (D) GFP channel, scale bar: 15µm. (D) Overlay of (A) with PI stained cell walls of the integuments, GFP in the outer integuments does not reach the distal end of the seed, scale bar: 35µm. (E, F) Magnification of the unloading zone with ending phloem and xylem, GFP signals in the outer integument and first two layers of the inner integument, scale bar: 20µm. (G) GFP fluorescence in the funiculus persists also in older stages of seed development, scale bar: 10µm. X (xylem), p (phloem).

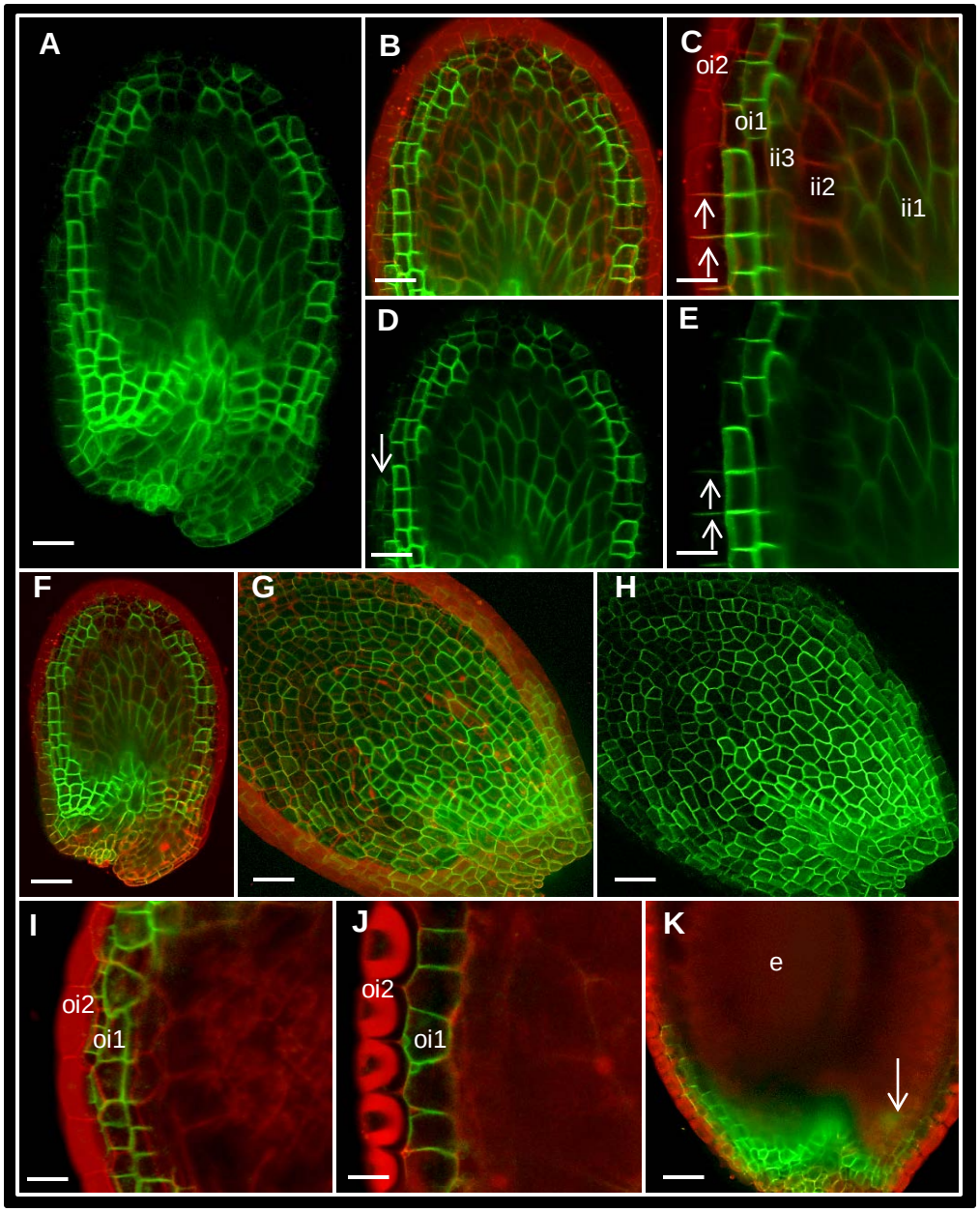

Figure 32. Localization of PIN3 in the seed during maturation of the seed. Localization study was done with the *PPIN3: PIN3-GFP* reporter line**.** (A, F) Maximum projection of a seed at about heart embryo stage, GFP strongest in the inner integument of the chalazal region, nearly all cells of the outer integument layer 1 show GFP expression, (A) GFP channel, (F) overlay with PI stained seed coat, scale bars: (A) 22µm (F) 52µm. (B, D) Maximum projection of the distal region of the same seed (B) overlay of (D) with PI stained seed coat. (D) GFP channel, GFP in the innermost integument layer and the outer integument layer 1, weak signals in the outer integument layer 2 only at the chalazal region (arrow), scale bars: 35µm. (C, E) Maximum projection with focus on the seed coat at the chalazal pole. (C) Overlay of (E) with PI stained seed coat. (E) GFP channel, GFP found in the outer integument layer 1 and 2 (polar distribution marked by arrow) and in the inner integument layer 1, scale bars: 13µm. (G, H) Seed at the beginning of the cotyledon bending stage. (H) GFP channel, (G) overlay of (H) with PI staining, GFP solely found in the outer integument layer1, scale bars: 40µm. (I) Maximum projection of the seed coat from a seed at about cotyledon bending stage, GFP only in the outer integument layer 1, scale bar: 25µm. (J) Seed coat almost at maturity, GFP in the first layer of the outer integument, scale bar: 15µm. (K) Old seed at late cotyledon bending stage, GFP solely found in the chalazal region and the first layer of the outer integument, weak GFP signals in the root of the embryo was also detected through the seed coat indicated by the arrow, scale bar: 50µm. E (embryo), oi (outer integument), ii (inner integument).

5.4.5. D6 protein kinase localization during seed development

PIN3 expression alone does not necessarily tell anything about the activity of the auxin efflux protein. It was already shown that D6 kinase is able to phosphorylate PIN3 (Zourelidou et al. 2014). In order to investigate in the seed the activation of PIN3 by the D6 protein kinase an expression analysis was done using a marker line for D6PK. The question was if expression of the D6 kinase occurred in the same cells where PIN3-positive cells were reported, which would indicate an activation of PIN3. A look at the fusion protein of YFP-D6PK under the control of its endogenous promoter showed that after fertilization signals were monitored in the unloading zone and the outer integument (Fig. 33 A, B, C). As the endosperm nuclei divide D6-YFP was found to be polar localized at the anticlinal walls of the two outer integuments (Fig. 33 D, E). During the cellularization of the endosperm the signal intensity of D6 gets weaker in the first layer of the outer integument (Fig. 33 F) and disappears completely as the seed develops further (Fig. 33 G). In later stages D6-YFP was still polar localized in the second layer of the outer integument (Fig. 33 H) and restricted exclusively to the outermost layer of the seed coat (Fig. 33 I). No YFP was ever observed in the innermost integument layer, where the strongest PIN3-GFP signals occurred.

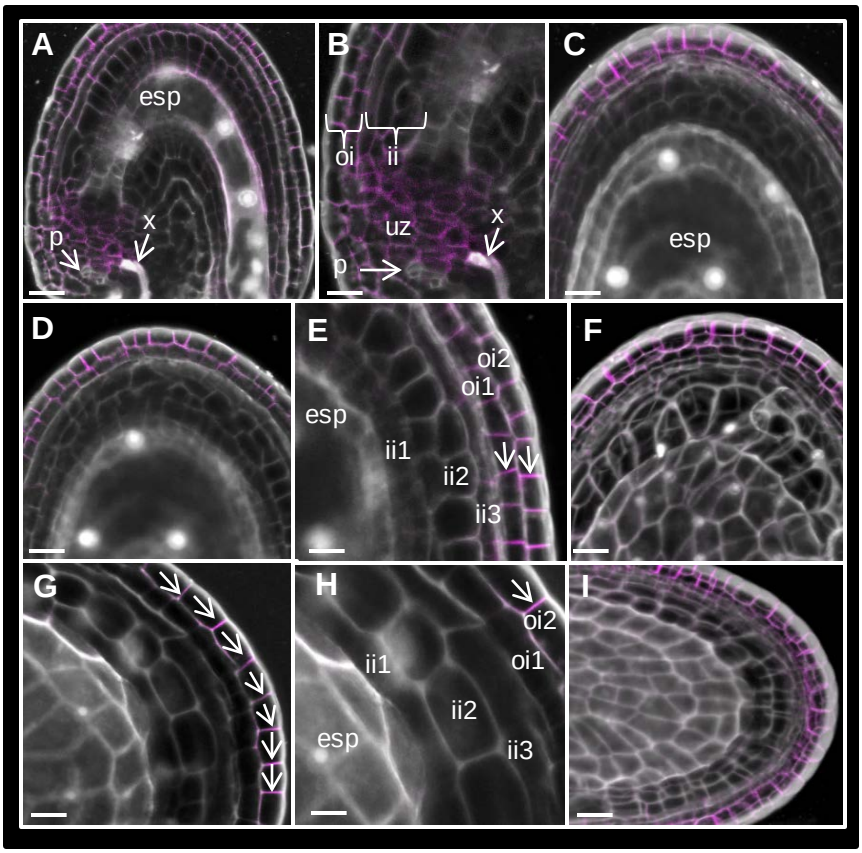

Figure 33. YFP-D6PK distribution in the seed. (A) Overview of a young seed, endosperm starts to develop, D6 in the unloading zone and outer integument, scale bar: 22µm. (B) Magnification of the unloading zone and seed coat, D6 absent from the inner integument, scale bar: 13µm. (C) Maximum projection of a seed with fully developed nucleated endosperm, D6-YFP restricted to the outer integument, scale bar: 14µm. (D, E) Single optical section of the seed coat showing YFP signals in the two layers of the outer integument, scale bar: (D) 17µm, (E) 9µm. (F) Distal end of the seed coat of a seed with cellularized endosperm, scale bar: 17µm. (G, H) Older seed after cellularization of the endosperm, D6-YFP restricted to the outermost seed coat layer. (H) Magnification of (G), D6-YFP shows polar distribution, scale bar: (G) 15µm, (H) 10µm. (I) Maximum projection of the seed coat after cellularization of the endosperm, YFP restricted to the outer integument, scale bar: 25µm. X (xylem), p (phloem), uz (unloading zone), ii (inner integument), oi (outer integument), esp (endosperm), arrows indicate polar distribution of YFP-D6PK.

5.5. Expression of *SCR* during ovule and seed development

Besides of hormones transcription factors play a central role in organ patterning and differentiation processes. SCARECROW (SCR) was analyzed during seed development to find out, if there is any specific expression in the seed coat or the unloading zone. In the aboveground tissue SCR is involved in the development of the bundle sheath cells, which are next to the vascular tissue. It was discussed that SCR is involved in cell division in those cells surrounding the vascular bundle (Wysocka-Diller et al. 2000). So far nothing is known about *SCR* expression in the maternal-female border occurring in the seed. To investigate if SCR could be involved in the development of the unloading zone a published marker line, which displayed ER-GFP driven by the *SCR* promoter was used (Wysocka-Diller et al. 2000). GFP was detected in the immature ovules of closed flowers and in the later stages of seed development (Fig. 34 A-E). It was also monitored in a limited number of cells of the inner integument (Fig. 34 J, M) and in few cells of the outer integument layer 1 from the chalazal pole (Fig. 34 K, L). No change of the promoter activity was seen comparing the mature ovule before fertilization (Fig. 34 F) with the stages after fertilization (Fig. 34 G, H, I). The specific cell file showing promoter activity of *SCR* was in distance to the unloading zone (Fig. 34 L, N, O). Also in later stages of embryo development the GFP signals did not change (Fig. 34 P).
SCR promoter activation was never seen in the phloem or unloading zone.
At the outer integument layer 2 promoter activity was missing at all, suggesting that the function of *SCR* in the reproductive tissue is limited to few cells surrounding the nucellus tissue and not involved in the differentiation process of the unloading zone.

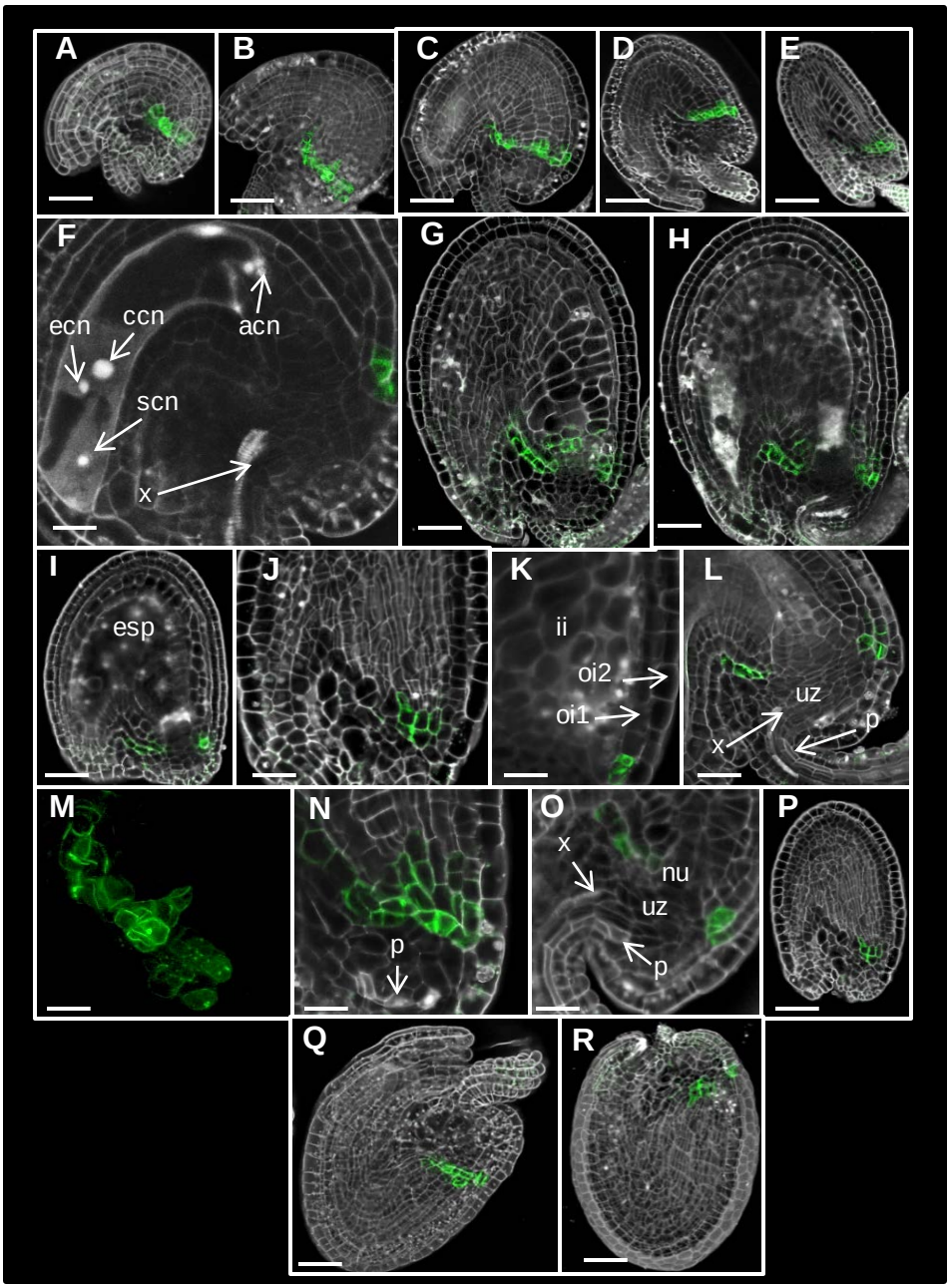

Figure 34. *P$_{SCR}$: ER-GFP* expression in the ovule and seed. (A-E) GFP signals at different stages of ovules in closed flowers (A, B), open flowers (C) and seeds (D, E), age increasing from (A) to (B), scale bars: (A, B) 50µm, (C) 25µm, (D) 35µm, (E) 70µm. (F) Optical section of an ovule, scale bar: 15µm. (G, H) Optical sections of an older seed, (G) focus on the integuments, (H) focus on endpoint of vasculature, scale bars: (G, H) 55µm. (I) Young seed with syncytial endosperm, scale bar: 45µm. (J) Magnification of (P) showing GFP in single cells of the outer integument at the chalazal tip, scale bar: 45µm. (K) GFP is found in single cells of the inner layer of theouter integument, scale bar: 20µm. (G) No GFP in the unloading zone and funiculus, but located in single cells of the outer and inner integument at the chalazal pole, scale bar: 25µm. (M) Maximum projection showing the chalazal cells decorated with GFP, scale bar: 12µm. (N) SCR-GFP fluorescence is detected in single cells of the outer integument layer 1 and in distance to the phloem, scale bar: 20µm. (O) Focus on the unloading zone after fertilization, GFP is restricted to the cells neighboring the nucellus, scale bar: 20µm. (P) Optical section of a seed with focus on integuments, scale bar.70µm. (Q, R) Maximum projection of a young (Q) and an old (R) seed, scale bars: (Q) 30µm, (R) 60µm. ECN (egg cell nucleus), sc (synergid cell nucleus), ccn (entral cell nucleus), can (antipodal cell nucleus), nu (nucellus), uz (unloading zone), x (xylem), p (phloem), oi (outer integument), ii (inner integument), esp (endosperm).

5.6. B-type cyclin expression in ovule and seed development

To address the question if also cell proliferation takes place in the phloem and at the unloading zone different markers for cell cycle were analyzed. Below the focus is on the dynamics in cell division during ovule and seed development. To monitor the cells undergoing mitosis the markers CYCB1.2 and CYCB1.3 were analyzed by reporter lines driving GFP under the control of the respective endogenous promoters (Schnittger personal communication). B-type cyclins trigger the transition form G2-to-M phase during mitosis (Colon-Carmona et al. 1999, Criqui et al. 2000). Although a high redundancy of B-type cyclins is discussed the subcellular localization showed differences. Whereas CYCB1.2 revealed a strong association with condensed chromatin the localization of CYCB1.3 is variable and occurs in the cytoplasm as well as on the chromatin (Bulankova et al.2013). Most data was based on the observation in roots. So far the different expression pattern of *CYCB1.2* and *CYCB1.3* during seed development was quite overlooked.

5.6.1. CYCB1.2

For CYCB1.2 was observed that in the immature ovule only single cells of the outer integument layer 2 showed GFP signals (Fig. 35 A, D), whereas additional signals in the inner integument appeared in the proceeded ovule (Fig. 35 B). Same findings were true for mature ovules before fertilization (Fig. 35 C). Altogether the presence of CYCB1.2-positive cells in the ovule shows a patchy pattern. Only single cells in both integument layers showed GFP signals (Fig 35 F, G) and this was always connected with mitotic events (Fig. 35 F, H).

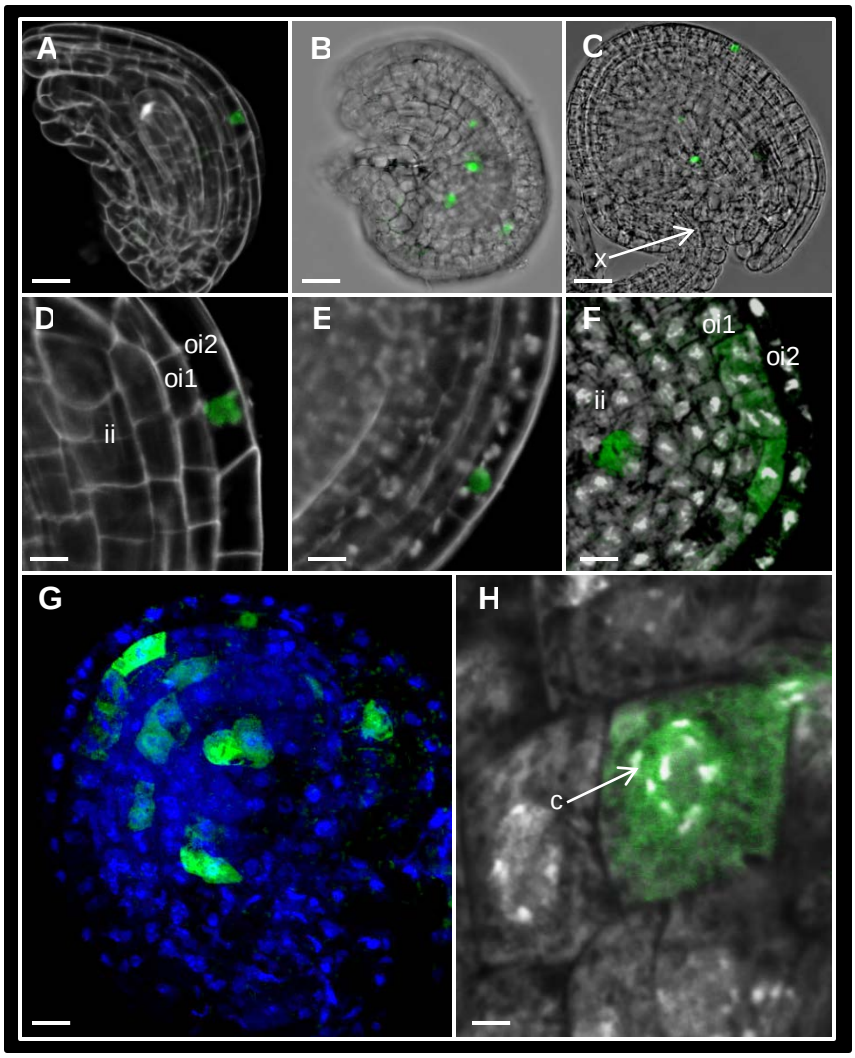

Figure 35. Localization of CYCB1.2 in the ovule. (A, D) Immature ovule of a closed flower. Localization study was done with the *P*$_{CYCB1.2}$*: CYCB1.2-GFP* reporter line**.** (A) Maximum projection of an ovule at about FG3 stage. (D) Magnification of the integuments, GFP detected in a single cell of the outer integument, scale bars: (A) 15µm, (D) 6µm. (B) Maximum projection of a proceeded ovule older than in (A), more cells show GFP fluorescence, scale bar: 24µm. (C, E) Mature ovule from an open flower. (C) GFP signals in single cells of the inner and outer integument. (E) Magnification of the integument area, scale bars: (C) 30µm, (E) 6µm. (F-H) Whole mount immunolocalization of ovules before fertilization, green cells: α-GFP, white and blue signals resulting from PI counterstaining of nuclei and cell compartments. (F) Signals in the inner and outer integument, cells show different stage of the cell cycle, scale bar: 8µm. (G) 3D reconstruction of an ovule showing several CYCB1.2-positive cells with differing intensity in the outer and inner integument, blue color: nuclei, scale bar. 12µm. (H) Magnification of a single cell of the integument with chromosomes, scale bar: 3µm. X (xylem), oi (outer integument), ii (inner integument), c

After fertilization and during seed development the GFP signal was seen in single cells of the funiculus and the two layers of the outer integument (Fig. 35 A). Also at the unloading zone fluorescence was observed (Fig. 35 B). Besides the very weak signals at the unloading zone, the fluorescence intensity in the two layers of the outer integument was very strong (Fig. 35 C, D), but GFP was present in more cells of outer integument layer 1 than layer 2 (Fig. 35 D, E). In later stages after syncytial stage of the endosperm signals were solely detected in the outer integument layer 1 (Fig. 35 F). The weak GFP fluorescence at the unloading zone was always found to occur in cells near the endpoint of the phloem (Fig. 35 G-I).

At heart embryo stage no further GFP expression was observed in the unloading zone or the integuments.

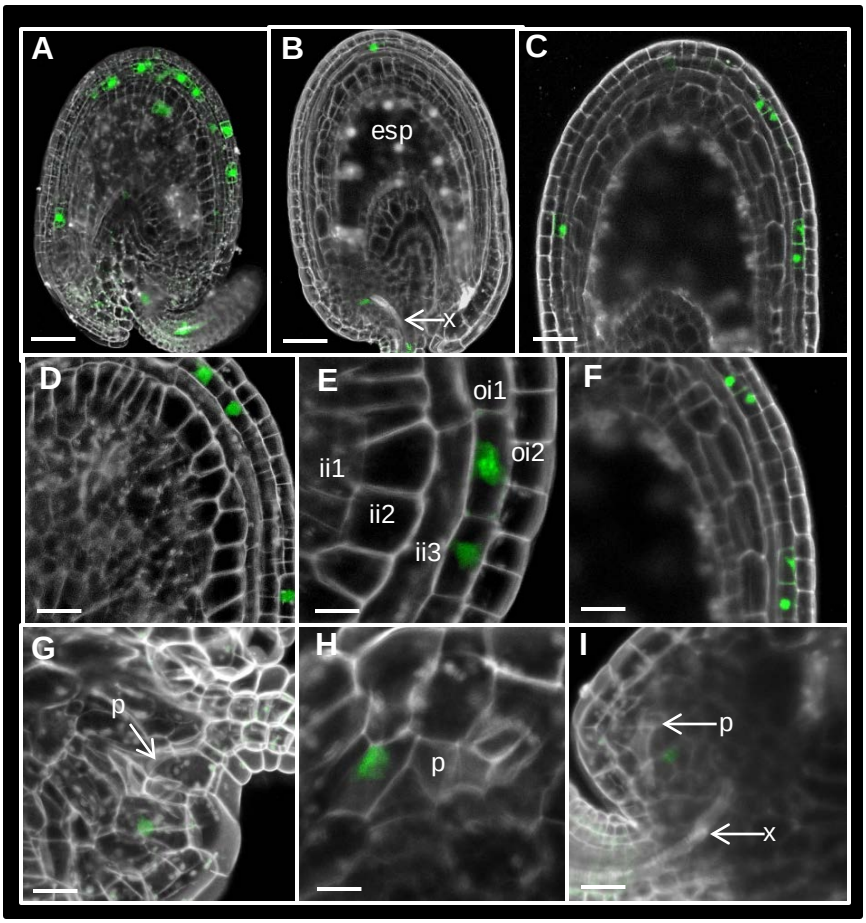

Figure 35. Localization of CYC B1.2 in the seed. Localization study was done with the *P*$_{CYCB1.2}$*: CYCB1.2-GFP* reporter line**.** (A) Seed right after fertilization CYCB1.2-GFP in the outer integument and funiculus, scale bar: 55µm. (B, C) Seed during endosperm development. (B) Maximum projection, GFP in outer integuments layer one and at the unloading zone, scale bar: 32µm. (C) Optical section, scale bar: 30µm. (D) CYCB1.2-GFP signals in seed of early stage endosperm development, GFP in single cells of both layers outer integument, scale bar: 18µm. (E) Magnification of a seed coat area, scale bar: 10µm. (F) GFP fluorescence in older seed with nucleated endosperm, scale bar: 25µm. (G-I) unloading zone. (G) Single cell of unloading zone with GFP signal, scale bar: 10µm. (H) CYCB1.2-positive phloem cell, scale bar: 6µm. (I) Unloading zone of the seed with endpoint of phloem and xylem and GFP signal in a single cell, seed at late globular embryo stage. X (xylem), p (phloem), oi (outer integument), ii (inner integument), esp (endosperm).

5.6.2. CYCB1.3

CYCB1.3 was completely different expressed during seed development. No GFP was detected in ovules. First signals appeared right after fertilization as the endosperm nuclei started to divide (Fig. 36 A). Accumulation of GFP was seen in the young embryo till early globular stage, too (Fig. 36 D). CYCB1.3-GFP remained solely in the nuclei of the endosperm until the syncytial phase was completed (Fig 36 B) and additionally it was detected in the borders of the endosperm cells during cellularization (Fig. 36 C, E-G, H). When the embryo reaches the heart stage the signals in the endosperm were much less clear and showed a diffuse signal pattern (Fig. 36 I). At this developmental stage the embryo showed no GFP signals and the GFP in the endosperm was marked by a fluid texture (Fig. 36 J). After consumption of the endosperm no further signals in older stages were monitored.

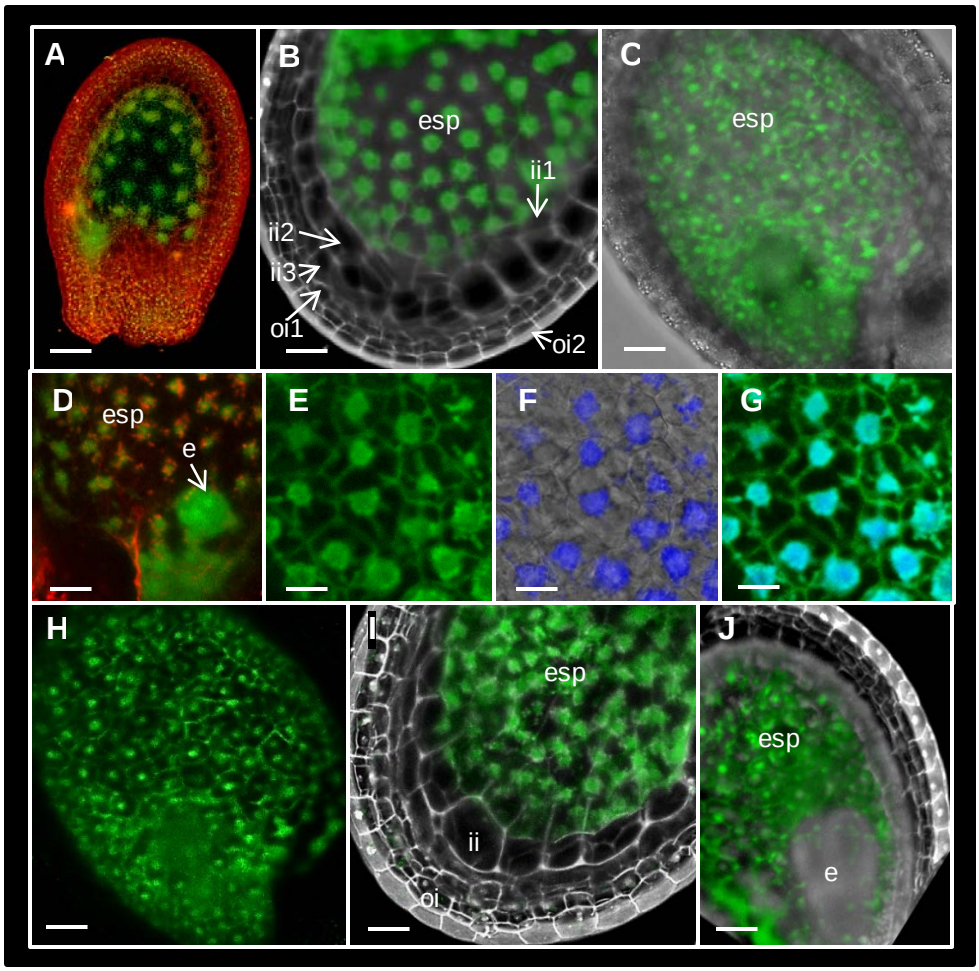

Figure 36. Localization of CYCB1.3 in the seed. Localization study was done with the *P*$_{CYCB1.3}$*: CYCB1.3-GFP* reporter line (A) Overview of a young seed at early globular embryo stage, maximum projection shows GFP restricted to the endosperm and accumulated at the micropylar area, scale bar: 45µm. (B) Maximum projection shows endosperm in the syncytial stage, scale bar: 30µm. (C) Endosperm during cellularization, scale bar: 40µm. (D) Maximum projection, GFP in the endosperm and embryo of a seed at about the same stage like in (A), scale bar: 30µm. (E-F) GFP signals in the cellularized endosperm. (E) GFP channel. (F) Bright field image with PI stained nuclei. (G) Overlay of GFP channel with PI channel, scale bars: 15µm. (H) GFP channel of (C) shows endosperm during cellularization, scale bar: 40µm. (I) Maximum projection of a seed at about heart embryo stage with fading endosperm, scale bar: 30µm. (J) 3D reconstruction of a seed at heart embryo stage showing embryo surrounded by the fading endosperm, no GFP fluorescence in the embryo, scale bar: 55µm. (E) embryo, esp (endosperm), oi (outer integument), ii (inner integument).

5.7. *UmamiTs* are plasma membrane localized and expressed in various tissues

According to the aramemnon database *UmamiT* candidate genes are predicted to harbor ten transmembrane domains and to localize at the plasma membrane. Furthermore public microarray data (BAR eFP browser) revealed a broad expression pattern with the seed as expression hotspot. In the following these predictions will be analyzed in detail.

5.7.1. Subcellular localization of *UmamiTs*

In order to investigate the subcellular localization of *UmamiTs* a transient expression assay of UmamiT-GFP was performed in tobacco (Fig. 37).

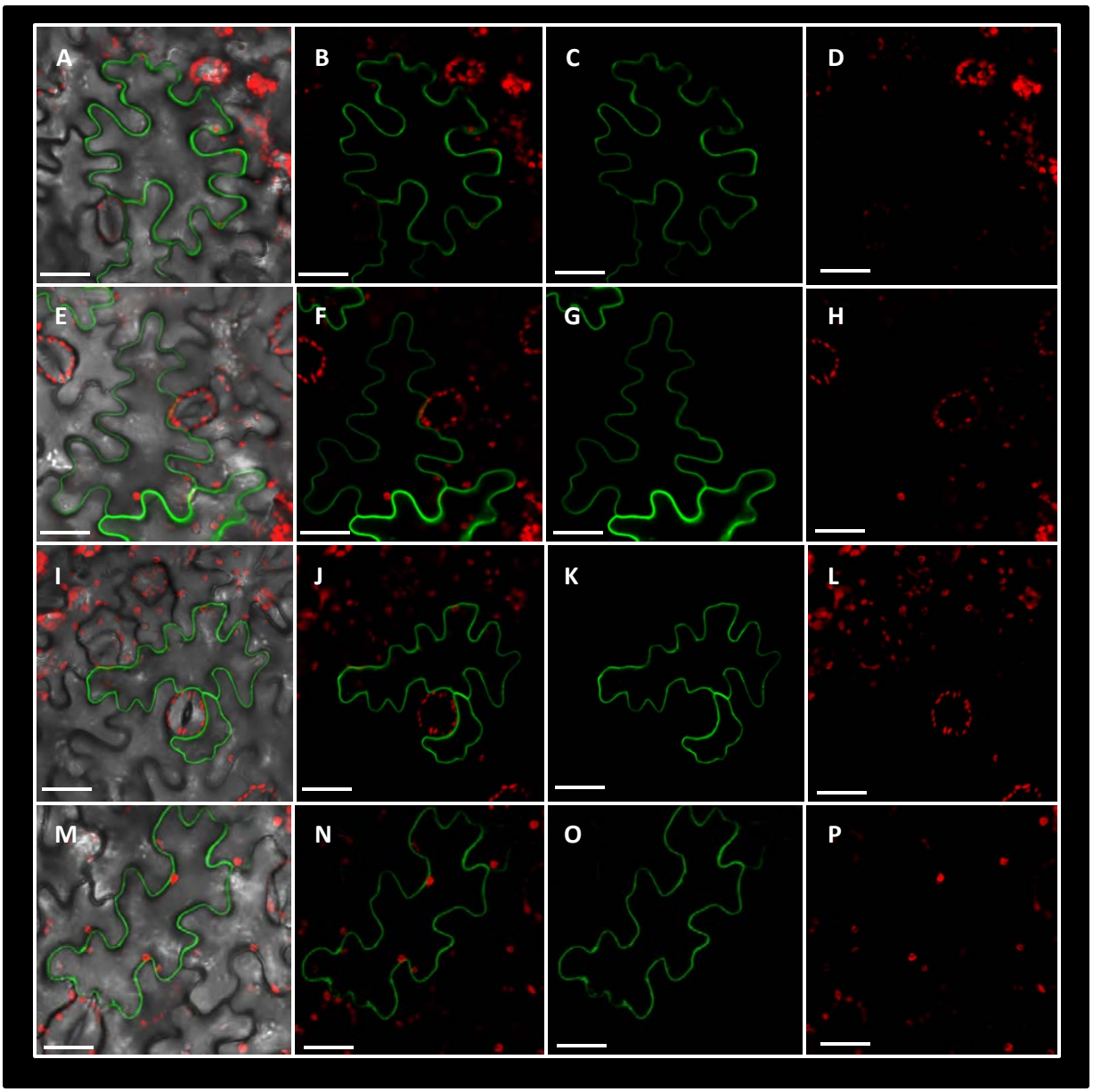

Figure 37. Transient expression of candidate *UmamiTs* in tobacco epidermal cells. *P35S: GFP-UmamiT; ch*annels are shown separately: (C, G, K, O) GFP channel, (D, H, L P) autoflourescence of chloroplasts, (B, F, J, N) overlays without bright field and (A, E, I, M) overlays with bright field. UmamiT14 (A-D), UmamiT11 (E-H), UmamiT29 (I-L), UmamiT28 (M-P), scale bars: 20µm.

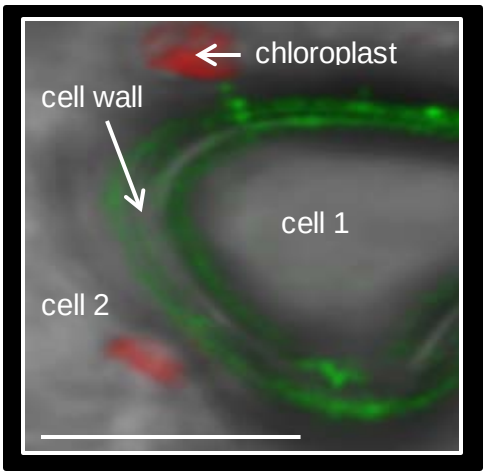

Figure 38. Magnification of tobacco epidermal cell showing UmamiT14-GFP. *P35S: UmamiT14-GFP.* Magnified region of the borders of two epidermal cells tagged with UmamiT14-GFP showing a clear gap between the two plasma membranes built by the cell wall. GFP signal was in distance to the chloroplast, scale bar: 10µm.

The epidermal cells were transiently transformed with agrobacteria harboring the expression vectors. These vectors contained the cDNA of the *UmamiT* candidates fused to GFP at the N-terminus (with stop codon) or at the C-terminus (without stop codon) under the control of the 35S promoter. For *UmamiT37* it was not possible to amplify the cDNA. Fig.37 shows an overview of the N terminal fusion with GFP of *UmamiT14* (A-D), *11* (E-F), *28* (I-L) and *29* (M-P). In all cases the fluorescence was detected as a thin line along the boundaries of the cell, assuming the fusion protein to be localized at the plasma membrane. Further indications for this assumption can be seen in Fig. 38, where a clear gap between the fusion protein and the chloroplast was obvious, thus ruling out localization to the tonoplast. In the case of a tonoplastic localization the GFP signal would be close to plastids without a visible gap in between.

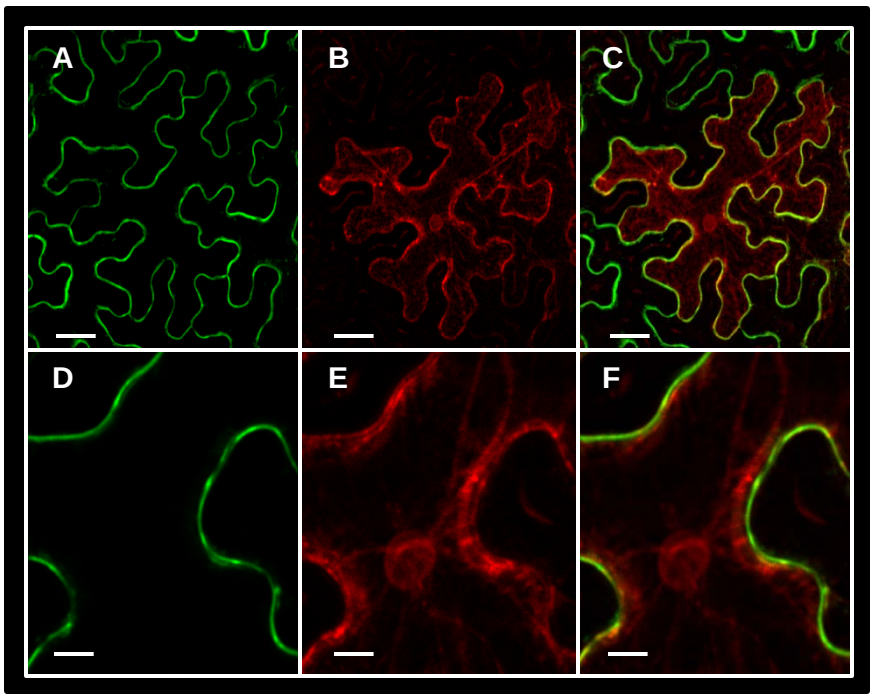

Figure 39. UmamiT-GFP does not localize to the ER. *P35S: UmamiT14-GFP;* UmamiT14- GFP (A, D), ER- RFP (B, D), merge (C, F), scale bar : 10µm

To validate the assumed plasma membrane localization, colocalization studies were done with already published compartment markers (Nelson et al. 2007). In the case of coexpression of UmamiT-GFP and a marker for ER (endoplasmatic reticulum) no overlap between the red and green channel was observed (Fig.39).

In contrast a clear colocalization with the plasma membrane marker could be detected. Fig.40 demonstrates the overview of single channels and the merges for clade I and clade III candidates. Additionally the amount of colocalizing pixels was quantified by statistics using Manders' colocalization coefficients and Pearsons R value. In all cases values >89 for M1 and M2, R >91 were obtained which supports that UmamiTs localize to the plasma membrane.

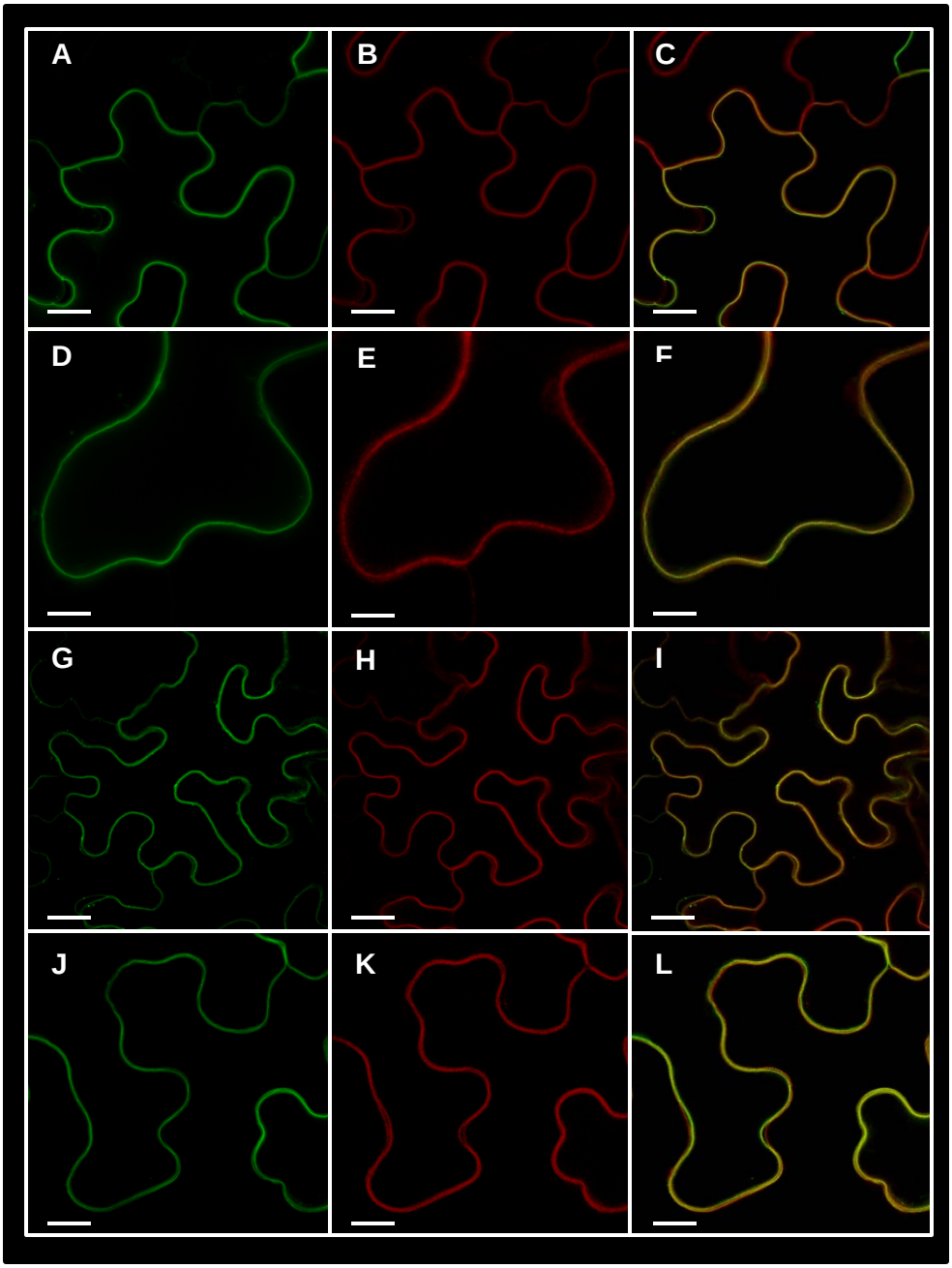

Figure 40. UmamiT-GFP localizes to the plasma membrane. *P_{35S}: UmamiT-GFP;* GFP channel (A, D, G, J), RFP channel (B, E, H , K), merge (C, F, I, L). *UmamiT14* (A. D), *UmamiT28* (G, J).Scale bars: (A-C): 15µm, (D-F): 5µm, (G-L): 10µm.

5.7.2. *UmamiT* expression in different tissues: focus on the RNA level and promoter activity

In order to investigate the tissue specific expression pattern of *UmamiT* candidate genes real-time RT-PCR and promoter reporter gene experiments were performed. The investigation of the expression level and tissue specific localization of GUS in the vegetative tissue is shown in Fig. 41. The overall RNA level in root and leaves was quite similar and relatively low compared to the seed. The promoter activity is associated with the vasculature in these tissues (Fig. 41 A, B). In flowers a much higher expression of *UmamiTs* could be detected, especially of *UmamiT14*, *UmamiT29* and *UmamiT37*. Furthermore the GUS staining showed a specific promoter activity not only in the vasculature of petals but also in anthers and stigmata.

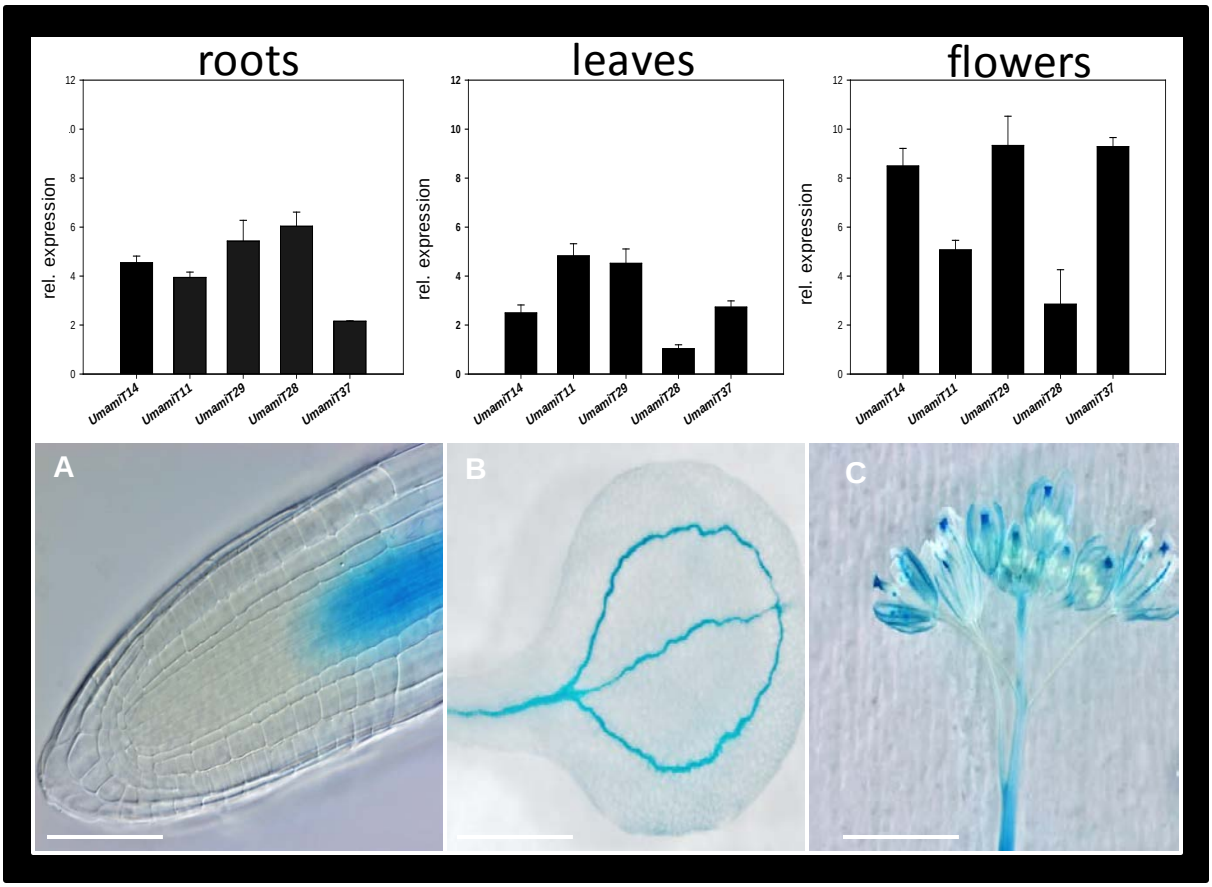

Figure 41. Expression of *UmamiTs* in roots, leaves and flowers. Semiquantitative real time PCR of roots, leaves and flowers normalized to UBQ10 (n=3 ± SD). P_{UmamiT}: *GUS* in (A) roots, (B) leaves and (C) flowers. Scale bars: (A) 80µm, (B) 200µm, (C) 800 µm.

In contrast to the lower expression values in roots and leaves a maximum was found in siliques (Fig.42.) Here the data revealed a divergent expression pattern for the selected candidates. The most striking finding was the absence of *UmamiT28* in young siliques and the highest abundance of the transcript in old siliques (Fig. 42 A, B), indicating specific roles of *UmamiTs* during seed development (Fig. 42 C, D, E).

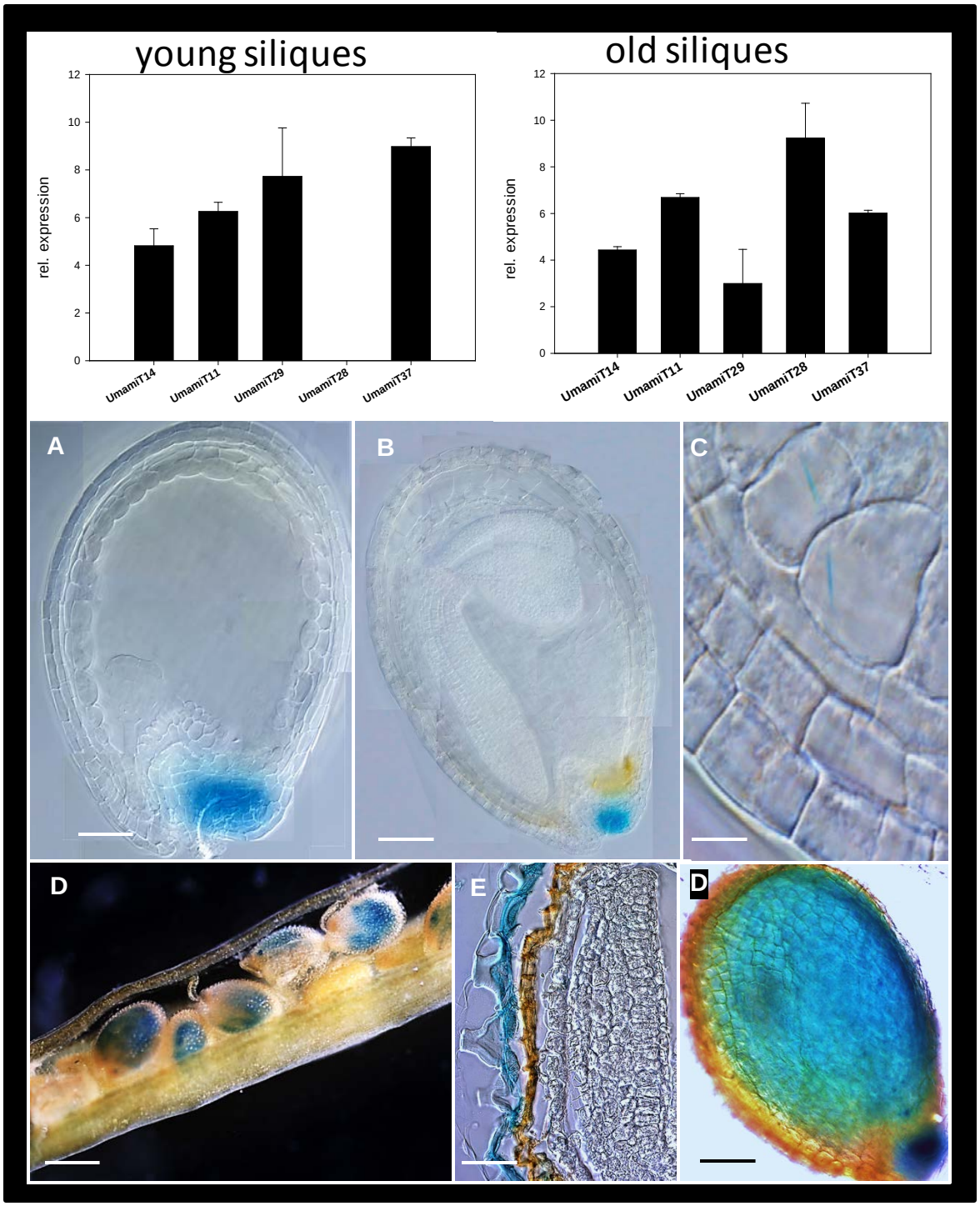

Figure 42. Expression of *UmamiTs* in young and old siliques. Semiquantitative real time PCR of siliques normalized to UBQ10 (n=3 ± SD). P_{UmamiT}: *GUS;* (A) *UmamiT14,* scale bar: 60µm. (B) *UmamiT11*, scale bar: 90µm. (C-E) *UmamiT29*, sale bar: (C) 40 µm, (D) 300µm, (E) 35µm. (D) *UmamiT28*, scale bar: 100µm.

5.8. *UmamiT* promoter activity and protein localization in *planta*

5.8.1. Leaves

In order to investigate the tissue specifc expression pattern of *UmamiTs* reporter lines for promoter activity and protein localization were examined. As shown in Fig.41 *UmamiT* RNA levels in the vegetative organs are remarkably similar. According to this, the following pictures always show representative images of all candidates concerning the promoter activity and protein localization in *Arabidopsis thaliana*. In leaves, the promoter analysis using *P-UmamiT: NLS 3xGFP* fusions revealed a very specific association with the vasculature (Fig. 43 B, C, D). The promoter activity was found in cells that are closest to the xylem but also in the larger neighboring parenchyma.

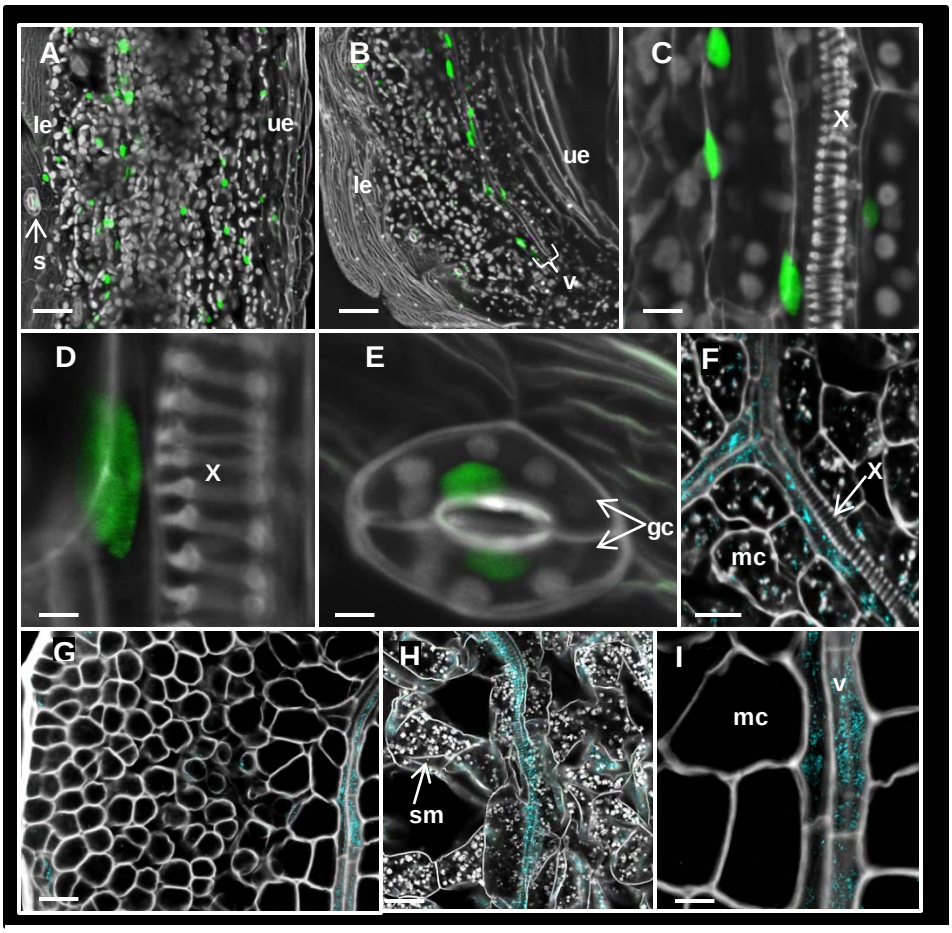

Figure 43. *UmamiT* promoter activity in leaves. Analysis of $P_{UmamiT29}$: *NLS3xGFP* (A) Optical section as z-stack starting from upper to lower epidermis, scale bar: 25µm. (B) Z-stack of leave with focus on the vasculature, scale bar: 25µm. (C, D) Vascular bundle in focus; (D) is a magnification of (C), scale bars: (C) 7µm, (D) 3µm. (E) Stoma of lower epidermis, scale bar: 5µm. (F-I) mPS-PI staining of leaves from P_{UmamiT}: *GUS* plants. (F) Mature leaf mesophyll cells with starch granules (based on Periodic acid-Schiff reaction), GUS crystals in the vasculature, scale bar: 22µm. (G) Leaf of a seedling, scale bar: 30µm. (H) Maximum projection of the spongy mesophyll in a mature leaf, GUS staining in the vasculature, scale bar: 20µm. (I) Magnification of the vascular bundle from a seedling leaf, GUS crystals restricted to the vasculature. S (stoma), le (lower epidermis), ue (upper epidermis), v (vasculature), x (xylem), gc (guard cell), sm (spongy mesophyll), mc (mesophyll cell).

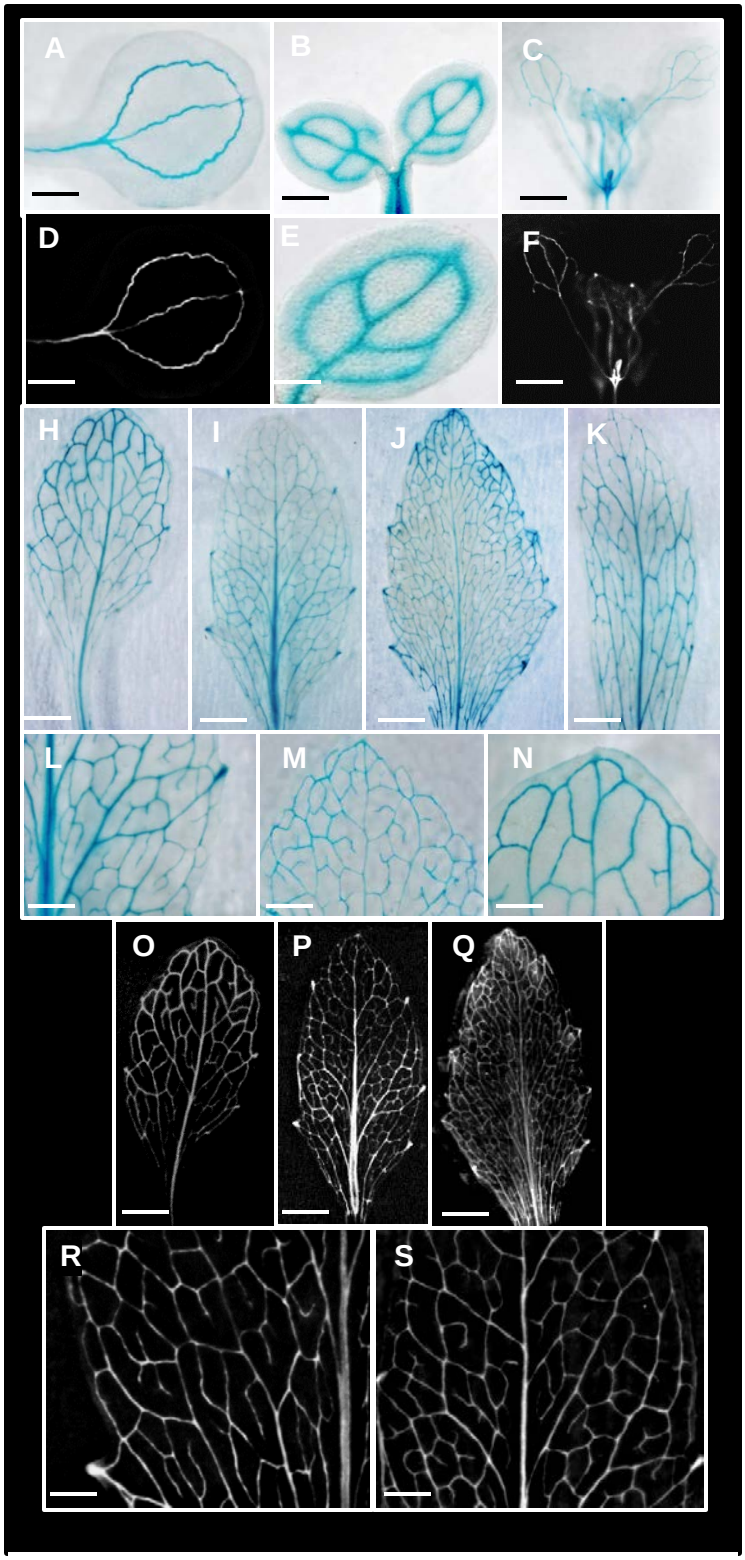

Figure 44. *UmamiT* expression in leaves indicated by GUS staining. *P*$_{UmamiT}$*: GUS, UmamiT14* (A, D) cotyledon, scale bar: 3mm, *UmamiT11* (B, C, E, F), (B, E) cotyledon, scale bar: (B) 2mm, (E) 1,5mm; (C, F) juvenile stage with first and second leaves, scale bar: 4mm. *UmamiT29* (H, J), third leave (H), cauline leaf (J), scale bars: 3mm (H), 2mm (J). *UmamiT28* (I, K, L, M, N), seventh leaf (I) scale bar: 2mm, leaf from the inflorescence shoot (K) 2mm. Magnifications of different leaf areas (L-N), scale bars: 2.2mm (L), 1.2mm (M), 1mm (N). (O-S) Inverse colored intensity pictures of (H, I, J) with the same scaling. Magnifications of vein patterning in (R) and (S), scale bars: (R) 1,5mm, (S) 1mm.

Additionally, a much weaker signal in the guard cells of the stomata was found (Fig. 43 E). Using mPS-PI staining proofed the vascular association of the promoter-GUS staining (Fig. 43 F, I). This was true for seedling leaves (Fig. 43 G,I) as well as for mature leaves (Fig. 43 F, H).

GUS staining in leaves showed that the promoter of all *UmamiT* candidates was active in the cotyledons of young seedlings after germination (Fig. 44 A, B, D, E). In the later stages of the juvenile plant, GUS staining was also obtained in the whole vascular system of the plant body (Fig. 44 C, F). GUS staining in the vasculature was seen in leaves from the rosette (Fig.44 H, I, J, O, P, Q) and from the inflorescence (Fig.44 K). Magnifications (Fig. 44 L, M, N) and inverse colored pictures (Fig. 44 O-S) illustrate the specificity of the GUS staining to the site of the vasculature in all veins of different orders (Fig. 44 R, S). The transcriptional fusion with GUS showed that *UmamiTs* were highly associated with the vascular tissue.

At next the the fusion protein P_{UmamiT}: *UmamiT-GFP* will be presented.

In this construct all introns are present and the expression is under the control of the endogenous promoter. It revealed that the protein localized to leave veins from seedling stage (Fig. 45 A, B) to the adult stage (Fig. 45 C, D). Longitudinal and cross sections detect UmamiT-GFP in cells close to the xylem (Fig. 45 E, F, G) and specifically restricted to the vasculature (Fig. 45 H, J, K, L). These overlapping findings between GUS staining and UmamiT-GFP indicate that all elements required for proper expression are found in the 5' region of the ATG.

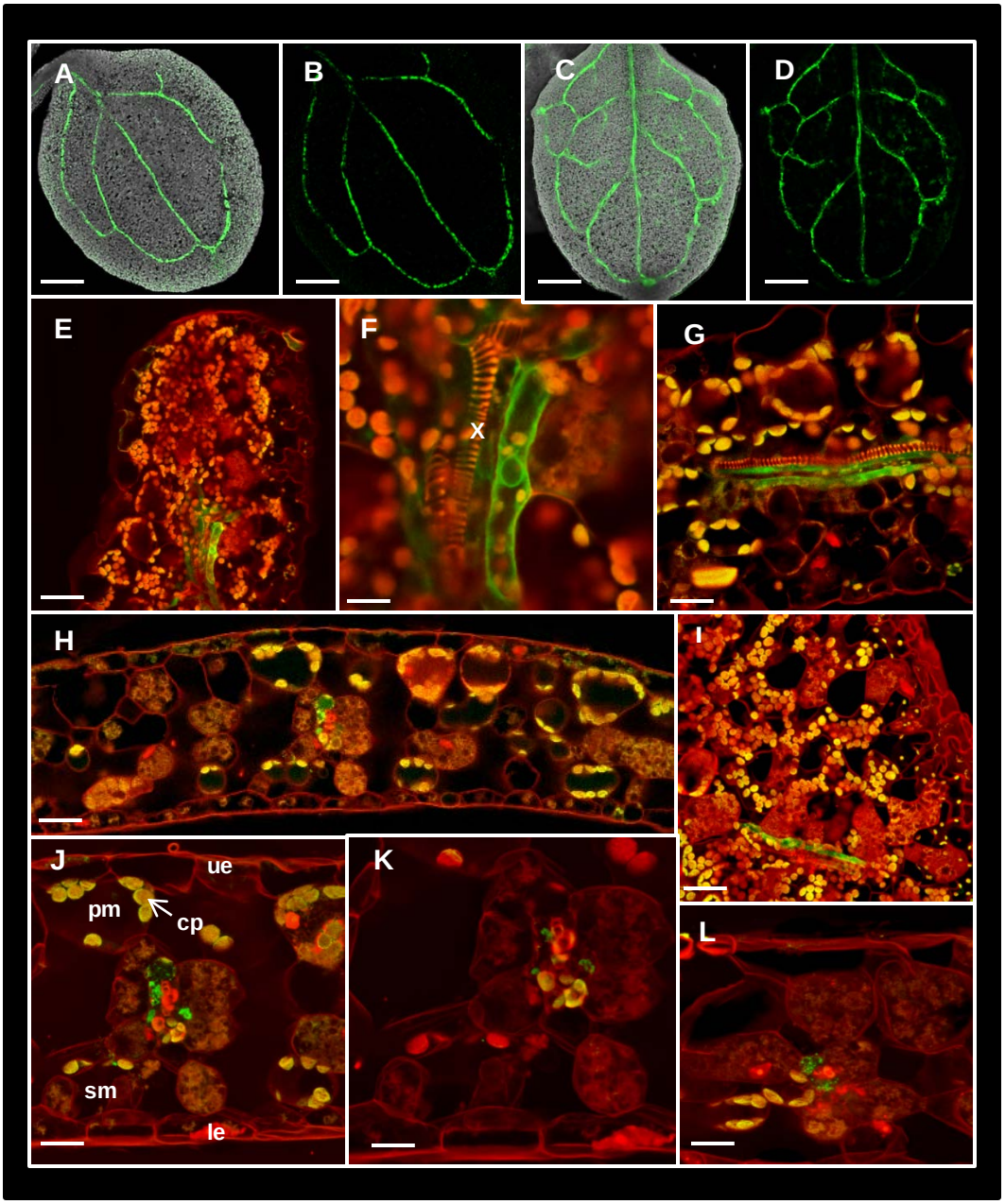

Figure 45. Tissue specificity of UmamiTs in leaves of P_{UmamiT}:*UmamiT-GFP* plants. (A-D) Overview of vascular decoration with UmamiT-GFP in a young (A-B) and older (C-D) leave. *UmamiT28* (A, B), scale bar: 250µm. *UmamiT29* (C, D) scale bar 250µm. (E-I) Vibratome sections. (I-L) Maximum projections, UmamiT-GFP always restricted to vascular associated cells. UmamiT11-GFP (G), scale bar: 20µm. UmamiT14-GFP (E, F, H, I, J, K, L), scale bar: (E) 50µm, (F) 10µm, (H, I) 30µm, (J, K) 13µm, (L) 16µm. X (xylem), ue (upper epidermis), le (lower epidermis), cp (chloroplast), pm (palisade mesophyll), sp (spongy mesophyll).

To define the cell types showing the GFP signal more precisely, cross sections of petioles of the main vein (Fig. 46 A), the major veins (Fig. 46 B, C) and the minor veins (Fig. 46 D) were prepared. In all cases, GFP could be detected in the zone of the phloem and the parenchymatic tissue of the xylem. To characterize the identity of these cells in the vasculature, immunolocalizations were performed using α-GFP (green signal) and an antibody against sieve elements, α-RS6 (red signal). Here, the results of the cross sections could be reproduced with the GFP antibody and furthermore a clear colocalization with sieve elements was documented in the cross section of the petiole as well as in the minor veins (Fig. 46 E-L). Taken together this results show that in leaves the vascular association of UmamiTs is in the phloem region corresponding with sieve elements. Their presence in the xylem parenchyma and phloem suggests a role in the distribution of amino acids and/or amino acid cycling.

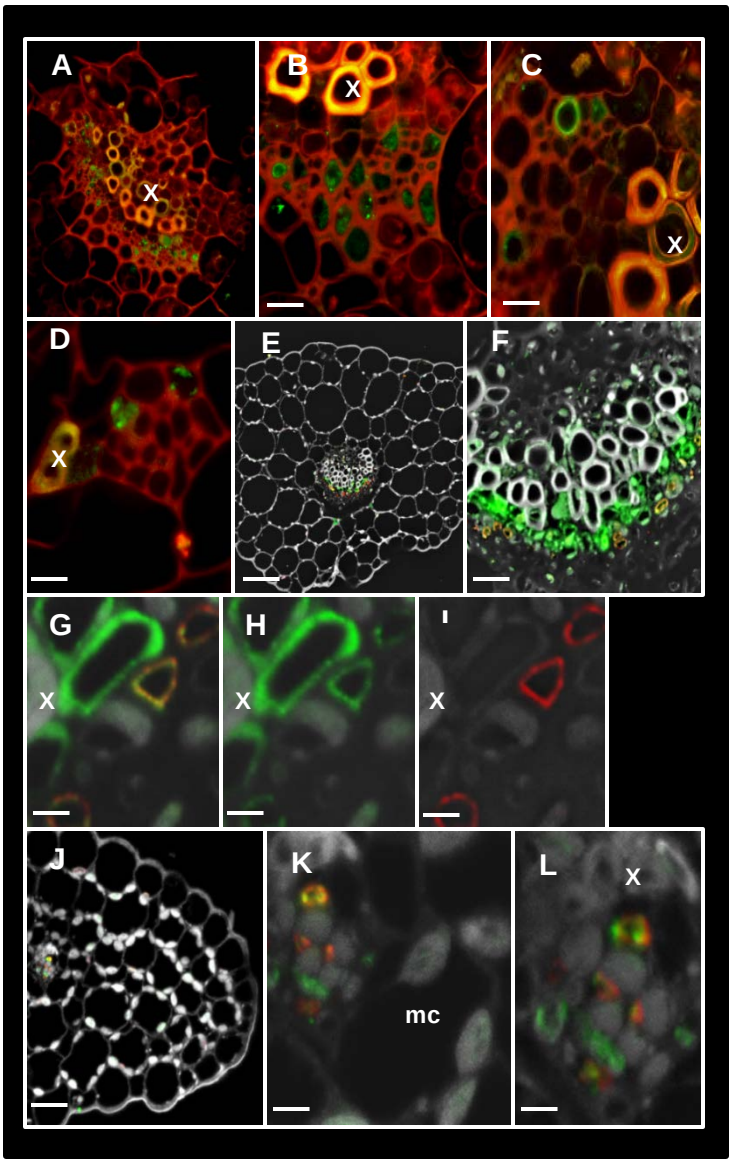

Figure 46. Cross sections and immunolocalization of UmamiTs in leaves. *P_{UmamiT}:UmamiT-GFP* ; (A-D) UmamiT14-GFP. Cross section of petiole (A), scale bar: 26µm. (B, C) Major vein, scale bar (B) 10µm, (C) 7µm. (D) Minor vein, scale bar 5µm. Immunolocalization of UmamiT11-GFP and RS6 (E-L). (E) Overview, scale bar: 37µm. (F) Magnification of (E), scale bar: 15µm. (G) Overlay of (H) and (I). (H) Green cells: α-GFP, detected with a CY2-antiserum, representing GFP positive cells; red cells: α-RS6 detected with an AF594-coupled antibody, representing sieve elements, white color: autofluorescence., scale bars (G-I): 3µm. (J) Cross section at the leave border area with a minor vein in the center, scale bar: 15µm. (K, L) Magnification of one minor vein, yellow cells indicate a colocalization between α-GFP and α-RS6. Scale bar: (K) 4µm, (L) 3µm. X (xylem), mc (mesophyll cell).

5.8.2. Stem

Long distance transport includes transport processes along the stem. In order to investigate if UmamiTs can be found there the promoter activity and fusion protein was analyzed. The GUS staining revealed a specific staining in the vasculature (Fig. 47 A, B, C). A detailed view of a cleared stem showed GUS crystals not only in the tissue of the xylem parenchmya and phloem parenchyma, but also within sieve elements. The fusion protein was detected at the same position (Fig. 47 D). The GFP signal was restricted to cells located in the vascular cylinder within a closed circle around big parenchyma cells. UmamiT-GFP seemed also there to be localized at the plasma membrane (Fig.47 F).

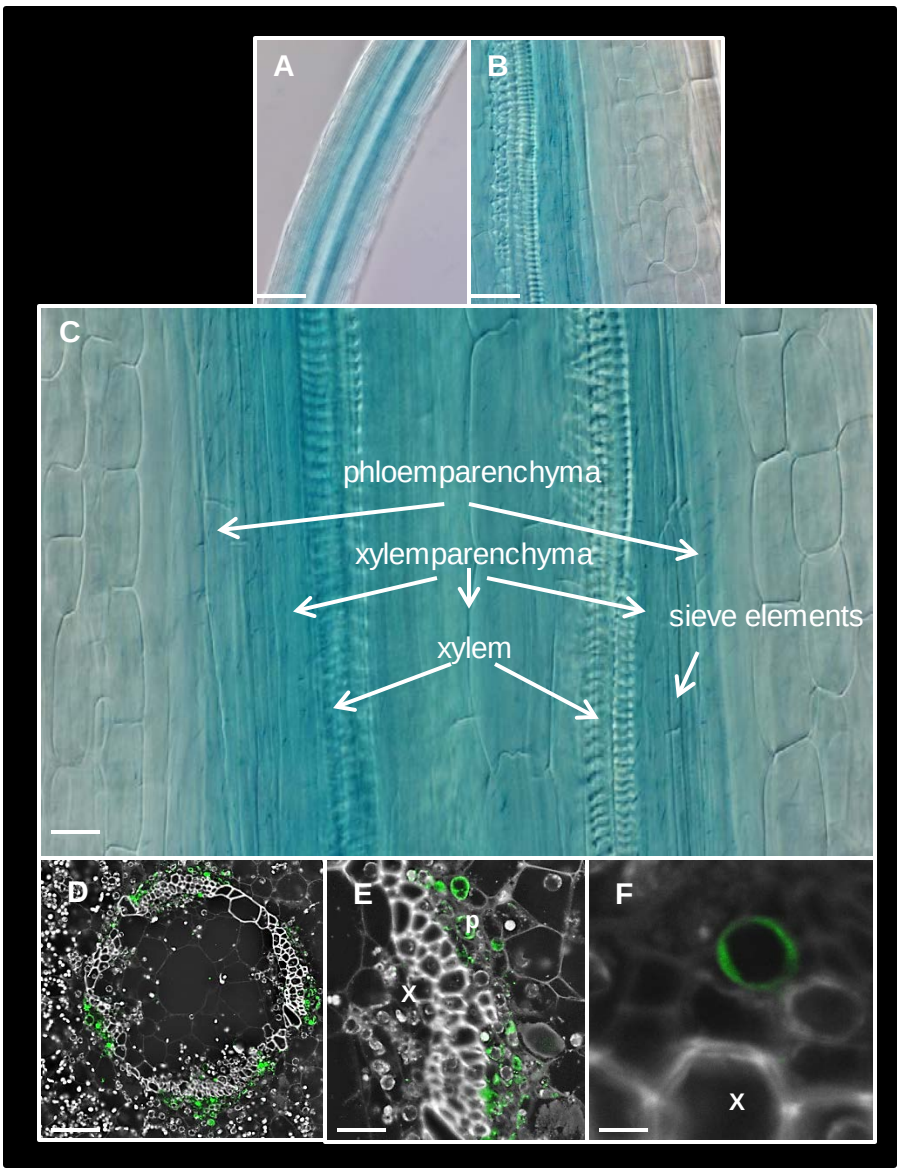

Figure 47. Tissue specificity of UmamiTs in stems. *P*$_{UmamiT29}$*: GUS* (A, B, C) and *P*$_{UmamiT29}$*: UmamiT29-GFP* (D, E, F), cross sections were done on a Vibratome. Scale bar: (A) 0.3 mm, (B) 70µm, (C) 400µm, (D) 50µm, (E) 20µm, (F) 4µm. GUS staining and UmamiT29-GFP fluorescence was found in the vasculature of stems in several cells of the phloem and cells close to the xylem. X (xylem), p (phloem).

Immunolocalizations on embedded tissue of young stems of flowers demonstrated again a specific expression of *UmamiT* in the vasculature. Colocalization with the RS6 marker was also obtained, but not in every sieve element (Fig.48). Interestingly, a developmental gradient from cells that show only the GFP decoration without colocalization, cells that harbored simultaneously UmamiT and RS6 and cells that were only labeled with RS6 could be seen (Fig. 48 E, I-L). These findings indicate a multiple origin of sieve elements from maybe different precursor cells or loss of the antigen over time.

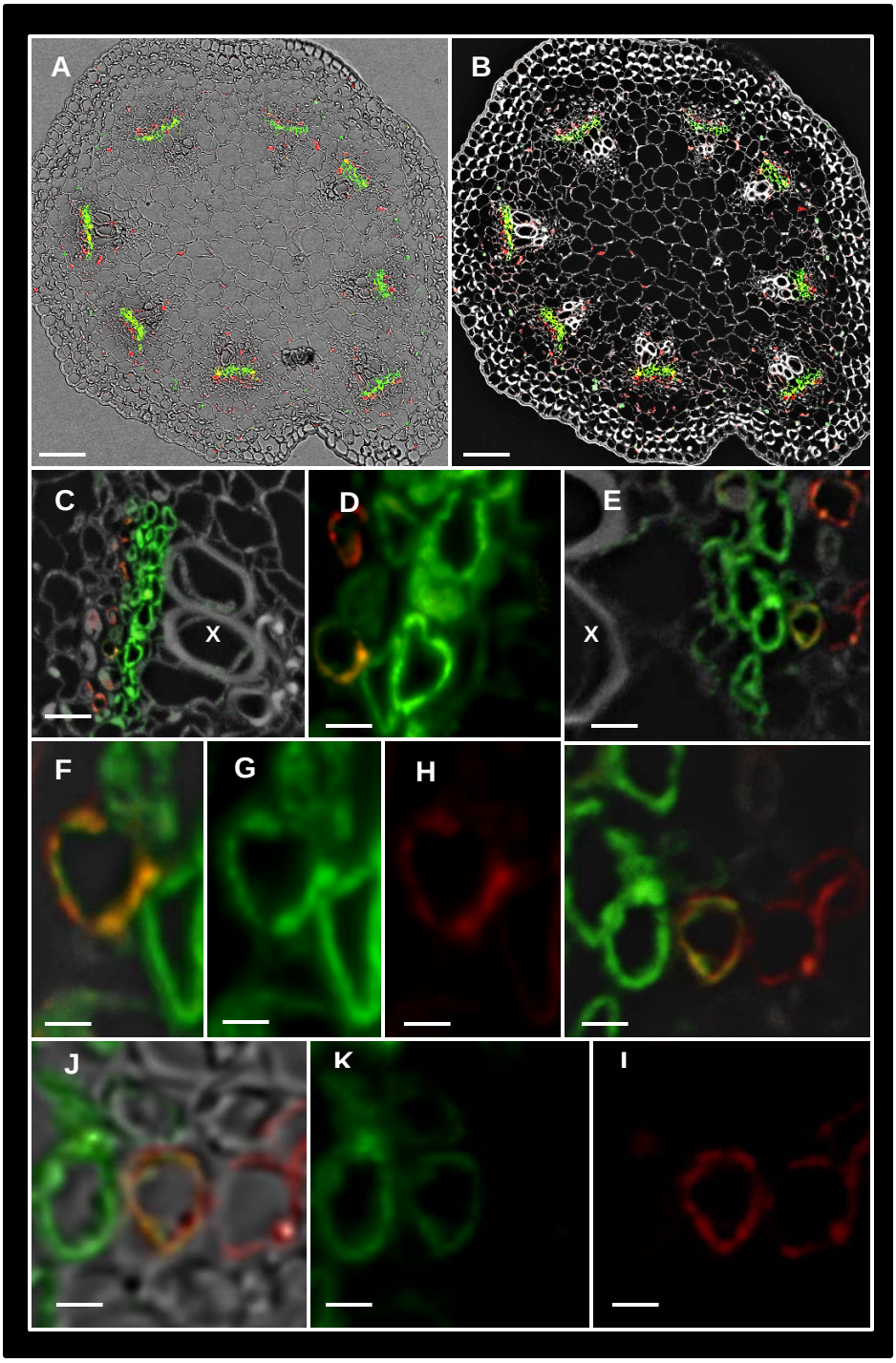

Figure 48. Immunolocalization of stem tissue of $P_{UmamiT28}$:*UmamiT28-GFP* plants. Overview of a complete cross section with brightfield image (A) and with autoflourescence (B) merged. Scale bar: 60µm. Green cells: α-GFP, detected with a CY2-antiserum, representing GFP positive cells; red cells: α-RS6 detected with an AF594-coupled antibody, representing sieve elements, white color: autofluorescence..Yellow signals indicate a colocalization. (C, D, F, G, H) Different magnifications of (B), scale bar: (C), 14µm, (D) 4µm, (F, G; H) 2µm. (E, I, J-L) Magnifications of a region showing sieve elements of different origin. Scale bars: (E) 4µm, (I) 2µm, (J-L) 1.5µm. X (xylem).

5.8.3. Inflorescence

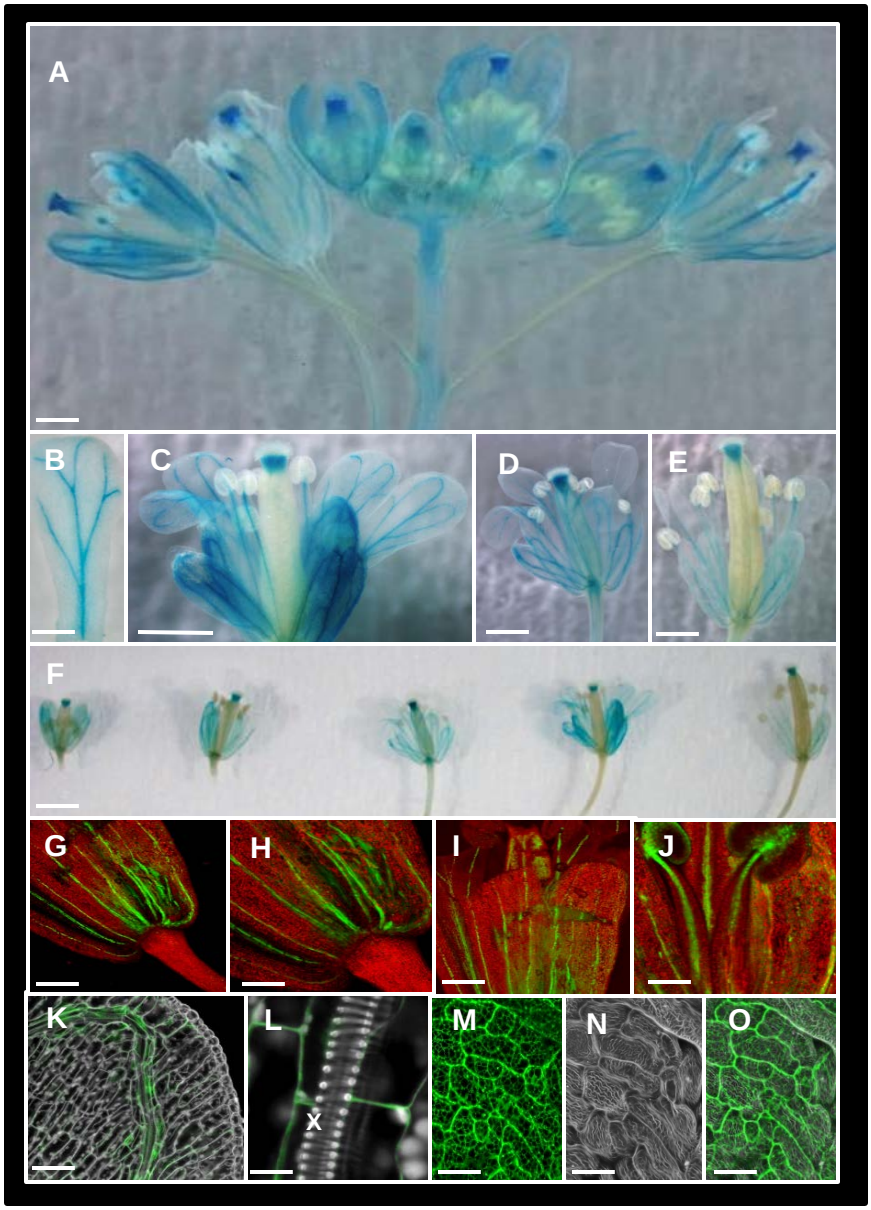

Figure 49. UmamiTs in the inflorescence. *P*$_{UmamiT14}$*: GUS*, (A) overview of a complete inflorescence, scale bar: 0.5mm; (B, C) *UmamiT11*, (B) petal and (C) open flower, scale bar: (B) 1mm, (C) 1.5mm. (D, E, F) *UmamiT28*, during anthesis (D) and after anthesis (E), (F) overview from floral stage 10-13 and stage after anthesis, scale bars: (D, E) 2mm, (F) 1.7mm. (G, H) *P*$_{UmamiT29}$*: UmamiT29-GFP* in veins of petals, scale bar: (G) 350µm, (H) 180µm; replum and anthers (I, J), scale bar: (I) 280µm, (J) 200µm. (K, L) UmamiT14-GFP in the vasculature of petals, scale bar (K) 17µm, (L) 6µm. (M, N, O) UmamiT29-GFP in epidermal cells of petals; (M) GFP channel, (N) PI stain, (O) overlay of (M) and (M), scale bar 30µm. X (xylem).

UmamiTs are broadly expressed in the vegetative tissues that are linked to reproduction (Fig. 49 A). GUS staining was found in flowers of different developmental stages (according to Smyth et al. 1990) starting from floral stage 8 to floral stage 13 (Fig. 49 A, F). Staining was detected in the veins of the petals (Fig. 49 B), the anthers and in the stigma (Fig. 49 B-E). At the same position the GFP fusion protein was detected: in the veins of petals (Fig. 49 G, H, K) and in the stigma and anthers (Fig. 49 I, J). The expression of UmamiT-GFP in the petals was again strongly associated with the vasculature (Fig. 49 K, L) and found in the cell file near the xylem. *UmamiT29* exclusively showed additional expression in the epidermal cells of petals (Fig. 49 M, N O).

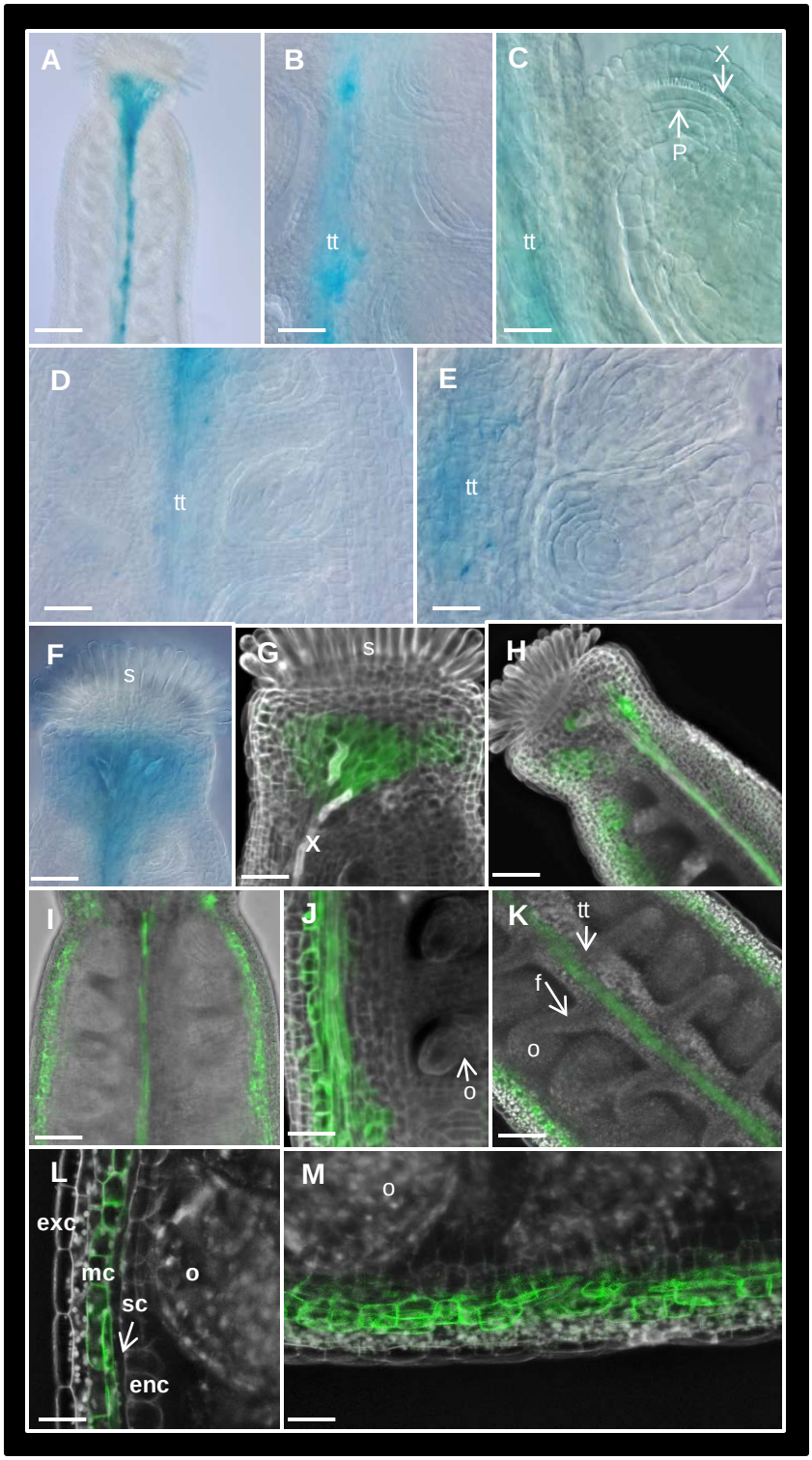

Figure 50 Tissue specificity of UmamiTs in flowers. *PUmamiT29: GUS* in closed flowers (D, E) and open flowers (A, B, C) staining in the transmitting tract before fertilization occurs, scale bars: (A) 200µm, (B) 60µm, (C) 30µm, (D) 60µm, (E) 20µm. (F) UmamiT11-GUS in the style, scale bar: 70µm. (G) UmamiT19-GFP in the style, scale bar: 40µm ; (H-M) UmamiT29-GFP in the flower. Scale bars: (H) 80µm, (I) 100µm, (J) 20µm, (K) 60µm. (L) 35µm, (M) 20µm. X (xylem), p (phloem), exc (exocarp), mc (mesocarp), sc (sclerenchyma), enc (endocarp), o (ovule), tt (transmitting tract), f (funiculus), s (stigma).

RNA levels of candidate *UmamiTs* in flowers were relatively high compared to root tissue (Fig. 41). In order to characterize their expression pattern before fertilization GUS staining and the GFP fusion protein was analyzed. Before fertilization, GUS staining was visible in the transmitting tract of the ovary (Fig. 50 A) in the closed flower (Fig. 50 D, E) as well as in the open flower (Fig. 50 B, D, C). The strongest GUS staining and detection of the GFP-protein was observed in the style directly behind the stigma (Fig. 50 F, G). All candidates showed a much weaker GFP signal in the transmitting tract as in the style. Expression in single cells of the carpels was also detected (Fig. 50 H-K) but *UmamiT29* exhibited the strongest signals there (Fig. 50 I-M). Optical sections illustrate that the specific cell file expressing *UmamiT* belongs to the mesocarp of the valve (Fig. 50 L, M).

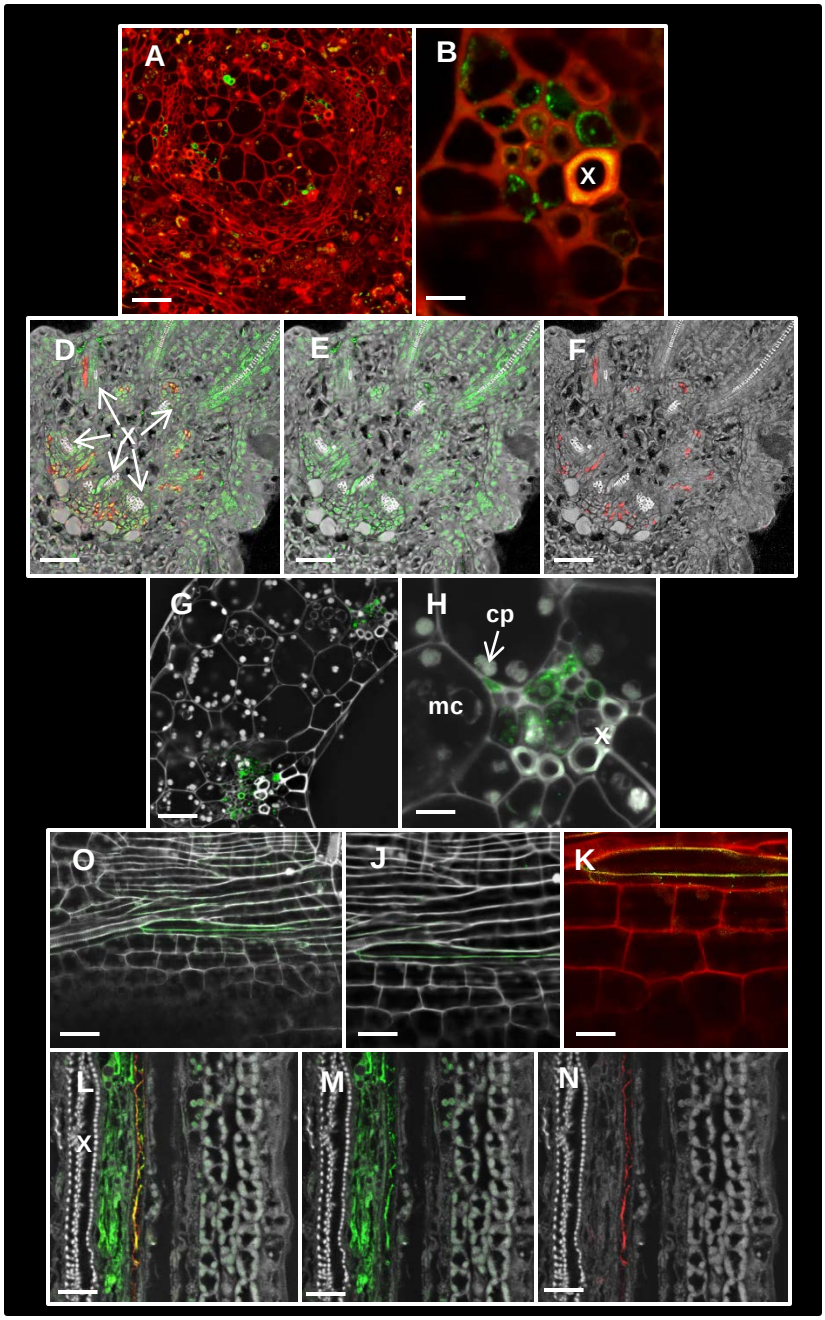

Figure 51. UmamiTs are located in the receptaculum of the flower. *P*$_{UmamiT14}$*: UmamiT14-GFP* in the vasculature of the basis of the petals (A, B); scale bar: (A) 35µm, (B) 5µm. UmamiT29-GFP in the vasculature of the silique (G, H); scale bar: (G) 40µm, (H) 10µm. UmamiT14-GFP in the mesocarp (O, J, K); (J, K) represent magnifications of (O); yellow colored membrane in (K) indicates a colocalization between UmamiT14-GFP and PI staining, scale bars: (O) 35µm, (J) 20µm, (K) 10µm. Immunolocalization of the same area of (A) shown in (D, E, F). Green cells: α-GFP, detected with a CY2-antiserum, representing GFP positive cells; red cells: α-RS6 detected with an AF594-coupled antibody, representing sieve elements, white color: autofluorescence. Yellow signals indicate a colocalization. Scale bar (D, E, F) 50µm. (L, M, N) Immunolocalization of veins from siliques, (M) UmamiT-positive cells, (N) sieve elements; scale bar 25µm. X (xylem), mc (mesocarp cell), cp (chloroplast).

Cross sections through the receptaculum (bottom area of the flower), where the carpels emerged showed a strong association of *UmamiT* expression with the vasculature (Fig. 51 A, B). As described before, UmamiT-GFP was also found in the lateral vascular bundles of the mesocarp (Fig. 51 G, H) as well as in parenchymatic tissues there (Fig. 51 O, J, K).

Immunolocalization of the bottom of the flower confirmed a strong association with the veins as detected in the reporter lines (Fig. 51 A, B, D, E, F). Not only there but also in the vascular bundles of the lateral veins in the mesocarp a colocalization with RS6 epitope was seen (Fig. 51 L, M, N).

5.8.4. Anthers

UmamiT expression was also found in developing anthers. GUS staining at the endpoint of the vasculature could be seen for all candidates (Fig. 52 A, K). Promoter activity was also reported in the vasculature of the filament (Fig. 52 B). Based on the RNA abundance *UmamiT29* represented the strongest candidate of clade III *UmamiTs* (Fig. 41) and showed additional expression of $P_{UmamiT29}$*:NLS-3xGFP* in the epidermal cells of the stamen in closed flowers (Fig. 52 C-F) and in stamen of open flowers (Fig. 52 G, H). The strongest signals according to the promoter activity was found in those cells, which are surrounding the ending xylem and forming an unloading zone there (Fig. 52 D, F, I) similar to the situation in the seed, see below. In ripe pollen sacs, promoter activity in distal position of the filament's unloading zone was restricted to epidermal cell files, whereas in immature pollen grains, *UmamiT29* promoter was also active in the tapetum layer next to the pollen (Fig. 52 K, L). These results indicate a role of *UmamiTs* in the nutrition of pollen grains.

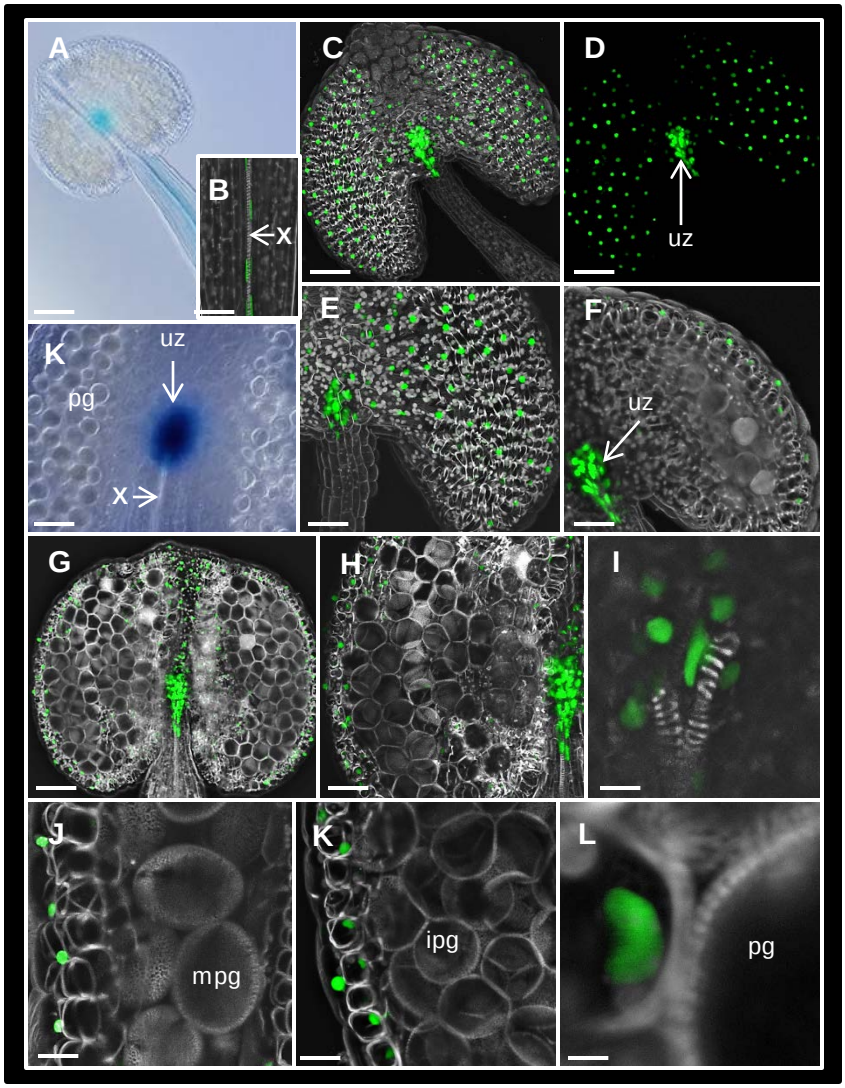

Figure 52. *UmamiT* expression in the anthers. $P_{UmamiT11}$*:GUS* in the filament (A) and anther (K). GUS staining in the vasculature and unloading zone, scale bar: (A) 120µm, (K) 40µm. $P_{UmamiT29}$*:NLS-3xGFP* in anthers of closed flowers: (C) overview, (D) GFP channel alone; scale bar: 90µm.(E) Z-stack of a young filament, scale bar: 50µm. (F) Optical section; scale bar: 40µm. (G, H) Ripe filament, scale bar: (G) 80µm, (H) 60µm. (I) Unloading zone of the anther, scale bar 6µm. (J) Anther with mature pollen, scale bar 12µm, (K, L) Anther with immature pollen, scale bar: 10µm. (L) Detail of tapetum cell with *UmamiT* promoter activity and a pollen grain, scale bar: 2µm. X (xylem), uz (unloading zone), pg (pollen grain) , ipg (immature pollen grain), mpg (mature pollen grain).

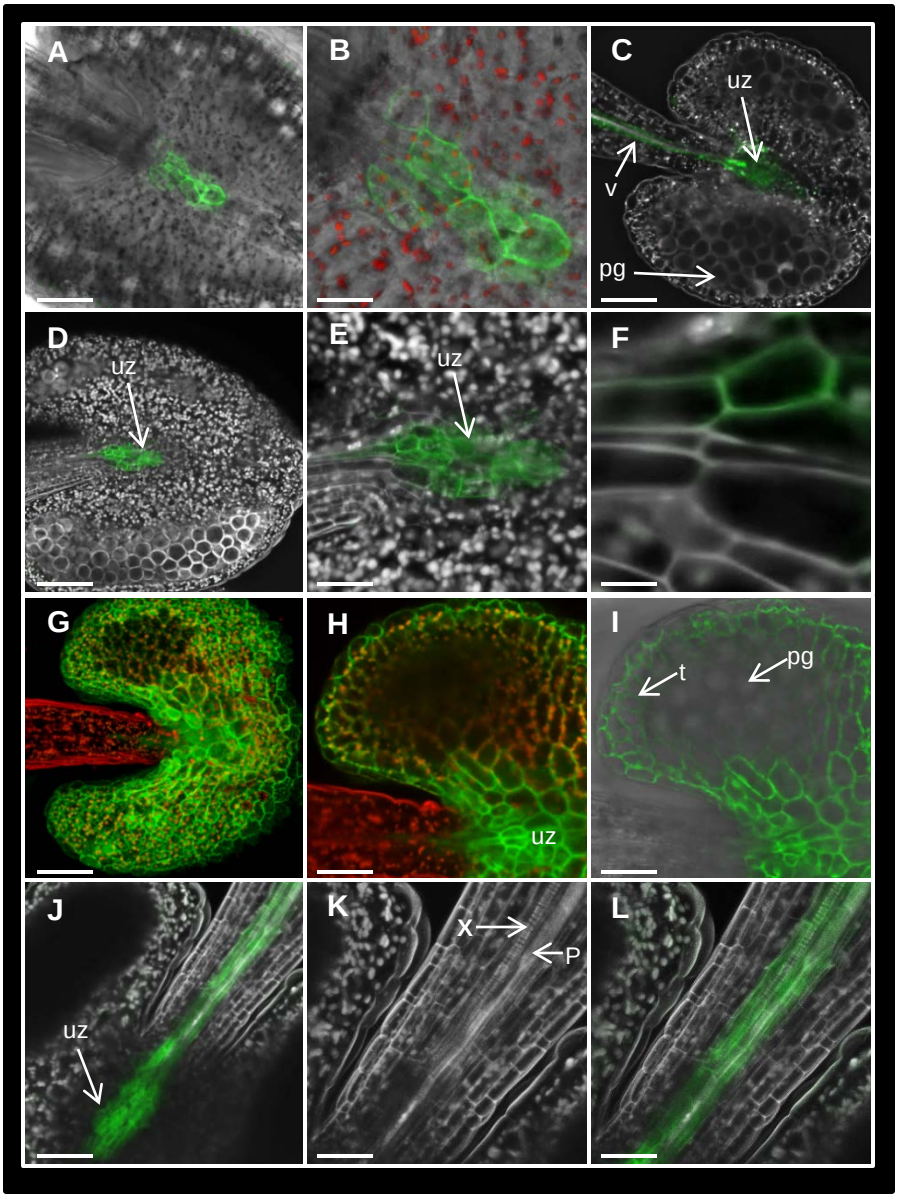

Figure 53. UmamiTs are differentially located in the anthers. *PUmamiT14:UmamiT14-GFP* (A-F); (A) open flower, scale bar: 60µm. (B) Magnification of the unloading zone in the anther, scale bar: 20µm. (C) Overview of an anther with mature pollen, scale bar: 70µm. (D) Anther of closed flower, scale bar: 90µm. (E) Magnification of the unloading zone, scale bar: 30µm. (F) Magnification of the unloading zone with focus at the phloem, scale bar: 3µm. (G-L) UmamiT29-GFP. (G) Maximum projection of an immature anther, scale bar: 70µm. (H, I) Magnification of an optical section from the unloading zone shows GFP signals in tissues around the pollen grains and at the unloading zone, scale bars: 35µm. (J-L) UmamiT29-GFP at the unloading zone and in the vasculature of the filament, maximum projection. (J) Overview, scale bar: 35µm. (K, L) Magnification of the vasculature form the filament, (L) overlay with GFP channel, scale bars: 20µm. X (xylem), p (phloem), pg (pollen grain), uz (unloading zone), v (vasculature), t (tapetum).

A look at the distribution of the fusion protein of UmamiT-GFP under the control of the endogenous promoter, showed differences between the *UmamiTs*. Clade I was specifically only detected at the unloading zone of the anther and in the vasculature of the funiculus (Fig. 53 A-F). This expression pattern was not changed during pollen grain maturation (Fig. 53 A, C, D). Clade III showed furthermore UmamiT-positive cells in the epidermal cells and the tapetum layer as well as in the vessels of the stamen and the endpoint of the vasculature (Fig. 53. G-I). The highest GFP intensity was found in the unloading zone and vasculature of the filament (Fig. 53 J-L).

To identify the distribution of UmamiT-positive cells and sieve elements at the endpoint of the vasculature of the filament, immunolocalizations were carried out on anthers with α-GFP and the sieve element antibody α-RS6. Signals could be specifically detected at the unloading zone of the stamen (Fig. 54 A, B, C). No colocalization in any sieve element was observed (Fig. 54 C, D). Maximum projections showed that UmamiT-positive cells were surrounded by sieve elements (Fig. 54 E) and stayed physically close to them (Fig. 54 F). UmamiT-positive cells are not restricted to the parenchyma around the xylem, but stretch also into the phloem regions without any colocalization with sieve elements, indicating a role of UmamiTs in the distribution of amino acids at the unloading zone in the anther (Fig. 54 G).

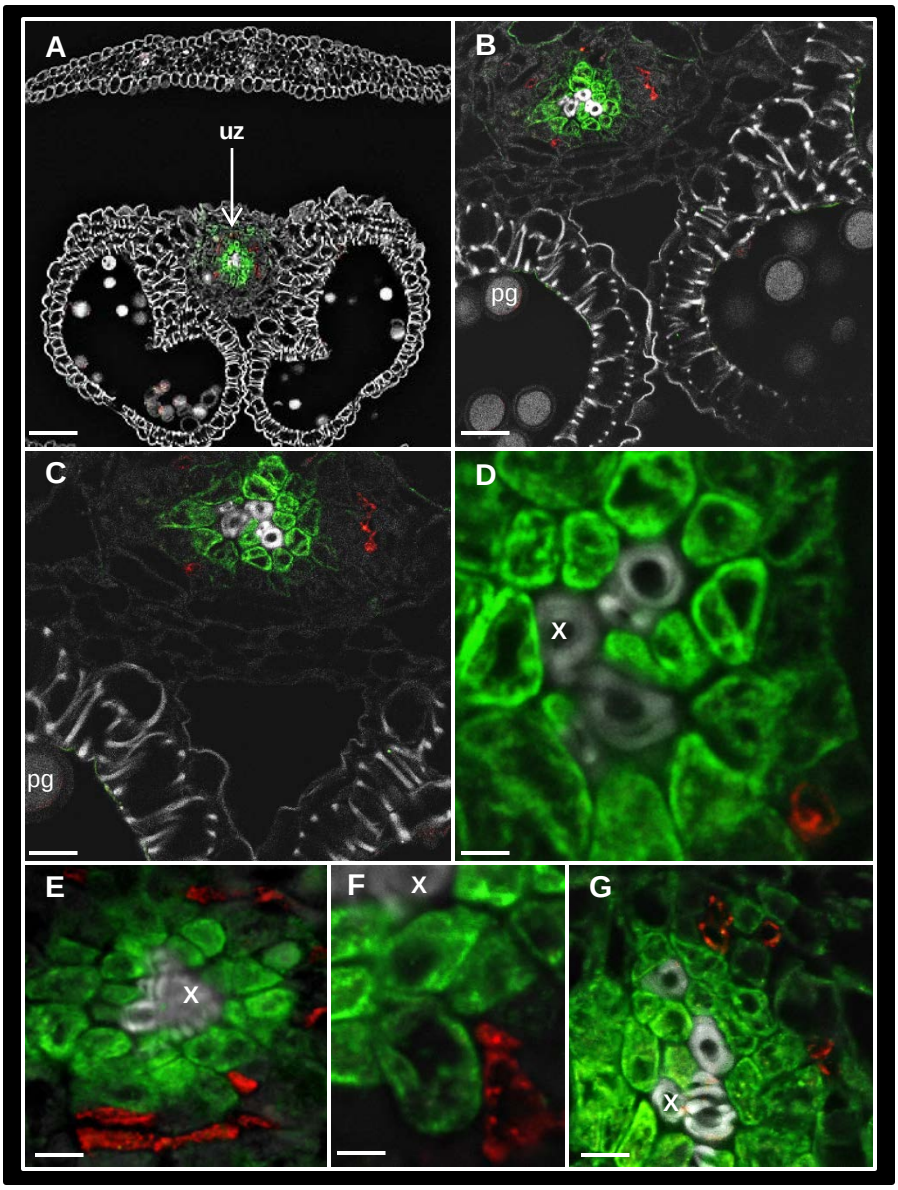

Figure 54. Characterization of UmamiTs in anthers by immunohistiochemistry. Green cells: α-GFP, detected with a CY2-antiserum, representing GFP positive cells; red cells: α-RS6 detected with an AF594-coupled antibody, representing sieve elements, white color: autofluorescence. (A) Overview: cross section through petal and anther, scale bar: 60µm. (B, C) Magnification of the unloading zone in the anther; scale bar: (B) 18µm, (C), 10µm. (D) Magnification of the endpoint of the xylem, scale bar: 2.5µm. (E) Z-stack of the unloading zone, scale bar: 10µm. (F) UmamiT-positive cells are located close to sieve elements, scale bar: 3.5µm. (G) Cells decorated with α-GFP are highly abundant around the xylem but also present in and behind the phloem region (G), scale bar: 5µm. X (xylem), uz (unloading zone), pg (pollen grain)

5.8.5. Replum, transmitting tract and funiculus

Before fertilization, *UmamiT* promoter activity was found in in the replum (Fig. 55 A). GUS staining of the transmitting tract in closed flowers (Fig. 55 B) and open flowers (Fig. 55 C) was obtained for all candidates. The presence of UmamiT-GFP was also observed in the same tissues (Fig. 55 D, G) where a partial polar distribution of the protein was detected.

In the funiculus GUS staining was seen within the vascular cylinder (Fig. 55 E, F). Although the fusion protein could be found there too, it was very weak and signals could not be detected in each funiculus (Fig. 55 H, I). Coexpression of SUC2-mCherry with UmamiT14-GFP proofed that the cell type there represents the companion cell indicating a role of UmamiTs in the long distance transport of amino acids into sink tissues (Fig. 55 J, K, L).

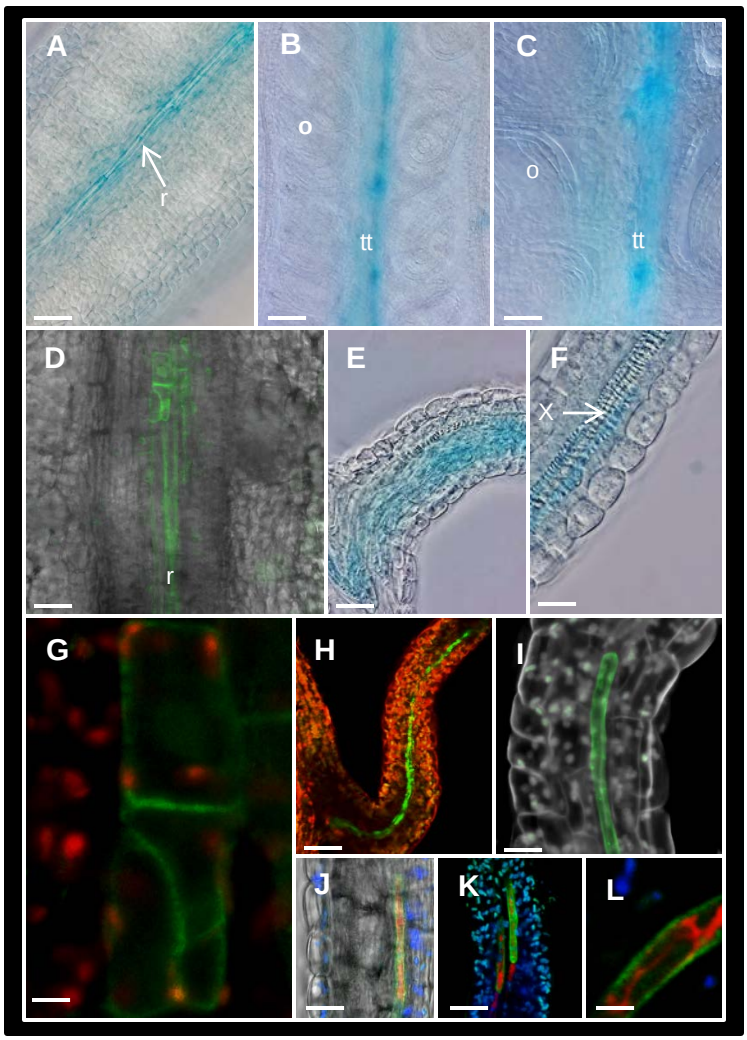

Figure 55. UmamiTs are found in the funiculus. (A) *P*$_{UmamiT29}$*:GUS* in the replum, scale bar: 60µm. Detail in (B) and (C) shows the stained transmitting tract, scale bars: (B) 50µm, (C) 30µm. (E, F) GUS staining in the funiculus, scale bars: (E) 20µm, (F) 10µm. (D) UmamiT29-GFP in the replum, scale bar 24µm. (G) Magnification of (D), scale bar 2µm. (H) UmamiT11-GFP in the funiculus, scale bar 30µm. (I) UmamiT14-GFP in the funiculus, scale bar 4µm. (J,K, L) In *P*$_{UmamiT14}$*: UmamiT14-GFP* x*P*$_{SUC2}$*: ER-mCherry* plants, some UmamiT14-positive cells show simultaneously mCherry; in the funiculus scale bars: (J) 10µm, (K) 30µm, (L) 3µm. X (xylem).

Due to the very weak signals of UmamiT-GFP in the transmitting tract and funiculus whole mount immunolocalization experiments were performed to elucidate the cell type, which contained the fusion protein. Detection of GFP by a fluorescent labeled secondary antibody leads to a signal amplification, due to the fact that the GFP-α-GFP complex has several binding sites for the secondary antibody. A specific signal was obtained within the transmitting tract by signal amplification (Fig. 56 A, B), where no overlap with the RS6 epitope was documented (Fig 56 C, D, E). Both cell types, UmamiT-positive cells (Fig 56 D) and sieve elements (Fig 56 E) were nucleated as indicated by DAPI staining. In the respective tissue both cell types were located very close to each other (Fig. 56 G, H).

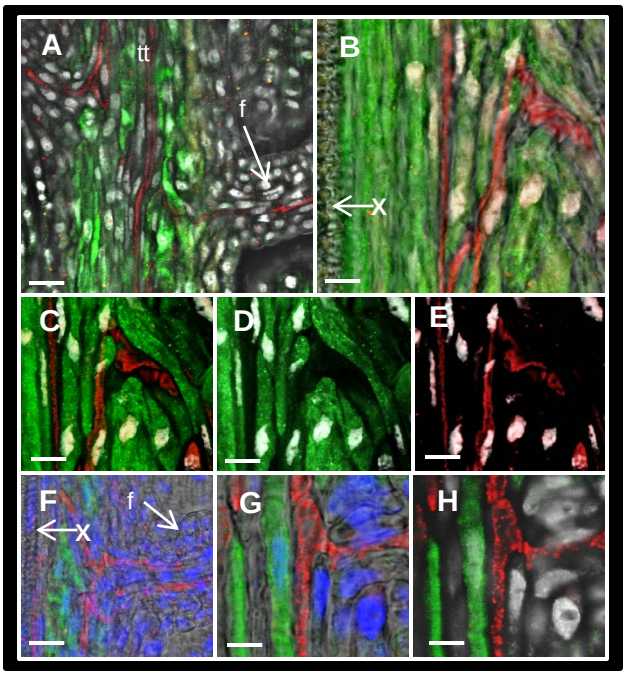

Figure 56. Whole mount immunolocalization of UmamiT14-GFP and sieve elements in the transmitting tract. Green cells: α-GFP, detected with a CY2-antiserum, representing GFP positive cells; red cells: α-RS6 detected with an AF594-coupled antibody, representing sieve elements. Blue and white color: DAPI. (A-D) Transmitting tract, UmamiT-positive cells close to sieve elements; no colocalization with RS6. (A) Overview, scale bar: 20µm. (B) Magnification of the vasculature in the transmitting tract, scale bar: 8µm. (C-E) Magnification of the fluorescence channels, (C) overlay of (D) and (E). (D) UmamiT–positive cells, (E) sieve elements, scale bars: 10µm. (F) UmamiT is detected at the branch point to the funiculus scale bar: 10µm. (G, H) Magnification of an area with (G) or without bright field image (H), scale bar: 7µm. X (xylem), tt (transmitting tract), f (funiculus).

The same was also true for the funiculus (Fig.57). The very striking difference here is, that only single cells very close to the sieve elements showed signals for α-GFP (Fig. 57 C, F, G). Phloem and xylem lay in collateral position to each other as reported for the stele in the root (Fig. 57 A, B). According to their position there and the previously shown colocalization with SUC2 (Fig. 55 J, K, L) it was concluded the cells to refer to companion cells.

Taken together the results suggest a role of UmamiTs in the amino acid transport along the transmitting tract and funiculus, where they are placed at strategically important positions for long distance transport.

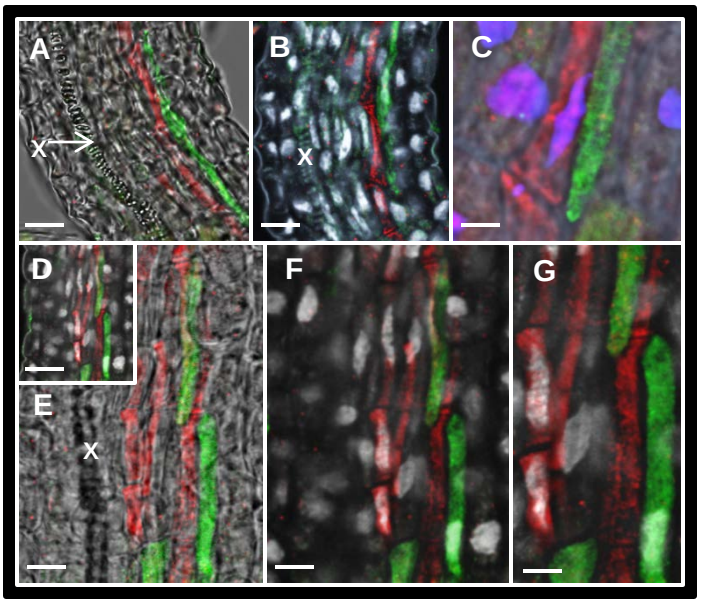

Figure 57. Whole mount immunolocalization of UmamiT14-GFP and sieve elements in the funiculus. Green cells: α-GFP, detected with a CY2-antiserum, representing GFP positive cells; red cells: α-RS6 detected with an AF594-coupled antibody, representing sieve elements. Blue and white color: DAPI. Nucleated sieve elements and companion cells are close to each other. (A) Overview with bright field image vasculature in funiculus, scale bar: 8µm. (B) Overlay with DAPI, scale bar: 10µm. (C) Nucleated sieve element next to UmamiT-positive cell, scale bar: 3µm. (D) Overview of (E, F) with DAPI; scale bar: (D) 25µm. (E, F) Magnification of (D). (E) Overlay with bright field image. (F) Overlay with DAPI, scale bars: 8µm. (G) Magnification of (F) showing nucleated sieve elements next to nucleated UmamiT-positive cell, scale bar: 5µm. X (xylem)

5.8.6. SAM

In order to study, if UmamiT-positive cells are associated with the shoot apical meristem, UmamiT marker lines for promoter activity and the GFP fusion protein were analyzed. As already shown *UmamiTs* are broadly expressed along the vasculature of the whole plant. A crossing point at the seedling stage is made by the shot apical meristem (SAM), where in a diagonal plane the vasculature expands into the leaves (Fig. 58 A). Promoter-GUS staining was observed very close to the SAM, which is independent of the age of the seedling or the developmental stage of the leaf primordia (Fig. 58 B-D, F). Not only cells close to the vasculature showed GUS staining, but even more parenchymatic tissues between the branch point of the vessels and the SAM (Fig. 58 D). High cellular resolution was reached using mPS-PI staining and the reflection mode of the confocal microscope (Fig. 58 E, G). Very specific GUS staining in the vessels was reported there, as well as single GUS crystals in the surrounding parenchymatic tissues at the bottom of the SAM. Altogether a strong promoter activity of *UmamiTs* was identified in the region close to the SAM indicating an additional role of *UmamiTs* in the supply of the SAM.

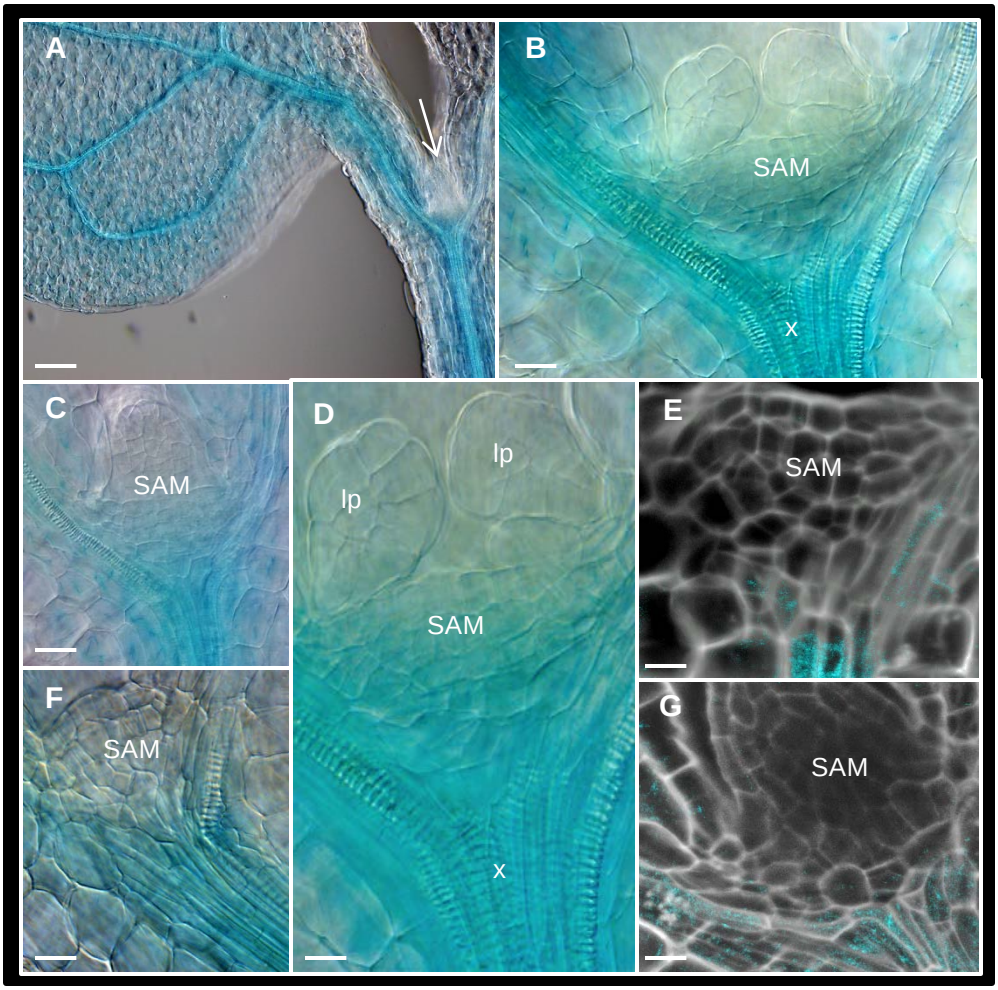

Figure 58. *UmamiT* promoter activity at the SAM. (A). Overview of a seedling showing staining in the vasculature of shoot and leaf, scale bar: 100µm. (B, C, D, F) Magnification of the SAM. (B, D) Ten day old seedling with visible leaf primordia, GUS staining in the vasculature and tissues close to the SAM, scale bars: (B) 18µm, (D)10µm. (C, F) Dome shape of the SAM with GUS staining in the surrounding cell files, scale bars: (C) 20µm, (F) 15µm. (E, G) mPS-PI staining of the SAM with GUS crystals in the vasculature and neighboring cells, scale bar: (E) 8µm, (G) 10µm. X (xylem), sam (shoot apical meristem), lp (leaf primordium).

The fusion protein of UmamiT-GFP at the plane of the SAM could also be detected in association with the vasculature (Fig. 59 A, B, F, G). The GFP signal ended right before the dome of the meristem was emerging from the shoot (Fig. 59 D, E, H). This was consistent with the findings in the mPS-PI staining of the SAM (Fig. 59 C), where most of the GUS crystals were placed in the cells of the vasculature.

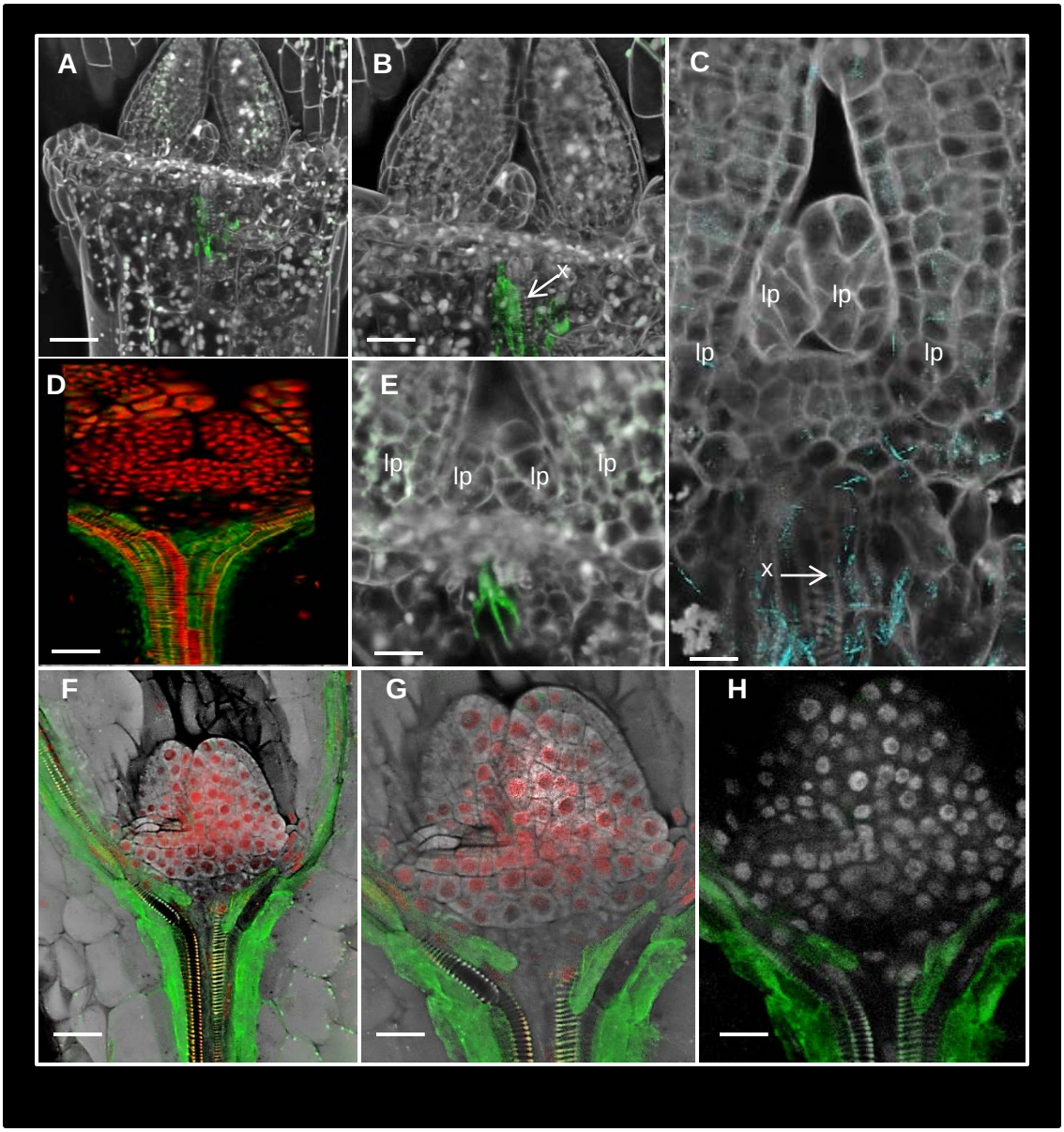

Figure 59. UmamiTs are closely located to the SAM . (A, B) Maximum projection of the shoot region of a ten day old seedling, showing UmamiT11-GFP fluorescence in the vascular tissue close to the leaf primordia, scale bars: (A) 50µm, (B) 35µm. (C) mPS-PI staining of a seedling at the same stage, scale bar: 20µm. (D) Maximum projection of the SAM with UmamiT28-GFP at the vascular tissue, close to the emerging meristem. DAPI stained nuclei and autofluorescence of xylem are shown in red, scale bar: 40µm. (E) UmamiT-11 GFP is very closely located to the emerging point of the leaf primordia, scale bar: 18µm. (F-G) UmamiT29-GFP fluorescence in the vasculature ended at the SAM, some cells share close vicinity to the meristem. Nuclei are stained with DAPI, colored in red (F, G) or white (H), scale bars: (F) 30µm, (G) 12µm, (H) 10µm. X (xylem), lp (leaf primordium), sam (shoot apical meristem).

To get a three dimensional impression about how the cells with UmamiT-GFP decoration are placed around the SAM immunolocalizations on cross sections were made.

Fig. 60 shows a section at the height of the shoot, where SAM and leaf primordia are located in the center. The SAM is encircled by green cells, which represent the UmamiT-positive cells. Sieve elements are found in the periphery in the vascular tissue and they do not colocalize with GFP-positive cells. This situation is similar to the already described unloading zone of the anthers, where UmamiT-positive cells are located close to sieve elements, but do not show an overlap between the GFP and RS6 decoration. *UmamiT* expression in parenchymatic cells around the SAM is clearly separated from cells differentiating to sieve elements and reaches close to the dome of the SAM.

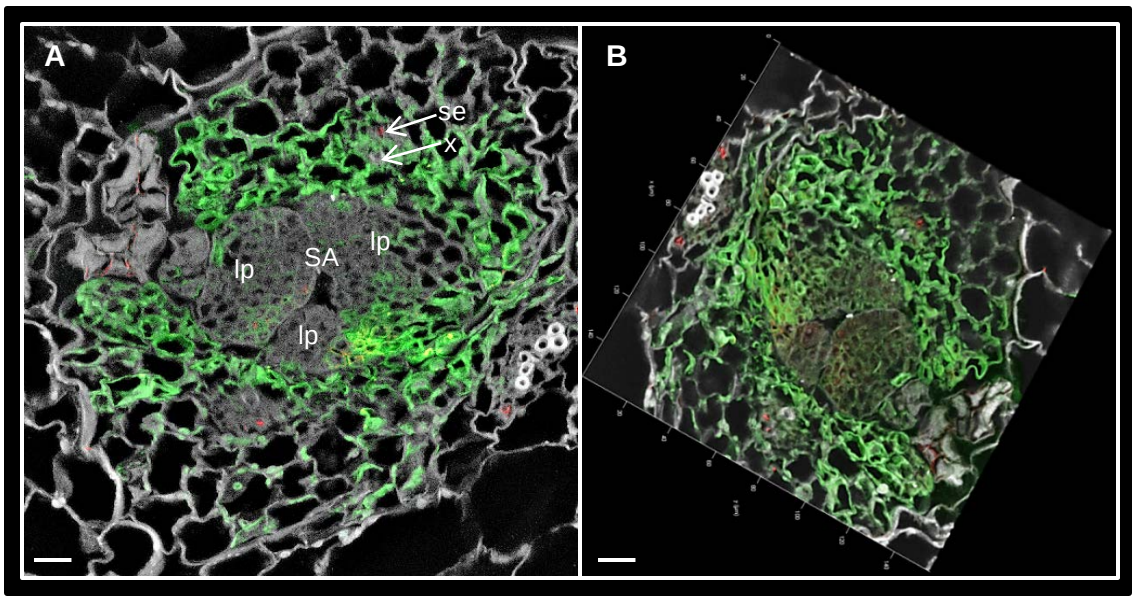

Figure 60. Immunolocalization at the SAM with *UmamiT-GFP* plants. Green cells: α-GFP, detected with a CY2-antiserum, representing GFP positive cells; red cells: α-RS6 detected with an AF594-coupled antibody, representing sieve elements, white color: autofluorescence**.** (A) Cross section through the SAM, UmamiT decoration in parenchymatic tissue surrounding the SAM, scale bar: 15µm. (B) 3D reconstruction of a cross section of the shoot at the level of the SAM, scale bar: 10µm. X (xylem), se (sieve element), lp (leaf primordium), sam (shoot apical meristem).

5.8.7. Hypocotyl

In order to characterize the cell type of UmamiT-positive cells in the hypocoty immunolocalizations of the stem near to the SAM (Fig. 61 A) were carried out, where the hypocotyl has already undergone secondary growth. Here, *UmamiT* expression was again observed in the parenchymatic tissue between sieve elements and the xylem. The same was true for the older hypocotyl more distal from the SAM (Fig. 61 B). In all cases, UmamiT-GFP was restricted to the parenchymatic tissue close to the xylem, forming an almost closed circle in the stele. Those cells did not colocalize with the sieve element marker RS6 (Fig. 61 C-F), indicating that *UmamiT* expression in the hypocotyl does not occur in sieve element progenitor cells.

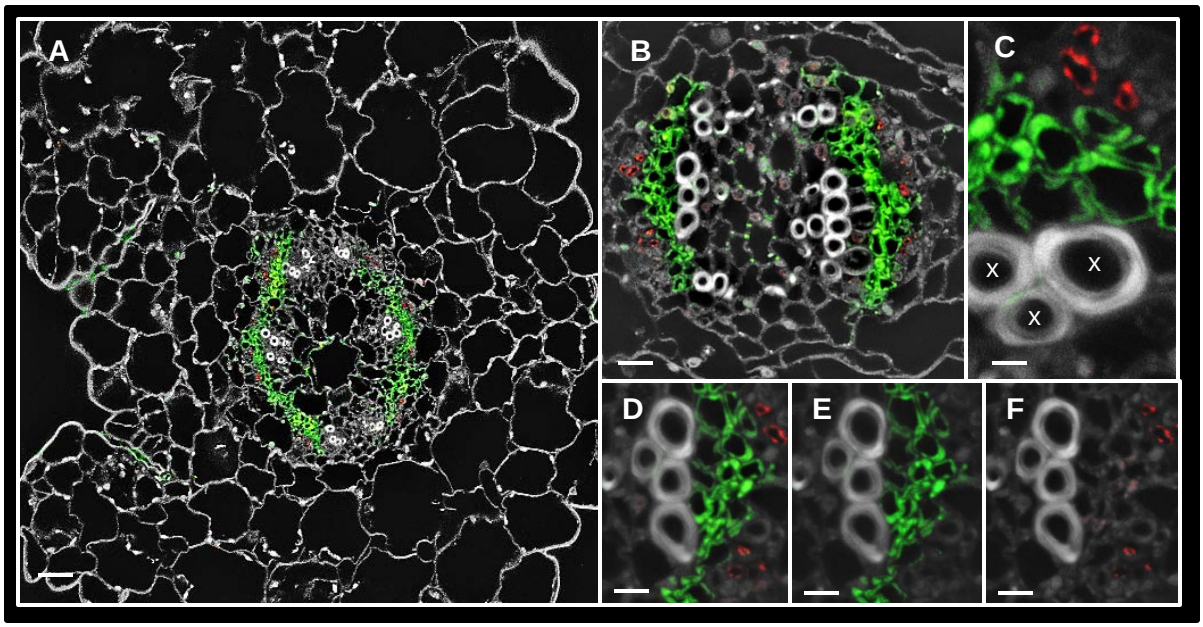

Figure 61. Characterization of UmamiT-positive cells in the hypocotyl by immunolocaization. UmamiT29-GFP reporter was used. Green cells: α-GFP, detected with a CY2-antiserum, representing GFP positive cells; red cells: α-RS6 detected with an AF594-coupled antibody, representing sieve elements, white color: autofluorescence. (A) Cross section through a part of the hypocotyl beneath the SAM. UmamiT-GFP in parenchymatic tissue of the vasculature, scale bar: 35µm. (B) Magnification of the stele in the hypocotyl, scale bar: 12µm. (C) UmamiT-positive cells between xylem and sieve elements, scale bar: 5µm. (D-E) Magnification of a part of the vascular tissue of the hypocotyl showing distinct labeling of UmamiTpositive-cells with only α-GFP (E) and sieve elements only decorated with α-RS6 (F), no colocalization with any sieve element was monitored. (D), scale bar: 8µm. X (xylem).

Distal from the SAM, UmamiT-GFP signals were also found in the hypocotyl (Fig. 62 A-C). This was true for members of clade I and III. A closer look at the site of GFP fluorescence in seedlings right after germination showed again a clear association of UmamiTs with the vascular tissue (Fig. 62 D-F). Cross sections showed GFP only in cells close to the stele. Those cells are ordered as a ring around xylem and phloem. No GFP signal was found in the phloem poles (Fig. 62 H, I). This lack of UmamiT-positive cells in the phloem validated the results obtained from the immunolocalization and indicated that sieve elements in the hypocotyl do not originate from UmamiT-positive cells, which are physiologically located in cells contributing to the long distance transport.

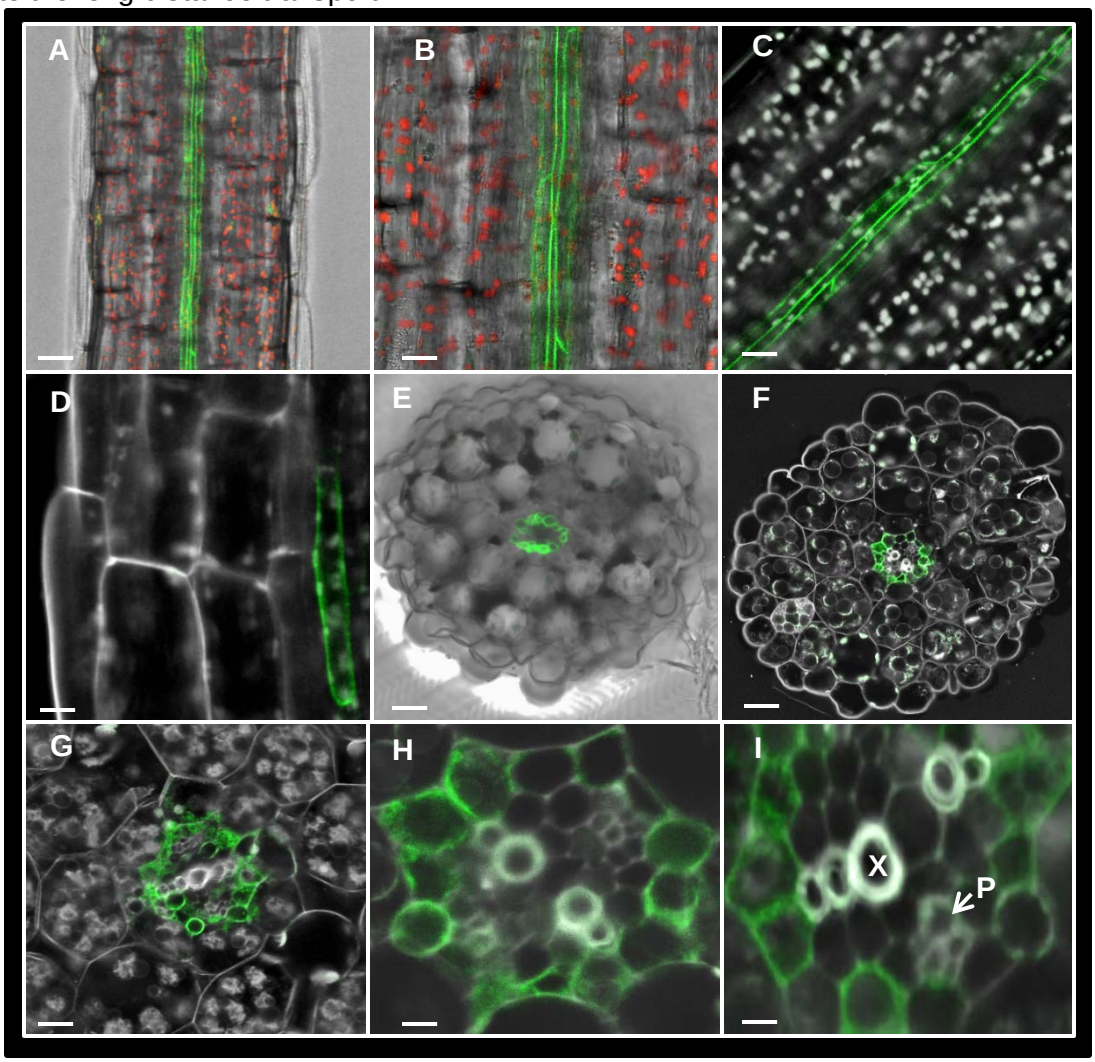

Figure 62. *P*$_{UmamiT}$*: UmamiT-GFP* expression in the hypocotyl. (A, B) UmamiT14-GFP in the vascular cylinder, scale bar: (A) 50µm, (B) 20µm. (C) UmamiT28-GFP in the hypocotyl, scale bar: 15µm. (D) Optical section showing epidermal cell files and UmamiT-GFP in the center of the hypocotyl, scale bar: 10µm. (E-I) Cross sections of the shoot. (E) Overlay with bright field image, UmamiT-GFP encircled the stele, scale bar: 20µm, (F-I) UmamiT-GFP restricted to the cells surrounding the stele of the young hypocotyl and absent from the phloem poles, scale bars: (F) 25µm, (G) 15 µm, (H) 8 µm, (I) 5µm. X (xylem), p (phloem).

5.8.8. Germination

UmamiT expression was found in the vasculature of the vegetative tissue in different position of the plant body. In order to investigate if UmamiTs are present in the seed coat and seedlings during germination, promoter activity and the GFP fusion protein was monitored before and after the rupture of the seed coat. In this chapter, the focus is on the few hours during the germination process. By promoter analysis it could be shown that especially *UmamiT28* is strongly expressed in the seed coat layer directly behind the remaining layer of the outer integument in imbibed seeds (Fig. 63 F). This layer is called aleurone or peripheral endosperm. GUS crystals were specifically found in this layer (Fig. 63 A, D). Analysis of promoter activity by GUS staining indicated that *UmamiT28* and *29* were expressed to highest degree in this tissue, whereas staining of the aleurone in the UmamiT11 and UmamiT14 reporter lines was quite weak and appeared only by after severe overstaining. This substantiates that the expression domains of clade I and clade III *UmamiTs* differs quite significantly. A few hours after germination, promoter activity of candidate *UmamiTs* was found in the stele of the radicle and hypocotyl (Fig. 63 B). At the moment the cotyledons were out of the seed, promoter activity was additionally broadly distributed in the cotyledons (Fig. 63 E). Within a few hours the GUS staining in the cotyledons was concentrated to the vascular tissue (Fig. 63 C). After expanding of the cotyledons the same expression pattern could be reported for the fusion protein. GFP was found in the vasculature of the root, the hypocotyl and the cotyledons (Fig. 63 H). *Promoter: NLS-3xGFP* analysis during germination revealed a high expression in the peripheral endosperm for *UmamiT29* (Fig. 63 G, I). This cell layer is a direct neighbor to the embryo (Fig. 63 J) and distinct from the thickened outer integument (Fig. 63 K). Promoter activity and the GFP fusion protein were detected in the same cells (Fig. 63 L-N). After cotyledons were out of the seed coat, the fusion protein in cells of the peripheral endosperm appeared in the ER in a patchy pattern (Fig. 63 N).

These results show that *UmamiTs* are expressed during germination and that especially clade III *UmamiTs* become directly activated as the seed imbibes. The specific association with the vasculature in the vegetative tissue was seen to shift from a ubiquitous expression in young cotyledons that were emerging out of the seed coat to a vascular tissue restricted expression pattern within few hours after germination.

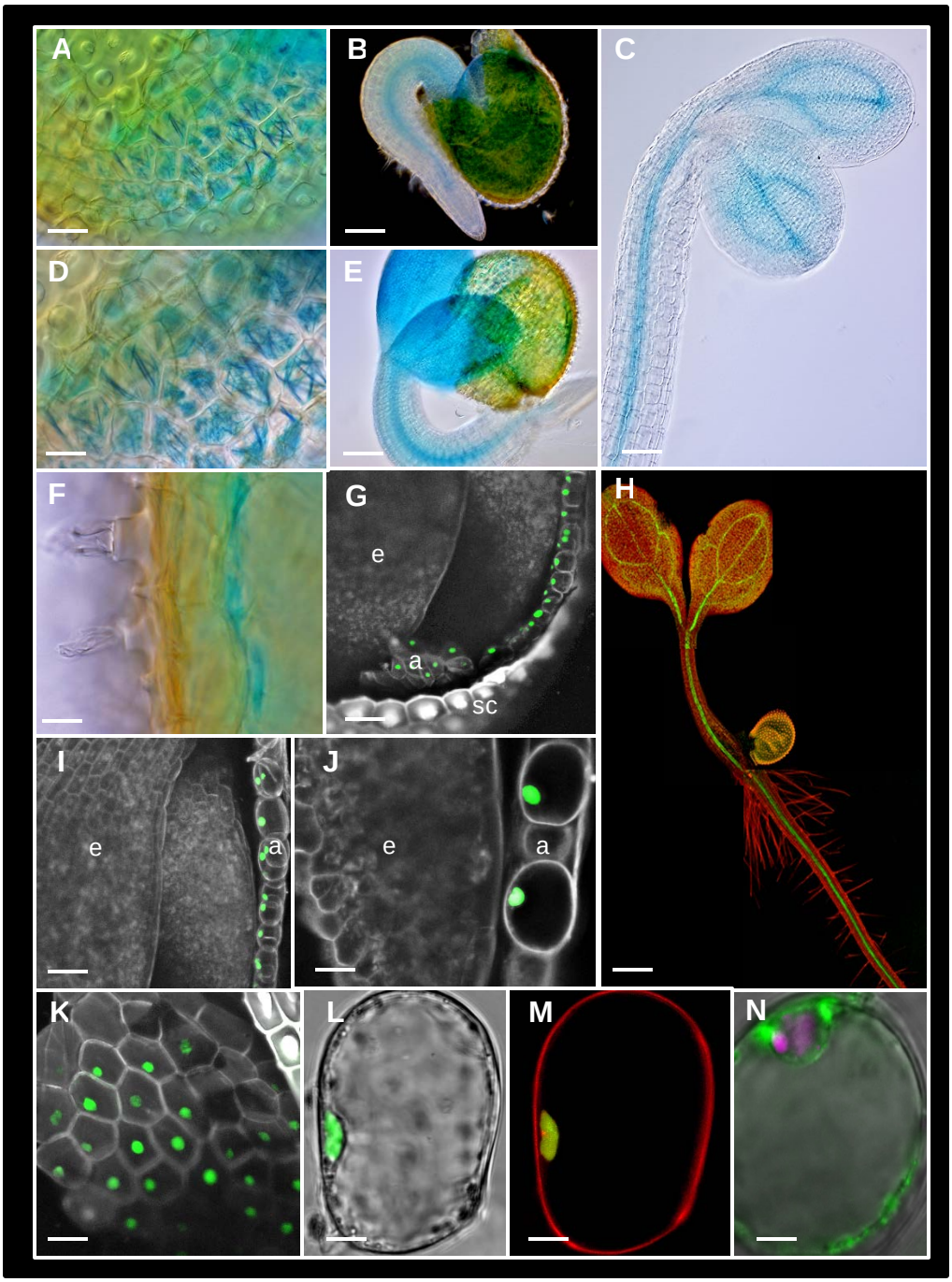

Figure 63. *UmamiTs* are expressed during germination. (A-F) *PUmamiT: GUS*, (H, N) *PUmamiT: UmamiT-GFP*, (G, I-M) *PUmamiT29: NLS-3xGFP*. (A, D, F) *UmamiT28-GUS* expressed in the aleurone layer of the seed coat, scale bars: (A) 40µm, (D) 30µm, (F) 20µm. (B, C, E) *PUmamiT: GUS* during germination. (B) Few hours after appearance of the radicle, scale bar: 100µm, (C) Two days after germination, scale bar: 50µm, (E) Few hours later than in (B), scale bar: 70µm. (H) Seedling after germination, UmamiT-GFP in the vasculature of root, hypocotyl and cotyledons, scale bar: 150µm. (G) UmamiT29 promoter activity in the germinating seed, scale bar: 55µm, (I) Maximum projection of an area excluding the outer integuments, GFP signals only found in the seed coat layer attached to the embryo, scale bar: 40µm. (J) Single optical section of the border between embryo tissue and peripheral endosperm, scale bar: 16µm. (K) GFP restricted to the peripheral aleurone, scale bar: 35µm. (L, M) One single aleurone cell. (L) Overlay with bright field image. (M) Overlay with PI, nucleus is stained yellow due to an costaining of the nucleus with GFP and PI, scale bar: 6µm, (N) UmamiT29-GFP expression in an isolated peripheral endosperm cell after germination, nucleus colored in magenta by PI staining, scale bar: 3µm. E (embryo), a (aleurone= peripheral endosperm), sc (seed coat).

5.8.9. Seed

According to the array data and the analysis of the RNA levels of *UmamiTs* in different tissues it turned out that they were prevalently expressed in seeds. In order to analyze the distinct localization of UmamiTs in the seed promoter activity and the GFP fusion protein was monitored during seed development. The order is according to the two major clades where first the candidate with the stronger expression will be analyzed.

One unique feature of all *UmamiT* candidate genes was that they were completely absent in the ovule before fertilization. Neither in the promoter GUS lines nor in the GFP reporter lines any signal could be detected.

5.8.9.1. UmamiT14 localization in the seed

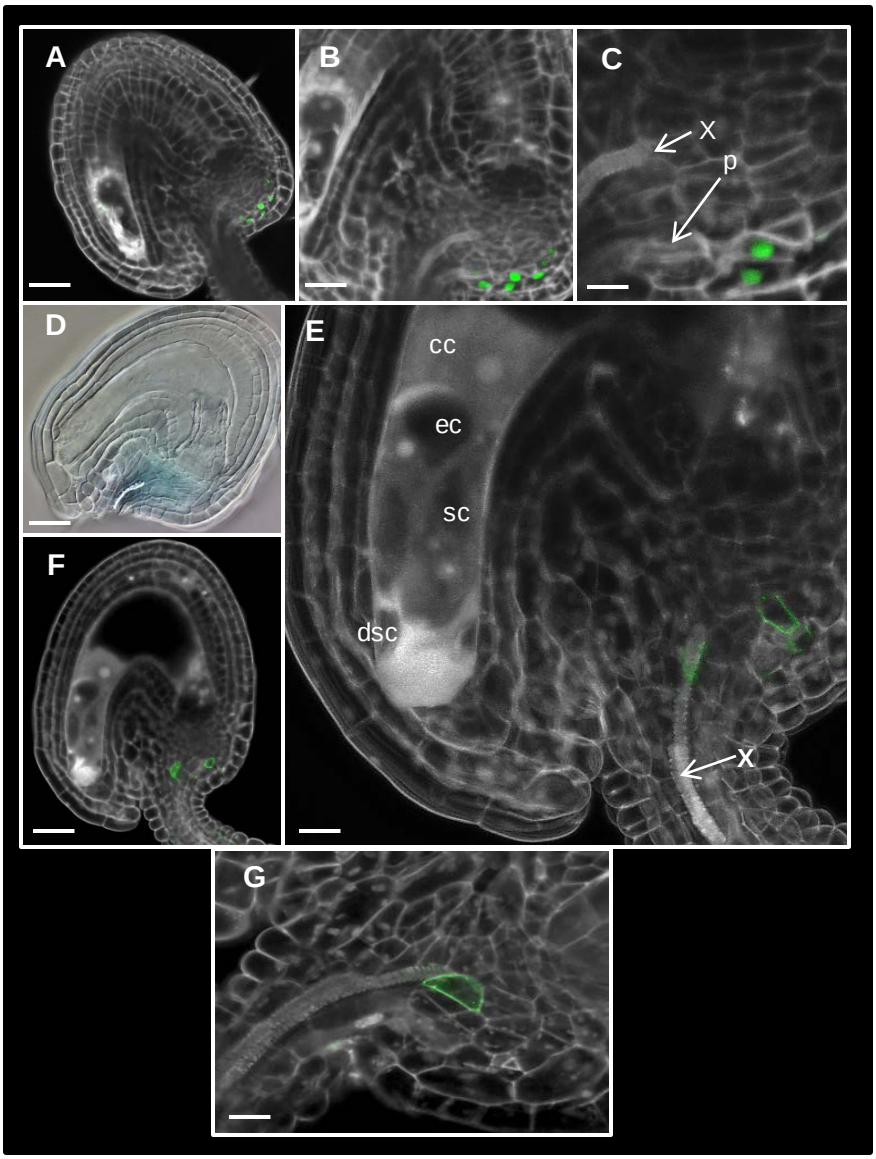

Figure 64. *UmamiT14* expression and localization of UmamiT14-GFP right after fertilization. $P_{UmamiT14}$*: NLS-3xGFP* after zygote formation. (A) Overview of the young seed, scale bar: 30µm; (B) Magnification shows promoter activity in the unloading zone; scale bar: 15µm. (C) *UmamiT* promoter activity close to phloem; scale bar: 7µm. (D) $P_{UmamiT14}$*: GUS;* GUS staining at the chalazal region after fertilization, scale bar: 30µm. (E, F) UmamiT14-GFP appeared right after fertilization; stage marked by degenerating synergid cell. (E) Maximum projection, scale bar: 8µm. (F) Overview of a fertilized ovule, scale bar: 30µm. (G) Magnification of the terminal vasculature, scale bar: 11µm. X (xylem), p (phloem, marked by thickened cell walls), sc (synergid cell), dsc (degenerating synergid cell), ec (egg cell), cc (central cell).

For *UmamiT14* the first promoter activity was documented at the chalazal region of the fertilized ovule (Fig. 64 A, D). It could be shown that the cells in which the promoter becomes activated are in close vicinity of the endpoint of the vasculature and near the phloem (Fig. 64 B, C). Using the translational fusions, it could be demonstrated that directly after fertilization (indicated by the degenerating synergid cell that shows accumulation of PI staining) only very few cells showed GFP (Fig. 64 E, F). These cells were close to the ending xylem and phloem (Fig. 64 G).

Later during seed development it was observed that much more cells at the chalazal pole showed strong GUS staining (Fig. 65 A-C). This did not change during the complete seed development starting from early globular stage to the cotyledon bending stage (Fig. 65 D-I). In all stages of seed maturation the promoter activity was very specifically restricted to those cells that are located at the endpoint of the vasculature, where the unloading zone is placed (Fig. 65 C, F).

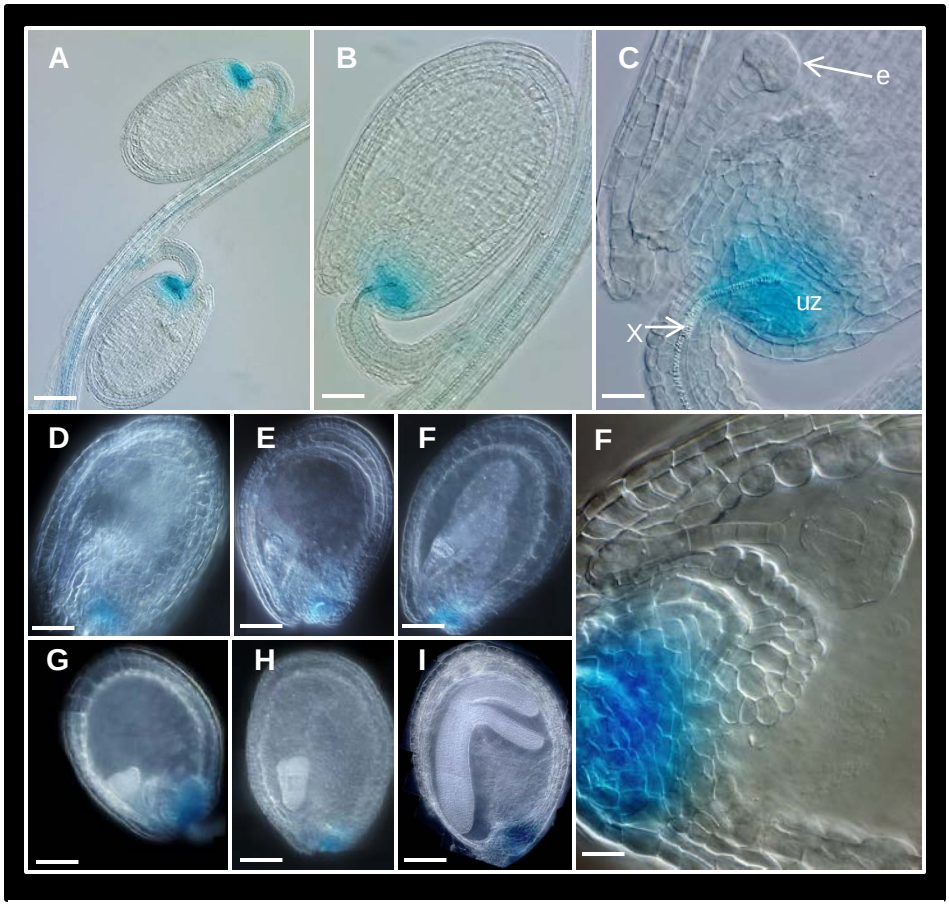

Figure 65. *UmamiT14* promoter activity is detected exclusively in the unloading zone throughout seed development. *P*$_{UmamiT14}$*: GUS* expression. (A) Open silique with seeds, strongest staining at the chalazal pole, only weak staining visible in the transmitting tract, scale bar: 100µm. (B) Magnification of one seed, scale bar: 50µm. (C) DIC image with focus on the unloading zone and globular embryo, scale bar: 15µm. (D-I) GUS staining throughout embryo development; scale bar: (D) 25µm, (E) 40µm, (F) 50µm, (G) 60µm, (H) 50µm, (I) 60µm. (F) DIC image with heart shaped embryo, scale bar: 10µm. X (xylem), e (embryo), uz (unloading zone).

Focusing now at the translational UmamiT14-GFP fusion, which contains all introns, demonstrated the specific GFP fluorescence at the chalazal region. This localization pattern took place throughout embryo development exclusively in the unloading zone (Fig. 66). Even in the very late stage when the embryo is at full maturity but the silique is still green and connected to the mother plant GFP was detected only in the chalazal pole at the unloading zone. The overlapping findings between GUS staining and UmamiT-GFP indicate that all elements required for proper expression are found in the 5' region of the ATG.

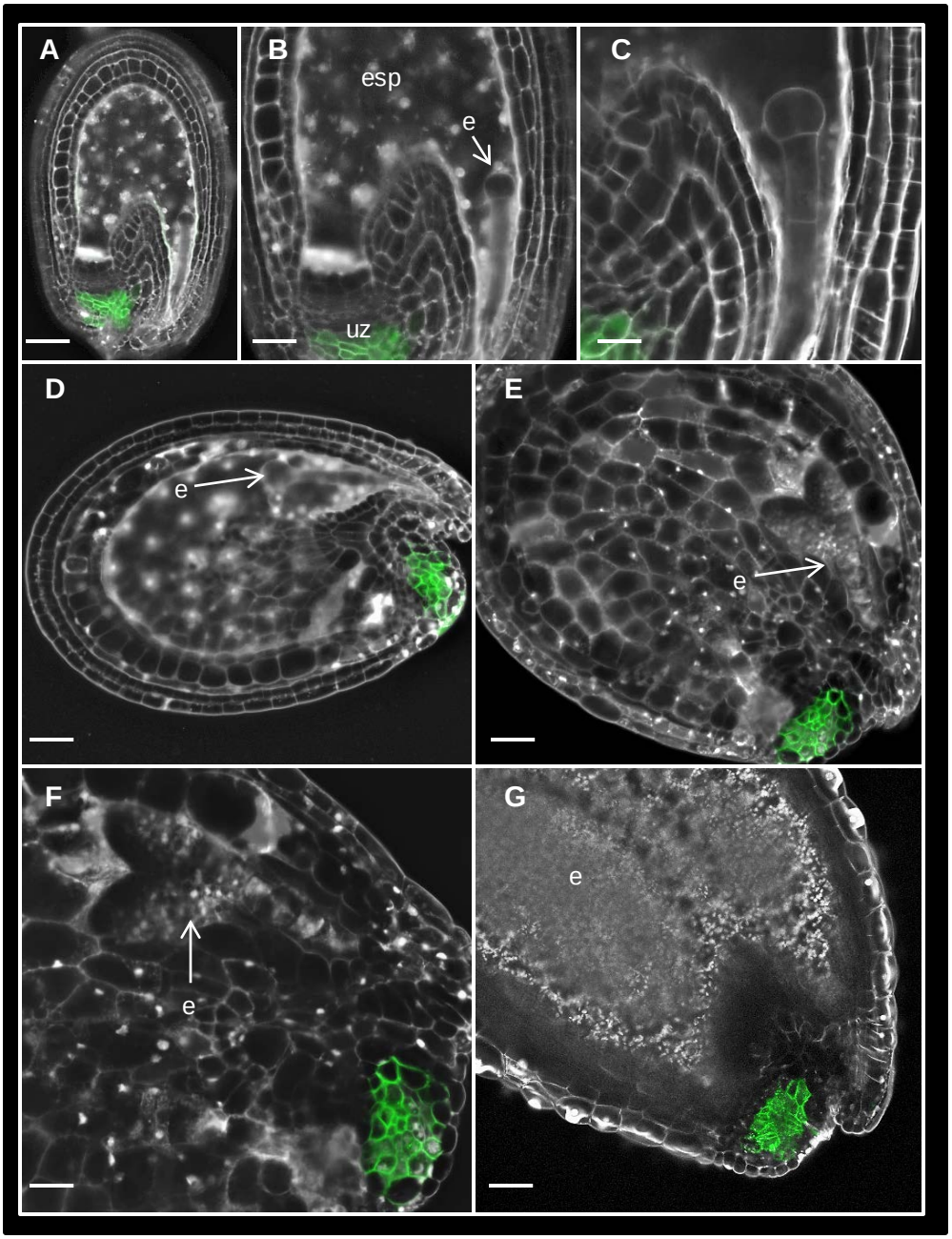

Figure 65. Analysis of tissue-specific UmamiT14 localization throughout embryo development. Localization studywas done with the $P_{UmamiT14}$: UmamiT14-GFP reporter line. (A-C) Early globular stage; (A) Overview of the seed as z-stack, scale bar: 50µm. (B) Magnification of (A), scale bar: 25µm. (C) UmamiT14-GFP at two cell stage, scale bar: 10µm. (D) Late globular stage, scale bar: 50µm. (E) heart stage, scale bar: 40µm. (F) Magnification of unloading zone of heart staged seed; scale bar: 18µm. (G) Late cotyledon bending stage, scale bar: 40µm. UZ (unloading zone), e (embryo) , esp (endosperm).

A closer look at this site of the seed revealed that the protein is located directly at the endpoint of the vasculature (Fig. 66 A, B). Z-stacks manifested that also cells in the periphery of the chalaza (Fig. 66 C, D) showed GFP but much weaker than those cells, which were directly associated with the endpoint of the vasculature (Fig. 66 E, F). These cells were nucleated (Fig. 66 G) and build the unloading zone where the xylem (Fig. 66 H) and phloem, represented by the nucleated sieve elements (Fig. 66 I), end.

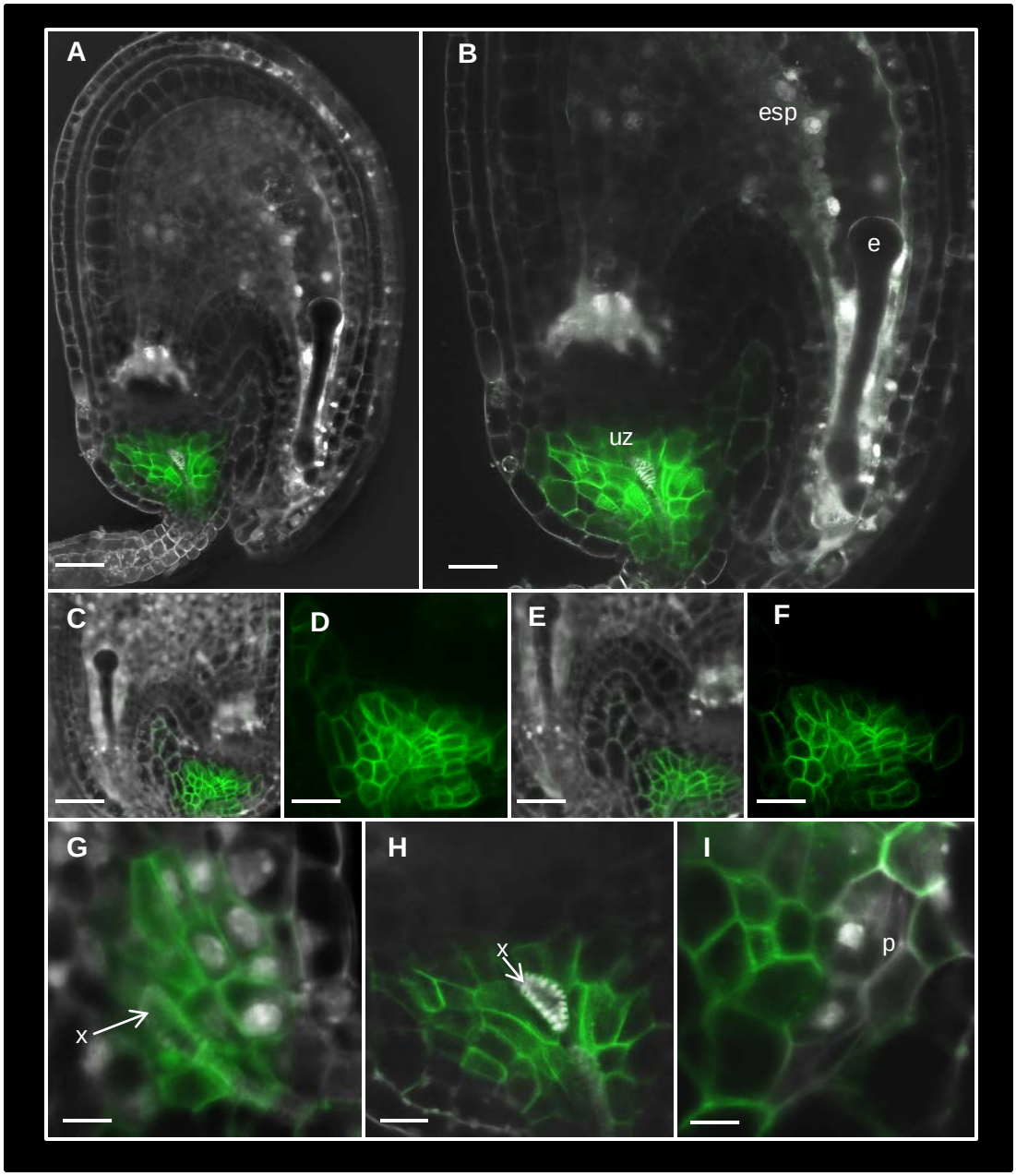

Figure 66. UmamiT14 is specifically localized at the unloading zone. Localization study was done with the $P_{UmamiT14}$: UmamiT14-GFP reporter line. (A) Overview of a seed with focus on the ending xylem at the chalaza, scale bar: 35µm. (B) Magnification at the unloading zone, scale bar: 20µm. (C) Z stack of the chalazal region, scale bar: 30µm. (D) GFP channel of (C), scale bar: 10µm. (E) Magnification of the unloading zone of (C) , scale bar: 35µm, (F) GFP channel of (E), scale bar: 20µm. (G) Nucleated GFP tagged cells at the vascular endpoint, cell nuclei stained by PI, scale bar: 10µm; (H) UmamiT14-GFP at the endpoint of the xylem, scale bar 15µm and (I) nucleated sieve elements/phloem , scale bar: 8µm. X (xylem), p (phloem), uz (unloading zone), esp (endosperm), e (embryo).

5.8.9.2. UmamiT11 localization in the seed

For *UmamiT14´*s close relative *UmamiT11* the same expression pattern was detected but with a slightly stronger expression in older stages of the seed (Fig. 67). The fusion protein was monitored directly at the chalazal region where the funiculus ends. This indicates that also UmamiT11-GFP is positioned in the unloading zone at a physiological important position for nutrient export into the sink tissue. Further investigations showed that UmamiT11 is supersimilar to UmamiT14 in terms of tissue specific localization .Therefore not everything is shown again

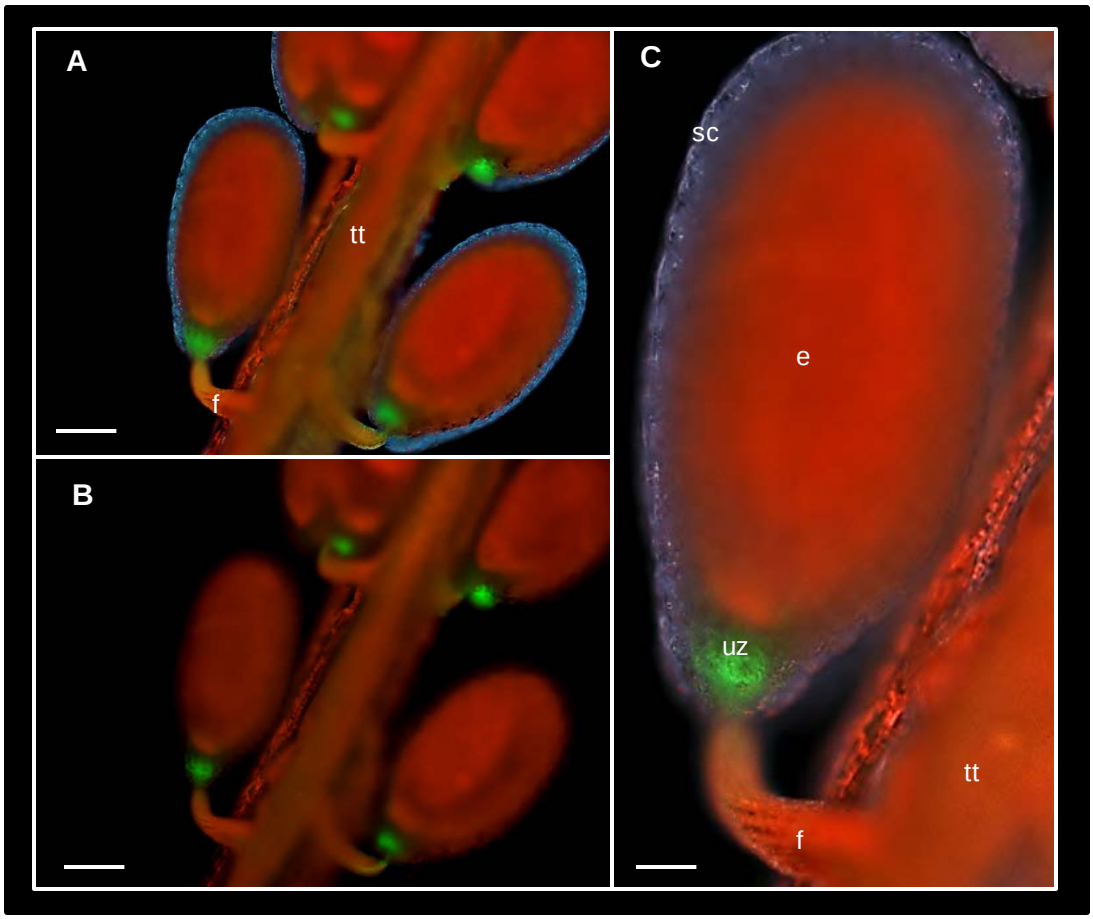

Figure 67. Analysis of tissue-specific UmamiT11 localization in the seed. Localization study was done with the $P_{UmamiT11}$: UmamiT11-GFP reporter line. (A and B) UmamiT11-GFP in seeds at cotyledon bending stage; seeds were left on the funiculus and transmitting tract. (A) Overlay with seed coat fluorescence, (B) GFP channel and autofluorescence, scale bar: 100µm. (C) Magnification of a seed from (A); scale bar: 60µm. TT (transmitting tract), f (funiculus), uz (unloading zone), e (embryo), sc (seed coat).

5.8.9.3. UmamiT29 localization in the seed

The first look at the promoter activity of *UmamiT29* with NLS 3xGFP revealed a completely different expression pattern as compared to the previously described *UmamiTs* of clade I. A very high signal intensity resulting from promoter activity was found specifically in the inner integument of young seeds till torpedo stage and later on during seed ripening in the first layer of the outer integument (Fig. 68).

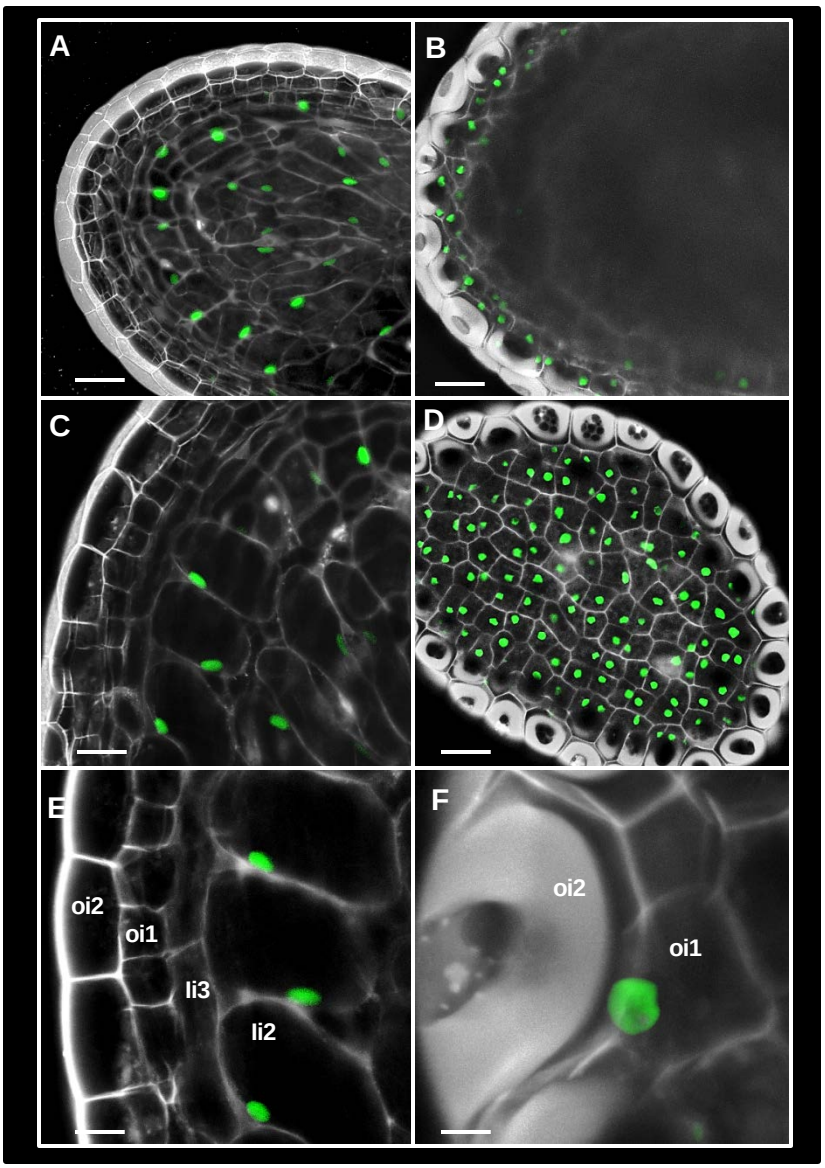

Figure 68. *UmamiT29* expression in young and old seeds. Analysis of *P*$_{UmamiT29}$*: NLS-3xGFP* plants**.** (A, C, D) Young seed; (B. D, F) old seed. (A) Z-stack through young seed coat, scale Bar: 60µm. (B) Z-stack through old seed coat; look at the mature outer integument and collapsed inner integuments, scale bar: 30µm. (C) Optical section of a young seed, scale bar: 30µm. (D) Optical section of mature seed coat with focus on the first layer of the outer integument, scale bar: 50µm. (E) Magnification of an optical section showing four layers of integuments; scale bar:18µm; (F) Magnification of the two outer integuments of an old seed, scale bar: 7µm. Oi (outer integument), ii (inner integument).

Analyzing the translational UmamiT29-GFP fusion revealed an overlap with the transcriptional fusion, indicating that all elements required for proper expression are found in the 5' region of the ATG. In the very early stages of embryo development UmamiT29-GFP was detected directly in the unloading domain at the end of xylem and phloem (Fig. 69). No GFP was monitored in any other cell layer of the seed coat. This tissue-specific localization pattern changes very soon as the embryo reaches the globular stage.

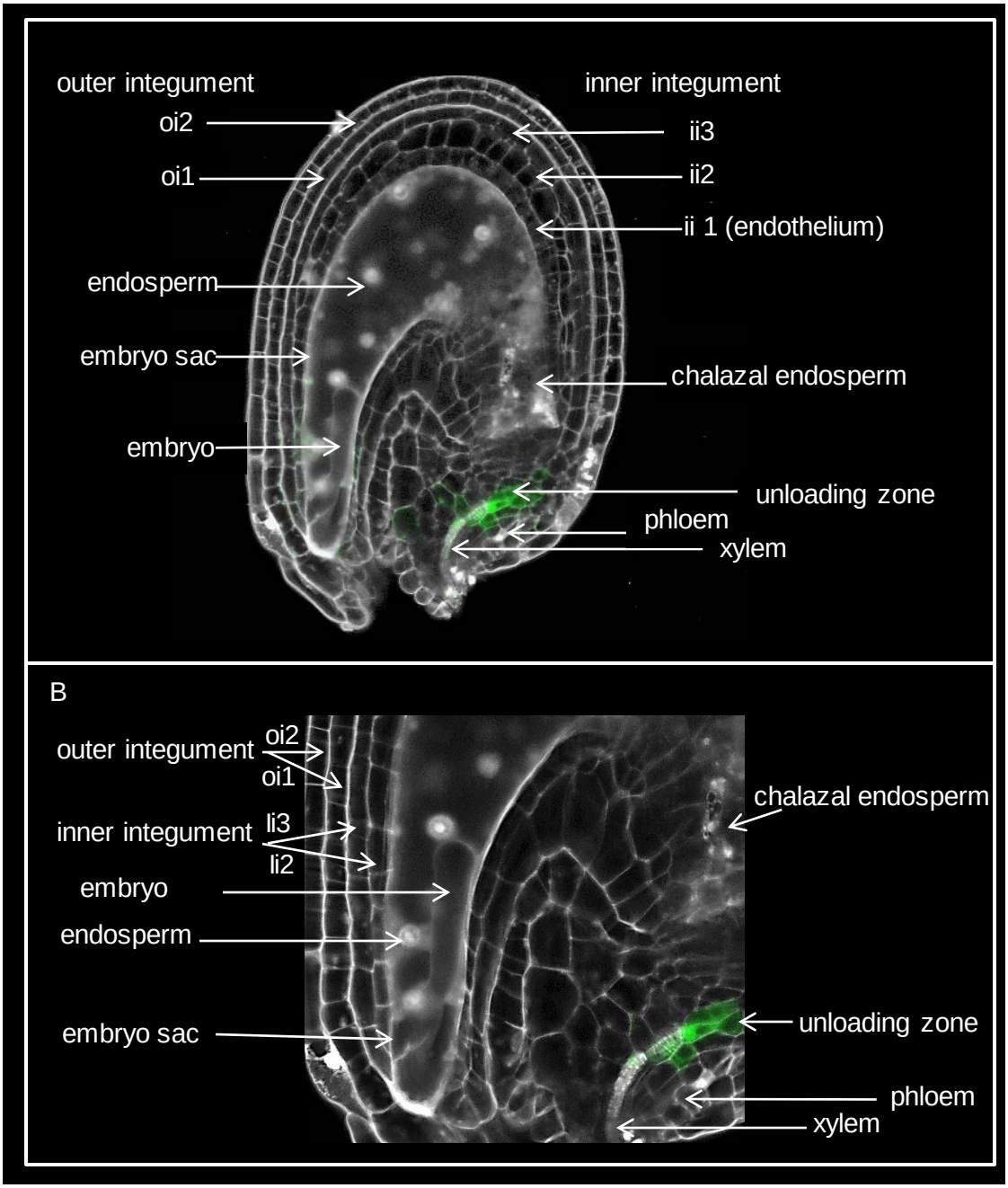

Figure. 69. UmamiT29 localization after fertilization at two cell embryo stage. Localization study was done with the $P_{UmamiT29}$: UmamiT29-GFP reporter line. (A) Overview of general seed anatomy at this stage and UmamiT29-GFP localization, scale bar: 20µm. (B) Magnification of a maximum projection of (A), Scale bar: 12µm.

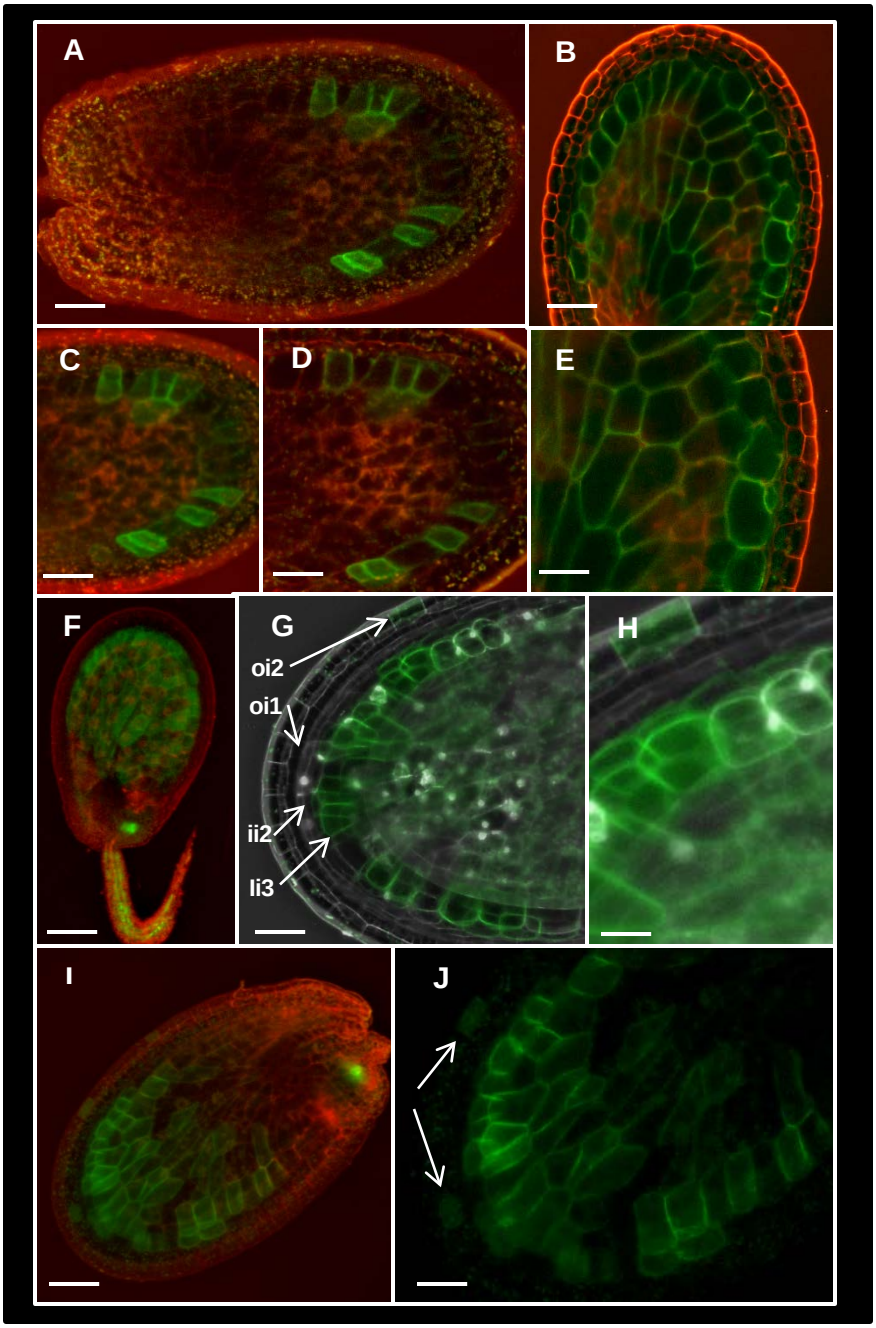

Figure 70. UmamiT29-GFP localization at young seed stages. Localization study was done with the $P_{UmamiT29}$: UmamiT29-GFP reporter line. (A) Young seed, UmamiT29-GFP shows up in single cells of the inner integument, scale bar: 35µm. (C) Maximum projection of several z-stacks of (A) , scale bar: 30µm. (D) Optical section with focus on the inner integument; scale bar: 25µm. (B, E) Older seed; scale bar: (B) 60µm, (E) 30µm. (F) Overview of a seed at late globular stage; scale bar: 100µm. (G, H) Maximum projection of a young seed, scale bar: 60µm. (H) Magnification of an area where UmamiT29-positive cells were found in the outer and inner integument, scale bar: 18µm. (I) Maximum projection of a seed at globular stage, scale bar: 80µm, (J) GFP channel of (I) magnified; scale bar: 30µm. Arrows indicate GFP-positive cells in the outer integument.

At early globular embryo stage, single cells of the inner integument layer 2 are decorated by UmamiT29-GFP in a seemingly random fashion (Fig. 70 A, C, D). This happens in a very short window of time and eventually results in a uniformly distributed GFP signal in all cells of the second layer of the inner integument during of seed maturation (Fig. 70 B, E). Interestingly, although the strongest GFP intensity was detected in the inner integument, it was possible to monitor also much weaker signals in the second layer of the outer integument at the same time (Fig. 70 G-J).

Nevertheless the most prominent expression of *UmamiT29* was detected in the second cell file of the inner integument (Fig. 71 A), surrounding the endosperm from the syncytial phase to the cellularized stage (Fig. 71 B, C). A closer look at the distribution of the protein in the inner integument revealed an obvious polar distribution in the plasma membrane along the anticlinal walls in about 70% (Fig. 71 D, E, F). At the point the embryo reaches the cotyledon bending stage a complete shift of UmamiT29-GFP to the first layer of the outer integument was observed (Fig. 71. G, H). Here, the complete cell layer shows GFP decoration at the same time point in those cells that lay directly beneath the mucilage producing cell files (Fig. 71, I, J, K).

To sum all the expression data of *UmamiT29* in the seed up it can be concluded from microscopy that the protein is transiently found in the unloading zone and the second layer of the outer integument but predominantly found in the inner integument as well as in the first layer of the outer integument. Anticlinal position suggests a role of UmamiT29 in the homogenous distribution of amino acids in the inner integument layer 2.

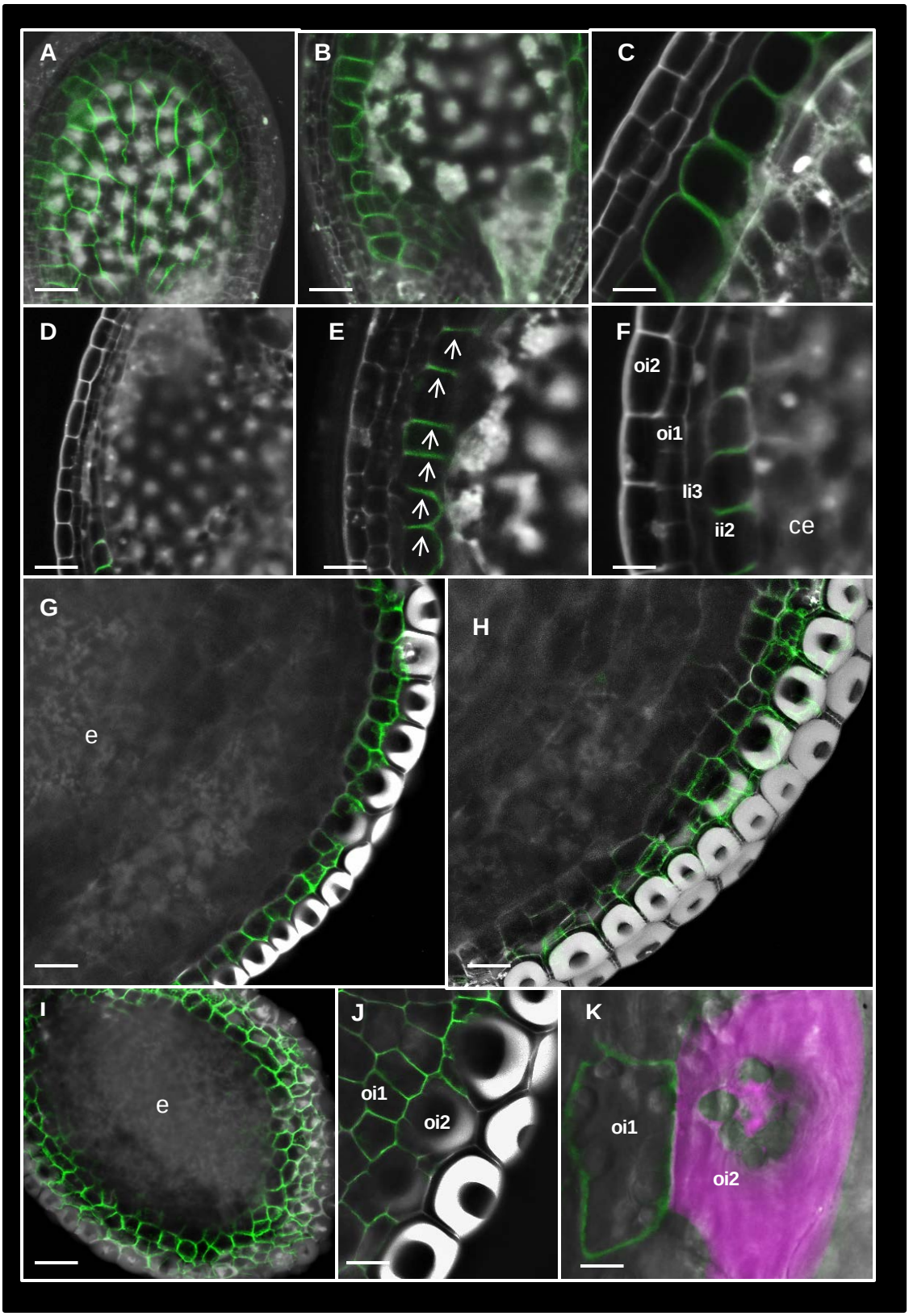

Figure 71. UmamiT29-GFP in the inner and outer integument. (A) Maximum projection with focus on seed coat, scale bar: 45µm. (B) Maximum projection with focus on embryo, scale bar: 50µm. (C) Seed coat at cellularized endosperm stage; scale bar: 15µm. (D, E, F) Young seed with polar distribution of UmamiT29-GFP indicated by arrows; scale bar: (D) 45µm, (E) 30µm, (F) 15µm. (G) UmamiT29-GFP in almost mature seed, scale bar: 40µm. (H) Maximum projection of (G) , scale bar: 30µm. (I) Optical section through a seed at cotyledon bending stage, scale bar: 80µm. (J) Magnification of outer integuments at almost mature stage, scale bar: 20µm. (K) Seed coat younger than (J), pink color represents autofluorescence of the mucilage layer in outer integument layer 2, scale bar: 8µm. OI (outer integument), ce (cellulaized endosperm), e (embryo)

5.8.9.4. UmamiT28 localization in the seed

A very special expression pattern was detected for *UmamiT28*. This candidate has its maximum of expression at later stages of embryo development after torpedo stage. A very clearly defined UmamiT28-GFP localization in the fading endosperm was observed at the early phase of the bending stage till the end phase of seed maturation (Fig. 71 A-E). Additionally, UmamiT28-psoitive cells were also found in the endothelium (Fig. 71 F) and the unloading zone (Fig. 71 G-I).

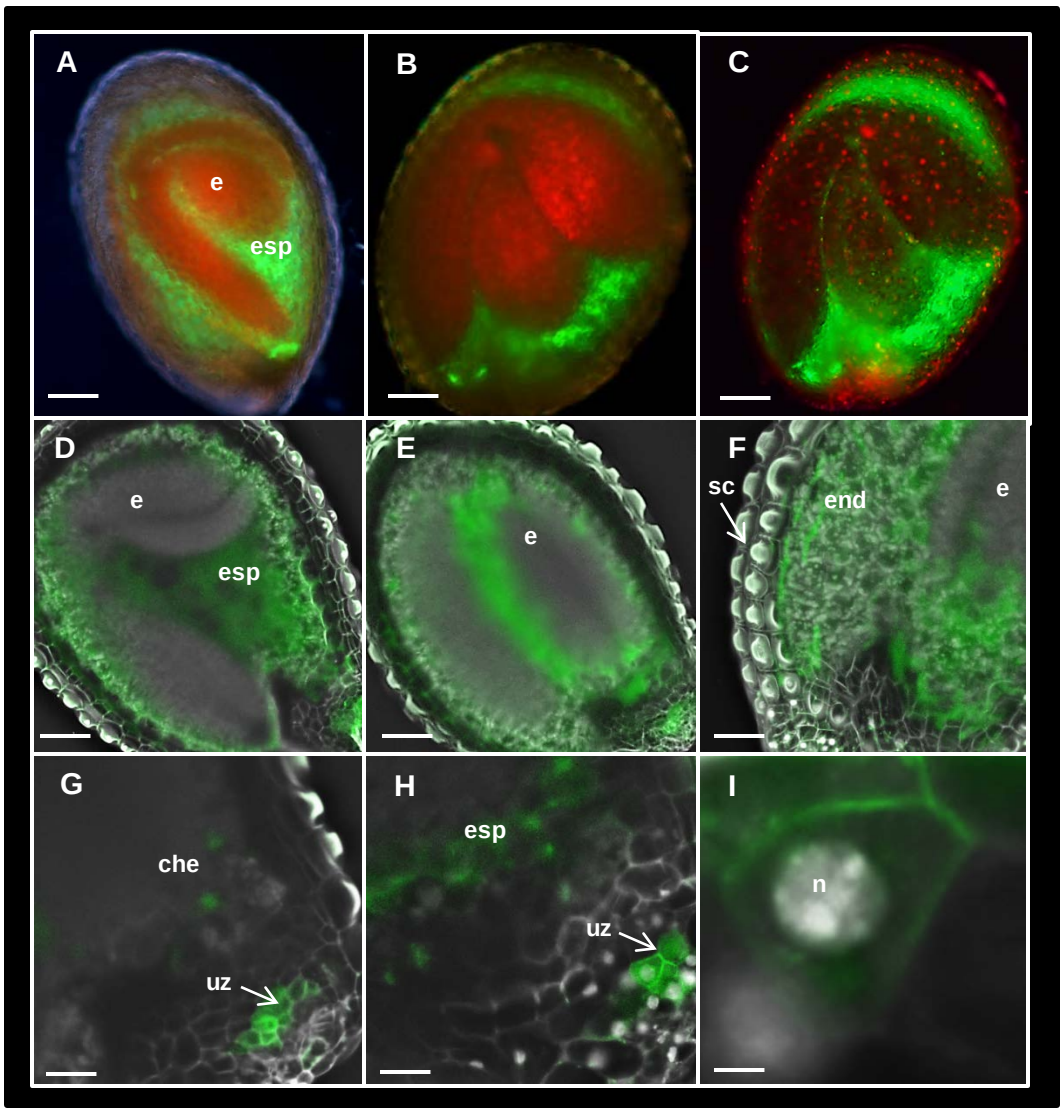

Figure 71. *UmamiT28* localization in the old seed stages. Localization study was done with the $P_{UmamiT28}$: UmamiT28-GFP reporter line. (A) Overview, early cotyledon bending stage, scale bar: 80µm. (B, C) Older cotyledon bending stage. (C) Overlay with autofluorescence of starch granules and mucilage, based on autofluorescence in the red spectrum, scale bar: 90µm. (D) Early bending stage. (E) Late bending stage, UmamiT28-GFP in the fading endosperm as well as the chalazal region, scale bar: 100µm. (F) Maximum projection, scale bar: 60µm. (G-I) UmamiT28-GFP at the unloading zone. Nucleus in (I) stained by PI. Scale bars: (G) 40µm, (H) 20µm, (I) 3µm. UZ (unloading zone), e (embryo), esp (endosperm), end (endothelium), seed coat, che (chalazal endosperm), n (nucleus).

A closer look at the cells marked by UmamiT28-GFP revealed a patchy pattern in the endosperm (Fig. 72 A-D). Signals in the endosperm appeared to be not only plasma membrane localized (Fig. 72 I), but also more ER-like (Fig. 72 F) indicating a high turnover of this protein in the endosperm for a rapid amino acid translocation to the embryo. In the middle phase of the cotyledon bending stage, before the seed coat was completely mature, UmamiT28-GFP was found in the fading endosperm as well as in the peripheral endosperm, named endothelium (Fig. 72 E, G). Whereas the signals in the endosperm were very diffuse at this point, a more defined localization as line marking the cell borders was found in cells of the peripheral zone. This was also true for the very late stage of seed maturation, where GFP could still be detected in the endothelium (Fig. 72 H). This results indicate a specific role of UmamiT28 during the end phase of seed maturation where amino acids from the endothelium are transported to the fading endosperm and from there to the embryo.

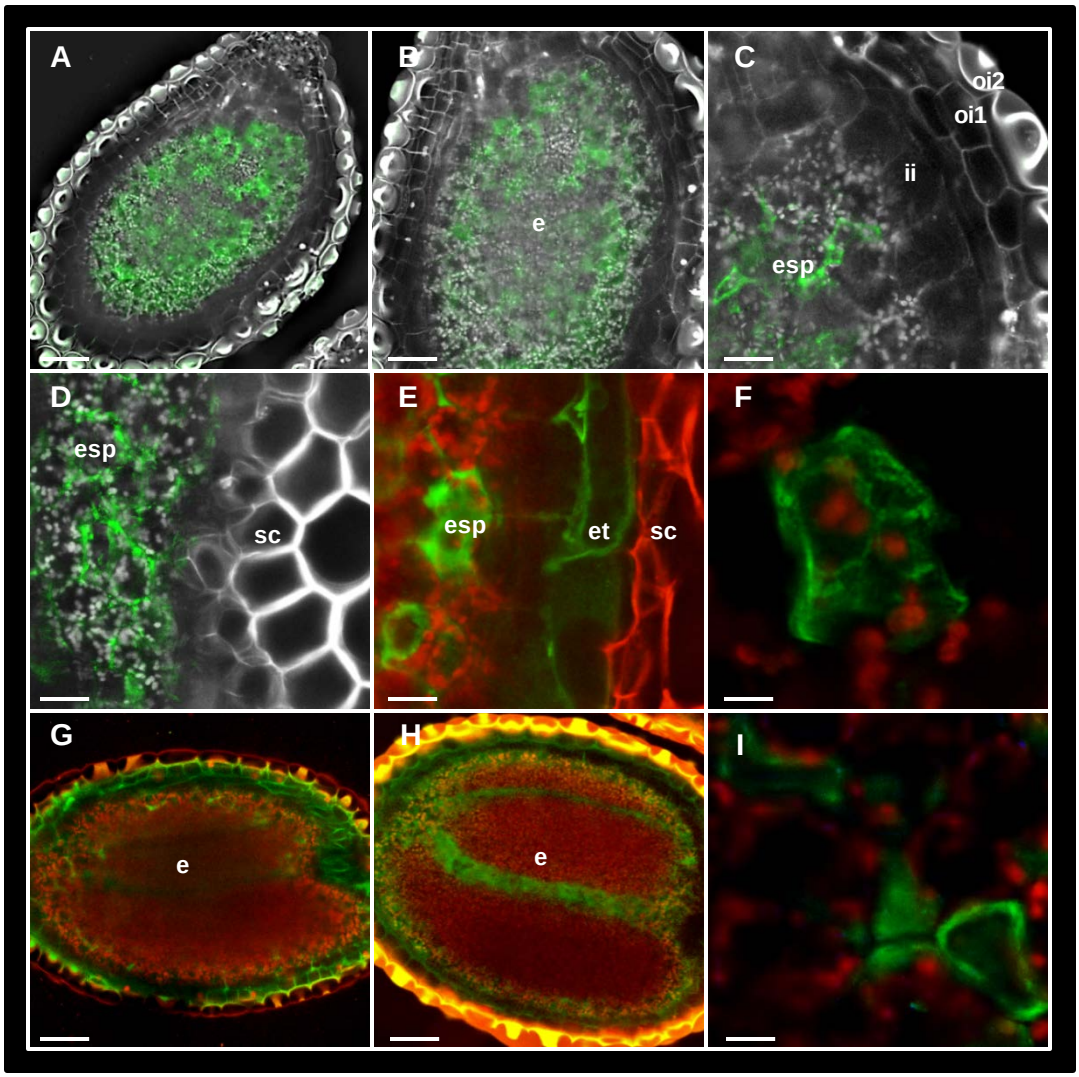

Figure 72. UmamiT28 localization in the endosperm and endothelium. Localization study was done with the $P_{UmamiT28}$: UmamiT28-GFP reporter line. (A) Maximum projection of a seed at early bending stage, focus at endosperm; scale bar: 40µm. (B) Magnification of same seed showing integument layers in the projection; scale bar: 50µm. (C, D) Optical sections; scale bar: (C) 25µm, (D) 15µm. (E) GFP signals in the endosperm and endothelium, scale bar: 10µm. (F, I) Endosperm cells, scale bar: (F) 2µm, (I) 5µm. (G, H) UmamiT28-GFP in the endothelium. (G) Seed immature stage. (H) Seed almost mature stage, scale bars: (G) 80µm, (H) 100µm. (E) embryo, esp (endosperm), et (endothelium), oi (outer integument), ii (inner integument), sc (seed coat).

5.8.9.5. UmamiT37 localization in the seed

Similar to UmamiT11 and UmamiT14 UmamiT37-GFP was detected at the unloading zone after fertilization (Fig. 73 A). During endosperm development additional signals were monitored in each cell from both layers of the outer integument (Fig. 73 B, C). In few cases a preference for a polar distribution of GFP in the outer integument layer 2 was observed (Fig. 73 D). In young stages of seed development GFP signals from the outer integument were co-localizing with PI, which supports the assumption that UmamiT37-GFP localizes to the plasma membrane (Fig. 73 H-J). As the embryo reaches the late cotyledon bending stage the GFP signal disappeared in the outer integument layer 2 (Fig. 73 E, F). During the maturation process of the seed coat the former plasma membrane localization of UmamiT37-GFP (Fig. 73 A, F) changed to a more diffuse pattern, where signals were also obtained within the cells of the outer integument layer 1 (Fig. 73 G). Here the GFP was not only detected at the borders of the cells but seemed to encircle plastids within the cells (Fig. 73 K).

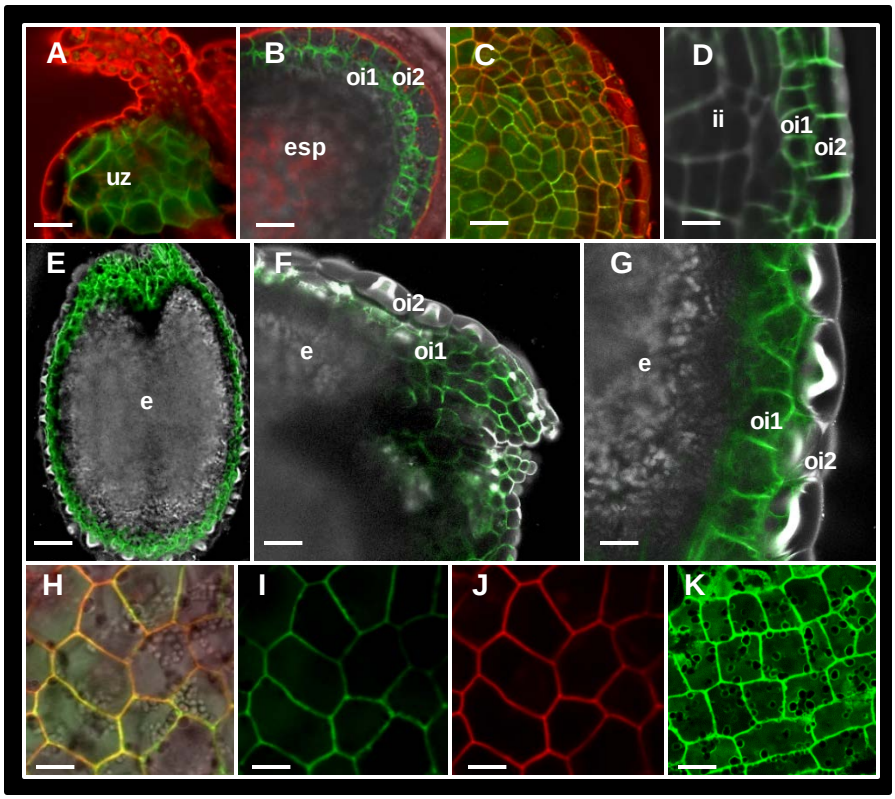

Figure 73. UmamiT37 localization in the seed. Localization study was done with the $P_{UmamiT37}$: UmamiT37-GFP reporter line. (A) Unloading zone, scale bar: 17µm. (B) UmamiT37-GFP in the outer integuments, scale bar: 35µm. (C) Maximum projection of the seed coat, scale bar: 40µm. (D) Magnification of the seed coat shows GFP in both layers of outer integument, scale bar: 22µm. (E-G) Old seed with embryo at late cotyledon bending stage, GFP in the outer integument layer 1. (E) Overview of the seed, scale bar: 80µm. (F) Magnification of the micropylar region, scale bar: 25µm. (G, K) Seed almost at maturity, GFP in the outer integument layer 1 shows additional signals around plastids, scale bars: 20µm. (H-J) GFP in the outer integument shows colocalization with PI stained cell walls, (H) overlay of bright field image with fluorescence channels, (I) GFP channel, (J) PI channel, scale bars: 16µm. UZ (unloading zone), esp (endosperm), oi (outer integument), ii (inner integument), e (embryo).

5.9. Characterization of the unloading zone

5.9.1. UmamiT localization in functional transfer cells

The unloading zone of the seed is located at the chalazal pole (Fig. 74 A), where the funiculus connects to the developing seed (Fig. 74 B). Here, a population of cells right at the endpoint of the vasculature (Fig. 74 C, D) forms a kind of nutrient unloading zone. These cells are close to the endpoint of phloem and xylem (Fig. 74 E) and share close physical connectivity with them. From an anatomical point of view the cells of the unloading zone are placed at a strategically important position to connect the vasculature with the seed coat and finally with the developing embryo as the driving force for the net import of assimilates. Several UmamiTs are found there at different time points after fertilization but not in unfertilized ovules. Whereas *UmamiT28*, *29* and *37* are only transiently expressed at the unloading zone, the GFP fusion protein of clade I-UmamiTs was present during the entire seed development (Fig. 74 A, I). *UmamiT14* showed the earliest expression at the unloading zone and the fusion protein was found to be at the highest degree. UmamiT14-GFP in the cell population of the unloading zone localized to the plasma membrane (Fig. 74 F, G) with a strong association to the endpoint of the phloem tissue (Fig. 74 H), which marks them as functional transfer cells for amino acid export.

In order to characterize the cell population of UmamiT14-positive cells, different phloem specific markers were coexpressed with UmamiT14-GFP to elucidate if the same phloem identity genes are also expressed in cells from the unloading zone.

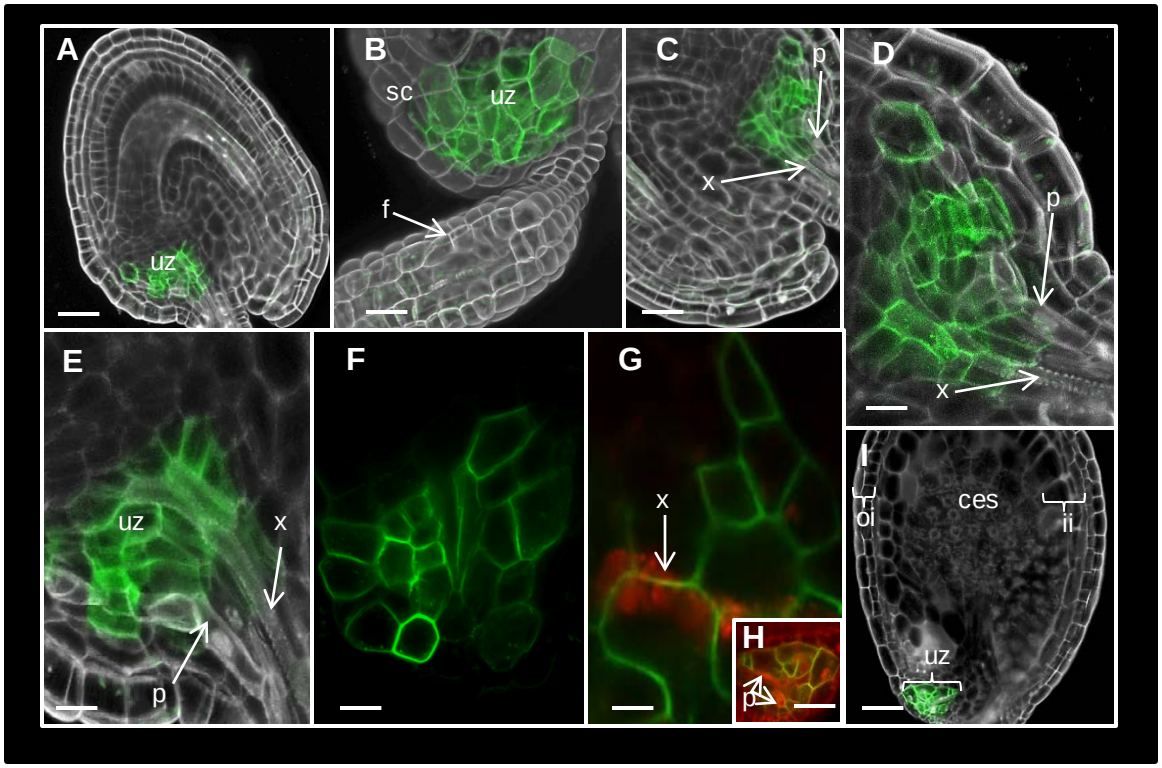

Figure 74. UmamiTs are localized in functional transfer cells at the unloading zone. Localization study was done with the $P_{UmamiT4}$: UmamiT14-GFP reporter line. (A) Young seed with GFP signals only at the chalazal pole in the unloading zone, scale bar: 25µm. (B) Maximum projection showing the funiculus and GFP signals at the unloading zone which is covered by the seed coat, scale bar: 17µm. (C, D) Maximum projection of the unloading zone shows GFP fluorescence restricted to the few cells at the endpoint of phloem and xylem, scale bars: (C) 20µm, (D), 7µm. (E) Optical section from the unloading zone, xylem vessel and nucleated phloem are surrounded by UmamiT14-positive cells, scale bar: 8µm. (F, G) UmamiT14-GFP shows putative plasma membrane localization, scale bars: (F) 10µm, (G) 3µm. (H) Magnification of the unloading zone from (I), nucleated phloem and UmamiT transfer cells share close physical vicinity, yellow color indicates a colocalization between PI and the membrane like GFP localization, scale bar: 30µm, (I) Strong GFP signal in the unloading zone of an older seed during cellularization of the endosperm, scale bar: 60µm. X (xylem), p (phloem), uz (unloading zone), f (funiculus), sc(seed coat), oi (outer integument), ii (inner integument), cesp (cellularizing endosperm)

5.9.2. Differentiation of UmamiT-positive cells is not regulated by APL

The MYB Transcription factor APL (Altered Phloem Development) was reported to have a key regulatory position for vascular differentiation in the root. In the presence of APL, phloem differentiation occurs (Bonke et al. 2003). Differentiation processes also take place in the unloading zone concerning the expression of *UmamiTs*. In order to address the question if APL could also play a role there, a marker line coexpressing UmamiT14-mCherry and APL-GFP was generated. APL-GFP was monitored in in a cell file of the funiculus of young and older seeds (Fig. 75 A, B). These nuclei of those cells belong to the phloem tissue. In the unloading zone, the signals of APL-GFP stopped very close to the transition zone from the funiculus into the seed, whereas UmamiT14-mCherry signals started to expand (Fig. 75 C). During seed maturation (Fig. 75 A, B, D), the localization pattern of APL and UmamiT14 did not change. APL-GFP was found in cells close to UmamiT14-positive cells (Fig. 75 E, F). According to their position and morphology the cells showing APL-GFP signals can be determined as phloem cells (in narrower sense sieve elements). In UmamiT14-positive cells a signal for APL-GFP was never found (Fig. 75 F). This result indicates that APL in the unloading zone is indeed restricted to the phloem tissue and does not interfere with the differentiation of the UmamiT-positive cells, which underlines the uniqueness of the unloading zone.

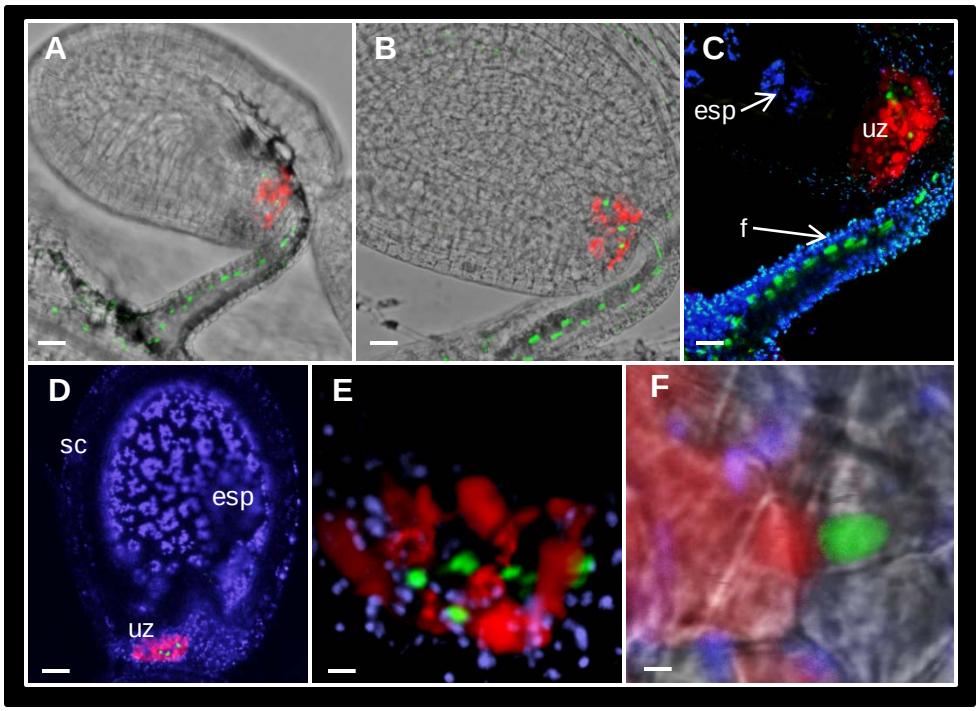

Figure 75. Coexpression of $P_{UmamiT14}$: *UmamiT14-mCherry* and P_{APL}: *APL-GFP* in the seed. (A) Young seed, UmamiT14-mCherry in the unloading zone, where the APL expression domain indicated by APL-GFP is ending, scale bar: 30µm. (B) Older seed, scale bar: 35µm. (C) Focus on funiculus and unloading zone, maximum projection, APL ends within the unloading zone, scale bar: 25µm. (D) Seed with fully differentiated endosperm, UmamiT14-mCherry and APL-GFP expression show no difference to younger stages, scale bar: 40µm. (E) Maximum projection of the unloading zone, UmamiT14-positive cells are neighboring cells with APL-GFP expression, scale bar: 4.5µm. (F) Optical section from the contact point of nucleated phloem cell with UmamiT14 transfer cell, scale bar: 3.5µm. Autofluorescence of plastids and the endosperm is colored in purple and blue. UZ (unloading zone), esp (endosperm), f (funiculus).

5.9.3. UmamiT postive cells are connected with companion cells

Phloem and xylem extend from the funiculus into the seed and end there. The expression analysis of all candidate *UmamiTs* showed that *UmamiT14* was expressed at the earliest time point and to the strongest degree. To characterize the relationship between phloem and UmamiT14-positive cells, coexpression analysis between UmamiT14-GFP and SUC2-mCherry, a companion cell specific marker, was performed. In the reproductive tissue, companion cells extend from the funiculus into the seed and end in the unloading domain (Fig. 76 A, B). They are positioned in juxtaposition of the xylem (Fig. 76 B, C, D) and constitute a single cell file without branch points (Fig. 76 E, F). At the unloading zone, only few companion cells extend into the population of UmamiT14-positive cells, but they are anatomically tightly connected with them(Fig. 76 G). This close physical proximity between UmamiT14-cells and companion cells (Fig. 76 H-J) supports the idea of a translocation event of assimilates between the companion cells and the unloading zone.

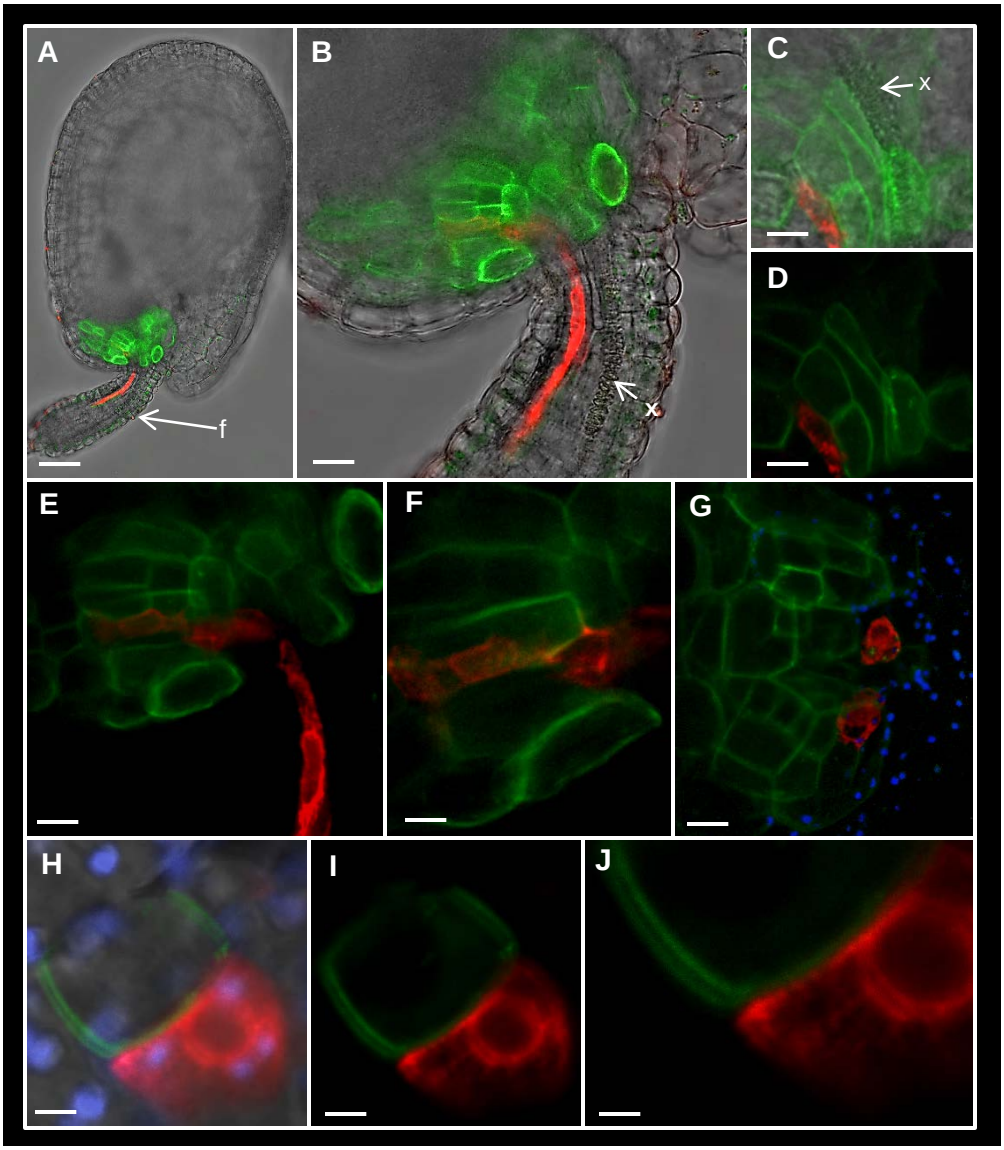

Figure 76. Coexpression of $P_{UmamiT14}$: *UmamiT14-GFP* and P_{suc2}: *ER-mCherry* in the seed. Green signals: UmamiT14-positive cells, red signals: companion cells. (A) Overview over the seed and funiculus, scale bar: 60µm. (B) Magnification of the unloading zone, companion cells and xylem extend into the population of UmamiT14-cells, scale bar: 12µm. (C, D) Xylem and companion cells are close to UmamiT14-positive cells and end in collateral position to each other, (C) Overlay of (D) with bright field image, scale bar: 7µm. (E) Companion cells extend from the funiculus and end in the unloading zone without branching, scale bar: 6µm. (F) Magnification of the endpoint of the companion cell file, scale bar: 3µm. (G) Maximum projection of the unloading zone in lateral view, blue color represents autofluorescence of plastids, scale bar: 10µm. (H-I) Companion cells and UmamiT14-positive cells share direct physical connectivity. (H) Overlay with bright field image;blue color: plastids. (I) Overlay of GFP and mCherry channel, scale bar: 2µm. (J) Magnification of (I) showing UmamiT14-GFP as thin green line in the cell borders close fitting to the companion cell, scale bar:1µm. F (funiculus), uz (unloading zone), x (xylem), cc (companion cell).

5.9.4. UmamiT-positive cells are connected with sieve elements

The phloem in the unloading zone does also consists of sieve elements, which led to the question, if the anatomical relationship between sieve elements and the localization of UmamiT14 is changing during seed maturation and embryo development. Therefore UmamiT14-mCherry was coexpressed with PD1-ER-GFP, a protophloem/sieve element marker. Fig. 77 shows the branching of the sieve elements into the unloading zone and how close this cells stay next to UmamiT14-positive cells in detail. Sieve elements stretch from the funiculus into the unloading zone (Fig. 77 A-C, E, F) and end there with the xylem vessels (Fig. 77 D). At this transition zone between the funiculus and seed the sieve elements form branches of higher order, which lay within the population of UmamiT14-positive cells (Fig. 77 C). In the unloading zone, sieve elements and cells expressing UmamiT14 are in close vicinity to each other, implicating from an anatomical point of view that nutrient unloading from the sieve elements into the transfer cells can occur (Fig. 77 G, H).

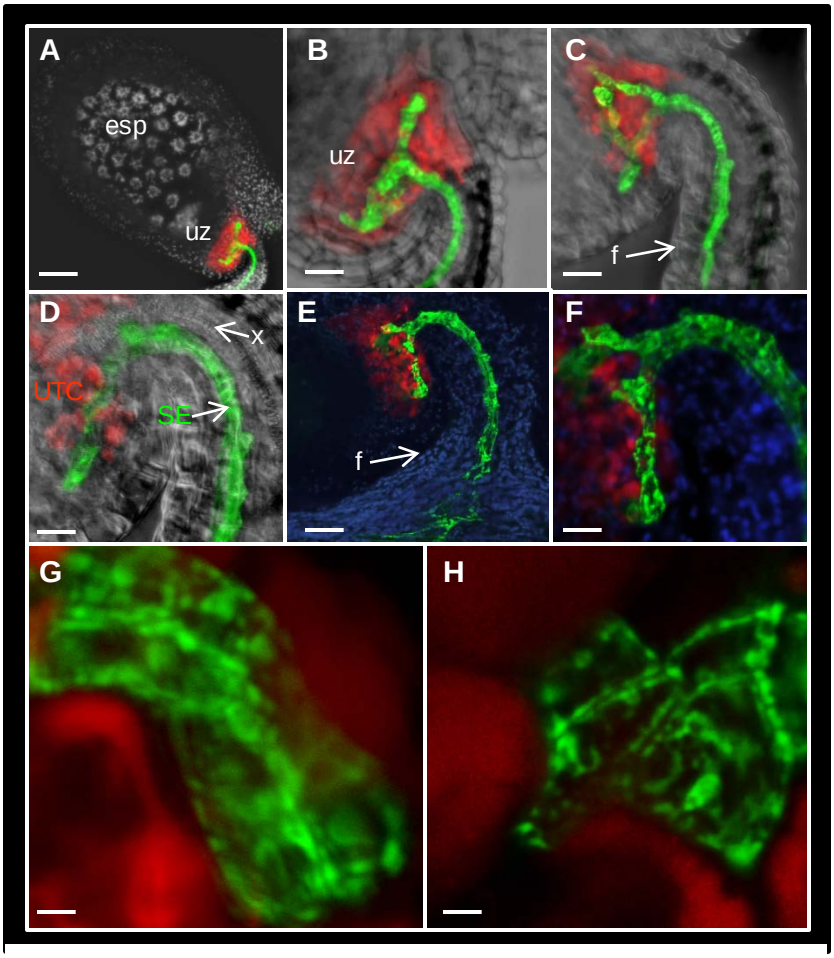

Figure 77. Coexpression of $P_{UmamiT14}$: *UmamiT14-mCherry* and P_{PD1}: *ER-GFP* at the unloading zone. (A) Seed with nucleated endosperm, white color results from autofluorescence, scale bar: 60µm. (B) Magnification of the unloading zone of the same seed, scale bar: 20µm. (C) Z-stack showing branching sieve elements in the unloading zone, scale bar: 15µm. (D) Optical section of the unloading zone including the xylem, scale bar: 20µm. (E) Sieve elements originating from the funiculus, scale bar 30µm; and (F) are ending in the unloading zone in front of UmamiT14-positive cells, purple and blue color result from autofluorescence, scale bar: 15µm. (G, H) Magnification of the contact point between sieve elements and UmamiT14-positive cells, (G) z-stack, (H) single optical section, scale bars: (G) 3µm, (H) 2µm. UZ (unloading zone), x (xylem), se (sieve element), utc (UmamiT14-positive cell), esp (endosperm).

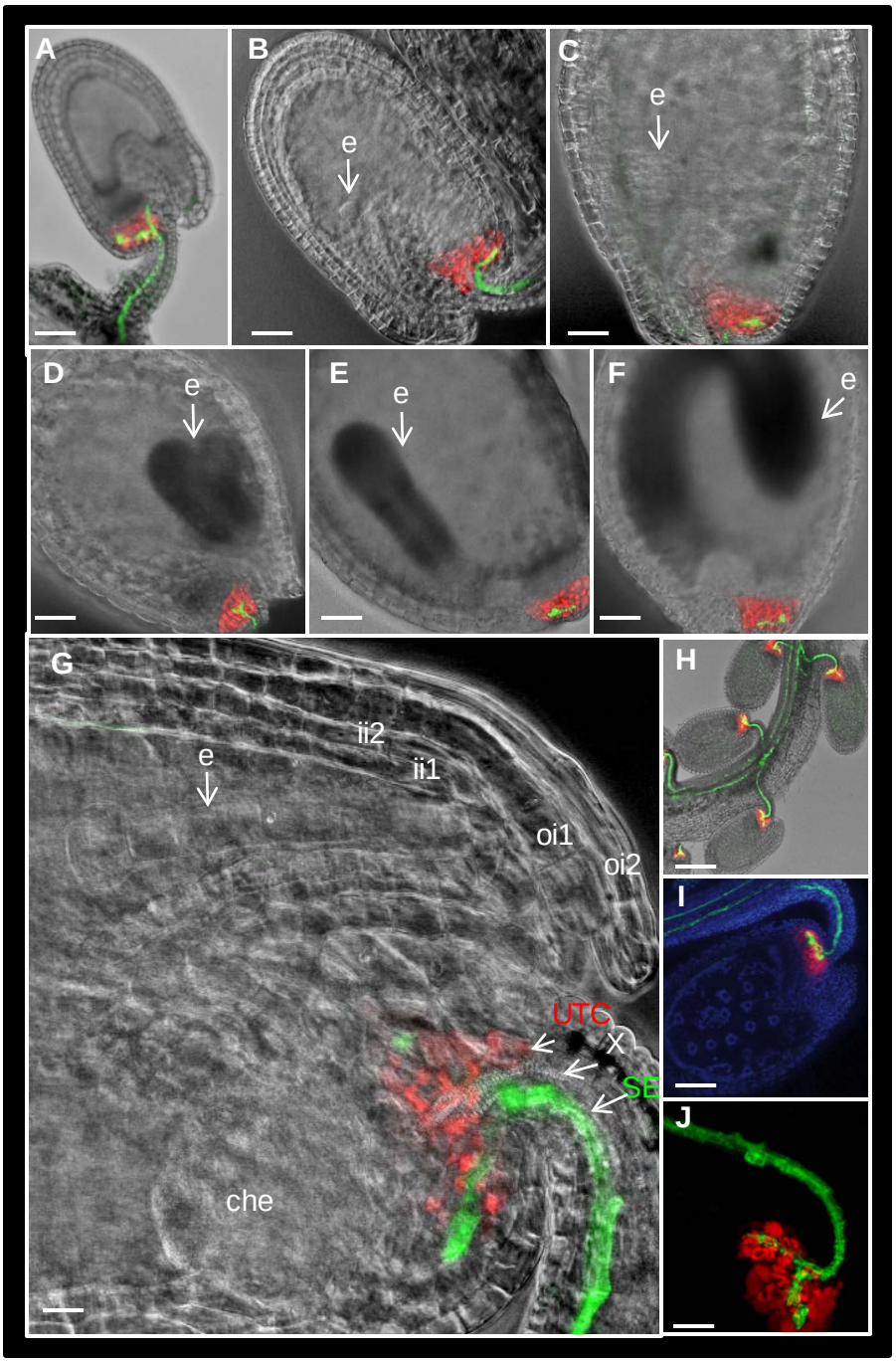

Figure 78. Coexpression of $P_{UmamiT14}$: *UmamiT14-mCherry* and P_{PD1}: *ER-GFP* in the seed. (A-F) The unloading zone and sieve elements show no morphological changes during embryo development starting with two cell embryo (A, B), scale bar: (A) 60µm, (B) 20µm. (C) Early heart stage, scale bar: 40µm. (D) Late heart stage, scale bar: 50mm. (E) Torpedo stage, scale bar: 50µm. (F) Cotyledon bending stage. scale bar: 60µm. (G) Overview of the seed anatomy with focus on the unloading zone, scale bar: 20µm. (H) Several seeds at the transmitting tract show sieve elements stretching into the seed, where the specific expression of UmamiT14-mCherry is visible, scale bar: 200µm. (I) Magnification of one seed showing endosperm at nucleated stage, blue color results from autofluorescence, scale bar: 60µm. (J) Magnification of unloading zone and sieve elements from the funiculus, scale bar: 15µm. UTC (UmamiT14- positive cell), x (xylem), se (sieve element), e (embryo), che (chalazal endosperm), ii (inner integument), oi (outer integument).

Looking at the morphology of the unloading zone concerning UmamiT14-mCherry and PD1-GFP localization during seed development no changes could be detected. After fertilization the sieve elements branch and stretch into the population of UmamiT14-positive cells, a situation that persists until the end of embryo development (Fig. 78 A-F, H). Xylem and sieve elements are in close proximity to UmamiT14-positive cells (Fig. 78 G) and form there a functional unloading point that is covered by *UmamiT14* expressing cells there. These results suggest that the increased assimilate demand of the embryo is met by increased transport acoss the membrane.

5.9.5. Whole mount immunolocalization of the unloading zone: sieve elements are nucleated and physically connected to UmamiT-positive cells

Additionally to the reporter lines whole mount immunolocalization experiments with antibodies against GFP and RS6, a sieve element specific epitope, were performed. UmamiT14 could be detected specifically in the unloading zone as well as the sieve element cell file (decorated by RS6) which extends from the funiculus and ends in the unloading zone (Fig. 79 A-C). Branching of sieve elements in the unloading domain was also observed (Fig. 79 D). UmamiT14 localization was again seen at the endpoint of the vasculature directly behind the xylem and sieve elements (Fig. 79 E, F). Sieve elements in the unloading zone are nucleated (Fig. 79 F-H) and share close physical proximity to nucleated UmamiT14-positive cells (Fig. 79. G-I). Altogether the results of the whole mount immunolocalization validated the findings taken from different coexpression studies and showed that the RS6 epitope is not present in UmamiT14-positive cells of the unloading zone. Additionally conclusions can be drawn by the finding that sieve elements extending into the unloading zone are nucleated, which reflects a similar situation found in the root tip.

These findings underline the uniqueness of the unloading zone in terms of differentiation and association with the vasculature.

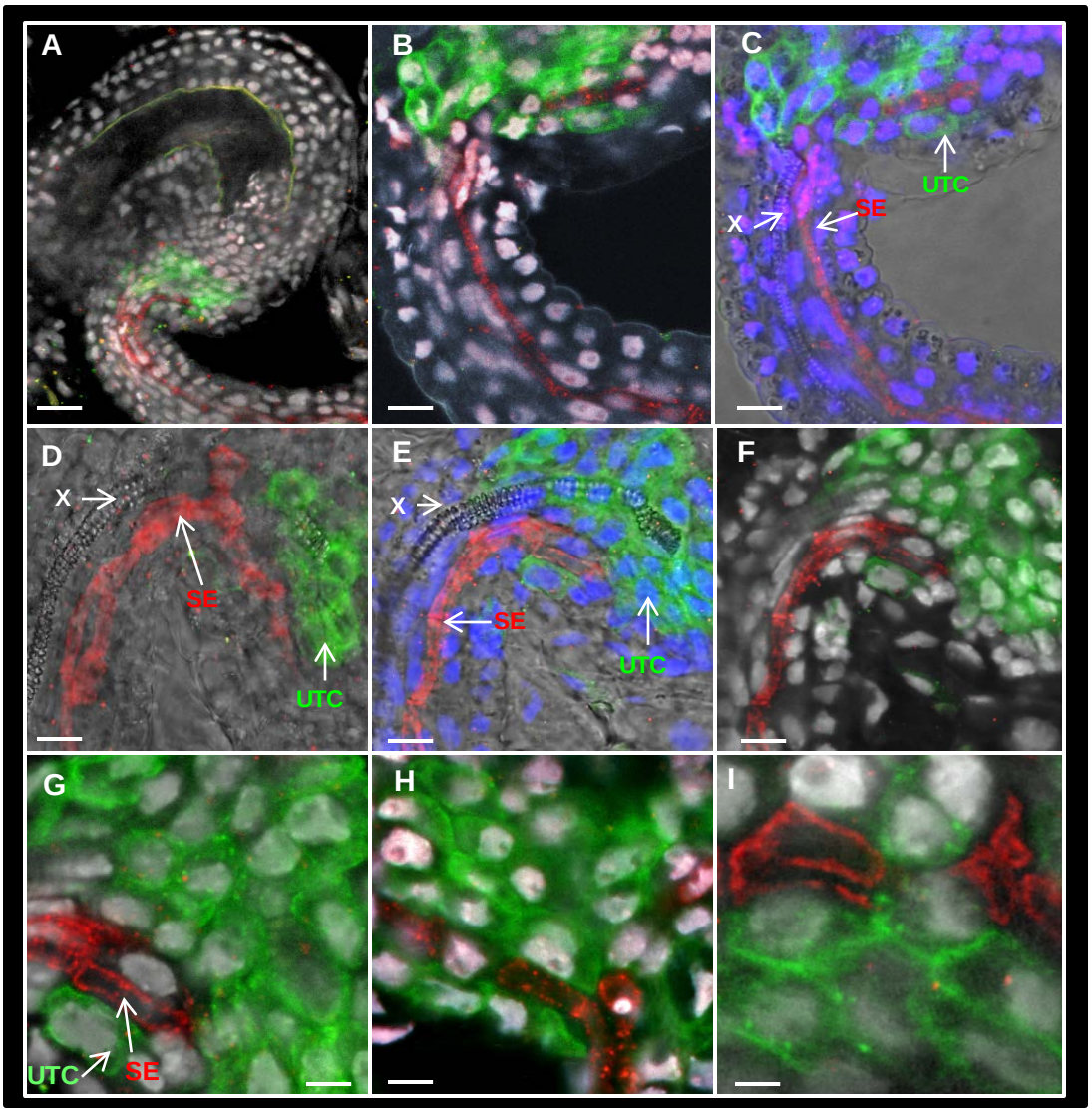

Figure 79. Localization of UmamiT14 and RS6 in seeds by whole mount immunolocalization. UmamiT14-GFP reporter was used. Green cells: α-GFP, detected with a CY2-antiserum, representing UmamiT14-positive cells; red cells: α-RS6 detected with an AF594-coupled antibody, representing sieve elements, white or blue color: DAPI. (A) Overview of a young seed at globular embryo stage showing specific detection of CY2 and AF594, scale bar: 18µm. (B, C) Magnification of the unloading zone including the vasculature of the funiculus. (B) Overlay of fluorescence channels, scale bar 12µm. (C) Overlay of (B) with bright field image, scale bar: 12µm. (D) Sieve elements are branching in the unloading zone, scale bar: 10µm. (E, F) Sieve elements and xylem are ending at the unloading zone. (E) Overlay of (F) with bright field image scale bars: 8µm. (G) Magnification of the ending sieve element, containing a nucleus as also seen in the surrounding UmamiT-positive cells, scale bar: 4µm. (H) Maximum projection showing branching nucleated sieve elements within a population of UmamiT14 transfer cells. Scale bar: 4.5µm. (I) Magnification of the contact point between the ending sieve elements and UmamiT14-positive cells, scale bar: 3µm. X (xylem), se (sieve element), utc (UmamiT14-positive cell).

5.9.6. UmamiT-positive cells at the unloading zone show colocalization with PIN3

In order to study what influence hormones take at the unloading zone auxin and cytokinin were focused. Cytokinin response was only detected in the endosperm, why the influence of auxin was investigated. Auxin is transported by PIN proteins, thus PIN1, 2, 3, 4, and 7-GFP reporter lines in the developing seed were screened. PIN3 was the only candidate to be found highly expressed as mentioned in Fig.27-32. To see if *UmamiT14* and *PIN3* expression show a spatial and temporal overlap, a reporter line coexpressing both genes with different fluorophores under the control of their endogenous promoter was generated. Before fertilization PIN3 was only monitored in the funiculus. Afterwards the signals were found in the outer and inner integument (Fig. 80 C) as well as in the unloading zone (Fig. 80 A, B, E). PIN3-GFP was uniformly distributed at the unloading zone without any preference of polar distribution as seen in the outer integuments (Fig. 80 D, E). In the unloading zone a colocalization between UmamiT14-mcherry and PIN3-GFP could be seen (Fig. 80 F-H), indicating that the unloading zone is UmamiT14- and PIN3-positive at the same time. This means that auxin could be distributed along the unloading zone and represent a possible factor for the induction of *UmamiT14* expression

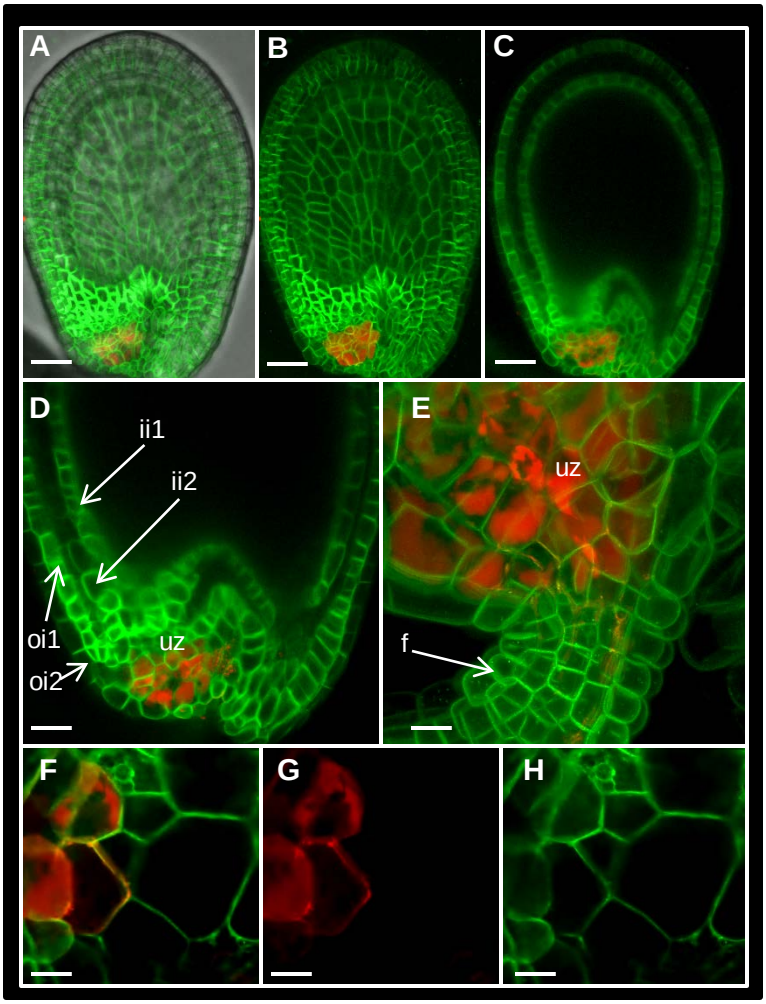

Figure 80. UmamiT14 and PIN3 show overlapping localization in seeds. Analysis of *P*$_{UmamiT14}$*: UmamiT14-mCherry* and *P*$_{PIN3}$*: PIN3-GFP* in the seed**.** (A, B) Maximum projection of a seed, (A) overlay of (B) with bright field image, scale bar: 50µm. (C) Optical section through a seed, PIN3 expression in the unloading zone, the outer integuments and the the inner integuments, UmamiT14 expression in the unloading zone, scale bar: 50µm. (D) Magnification of the unloading zone including the integuments, PIN3 with polar distribution at the outer integument, scale bar: 30µm. (E) Z-stack of the unloading zone including the funiculus, scale bar: 15µm. (F-G) PIN3-GFP and UmamiT14-mCherry colocalize at the unloading zone, (F) merge of (G) and (H). (G) mCherry channel (UmamiT14 expression), (H) GFP channel (PIN3 expression), scale bars: 6µm. F (funiculus), uz (unloading zone), ii (inner integument), oi (outer integument).

5.9.7. Auxin response in UmamiT14-positive cells during seed development

As suggested by the presence of PIN3, auxin is distributed along the unloading zone. The next step was to analyze the auxin response in the UmamiT14-mCherry line. It was investigated if auxin response takes place in the same cells with *UmamiT14* expression. To visualize auxin response P_{DR5}*: ER-GFP* plants were used. Fig. 81 summarizes the changes of auxin response together with UmamiT14-mCherry localization during embryo development. Shortly after fertilization no auxin response could be detected in most cells of the unloading domain, but signals of DR5-GFP were culminating in cells really close to the xylem vessel; only in a few of those xylem associated cells UmamiT14-mCherry was found (Fig. 81 A-C). After globular stage of the embryo auxin response was detected in single cells of the inner integument facing the chalazal pole. Additionally, a very strong auxin response appeared suddenly in the unloading zone, where all cells with UmamiT14-mCherry expression also colocalized with DR5-GFP (Fig. 81 D-F). During the heart stage, strong auxin response was seen in the second layer of the inner integument, as well as in the embryo. The signal intensity of DR5-GFP at the unloading zone was weaker than before at this stage (Fig. 81 G, H). Later on signals in the outer integument appeared in a patchy pattern and the intensity of GFP in the funiculus and unloading zone decreased further (Fig. 81 I). For a short time window before torpedo stage of the embryo, auxin response could be observed in the funiculus, the unloading zone, the second layer of the inner integuments and both layers of the outer integument (Fig. 81 J). UmamiT14-mCherry was still present at this stage but only few cells showed colocalization. At the end phase of embryo development, auxin response in the outer integument disappeared completely and was at highest expressed in the endothelium. In the unloading zone DR5-ER-GFP was still found but in much fewer cells and also colocalization with UmamiT14-mCherry was very limited to single cells (Fig. 81 K, L).

Auxin response was found to occur in the unloading zone in the same cells showing UmamiT14 after fertilization. But this happened only in a narrow time window of the young seed at about globular embryo sage. Afterwards the signals for UmamiT14-mCherry were still strong but DR5-GFP intensity decreases and only few cells with colocalization of both fluorophores were detected.

The presence of PIN3 and DR5 in the same UmamiT-positive cell population of the unloading zone after fertilization indicates that the differentiation of these cells may be regulated by the distribution of auxin, which can function as an inducer of *UmamiT14* expression.

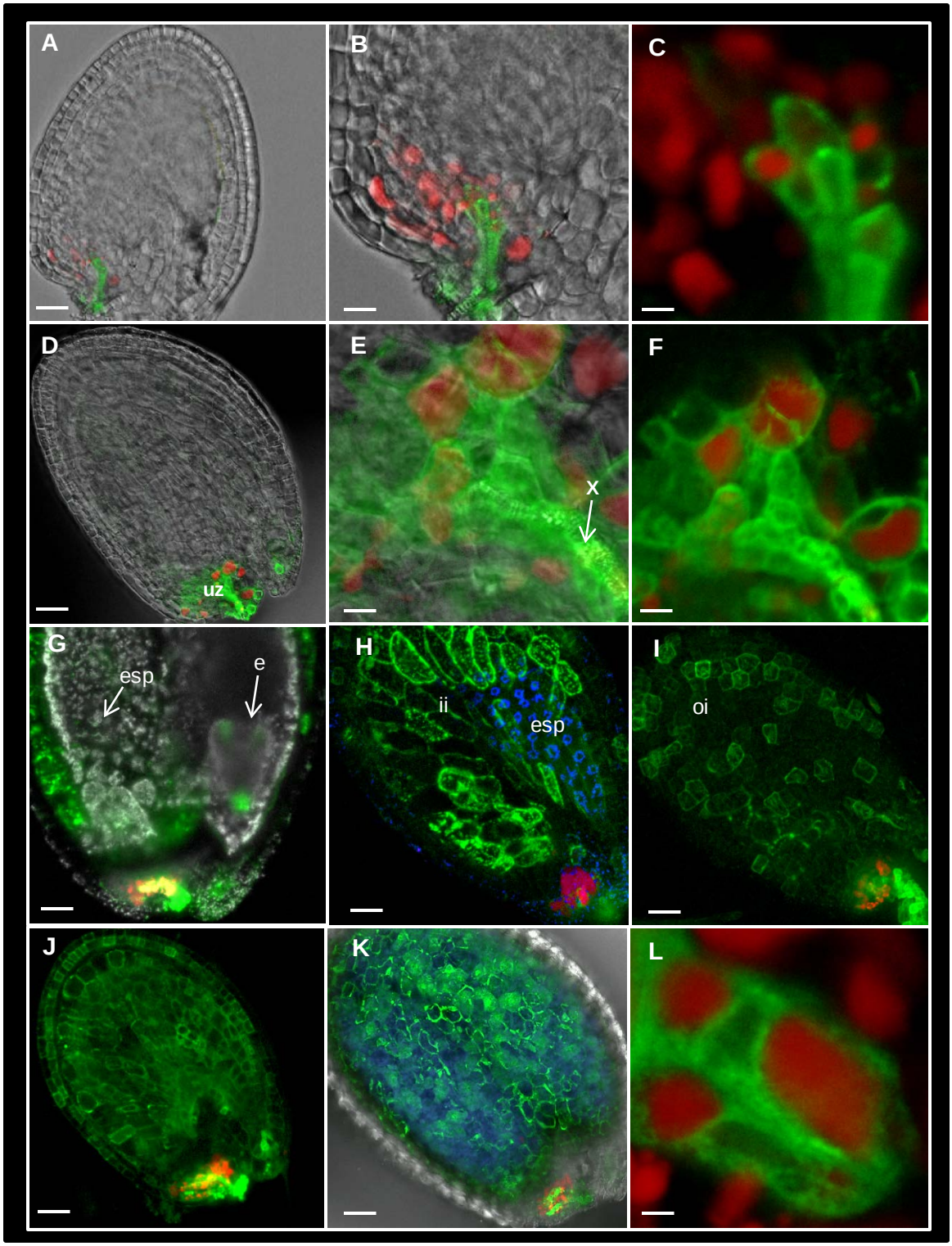

Figure 81. UmamiT-positive cells in the unloading zone show auxin response during seed development. Analysis of *P*$_{UmamiT14}$*: UmamiT14-mCherry* and *P*$_{DR5}$*: ER-GFP* in the seed**.** (A-C) Seed shortly after fertilization, GFP signals concentrated to cells close to the xylem, scale bars: (A) 30µm, (B) 10µm, (C) 4.5µm. (D-F) Seed after globular embryo stage, intense DR5-GFP fluorescence intensity and colocalization with UmamiT14-mCherry in the unloading zone, scale bars: (D) 30µm, (E) 7µm, (F) 6µm. (G, H) Seed at heart embryo stage, DR5-GFP expression in the inner integument and unloading zone overlapping with UmamiT14-mCherry signals, scale bars: (G) 50µm, (H) 25µm. (I) Patchy pattern of GFP signals in the outer integument at later stages, DR5-GFP decreased in the funiculus and unloading zone, scale bar: 40µm. (J) Maximum projection of a seed before torpedo embryo stage, auxin response in outer integuments, the second layer of the inner integument and the unloading zone, scale bar: 30µm. (K) Seed at cotyledon bending stage, scale bar: 40µm. (L) UmamiT14-mCherry and DR5-GFP in a cell of the unloading zone, scale bar: 2µm. Blue and white color results from autofluorescence. X (xylem), uz (unloading zone), ii (inner integument), oi (outer integument), e (embryo), esp (endosperm).

5.10. Root

5.10.1.1. Introduction of the marker lines in roots used in this thesis

In terms of the analysis of juvenile phloem development in the pathogenic situation different published marker lines were analyzed. To ensure a proper expression as described in the corresponding publication the lines were screened in the uninfected root (Fig. 82-84). In most cases the published data based on observations of the first 50µm of the root tip few days after germination. In this thesis the lines were also analyzed in more differentiated parts of the root and especially in root tissue that has undergone secondary thickening. At this developmental stage some differences in the expression pattern were visible that play a role especially during pathogenesis with root-knot nematodes during the differentiation process of the juvenile phloem (Absmanner et al. 2013). The data obtained were also used to identify the cells, where *UmamiT* promoter activity and the UmamiT-GFP fusion protein was found.

Table 3. Overview about the investigated marker lines

line	marker of	published
P_{DR5}: ER-GFP	auxin response (low affinity elements)	Ottenschlager et al.2003
P_{DR5v2}: NLS-Venus	auxin response (high affinity elements)	Liao et al. 2015
R2D2	auxin dynamics	Liao et al. 2015
P_{PIN3}: PIN3-GFP	auxin efflux transporter PIN3	Zádniková et al. 2010
P_{D6PK}: YFP-D6PK	protein kinase D6	Zourelidou et al. 2009
P_{TCS}: ER-GFP	cytokinin response	Zürcher et al. 2013
P_{CAT6}: CAT6-GFP	cationic amino acid transporter CAT6	unpublished, based on Hammes et al.2006
$P_{CYCB1.2}$:CYCB1.2-GFP	mitosis (G2-M phase), CYCB1.2 on chromatin	Schnittger, personal communication
$P_{CYCB1.3}$:CYCB1.3-GFP	mitosis (G2-M phase), CYCB1.3 on chromatin and cytosol	Schnittger, personal communication
P_{PLT1}: ER-CFP	stem cell transcription factor PLT1	Galinha et al. 2007
P_{APL}: APL-GFP	phloem identity transcription factor APL	Bonke et al. 2003
P_{PD1}: ER-GFP	protophloem and sieve elements	Bauby et al. 2006
P_{PD1}: PD1-ER-GFP x P_{SUC2}: ER-mCherry	protophloem, sieve elements and companion cells	Müller et al. 2015
P_{35S}: MP17-GFP	branched, likely secondary plasmodesmata	Hofius et al. 2001

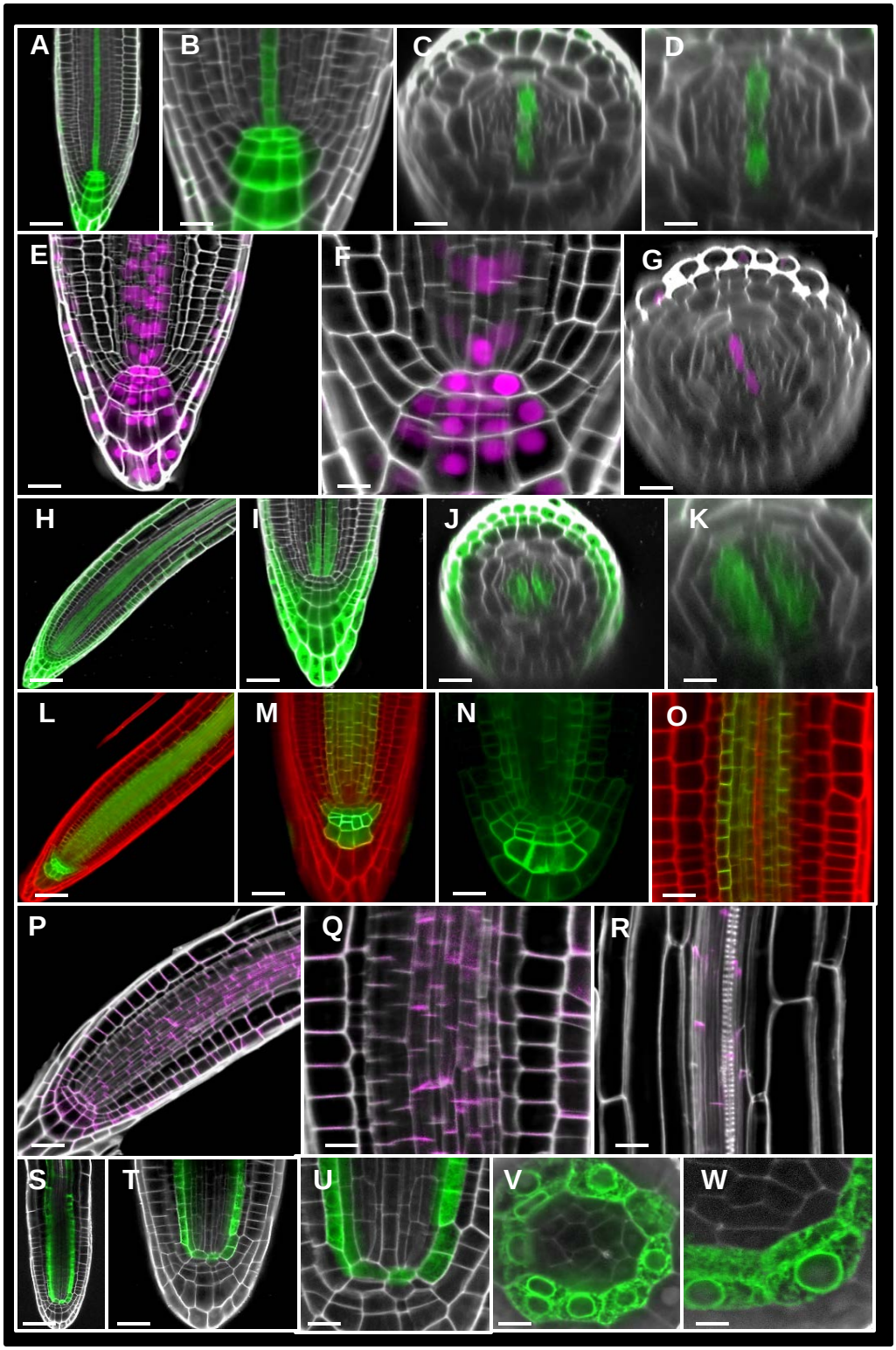

Figure 82. Expression of different marker lines in the root. (A-C) *P_{DR5}: ER-GFP.* (A) Overview, scale bar: 45µm. (B) Magnification of the tip, scale bar: 8µm. (C, D) Optical sections, scale bars: (C) 14µm, (D) 10µm. (E-G) *P_{DR5v2}: NLS-VENUS.* (E) Maximum projection as overview, scale bar: 20µm. (F) Magnification of the stem cell niche of the root, scale bar: 6µm. (G) Optical section, scale bar: 11µm. (H-K) *P_{TCS}: ER-GFP.* (H) Overview, scale bar: 50µm. (I) Magnification of the tip, scale bar: 22µm. (J, K) Optical sections, scale bars: (J) 16µm, (K) 8µm. (L-O) *P_{PIN3}: PIN3-GFP.* (L) Overview, scale bar: 45µm. (M) Magnification of the tip, scale bar: 28µm. (N) Maximum projection of the root tip, GFP channel, scale bar: 12µm. (O) Magnification of the differentiation zone, scale bar: 16µm. (P-R) *P_{D6PK}: YFP-D6PK*. (P) Overview, scale bar: 20µm. (Q) Magnification of the differentiation zone, scale bar: 7µm. (R) Magnification of the vasculature with phloem and xylem, scale bar: 15µm. (S-T) *P_{SCR}: ER-GFP.* (S) Overview, GFP detected from meristematic to differentiation zone, scale bar: 60µm. (T) Root tip, SCR-GFP found in the endodermis and QC, scale bar: 20µm. (U) Magnification of the QC area, scale bar: 10µm. (V, W) Optical sections, scale bars: (V): 6µm, (W) 4µm.

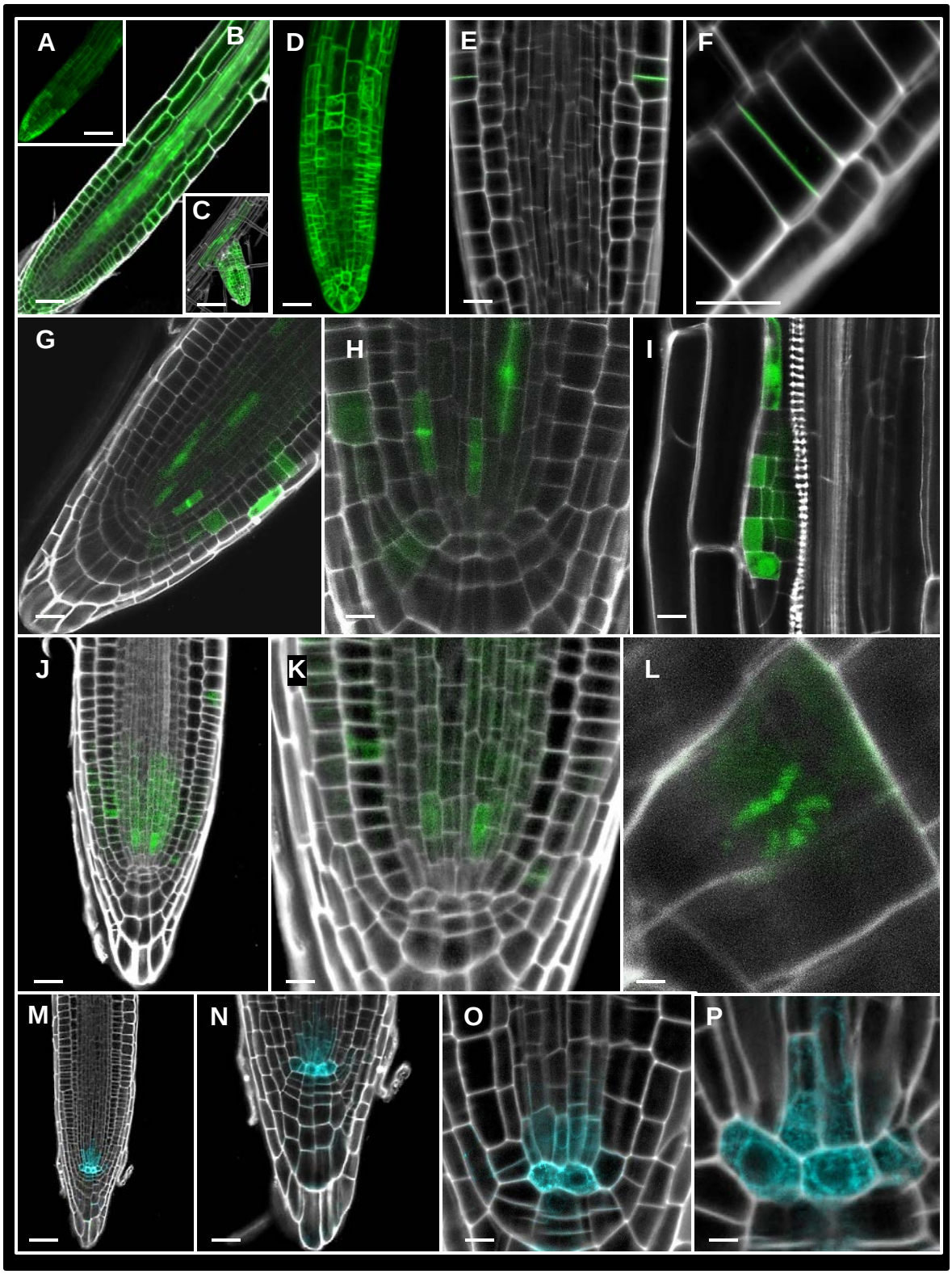

Figure 83. Expression of different marker lines in the root. (A-F) *PCAT6: CAT6-GFP.* (A) Overview, maximum projection, polar distribution of GFP in the meristematic zone, scale bar: 100µm. (B) Optical section, scale bar: 45µm. (C) Maximum projection of an emerging lateral root ,scale bar: 100µm. (D) Maximum projection of the root tip, many cells of the meristematic zone show polar distribution of GFP, scale bar: 40µm. (E, F) Polar distribution of GFP is restricted to the rhizodermis, scale bars: (E) 15µm, (F) 8µm. (G-I) *PCYCB1.2: CYCB1.2-GFP.* (G) Optical section of a root tip, scale bar: 15µm. (H) Focus on the QC, scale bar: 7µm. (I) Expression during lateral root emergence, scale bar: 10µm. (J-L) *PCYCB1.3: CYCB1.3-GFP*. (J) Overview of the root tip, scale bar: 20µm, (K) Magnifications of the area near the QC, scale bars: 8µm. (L) Dividing cell shows GFP signals at the chromosomes and weak in the cytosol, scale bar: 2µm. (M-P) *PPLT1: PLT1-CFP.* (M) Overview, scale bar: 50µm. (N) Magnification of the root tip, scale bar: 20µm. (O) Focus on the QC, scale bar: 7µm. (P) Maximum of CFP detected in the QC and few cells upwards from there, scale bar: 3µm.

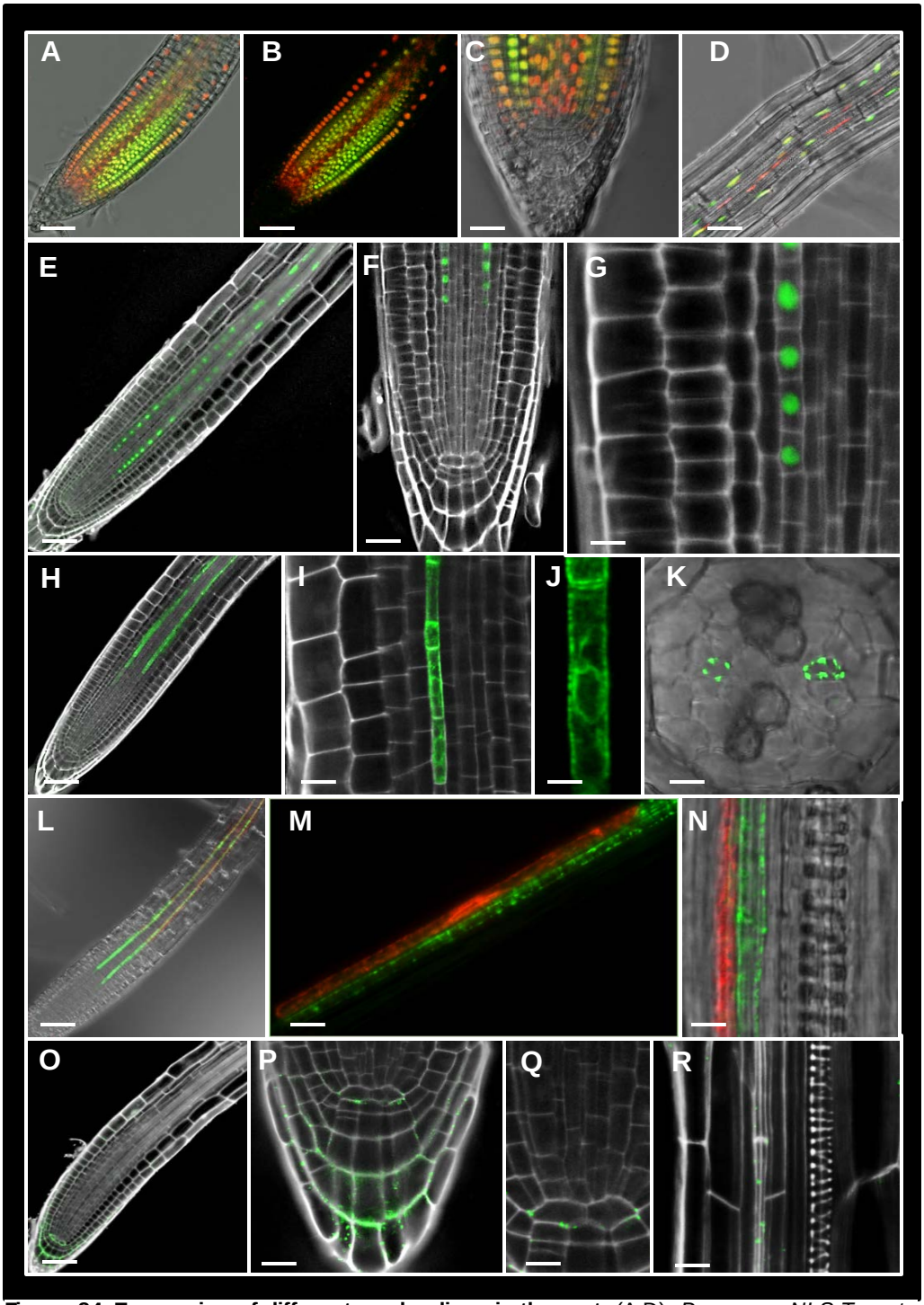

Figure 84. Expression of different marker lines in the root. (A-D) *PRPS5A-mDII: NLS-Tomato/ PRPS5A-DII: NLS-3xVenus* red nuclei indicate auxin maxima, green nuclei auxin minima. (A, B) Overview of the root, (B) fluorescence channel, scale bars: 50µm. (C) magnification of the root tip, scale bar: 30µm. (D) Auxin distribution along the root hair zone, scale bar: 40µm. (E-G) *PAPL: APL-GFP*. (E) Maximum projection, overview of the root, morphology of protophloem nuclei is changing during differentiation along the root, scale bar: 50µm. (F) Root tip, APL expression occurs in about 75µm distance to the QC, scale bar: 24µm. (G) APL expression in the fifth cell file beneath the rhizodermis, scale bar: 7µm. (H-K) *PPD1: ER-GFP.* (H) Root tip showing the two protophloem files, scale bar: 60µm. (I) PD1 expression in the fifth cell layer beneath the rhizodermis, scale bar: 5µm. (J) Magnification of the GFP channel from I, scale bar: 3.4µm. (K) Cross section, expression of PD1 in the metaphloem, scale bar: 7µm. (L-N) PD1: ER-GFP x PSUC2: mCherry. (L) Maximum projection of the root tip, scale bar: 70µm. (M) Magnification of one companion cell and sieve element from the root tip, scale bar: 5µm. (N) Root vasculature with phloem and xylem, scale bar: 6µm. (O-R) *P35S: MP17-GFP*. (O) Overview of the root, scale bar: 50µm. (P) Magnification of the root tip, scale bar: 11µm. (Q) Magnification of the QC, scale bar: 5µm. (R) Root vasculature, MP17 in the phloem, scale bar. 10µm.

5.10.1.2. Promoter activity of *UmamiTs* in the root

In order to support the distinct expression pattern described so far for seeds and the the previously shown results of the qRT-PCR (Fig. 41) the promoter activity of *UmamiTs* was studied in roots. Looking at the RNA level in roots, it was obvious that the overall expression intensity was much lower and seemed to be in the same range for candidates of the same clade. This could also be confirmed in *promoter:GUS* reporter lines. Unless stated otherwise, the figures show representative images that are identical for each candidate analyzed. An overlapping promoter activity in the vasculature for each *UmamiT* candidate was monitored. GUS staining was observed in seedling roots tips (Fig. 85 A) as well as in root tips of older plants where starch statholiths were already present (Fig. 85 C). Promoter activity was also observed behind the differentiation and elongation zone along the whole root system (Fig. 85 B). GUS crystals could be seen clearly in those cells neighboring the xylem (Fig. 85 D). Cross sections showed promoter activity, which was not only restricted to cells near the xylem, but also present at the phloem poles and the pericycle (Fig. 85 F). Using mPS-PI staining and the reflection mode of the confocal microscope it was possible to visualize the crystals in a better cellular resolution. Herein the GUS staining could again be seen in parenchymatic cells that were positioned around the xylem (Fig. 85 E). Additionally, also in the sieve elements distinct GUS crystals were seen (Fig 85 G).

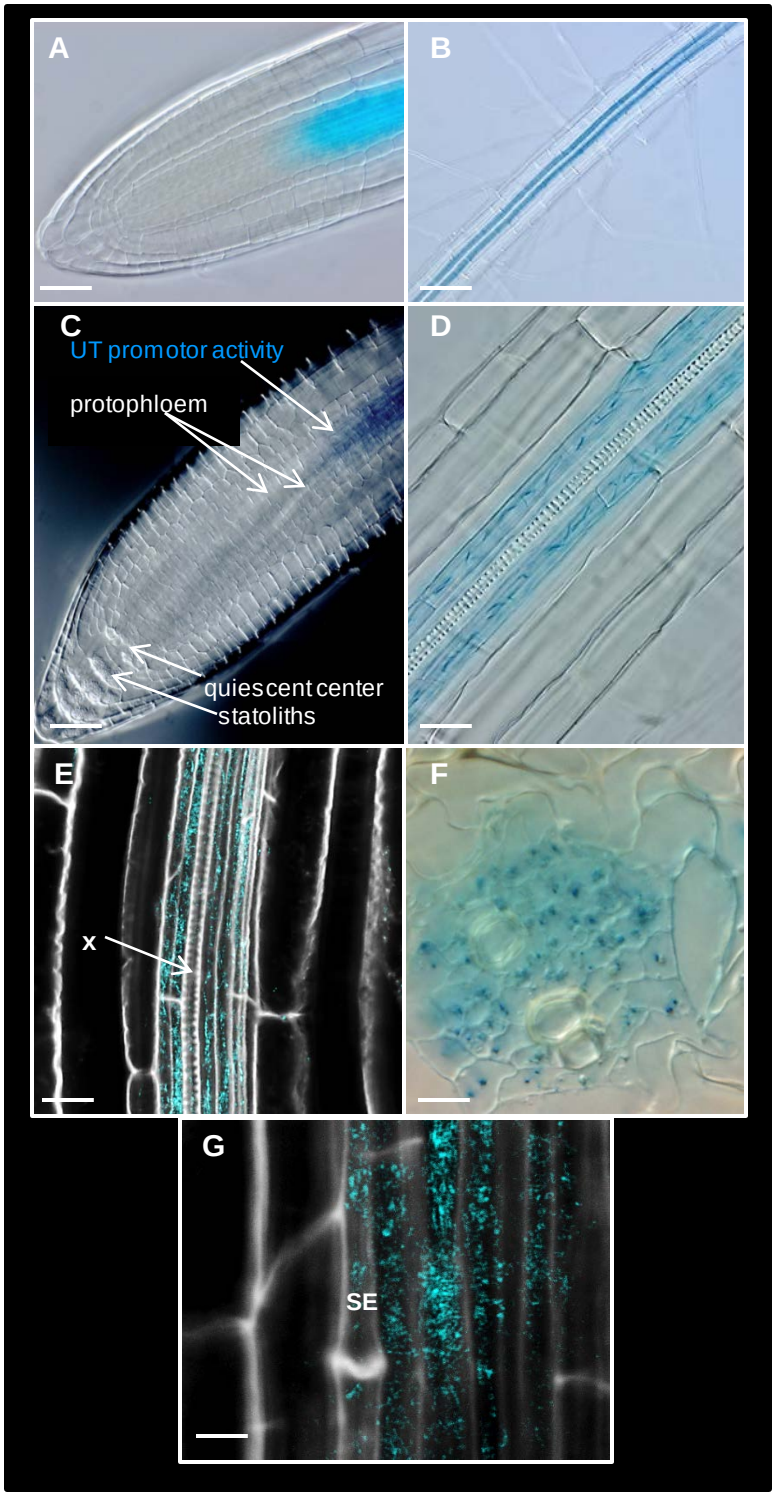

Figure 85. *UmamiT expression* in the root indicated by GUS staining. (A) GUS staining in a root few hours after germination, scale bar: 40µm. (B) GUS staining in the vascular cylinder along root hair zone; scale bar: 100µm. (C) Root of a plant two weeks after germination; scale bar: 25µm. (D) GUS staining specific in the vascular cells; scale bar: 20µm. (E, G) mPS-PI staining, showing cellular resolution of GUS staining pattern in the stele (E) and (G) additionally in the sieve elements (accumulation of staining at the putative sieve plate) scale bar: (E) 10µm, (G) 4µm. (F) Cross section, scale bar: 5µm. X (xylem), se (sieve element).

GUS signals could also be obtained in the vasculature if a lateral root was emerging (Fig 86 A). Although GUS crystals were seen in sieve elements as shown before, only weak staining was found in the protophloem (Fig 86 B, C).

The same expression pattern in the root was true for the NLS-3xGFP version for visualization of promoter activity (Fig. 86 D-F). Only in the case of the promoter of *UmamiT29* the GFP was very clearly detected in the protophloem and adjacent cell types (Fig. 86 G, H), see also below.

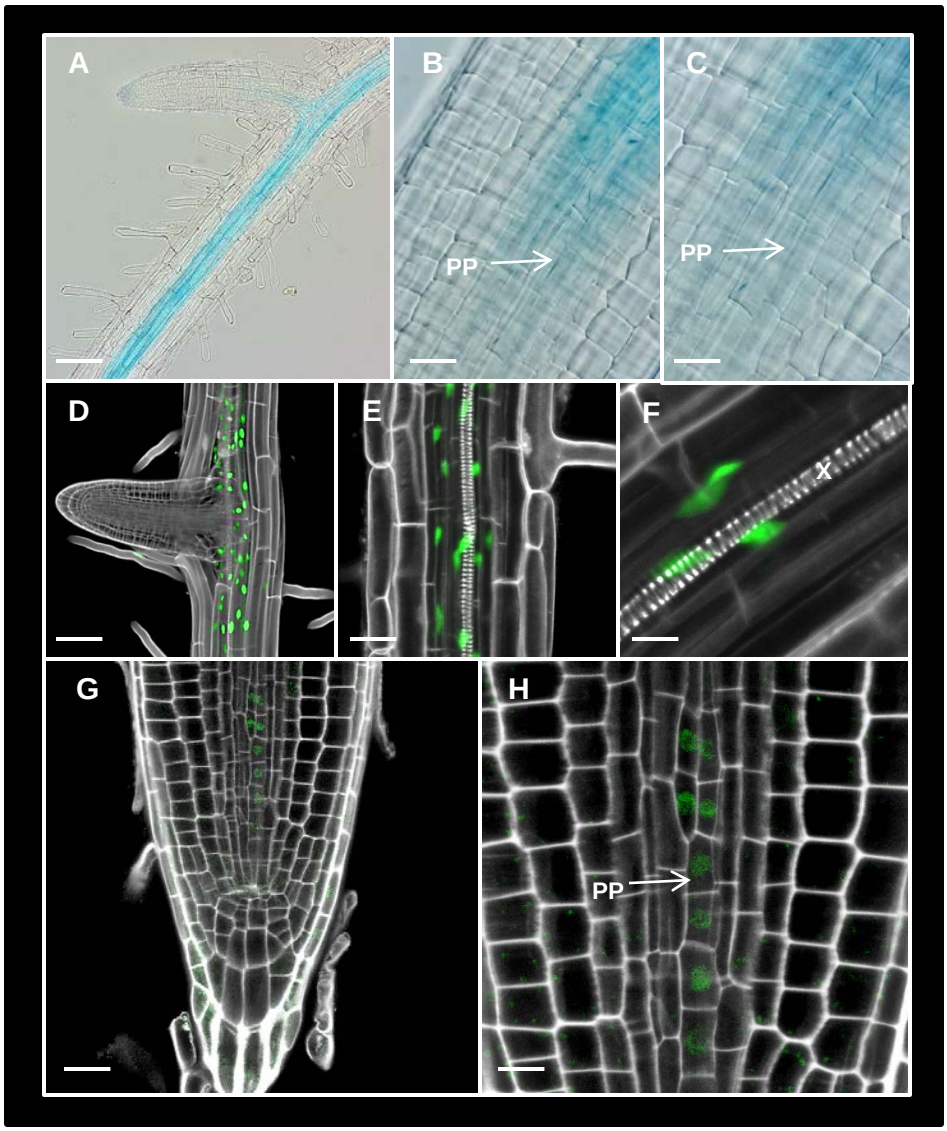

Figure 86. *UmamiT* promoter activity in lateral root and protophloem. *P$_{UmamiT14}$: GUS* (A-C), (A) GUS staining at lateral root formation, scale bar: 80µm. (B, C) Earliest staining observed in protophloem cells, scale bar: (B) 12µm, (C) 7µm. (D-H) *P$_{UmamiT29}$: NLS-3xGFP.* (D-F) Strongest signals in the stele in xylem surrounding cells; scale bars: (D) 50µm, (E) 30µm, (F) 7µm. (G) Early signals at the root tip, scale bar: 20µm; (H) Promoter activity in the young protophloem cells, scale bar: 7µm. X (xylem), PP (protophloem).

Coexpression of a marker for promoter activity of *SUC2* and *UmamiT14* showed no colocalization at all (Fig 87 D-F). But the cell types were in close vicinity to each other, indicating that *UmamiT* promoter activity was not only restricted to xylem parenchyma cells (Fig. 87 A-C), but also detectable in the phloem poles.

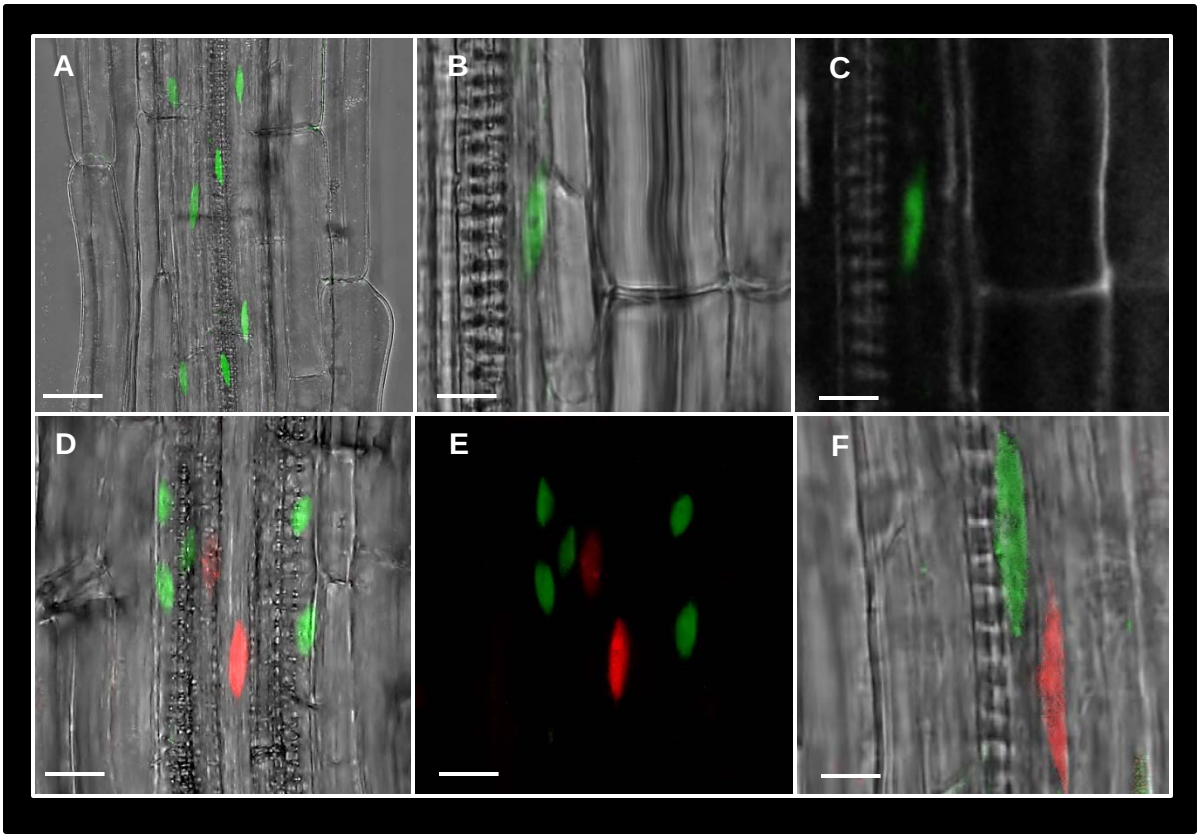

Figure 87. *$P_{UmamiT14}$: NLS-3xGFP and P_{suc2}: NLS-mCherry* distribution in the root. (A-C) *$P_{umamiT14}$: NLS-3xGFP* expression in the root. (A) Maximum projection, signals specific in the stele, scale bar: 20µm. (B, C) Optical section, focus at the stele. (B) With bright field image. (C) With autoflourescence channel; scale bar: 5µm. (D-F) Coexpression of *$P_{umamiT14}$: NLS-3xGFP and P_{suc2}: NLS-mCherry.* (D, E) Maximum projection, (E) GFP and mCherry channel merged, scale bar: 10µm. (F) Magnification of two nuclei from neighboring cells, scale bar: 4µm.

As previously stated, the promoter activity of *UmamiT29* displayed unique features. For this candidate signals in the root cells near the quiescent center (QC) were found (Fig 88 A). The strongest GFP fluorescence was detected in a thin cell file, the protophloem (Fig. 88 B, C). The fluorescence disappeared suddenly as the protophloem becomes mature (Fig. 88 D). Much weaker signals were also found in single cells of the provascular cells (Fig. 88 E). The first appearance of the transcriptional fusion with NLS-3xGFP was reported two cells upwards from the QC (Fig. 88 F). To obtain higher sensitivity for weak signals indicating promoter activity, the $P_{UmamiT29}$*:GUS* reporter line was used. Strongest GUS staining was seen as described before at the differentiation zone of the root tip (Fig. 88 G). Intensity in the frequency of GUS crystals increased in the vascular cells from elongation to differentiation zone (Fig. 88 H). Very weak signals could be also obtained in the meristematic zone of the root harboring the QC (Fig. 88 I). Here cells forming the provascular parenchymatic tissue showed promoter activity for *UmamiT29*. These cells were located right behind the QC (Fig. 88 J), indicating that amino acid transport by UmamiTs occurs also in the stem cell niche.

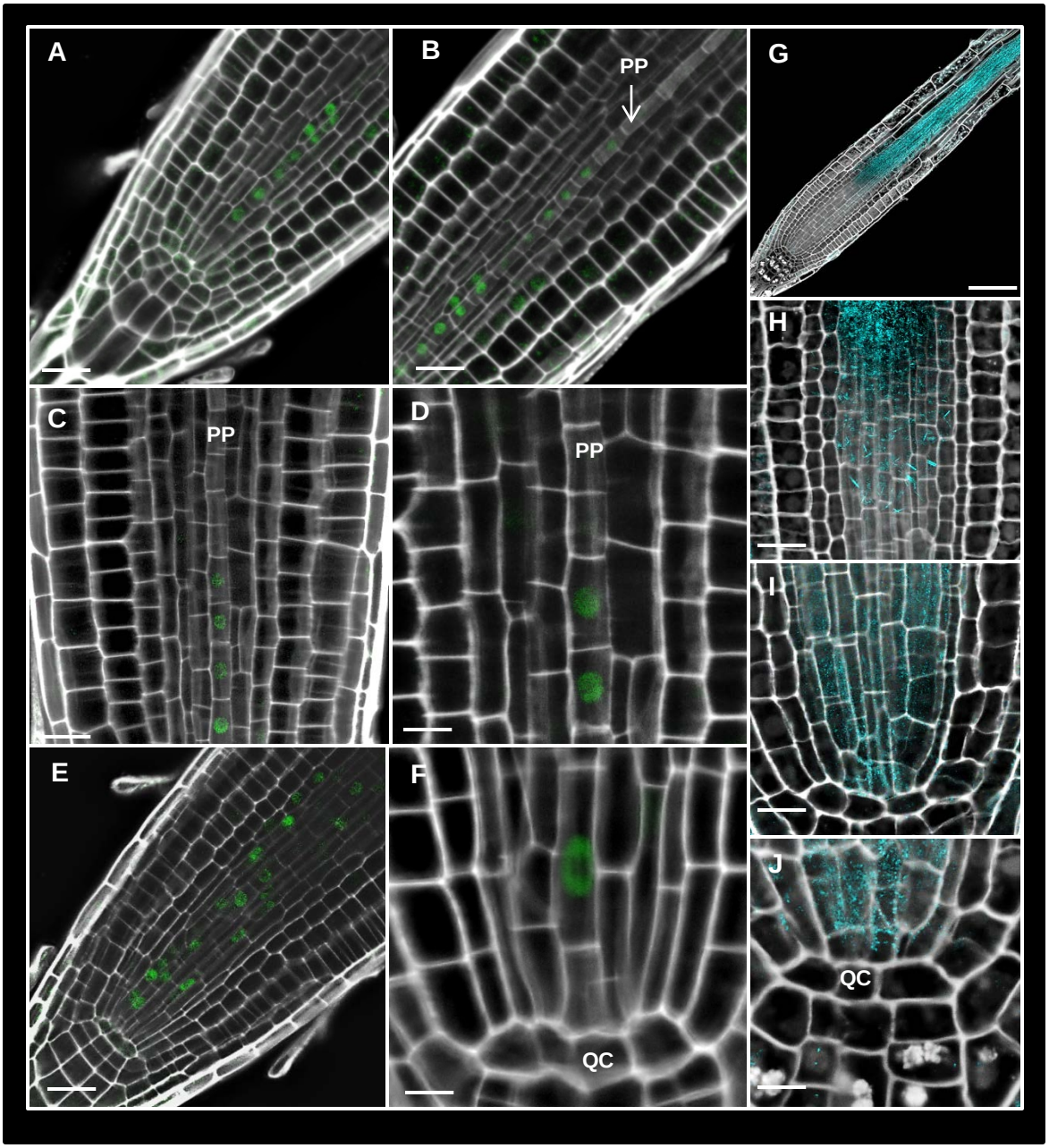

Figure 88. *UmamiT29* expression in the provasculature and protophloem. Analysis of the marker line *P*$_{UmamiT29}$*: NLS-3xGFP/GUS* (A) Overview of root tip, scale bar: 20µm; (B) Signals in protophloem cells file before differentiation takes place, scale bar: 10µm. (C, D) GFP signals are only found in the young protophloem cells and disappeared in the differentiated cells, scale bars: (C) 12µm, (D) 7µm. (E) *UmamiT29* promoter active in several provascular cells, scale bar: 20µm. (F) Magnification of a region right behind the quiescent center; scale bar: 5µm. (G) Overview of root with strong GUS staining in the vasculature, scale bar: 70µm. (H) Transition area from the elongation to the differentiation zone, scale bar: 18µm. (I) Meristematic zone shows weak GUS staining in the provascular parenchyma cells, scale bar: 12µm. (J) Magnification of the area around the QC, GUS crystals were found right behind the root meristem, scale bar: 10µm. PP (protophloem), QC (quiescent center).

5.10.1.3. Tissue specific localization of UmamiTs in the root

In order to support the data obtained by the promoter analysis the distribution of the fusion protein in the root was monitored. Analysis of UmamiT localization in the root was done by using plants harboring the full length GFP fusion protein, containing all introns. The distribution of GFP in the roots showed that all candidate UmamiTs were located in the vascular tissue of the differentiating zone (Fig. 89 A, B, D, E). UmamiT-GFP was then continuously detected in the vasculature along the root hair zone and also in older parts (Fig. 89 G, H). Co-staining with FM4-64 confirmed in this tissue a plasma membrane localization (Fig 89 C, F, I).

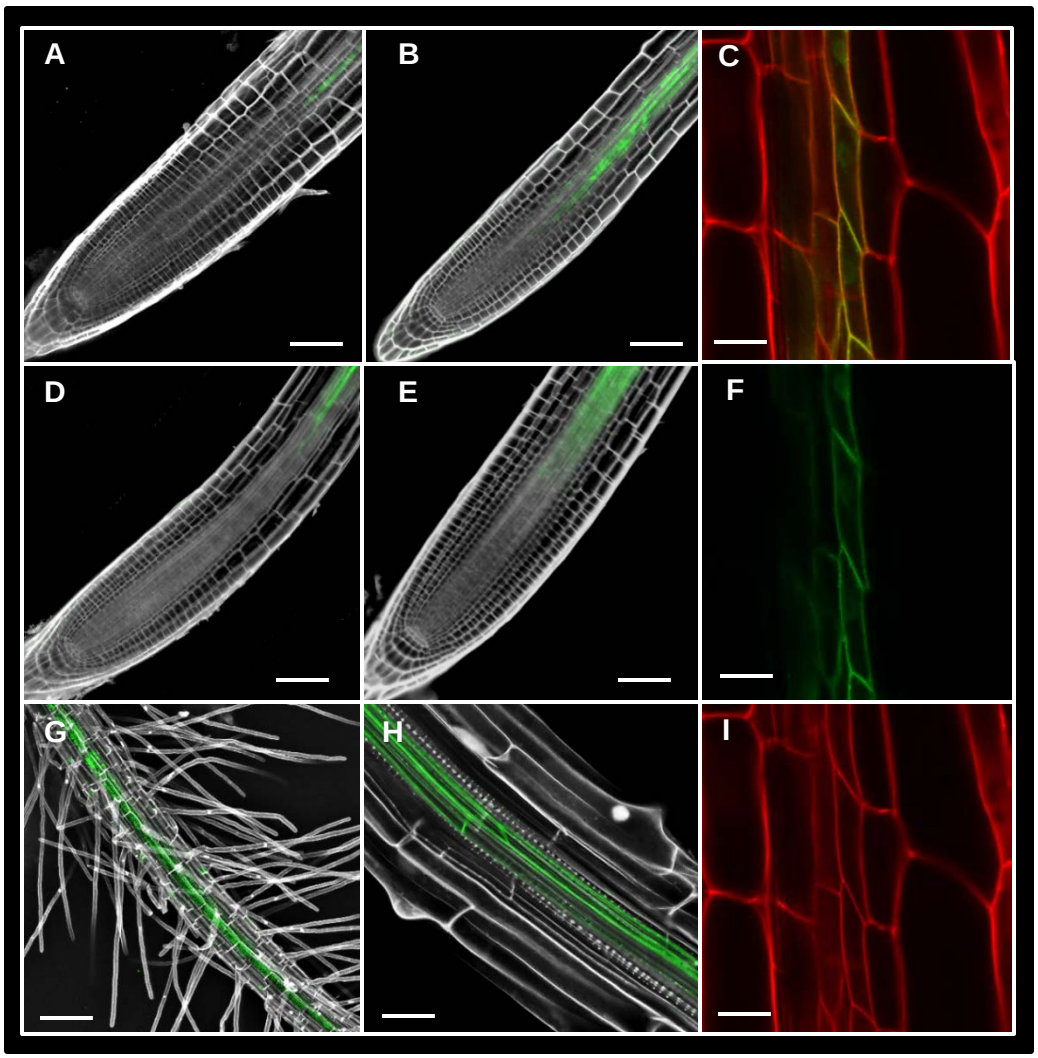

Figure 89. Localization of UmamiTs in the root. ***P*$_{UmamiT}$*: UmamiT-GFP* **was screened for each candidate.** (A) UmamiT14-GFP. (B) UmamiT11-GFP, (D) UmamiT28-GFP, (E) UmamiT29-GFP; scale bars: 50µm. (C, F, I) Co-staining of UmamiT28-GFP with FM4-64. Yellow color in C indicates colocalization. (C) Overlay of GFP channel (F) with FM4-64 signals (I) indicating colocalization, scale bars: 15µm. (G) UmamiT29-GFP, maximum projection at the root hair zone, scale bar: 100µm. (H) UmamiT14-GFP in the stele; scale bar: 30µm.

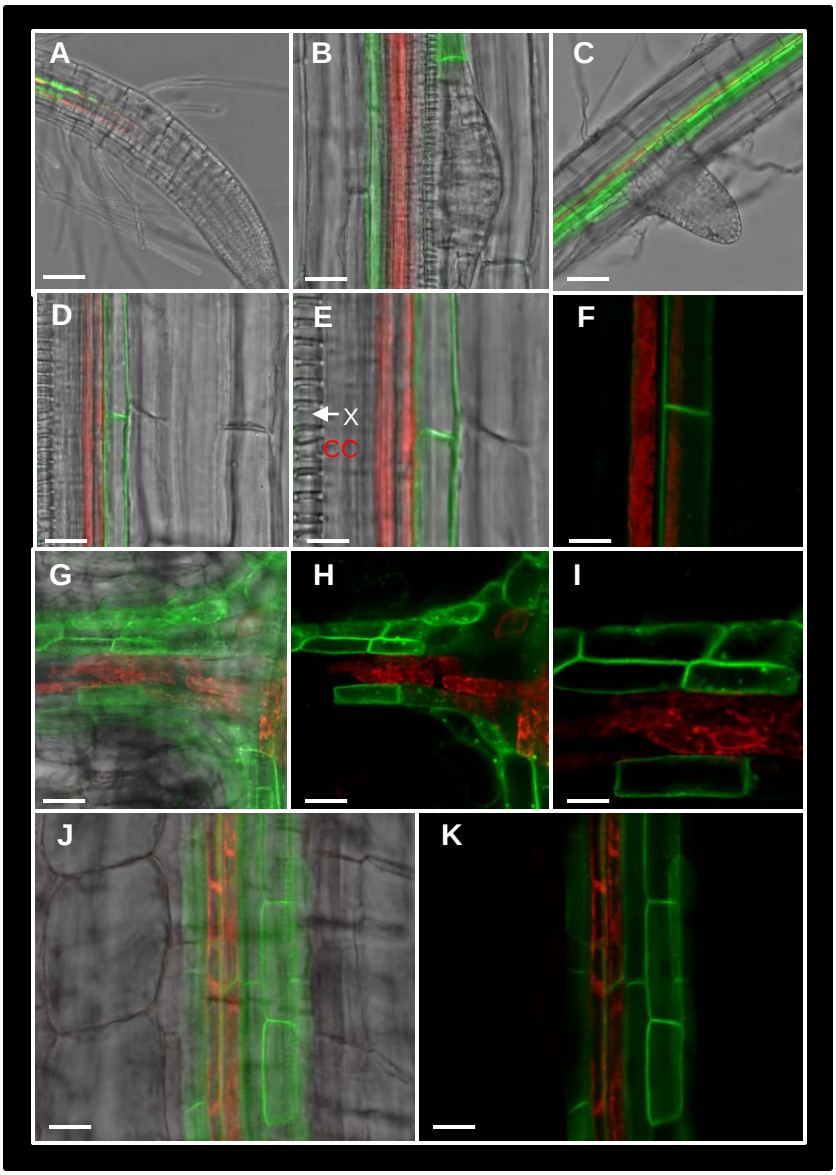

Figure 90. Coexpression of $P_{UmamiT14}$: *UmamiT14-GFP* and P_{suc2}: *ER-mCherry* in the root. Green signals: UmamiT14-GFP, red signals: SUC2-mCherry (A) Overview of the root tip, scale bar: 50µm. (B) Early stage of lateral root formation; scale bar: 20µm. (C) Later stage of lateral root emergence; scale bar: 40µm. (D-F) Polar distribution of UmamiT14 in the stele. (D) Stele with companion cell file next to UmamiT14 expressing cell; higher GFP intensity at the anticlinal wall indicated by arrow, scale bar: 18µm. (E) Magnification of (D), scale bar: 10µm. (F) Overlay of the fluorescence channel for GFP and mCherry, higher GFP intensity at the anticlinal wall indicated by arrow; scale bar: 7µm. (G-I) Branch point of a differentiated lateral root; companion cells and UmamiT14 positive cells close to each other but no overlap of the signals occurred. (G, H) Maximum projection with bright field image (G) and without (H) scale bar: 20µm. (I) Single optical section of the same root; scale bar: 8µm. (J, K) Maximum projection of the main root; UmamiT14-GFP was detected in several cells of the phloem region around companion cells; (J) Merge with bright field image. (K) Merge of GFP and mCherry channel scale bar: 8µm. X (xylem), cc (companion cell).

In order to characterize the UmamiT-positive cells, a marker line coexpressing UmamiT14-GFP and SUC2-mCherry was generated. It could be shown that *SUC2* appeared much earlier in the root than UmamiT14 (Fig. 90 A). A clear fluorescence “gap” in the stele was seen at the positions where lateral roots formed (Fig. 90 B, C). These lateral roots were later on connected to the central cylinder and GFP and mCherry were monitored again at the site of outgrowth of the lateral root (Fig 90 G, H, I). Altogether no colocalization between UmamiT14-GFP and SUC2-mCherry was found, but a very distinct localization pattern. A tendency for polar distribution of UmamiT14-GFP was also documented for the anticlinal membranes (Fig. 90 D-F). Z stacks showed again the widespread distribution of UmamiT14 in several cell files around the companion cells (Fig

91. J, K). This indicates that UmamiT-GFP is not only found in cells close to the xylem but also in parenchymatic cells close to the phloem.

To find out if UmamiT-positive cells in roots are positioned in the same cell file independent of the age, optical cross sections were done, starting from the first visible expression (Fig. 91). Near the root tip signals in the region of the phloem poles were identified that were spreading in the upper regions towards the whole stele. In the more differentiated part of the root GFP was seen to be associated with the xylem vessels.

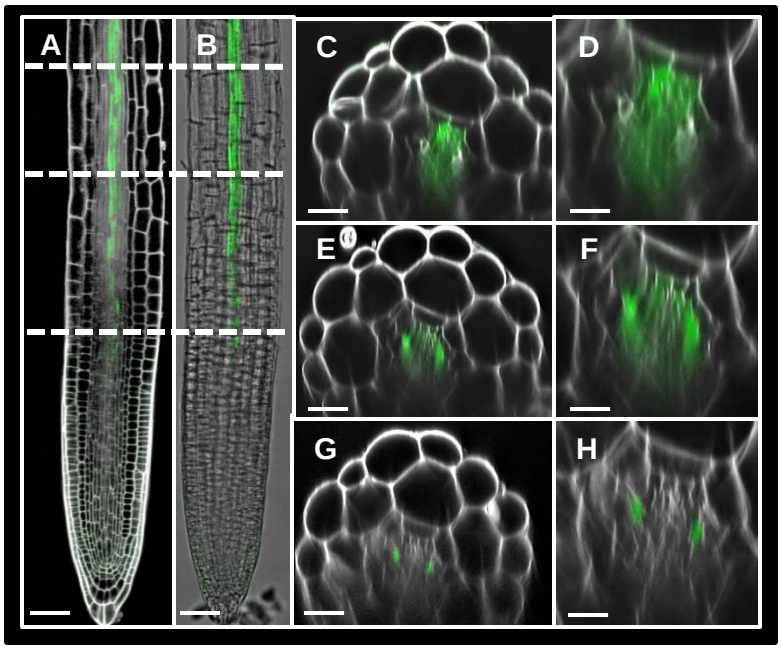

Figure 91. Optical cross sections along the root. *P*$_{UmamiT28}$*: UmamiT28-GFP* reporter line was analyzed. (A, B) Overview of UmamiT-GFP signals in the root, scale bar: 30µm. (C, D) Optical section in the upper region marked in (A, B) by a white punctuated line. (D) Magnification of the central cylinder of (C), scale bars: (C) 30µm, (D) 15µm. (E, F) Optical section through the middle part of the marked root from (A, B). (F) Magnification of the central cylinder of (E), scale bars: (E) 20µm, (F) 10µm. (G, H) Optical section through the youngest part. (H) Magnification of (G), scale bars: (G) 17µm, (H) 10µm.

The same results were obtained in cross sections of the reporter lines (Fig. 92). Here first signals in the phloem regions were detected (Fig. 92 A, C, E). According to their anatomical position, i.e. not directly adjacent to the pericycle, these cells can be classified as metaphloem (Esau 1969). Later on GFP gets more homogeneously distributed in the stele (Fig. 92 B, D, F). Signals in the young metaphloem were weak compared to the signal intensity in the pericycle or parenchymatic tissue of the older root and seemed to be transiently expressed in these cells, whereas signals in the parenchyma of xylem and phloem were observed throughout the differentiated root. These observations indicate that UmamiTs are placed in cells that contribute to the long distance transport of amino acids.

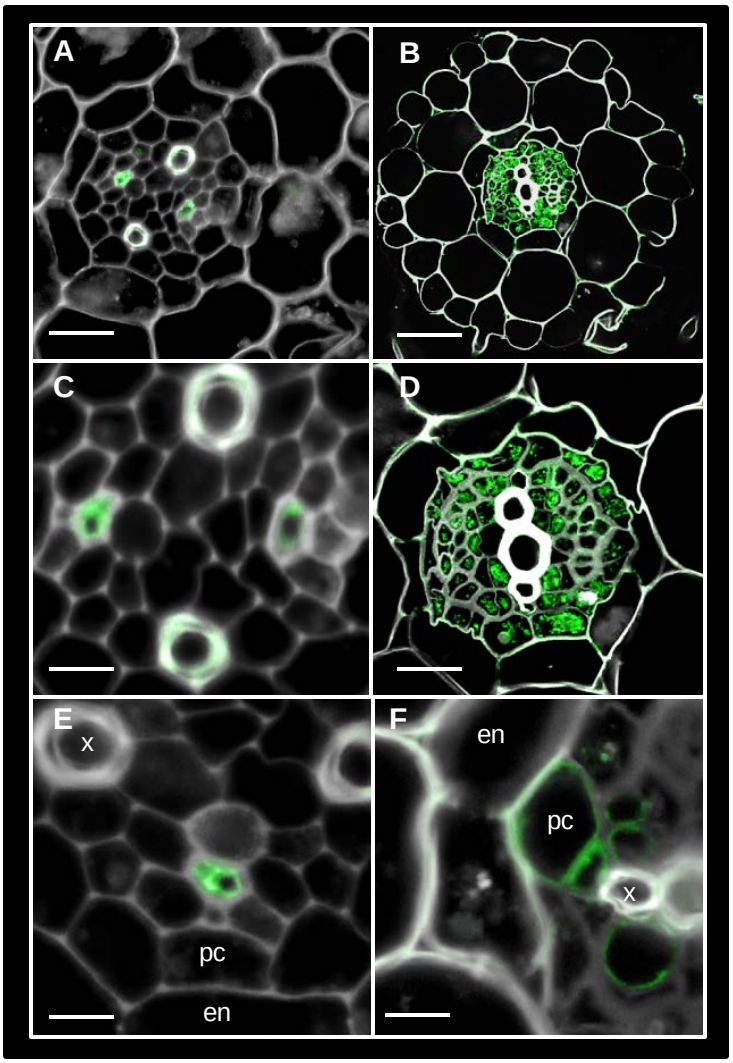

Figure 92. Localization of UmamiT in cross sections along the root. Used reporter line: *$P_{UmamiT14}$: UmamiT14-GFP*. (A, B) Overview of a cross section through a young root (A) and an fully differentiated root (B), scale bars: (A) 12µm, (B) 30µm. (C, D) Magnification of (A) and (D) , scale bars: (C) 5µm, (D) 15µm. (E) Detail of the phloem pole it's in the metaphloem, scale bar: 5µm. (F) Detail of pericycle and xylem parenchyma, scale bar: 6µm. X (xylem), pc (pericycle), en (endodermis).

The GFP fusion protein was found distal from the root tip until the root showed secondary growth and got connected to the hypocotyl (Fig. 93 A,-C). GFP fluorescence was visible in parenchymatic cells of the xylem as well as in several cells of the secondary phloem (Fig. 93 C). Additionally it was documented that UmamiT-positive cells were placed between xylem elements of already secondary thickened roots (Fig. 93 D). Immunolocalization of these tissues could demonstrate how close those cells stand to the xylem vessels and that the fusion protein is attached to the borders of the cell, indicating a plasma membrane localization there (Fig. 93 E-H). According to their close position to the vessels it can be suggested that UmamiTs in the xylem parenchyma contribute to the retrieval and/or feeding of amino acids for the long distance transport or the distribution of amino acids to the surrounding tissues.

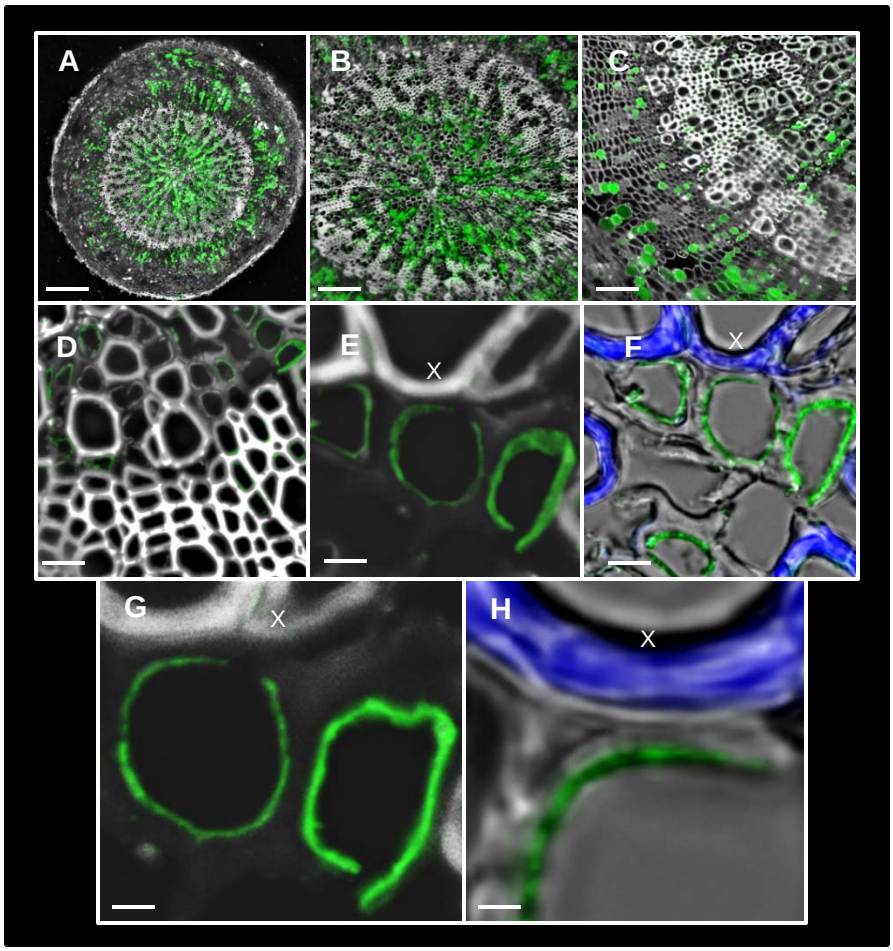

Figure 93. Localization of UmamiT11-GFP in the secondary root. (A) Overview, scale bar 250µm. (B) Magnification of the xylem circle, scale bar: 120µm. (C) Optical section of the vascular cylinder of a secondary root, signals in the xylem region magnified in (D), scale bar: 50µm. (D) UmamiT-GFP in the xylem parenchyma of the secondary root, scale bar: 25µm. (E-H) Immunolocalization of the xylem parenchyma at the secondary root stage; white and blue color: autofluorescence; Green cells: α-GFP, detected with a CY2-antiserum, representing GFP positive cells. Scale bars: (E) 5µm, (F) 5µm, (G) 2µm, (H) 1.5µm. X (xylem).

5.10.1.4. Polar distribution of UmamiT14 in the root

Expression of *UmamiTs* in the root was detected along the root in the stele (Fig. 94 A) with a plasma membrane localization of the fusion protein (Fig. 94 B-D, G). GFP was found in parenchymatic cells close to the xylem (Fig. 94 E, H), which was the case for each candidate. Only for UmamiT14-GFP a tendency for polar distribution could be observed (Fig. 94 F). This asymmetry in the distribution of GFP was detected at the anticlinal walls (Fig. 94 I, J). Although the GFP signal occurred as a thin line across the cell borders over the whole cell (Fig. 94 K) the maximum intensity of GFP was detected in the anticlinal position (Fig. 94. J, L), suggesting a role of *UmamiT14* in the directed translocation of amino acids for long distance transport. Furthermore one possible physiological role could be in the export of amino acids from the vascular parenchymatic tissue into the xylem.

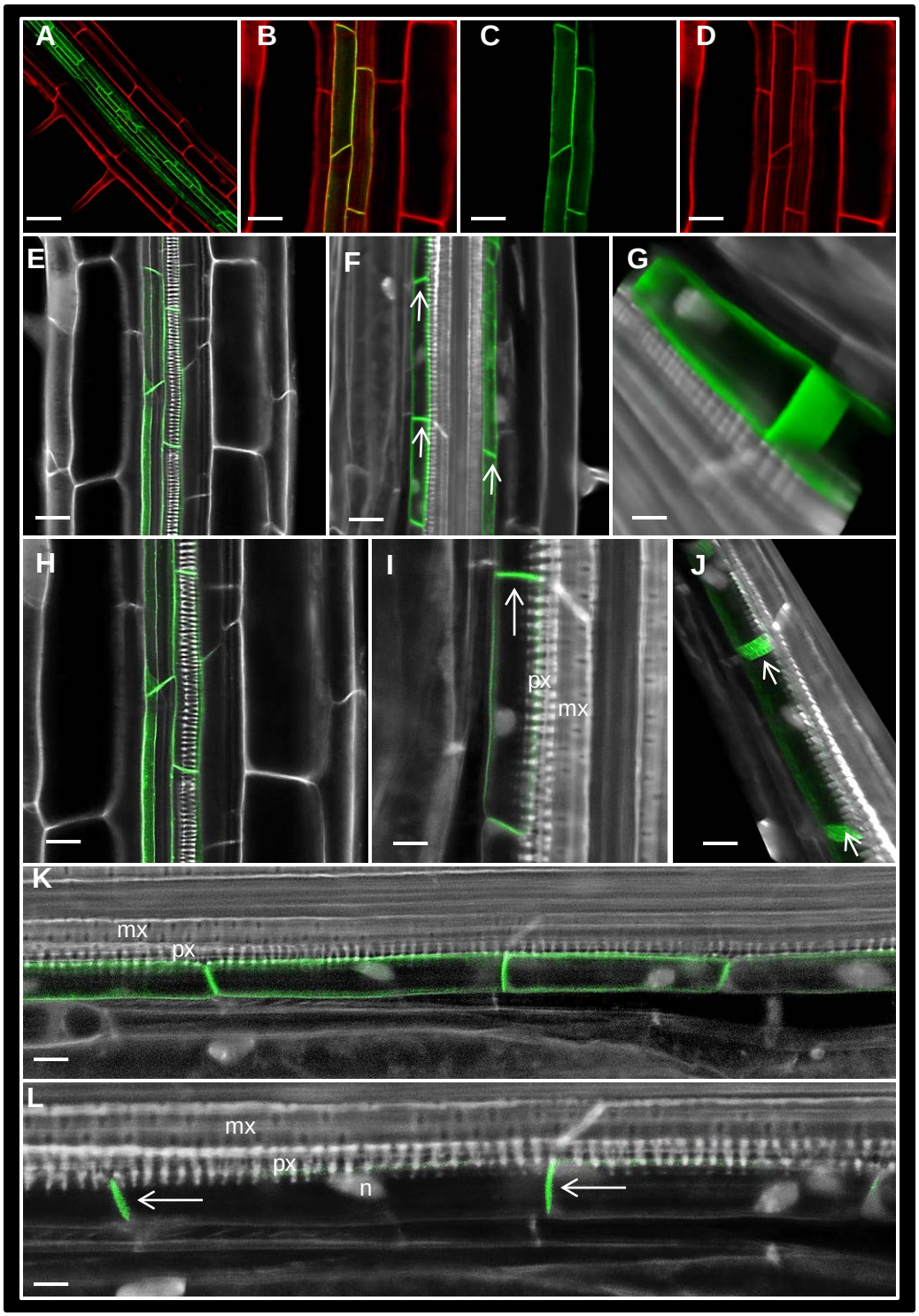

Figure 94. Polar localization of UmamiT14-GFP in the root. (A-L) *$P_{UmamiT14}$: UmamiT14-GFP.* (A) Overview as maximum projection, UmamiT14-GFP found in the stele, scale bar: 65µm. (B-D) UmamiT14-GFP localizes to the plasma membrane. (B) Overlay of (C) and (D). (C) GFP channel. (D) PI channel, scale bars: 23µm. (E, H) GFP signals in several cells of the vasculature, closely associated to the xylem, scale bars: (E) 21µm, (H) 14µm. (F) UmamiT14-GFP in the stele with a slightly polarized distribution, scale bar: 17µm. (G) 3D reconstruction of a vascular UmamiT14-positive cell, scale bar: 6µm. (I) Single cell from the vascular parenchyma displaying a slightly polarized distribution of UmamiT14-GFP, scale bar: 8µm. (J) 3D reconstruction of several UmamiT14-positive cells along the xylem vessels with polar distribution of GFP, scale bar: 10µm. (K) UmamiT14-GFP in a cell file next to the xylem, scale bar: 10µm. (L) GFP found in anticlinal position of the cells indicating a polar localization of UmamiT14, scale bar: 5µm. N (nucleus), px (protoxylem), mx (metaxylem), arrows mark polarized GFP signals.

5.10.1.5. UmamiTs and the protophloem paradoxon

In order to investigate the association of UmamiTs with the protophloem, which was already supposed by promoter activity and cross sections, the earliest detectable presence of the fusion protein in the root tip was studied. As shown before, UmamiT-positive cells were found at the late elongation zone of the root (Fig. 95 A, C). Although highest GFP intensity was monitored at the moment the xylem axis was closed, it was possible to identify signals also in much younger stages in the stele (Fig. 95 C). There, cross sections indicated expression of *UmamiT* in the metaphloem (Fig. 95 B). A look at the GFP signals in the root at the level of the differentiating protophloem showed that fluorescence was found distant from the protophloem (Fig. 95 D). Several cells of the stele displayed strong UmamiT-GFP signals also in a single cell file in distance to the protophloem (Fig. 95 E). Interestingly, GFP was also found in a cell file in neighborhood to the protophloem (Fig. 95 G). Looking at the two protophloem cell files simultaneously it could be documented that GFP signals were asymmetrically distributed in the cells next to the differentiating protophloem in the fourth cell file beneath the rhizodermis (Fig. 95 F, H). UmamiT-GFP was present weakly in one single cell next to one protophloem strand whereas no GFP was found in the opposite cell file (Fig. 95 F). This is probably a result of the low expression of *UmamiTs* in those cells or a result of a transient expression concerted with a fast protein degradation. With this result it can be explained, why in most cases no GFP was ever found in the phloem poles of young roots regarding the focus on the strong GFP in the stele near the xylem.

In summary, only for UmamiT29-GFP weak fluorescence in the protophloem could be monitored (Fig. 95 I) but not for any other UmamiT. As already shown for the promoter activity in this cell file (Fig. 98), it could be established that also the fusion protein was transiently found in this position. Only a single young protophloem cell showed GFP (Fig. 95 K), whereas the main GFP intensity was placed more distal in the root (Fig. 95 J). Older protophloem cells completely lack of GFP signals (Fig. 95 K).

This supported the already mentioned idea of a transient expression of *UmamiTs* in the protophloem cells and supported the results obtained from cross sections, where never any signals of UmamiT-GFP could be observed in the protophloem.

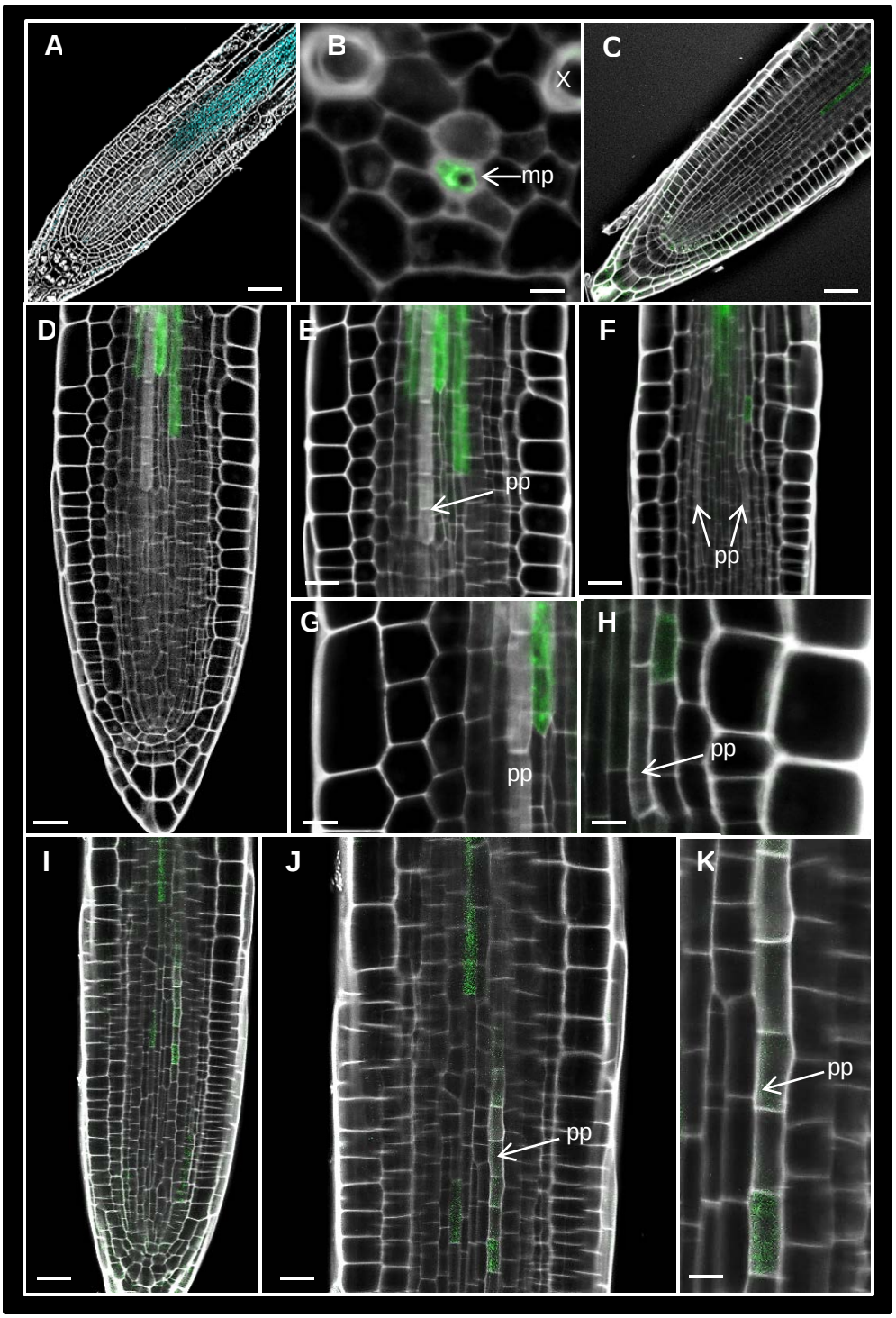

Figure 95. UmamiT localization in the root tip: focus on protophloem. (A) mPS-PI stained P_{UmamiT}: GUS root, scale bar: 45µm. (B) Cross section of a P_{UmamiT}: UmamiT-GFP root at the very tip, scale bar: 2µm. (C) root tip of a P_{UmamiT}: UmamiT-GFP seedling. (D-H) UmamiT-GFP not found in the protophloem. (D) Overview, one protophloem file is visible, UmamiT-GFP positive cells next to protophloem and in a cell file near the center of the stele, scale bar: 17µm. (E) Magnification of (D), scale bar: 12µm. (E) Root where both protophloem files are visible, scale bar: 15µm. (G) Single optical section with focus on protophloem, UmamiT-GFP is not present in the protophloem, scale bar: 7µm. (H) Magnification of (H) showing UmamiT-GFP expression in one cell next to the protophloem, scale bar: 6µm. (I) Root tip of a plant expressing UmamiT29-GFP, scale bar: 25µm, (J) Magnification of (I), only very weak GFP signals in one protophloem cell and one cell in the center of the stele, scale bar: 15µm. (K) Magnification of a protophloem cell file, GFP was found only in the youngest cell near root tip, scale bar: 5µm. X (xylem), pp (protophloem), mp (metaphloem).

5.10.1.6. Analysis of UmamiT-GFP overexpression in the root

In order to overcome the very weak GFP signals of the translational fusions at the meristematic zone of the root, overexpression lines were generated by exchanging the promoter. Overexpressors were also generated to analyze seed development and root length. It is important to note that *P*$_{UBQ10}$*: UmamiT-GFP* harbors also all introns, meaning that the full length gene is under control of the ubiquitin 10 promoter. RNA levels for each candidate were elevated by a factor of three in the overexpression lines compared to the WT (Fig. 96). In the overexpression lines bright GFP signals were found in the columella and lateral root cap cells (Fig. 97 A, B). In the columella stem cell file right behind the QC no signals could be detected (Fig. 97 B, F). A very low GFP intensity was seen directly in the QC and adjacent cells of the endodermis.(Fig. 97 F, G), where at some points a preference for polar distribution was monitored (Fig. 97 G). Looking at the whole root it was obvious that strong GFP singals were found in the two protophloem cell files (Fig. 97 A). A closer look at this area revealed that GFP signals started to appear in more differentiated cells of the protophloem strand (Fig. 97 D, I-K). Maximum of GFP intensity showed in young differentiated protophloem cells a polar distribution at the anticlinal position (Fig. 197 D), which was distinct from the cell wall (Fig. 97 C, E, H).

This results support the previously shown findings and indicate that UmamiTs can be invovled in the directed transport of amino acids in the protophloem in direction to the root tip and furthermore play a role in the distribution of amino acids in stem cells of the QC.

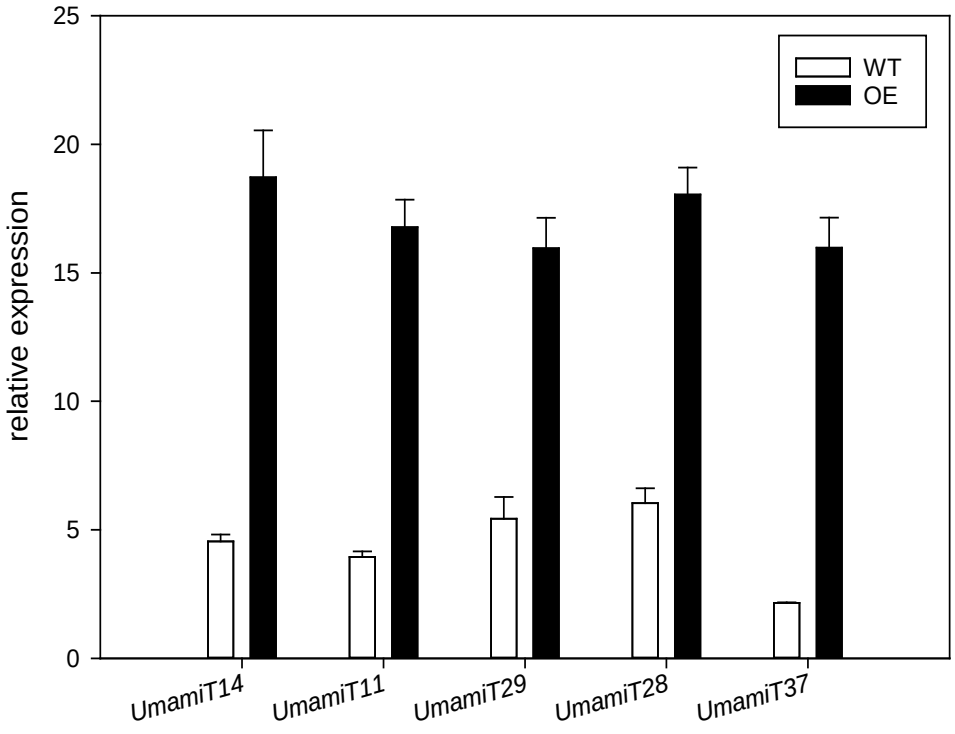

Figure 96. Overxpression of *UmamiTs* in roots. Semiquantitative real time PCR of roots from WT and *P*$_{UBQ10}$*: UmamiT-GFP* lines, normalized to UBQ10 (n=3 ± SD). Expression levels were increased by a factor of three.

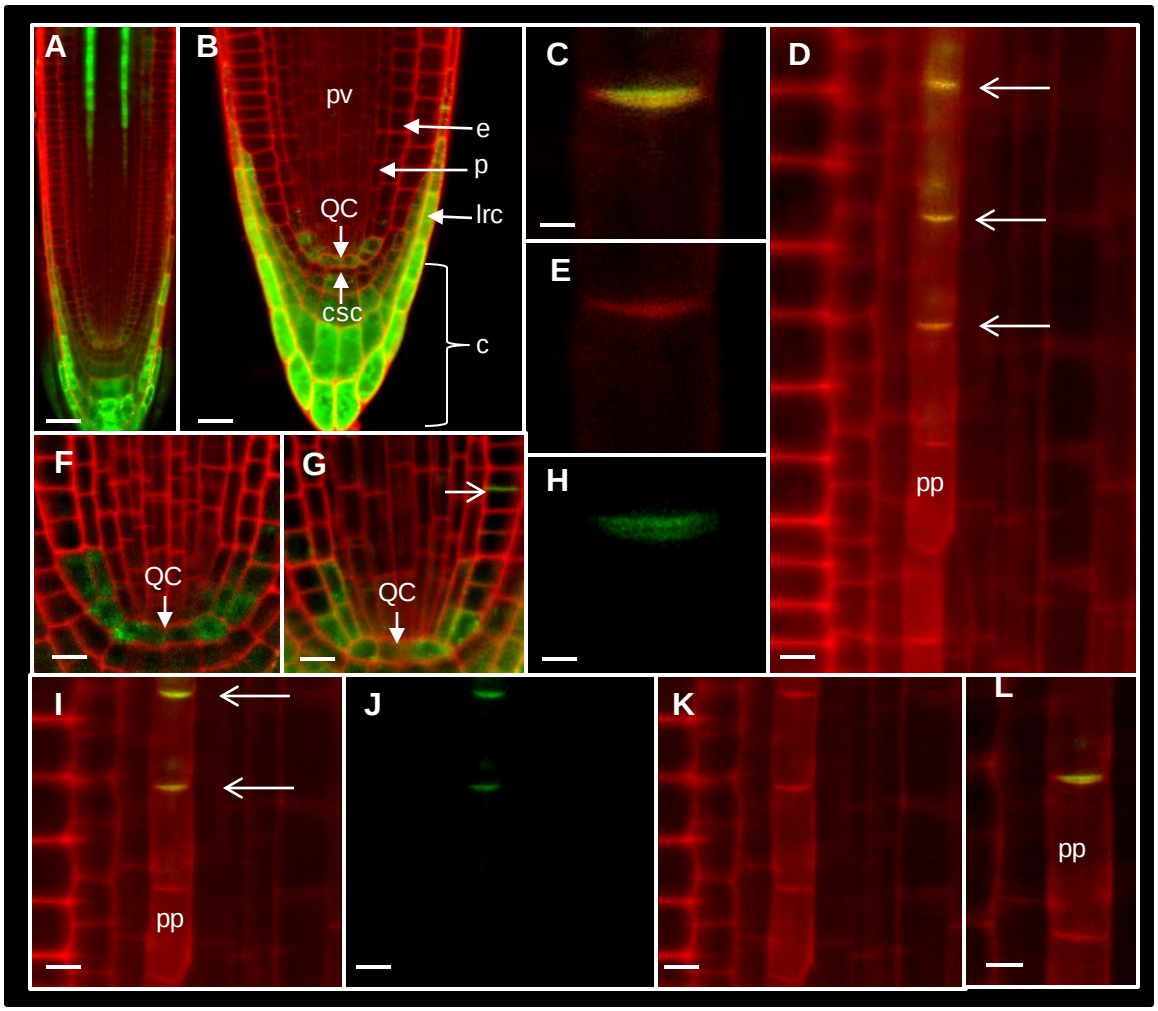

Figure 97. UmamiT-GFP overexpression in the root. (A-L) *PUBQ10: UmamiT-GFP.* (A) Overview, maximum projection, strong UmamiT-GFP signals in the columella cells, lateral root cap and the two protophloem cell files. Much weaker GFP signals in the meristematic zone, scale bar: 37µm. (B) Magnification of a root tip, scale bars: 15µm. (C, E, H) Details of the GFP distribution in anticlinal position between two protophloem cells. (C) Overlay of PI channel (E) with GFP channel (H), scale bars: 2µm. (D) UmamiT-GFP overexpression in the protophloem displayed polar distribution in the anticlinal position of older cells (arrows), scale bar: 5.5µm. (F) Magnification of the QC area from a root tip, GFP signals in the QC and adjacent cells of the endodermis, scale bar: 6µm. (G) Additional signal in the anticlinal position of an endodermis cell (arrow), scale bar: 8µm. (I-K) Magnification of one protophloem cell file showing polar distribution of GFP in more differentiated cells (arrows). (I) Overlay of GFP channel (J) with PI channel (K), scale bars: 6µm. (L) Magnification of the first protophloem cell with UmamiT-GFP signal, scale bar: 4µm. QC (quiescent center), csc (columela stem cells), lrc, (lateral root cap), p (pericycle), e (endodermis), pv (provascular cells), pp (protophloem).

5.10.1.7. UmamiTs in the root: interplay with auxin

In order to investigate if UmamiTs are regulated by phytohormones a hormonal interplay study was performed in roots to. According to the results obtained in the GUS und GFP reporter lines the comparison with the introduced marker lines strongly suggested that *UmamiT* expression is influenced by the master regulator auxin. Therefore a GUS assay was performed using plants with the GUS construct on control plates without auxin and on plates supplemented with 0.1 or 10 µM auxin. A clear correlation between the strength of GUS staining and the concentration of auxin on the plate was recognizable (Fig. 98 A-C). To quantify the result, qRT-PCR on WT plants, grown under the same conditions, was performed (Fig. 98). Again for all candidates an increase of the *UmamiT* RNA level by the additional supply of auxin could be seen. The relative expression level was increased 1.4 fold for *UmamiTs* of clade I (*UmamiT14*, *UmamiT11*), 1.6 fold for *UmamiT29* and 1.9 fold for *UmamiT28*.

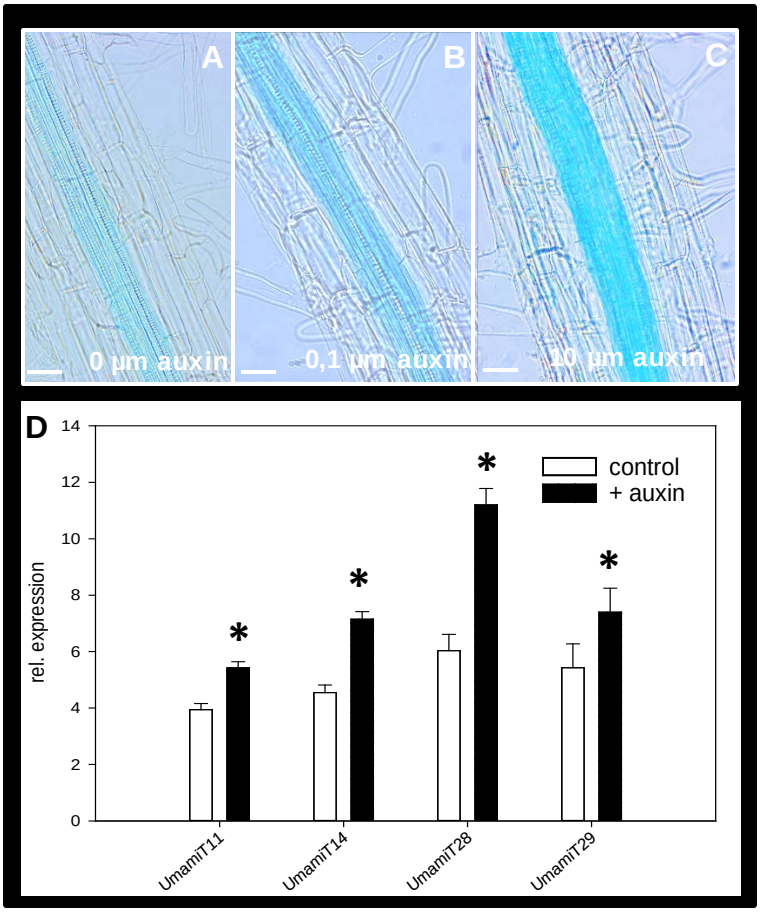

Figure 98. UmamiTs respond to auxin. (A-C) *P*$_{UmamiT}$*: GUS.* Roots of different treatments were simultaneously stained. Staining was stopped at the moment the first blue signals appeared in the vasculature of the control plants. Staining intensity increased by the addition of auxin. Scale bars: (A), (B) 35µm, (C) 25µm. (D) Semiquantitative real time PCR of roots grown on media without (control) or supplemented with 10µM auxin. Normalized to UBQ10 (n=3 ± SD). One way ANOVA followed by Holm-Sidak post hoc test.

To investigate further how this effect could be explained at the cellular level, analysis of different auxin related markers in combination with the translational fusion of UmamiT14 the root was done. Fig 99 shows a co-labeling of UmamiT14-mCherry with PIN3-GFP. An overlap of fluorescence upon the differentiation zone between PIN3 and UmamiT14 was visible (Fig. 99 A, B). It was possible to document a clear colocalization between UmamiT14 and PIN3 (Fig. 99 C-E).

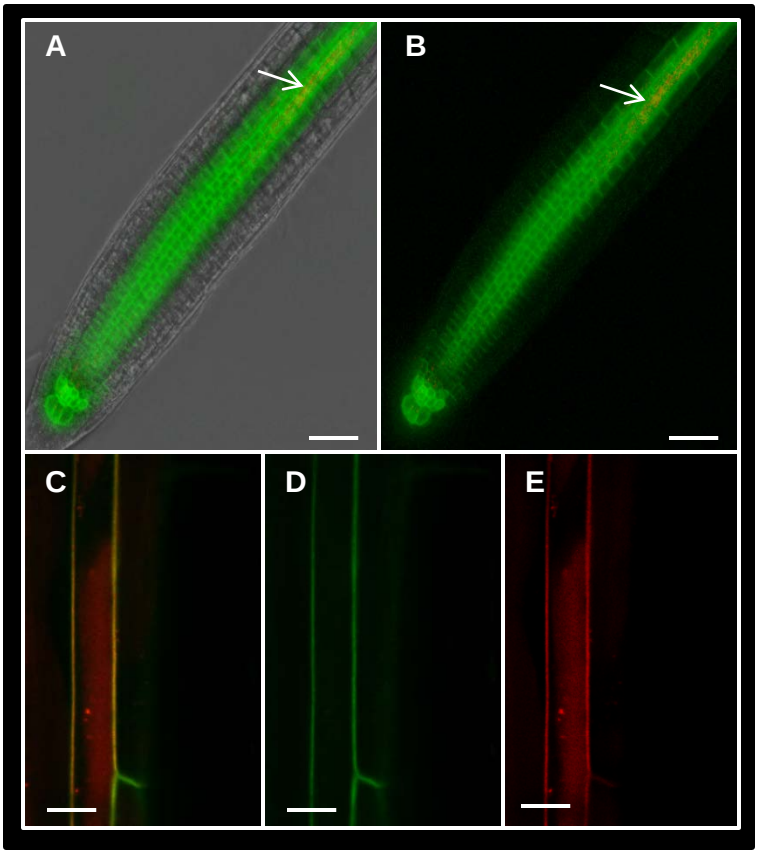

Figure 99. Coexpression of P_{PIN3}: *PIN3-GFP* and $P_{UmamiT14}$: *UmamiT14-mCherry* in the root. (A, B) Maximum projection, showing polar distribution of PIN3-GFP and signals of UmamiT14-mCherry at the differentiation zone (marked by an arrow). (A) Overlay of green and red channel with bright field image. (B) Overlay of GFP and mCherry channel; scale bars: 60µm. (C-E) Magnification of cells from the stele; assumed membrane localization of PIN3-GFP (D) and UmamiT14-mCherry (E) can be seen; (C) overlay of (D) and (E) showing the colocalization between PIN3 and UmamiT14 at the putative plasma membrane, indicated by the yellow color, scale bars: 8µm.

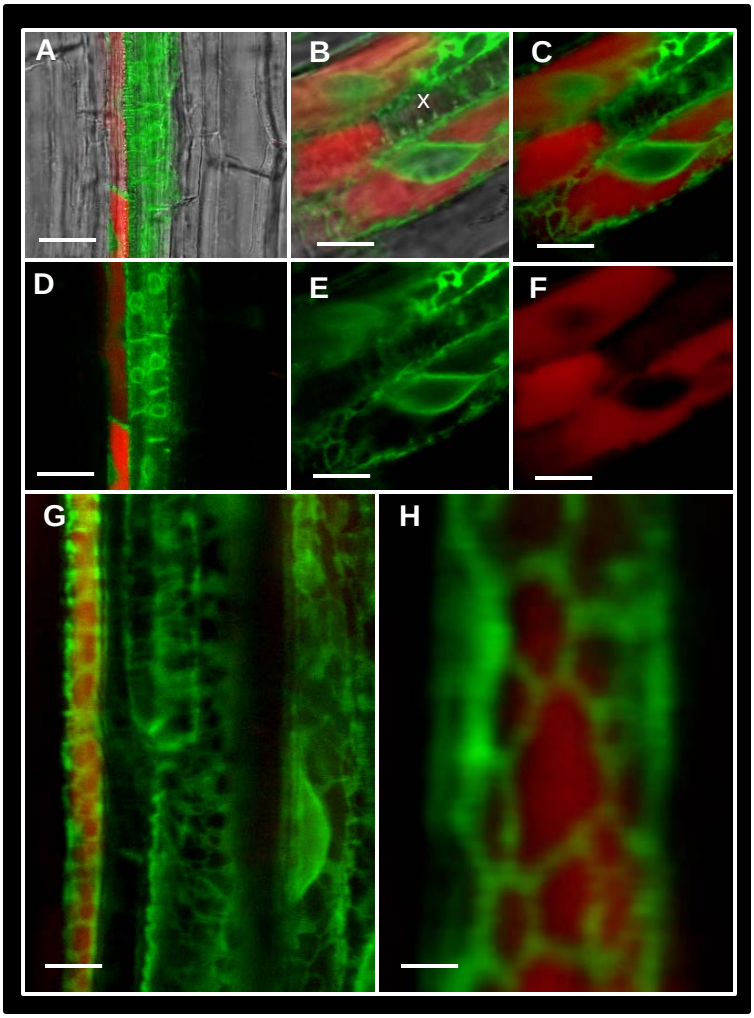

Figure 100. Coexpression of P_{DR5}: *ER-GFP* and $P_{UmamiT14}$: *UmamiT14-mCherry* in the root. (A, D) Central cylinder of a root part near tip showed intense auxin response in vascular associated cells, scale bar: 40µm. (B, C, E, F) UmamiT14-positive cells around the xylem in a part behind differentiation zone showing intense auxin response. (B) Overlay of (E, F) with bright field image. (C) Overlay of GFP and mCherry channel. (E) DR5-positive cells. (F) UmamiT14-positive cells, scale bars: 10µm. (G, H) close up from the stele shows widespread distributed DR5-GFP signals also in differentiated UmamiT14 positive cells, scale bars. (G) 5µm, (H) 1µm. X (xylem).

The next issue was to take a look at the result of polar auxin distribution, the auxin response. As a marker DR5-GFP was used. In the DR5-GFP x UmamiT14-mCherry reporter line auxin response in roots was more widespread distributed than the expression of UmamiT14 (Fig. 100 A, D). The maximum of GFP was seen in the cell files of the stele. In those cells that showed UmamiT14-mCherry an auxin response was noticeable, visualized by the ER bounded GFP (Fig. 100 B, C, E, F). This shows that indeed UmamiT14-positive cells respond to auxin. These new findings explain why an activation of promoter activity by the additional supply of auxin on plates could be monitored and why the *UmamiT* RNA levels were elevated if more auxin was distributed along the root, suggesting that the expression dynamics of *UmamiTs* in roots is actively and fast regulated by the phytohormone auxin and thus capable to respond to the demand of amino acids.

5.10.1.8. Immunolocalization of different marker lines in roots

In order to characterize the cell type of DR5, PIN3, TCS, PD1 and SCR positive cells in the root immunolocalization experiments using α-GFP and α-RS6 as a marker for sieve elements were performed. The big advantage of cross sections also in older root tissues is to see where the cells of the different markers are positioned in the stele and how they are associated with sieve elements. By this method it is possible to investigate if sieve elements clolocalize with any marker and to draw conclusions about their origin in the tissue. In the vasculature it was observed that cells showing auxin response were located in the parenchyma tissue but no colocalization between the α-GFP and α-RS6 epitope in sieve element was detected (Fig. 101 A-H). This indicates that auxin response was restricted to the vascular cylinder, as previously suggested (Absmanner et al. 2013). Similar results were obtained for the histological localization of PIN3 in the root at the position where the xylem axis is closed. Additionally, colocalization in the phloem poles in sieve elements was found in older roots (Fig. 101 L, M). In younger roots, PIN3-GFP signals were restricted to the xylem parenchyma and not found to be located at the phloem (Fig. 101 I-K), suggesting that the newly formed sieve elements originate from parenchyma tissues. In contrast to auxin response signals for cytokinin response were differently distributed along the root. TCS-positive cells were found exclusively in the phloem pole, where many of them showed colocalization with sieve elements next to cells that were decorated exclusively with GFP (Fig. 102 A-D). This could be a further hint that these sieve elements originated from the phloem parenchyma. The protophloem/sieve element marker PD1 was also located in the phloem poles. GFP-marked cells in the cross section were perfectly colocalizing with RS6 (Fig. 102 E-K). According to their anatomical position, i.e. not directly adjacent to the pericycle, these cells can be classified as metaphloem (Esau 1969). In younger parts of the root that were closer to the root tip it was possible to find simultaneously signals of PD1 in the protophloem cells besides the colocalization with RS6 in the metaphloem (Fig. 102 L-P). This indicates that PD1-GFP signals are found in sieve elements due to the differentiation process of the protophloem, where signals of PD1 disappeared as it gets mature. As expected and previously shown, SCR-GFP was restricted to the endodermis and did not show colocalization with cells from the phloem poles or any other cell from the vascular tissues (Fig. 103 A-D).

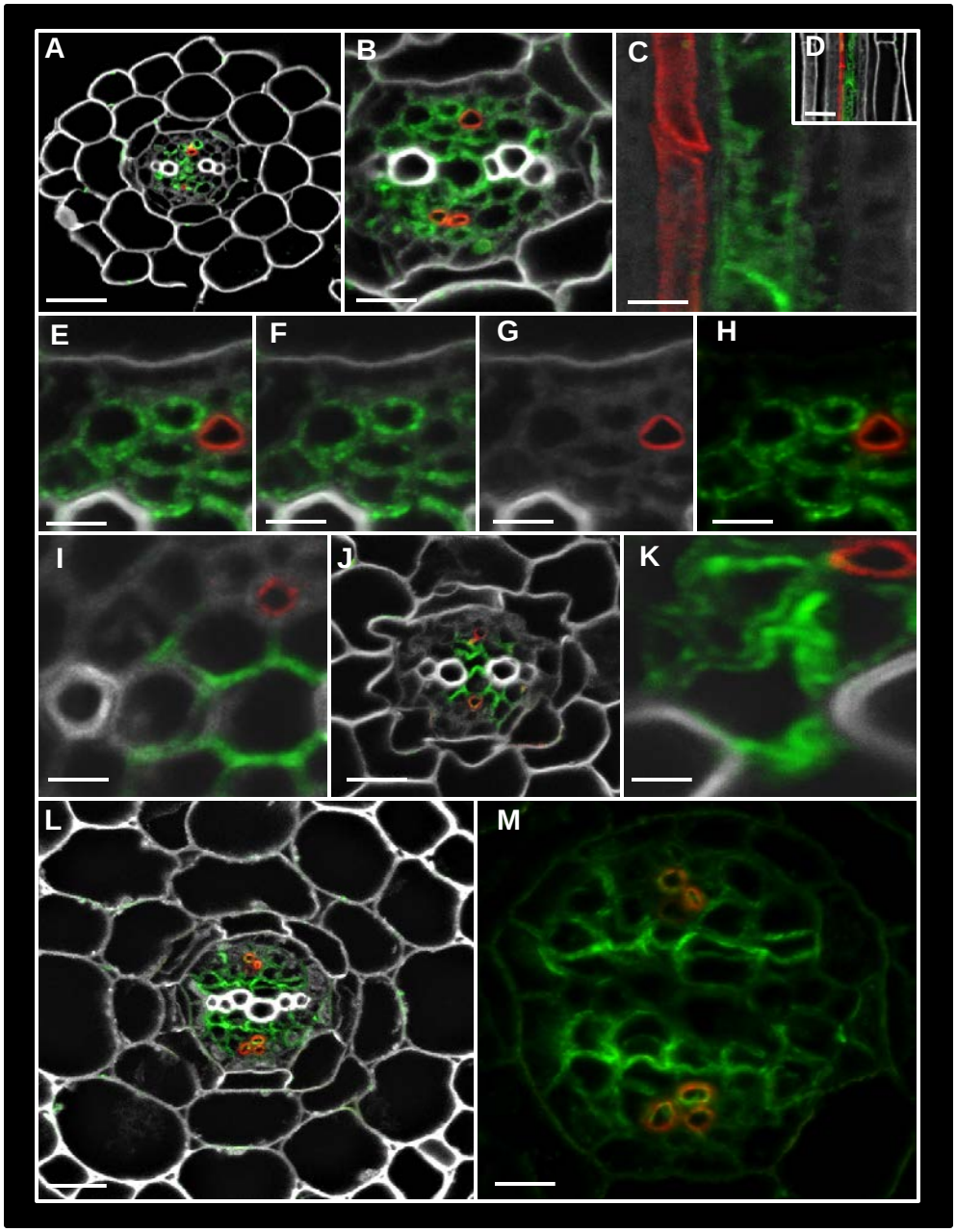

Figure 101. Immunolocalization of DR5 and PIN3 positive cells in the root. Green cells: α-GFP, detected with a CY2-antiserum, representing GFP positive cells; red cells: α-RS6 detected with an AF594-coupled antibody, representing sieve elements, white color: autofluorescence. (A-H) Immunolocalization of DR5-GFP. (A) Overview of a cross section from a young root, scale bar: 24µ. (B) Magnification of the stele, DR5 positive cells in parenchymatic tissue and the phloem poles, scale bar: 10µm. (C, D) Longitudinal section shows distinct signals for DR5-GFP and RS6 in different cells that were neighboring each other. (C) Magnification from the overview shown in (D), scale bars: (C) 5.5µm, (D) 20µm. (E-H) DR5 positive cells show no colocalization with sieve element. (E) Overlay of fluorescence channel (H) with autofluorescence channel. (F) DR5 positive cells. (G) Sieve elements. Scale bars: 4.5µm. (I-M) Immunolocalization of PIN3-GFP. (I) Magnification of the vascular tissue before metaxylem differentiated, PIN3-GFP shows signals in the vascular parenchyma at the xylem axis, scale bar: 12µm. (J) Overview of a cross section from a young root, PIN3 located in the parenchymatic cells distinct from sieve elements, scale bar: 20µm. (K) Magnification of the stele shows that PIN3 positive cells are close to sieve elements but do not colocalize with them in roots where the xylem axix ist not closed, scale bar: 6µm. (L) Overview of a cross section from a root with closed xylem axis, scale bar: 20µm. (M) Magnification of the stele, overlay of green and red channel shows colocalization in the phloem poles with sieve elements, scale bar: 6.5µm.

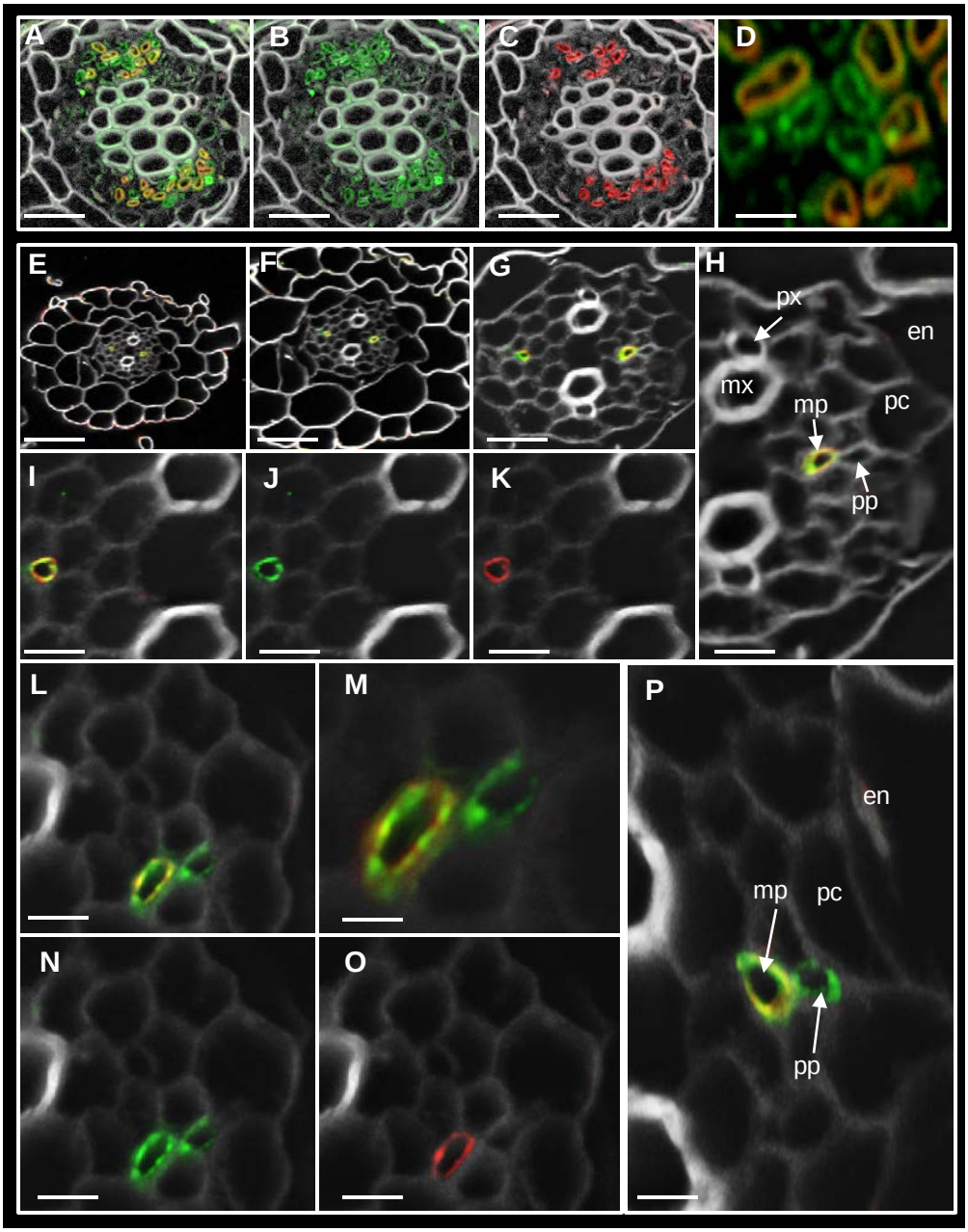

Figure 102. Immunolocalization of TCS and PD1 positive cells in the root. Green cells: α-GFP, detected with a CY2-antiserum, representing GFP positive cells; red cells: α-RS6 detected with an AF594-coupled antibody, representing sieve elements, white color: autofluorescence, yellow color: colocalization between α-GFP and α-RS6. (A-D) Immunolocalization of TCS-GFP. (A) TCS positive cells found in the phloem poles, where they are partially colocalizing with sieve elements. (B) TCS positive cells in the two phloem poles. (C) Sieve elements, scale bars: 17µm. (D) Magnification of one phloem pole; cells with double decoration of GFP and RS6 are next to cells only marked by α-GFP, scale bar: 4 µm. (E-P) Immunolocalization of PD1-GFP. (E) Overview of a cross section, scale bar: 37µm. (F, G) Magnifications of the stele, overlay of green and red channel shows colocalization in the phloem poles with sieve elements, scale bars: (F) 26µm, (G) 12µm. (H) Magnified segment of the stele, colocalization occurs in the sieve element belonging to the metaphloem, scale bar: 8µm. (I-K) Overlay of PD1 positive cells (J) with sieve element (K), scale bars: 6µm. (L-P) Part of the root little bit younger than (E). A clear colocalization between PD1 and RS6 appeared in the metaphloem. Protophloem is only decorated by PD1. (L) Overlay of PD1 psoitive cells (N) with sieve elements (O), scale bar: 5µm. (M) Magnification of protophloem and metaphloem cell form (L), scale bar: 2µm. (P) Magnified segment of the stele, colocalization occurs in the sieve element belonging to the metaphloem, protophloem only PD1 positive, scale bar: 4µm PX (protoxylem), mx (metaxylem), pp (protophloem), mp (metaphloem), en (endodermis), pc (pericycle).

5.10.1.9. Characterization of UmamiT-positive cells in the root by immunolocalization

In order to investigate if UmamiTs are colocalizing with SEs in the root, immunolocalization experiments with α-GFP to detect UmamiT-GFP and α-RS6 (sieve element epitope) were done. In the young primary roots, UmamiTs were found exclusively in the xylem parenchyma and no overlap with signals in the phloem poles, marked by the RS6 labeled sieve elements was observed (Fig. 104). This was true for all clade I and clade III UmamiTs.

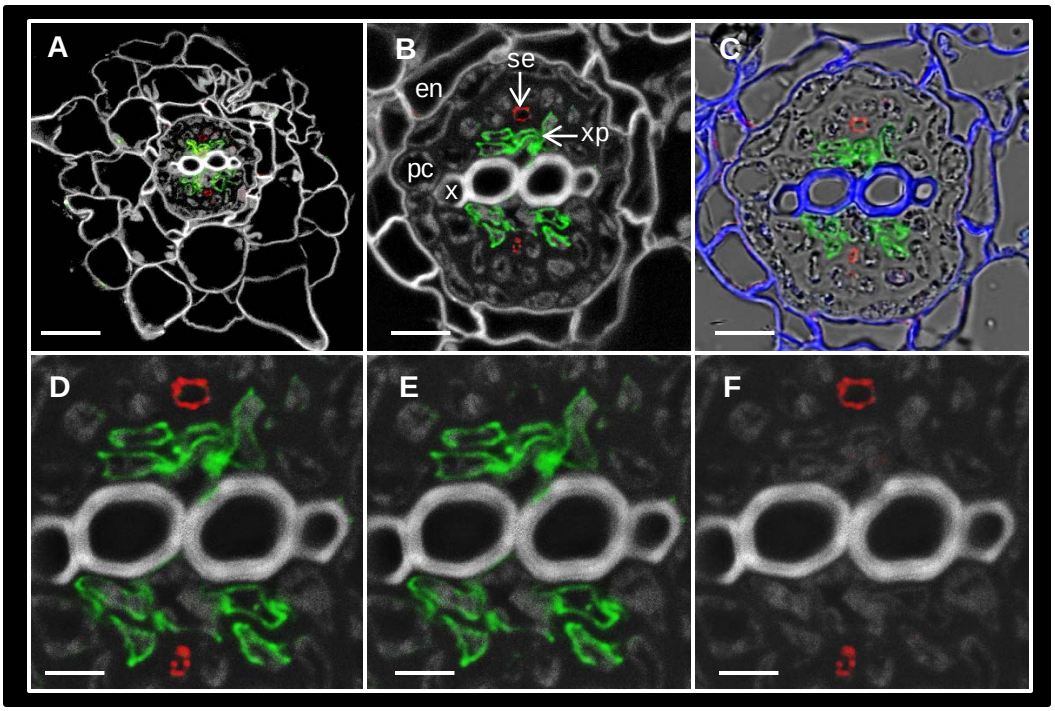

Figure 104. UmamiTs are not SE-localized in the primary root. Immunolocalization of a primary root at the root hair zone. Green cells: α-GFP, detected with a CY2-antiserum, representing UmamiT-GFP positive cells; red cells: α-RS6 detected with an AF594-coupled antibody, representing sieve elements, white color: autofluorescence. (A) Cross section at root hair zone, scale bar: 18µm. (B) Central cylinder of the cross section showing endodermis, pericycle and vascular cylinder, (C) Overlay with bright field image, blue color: lignified cells, scale bar: 7µm. (D-F) No colocalziation between sieve elements and UmamiT-positive cells. (D) Overlay of (E) α-GFP signals and (F) α-RS6 decorated cells, scale bar: 3.5µm. X (xylem), se (sieve element), xp (xylem parenchyma), en (endodermis), pc (pericycle).

Colocalization between the sieve elements and UmamiTs first appeared when five mature metaxylem vessels in exist in the xylem axis, (Fig. 105 A, B). This colocalization persisted when the root started to enter the secondary state (Fig. 105 C). Also in very old parts of the roots, when a severe increase of the xylem vessel diameter occurred, the colocalization with sieve element marker RS6 in the phloem tissue could be observed (Fig. 105 D, E).

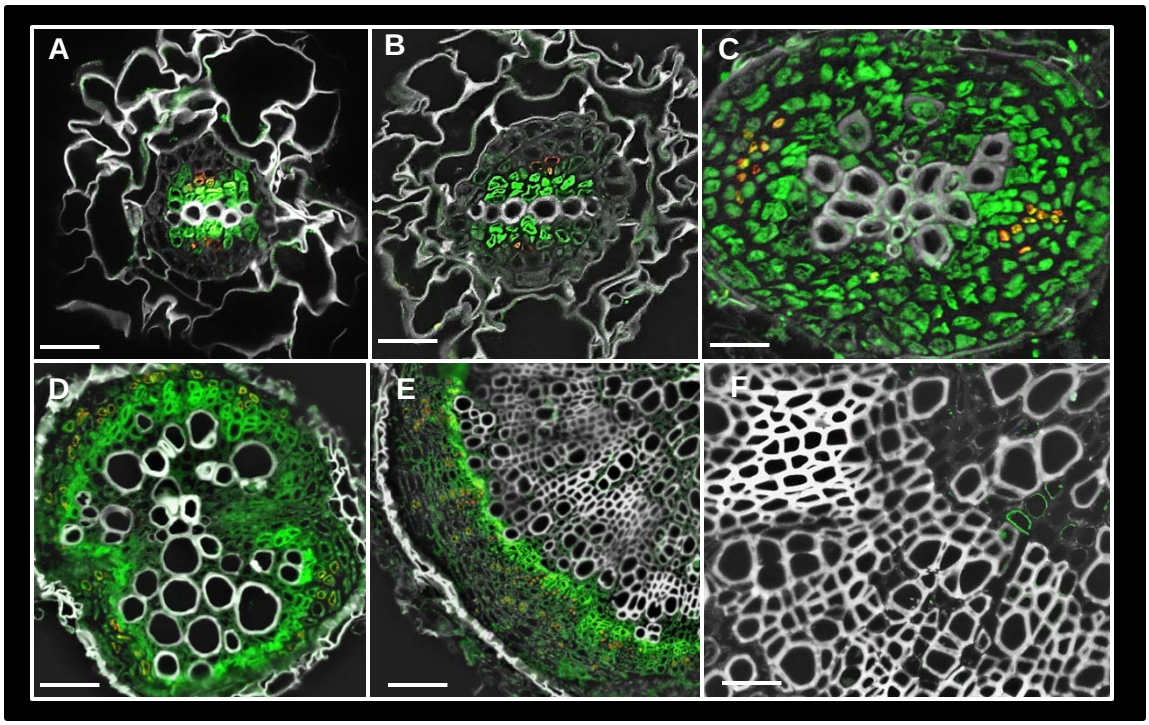

Figure 105. UmamiTs are found in SEs of roots from the onset of secondary growth. (A-E) Cross-sections of roots of different ages. (A) About 700µm behind the root tip, (E) 500 µm in front of the hypocotyl, at (C) secondary growth. (F) Magnification of the xylem vessel population in a root that has undergone extensive secondary growth showing few UmamiT-positive cells. Green cells: α-GFP, detected with a CY2-antiserum, representing UmamiT-GFP positive cells; red cells: α-RS6 detected with an AF594-coupled antibody, representing sieve elements, white color: autofluorescence. Scale bars: (A) 30µm, (B) 24µm, (C) 20µm, (D) 25µm, (E) 50µm. (F) 20µm.

Figure 113 shows the results of the immunolocalization of older roots, where colocalization was apparent in detail. Even before the secondary stage in the root was observed (Fig. 106, A-C) a colocalization between sieve element marker RS6 and UmamiT-GFP was documented (Fig. 106 D-L).

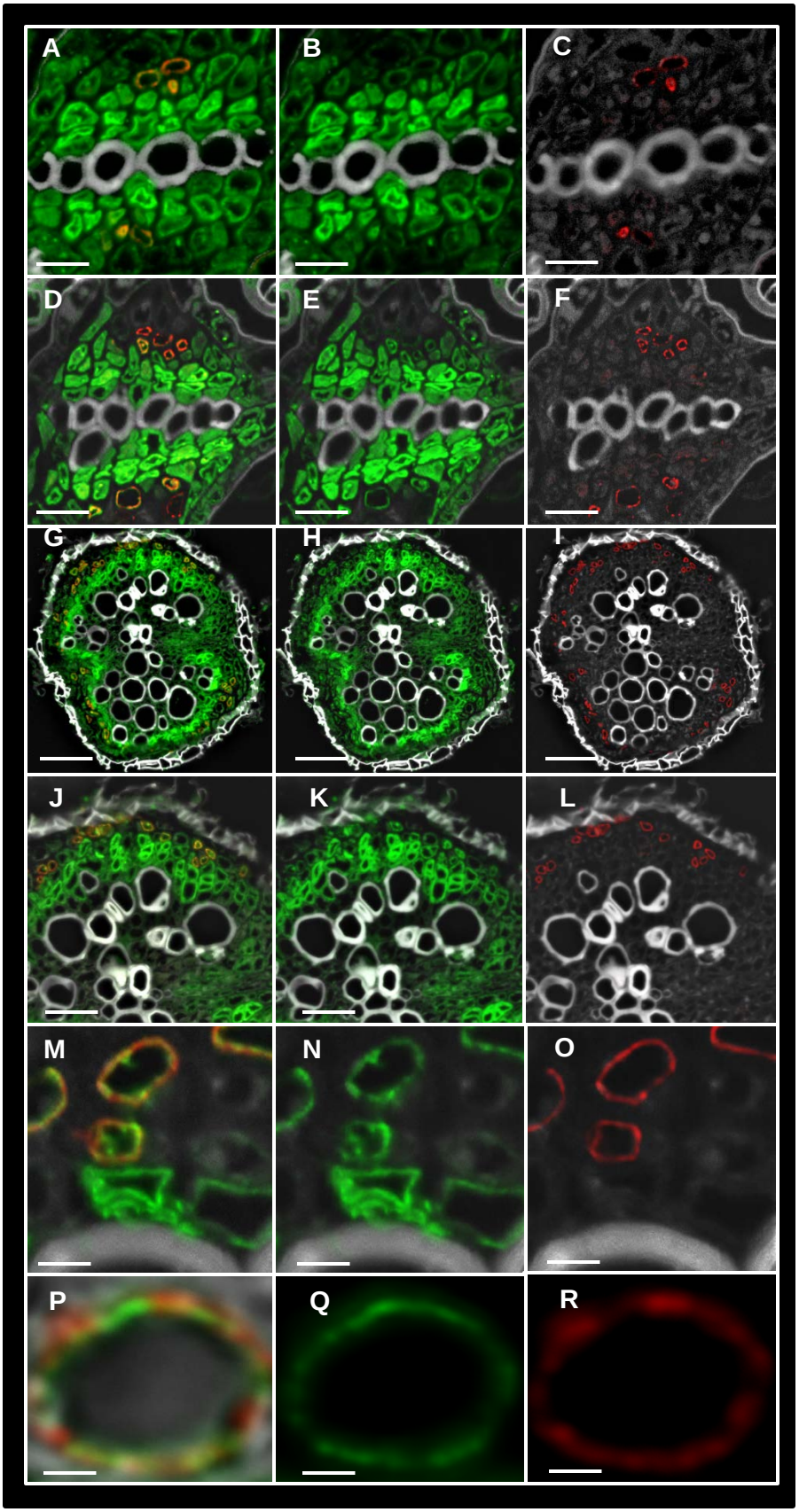

Figure 106 UmamiTs are found in SEs of roots from the onset of secondary growth. Immunolocalization of older roots, increasing age from top to bottom; Green cells: α-GFP, detected with a CY2-antiserum, representing UmamiT-GFP positive cells; red cells: α-RS6 detected with an AF594-coupled antibody, representing sieve elements, yellow color: colocalization between α-GFP and α-RS6, white color: autofluorescence. (A, D, G, J, M, P) Merge of α-GFP and α-RS6. (B, E, H, K, N, Q) signals coming from α-GFP (UmamiT positive cells). (C, F, I, L O, R) Sieve elements. Scale bars: (A-C) 10µm, (D-F) 12µm, (G-I) 40µm, (J-L) 20µm, (M-O) 5µm, (P-R) 1µm.

In the roots that had undergone extensive secondary growth, it could be observed very clearly how UmamiT-positive cells originate near the xylem and then are pushed to the periphery, where most of them differentiated to sieve elements (Fig. 107 A-D).This observation, based on immunolocalization, was uniformly distributed across the complete surface of the cross section (Fig. 107 E-J). How close differentiated sieve elements and parenchymatic cells of different size stand together is illustrated in Fig. 107 K-M. Colocalization between α-RS6 and α-GFP indicated again that at least in the precursor cell UmamiT-GFP was present.

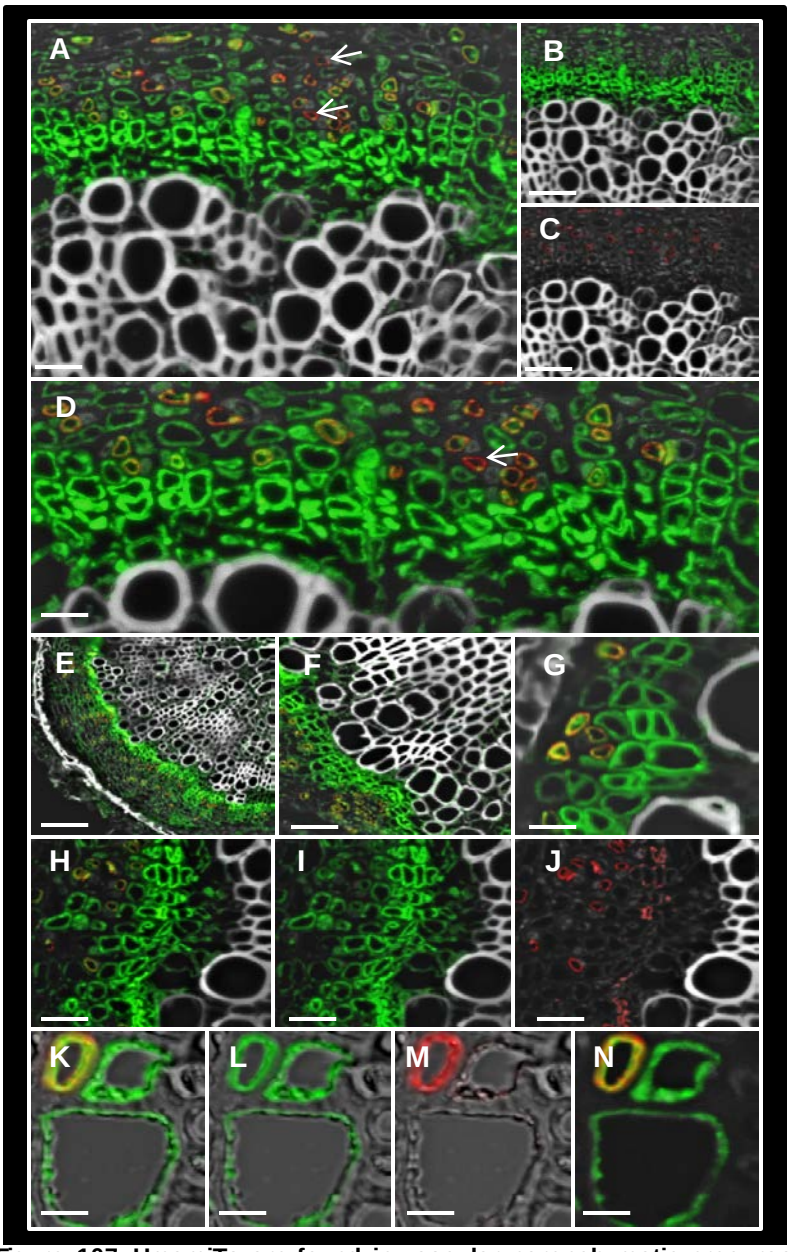

Figure 107. UmamiTs are found in vascular parenchymatic precursor cells for sieve elements. (A-D) Magnification of the central vascular cylinder of a root that has undergone secondary growth showing differentiating parenchyma cells in the phloem region, note the distribution of green UmamiT cells and the presence of some sieve elements without double decoration (only red, not yellow colored indicated by an arrow), scale bars: (A) 20µm, (B, C) 35µm. (D) Magnification of (A), scale bar: 12µm. (E, F) Segment of a very old root cylinder; accumulation of UmamiT positive cells at the xylem, colocalization in the phloem region with sieve elements detected; scale bars: (E) 60µm, (F) 15µm. (G) Detail of a younger secondary root, scale bar: 10µm. (H-J) A little bit older stage than (G), UmamiT positive cells more distributed in the peripheral tissues, scale bar:18µm. (K-O) Three cells of different size at the transition zone to the phloem, all show α-GFP decoration; one cells is colabeled with α-RS6 epitope. (K) Overlay with bright field image; (L) CY2 channel (cells with UmamiT-GFP decoration), (M) AF594 channel (sieve element). (O) Overlay of (L) and (M) with autofluorescence, scale bar: 5µm.

5.10.1.10. Validation of the sieve element identitiy of UmamiT positive cells by marker lines

The previous immunolocalization data showed that, after secondary growth in roots, UmamiT-GFP was associated with the vascular parenchyma and displayed colocalization in sieve elements decorated with the RS6 epitope. A consideration that should be taken into account is that in immunolocalizations there is a risk to detect only the remaining epitope that was built in the cell in earlier times. To overcome this constrain, several coexpression studies with phloem or sieve element specific markers were done, that allowed a much clearer temporal resolution between the appearance of UmamiTs and the sieve element marker. Due to the observation that *UmamiTs* had an overlapping expression in the root all investigations for this study were performed using UmamiT14-mCherry as a representative example. This construct showed predominantly a vacuolar localization of the fusion protein, due to the different turnover of mCherry in the cell and the degradation of the fluorophore in the vacuole.

1.1.1.3.1. UmamiT14 colocalized in cells with SE-ENOD promoter activity

Sieve elements accumulate a nodulin-like (SE-ENOD, RS6) protein in the plasma membrane before they differentiate (Khan et al. 2007). The promoter of this protein was fused to ER-localized GFP (Werner 2011) in order to visualize the expression pattern in young sieve elements before the RS6 epitope was present. Coexpression with UmamiT14-mCherry showed that, in the vascular tissue of roots, promoter was found in single cells in collateral position to the xylem, which was surrounded by a population of cells exclusively labeled by UmamiT14-mCherry (Fig. 108 A, B). In roots of about 1mm distance to the tip, it could be documented that cells showing SE-ENOD promoter activity were UmamiT14-positive and close to parenchymatic cells only showing UmamiT14-mCherry signals (Fig. 108 D-F).
This indicates that some cells of the UmamiT14 cell population started to differentiate into sieve elements.

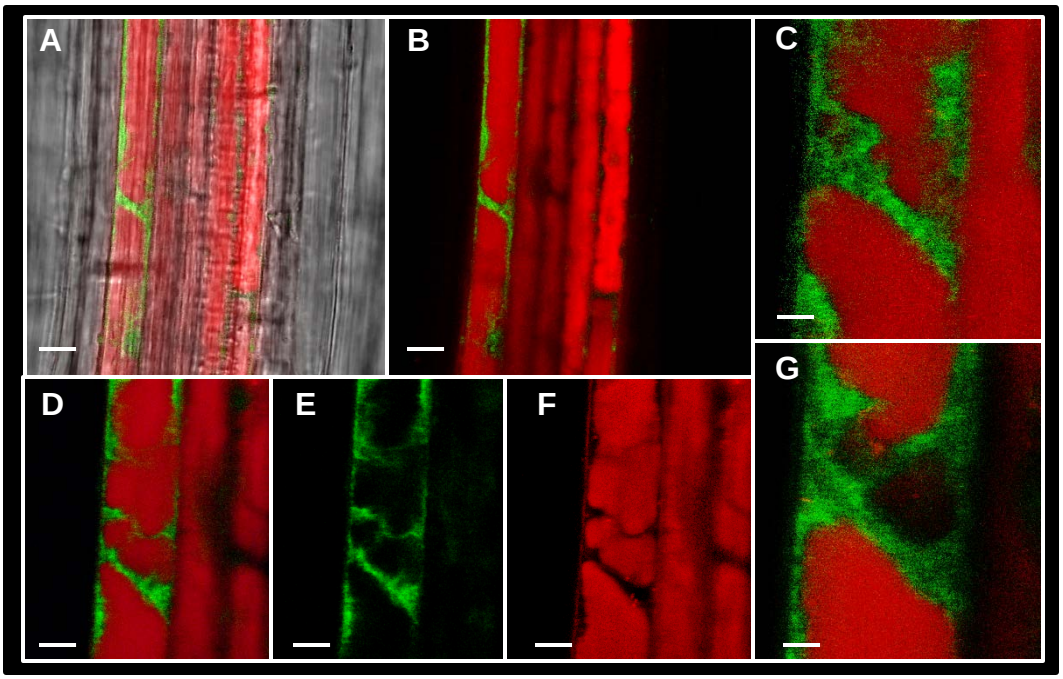

Figure 108. Coexpression of $P_{UmamiT14}$: *UmamiT14-mCherry* and $P_{SE\text{-}ENOD}$: *ER-GFP* in the root. (A, B) Optical section through the stele of a root, ER bound GFP seen in two cells from the vasculature with mCherry signals. (A) Overlay of fluorescence channel (B) with bright field image, scale bars: 10µm. (C, G) Magnifications of cells with overlapping signals of ENOD-GFP and UmamiT14-mCherry. (C) Two cells of the stele, only the border cells shows coexpression, scale bar: 2.2µm. (G) magnification of a single cell, scale bar: 2µm. (D-F) Coexpression occurs only in a single cell file within the vascular tissue. (D) Overlay of GFP channel (E) with mCherry channel (F), scale bars: 5.5µm.

1.1.1.3.2. UmamiT14 colocalized with APL in differentiating sieve elements

APL (Altered Phloem Development) is a MYB transcription factor involved in phloem differentiation (Bonke et al. 2003). Its expression is highly similar to the protophloem marker PD1 but occurred before PD1. Coexpression with UmamiT14-mCherry showed, that in roots of about 400µm distance to the tip, there is no overlap with APL-GFP. Sieve elements and parenchyma cells were close to each other but showed distinct signals of GFP and mCherry (Fig. 109 A, B). In roots behind the root hair zone more cells were UmamiT14-positive and in some of them coexpression between APL-GFP and UmamiT14-mCherry (Fig. 109 C, D) could be documented. This indicates that UmamiT-positive cells started behind the root hair zone to differenciate into sieve elements. Also in root tissue of about 1mm distance to the tip only a limited number of cells depicted coexpression next to cells where only signals form UmamiT14-mCherry occurred (Fig. 109 E-G). UmamiT14 and APL co-occur in single cells of the vasculature, indicating a differentiation of UmamiT14-positive cells to sieve elements.

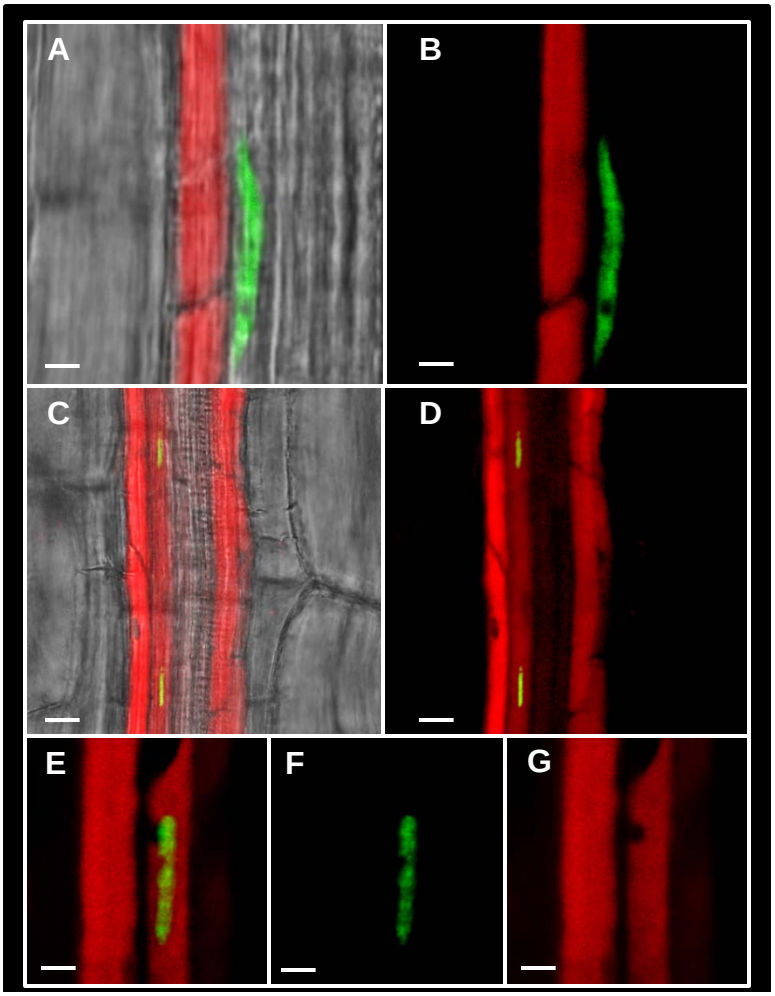

Figure 109. Coexpression of $P_{UmamiT14}$: *UmamiT14-mCherry* and P_{APL}: *APL-GFP* in the root. (A, B) Young root in about 400µm distance to the root tip shows distinct signals of UmamiT14-mCherry and APL-GFP in the vascular tissue. (A) Overlay of (B) with bright field image, scale bars: 2.8µm. (C, D) Older root in about 1mm distance to the root tip. More cells in the stele were UmamiT14 positive, coexpression with APL-GFP occurred in two cells. (C) Overlay of (D) with bright field image, scale bars: 14µm. (E-G) Magnification of two cells, coexpression with APL occurred in one cell. (E) Overlay of (F) GFP channel with (G) mCherry channel, scale bars: 5µm.

1.1.1.3.3. UmamiT14 colocalized with PD1 in sieve elements

Additionally to the presence of APL in sieve elements the marker PD1 was also studied, because this marker is also present in the metaphloem and thus marking also already differentiated sieve elements. One advantage to use an additional marker for the phloem is that APL and PD1 have a different temporal expression pattern and enable a detailed view on the time window where the colocalization with UmamiTs appeard. The protophloem marker PD1-GFP (Bauby et al. 2006) is located also in sieve elements and is thus suitable to validate the presence of UmamiT14-mCherry in sieve elements. Coexpression of PD1-GFP with UmamiT14-mCherry showed in the primary root no overlap as reported before by immunolocalization (Fig. 104). As the xylem showed secondary thickening in young roots, first red spots appeared in the sieve element cell file (Fig. 110 B, C). In about 1mm distance from the tip of the root, the same observations were made, but more vesicular UmamiT14-mCherry spots were seen within sieve elements marked by PD1-GFP (Fig. 110 E-H). Also the number of cells with UmamiT14-mCherry decoration increased with the age of the root (Fig. 110 J-L). Cross sections of roots that had undergone extensive secondary growth (Fig. 110 M) showed colocalization of UmamiT14-mCherry with PD1-GFP marked cells in the phloem (Fig. 110 N-P). Beside that it was monitored that also some cells within the phloem population showed exclusively m-Cherry fluorescence without an overlap with GFP (Fig. 110 M, N). Sieve elements positive for UmamiT14 and PD1 showed independent of the age vesicular red spots in primary roots above the root hair zone (Fig. 110 I) and in the vasculature of roots that had undergone secondary growth (Fig. 110 D). The ER localization of PD1 revealed that those vesicles were surrounded by the ER (Fig. 110 A).
This results indicate that UmamiTs are found in functional sieve elements where they can play a role in the amino acid export from the phloem. Furthermore it is possible that UmamiT-positive cells function as progenitor cells for sieve elements.

In summary the results revealed that parenchymatic UmamiT-positive cells can differentiate into sieve elements, which means that similar to the RS6 epitope UmamiTs are built in the undifferentiated parenchymatic cells and remain later on in the differentiated sieve elements, from where they were detected by immunolocalization.

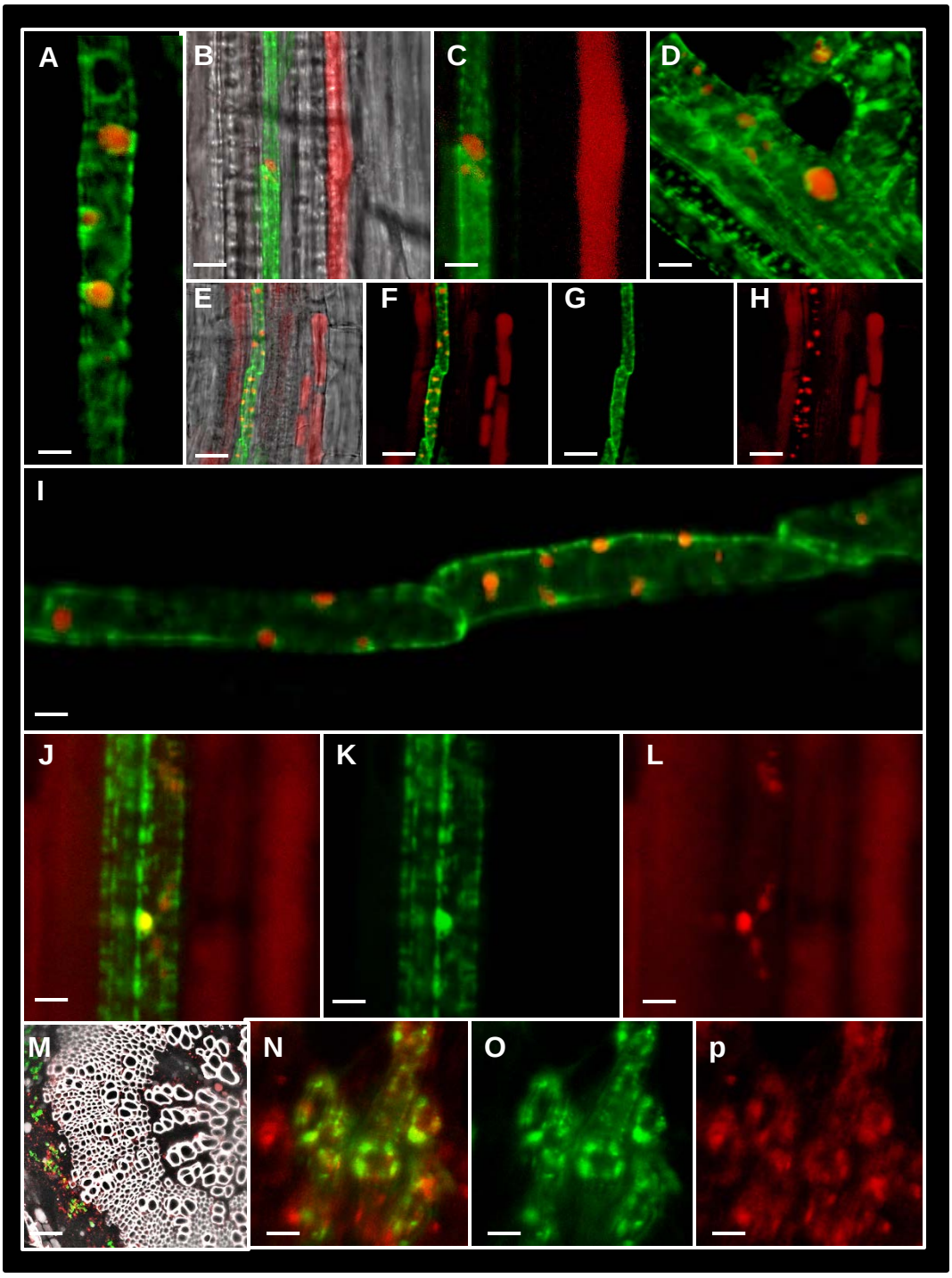

Figure 110. Sieve elements are UmamiT and PD1 positive. Colabeling of sieve elements with *P*$_{UmamiT14}$*: UmamiT14-mCherry* and *P*$_{PD1}$*: ER-GFP* in the root**.** (A) Single sieve element with red vacuole like spots, scale bar: 3µm. (B, C) Primary root. (B) Overlay with bright field image. (C) Magnification of the fluorescence channel, small red spots in the young sieve element, scale bars: (B) 7µm, (C) 4µm. (D) Sieve elements from a root that has undergone secondary thickening, mCherry spots still visible inside the cells, scale bar: 5µm. (E-H) Older root, that has undergone secondary thickening, shows brighter signals of UmamiT14-mCherry and red spots inside the sieve element file, marked by PD1. (E) Overlay of (F) with bright field image. (F) Overlay of the GFP channel (G) with mCherry channel (H), scale bars: 10µm. (I) Magnification of (F) shows distinct red spots inside mature sieve elements, scale bar: 3µm. (J-L) Vasculature from an old root with several sieve element cell files. (J) Overlay of GFP channel (K) and mCherry channel (L), scale bars: 2.5µm. (M) Cross section from an old secondary root, scale bar: 60µm. (N-P) Magnification of a population of cells from a cross section shows in many cells cololcalization between PD1-GFP signals in sieve elements and UmamiT14-mCherry. (N) Overlay of GFP channel (O) and mCherry channel (P), scale bars: 4µm.

5.11. Analysis of the root-knot nematode feeding site by different marker lines: focus on giant cell associated tissue

The infection with the nematode *Meloidogyne incognita* leads to the formation of a pathogenic feeding site, called root-knot. Root knots are a tumor like structure of the root which originates from the vascular cylinder. The extreme changes in the morphology are encompassing dramatic changes in the hormonal homeostasis, the distribution of transport proteins and the formation of phloem tissue in the feeding site. Key regulators in this process are the phytohormones auxin and cytokinin. To investigate which cells respond to auxin and cytokinin during infection the already introduced DR5-GFP and the improved version of the TCS-GFP marker line were monitored. Concerning auxin the results of Absmanner (2013) could be verified. Cytokinin response occurred in the tissue surrounding the giant cells (Fig. 111 A-D). Accumulation of GFP was seen in the population of cells neighboring giant cells (Fig. 111 D). No auxin response or cytokinin response was seen in the mature giant cells.

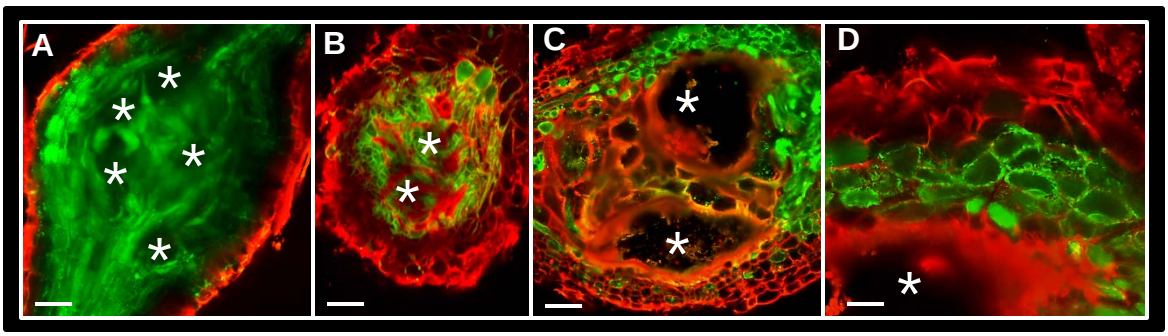

Figure 111. Cytokinin response in root-knots. (A-D) Cytokinin response visualized by *PTCS: ER-GFP*. (A) Overview of a gall with several giant cells, scale bar: 60µm. (B) Cross section above the giant cells; GFP signals in the vascular tissue, scale bar: 35µm. (C, D) Cross section from a root-knot. TCS-GFP in cells adjacent to giant cells but not inside giant cells, scale bars: (C) 40µm, (D) 15µm. Asterisks mark giant cell.

To extend the results obtained previously (Absmanner et al. 2013) and to get an impression about the auxin fluxes at the feeding site the GFP distribution of PIN3-GFP and PIN7-GFP marker lines were monitored. Accrding to array data from Hammes (2006), these transporters were induced in the root-knot upon infection. At the very beginning of giant cell development a GFP signal for PIN3 was obtained in the vasculature and in some of the giant cell precursors (Fig. 112 A, C, D), which were located in center of the stele surrounded by non-fluorescent cells (Fig. 112 B). After establishment of the feeding site the GFP signal was not seen any more in the giant cells, but in tissues neighboring them (Fig, 112 E-G). A similar result was obtained for PIN7-GFP (Fig. 112 H). Cross sections showed that in the mature root knot the GFP signal for PIN proteins was located in cells next to the giant cells and completely absent from giant cells (Fig. 112 I).

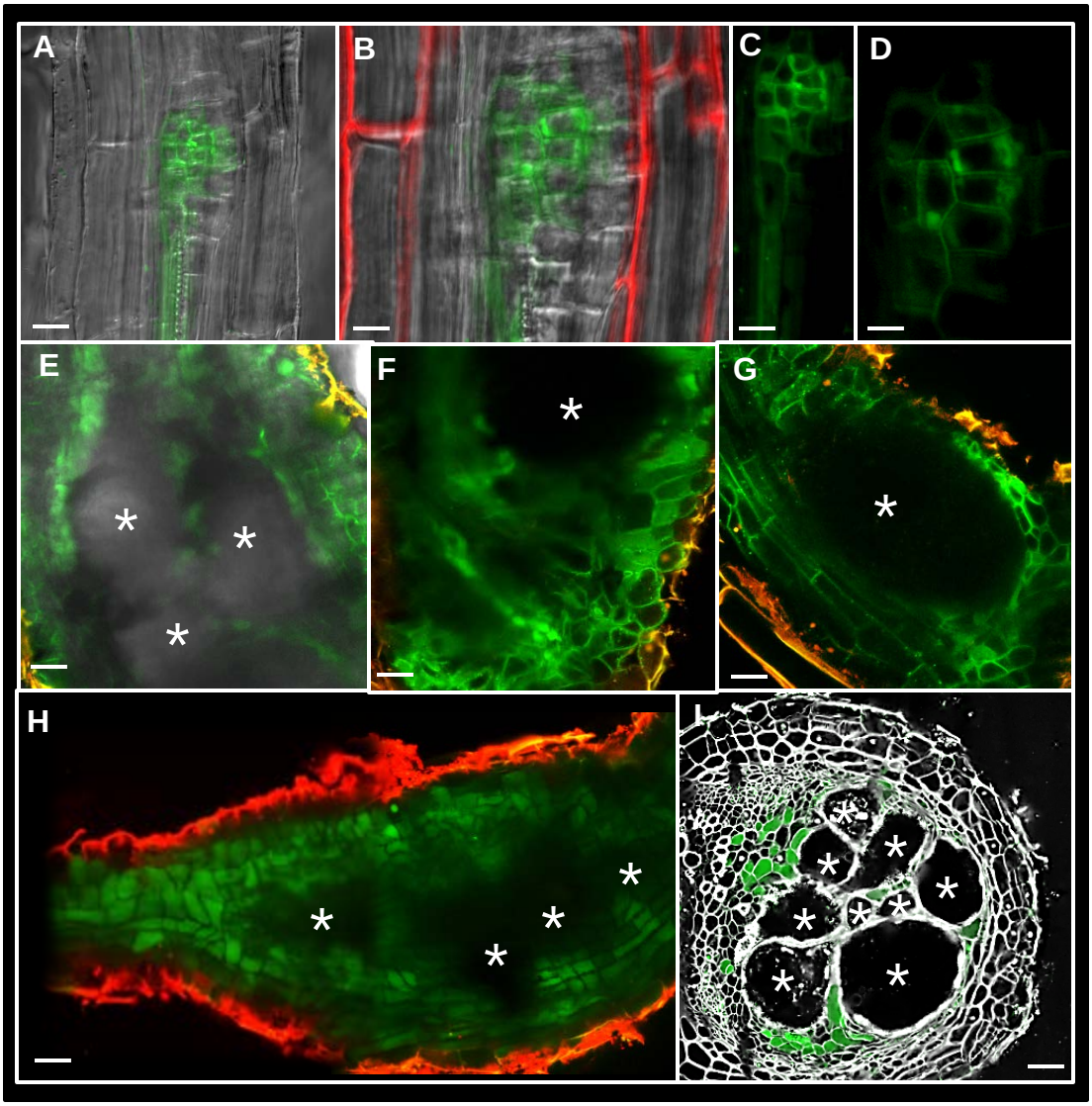

Figure 112. Distribution of PIN3 and PIN7 at the nematode feeding site. (A-G) PIN3-GFP. (A-D) Young root knot at the initiation phase of feeding site formation; GFP signals found in some cells of the young knot. (C, D) Magnification of theGFP channel from (A) and (B). (E) Overlay of GFP channel and PI stained cell walls of the rhizodermis, scale bars: (A) 10µm, (B) 8µm, (C) 9µm, (D) 4.5µm. (E-G) Mature root-knot with giant cells, GFP signals found in cells surrounding the giant cells, scale bars: (E) 30µm, (F) 22µm, (G) 25µm. (H) PIN7-GFP. (H) Mature root knot shows GFP signals outside of the giant cells, scale bar: 35µm. (I) Cross sections of an old root knot; PIN7-GFP positive cells are neighboring the giant cells, scale bar: 30µm. Asterisks mark giant cell.

The intense auxin response observed in the root knot during feeding site formation does not reflect the precise distribution of auxin between the different tissues. To monitor the auxin level in the feeding site the R2D2 marker was analyzed during infection. Green nuclei indicate auxin minima, red cell nuclei show auxin maxima. In young root knots, an asymmetry of the auxin distribution was found (Fig. 113 A-C, F). In younger root knots, higher auxin levels were observed in cells next to giant cells than in giant cells themselves (Fig, 113 F). In older root knots, giant cells and surrounding tissues both display high auxin levels (Fig. 113 G, H). In the rhizodermis and cells in the periphery of the vasculature low auxin concentrations were observed. In contrast, the maxima were found in the center of the feeding site. The red nuclei of the giant cells (Fig. 113 C) indicate high auxin levels in the giant cells. Over time, the amount of yellow and green cell nuclei decreased and most cells showed high auxin levels (Fig. 113 D). In very old root knots a clear contrast of auxin dynamics between the feeding site and the remaining root system was obvious (Fig. 113 E). Auxin maxima were concentrated at the center of the feeding site, minima were found in the periphery. Although in young root-knots high auxin levels were found inside the giant cells the auxin response, visualized by DR5, was never observed there.

In summary, it can be concluded that especially in the tissues surrounding the giant cells a high level of auxin was seen throughout the development of the root-knot, underpinning the role of auxin in the differentiation process of these cells to phloem.

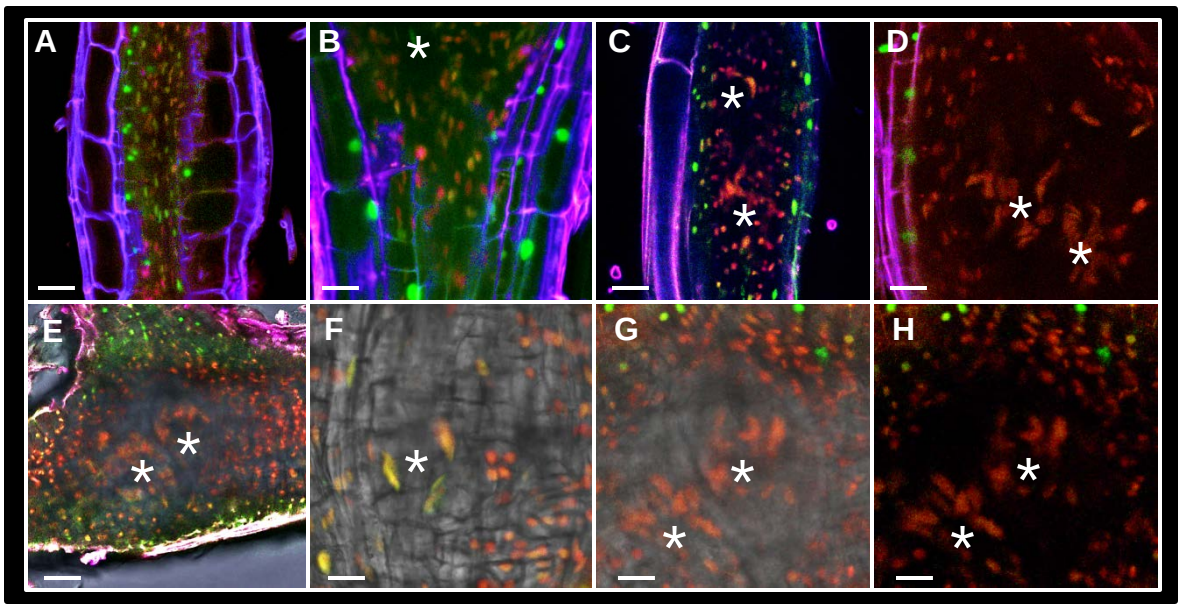

Figure 113. Distribution of auxin in root-knots. R2D2 reporter line visualized distribution of auxin in the tissue. Green nuclei indicate auxin minima, red nuclei represent auxin maxima. (A-C) Young root-knot: high auxin levels in the vascular tissue and giant cells, low auxin levels in the rhizodermis. Giant cell out of focus in (A), scale bars: (A) 20µm, (B) 10µm, (C) 15µm. (D) Magnification of an area from the root knot with small nuclei from the vascular tissue and bigger nuclei of the giant cells; high auxin levels in the feeding site, scale bar: 22µm. (E) Old root-knot, green nuclei in the periphery, high auxin level in the center of the feeding site indicated by red nuclei, scale bar: 40µm. (F) Young giant cells with smaller neighboring cells, auxin minima in the giant cell, auxin maxima in the surrounding cells, scale bar: 12µm. (G, H) Multinucleated giant cell with surrounding smaller cells. Auxin accumulation at the feeding site, only few cells in the periphery show low auxin levels. (G) Overlay of merged fluorescence channels (H) with bright field image, scale bars: 4µm. Asterisks mark giant cell.

The giant cell-associated juvenile phloem cells were furthermore characterized by the already introduced transcription factor SCR. In young root knots, SCR-GFP was located at the periphery of the feeding site in the endodermis cell files (Fig. 114 A, B), indicating that SCR plays during early stages of root knot formation no role in phloem differentiation and is found in a tissue that is consistent with previous data. This is comparable to the situation found in the root tip. The situation changes as the young gall gets mature and building a massive tumor like structure harboring several giant cells. There, SCR-GFP was detected not only in the cortex of the gall but also in tissues close to giant cells (Fig. 114 C, D). Cells of these tissues were close to xylem elements and positioned next to the membrane of the giant cell (Fig. 114 E, F).

The results obtained indicate that *SCR* plays no role in early events of the infection but is later on highly expressed in small cells neighboring the giant cells. This suggests a role of SCR in the differentiation process of parenchyma tissue into juvenile phloem and underlines the uniqueness of this phloem cells.

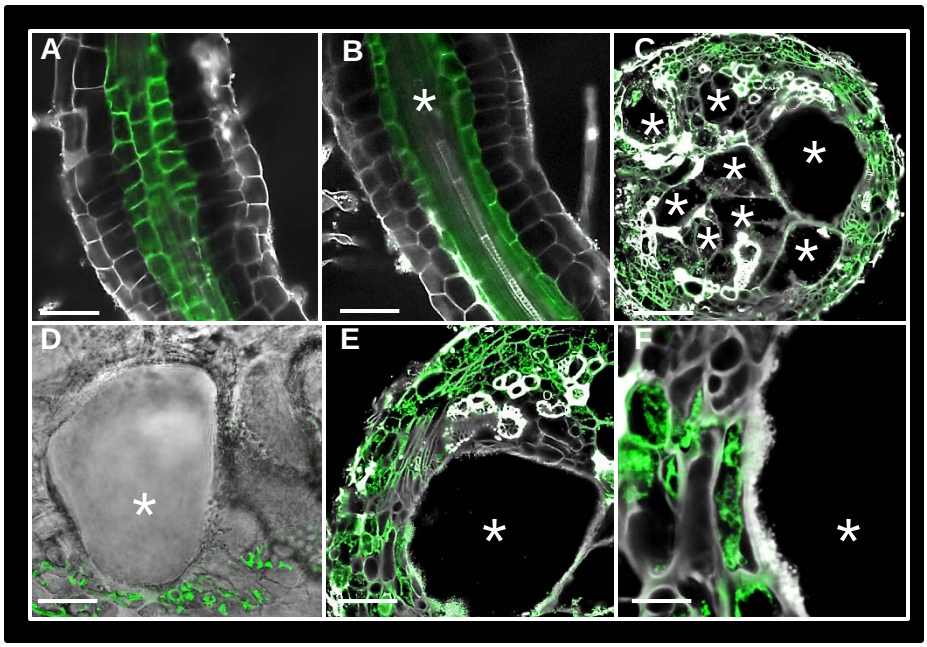

Figure 114. *SCR* promoter activity in root-knots. Infected P_{SCR}: ER-GFP plants were analyzed. (A, B) Young root-knot, GFP detected in the endodermis, scale bars: (A) 42µm, (B) 48µm. (C) Cross section through a mature gall, several giant cells, surrounded by SCR positive cells, are visible, scale bar: 80µm. (D) Magnification of one giant cell, scale bar: 20µm. (E) Segment of a sectioned root knot showing a mature giant cell, embedded in xylem elements and cells with GFP decoration, scale bar: 50µm. (F) Magnification of SCR-positive cells close to a giant cells, scale bar: 9µm. Asterisks indicate giant cell.

In order to characterize the phloem differentiation during the infection with root-knot nematodes, different phloem markers were studied. It was found that the phloem-specific transcription factor APL was located in several cells of the vasculature in the mature root- knot (Fig. 115 A). These phloem cells were found in close vicinity of the giant cells (Fig. 115 B-D). APL-GFP signals in these cells indicate that the translational fusion shows the same pattern as already described for the transcriptional fusion (Absmanner et al. 2013). Furthermore, APL seemed to play a role in the differentiation process of parenchyma to phloem cells during root-knot formation. Also another early phloem marker, PD1, was monitored in the feeding site. PD1-GFP was seen in the root-knot (Fig. 115 H, I) in cells that were in close vicinity to the giant cells (Fig. 115 J, K). The presence of this marker in the parenchymatic tissues at the feeding site supports the idea that the GFP marked cells share the characteristics of juvenile phloem. At the same position, promoter activity of ENOD-GFP was seen (Fig. 115 E-G), suggesting that the resulting translation of RS6, a sieve element epitope is built in the same cells, which is an additional hint for the phloem identity in the small cells adjacent to the giant cells. All investigated phloem marker lines showed signals in the same tissue of the gall. High similarity was seen between ENOD and PD1, which appeared in more cells than APL, suggesting that APL activity is present in undifferentiated parenchymatic tissues that will later on differentiate to juvenile phloem.

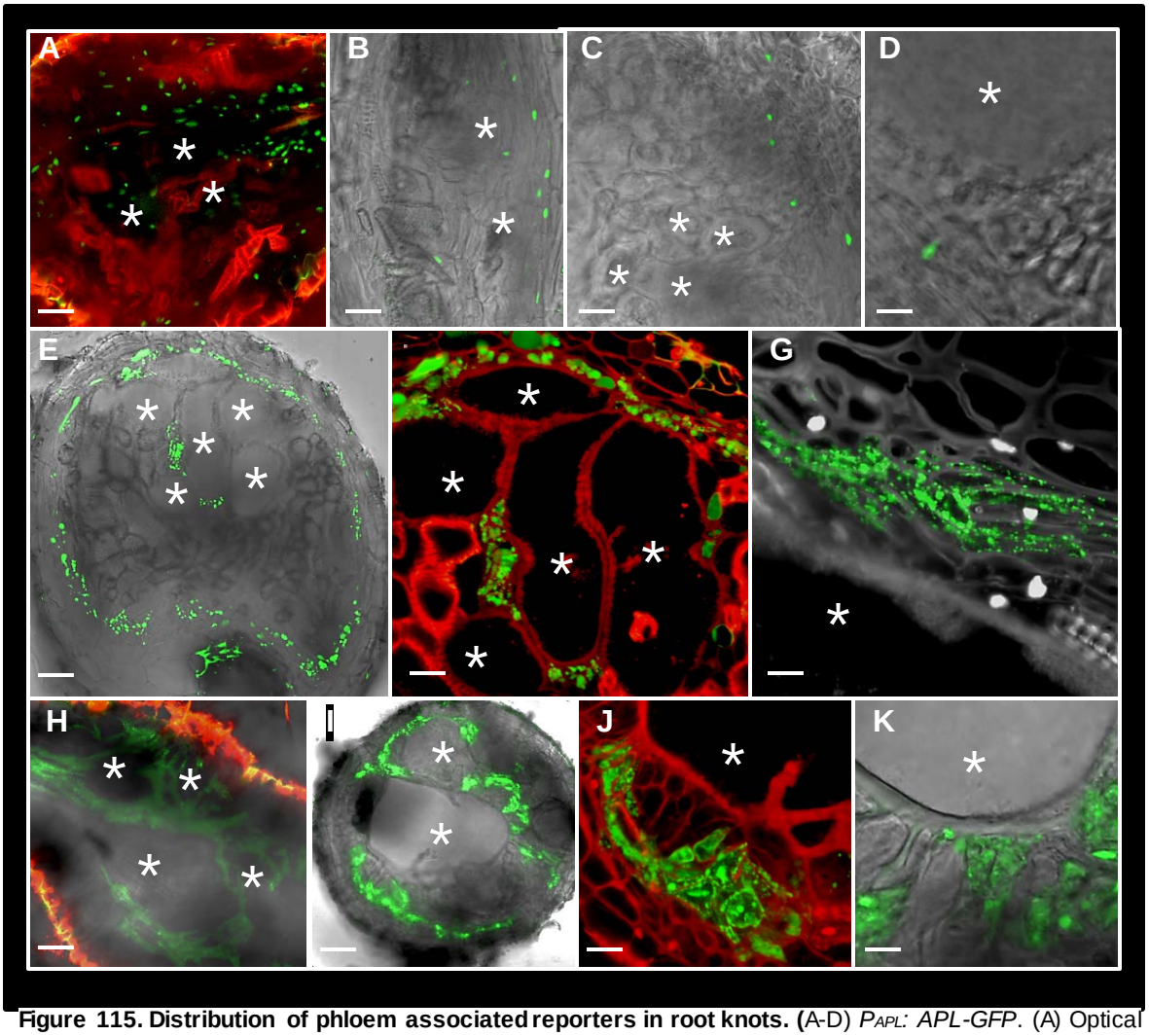

Figure 115. Distribution of phloem associated reporters in root knots. (A-D) *P_{APL}: APL-GFP*. (A) Optical section shows several GFP signals in the feeding site, scale bar: 30µm. (B) Cross section above the giant cells, APL-GFP in the phloem pole, scale bar: 25µm. (C) Magnification of a section from a young root-knot with immature giant cells, GFP only found in the phloem pole, scale bar: 20µm. (D) Mature giant cell with associated cells, scale bar: 10µm. (E-G) *P_{ENOD}: ER-GFP*. (E) Cross section through a root-knot, ENOD-GFP in the phloem, scale bar: 25µm. (F) Magnification of giant cells from (E), GFP visible in cells next to giant cells, scale bar: 20µm. (G) Focus on the close physical vicinity of ENOD-positive cells to a giant cell, scale bar: 4µm. (H-K) *P_{PD1}: ER-GFP*. (H) Optical section through root knot, GFP outside of giant cells, scale bar: 30µm. (I) Cross section, GFP signals surround giant cells, scale bar: 20µm. (J, K) PD1-positive cells are closely associated with giant cells, scale bars: (J) 15µm, (K) 9µm. Asterisks mark giant cell.

5.12. Expression of *UmamiTs* during root knot nematode infestation

In order to investigate in which tissues *UmamiT* expression took place during pathogenesis with root knot-nematodes the promoter activity and the distribution of the fusion protein, containing all introns, was analyzed.

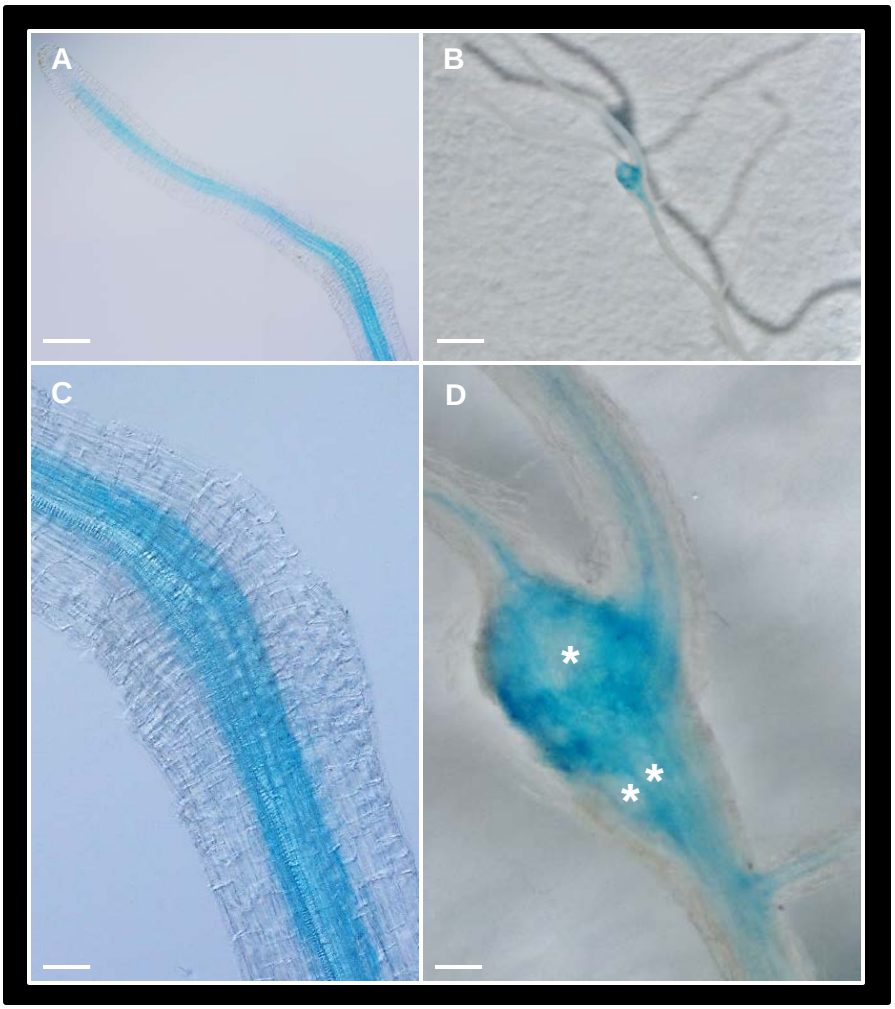

Figure 116. *UmamiT* promoter activity during infection with *Meloidogyne incognita*. $P_{UmamiT28}$: *GUS* was analyzed. (A, C) Root infected with *M. incognita*, very early stage. Swelling of the infection side, scale bars: (A) 100µm, (C) 30µm. (B, D) Root with differentiated root-knot; scale bars: (B) 500µm, (D) 60µm. Asterisks mark giant cells.

Unless stated otherwise, the figures show representative images that are identical for each candidate analyzed. According to transcriptom data from seeds and root knots, *UmamiTs* were identified as possible candidates for exporters in symplasmically isolated tissues. Giant cells of root-knots are symplasmically isolated from the surrounding tissues which underlines the importance of plamsma membrane guided transport processes. Using the set of marker lines at hand, analysis of *UmamiT* promoter activity and protein localization in the root-knot system was performed. Promoter activity was documented in the very young knot, when the swelling of the infected root part became visible (Fig. 116 A, C). Furthermore GUS staining was seen in the mature knot with visible giant cells, which were completely free from staining (Fig.116 B, D). Staining was observed before parts of the remaining root vascular system started to become stained (Fig. 116 B).

In the very young root, all cells of the central cylinder with exception of the xylem and giant cells were stained (Fig. 117 A, B). A cross section through the root-knot showed specific promoter activity in the cells around the giant cells (Fig. 117 C), indicating that gene expression of *UmamiTs* gets activated upon infection

To quantify the different RNA levels of *UmamiTs* before and during pathogenesis in the root knot qRT-PCR of uninfected roots, part of infected roots without the knot and solely the root knot was done (Fig. 117 D).

The results of this analysis showed that all *UmamiTs* were induced during infection and displayed significantly higher RNA levels compared to the uninfected roots, even in the infected parts without knots. In detail, the two clades of *UmamiTs* behave a little bit divergent. *UmamiTs* of clade I (*UmamiT14* and *UmamiT11*) show the RNA maximum only in the root-knot, whereas both *UmamiTs* from clade III (*UmamiT29* and *28*) are upregulated in the infected roots in tissues right next to the knot as well as in the knot itself.

These results validate the transcriptome data and confirm the observations indicated by the GUS staining, where staining was earlier visible in the root-knot than in the remaining root system, based on a higher promoter activity in the feeding site compared to the remaining root system.

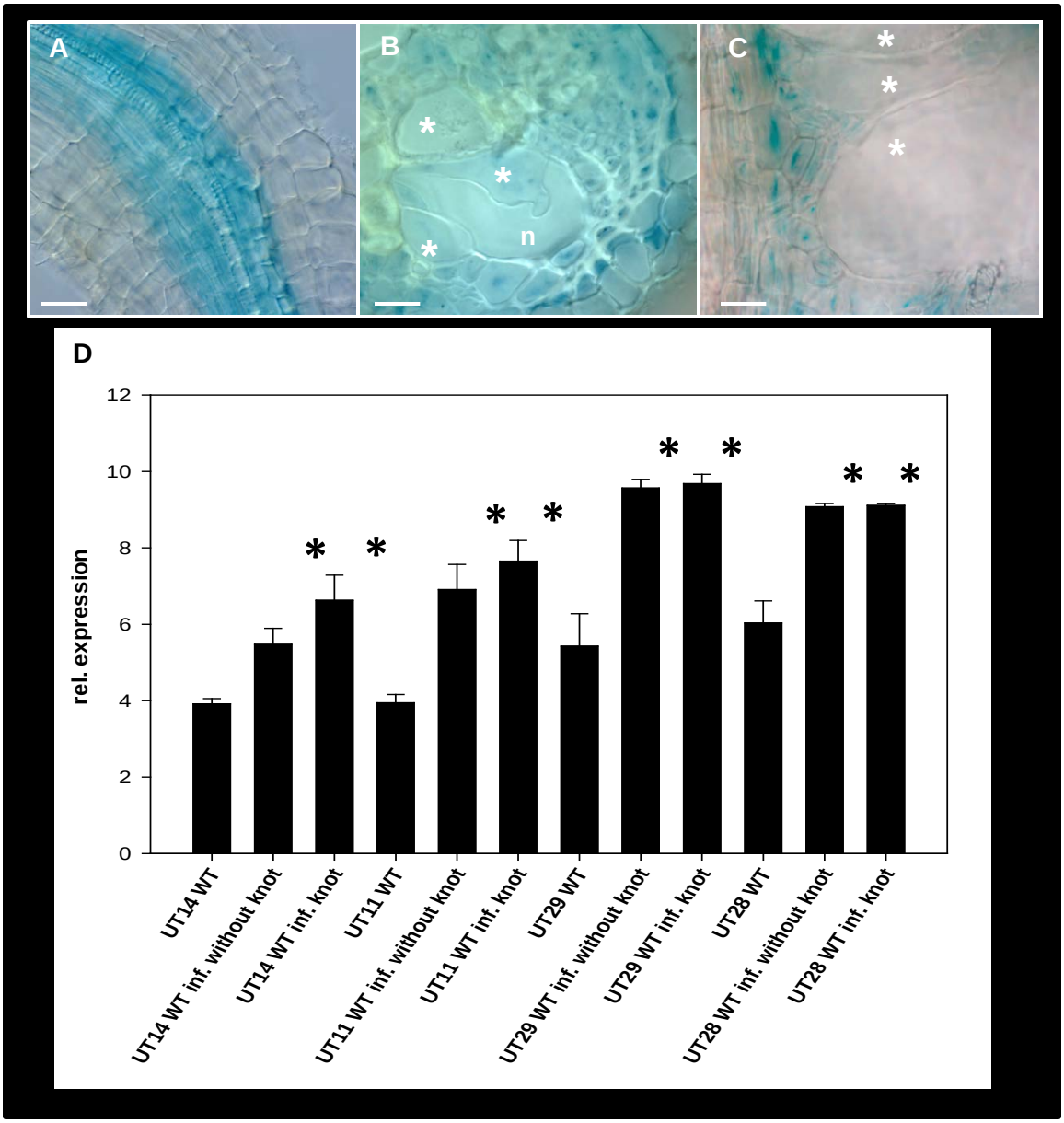

Figure 117. *UmamiTs* are induced during infection with *M. incognica* in the feeding site. (A) Young root knot, swelling of the vascular tissue apparent, scale bar: 30µm. (B) Cross section through a root knot, nematode and giant cells are embedded in tissues showing GUS staining scale bar: 20µm. (C) GUS staining in an older root-knot, promoter activity specifically found in cells surrounding the giant cells, no GUS crystals at the membrane of giant cell or inside, scale bar: 18µm. Asterisks mark giant cells, n (nematode). (D) Semi quantitative real time PCR of uninfected roots, infected roots without knot and solely root-knot, normalized to UBQ10 (n=3 ± D), ANOVA, $p<0.05$.

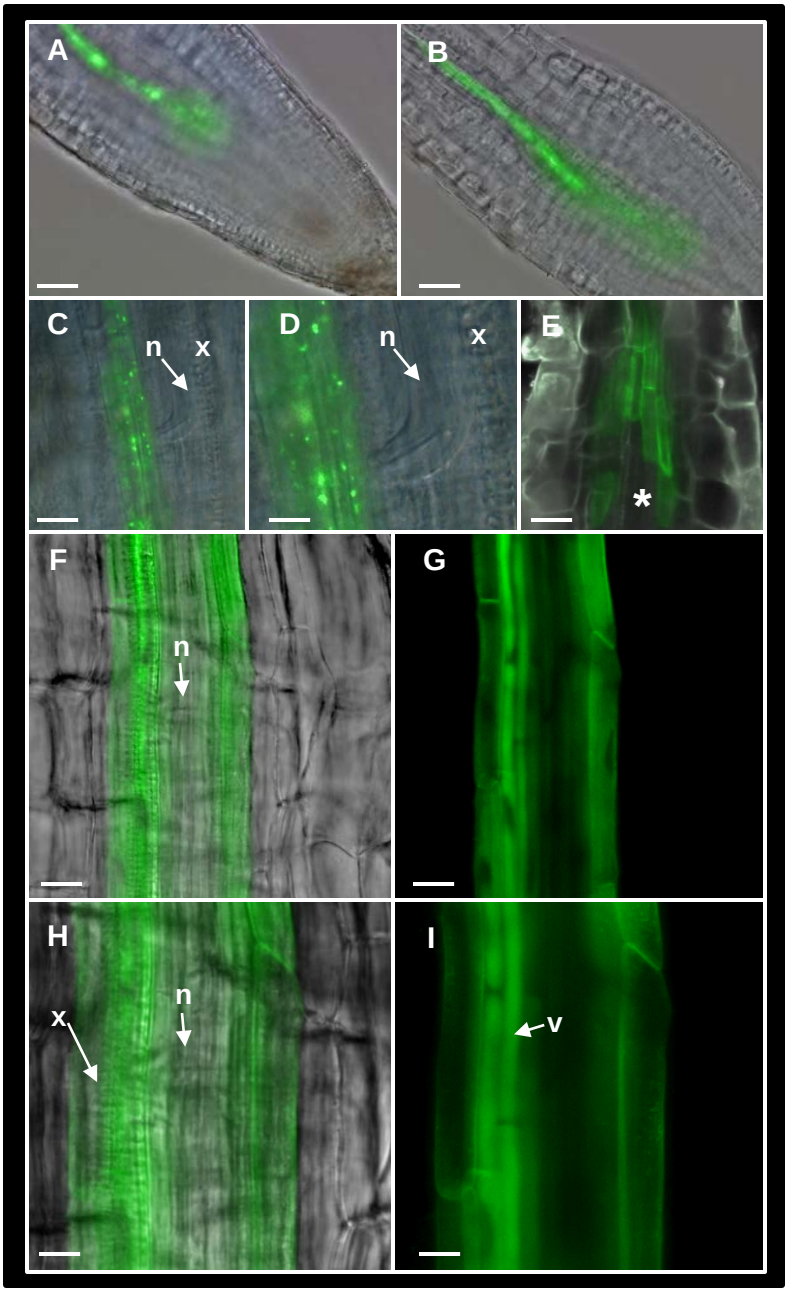

Figure 118. Localization *of* UmamiTs at the beginning of feeding site formation. *$P_{UmamiT14}$: UmamiT14-GFP reporter line was analyzed.* (A, B) Starting point of infection with *M. incognita*; infection zone starts swelling, scale bars (A) 20µm, (B) 15µm. (C, D) Root-knot nematode visible in the central cylinder; scale bar: (C) 12µm, (D) 5µm. (E) Young root knot with UmamiT14-GFP around the forming feeding site, scale bar: 18µm. (F-I) Maximum projections of an older part of the root infected by the nematode; tapped cells show accumulation of GFP in the vacuole. (G, I) GFP channel, scale bars: (F, G) 15µm, (H, I) 11µm. Asterisks mark giant cells, n (nematode), x (xylem), v (vacuole).

A look at the fusion protein, which contains all introns, during infection shows UmamiT-GFP in the vasculature of very young stages of root knot development when the cells of the elongation-differentiation zone get reorganized by the size increment of the reprogrammed pericycle cells (Fig. 118 A, B).

The nematode moves from the root tip to the pericycle cells and taps one of those cells that started to form a multinucleated giant cell at this moment, which leads to swelling of the whole stele (Fig. 118 C-E). At the site the nematode infected the root, the plasma membrane localization disappeared and GFP was found to accumulate in the vacuoles (Fig. 118 F-I), indicating a possible higher turnover rate of the fusion protein. These findings are in line with the GUS staining data and indicate, that all elements required for proper expression are found in the 5' region before the ATG.

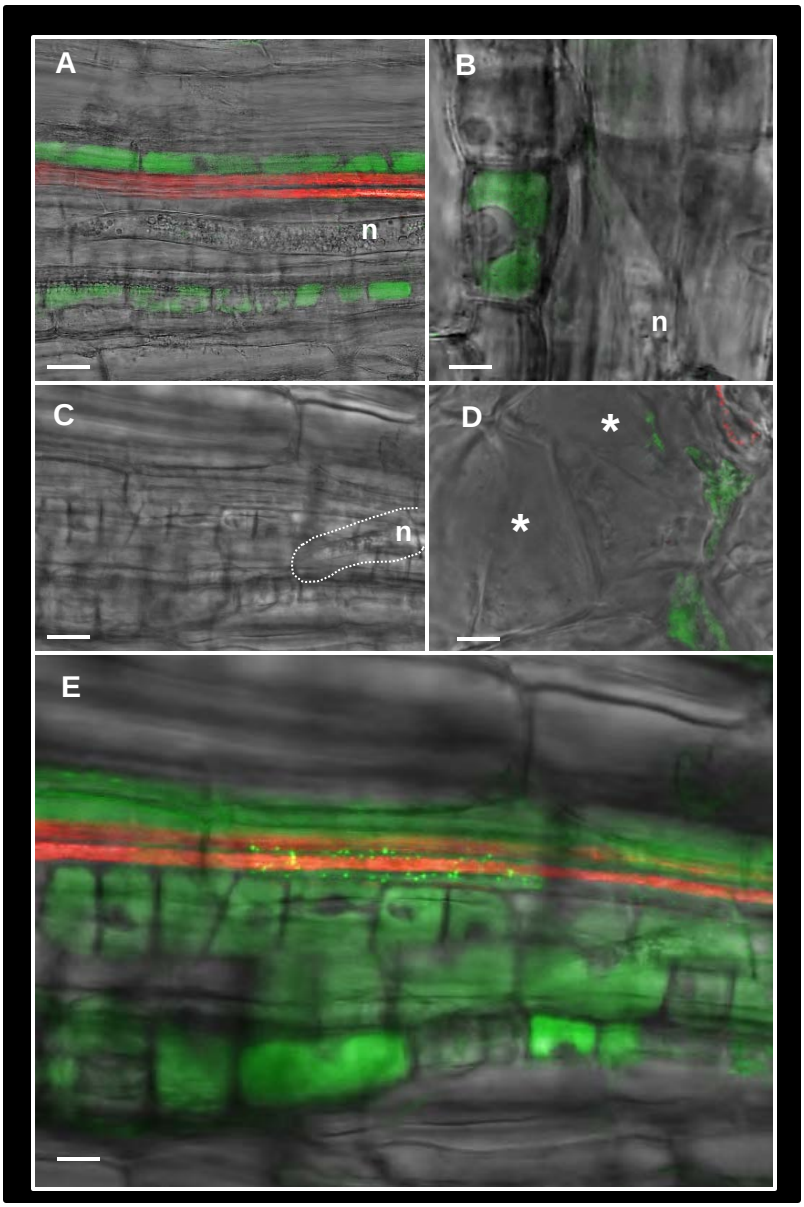

Figure 119. Coexpression of $P_{UmamiT14}$: *UmamiT14-GFP* and P_{suc2}: *ER-mCherry* in the young root- knot. (A) Nematode in the root, near feeding site, scale bar: 20µm. (B) Nematode at the pericycle, trapping one cell, UmamiT14-GFP in the neighboring cell; scale bar: 7µm. (C) Bright field image of a maximum projection of (E) to show the position of the nematode at the feeding site. Nematode is marked by a dotted line; scale bar: 20µm. (D) Young giant cells next to UmamiT-positive cells and at the periphery companion cells; scale bar:8µm. (E) Maximum projection of a young root-knot; companion cells present only in the periphery; UmamiT14- positive cells surround young giant cells; scale bar: 15µm. Asterisks mark giant cells, n (nematode).

Later on during feeding site development the reprogrammed cell of the pericycle differentiated to the giant cell and lost completely GFP signals (Fig 119 B). In order to show the distribution of companion cells and UmamiT-positive cells a marker line coexpressing mCherry driven by the *SUC2* promoter and UmamiT14-GFP was monitored. During young stages it could be shown that companion cells are placed only in the periphery of the root-knot, whereas UmamiT14-positive cells are found directly around the forming giant cells (Fig. 119 D, E).

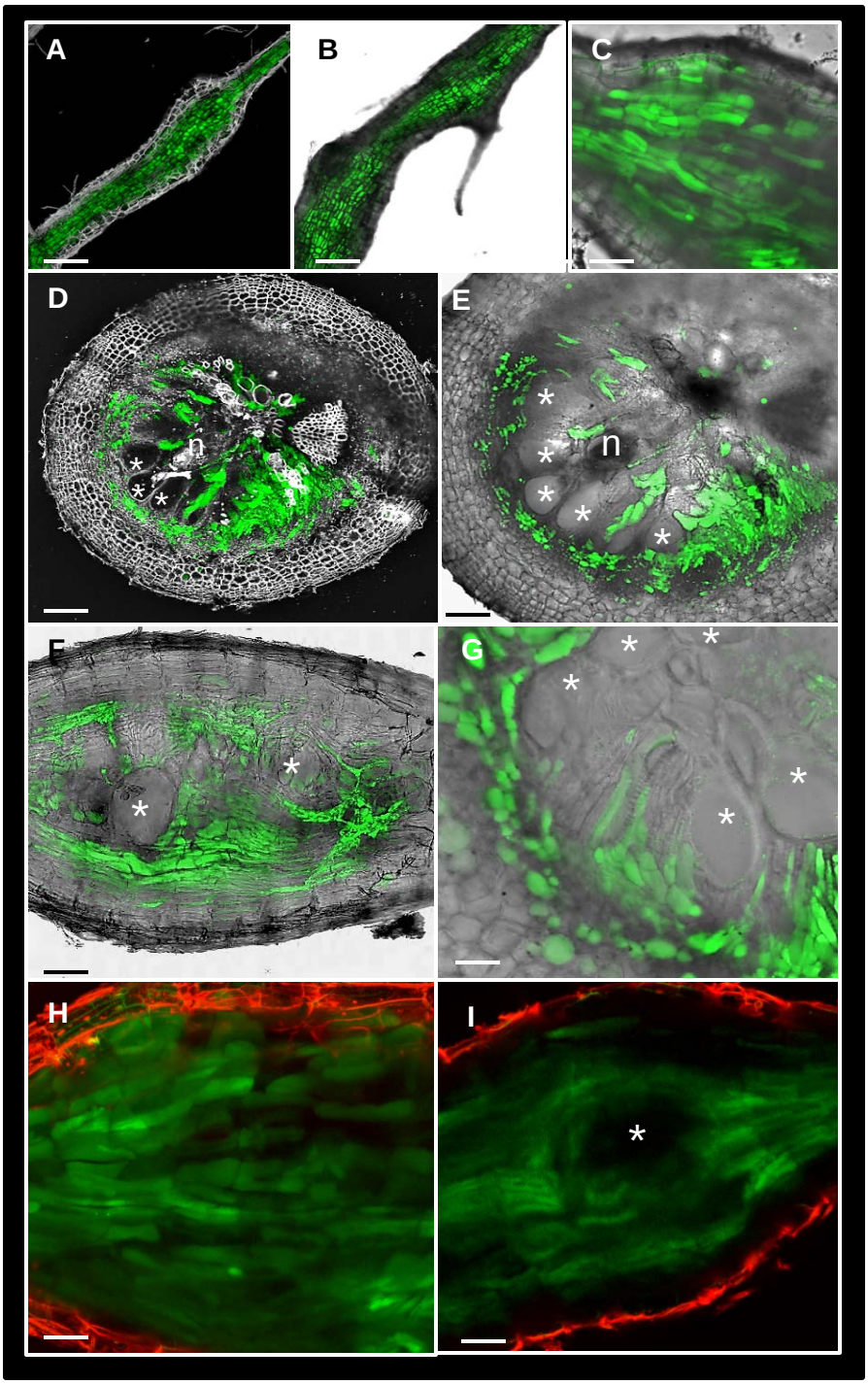

Figure 120. Localization of UmamiTs in the mature root-knot.

(A) UmamiT29-GFP in the infected root with one root- knot; scale bar: 100µm, (B) Infected root with two root-knots in tandem position, strong UmamiT29-GFP signals at the feeding site of the nematode, scale bar: 200µm. (C) Optical section through a root-knot; UmamiT29-GFP in several cells around the feeding site, scale bar: 60µm. (D, E) Cross section through a mature feeding site with the nematode in the center, the giant cells around the nematode and green UmamiT14-positive cells next to the giant cells; scale bars: (D) 150µm, (E) 100µm. (F) Longitudinal section through a root-knot, strong UmamiT28-GFP signals in the feeding site, scale bar: 50µm.(G) Transversal section through root-knot, giant cells embedded in UmamiT14-positive cells, scale bar: 20µm. (H) Maximum projection of a root-knot, scale bar: 25µm. (I) Optical section through a root-knot showing the black whole inside the knot which represents the giant cell that is surrounded by UmamiT positive-cells, scale bar: 30µm. Asterisks mark giant cells, n (nematode).

In later stages of the root-knot development, fluorescence was detected along the whole root in the vascular tissue surrounding the giant cells (Fig. 120 A-C, H, I). Cross sections showed that UmamiT-GFP was located preferentially within the thickened vascular cylinder (Fig. 120 D, E). Longitudinal sections (Fig. 120 F, G) also proofed that giant cells were completely devoid of GFP and signals were specific to those cells positioned adjacent to the giant cells.

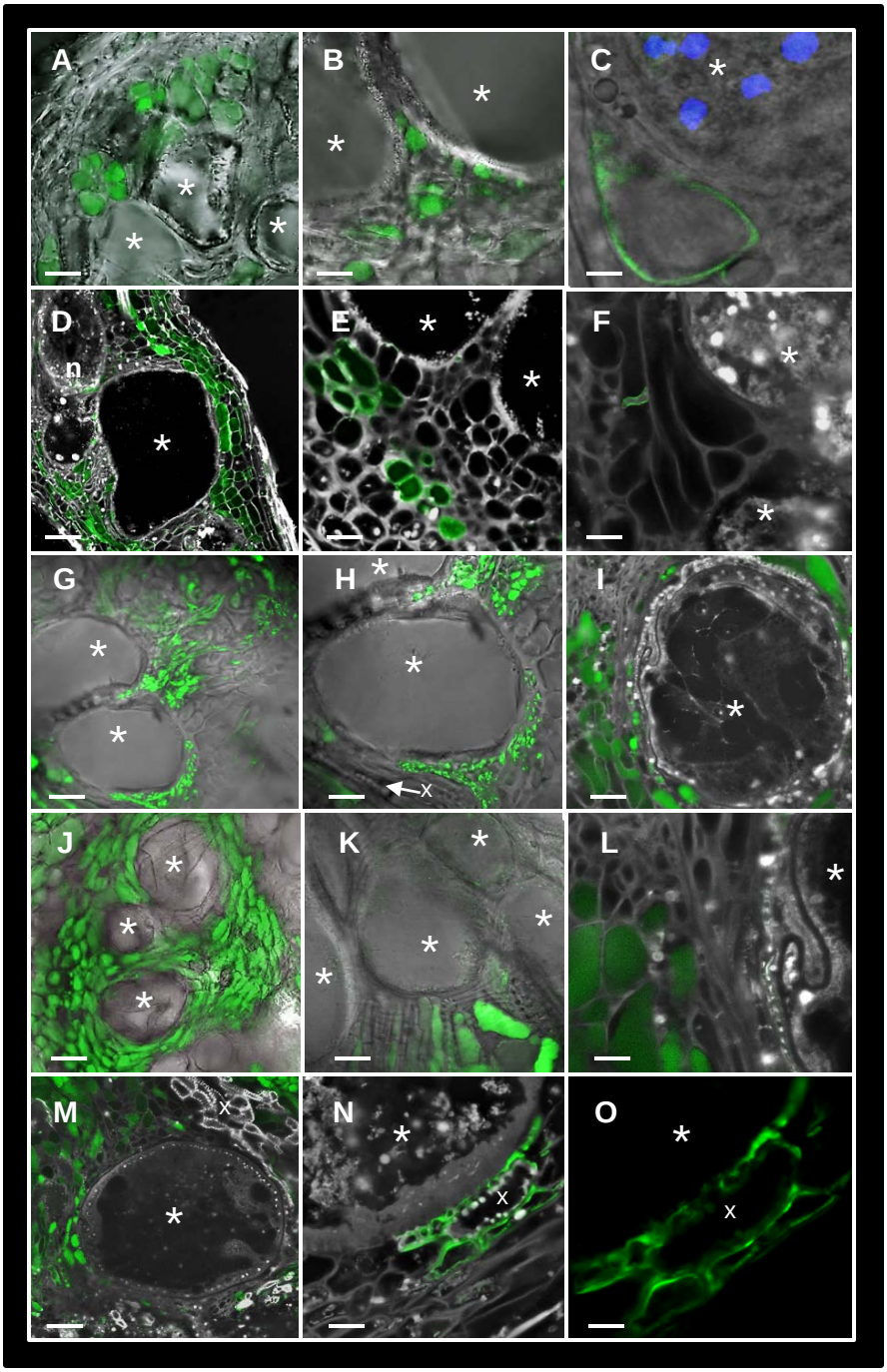

Figure 121. P_{umamiT}: *UmamiT-GFP* at the giant cells. (A, B) Clade I: UmamiT14-GFP in distinct cells around giant cells, scale bars (A) 35µm, (B) 20µm. (C) UmamiT11-GFP next to multinucleated giant cell, blue color: PI marked nuclei, scale bar: 3,5µm. (D) Clade III: UmamiT29-GFP around giant cell, scale bar: 40µm. (E) Magnification of parenchymatic cells around giant cells, scale bar: 20µm. (F) Zoom out of same area from (C) focusing only to the brightest signal of UmamiT-GFP between two cells. (G, H) UmamiT28-GFP found around giant cells; scale bars: (G) 30µm, (H) 18µm. (J) UmamiT14-GFP, (K) UmamiT11-GFP around giant cells, scale bars: (J) 35µm, (K) 15µm. (I, L,) Very old giant cell with membrane invaginations at the side where UmamiT positive cells are located, scale bars: (I) 25µm, (L) 10µm. (M) Giant cells encaged by big xylem vessels, scale bar: 30µm. (N,O) UmamiT-GFP next to the membrane of a giant cell and a xylem vessel, (O) GFP fluorescence shows membrane like localization of GFP; scale bars: (N) 10µm, (O) 5µm. Asterisks mark giant cells, n (nematode), x (xylem).

Focusing only on the giant cells it was possible to document the same GFP fluorescence pattern for all candidates (Fig. 121). UmamiT-GFP was found in those cells sharing close physical vicinity to the multinucleated giant cells (Fig.121 C, F). A very prominent accumulation of GFP fluorescence around the giant cells was obvious (Fig. 121 A, D, J). Especially very small cells around the giant cells showed a bright fluorescence (Fig. G, H). Those cells were next to the membrane of the giant cells and close to xylem vessels and showed GFP signals across the putative plasma membrane (Fig. 121 N, O).

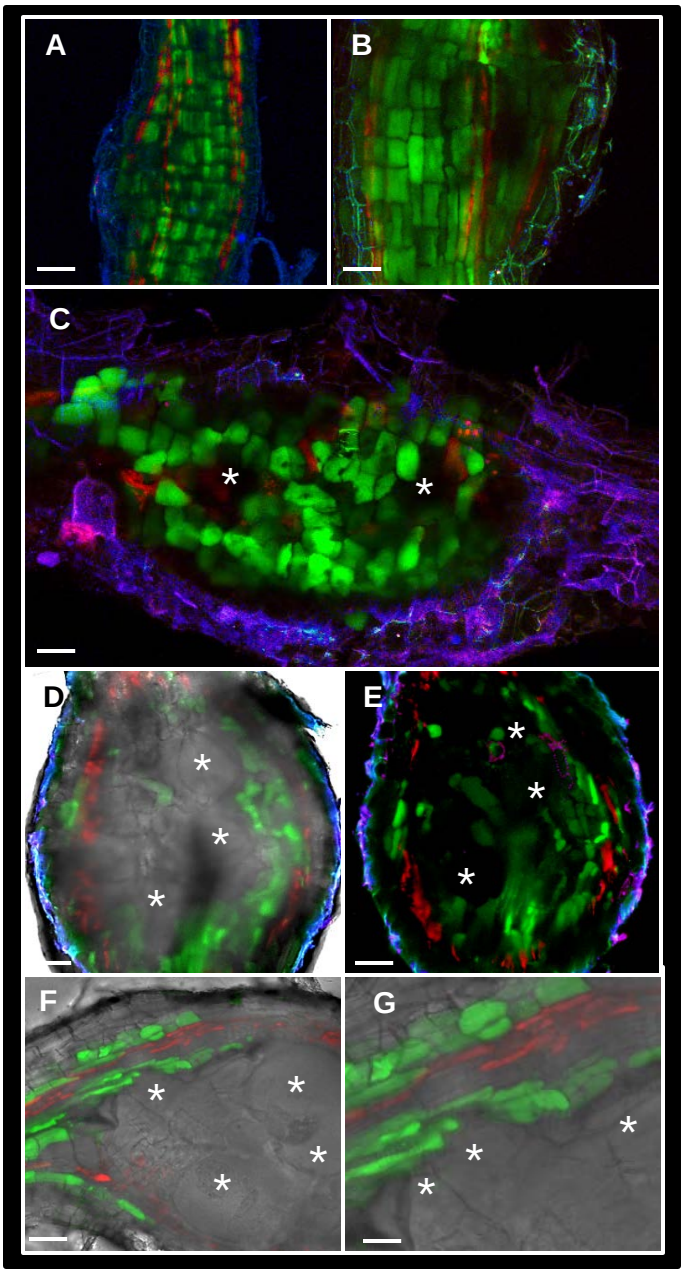

Figure 122. Coexpression of *P*$_{UmamiT14}$*: UmamiT14-GFP* and *P*$_{suc2}$*: ER-mCherry* in the mature root-knot. (A) Maximum projection showing UmamiT14-GFP and SUC2-mCherry, companion cells at the lateral site of the root-knot; scale bar: 80µm. (B) Maximum projection with focus at the giant cells; giant cell visible as fluorescence free black hole in the projection, scale bar: 50µm. (C) Lateral view of the root-knot, numerous UmamiT-positive present in the feeding site surrounding the giant cells; companion cells mostly found at the edges of the feeding site; giant cells close to UmamiT positive cells; scale bar: 18µm. (D, E) Cross section. (D) Overlay with bright field image. (E) Overlay of fluorescence channels, UmamiT14-GFP close to giant cells; companion cells present in lateral bundles away from the feeding site, scale bar: 60µm. (F, G) Lateral section showing companion cells grouped in a cell file distinct from the UmamiT14-positive cells, giant cells always associated with cells decorated by GFP, scale bars: (F) 60µm, (G) 25µm. Asterisks mark giant cells.

To investigate the histological relationship between companion cells and UmamiT14-positive cells in the mature knot a line coexpressing *P*$_{UmamiT14}$*: UmamiT14-GFP* and *P*$_{suc2}$*: ER-mCherry* was analyzed. It was apparent that the situation shifted with the age of the root knot (→Fig. 119). Whereas in young infected roots the strand of companion cells was absent at the infection site, in older knots a file of companion cells started to surround the feeding site (Fig.122 A-C). Cross sections visualized that only UmamiT14-GFP signals were found next to giant cells. Fluorescence resulting from promoter activity of *SUC2* was not observed in this position (Fig. 122 D, E). Longitudinal sections (Fig. 122 F, G) showed on the one hand companion cells to be present in root knots, but only in the vasculature distant from the giant cells, not directly connected to them. On the other hand, UmamiT14-positive cells were not only present in the stele next to companion cells, as mentioned before (→Fig. 119), but they were even more directly linked next to giant cells, which marks them simply by their position in the feeding site as important players for the allocation of amino acids across membranes to the sinks there.

5.12.1. Characterization of UmamiT-positive cells in the root-knot by immunolocalization

In order to characterize those cells with UmamiT-GFP decoration in the root-knot, immunolocalization studies with α-GFP and α-RS6, a sieve element marker, were performed. Using this method, the characterization of the cell type of UmamiT-positive cells was possible. Many cells around young giant cells colocalize with RS6 (Fig. 123 A-F). But besides that a significant portion of cells only labeled by α-GFP was located in the same population where colocalization occurred. This was also true in slightly older root-knot tissue, when the xylem started to cage the giant cell complex with thick vessels (Fig. 123 G-L).

This observation was also made in root knot tissue that underwent secondary growth according to the gall maturation (Fig. 124). Although the root tissue was quite old, cells that were only carrying the GFP epitope without harboring RS6 were found. Due to these findings it can be concluded that differentiation of parenchymatic cells to sieve elements happened during root knot formation.For nearly all cells surrounding the giant cell a colocalization of α-GFP with α-RS6 was detected.

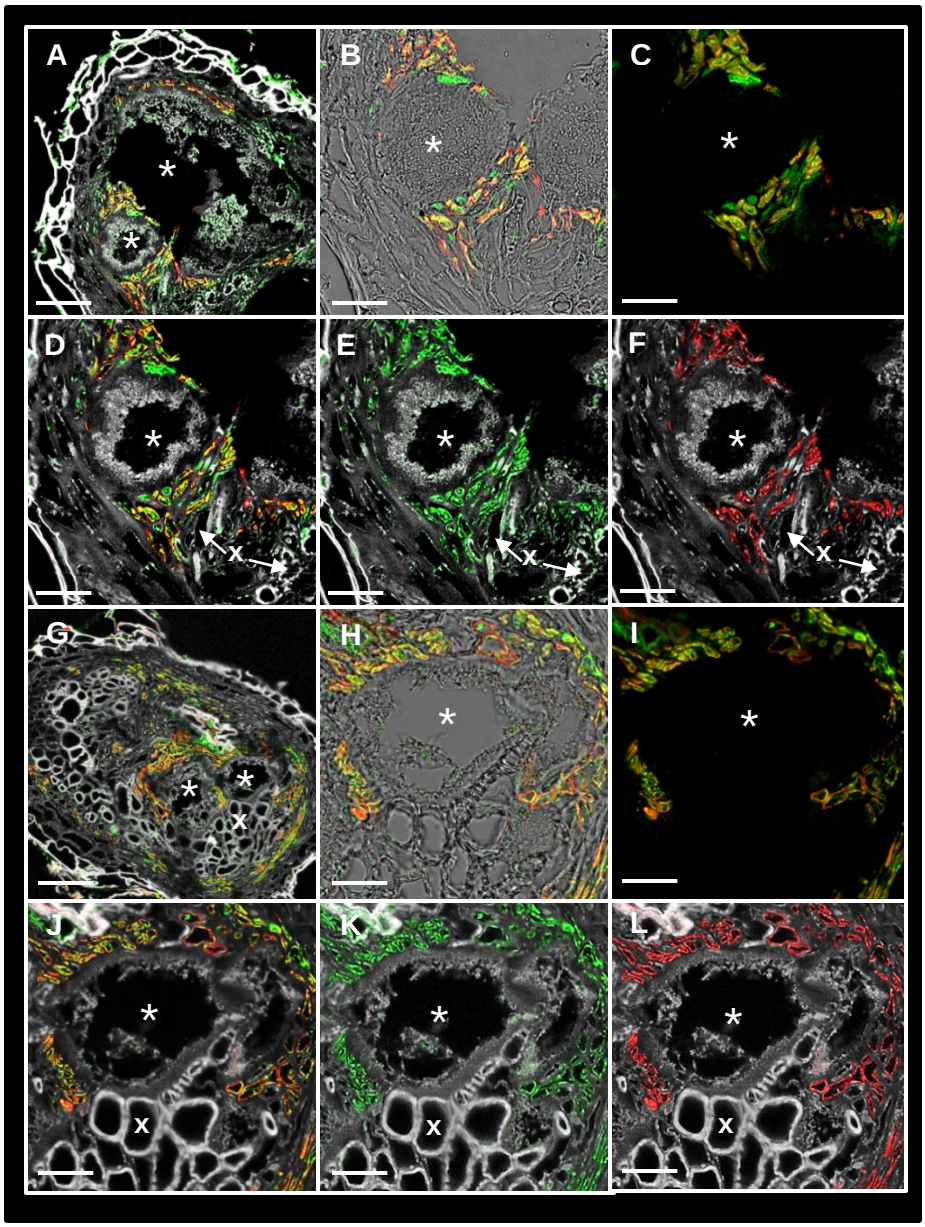

Figure 123. Immunolocalization of root-knots from *P_{UmamiT}: UmamiT-GFP* plants. Green cells: α-GFP, detected with a CY2-antiserum, representing UmamiT-GFP positive cells; red cells: α-RS6 detected with an AF594-coupled antibody, representing sieve elements, yellow color: colocalization between α-GFP and α-RS6, white color: autofluorescence. (A-F) UmamiT28-GFP, (G-L) UmamiT14-GFP. (A) Overview of a cross section through a young root knot with a developing giant cell, scale bar: 70µm. (B-F) Young giant cell embedded in tissues decorated by UmamiT-GFP and RS6, but also cells without RS6 epitope detectable. (B) Overlay with bright field image. (C) Overlay of the green and red channel; (D-F) Overlay with auotflourescence. (E) Cells marked by α-GFP. (F) Sieve elements, marked by α-RS6, scale bars: 25µm. (G) Overview of an older root- knot with secondary growth and massive xylem elements around giant cells, scale bar: 60µm. (H-L) Mature giant cell surrounded by cells showing colocalization between α-GFP and α-RS6 epitope. (H) Overlay with bright field image. (I) Overlay of the green and red channel. (J-L) Overlay with auotflourescence, (E) Cells marked by α-GFP. (F) Sieve elements, marked by α-RS6, scale bars: 20µm. Asterisks mark giant cells, x (xylem).

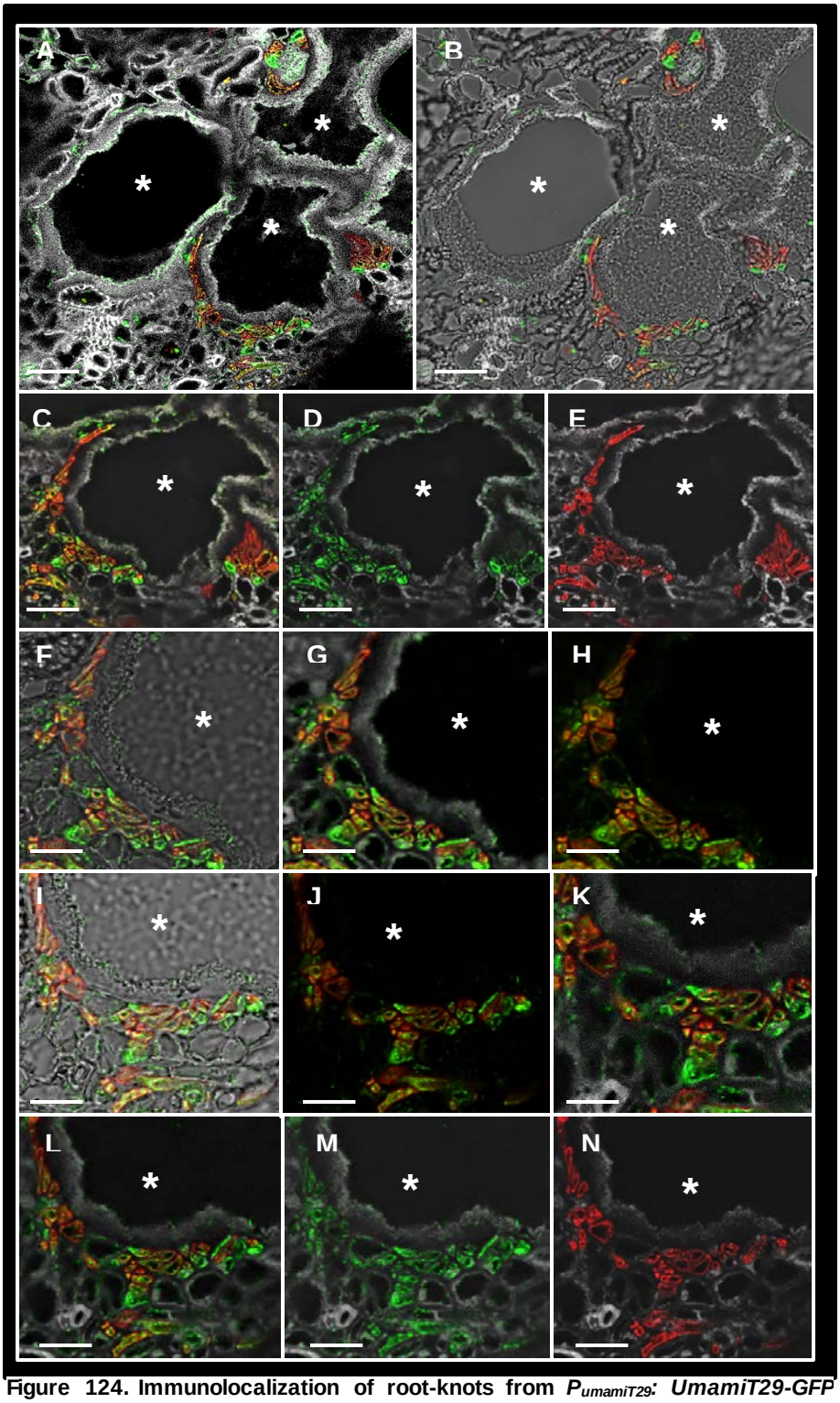

Figure 124. Immunolocalization of root-knots from *P*$_{umamiT29}$*: UmamiT29-GFP* plants at secondary stage. Green cells: α-GFP, detected with a CY2-antiserum, representing UmamiT-GFP positive cells; red cells: α-RS6 detected with an AF594-coupled antibody, representing sieve elements, yellow color: colocalization between α-GFP and α-RS6, white color: autofluorescence. (A, B) Infected root that has undergone secondary thickening. (B) Merge with bright field image; scale bar: 27µm. (C-E) Mature giant cell of an old root. (C) Overlay of α-GFP and α-RS6 signals. (D) α-GFP cells. (E) α-RS6 cells, scale bar: 20µm. (F-H) Magnification of (C-E). (F) Merge with bright field image; (G) merge with autofluorescence channel, (H) overlay of green and red channel alone scale bar: 10µm. (I, J, L-N) Area with big xylem vessels around colocalizing cells. (I) Overlay with bright field image. (J) Overlay of only the green and red channel. (L) Overlay with autoflourescence channel. (M) Cells marked by α-GFP. (N) Cells marked by α-RS6, scale bar: 12µm. Asterisks mark giant cells.

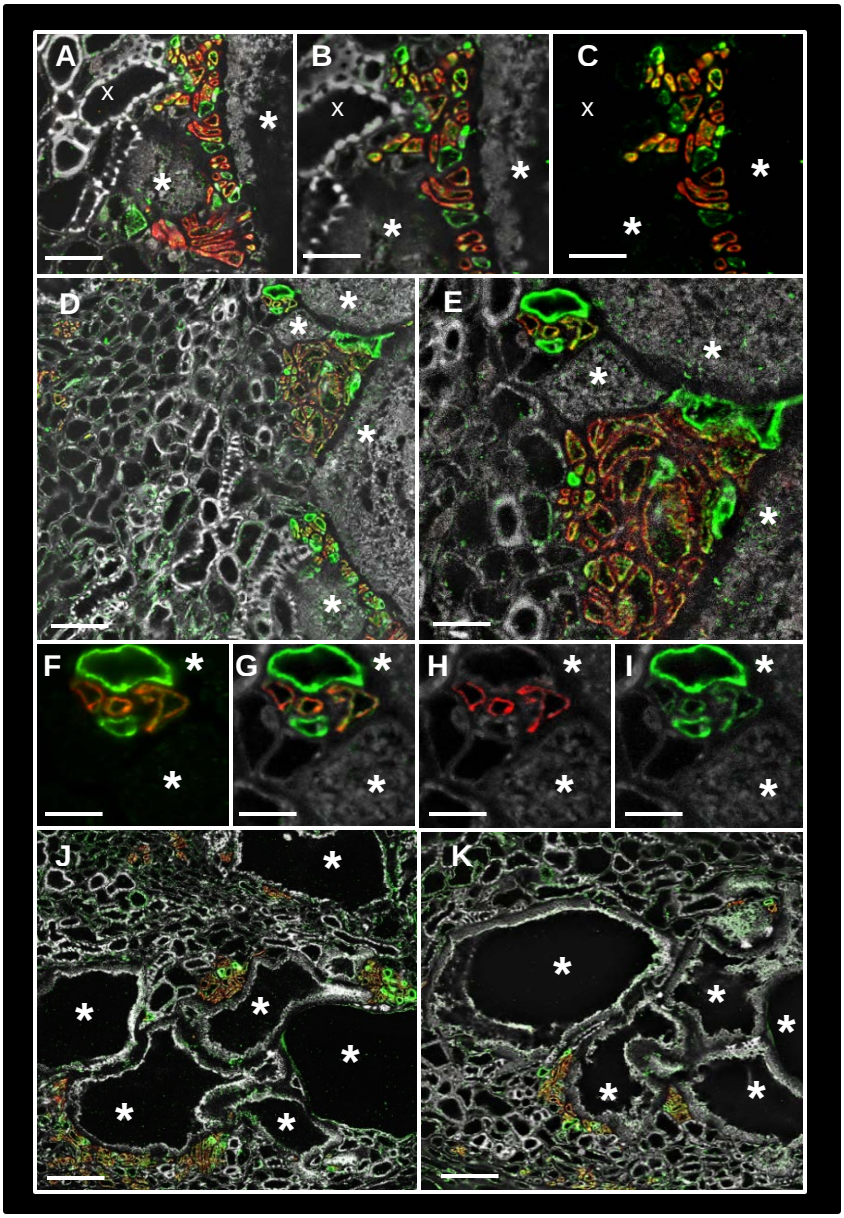

Figure 125. Immunolocalization of root-knots at secondary growth expressing $P_{umamiT29}$: *UmamiT29-GFP*: focus on the cell population around giant cells. Green cells: α-GFP, labeled with CY2, representing UmamiT-GFP cells; red cells: α-RS6 labeled with AF594, representing sieve elements, yellow color: colocalization, white color: autoflourescence. (A) Overview of cell decoration of giant cells in a mature root-knot, scale bar: 25µm. (B, C) Magnification of (A) showing besides yellow cells a number of cells only labeled by α-GFP. (C) Overlay of green and red channel alone, scale bar: 20µm. (D) Extreme old root-knot with very thick xylem vessels encaging the smaller, colored cells and giant cells; scale bar: 25µm. (E) Magnification of the small cells tightly packed around the giant cells, all sieve elements colocalize with α-GFP epitope, a number of cells remains undifferentiated and shows solely UmamiT expression in green, scale bar: 12µm. (F-I) Sieve elements have similar size, cells only UmamiT-positive differ in size. (F) Overlay of green and red channel. (G) Overlay of (F) with autofluorescence channel. (H) Sieve elements in red; (I) UmamiT –positive cells in green, scale bar: 7µm. (J, K) Even in root-knots older than two months colocalization can be observed as well as single cells only with α-GFP decoration, scale bar: 40µm. Asterisks mark giant cells, x (xylem).

A detailed view of the more developed feeding site (Fig 125.) revealed that even at this stage, a limited number of cells still can be classified as parenchyma without differentiation into functional sieve elements (Fig. 125 D-I). As no unlabeled small cells around the giant cells were found and, in contrast to roots, also no sieve element without GFP epitope indicates that every newly formed sieve element around the giant cells is a direct descendant of parenchymatic UmamiT-positive cells.

Although those parenchymatic tissues differentiate into sieve elements, they remain nucleated as shown by DAPI staining (Fig. 126), which characterizes this cell type as juvenile phloem. Additionally, it was possible to show signals for the phloem specific transcription factor APL in the nuclei of those cells (Fig. 127 A-H). Furthermore, the same tissue with RS6 identity showed promoter activity of the transcription factor *SCR* (Fig. 127 I-M). All giant cells surrounding sieve elements showed colocalization with SCR but there were still cells remaining which showed only decoration by α-GFP (Fig. 127 J). Undifferentiated SCR- positive cells were next to differentiated sieve elements but never in direct contact to the giant cells (Fig. 127 J).
These results underline the idea that phloem cells of the feeding site differentiate from parenchymatic cells and represent a discrete cell population in contrast to the phloem originated from the vasculature.

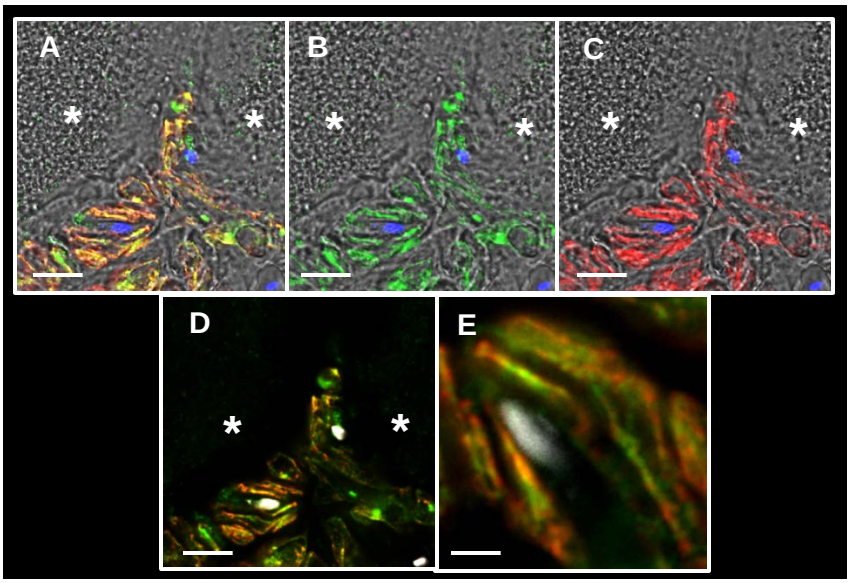

Figure 126. Immunolocalization of root-knots from *P*$_{UmamiT14}$*: UmamiT14-GFP* plants: cell population around giant cells defined as juvenile phloem. Green cells: α-GFP, detected with a CY2-antiserum, representing UmamiT-GFP positive cells; red cells: α-RS6 detected with an AF594-coupled antibody, representing sieve elements, yellow color: colocalization between α-GFP and α-RS6, blue, white color: DAPI. (A-D) Nucleated sieve elements around giant cells with UmamiT identity. (A) Merge of green and red channel. (B) Cells with α-GFP decoration. (C) Sieve elements. (D) Overlay of green and red channel with DAPI, scale bars: 10µm; (E) Single nucleated protophloem cell with RS6 and GFP epitope; scale bar: 2µm. Asterisks mark giant cells.

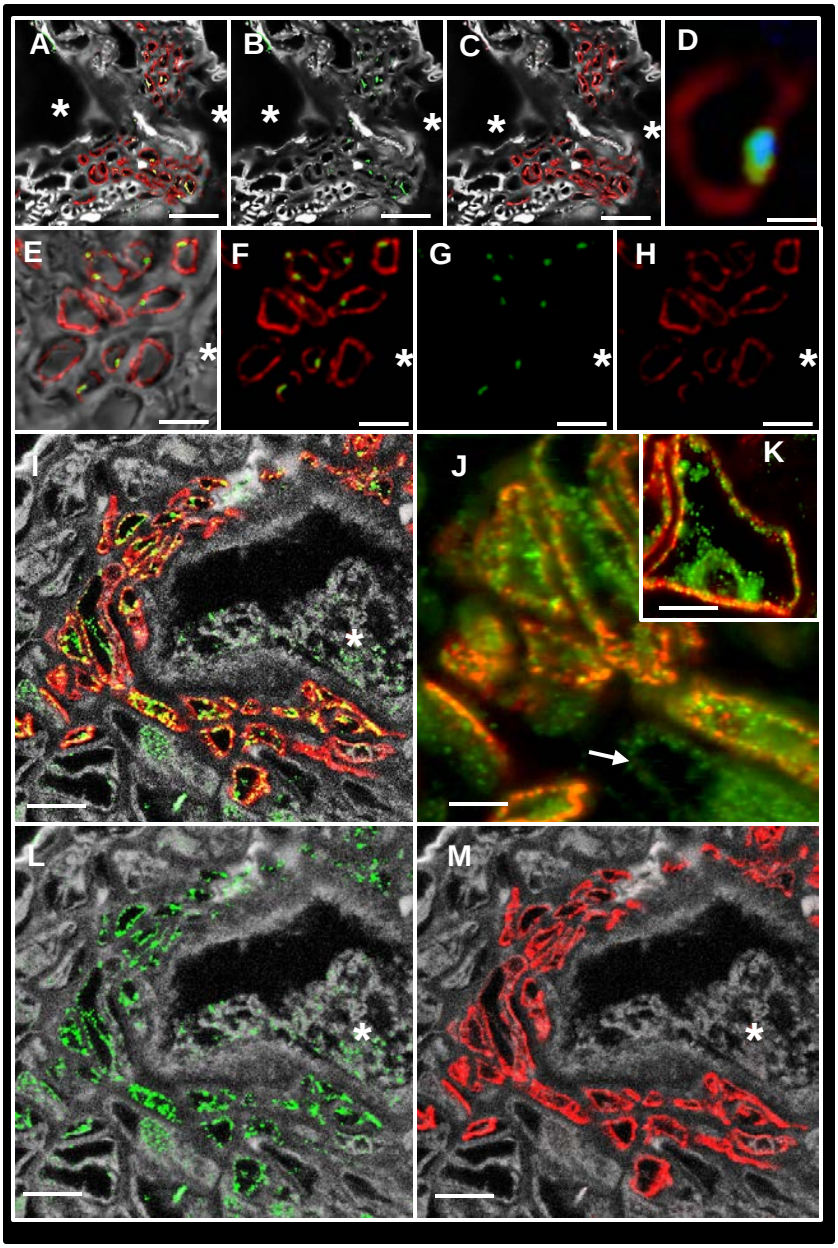

Figure 127. APL localization and *SCR* promoter activity in root knots are found in juvenile phloem. Immunolocalization of root-knots from *P*$_{APL}$*: APL-GFP* (A-H) and *P*$_{SCR}$*:GFP* (I-M) plants: focus on protophloem-like cells. Green cells: α-GFP, labeled with CY2, representing GFP positive cells; red cells: α-RS6 labeled with AF594, representing sieve elements, blue color: DAPI, white color: autofluorescence. (A-C) Sieve elements surround giant cells and harbor nuclei with APL-GFP signals. (A) Merge of green and red channel. (B) Cells with a-GFP decoration. (C) Sieve elements, scale bars: 28µm. (D) Magnification of one phloem cell from a cell population at the feeding site, merge of green and red channel with DAPI, scale bars 6µm; (E-H) Several nucleated phloem cells with RS6 and GFP epitope in the nucleus.; (E) Merge of bright field with (F). (F) Merge of green and red channel. (G) Cells with α-GFP decoration in the supposed nucleus. (H) Sieve elements, scale bars: 15µm. Asterisks mark giant cells. (I, J, L, M) Cross section of a root-knot. (I) Overlay of SCR positive cells (L) with sieve elements (M) , scale bars: 11µm. (J) Every sieve element shows colocalization with SCR, in some cases cells with solely GFP decoration were found (marked by an arrow), scale bar: 3.5µm. (K) Detail image of one sieve element colocalizing with SCR-GFP, scale bar: 5µm. Asterisks indicate giant cells.

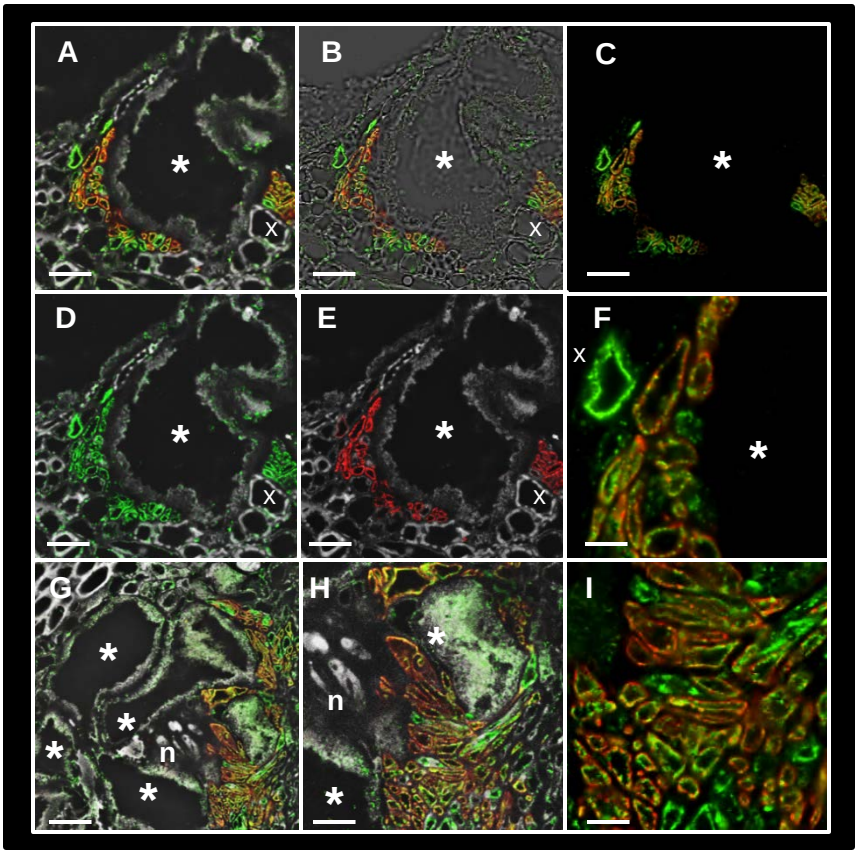

Figure 128. Immunolocalization of root-knots at secondary growth from *$P_{UmamiT29}$: UmamiT29-GFP* plants: focus on the cell population around giant cells. Green cells: α-GFP, labeled with CY2, representing UmamiT-GFP cells; red cells: α-RS6 labeled with AF594, representing sieve elements, yellow color: colocalization, white color: autoflourescence. (A-E) Giant cell embedded in cells colocalizing with α-GFP and a-RS6; feeding site surrounded by massive xylem elements; cells next to xylem mostly undifferentiated. (A) Overlay between autoflourescence, green and red channel. (B) Overlay with bright field picture. (C) Overlay between green and red channel. (D) Cells marked by α-GFP. (E) Sieve elements marked by α-RS6, scale bar: 15µm. (F) Magnification of cells with different size and epitope decoration, scale bar: 5µm. (G-I) Colocalizing cells appear in much higher frequency in older root knots. (G) Feeding site built by xylem cage, giant cells, nematode in the center and small protophloem cells in between, scale bar: 30µm. (H) Magnification of (G) with a very young giant cell embedded in small protophloem cells, scale bar: 20µm. (I) Overlay of green and red channel shows a mixture of cells in the old root knot of (G), high amount of protophloem cells with double decoration of α-GFP and α-RS6; cells without sieve element decoration still present, scale bar: 15µm. Asterisks mark giant cells, n (nematode).

Looking at the anatomical position of these juvenile phloem cells demonstrates their vicinity to the membrane of the giant cell and their functional position next to the xylem (Fig. 128. A-E). Cells next to the xylem remain undifferentiated in higher frequency. Due to this cellular organization the giant cells get connected to the vasculature of the former root. Those cells without the RS6 epitope differ also in size; undifferentiated cells next to the xylem are bigger than those cells appearing directly attaching the giant cells (Fig. 128. F).

Supply of the giant cell complex with the nematode in its center is therefore achieved by the intense differentiation of parenchymatic cells into functional sieve elements (Fig. 128 G-I), which always occurrs at the same place in those tissues next to the giant cells.

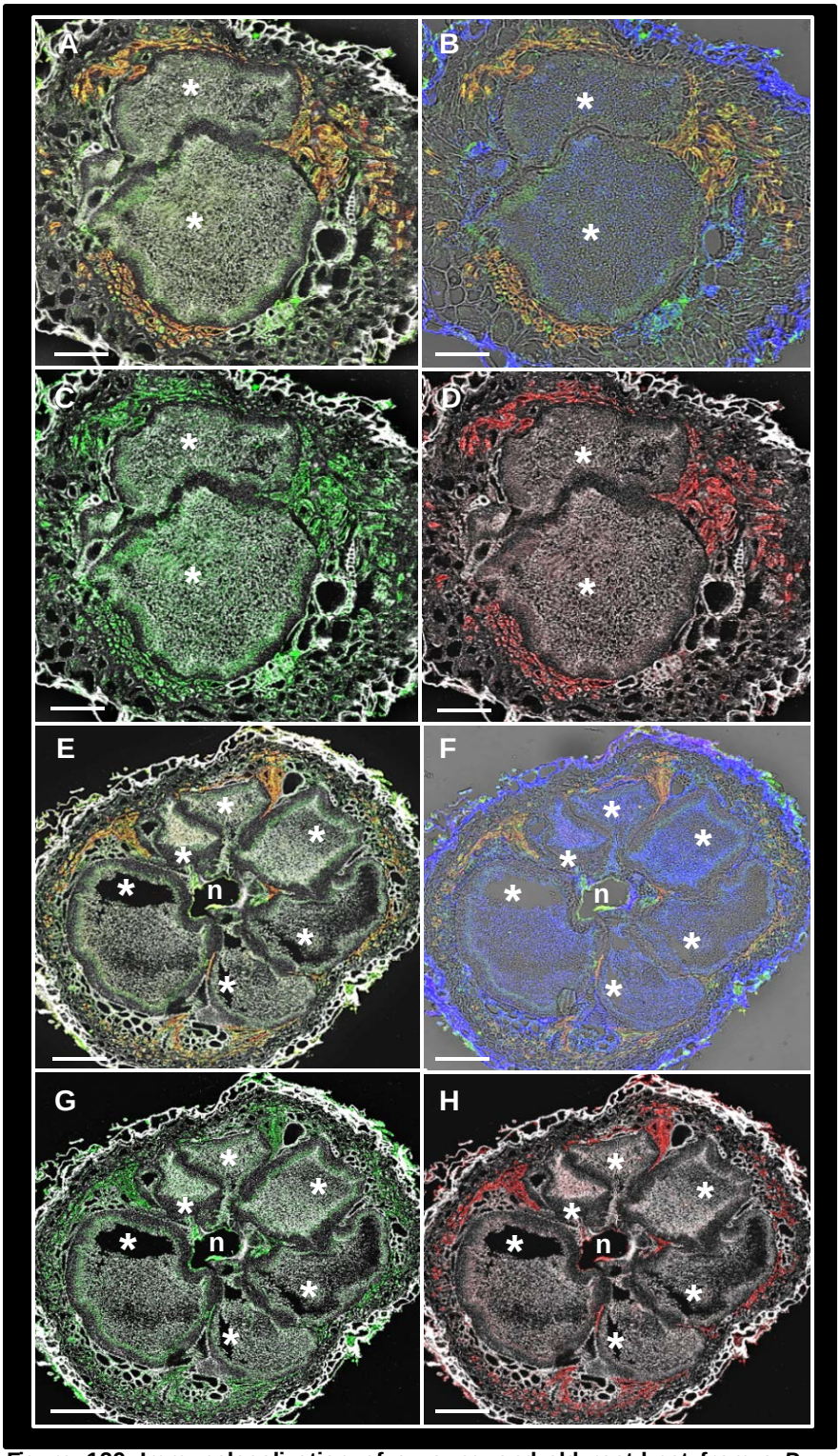

The higher amount of these juvenile phloem cells in older root-knots indicates, that the differentiation process is a consequence of the intense demand of nutrients and a response to the strong sink tissue that was formed there. This enables the nematode to form more and more giant cells within one root knot and to sustain a continuous sink organ there (Fig. 129).

Figure 129. Immunolocalization of a young and old root-knot from a *P*$_{UmamiT29}$*:UmamiT29-GFP* plant. Green cells: α-GFP, labeled with CY2, representing cells that had expressed UmamiT-GFP; red cells: α-RS6 labeled with AF594, representing sieve elements, yellow color: colocalization, blue or white color: autoflourescence. (A-D) Young root-knot with fully differentiated giant cells, xylem cage not completely formed. (A, B) Overlay of green and red channel with (A) autofluorescence and (B) bright field image. (C) Cells with α-GFP decoration. (D) Cells with α-RS6 decoration. Cells around giant cells show colocalization, scale bar: 30µm. (E-H) Very old root-knot with many more giant cells than in (A-D), xylem cage completely built around giant cells, colocalizing cells around giant cells. (E, F) Overlay of green and red channel with (E) autofluorescence and (F) bright field image. (G) Cells with α-GFP decoration; (H) sieve elements, scale bar: 65µm. Asterisks mark giant cells, n (nematode).

5.13. Characterization of knock-out plants

To analyze the physiological function of *UmamiT* candidate genes, single knock-outs of T-DNA insertion lines were identified. Genotyping showed a distinct band pattern for different *UmamiTs*. The predicted fragment for the insert (Fig. 131) could be amplified in the knock-out (KO) but not in the wild type (Fig. 130 A). Using qRT-PCR a severe reduction of the transcript level near zero was observed (Fig. 130 D). Furthermore, the absence of *UmamiT14* and *UmamiT11* transcript at the unloading zone was confirmed by whole-mount *in situ* RNA hybridization (Fig. 130 B-D, Müller et al. 2015, data by Andrea Bleckmann).

Furthermore, in order to complement the mutants, the corresponding UmamiT-GFP construct, containing all introns, was introduced in the KO background.

Before any experiment was started, the seed batch of WT (Col0), the single KOs as well as the complementation lines were synchronized, meaning that all genotypes were grown together at the same time in the same climate chamber and the seeds were harvested simultaneously at maturity.

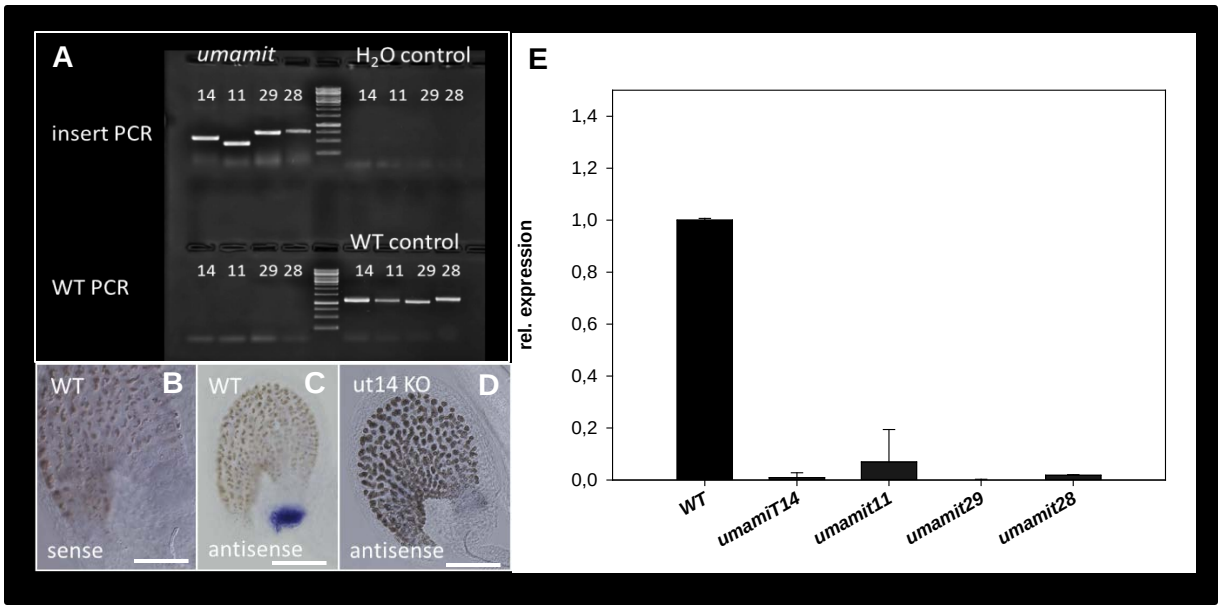

Figure 130. Identification of loss-of-function mutants of the candidate *UmamiTs*. (A) Genotyping PCR shows homozygous individuals for each candidate. Upper row: insert PCR amplified the right band of the insertion using gene specific primers in combination with a primer sitting in the T-DNA. H_2O control was empty. Bottom line: PCR with gene specific primers for the full-length amplicon. Using the same DNA as in the upper panel no amplicon for the homozygous lines was produced, whereas in the control with WT gDNA all bands at the predicted size could be obtained. (B-C) Whole mount *in situ* RNA hybridization using UmamiT14 antisense probe to show that no RNA was left in the unloading zone for this candidate, scale bars: (B) 50µm, (C, D) 40µm. (E) RT-PCR shows severe reduction of the transcript of all mutants near to the detection limit, normalized to UBQ10 (n=3 ± SD).

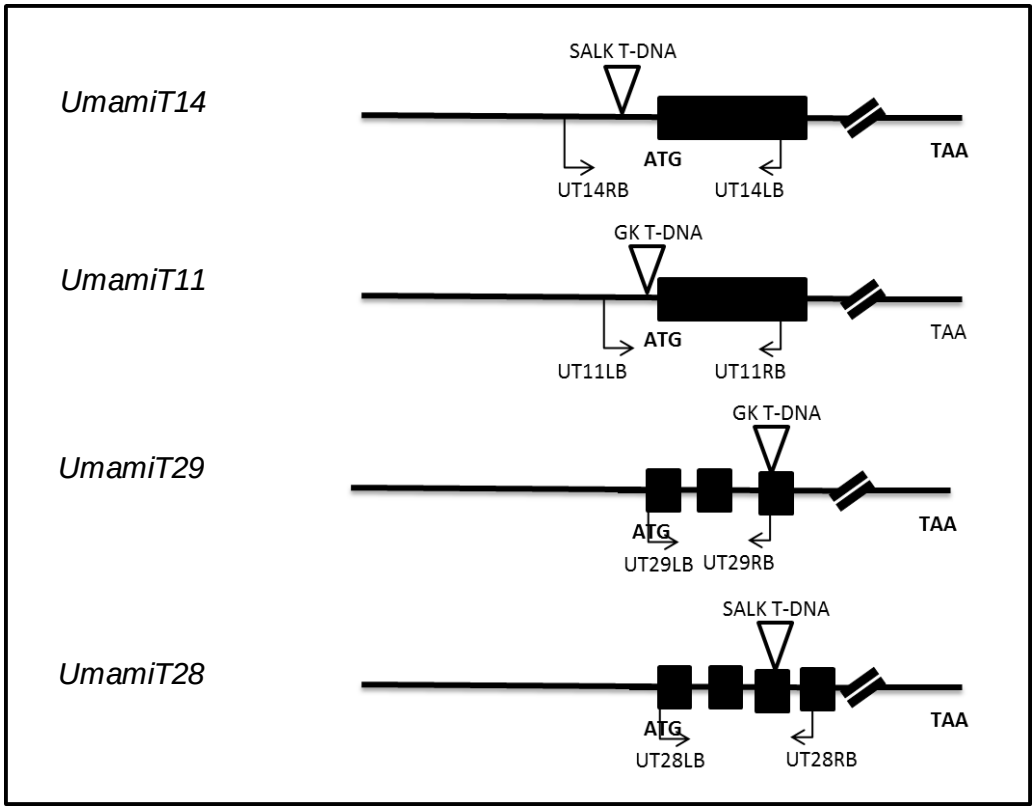

Figure 131. Location of the T-DNA for the isolated *UmamiT* insertion lines. Black boxes represent the exons, white triangle shows place of insertion; position of primers used for genotyping PCR is marked by arrows.

None of the knock-out plants showed any phenotype during the growth and reproduction phase (Fig. 133). The time point of flowering was always quite simultaneously dated with the corresponding WT plants and also the seed set was not affected by the mutation at all. Additionally the embryo development in WT and single knock outs was monitored but also in this study no phenotype or variance compared with the WT could be documented (Fig. 132).

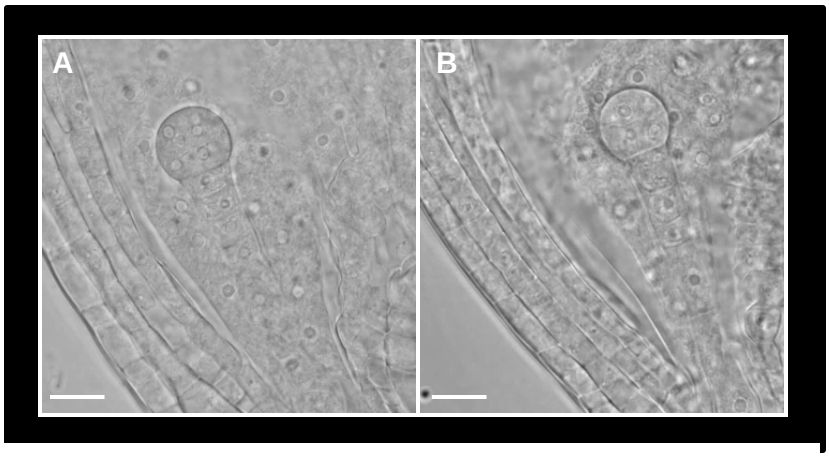

Figure 132. Cleared seed of WT and *umamit14*. No differences in embryo development were found between seeds of WT (A) and *umamit* mutants, represented here by *umamit14* (B), scale bar (A, B) 15µm

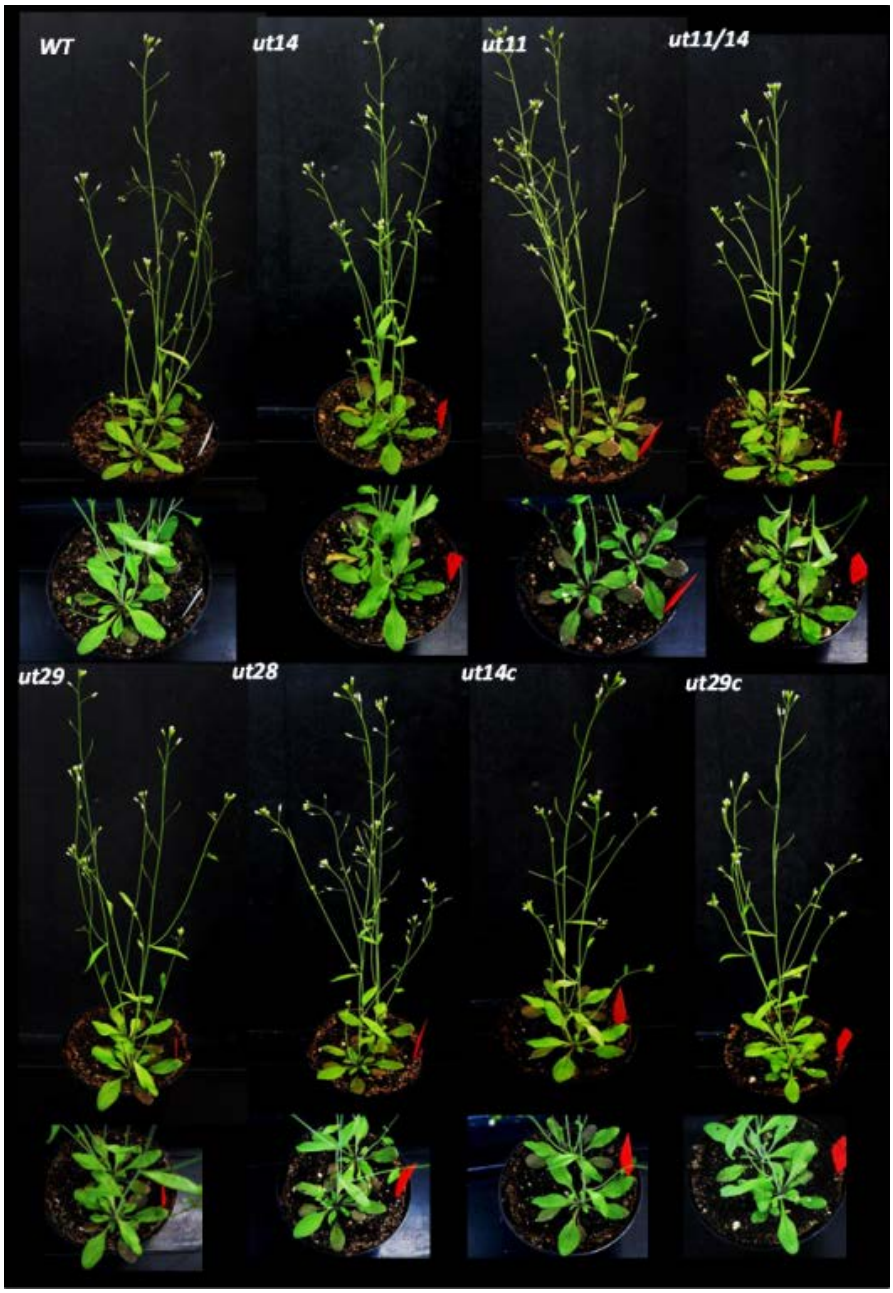

Figure 133. Comparison of growth phenotype between WT, *umamit* knock- outs and one complementation line for clade I (ut14c) and clade III (ut29c). No differences in vegetative growth were seen, flowering time and inflorescence branching was the same for all lines; leave color and size of the plants was the same in all lines.

5.13.1. Analysis of the level of free amino acids

In order to investigate the influence of the loss-of-function of UmamiT proteins in the unloading domain and the integuments, an analysis of the amount of free amino acids in the silique was established. Rationale was that the mutation would result in elevated levels of free amino acids, because they would not be exported out of the unloading zone or the integuments into the embryo, where they would be metabolized into proteins. The preparation of the probes and the LC-MS analysis was outsourced to the lab of the cooperation partner Prof. Dr. Wilfried Schwab at the TUM.

Siliques of the same age were harvested between 10 o´clock and 12 o´clok to allow the plants to recover from the night. The results of amino acids that were present in higher concentration in the seeds are shown in Fig 134. In most cases a higher amount of free amino acids in the mutants compared to the WT plants was noticed.

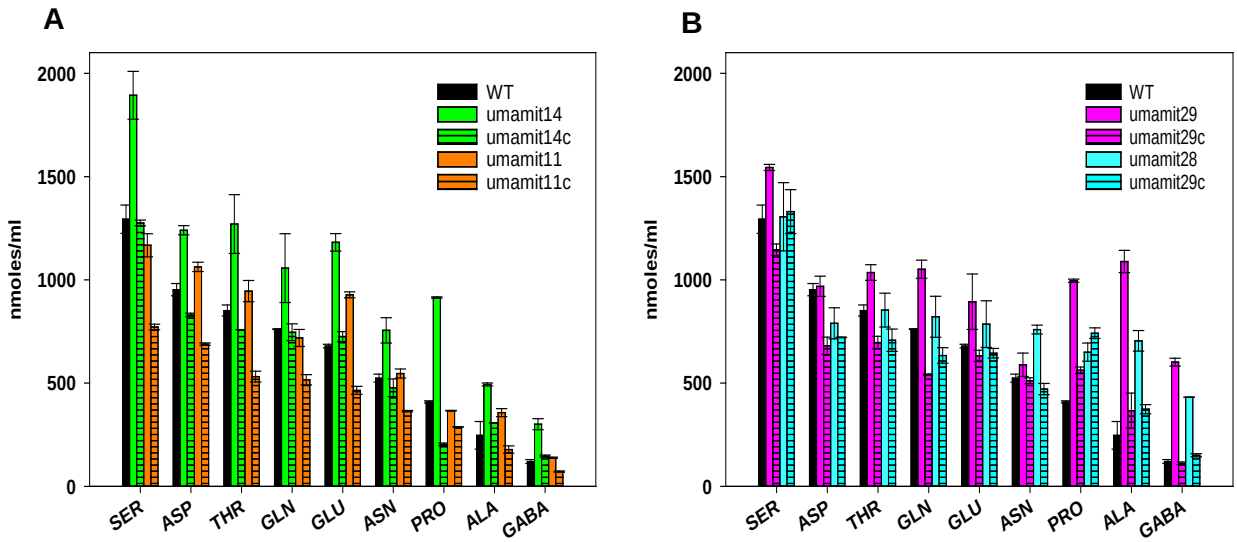

Figure 134. Level of free amino acids in siliques of WT and *umamits* determined by LC-MS. (A) Clade I UmamiTs, (B) clade III UmamiTs. In most cases complementation of mutants resulted in a titer of free amino acids comparable to WT level. Differences were seen between UmamiTs from different clades; UmamiTs from the same clade behave similar compared to members from another clade.

Complementation was also possible for the single knock out, which shows that on the one hand the UmamiT-GFP fusion protein is functional in plants and on the other hand that changes in the amino acid level were due to the knock-out of the corresponding *UmamiT* gene. The amino acid profile varied between members of different clades. UmamiTs from clade I apparently transport different amino acids than UmamiTs from clade III in the seed. This suggests that members among one clade behave more similar than in comparison with members of other clades. Knock-out of *UmamiT11* showed the mildest effect on changes in

amino acid levels. Amino acids that were found in high amounts in WT increased furthermore in *UmamiT14* and *11* mutant background, whereas only a mild effect on these amino acids in *UmamiTs* of clade III was detected.

All knock-outs showed elevated levels of glutamate. Looking at the substrate specificity the two clades displayed differences. UmamiTs of clade III seemed to transport preferentially small and nonpolar amino acids and to a much lower extend amino acids that were strongly increased in *umamit14* from clade I.

Additionally, an analysis was done in a higher order mutant of *umamit14/11* (Fig. 135). Here a striking elevation of the level of free amino acids was seen in the ho/he mutant. The greatest impact of the additive effect of the downregulation of two *UmamiTs* was seen for Ser, Asp, Thr, Gln and Glu. For the other amino acids, the accumulation of free amino acids was not that pronounced and comparable to the single knock out of *UmamiT14*. Fig. 134 shows that UmamiT14 had a stronger impact on amino acid levels than UmamiT11. Judging from the results of the single knock-out, the additive effect seen in Fig. 135 is higher than expected. These results show that indeed higher order mutants do have a higher level of free amino acids. The level is more than twice the amount of the single knock-outs, suggesting that there may be an interaction at the protein level between UmamiT11 and UmamiT14.

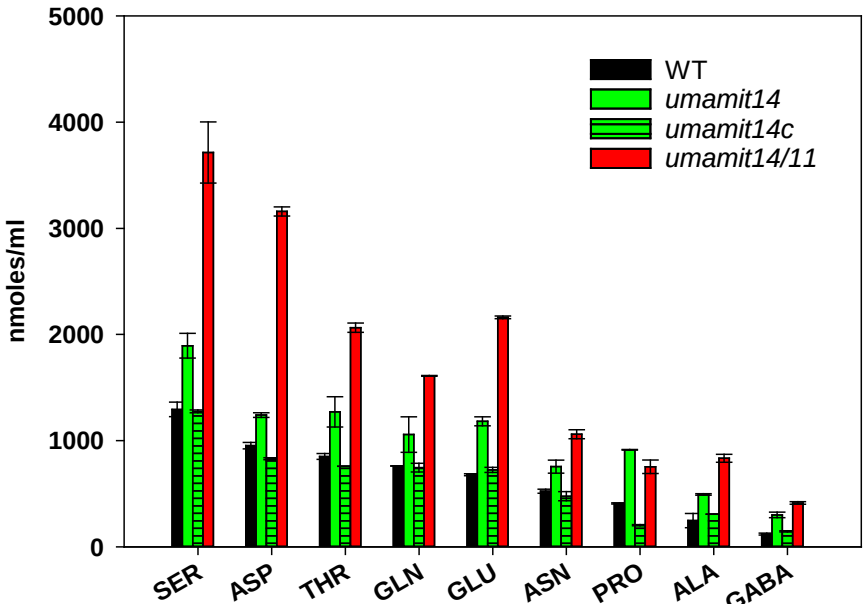

Figure 135. Level of free amino acids in siliques of WT, single and double mutants of clade I determined by LC-MS. Additive effect in the higher ordered mutant of clade I UmamiTs.

Although this metabolic phenotype was found in the knock-out plants, no impact on seed set could be observed. Therefore investigation of seed size by measuring length and width of the mature seeds was done. Indeed, there was a significant difference for both parameters. Furthermore, the seed volume was calculated from this measurements (Fig. 136). Seeds of the mutants were significantly smaller compared to WT or the complementation lines (ANOVA, $p<0.001$). As already observed in the amino acid levels, the effect of the mutation of *UmamiT11* was weakest compared to the other *UmamiTs* including its close relative *UmamiT14*. This result demonstrates that transport processes in the unloading domain and the integuments during seed development are linked with yield, indicating that amino acid transport in the seed is significantly managed by UmamiTs.

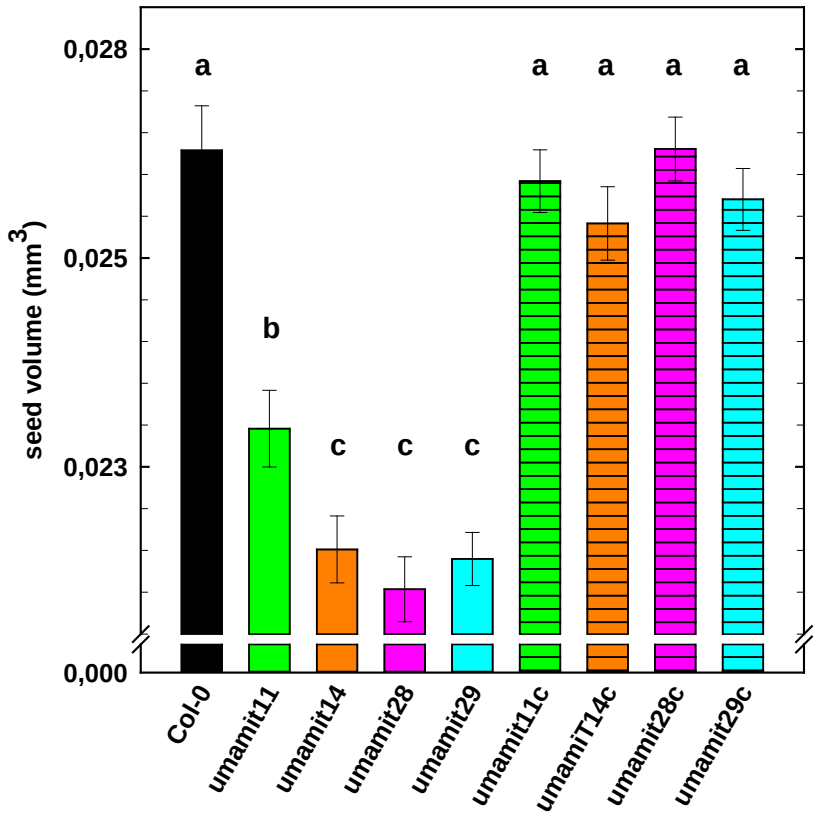

Figure 136. Seed volume determination. Seed Volume of WT, u*mamit* mutants and complementation lines were calculated using measurements of length and width of the seed. ($p<0.001$, $n>40$±SE, one way ANOVA followed by Holm-Sidak post hoc test)

5.13.2. Phenotypical characterization of roots in *umamit* mutants

5.13.2.1. Root length in single knock-out background

Although the aboveground vegetative growth was not influenced, the effect of the T-DNA insertion on the root system was investigated on plates. Plants with a root system comparable to WT were found, but also in higher extend individuals with shortened roots for each T-DNA genotype. The mutant plants showed a significantly reduced root length (ANOVA, $p<0.001$) compared to WT or the corresponding complementation line (Fig. 137). *UmamiTs* of the same clade (*umamit11,14* and *umamit28, 29,* respectively) behaved more similar to each other than members of different clades. This phenotype disappeared latest after 21 days and the roots of mutants reached the same size as the WT.

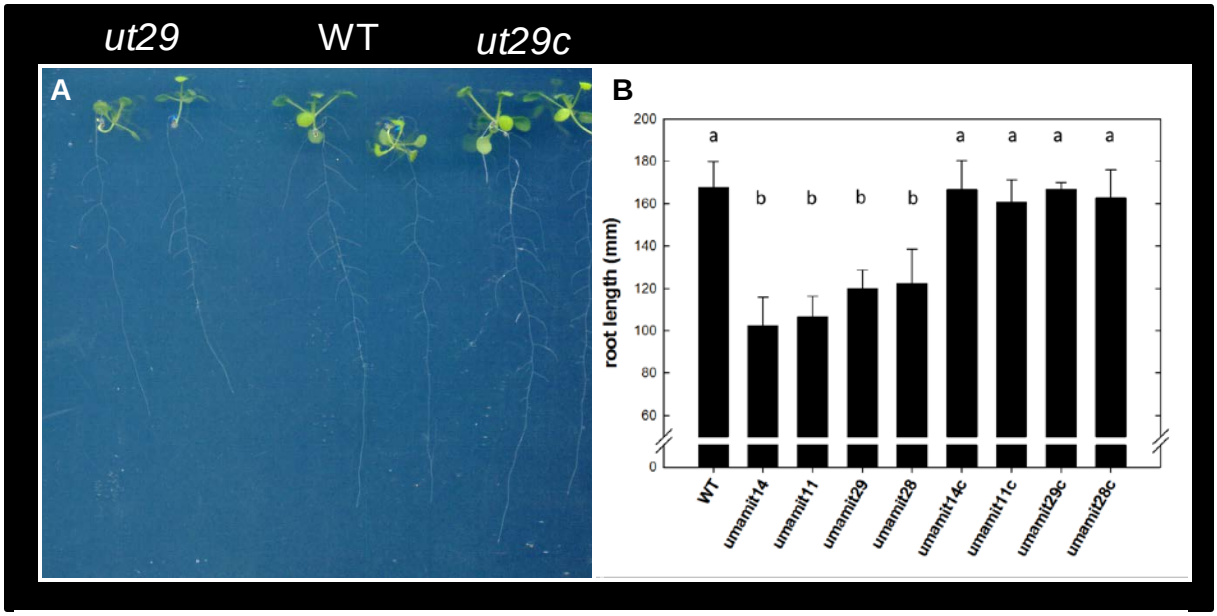

Figure 137. Root length of WT, *umamit* mutants and complementation lines. (A) Single knock-out growing next to WT and complementation line, scale bar: 500µm. (B) Determination of root length of WT, umamits and the corresponding complementation lines. ($p<0.001$, $n>17\pm SE$, one way ANOVA followed by Holm-Sidak post hoc test)

Furthermore, double knock-outs were created for *umamit11* and *umamit14*, as well as for the pair *umamit14* and *umamit29*. The double-knock out of *umamit28* and *umamit29* was in progress but not analyzed so far due to time limitation. Additionally, in the *umamit14* mutant background crosses of the insertion of the already published SIAR1 (Ladwig et al. 2012) or CAT6 (Hammes et al. 2006) were generated. By crossing was also a double knock out between *cat6* and *umamit29* created. The rational of these crosses was to analyze the effect of a loss-of-function of an amino acids exporter and importer on the plant growth, seed development and root morphology.

5.13.2.2. Cripple plants in the double knock-out background

In the case of the double knock-out of *umamit14* and *umamit11* homozygous plants were never obtained on soil. Vegetative growth and seed set was also not significantly affected. Nevertheless, empty spaces in the siliques were not observed in the parental plants. On plates, it could be observed that some seeds germinated much later and the plants arising from those seeds were less vital than the sister plants on the same plate. According to their look they were called “cripple” plants. The frequency in which those plants appeared was less than 11%. Genoyping of the cripple plants identified them as homozygous mutants. A longer cultivation on plates revealed that the vegetative growth was severely reduced. The root stopped growth eventually and also no additional leaves were made (Fig. 138). Cripple plants started to become pale after two weeks and finally died. Several runs of rescue experiments were performed to obtain seeds form homozygous plants. Cripple plants were cultivated together with the “normal” looking sister plants on plates supplemented with glutamate or aspartate alone. Also a combination of both amino acids was used with and without sucrose. None of these experiments lead to a rescue of the cripple plants, whereas the WT-like plants showed a normal growth (data not shown). In addition, because promoter activity and RNA level increased after application of auxin, it was tried to rescue the mutants by application of auxin. But also in this case no rescue was possible for the mutants, whereas normal looking sister plants could grow well on the plates (data not shown).

Furthermore, it was tested if *UmamiT11* and *UmamiT14* compensate for each other. As Fig. 139 shows, there was no difference in the RNA level of *UmamiT14* found in WT and in the *umamit11*. The same was true for the close relative *UmamiT11*. This indicates that a rescue by compensation mechanisms with the genetically closest relative was not achieved and that RNA levels of each candidate stay unaffected in the sister knock-out.

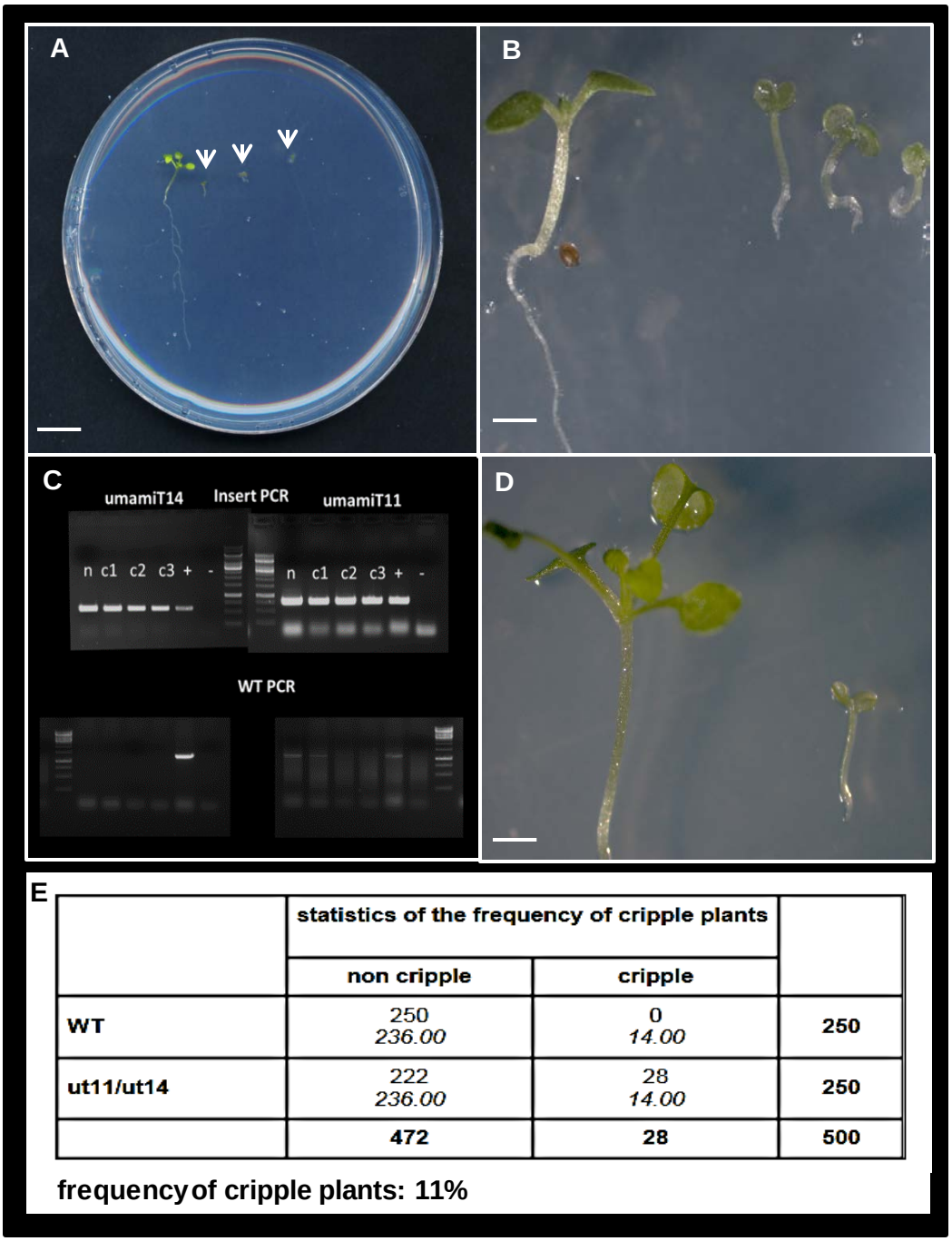

E

	statistics of the frequency of cripple plants		
	non cripple	cripple	
WT	250 *236.00*	0 *14.00*	250
ut11/ut14	222 *236.00*	28 *14.00*	250
	472	28	500

frequency of cripple plants: 11%

Figure138.Characterization of *umamit* double knock-out. (A) Comparison of vegetative growth between normal looking WT-like- double knock out and cripple plants, scale bar: 500µm. (B) severe root phenotype in the cripple plants, scale bar 300µm. (C) genotyping PCR of normal looking plants and cripple plants. Upper row: insert PCR, lower row: WT PCR, +: positive control, -: water control. (D) Comparison of growth phenotype of individual plants from (A) after three weeks. Cripple plants don't develop further in the shoot and show severe root phenotype. Also the color of the cotyledons changed to pale green, which indicates dying of the seedling. Scale bar: 300µm. (E) Chi^2 statistics on the frequency of cripple plants, expected values are displayed in *italics.* P<0.001, χ^2= 29.666, df=1, n=250.

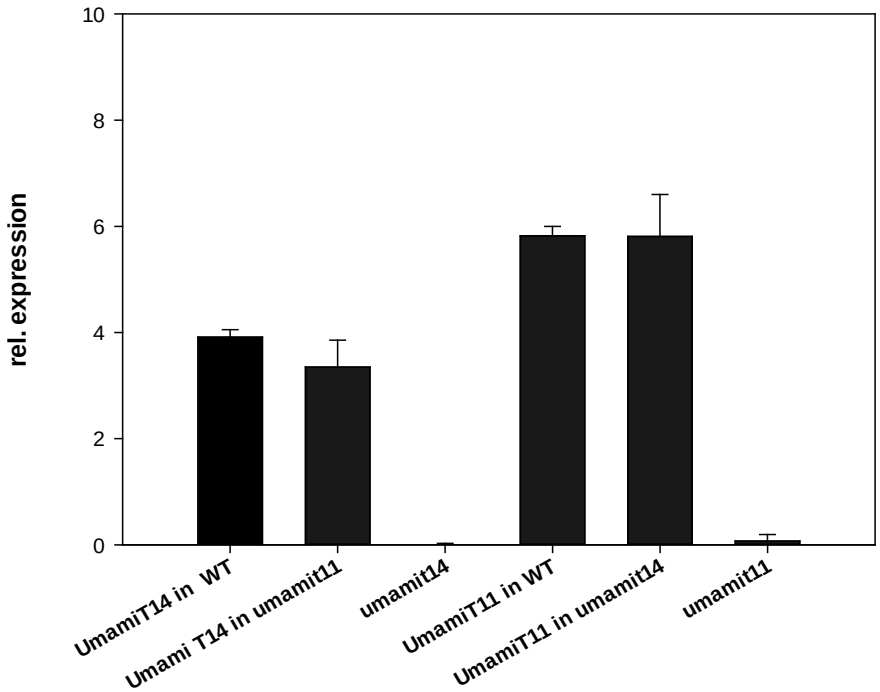

Figure 139. Real time PCR to quantify the amount of transcript of the sister *UmamiT* in the *umamit background*, normalized to UBQ10 (n=3 ± SD).

The lack of a compensation of the mutation in the roots led to an arrest of root elongation in the cripple plants. First the roots of those cripple plants were characterized by PI staining in comparison with WT and a deorganized root tip and a lack of a functional columella cell file were found (Fig. 140). According to the anatomical position it was not possible to find any cells that displayed the same morphological character as a QC or stem cells. Instead, more or less uniformely shaped cells in the root tip were found and no functional organizing center (Fig. 140 E, F).

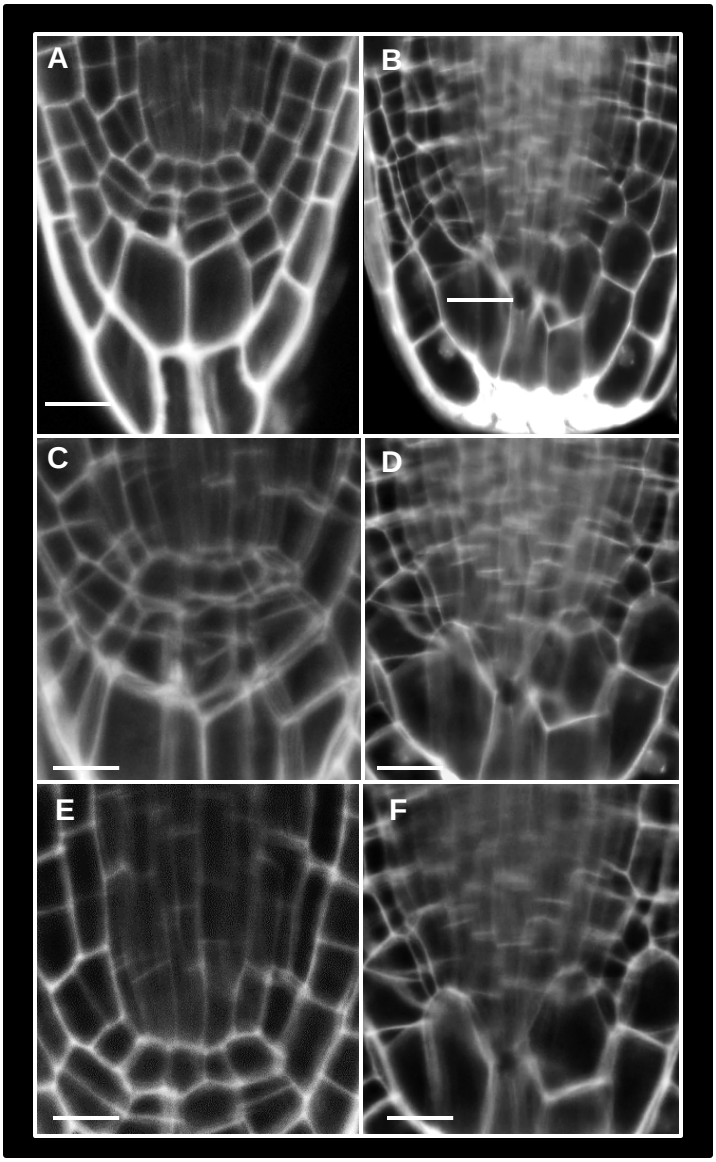

Figure 140. PI staining of WT root compared with cripple plant. (A, C, E) WT, (B, D, F) cripple plant, (A, B) focus at the QC, scale bars. (A) 15µm, (B) 18µm. (C, D) maximum projection, scale bars: (C) 10µm, (D) 12µm; (E, F) magnification of the area around the QC, scale bars: 10µm.

5.13.2.3. Lugol staining of roots from *umamit* mutants

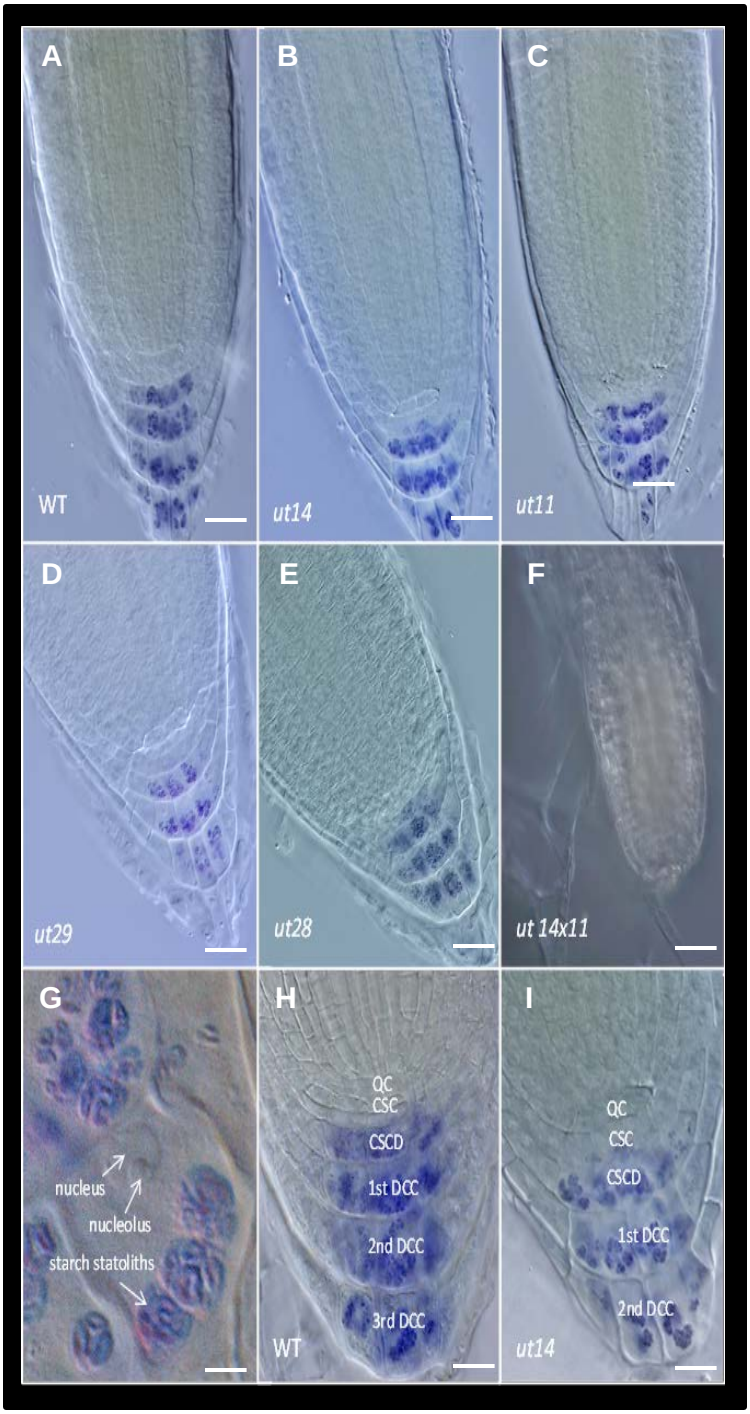

Figure 141. Lugol staining of roots from WT and *umamits*. (A) WT, scale bar: 25µm, (B-F) *umamit* mutants, scale bar (B, C) 20µm, (D) 15µm, (E) 20µm, (F) 40µm. (G) Magnification of a columella cell where specific staining was found in the starch statholiths, scale bar: 2µm. (H, I) Magnification of the root tip from a WT root (H) and *umamit* mutant root (I), scale bars: (H) 15µm, (I) 12µm. QC (quiescent center), csc (columella stem cells), cscd (differentiating columella stem cell daughters), dcc (differentiated columella stem cells).

The observations from the PI staining indicated that stem cell maintenance and differentiation of columella root cap cells was compromised. In order to visualize the presence of a functional columella also in single knock-outs Lugol staining was performed. The specifc staining of the starch statholoths (Fig. 141 G) showed that there were no differences in the proportion of starch granuels in the differentiated columella cells in WT and single knock-out plants (Fig. 141). Also the shape and number of columella cells was not altered in the single knock-outs. As observed before in the PI staining, no functional columella cells in the cripple plants could be found. Altogehter these results show that the formation of the columella was not affected by the loss of function of one *UmamiT* candidate in the root. Due to the limitations of light microscopy the cellular resolution in this case was not that good to see smaller differences that may occur in the anatomy of the deeper laying tissues around the stem cells.

5.13.2.4. mPS-PI staining of roots from umamit mutants

To overcome these limitations, mPS-PI staining was done for WT and single-knock outs. This allows the simultanous visualization of the starch statholiths as well as the cellular organization of the very root tip. No strinking differences in the number of cell files with starch granules between WT plants and the single knock-outs could be observed (Fig. 142 A-C). The overal morphology of the root was not altered compared to WT. Also a closer look at the protophloem cell file, which always appeard in about 150µm distance from the root tip and is characterized by cell wall thickening, revealed no striking differences between the anatomy of the single knock-out compared to the WT (Fig. 142 D, E). Protophloem cells always lay in the fifth cell layer under the rhizodermis (Fig. 142 F, G).

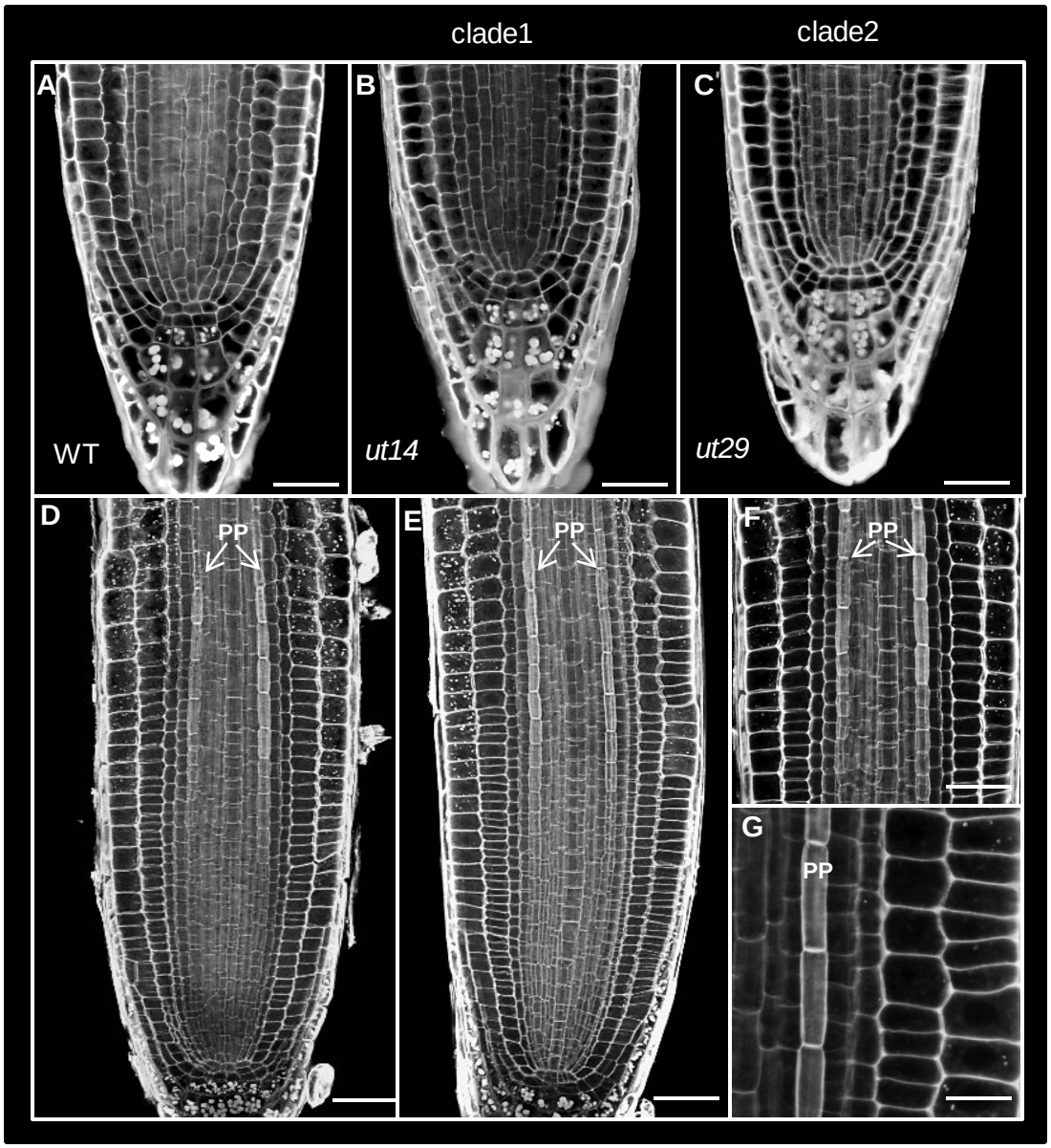

Figure 142. mPS-PI staining of roots from WT and *umamits*. (A-C) Root tips, (A) WT, scale bar: 30µm, (B) *umamit14*, scale bar: 25µm, (C) *umamit29*, scale bar: 20µm. (D-G) Protophloem in focus, (D) WT, scale bar: 40µm, (E) *umamit29*, scale bar: 35µm, (F) maximum projection of *umamit29* differentiation zone, scale bar: 33µm. (G) Single optical section, showing the position of the protophloem file in the fifth cell layer beneath the rhizodermis, scale bar: 16µm. PP (protophloem).

The organziation of the cells around the QC was in most cases comparable to each other (Fig. 142 A-C), meaning that after the QC one cell file of columella stem cells (CSC) appeared, followed by the zone of differentiating columella stem cells daughters (CDSD) with starch statholits, that appeard very prominent in the next cell layers, the so called differentiated columella cells (DCC) (Fig. 143. A). In very few cases (<7%) opposite differences were observed concerning the differentiation of the columella stem cells in both clades.

For *umamit11* and *umamit14* first starch granules appeared already in the columella stem cells (Fig. 143 B-D). This indicates that the diffentiation zone of the root cap is shifted towards the QC (Fig. 143 D). In the CSC of WT roots never any starch granules were detected, wherease *umamits* of clade I showed an accumulation of small granules already in the stem cell zone. The opposite effect was monitored in *umamit28* and *umamit29*. In those roots an increase of columella stem cells was observed (Fig. 143 E-G). Instead of one layer like in WT, two cell layers could be seen. Although these findings were only apparent in rare cases, they could be documented. They show that mutations of *UmamiTs* lead to different effects in the root tip concerning clade I and clade III *UmamiTs* (Fig. 143 H-I). These results for clade I correspond to the phenotype of the cripple plants that completely lack a functional columella. This is an indication, that the complete differentiation of stem cells in the root may be responsible for the observed phenotype and that this “accident” was already found in the single knock outs, where an unusual shift of differentiated cell layers towards the QC happened.

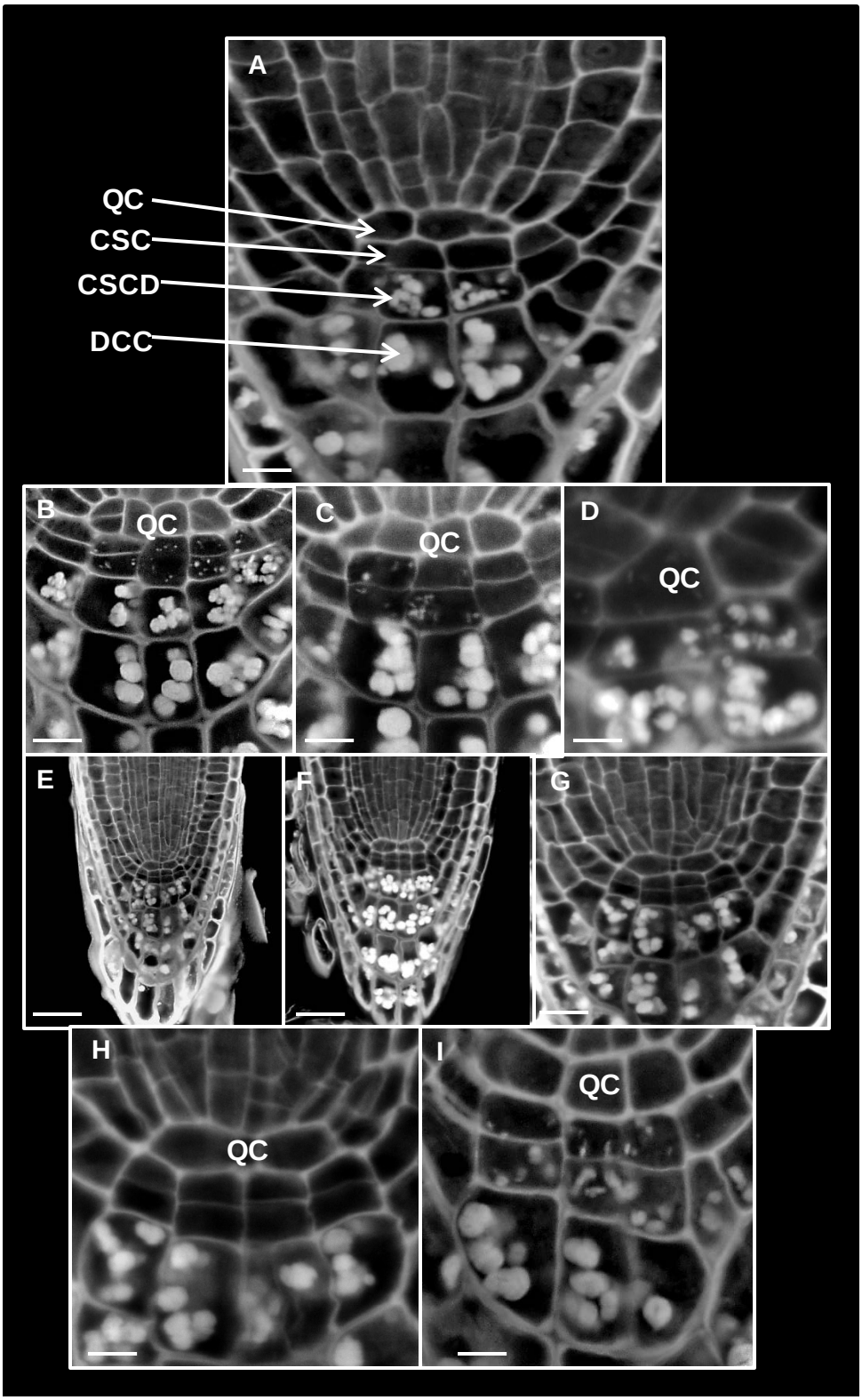

Figure 143. Root stem cell phenotype of *umamit* mutant plants. (A) Overview of the organization of the root tip in WT, scale bar: 7µm. (B-D) *umamit* clade I phenotype, (B) *umamit14*, scale bar: 8µm, (C) *umamit11*, scale bar: 6µm, (D) extreme phenotype of *clade I umamits*, scale bar: 2µm. (H-G) *umamit* clade III phenotype, (E) *umamiT29*, scale bar: 22µm, (F) *umamit28*, scale bar: 20µm, (G) magnification of (E) scale bar: 7µm, (H, I) opposite effect on roots in clade I and clade III mutants; (H) *umamit29*, scale bar: 3µm, (I) *umamiT14*, scale bar: 5µm.QC (quiescent center), csc (columella stem cells), cscd (differentiating columella stem cell daughters), dcc (differentiated columella stem cells).

5.13.2.5. Whole-mount *in situ* RNA hybridization in the mutant background of *UmamiTs*

A single knock out of *UmamiT* genes has a positional effect on the organization of root tip cell layers, as it was shown before. In the cripple plants there were several hints, that the loss of the meristem was the reason of the phenotype. In order to analyze the pleiotropic effects of the mutation whole-mount *in situ* RNA hybridization experiments were performed. This method enables to visualize the distribution of mRNA and is therefore suitable to monitor more precisely the effect of UmamiTs on the gene expression in the root meristem. Harvesting and analyzing probes at the same time and using mastermixes for all specimens of sense and antisense probes allows furthermore to make statements about the strength of RNA expression in the tissues. First *in situs* with *PLT1*, a transcription factor important for stem cell activity in the QC, were performed (Fig. 145).

As published, the maximum of *PLT1* RNA detected was found in the QC and the columella stem cells (Fig. 144 A). In WT and the single knock-out lines no negative effect of the mutation could be seen on the staining intensity of *PLT1* at the root tip (Fig. 144 B-F).

Double knock-out combinations of *umamit14* and *umamit29* showed a slight reduction of signal intensity (Fig. 144 G).

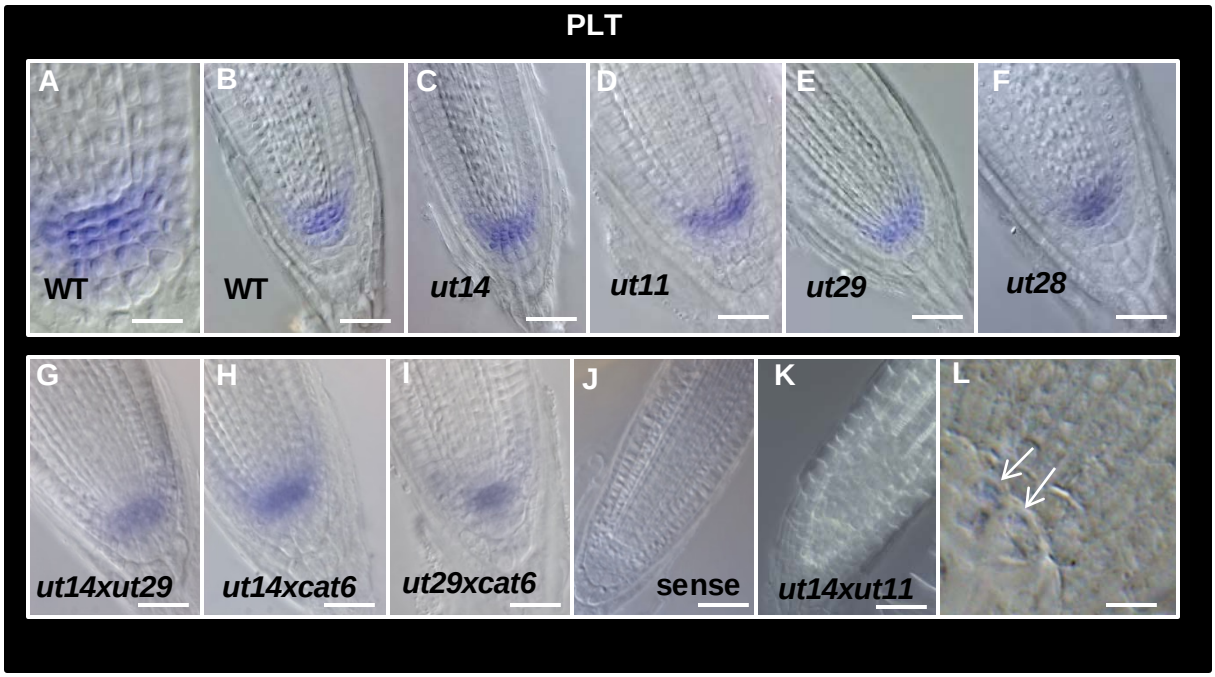

Figure 144. Whole mount *in situ* RNA hybridization using *PLT1* antisense probe. (A, B) WT, scale bar: (A) 15µm, (B) 30µm. (C) *umamit14*, scale bar: 30µm, (D) *umamit11*, scale bar: 40µm. (E) *umamit29*, scale bar: 25µm. (F) *umamit28*, scale bar: 20µm, (G) *umamit14/umamit29*, scale bar: 25µm. (H) *umamit14/cat6*, scale bar: 18µm. (I) umamit29/cat6, scale bar: 25µm. (J) Sense probe, scale bar: 40µm. (K) *umamit14/umamit11*, scale bar: 30µm. (L) *umamit14/umamit11*, scale bar: 10µm.

The same was true, if a knock-out of the strongest candidate of from clade I or III together with the gene encoding the cationic amino acid transporter AtCAT6 was analyzed (Fig. 14 H, I).In the mutant situation of *umamiT11/14*($\frac{umamit11}{bumamit11}/\frac{UmamiT14}{umamit14}$ and $\frac{UmamiT11}{bumamit11}/\frac{Umamit14}{umamit14}$) hardly any signal for *PLT1* could be detected. In one of eight cases, a very weak signal was detected at the QC, whereas in most probes no signal at all was found (Fig. 144 J-L). This supported the idea, that a loss-of-function of a combination of *UmamiTs* affects the stem cell niche and leads to a loss of the QC.

To specify this scenario in more detail, the same experiment was done with probes for the QC marker *WOX5*. Distinct signals in punctuated fashion only in the QC were found in the root tip (Fig. 145 A). The genotype had no influence on the position of expression or strength of the signals. All single knock-outs as well as combinations with *cat6* showed *WOX5* expression in the QC (Fig. 145 B-F, H.I). The double mutant of *umamit14*x*umamit29* was also comparable to WT (Fig. 145 G). Only in the knock-out of *umamit14*x*umamit11* no signal was observed and the specimens looked like the sense probes (Fig. 145 K). This result supported the previously reported findings about *PLT1* and the idea, that a loss of *UmamiTs* in the roots affects processes occurring in stem cell maintenance.

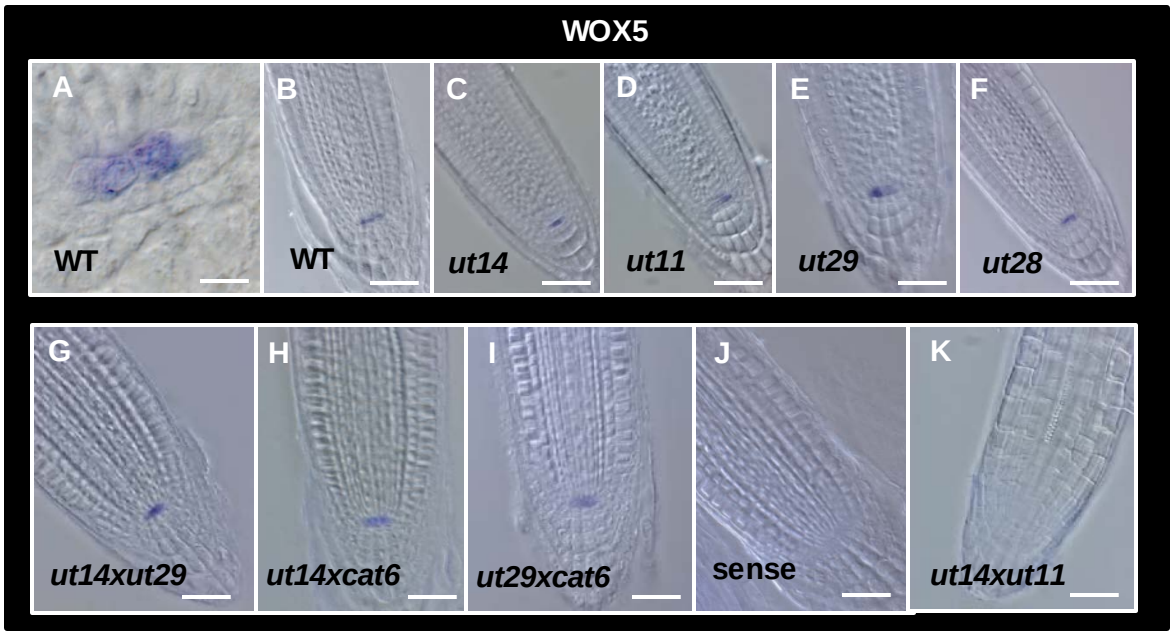

Figure 145. Whole mount *in situ* RNA hybridization using *WOX5* antisense probe. (A, B) WT, scale bars: (A) 6µm, (B) 40µm. (C) umamit14, scale bar: 40µm, (D) *umamit11*, scale bar: 40µm. (E) *umamit29*, scale bar: 30µm. (F) *umamit28*, scale bar: 25µm, (G) *umamit14/umamit29*, scale bar: 40µm. (H) *umamit14/cat6*, scale bar: 40µm. (I) *umamit29/cat6*, scale bar: 40µm. (J) Sense probe, scale bar: 25µm. (K) *umamit14/umamit11*, scale bar: 50µm.

UmamiT knock-out plants showed reduced root length compared to WT or complementation lines. A reduction of root length could be a result of a smaller cell size or a reduced cell number. To address this question whole mount *in situ* RNA hybridization experiments using the cell cycle marker *CYCB1.3* were performed (Fig. 146). Differences in staining intensity and number of cells with positive staining were found. Whereas in the WT plants a strong staining in several cells of the rhizodermal layer and the cells belonging to the provasculature was observed (Fig. 146 B), a much weaker staining pattern was documented for *umamit14*, *28* and *29* (Fig. 146 D, E, F). *umamit11* mutants showed a less clear reduction in staining intensity (Fig. 146 D) and thus were more similarto WT. In *umamit* mutants of higher order (Fig. 146 G, H) a weaker staining pattern was observed, with exception of u*mamit14xumamit11*, where no staining in the cripple plants was seen. The tendency to show an altered staining pattern compared to WT was also true for the knock-outs between the strongest candidate of each UmamiT clade and the cat6 knock-out of (Fig. 146 I, J).

In order to quantify the observed staining pattern z-stacks through the whole root tip were performed for WT and umamit mutants. The quantification of the number of cells with strong staining over the whole root tip validated the already mentioned differences between *umamit* plants compared to WT. With exception of *umamit11* all knock-out plants showed a significantly reduced number of cells being in the mitotic state in the root tip (Fig. 148). This indicates that the weaker staining pattern and the reduced number of mitotic cells could be a possible reason for the shorter roots in young seedling plants. The presented results indicate that the amino acids transport by UmamiTs influences mitosis in the meristemtaic zone of the root tip.

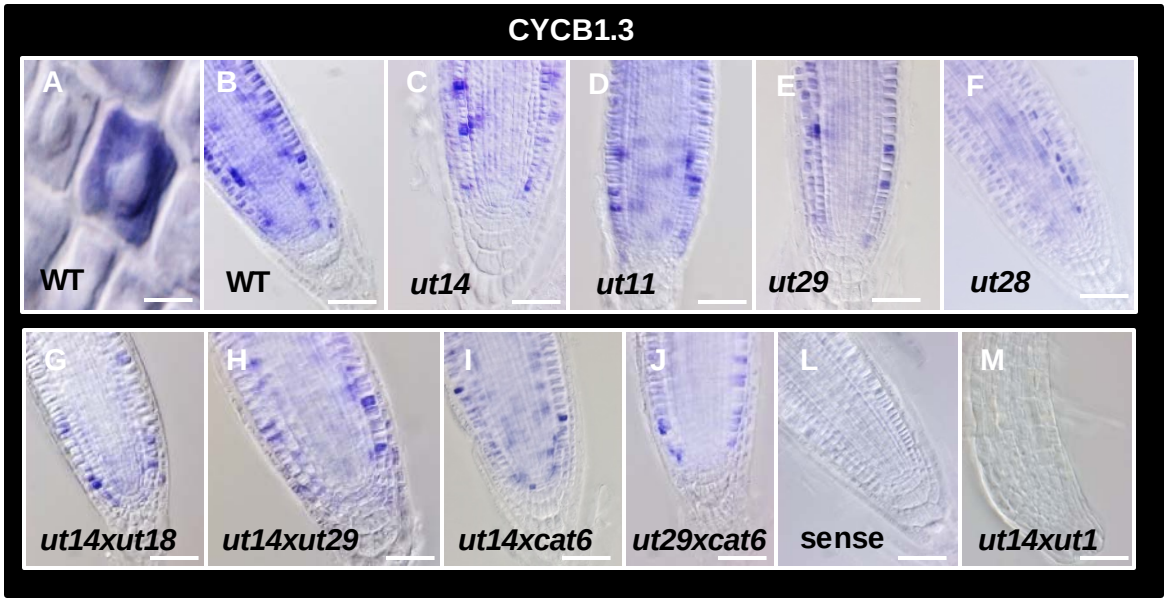

Figure 147. Whole mount *in situ* RNA hybridization using *CYCB1.3* antisense probe. (A, B) WT, scale bars: (A) 6µm, (B) 50µm. (C) umamit14, scale bar: 40µm, (D) *umamit11*, scale bar: 40µm. (E) *umamit29*, scale bar: 40µm. (F) *umamit28*, scale bar: 45µm, (G) *umamit14/umamit18*, scale bar: 40µm. (H) *umamit14/umamit29*, scale bar: 35µm. (I) *umamit14/cat6*, scale bar: 40µm. (J) *umamit29/cat6*, scale bar: 40µm. (L) Sense probe, scale bar: 25µm. (M) *umamit14/umamit11*, scale bar: 40µm.

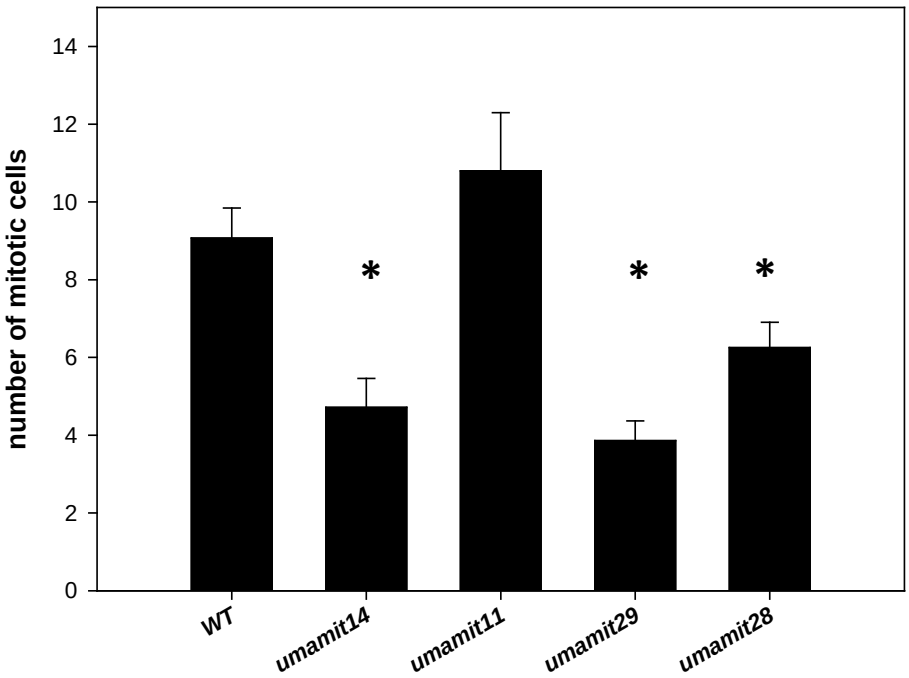

Figure 148. Calculation of the number of mitotic cells in the root tip. Signals for counting were obtained from the whole mount *in situ* RNA hybridization of *CYCB1.3*. Analysis was done using z-stacks of the complete root tip; n>6±SE, one way ANOVA followed by Holm-Sidak post hoc test.

5.14. UmamiTs: filling the gaps

The candidates characterized in this thesis demonstrated the importance of amino acid export by UmamiTs in developing seeds. Looking at the complex route of amino acids out of phloem and xylem into the seed coat and embryo underpins the uniqueness of *UmamiTs* at the unloading zone and their distinct expression pattern in the integuments. Although the candidates presented from UmamiT clade I and III can at least partially explain the mechanism of seed filling with amino acids, it was quite obvious that there are many time points and positions within the seed, where none of the UmamiTs investigated was detected. It was shown that after fertilization UmamiT11 and UmamiT14 function as exporters of amino acids out of the unloading zone into the outer integument (Müller et al. 2015). At this time, only UmamiT29 appeared in very few cells of the outer integument layer 2, suggesting that other candidates are needed for an even distribution of amino acids along the integument and for an effective export into the next layer. According to the size of the family (44 members) it appeared obvious that other UmamiTs would be closing the gaps observed. Additionally, hints were given by the analysis of the translational fusion of the amino acid importer CAT6, which was created based on the promoter analysis of Hammes (2006). CAT6-GFP appeared during seed development in exactly those cell files, where import of amino acids, based on export activity by the investigated UmamiTs, would be needed for a translocation of amino acids across the integuments (Fig. 149). *CAT6* expression was also detected in the endosperm, in line with the idea that subsequent export and import events in the seed are the required during seed filling. The only concern about the results obtained is that the time frame in which CAT6-GFP was seen is not always covered by the expression pattern of the characterized *UmamiTs* in this thesis, indicating that other amino acid exporters are needed to close this gap. In order to find possible candidates public microarray data (BAR eFP browser (Toufighi et al. 2005)) was screened under the focus of the predicted time frame and tissue specific expression in seeds. This screen revealed that several other members from different UmamiT clades fulfilled the criteria mentioned (table 4).

Table 4: Overview about the selected candidates located in the "gap" positions of the seed

old nomenclature	new nomenclature	AGI identifier
BAF38	UmamiT41	AT3G28050
BAF5	UmamiT15	AT5G13670
BAF15	UmamiT2	AT4G19185
BAF9	UmamiT25	AT1G09380
BAF24	UmamiT21	AT5G64700
BAF26	UmamiT10	AT3G56620
BAF32	UmamiT34	AT4G30420
BAF22	UmamiT23	AT1G68170
BAF16	UmamiT1	AT5G45370

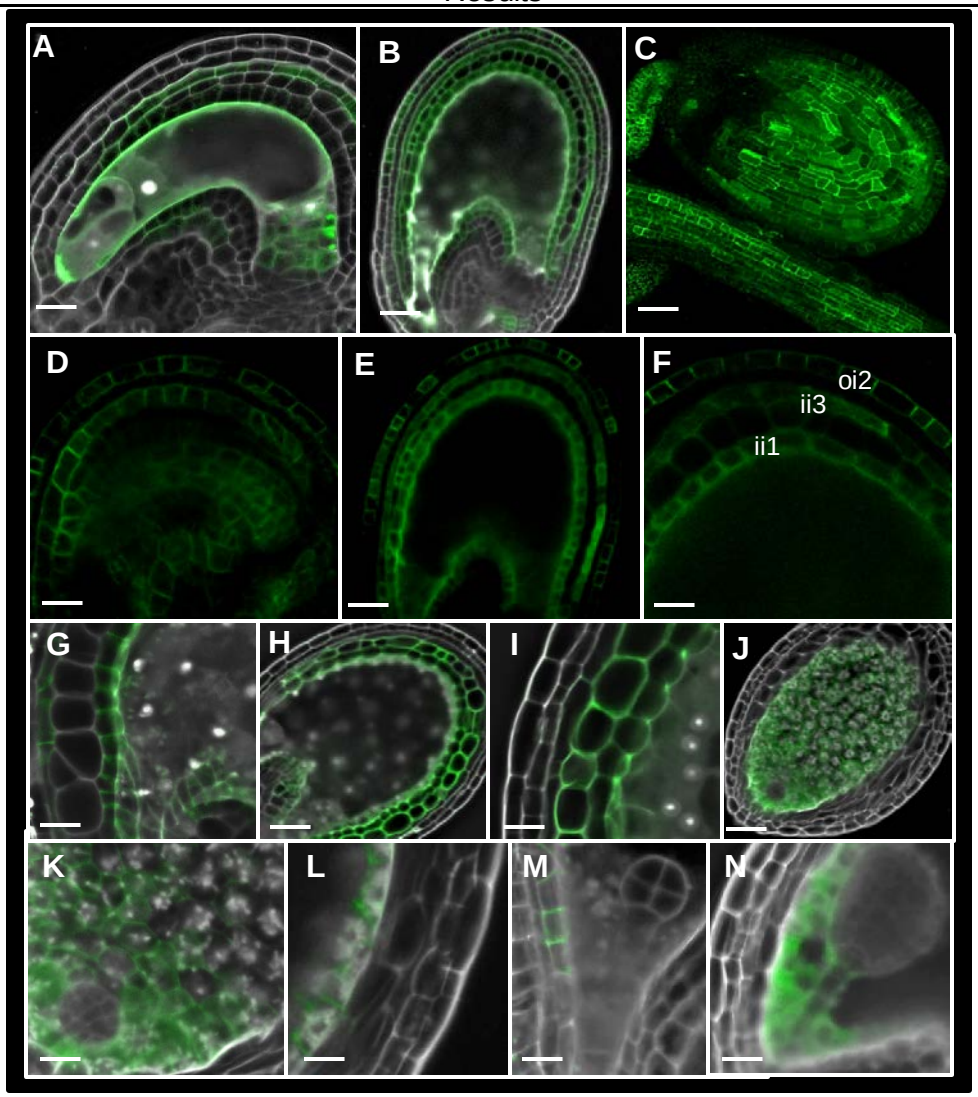

Figure 149. Localization of CAT6-GFP before fertilization and during seed development. *P*$_{CAT6}$*: CAT6-GFP* reporter line was analyzed. (A) Before fertilization. CAT6-GFP detected in the central cell and in the inner integument layer 2 and nucellus, scale bar: 20µm. (B) After fertilization. CAT6-GFP appeared in few cells of the unloading zone, the outer and the inner integument, scale bar: 50µm. (C) Maximum projection shows GFP decoration of the seed, the funiculus and the transmitting tract, scale bar: 70µm. (D-F) GFP channel from seeds right after fertilization (D) and at early globular embryo stage (E, F). CAT6-GFP appeared in the outer integument layer 2, the inner integument layer 3 and in the innermost integument layer 1, scale bars: (D) 20µm, (E) 40µm, (F) 30µm. (G) Early stage of endosperm development, CAT6-GFP located in the inner integument layer 1 and 3, scale bar: 18µm. (H) Syncytial phase of the endosperm, chalazal endosperm and embryo at the opposite direction are visible, CAT6-GFP detected in the inner integument layer 1 and 2, scale bar: 50µm. (I) Magnification of the seed coat in the same developmental stage as in (H); GFP was monitored in the two layers of the inner integument closest to the endosperm, scale bar: 20µm. (J) CAT6-GFP specifically localizing in the cellularizing, scale bar: 80µm. (K) Magnification of the endosperm region that contained the embryo, scale bar: 35µm. (L) Optical section through the seed coat showed specific localization of CAT6-GFP in the endosperm during cellularization, scale bar: 25µm. (M) Embryo at four cell stage, CAT6-GFP is absent from the endospem but detected in the innermost integument layer, scale bar: 15µm. (N) In later developmental stages of the embryo, GFP was located in the endosperm with highest fluorescence intensity at the region surrounding the embryo. Picture shows embryo at early heart stage, scale bar: 18µm. Oi (outer integument), ii (inner integument).

5.14.1. Localization of UmamiT41 in the seed and silique

A possible candidate for closing the “gap” in the outer integument could be UmamiT41 (Fig. 150 A-F). In seeds, UmamiT41-positive cells were found in both layers of the outer integument at a time point, where none of the candidates described above was located. This could indicate, that export of amino acids into the inner integument and/or the even distribution is done by UmamiT41. In seeds, the GFP-fusion protein showed a lower ER “background” than in the epidermal tissues of the silique, were the protein was found predominantly in the ER.

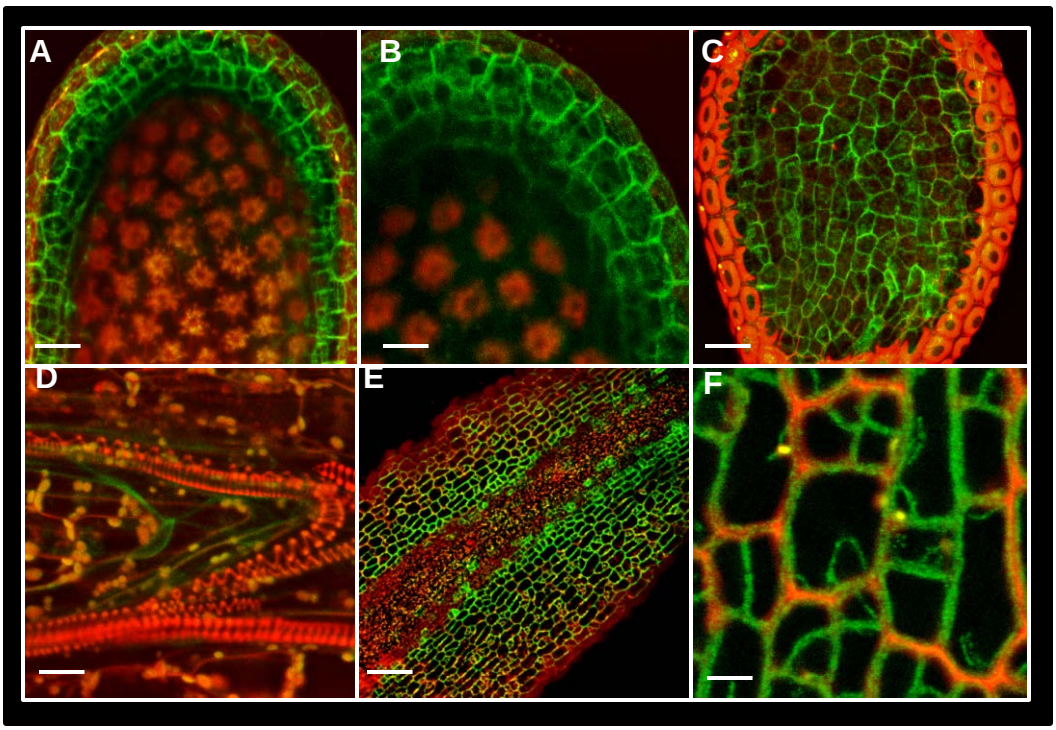

Figure 150. Localization of UmamiT41 in seeds and the silique. *P*$_{UmamiT41}$*: UmamiT41-GFP* was analyzed. (A, B) UmamiT41-GFP signals found right after fertilization in both layers of the outer integument. Both pictures show a maximum intensity projection, scale bars: (A) 50µm, (B) 22µm. (C) Seed close to maturity, GFP restricted to the outer integument layer 1, scale bar: 45µm. (D) Silique parenchyma shows GFP signals close to the xylem, scale bar: 14µm. (E, F) GFP in epidermal cells of the valve, scale bars: (E) 45µm, (F) 7µm.

5.14.2. Localization of UmamiT15 in the seed

During the process of the even distribution of assimilates along the integuments the flux is directed towards the micropylar pole of the seed. There another new member, UmamiT15, was found only in very few cells of the outer integument that are directly attached to the inner integument (Fig. 151). This implicates a very concentrated export of amino acids into the inner integument at the micropylar pole of the seed that is corresponding to the route amino acids take along the outer integument. In later developmental stages UmamiT15 GFP was additionally seen in the whole outer integument layer 1.

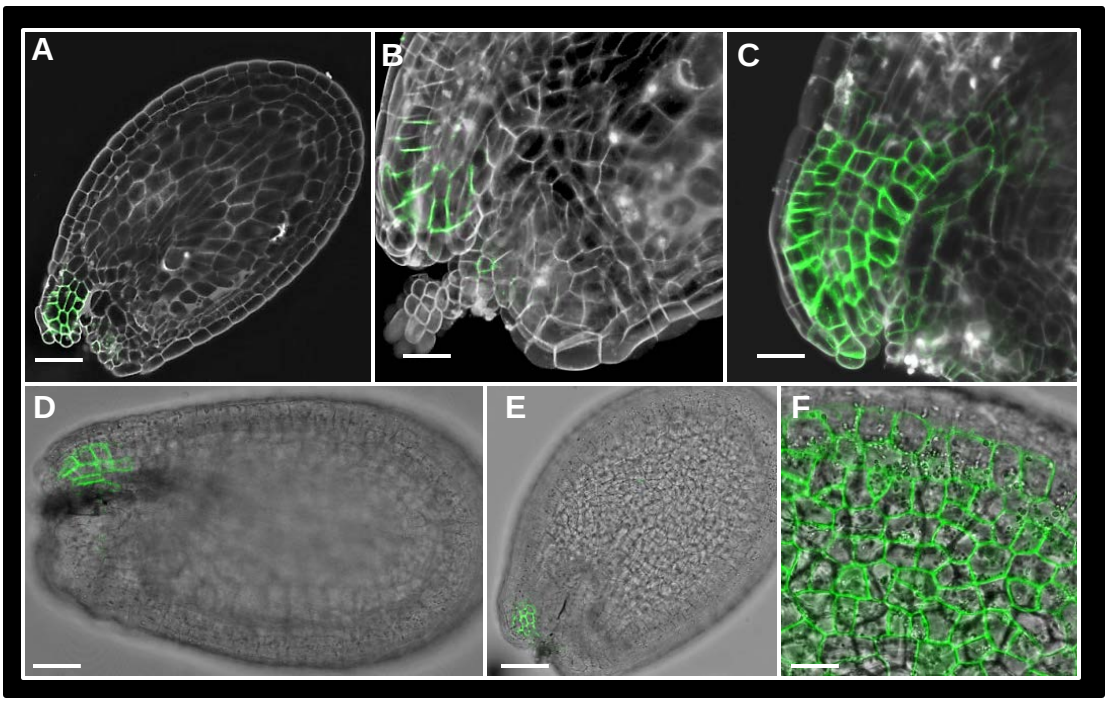

Figure 151. Localization of UmamiT15 in seeds. $P_{UmamiT15}$: *UmamiT15-GFP* marker line was analyzed. (A-C) UmamiT15-GFP is specifically detected in cells of the outer integument layer 1 positioned at the micropylar pole of the seed. In some cases an anticlinal polar distribution of the fusion protein was observed, shown in (B), scale bars: (A) 45µm, (B) 23µm, (C) 20µm. (D, E) In young stages of seed development only few cells at the micropylar pole show GFP signals, in older seeds (F) signals were found in every cell of the outer integument layer 1, scale bars: (D) 40µm,(E) 44µm, (F) 20µm.

5.14.3. Localization of UmamiT2 in the seed

Amino acids of high abundance coming from the phloem were translocated by UmamiT11 and UmamiT14 into the outer integument. Synthesis of amino acids that are found in much lower concentration happened in plastids of the outer integument. There at the subcellular level amino acid export plays a role, meaning that export out of plastids is a key step to provide amino acids for intercellular trafficking. A possible function in this sense could be exhibited by UmamiT2. This candidate was specifically found in plastids of the outer integument (Fig. 152 A-G). One possible explanation would be that amino acids are not only delivered by the vasculature, but also synthesized *de novo* in the seed coat to deal with the increasing demand of nutrition of the embryo. Furthermore, these amino acids are also needed for the differentiation of the outer integument for mucilage production. Amino acids that were translocated into the inner integument are subsequently exported in direction to the endosperm.

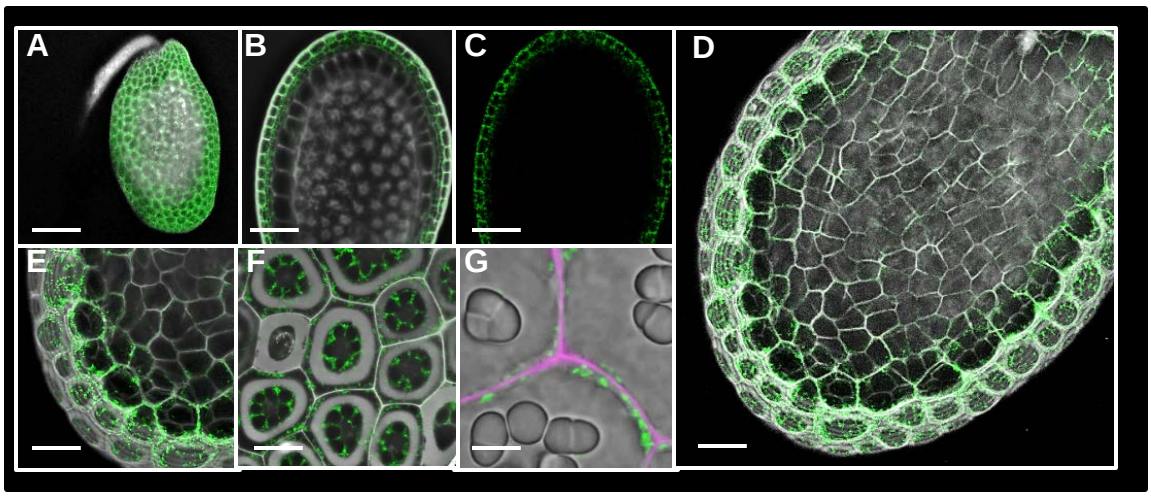

Figure 152. Localization of UmamiT2 in the seed. $P_{UmamiT2}$: *UmamiT2-GFP* reporters was monitored. (A) GFP is found in the seed coat, scale bar: 230µm. (B) Magnification of the seed coat shows GFP specifically located in the outer integument. (C) GFP channel of (B), scale bars: 110µm. (D) Maximum projection of the seed coat when the outer integument starts secretion of mucilage, scale bar: 53µm. (E) Magnification of (D), scale bar: 45µm. (F) View from the top at the outer integument layer 2 with GFP located in distinct foci, scale bar: 25µm. (G) Magnification of the outer integument layer 2, GFP in plastids, scale bar: 5µm

5.14.4. Localization of UmamiT25 in the seed

Also the transfer from the endosperm to the embryo is a central aspect in nutrient supply of seeds. *UmamiT25* showed an interesting dual expression pattern (Fig. 153), because it appeared in the area of the endosperm, where the embryo was located. During seed development, fluorescence was also detected in the inner integument layer 2 and, in a spotty pattern, in the outer integument, when the seed was close to maturity. The finding, that this candidate is present in the endosperm at all stages of embryo development indicates that amino acid supply of the developing endosperm and embryo may be facilitated by UmamiT25.

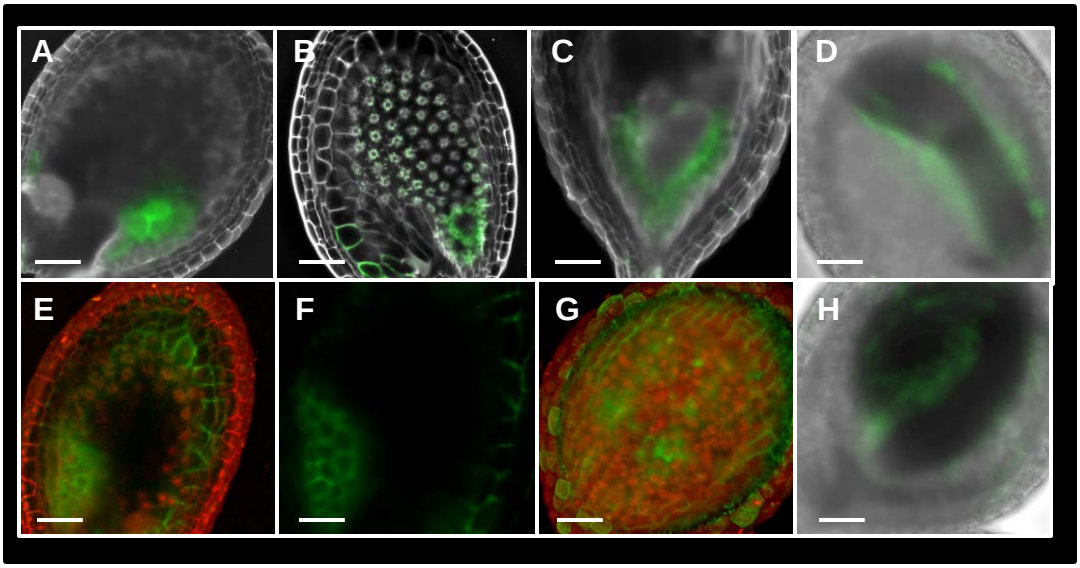

Figure 153. Localization of UmamiT25 in seeds. $P_{UmamiT25}$: *UmamiT25-GFP* reporter was analyzed. UmamiT25-GFP during seed development located in the inner integument layer 2 and the endosperm. (A) Early globular stage, scale bar: 60µm. (B) Late globular stage, scale bar: 70µm. (C) Heart stage, scale bar: 50µm. (D) Late torpedo stage, scale bar: 80µm. (I) Late cotyledon bending stage, scale bar: 80µm. (E) During embryo globular stage UmamiT25-GFP is found in the inner integument layer 2 and the endosperm, scale bar: 60µm. (F) Magnification of the GFP channel in (E), scale bar: 50µm. (G) Old seed near maturity; patchy distribution of GFP in the outer integument.

5.14.5. Localization of UmamiT21 in the seed and siliques

Another candidate, UmamiT21, was detected only in very few cells of the unloading zone, but additionally signals were found in the funiculus (Fig. 154 P-R). Also pavement cells in the epidermis of siliques and cells of the mesocarp were UmamiT23-positive, indicating that amino acid facilitation also occurs into or from symplasmically isolated stomata and in the protecting layer of the developing ovules and seeds.

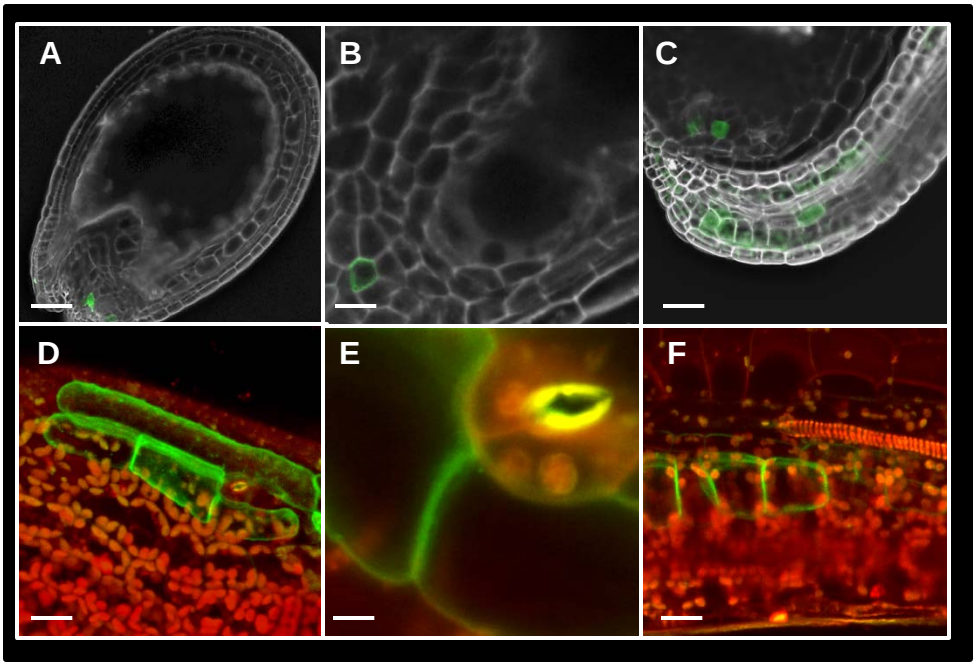

Figure 154. Localization of UmamiT21 in seeds and the silique. *P*$_{UmamiT21}$*: UmamiT21-GFP* reporter was analyzed- (A) UmamiT21-GFP in singular cells of the unloading zone, scale bar: 60µm. (B) Magnification of the chalazal pole, only one single cell from the unloading zone shows GFP signal, scale bar: 12µm. (C) GFP appeared also in parenchymatic cells of the funiculus close to the vasculature, scale bar: 17µm. (D) UmamiT21-GFP in pavement cells of the epidermis from siliques, scale bar: 12µm. (E) Detailed picture, GFP showed putative plasma membrane localization in pavement cells, scale bar: 2.7µm. (F) UmamiT21-positive cells in the mesocarp tissue of siliques, scale bar: 18µm.

5.14.6. Localization of UmamiT10 in the seed

A somewhat special expression pattern was seen for *UmamiT10* (Fig. 155). This candidate appeared in the unloading zone and in the suspensor of the developing embryo. Until now amino acid supply of the embryo by the suspensor seemed to be an unknown phenomena and UmamiT10 could be the first candidate which exhibits transfer function of amino acids coming from the micropylar pole or the endosperm in direction to the developing embryo, which would link hormonal transport of auxin into the embryo with amino acid export into seeds. This route of amino acids from the unloading zone into the embryo is similar to the suggested mechanism for seed filling with sugar (Lafon-Placette and Köhler 2014).

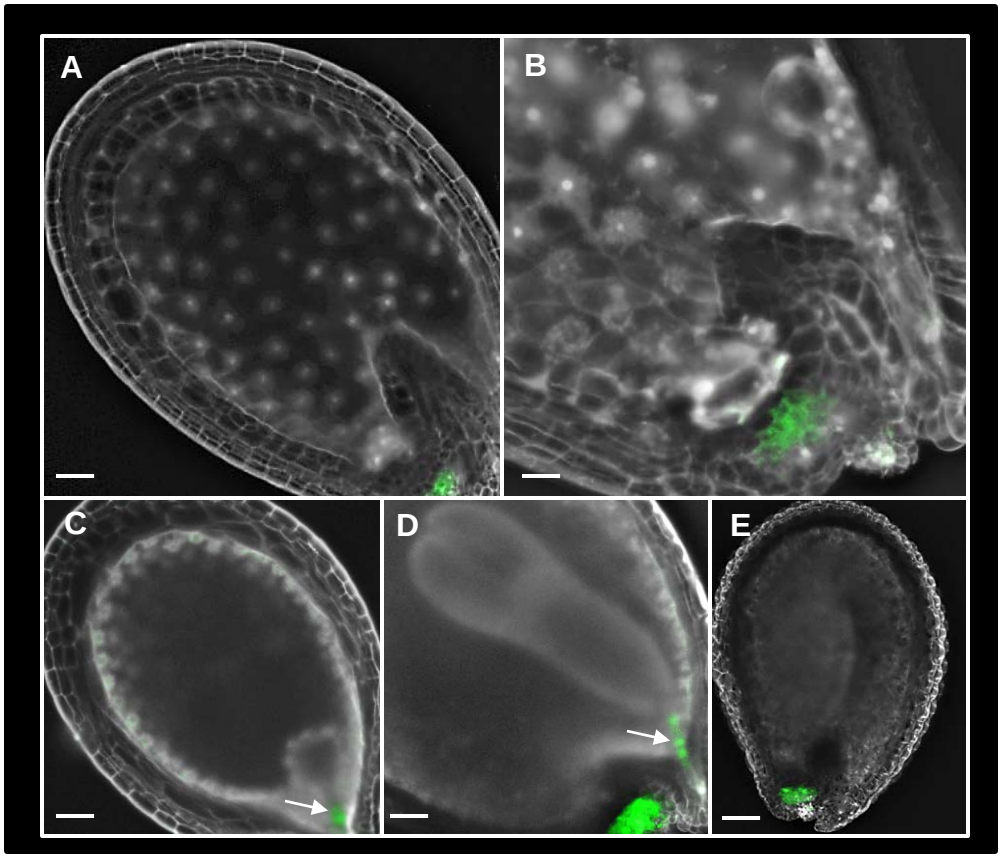

Figure 155. Localization of UmamiT10-GFP. (A-E) *P*$_{UmamiT10}$*: UmamiT10-GFP* reporter line was analyzed. (A, B) Seed at early globular stage, GFP specifically detected at the unloading zone, scale bars: (A) 30µm, (B) 15µm. (C) During late globular stage UmamiT10-GFP appeared in the suspensor (arrow), scale bar: 40µm. (D) fluorescence in the suspensor was seen until torpedo stage of the embryo. Scale bar: 45µm. (E) Seed almost at maturity. UmamiT10-GFP was restricted to the unloading zone, scale bar: 90µm.

5.14.7. Localization of UmamiT34 in the seed

At the moment the seed coat starts to differentiate, the candidate UmamiT34 appeared in the outer integument layer 1 (Fig. 156). The reporter line showed GFP surrounding plastids and a vacuole-like distribution at the borders of the cells. Although co-localization experiments still have to be carried out it seems that this particular candidate could play a role in amino acid transport across the tonoplast, perhaps amino acid loading into the vacuole. It is worth noting that the molecular identity of this activity is unknown to date. A function for import of amino acids into the vacuole or export out of the tonoplast might be possible, linking amino acid compartmentation and tissue differentiation of the outer integument together.

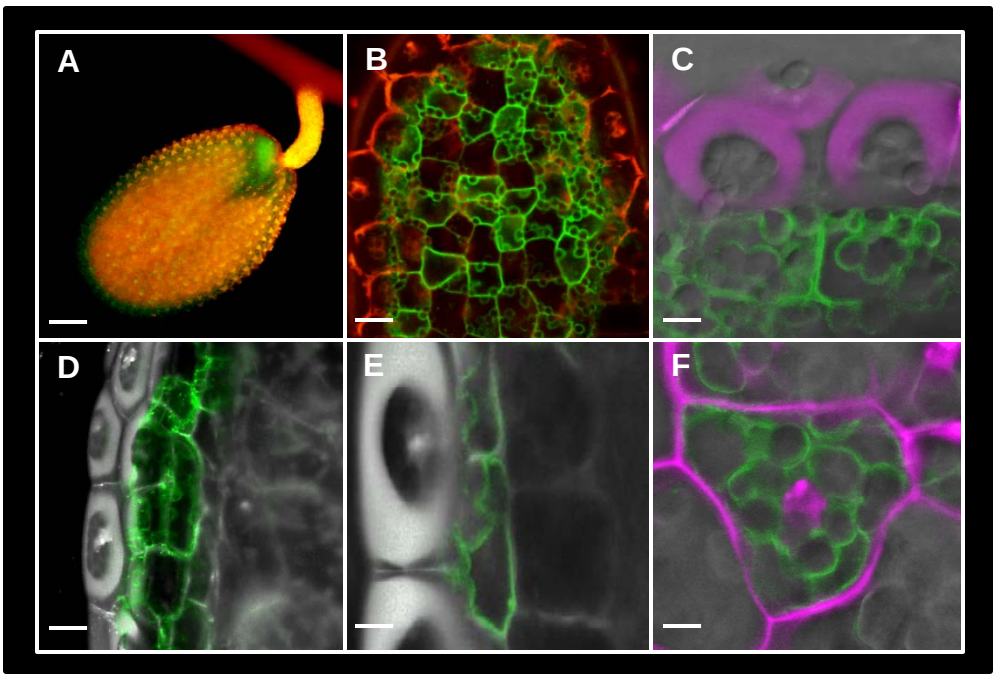

Figure 156. Localization of UmamiT34-GFP in seeds. (A-E) *P*$_{UmamiT34}$*: UmamiT34-GFP* reporter line was studied. (A) UmamiT34-GFP appeared at late seed developmental stage, when the seed coat starts to differentiate, scale bar: 80µm. (B) Maximum projection of the outer integument of the seed coat, fluorescence was detected in the first layer of the outer integument, scale bar: 25µm. (C) Optical section of the outer integument shows differentiated outer integument layer 2, indicated by the PI stained mucilage, colored in magenta. Fluorescence was specifically observed in the first layer of the outer integument, scale bar: 5µm. (D) Maximum projection of the seed curvature, GFP located in the outer integument layer 1. (E) Optical section reveals specific GFP signals in the first layer of the outer integument, which was distinct from the inner integument, scale bar: 8µm. (F) Single cell from the outer integument layer 1 with PI stained cell wall and nucleus colored in magenta. GFP encircled plastids, scale bar: 2µm.

5.14.8. Localization of UmamiT23 in the seed and embryo

The only candidate UmamiT with a dual localization in the unloading zone and embryo identified so far is UmamiT23 (Fig. 157). After fertilization only a single cell in the unloading zone, distinct from the phloem and xylem, showed fluorescence. During the further developmental stages more cells of the unloading zone showed fluorescence and additionally weak signals appeared also in the phloem. A very remarkable aspect of the expression pattern of this candidate was the presence of the fusion protein in the embryo tissue, right after heart stage. During the maturation phase of the embryo, more and more cells showed fluorescence. At the cotyledon bending stage, every epidermal cell of the embryo was UmamiT23-positive. These findings also close an important “gap” of the seed story: amino acids are imported into the embryo by the translocation of amino acids from the endosperm or *via* the suspensor route. But then an efficient distribution of amino acids into different embryo regions of enhanced growth must be given to keep the steepness of the import gradient between the extra-embryo space and the embryonic tissue. UmamiT23 could be a possible candidate to distribute amino acids within the embryo tissue.

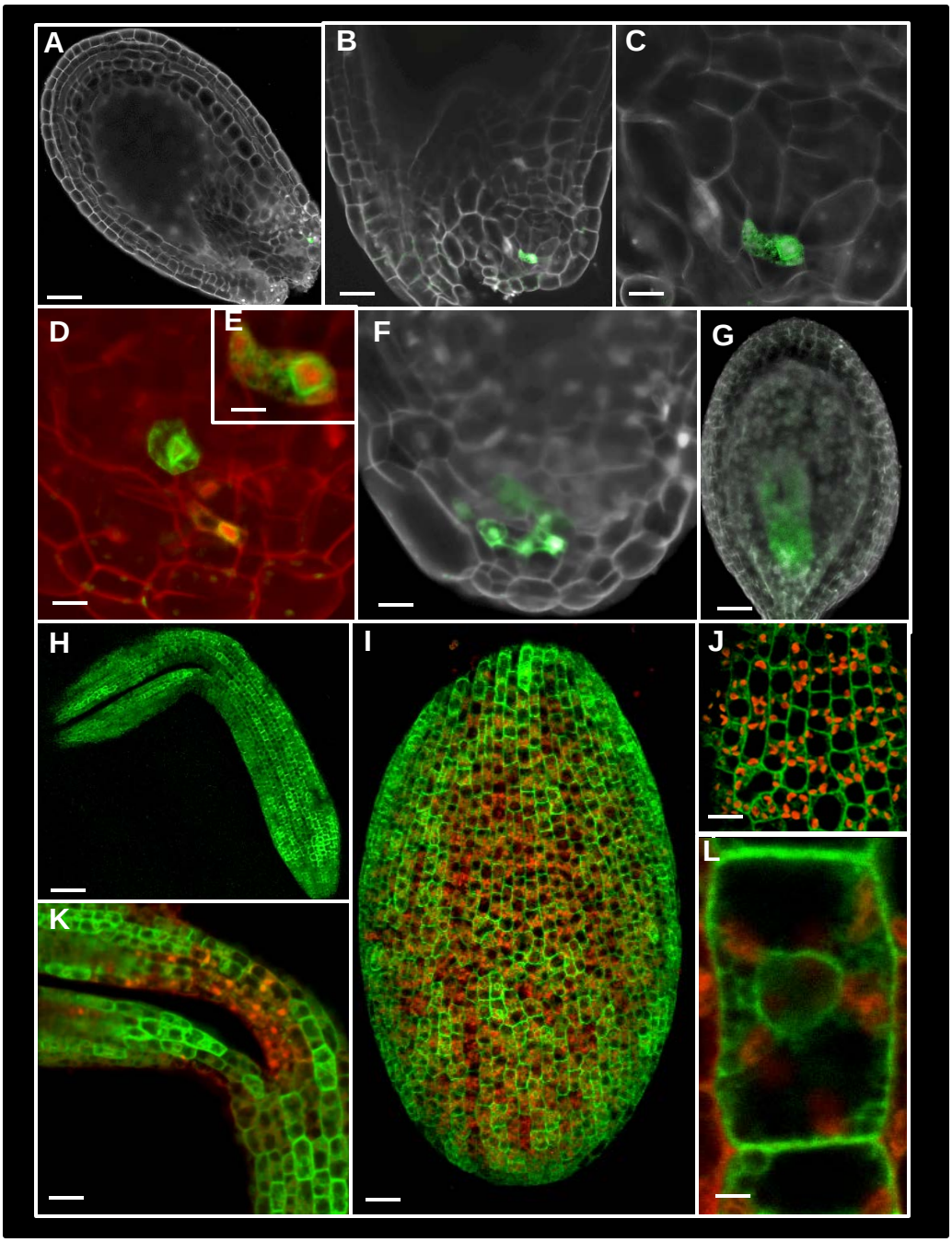

Figure 157. Localization of UmamiT23-GFP in seeds and the embryo. (A-E) *P*$_{UmamiT23}$*: UmamiT23-GFP* was analyzed. (A-C) After fertilization. A single cell, distict from the phloem, at the unloading zone shows fluorescence. Scale bars: (A) 35µm, (B) 25µm, (C) 12µm. (D-F) Later during seed development more cells at the unloading zone show fluorescence. In some phloem cells fluorescence was detected: (E) Magnification of a phloem cell. Scale bars: (D) 15µm, (E) 3µm, (F) 12µm. (G-L) In later stages of seed development fluorescence appeared in the embryo, starting from torpedo embryo stage (G), until cotyledon bending stage (H); scale bars: (G) 80µm, (H) 40µm. (I) UmamiT23-GFP in the cotyledon of an embryo, scale bar: 30µm. (J) Magnification of the epidermal cells of the embryo, fluorescence was distinctly located from plastids shown in red, scale bar: 20µm. (K) In early bending stages fluorescence was widely distributed in the embryo, but some cells were undecorated with UmamiT23-GFP, scale bar: 25µm. (L) Magnification of one single cell from the embryo shows ER-like localization of UmamiT23-GFP, indicated by the reticular signal pattern and the nuclear envelope, scale bar: 1.5µm.

5.14.9. Localization of UmamiT1 in the seed and embryo

Finally, with *UmamiT1* a candidate with a dual expression pattern for the outer integument and embryo was identified. In both tissues the protein is likely localized to the tonoplast. (Fig. 158). In embryos at heart stage fluorescence was detected in the cotyledons and the hypophysis that is connected with the embryo. At the final stage of seed development, UmamiT1-GFP was found along the epidermal layer of the embryo with obvious brighter signals in the cotyledons and the protoderm of the root apex. The specific expression pattern of *UmamiT1* in tissues, where amino acids are imported or metabolized could be a hint for the function of this candidate UmamiT in the intracellular compartmentation into the vacuole or a transport of amino acids outside into the cytosol. This may help to storage amino acids in the vacuole for differentiation processes during embryo development or growth after germination.

The candidate UmamiTs presented in this chapter visualize a possible path for the future research on UmamiTs in seeds. Characterization of mutants will help to analyze the function these transporters have during seed development. Their very distinct und highly regulated expression pattern at time points and in tissues, where none of the candidates of clade I and III selected was present, underlines the evolutionary specified function and the uniqueness of UmamiTs in the supply of symplasmically isolated tissues during the reproductive phase of the life cycle. This issue will help to go deeper into the mechanisms of seed filling with amino acids and provides candidates under the aspect of yield stability and safety for the future.

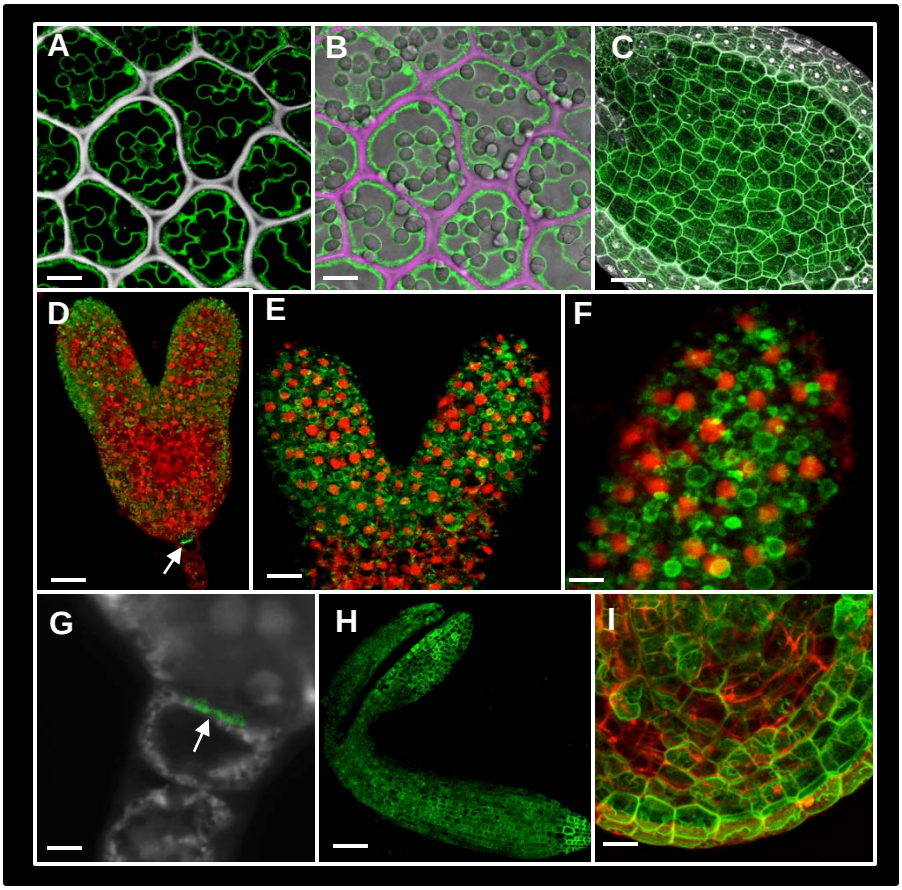

Figure 158. Localization of UmamiT1-GFP in seeds and the embryo. (A-E) *P*$_{UmamiT1}$*: UmamiT1-GFP* reporter line was studied. (A, B) Outer integument layer 2, UmamiT1-GFP showed a putative vacuolar localization pattern. PI stained cell walls are colored in white (A) or magenta with the overlay of the bright field picture (B), scale bars: 12µm. (C) Maximum projection. Fluorescence in both layers of the outer integument, scale bar: 50µm. (D) Embryo at heart stage. UmamiT1-GFP in the cotyledons and in a bright spot at the suspensor (arrow), scale bar. 25µm. (E, F) Magnification of the cotyledons shown in (D). GFP signals formed circular structures. Bright red spots are PI-stained cell nuclei. Scale bars: (E) 12µm, (F) 6µm. (G) Hypophysis (arrow), polarly localized UmamiT1-GFP directed towards the embryo, scale bar: 3.5µm. (H) Mature embryo. Fluorescence distributed along the whole embryo. Hotspots of florescence were detected in the cotyledons and the protoderm of the root apex, scale bar: 50µm. (I) Maximum projection of the seed coat before differentiation. GFP appeared in all cells of the outer integument layer 2 but in a patchier pattern in layer 1, scale bar: 25µm.

6. Discussion

The focus of this work was to elucidate how amino acids are unloaded from the vasculature in sink tissues. The first chapter was the investigation how amino acids are translocated from the mother plant into the seed by UmamiTs and how these processes are regulated by phytohormones during seed development.
Seeds show unique anatomical properties for nutrient exchange between the unloading phloem, the unloading zone and the integuments. Besides that, phytohormones were found to be asymmetrically distributed after fertilization and dynamically changed during seed development. In the following the possible route amino acids can take to get incorporated into the embryo and how seed development is regulated by cytokinin and auxin will be discussed. The second chapter centralizes the function of UmamiTs in the supply of sink tissues represented by seeds and root-knots. Furthermore, a possible characterization as unique cells with transfer function and a role in the nutrition of stem cells will be discussed.

6.1. The seed: nutrients on a complex route.

Seeds contain and protect the developing embryo which is an endogenous sink tissue (Imlau et al. 1999). The transport of assimilates and nutrients into this sink is facilitated by the vasculature. Sugars and amino acids are transported by the phloem and water, minerals and amino acids are translocated by the xylem. In order to supply the seed, the vasculature is extending from the funiculus into the chalazal region. In this work was shown that after fertilization sieve elements start to branch and form branch points of higher order whereas companion cells are only poorly branched (Müller et al. 2015). By this way, the surface area for nutrient exchange with the unloading zone can be increased. But the morphology of the phloem remained the same until the seed becomes mature and is quite small compared to the overall size of the seed. The number of cells at the unloading zone is referred to be constant after fertilization because none of the cell cycle makers analyzed (*CYCB1.2*, *CYCB1.3*) was expressed in the phloem of the seed. This immediately suggests that the increasing demand of nutrients by the embryo cannot be covered by a proliferation event but by differentiation processes of the chalazal cells and an increasing transporter activity around the unloading sieve elements. The unloading of assimilates from the sieve elements can occur by the symplasm by mass flow and diffusion or by an active transport *via* transport proteins, that lead to a translocation of nutrients across the intracellular space (Offler et al. 2002, Patrick and Offler 1995). In the reproductive tissue of *Arabidopsis,* the phloem in ovules is symplasmically isolated from the chalazal pole. After fertilization, symplasmic unloading gets restored by newly

formed plasmodesmata (Werner et al. 2011). Plasmodesmal conductance is a highly regulated phenomenon, influenced by phytohormones (Cosgrove 1999), calcium ions (Holdaway-Clarke et al. 2000), the resulting changes in callose deposition (Baluska et al. 2001) and the cytoskeleton (Baluska et al. 2001). These factors influence the size exclusion limit of plasmodesmata. Experiments of Stadler (2005) showed that soluble GFP, expressed by the strong companion cell specific *SUC2* promoter, is unloaded from the phloem through plasmodesmata into the unloading zone and translocated from there into the outer integument. It was suggested that this is also the route for nutrients and assimilates. In contrast to that, the findings in this work indicate that soluble GFP in the unloading zone cannot get out of there, if an unloading zone specific promoter is used. This means that the already published data concerning the symplasmic flow of GFP from the unloading zone into the outer integuments is conducted by the phloem pressure and reflects a possible route for a non-osmotic compound. But the situation *in natura* can be different for osmotically active assimilates. In the case of amino acids nothing is known about their ability to move into the integuments by the symplasmic route. Amino acids are much smaller than GFP for which the size exclusion limit in the unloading phloem was determined. If this was the case an equal distribution of amino acids across the unloading zone and the integuments of the seed comparing the possible route of GFP with amino acids must be postulated. But, looking at the seed phenotype described later and the fact that amino acids are metabolized and compartmented, that does not seem to be the case. The results obtained by the analysis of soluble GFP driven from the *UmamiT* promoters active in the unloading zone indicate that a possible route for GFP across plasmodesmata exists which is likely different for assimilates. Amino acids of higher abundance are delivered by the phloem and unloaded via the phloem pressure into the unloading zone from where they can be selectively exported into the outer integument. This supports the findings of Stadler (2005) and indicates that the pressure component of the phloem is a driving force for the unloading of assimilates into the unloading zone. But at this point the route of assimilates from the unloading zone into the outer integument must be considered to be more complex than visualized by the flow of soluble GFP. The difference at this point between the results in this thesis and Stadler (2005) strongly depend by the choice of the promoter and explain that the unnatural overloading of the unloading zone with GFP by the phloem pressure does not reflect the mechanism of seed filling with amino acids. Additionally, it should be considered that so far nothing is known about the importance of an apoplastic unloading of the phloem as it occurred in the so called “fleshy fruity” species (Zhang et al. 2004). The data obtained during this thesis, strongly suggest the requirement for transporters, which are involved in the phloem unloading process and capable of translocation of amino acids from the chalazal region into the outer integument. In the outer integument layer 2, MP17-GFP was monitored and cytosolic GFP was seen only in this integument layer and

never occurred in the first layer of the outer integument, using an integument specific promoter. This observation leads to the suggestion that once compounds are transported to the outer integument they can get homogenously distributed in lateral direction within the outer integument layer 2 from where they are translocated to the outer integument layer 1. The “big gap” of nutrient translocation is present between the outer and inner integument, which results from the planar growth pattern during early ovule development (Schneitz et al. 1995): the inner integument arises from cells which were ordered as a ring around the ovule primordium. These cells start to initiate by a symmetrical growth until they surround the nucellus. At this moment the outer integument starts to initiate at the base of the carpel with an asymmetric growth pattern. This means that inner and outer integument are formed by planar growth and due to the asymmetric growth pattern they do not share a cell wall that resulted from a common phragmoblast. As a result, plasmodesmata do not form between inner integument and outer integument. In consequence, nutrient flow in this scenario requires an apoplastic step to translocate compounds from the outer integument into the inner integument. From there, the translocated compounds can again homogenously be distributed in lateral dimension, which can be explained by the presence of MP17-GFP in this layer, which is at some stages even polarly localized at the anticlinal position, as well as the later described PIN3 and UmamiT29. Endosperm and inner integument were found to be also symplasmically isolated from each other, which is in concordance to the findings of Stadler (2005) and Creff (2014). This means that also here, an apoplastic step of export from the inner integument and import into the endosperm is required.

Altogether, the results show that in the seed the cells of the unloading zone are interconnected by plasmodesmata also with the phloem, where symplasmic unloading occurs. Outer and inner integument are also isolated from each other, as well as the inner integument from the endosperm. Nutrients that were translocated form the unloading zone into the outer integument can be homogenously distributed in lateral direction before they are exported into the apoplast between outer and inner integument. Nutrients which are imported from the inner integument can also be homogenously distributed within the whole cell layer, which would result in a uniform distribution from where the export into the endosperm can occur. From a physiological point of view this uniform distribution of assimilates resulted in a syncytium at lateral dimension, where compounds can equally be translocated from the outer integument to the inner integument and from there into the endosperm.

This complex route of assimilates across the seed underlines the need of (UmamiT) transporters especially at the unloading zone and integument layers, where a symplasmically isolation of these tissues is apparent.

Transport processes are also regulated by phytohormones. During seed development a strong change of hormonal distribution and concentration was monitored. Simultaneously, the

translocation of assimilates is also occurring at the same time point in different integument layers. The amino acid supply of the developing seed by UmamiTs is a complex and completely new story and their spatio-temporal regulation is linked with the hormonal dynamics during seed development.

6.2. Hormonal dynamics during seed development

Phytohormones play a central role in the initiation and organ pattern formation of the reproductive tissues (Nole-Wilson et al. 2010). It is well described that auxin synthesis, transport and degradation are responsible for the establishment of a tissue-specific gradient (Robert et al. 2015). In the last years, the main focus was on the development of the female gametophyte, whereas seed development was quite overlooked. In contrast to seeds, there is no auxin gradient present in the angiosperm female gametophyte (Lituiev et al. 2013). These findings were mostly based on the observation of auxin response and auxin biosynthesis. In this work it was possible to reproduce the data for the reproductive tissue before fertilization by the auxin sensor R2D2, which gives information about auxin abundance. Auxin was completely absent in the functional mega spore mother cell and all further developmental stages leading to the receptive female gametophyte. In contrast, during seed development, auxin concentration was highly dynamic in the integuments and the unloading zone. After fertilization, auxin maxima could be detected in the funiculus and the unloading zone. These maxima were later on also found in all integument layers. Auxin presence, as indicated by R2D2 was not detected in the endosperm at all developmental stages. In line with these findings, no auxin response was found in the endosperm using the DR5-GFP and DR5v2 reporter. On the other hand, a strong cytokinin response was observed there using the TCS-GFP reporter. This auxin gradient between the unloading zone, the integuments and the endosperm diminished over time as the embryo reached heart stage. At this moment, auxin maxima were only seen in the unloading zone, whereas in the integuments the signals indicating high auxin levels disappeared. The dynamic change of auxin distribution across the integuments was seen in the innermost integument layer and the outer integument, where, during seed development, some cells contained high and others low auxin levels, indicating that a mechanism for asymmetric auxin transport must exist in the integuments leading to cells with different auxin levels and thus differing gene expression. These findings raise the question what the source of auxin is after fertilization. At the moment no data about auxin biosynthesis during seed development is available. In the ovule, several members of the *YUCCA* gene family are dynamically expressed (Panoli et al. 2015). Members of this family encode key enzymes for auxin biosynthesis (Cheng et al.2007). It was found that *YUC1*, *YUC2* and *YUC8* are asymmetrically expressed in the embryo sac and ovule (Panoli et al. 2015). The same is

true for members of the *TAA* gene family (*TAA1* and *TAR2*). They act as key enzymes in the first step of the conversion of tryptophan to indole-3-pyruvate (IPA), which is synthesized to IAA by the enzymes encoded by the *YUCCA* genes (Mashiguchi et al. 2011). Mutations of members of both families cause morphological defects in the ovules including defects in the nuclear proliferation and anisotropic growth (Panoli et al. 2015). The findings that several members of the YUCCA/TAA family are located in the female gametophyte and ovule indicates that there is a pool of gametophytic synthesized auxin present before fertilization. At this developmental stage, the only member of the auxin efflux PIN family, which showed expression in the ovule, was *PIN3.* It was expressed in the funiculus and showed a polar localization at the anticlinal position in the cell especially in cells adjacent to the xylem, which indicates a contribution to long distance transport of auxin towards the ovule. A dramatic change of expression happened after fertilization, where PIN3-GFP showed signals in the innermost layer of the integuments and the unloading zone. An asymmetry of expression was seen also in later stages of seed development. Only cells of the outer integument that were positioned at the chalazal region showed polar distribution of PIN3-GFP, whereas no signals were obtained in the distal parts of the seed or the micropylar region. This was also true for the inner integument layer 2. The polar distribution of PIN3-GFP in the outer integument and the inner integument layer 1 and 2 indicates that a directed flow of auxin happened at the one hand from the inner integument towards the outer layer and on the other hand from the unloading zone to the micropylar pole of the seed. These data correspond well with the results obtained by R2D2. In young stages, the presence of an auxin maximum was observed in the unloading zone and the integuments and diminished later on during seed maturation. The accumulation of auxin at the unloading zone could be a result of the co-occurrence of two auxin fluxes in the seed, which could function as a signal for the trans-differentiation of parenchymatic cells at the unloading zone. One pulse is coming from export of auxin out of the inner integument towards the unloading zone and the other is coming from the funiculus into the unloading zone. PIN3 shows no polar distribution in the unloading zone, indicating that auxin is homogenously distributed there and later on directionally transported along the integuments. These findings fit well with the presence of the PIN3 activating kinase D6PK. This kinase is homogenously distributed at the walls of the unloading zone and gets polarized in the outer integument, where PIN3-GFP showed also polar distribution. However D6PK was not seen in the innermost layer of the inner integument, where the highest intensity of PIN3-GFP was reported, indicating that other kinases must be present in this cell layer to activate PIN3 mediated auxin efflux. Possible candidates could be other kinases from the AGCVIII superfamily, PINOID and WAG1 and 2 the D6 PROTEIN KINASE LIKE1 to 3, as well as the remaining mambers of the D6-clade of AGCVIII kinases (Zourelidou et al. 2014, Benjamins et al. 2001) and possibly additional, not yet identified kinases. The massive auxin accumulation in the developing seed validated

observations using the auxin response marker DR5-GFP. Directly after fertilization, high auxin response was detected in the funiculus and the unloading zone, which could be a result of the auxin accumulation that was already seen in the PIN3-GFP and R2D2 reporter line. The finding that even the much more sensitive DR5v2 showed up later in the inner integument than in the outer integument could be a result of the export activity of PIN3 in the innermost integument layer. Signals in the integuments showed a patchy pattern for a short window of time before all cells of the same layer were decorated with GFP. Signals in the outer integument appeared earlier than in the inner integument, suggesting that auxin is first transported from the chalazal region into the outer integument and from there translocated to the inner integument, suggesting that auxin follows the assimilate route.

In summary after fertilization a massive accumulation of auxin occurred in the seed. This can be explained by PIN3 mediated dual auxin flux from the innermost integument layer to the chalazal region and from the funiculus into the unloading zone and across the whole seed. The directed flux of auxin can furthermore be supported by the detection of auxin maxima in the unloading zone directly after fertilization and the polarized signals of D6PK in the outer integument, where during seed development the auxin gradient diminished as a consequence of PIN3 activation.
The consequences of the hormonal dynamics during seed development for nutrient partitioning and differentiation of UmamiT-positive cells will be elucidated in chapter 1.3.3.

6.3. UmamiTs: the missing link in the amino acid supply of symplasmically isolated sink tissues and nitrogen cycling between xylem and phloem.

The big aim of the UmamiT project was to identify candidate exporters, responsible for the amino acid supply of symplasmically isolated sink tissues in *Arabidopsis*. According to array data derived from internal sink tissues (seed) and external induced sink tissues (root-knot) five candidate genes were selected belonging to the DMT-superfamily. The plant specific clade of this family comprises of the *UmamiT* genes, which are only present in higher plants and were so far completely uncharacterized.

6.3.1. Candidate UmamiTs are plasma membrane localized and broadly expressed in the vasculature of the above ground vegetative tissue.

Colocalization experiments in tobacco demonstrated a subcellular localization of the UmamiT proteins at the plasma membrane for clade I and clade III candidates. This is consistent with the bioinformatic predictions of the plant membrane protein database (Schwacke et al. 2003, http://aramemnon.uni-koeln.de) and with the already published SlAR1 (Ladwig et al. 2012), a member of the UmamiT clade, which was shown to be a plasma membrane localized transporter. In line with a plasma membrane localization, UmamiTs can act as transport proteins for amino acids into and out of the cell. Biochemical studies of Astrid Fastner proofed that it was possible to receive a selective uptake and import activity of certain amino acids, like glutamate and citrulline (Müller et al. 2015). Furthermore, Astrid Fastner could show that the uptake of glutamate occurred in the acidic range and is working at a K_M of 15 mM, which is in the physiological range (Müller et al. 2015, Zhu et al. 2005). The function of UmamiTs as bidirectional transporters makes them quite unique compared to the big amino acid transporter families (AAPs and ATFs), which are described as importers, working as proton-coupled symporters (Fischer et al. 2002, Hirner et al. 2006, Hammes et al. 2006). Bidirectional amino acid transport is a special kind of translocation process in animals, too. Best described are transporters acting across mammalian intestinal and renal epithelia, where in most cases amino acids are taken up by a sodium dependent symport (Bröer 2008). For animals essential amino acids are known to be the limiting factors concerning cell growth and translation (Wang et al. 1998). These transporters which translocate essential amino acids are indeed of high relevance for the homeostasis of the plasma amino acid levels. Nicklin et al. (2009) could show for mammalian cells that bidirectional amino acid transport of L-glutamine and L-leucine regulates the activation of a kinase responsible for protein translation and cell growth. This

mechanism enables an animal cell to respond to the current nutrient state. So far in plants the only published bidirectional amino acid transporter is BAT1 (Dundar and Bush 2009) and SIAR1 (Ladwig et al.2012). In the case of sugar and nitrogen more investigation was recently done showing how important the export and reuptake of sugars by SWEETs (Chen et al. 2012, Eom et al. 2015) and of nitrogen by members of the NRT family (Leran et al. 2013) is. Inorganic nitrogen is furthermore assimilated to amino acids in the leaves (Crawford, 1995, Pratelli and Pilot 2014). By q-RT PCR it could be shown that all candidate *UmamiTs* have similar RNA levels in the leaves and also activity of the promoter occurs in the vascular tissue in seedlings as well as in leaves of mature plants in different position at the plant body, i.e. source and sink leaves. The GFP fusion protein was found within the leaf tissue in parenchymatic cells close to the xylem and in the phloem. Additionally, by immunolocalization a number of cells were identified, which showed coexpression of UmamiT-GFP and the sieve element marker RS6. Most of the cells in the leaf vasculature with UmamiT decoration were placed within the xylem parenchyma. The double decoration with RS6 and UmamiT-GFP was seen for major veins and minor veins, where the loading of the phloem occurs (Slewinski et al. 2013). Only looking at this tissue specific distribution of UmamiTs in the vegetative tissue and taking their ability to facilitate the uptake and export of amino acids into account illustrates their relevance in the amino acid transport across the vasculature. Especially the parenchymatic tissue between xylem and phloem is an important gateway for the exchange of amino acids between those two vasculature types. The additional expression of high affinity importers in those cells (Okumoto et al. 2002) allows the uptake of low concentrated amino acids directly from the xylem sap, where they could be exported by UmamiTs to the surrounding cells. The occurrence of UmamiTs in the sieve elements of the phloem and parenchymatic tissue around the sieve elements made them interesting in the case of phloem loading with amino acids or their retrieval for long distance transport. Amino acids represent the main mobile form of nitrogen in the plant body and they are delivered to the sink tissues by the vascular system (Pate et al. 1981). Okumoto and Pilot (2011) already discussed the importance of amino acid export in source tissues and that the so far unknown players can close the gap in the nitrogen cycling between xylem and phloem. Exactly in this obvious gap *UmamiT* expression takes place and was found to occur in parenchymatic tissues which are the chokepoint of compound cycling between xylem and phloem from a histological and biochemical point of view (Cooper et al. 1986, Schneider et al. 1994). The physiological importance of this process is obvious, because it enables the plant to get an optimal nitrogen allocation to the sink tissues by enriching the amino acid content of the phloem sap as it moves to the sink tissues (Franceschi and Tarlyn 2002). Not only the expression of *UmamiTs* in the source and sink leave tissue can support this idea. Furthermore, they also were found along the hypocotyl, shoot, stem and in the vegetative tissues of the silique, which underlines their physiological function in the long

distance transport of amino acids and phloem/xylem cross-transfer. In all organs, UmamiTs were associated with the vasculature. Interestingly, in stems not every sieve element showed colocalization with UmamiT-GFP. Sometimes sieve elements with double decoration by α-GFP and α-RS6 directly neighboring sieve elements with only a-RS6 labelling were found. These findings are in agreement with the idea, that sieve elements can have different origins. Sieve elements, which showed colocalization were always close to parenchymatic cells only with α-GFP decoration, an observation that supports the publications of Lucas et al. (2013) and Furuta et al. (2014). Here, it was postulated that newly formed sieve elements can have parenchymatic cells as ancestors.

It can be concluded by the expression profile of *UmamiTs* in the vasculature of the vegetative tissue and their association with the phloem that they function in the spatial distribution of amino acids along the plant to optimize the support of the sink tissues. This process is guaranteed by the close physical vicinity between UmamiT-positive cells in xylem parenchyma and the direct neighborhood of those cells to sieve elements. From an anatomical perspective UmamiTs are placed in the vegetative tissues in order to link xylem and phloem to each other. Thereby, they contribute to the amino acid cycling within the plant by their capacity to take up amino acids and release them into the apoplast.

6.3.2. UmamiTs are spatio-temporally distinct expressed in the seed and impact amino acid composition and yield

In contrast to the overlapping expression profile of *UmamiTs* in the vasculature of the vegetative tissue, they were found to be highly specific and distinctly expressed during seed development. The starting point of the import of compounds into the seed is the structural change at the unloading zone after fertilization. Immediately after fertilization the phloem becomes symplasmically connected to the surrounding cells by the new formation of plasmodesmata (Werner et al. 2011). This process contributes to the unloading of assimilates into the seed and to translocate of compounds into the embryo. The morphology of the seed shows that the embryo is enclosed in two layers of outer integument and three layers of inner integument (Schneitz et al. 1995). Outer and inner integument are symplasmically isolated from each other (Schneitz et al. 1995, Stadler et al. 2005, Creff et al. 2014) and it was additionally shown in this work that the two layers of the outer integument are isolated from each other, as well as the inner integument layer two and three. This means, that indeed an export of compounds must happen in the integuments to overcome the poor symplasmic connectivity. But the most critical point is set far before the integuments in the unloading zone. Before compounds can be found in the integuments, they are delivered into the unloading zone (Stadler et al. 2005, Werner et al. 2011) The data presented demonstrate that also this domain is unique in terms of connection to the integuments, indicating that all further transport processes are underlying the major “hub” of those cells. It was observed that candidate genes of clade I (*UmamiT11*, *UmamiT14*) are specifically expressed in the unloading zone after fertilization and during the complete embryo development till the end of seed maturation. *UmamiT14* shows the highest RNA level there and the population of cells showing *UmamiT14* expression stays in close contact to the endpoint of xylem and phloem, similar to SIAR1 (Ladwig et al. 2012). This physical connectivity between the ending vasculature and the UmamiT-positive cells enhances the unloading process and, although nothing is known about their structural decoration with cell wall ingrowths, they are functionally equivalent to transfer cells. These cells take up amino acids from the endpoint of the vasculature and export them into the integuments to overcome the maternal-filial barrier (Patrick et Offler 1995, McCurdy and Hueros 2014). Although the nutrient demand increases with embryo size, the expression of *UmamiT11* and *UmamiT14* at the unloading zone did not change. Furthermore, it was observed that cell division, indicated by *CYCB1.2* and *CYCB1.3* expression, does not occur in the unloading zone. These findings indicate, that the increased assimilate demand of the embryo is met by increased transport across the membrane. This makes the cells of the unloading zone quite unique because they undergo right after fertilization the

transdifferentiation into UmamiT-positive cells to facilitate the amino acid export out of the unloading zone. In the next step, amino acids are exported into the outer integument. From there, export and reuptake events between the outer integument, the inner integument, the endosperm and the embryo tissue are needed to translocate amino acids from the unloading zone into the new plant generation. In the case of sugars several candidates of the exporter family SWEETs were identified to act in seed filling with carbohydrates by differential expression of SWEETs in the integuments (Chen et al. 2015). But for amino acid export in the integuments nothing was known so far. Many importers for amino acids acting in the integuments are already described (Okumoto et al. 2002, Hammes et al.2006) but the core players responsible for the export in the integuments were still unknown. UmamiT28 and UmamiT29 were identified as two candidates acting during this process in different layers of the seed coat. *UmamiT28* is strongly expressed in older seed stages (cotyledon bending stage) and located in the unloading zone, the endothelium layer and in the cellularized endosperm. The importance of endosperm transfer cells for seed filling was already reported by Thiel (2014). Moreover, amino acid transfer from the maternal-filial boundary into the seeds of barley revealed a concerted action of genes involved in amino acid metabolism and amino acid transport in the aleurone (Thiel et al. 2009), which is the functional analogue to those cells in the *Arabidopsis* seed, where *UmamiT28* expression occurs. In the integuments *UmamiT29* was the only candidate of clade III with a spatially and temporally different expression profile. After fertilization, until the early globular stage of the embryo the candidate is exclusively expressed in the unloading zone. After that, the protein was additionally found in single cells of the second layer of the inner integument. As the seed matures, all cells of the inner integument showed expression of *UmamiT29* and in rare cases expression was also found in single cells of the second layer of the outer integument, where at the same time point UmamiT37 was located too. During the late globular stage till the late torpedo stage UmamiT29 was exclusively found in the inner integument and expression in the unloading zone disappeared. A polar distribution of UmamiT29 was found in some cells of the second layer of the inner integument. Here, the protein was located at the anticlinal membranes and at the membranes facing the endosperm, which fits into the physiological context of an equal distribution of amino acids along the inner integument and the translocation of them in the direction of the embryo. During the last steps of embryo development at bending cotyledon stage UmamiT29 disappeared from the inner integument and was exclusively detected in the first layer of the outer integument. This time depending variable expression of UmamiT29 showed how finely tuned the induction of UmamiTs during seed maturation is.

Altogether the expression data demonstrate that all *UmamiT* candidates are spatial-temporally distinct expressed in the seed and located in cell files, where unloading of amino acids must

occur to overcome the symplasmic barrier. Post sieve-element transport of assimilates into sink tissues is a common phenomenon especially in seeds.

The principle of transfer processes at the endpoint of the vasculature in seeds seems to be an evolutionary conserved mechanism, because the process described in *Arabidopsis* was found also in distantly related plant families like legumes (Patrick and Offler 2001), rosids (Zhang et al. 2004) and monocots (Weschke et al. 2000, Sosso et al. 2015): from the unloading zone, assimilates are transported into specialized cells with transfer function to get incorporated by the endosperm and developing embryo. In *Arabidopsis,* amino acids were exported out of the unloading domain into the outer integument by UmamiT-positive cells (Fig. 159). There, they are homogenously distributed and subsequently translocated into the inner integument, where again an even distribution of the amino acids arriving across the integument layer can occur, as it is indicated by the polar distribution of UmamiT29 and MP17 in anticlinal position of the cells. In the final step, amino acids are delivered to the endosperm and incorporated by the embryo. Each translocation event in the seed coat needs the subsequent export and re-uptake of amino acids. This is in line with the export function of UmamiTs (Müller et al. 2015) and the presence of amino acid importers like CAT6 in integuments and the endosperm (Hammes et al. 2006) and AAP1 in the embryo (Sanders et al. 2009). A similar scenario was published for the seed filling mechanism with sugars by members of the SWEET family, which function as sugar exporters in the symplasmically isolated tissues of the seed coat of *Arabidopsis* (Chen et al. 2015) and in the basal endosperm transfer cells of maize and rice (Sosso et al. 2015). Also in barley an apoplastic barrier exists between the genetically distinct maternal tissue, endosperm and embryo. Similar to *Arabidopsis,* nutrients are symplasmically unloaded into the nucellar projection cells, which are symplasmically isolated from the endosperm (Borg et al. 2009), implicating that export of assimilates is a crucial mechanism for seed filling. Also in the morphologically highly variable seed coat of legumes transfer cells exist that allow the export of assimilates into the cotyledons of the embryo (Patrick and Offler 2001), although the symplasmic route between the vascular tissue and the integuments is more emphasized than in *Arabidopsis* (Patrick et Offler 1995), which is perhaps a reason for the reduction in the number of integument layers there.

This indicates that in angiosperms the basic mechanism of seed filling with assimilates shows evolutionary parallelisms between plant families but also various modifications for each taxon according to the underlying seed anatomy (number of integuments, vascular projection) and the used nutrient storage compound.

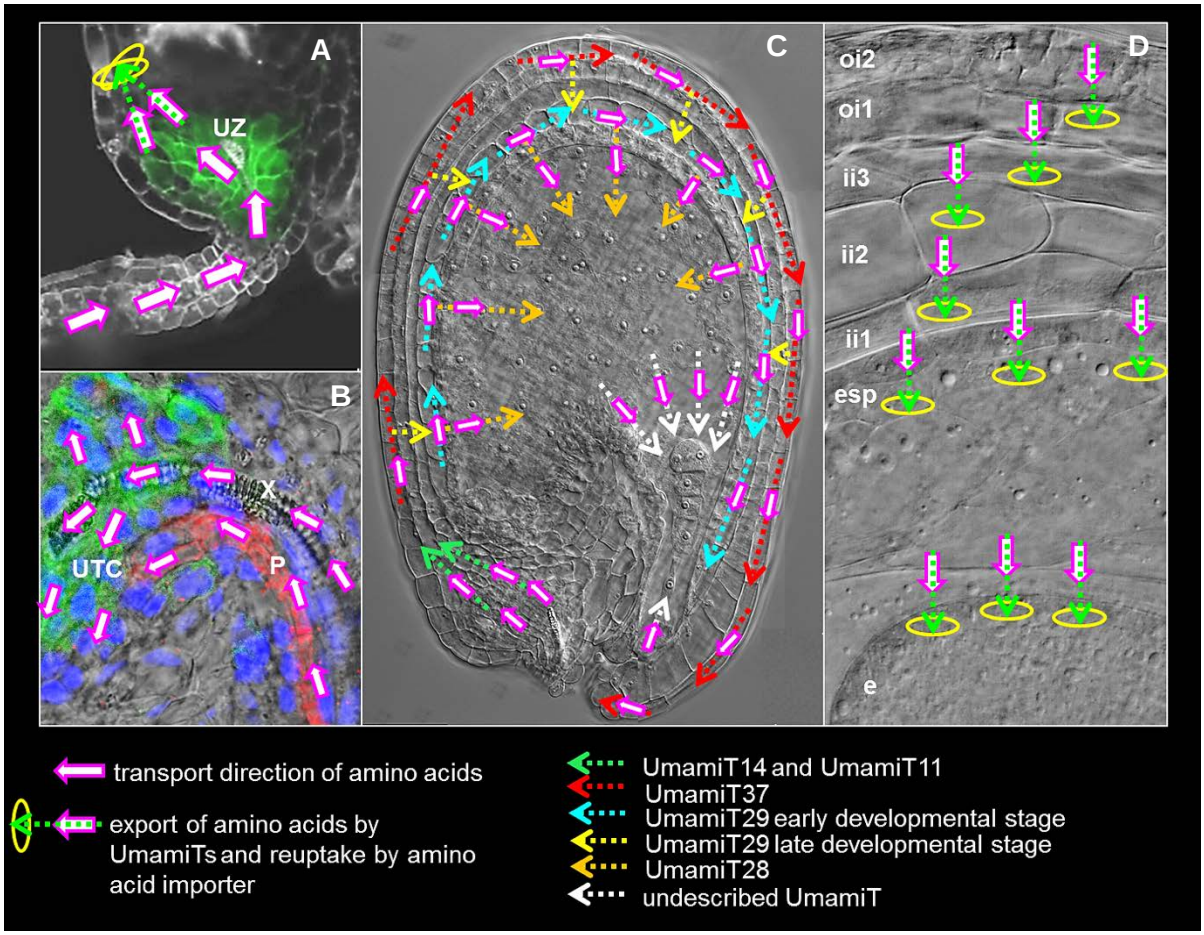

Figure 159. Model about the complex route of amino acids in the seed and the localization of the individual UmamiTs in the symplasmically isolated domains. (A) Amino acids are delivered by the vasculature in the funiculus into the unloading zone (UZ) and exported by UmamiTs (green cells), into the outer integument. (B) Amino acids are transported by the phloem (P) and xylem (X) into the unloading zone, where UmamiT-positive cells (UTC) are located in close contact to the endpoint of the vasculature. (C) Illustration of the complex route amino acids take to reach the embryo. UmamiTs export amino acids out of the unloading zone into the seed coat. In each integument layer of the seed coat amino acids can be homogenously distributed along the cell file they get imported. Several export steps in the seed coat are necessary to transfer amino acids into the endosperm. Each export step between the symplasmically isolated integuments is facilitated by different UmamiTs, indicated by colored arrows. (D) Detailed view on the different export/reimport steps that are needed to translocate amino acids from the seed coat into the endosperm and embryo. For each export step UmamiTs are needed. E (embryo), esp (endosperm), ii (inner integument), oi (outer integument).

The physiological relevance of these results could be shown by analyses of *umamit* mutants. The hypothesis was that loss-of-function of the UmamiT transporters in their respective expression domain would lead to an accumulation of free amino acids in the seeds, because they are not transferred into the embryo and metabolized further into proteins while the flow of sucrose, which is responsible for pressure-flow is still taking place at unaltered rates. Indeed, elevated levels of free amino acids were found in the siliques of mutants compared to WT or

the corresponding complementation lines. Similar results were obtained in the analysis of *aap1* mutants (Sanders et al. 2009). AAP1 is an amino acid importer localized in embryos. It was found that aap1 mutants have an increased amount of free amino acids that were accumulating in the embryo and seed coat. This is in line with the *umamit* mutants suggesting that exporters and importers act together to supply the embryo with amino acids. To understand the complexity how amino acid exporters and importers act together, higher-order mutants between UmamiTs and amino acid importers, such as AAP1 are needed to characterize the flux of amino acids from the unloading zone into the embryo in more detail. Furthermore, also differences in the amino acid spectrum between the single knock-outs of clade I and clade III UmamiTs could be observed. In *umamit29* and *umamit28* small and polar amino acids were more different to WT as in *umamit11* and *umamit14*. Amino acids, which were delivered by the vasculature are transported by the unloading zone specific. This indicates different substrate specificity for those two clades *in planta*. In the unloading zone UmamiT11 and UmamiT14 transport amino acids, which had higher concentration in the vasculature. From the unloading zone amino acids are translocated into the outer integument. The outer integument is also able to metabolize amino acids, which means that amino acids are not only delivered by the vasculature, but also synthesized *de novo* in the seed coat to deal with the increasing demand of nutrition of the embryo. This underlines that export out of plastids is a key step to provide amino acids for intercellular trafficking, which could be managed by UmamiT2, a newly selected candidate, which localized in the plastids of the outer integument. By this mechanism it is a rational consequence that the spectrum of amino acids, which accumulates in *umamit28* and *umamit29*, is different from the spectrum that is affected by umamit11 and umamit14. Taken together, a clear effect of the mutation on the level of free amino acids in the siliques was seen and members within one clade showed a similar effect compared to members of the other clade. Demonstrating that members of one clade are physiologically similar to each other compared to sister UmamiT clades. It was also possible to report an additive effect of a double knock-out between *umamit11* and *umamit14*, where the amino acid composition showed higher levels of free amino acids than it was expected according to the levels in the single knock-outs. Using qRT-PCR it was proven that the loss-of-function of one *UmamiT* is not compensated for by induction of the sister gene. This leads to the interpretation that protein-protein interaction of UmamiTs of the same clade could occur. A similar phenomenon was recently described for a nitrate transporter (NRT1.1). It was found that NRT1.1 is a dual-affinity nitrate transporter that changes its affinity in the availability of nitrate by phosphorylation of a threonine residue in the homodimer (Sun et al. 2014). These results show that posttranslational modifications of transporters from the major facilitator superfamiliy to which NRT1.1 and UmamiTs belong could be a mechanism to extend the transporter flexibility in the physiological

context. Preliminary FRET studies carried out during the writing of this thesis support that hypothesis.

Although there were elevated levels of free amino acids in the seeds of mutants, the plants showed full seed set without any obvious difference to the WT. Investigation of the length and width of the seeds revealed differences between WT, single knock-outs and the complementation lines. Seeds of the knock-outs were smaller than in WT or the complementation lines. This becomes more obvious as calculation of the seed volume was done: a significant reduction of the seed volume in mutants appeared. It was already shown in *Arabidopsis* that seed size is a very complex trait and determined by endosperm growth and the integument cell elongation (Gracia et al. 2004, Lafon-Placette and Köhler 2013, Creff et al. 2015, Figueiredo et al. 2015). Mutation of *TTG2* (transparent testa glabra 2) prevents cell elongation in the outer integuments and leads to smaller seeds in the mutants. The same effect was obtained if the HAIKU pathway of the endosperm was mutated, a regulator of proliferation in this tissue (Gracia et al. 2003). Also hormones influence seed size. For auxin no direct link to seed size was shown so far. The findings of high auxin levels and auxin response at the unloading zone and the integuments indicated that *UmamiT* expression is triggered by auxin as shown in this thesis. This enables the plant to regulate the amino acid transport by modulating the different UmamiTs and thus react to the demand of nutrients consumed by the embryo. Mutation of cytokinin receptors leads to a bigger seed size, which can be mainly explained by bigger embryos (Riefler et al. 2006). Until now it was not investigated that the amino acid level in a developing seed can influence seed size too. The new findings of the research on UmamiTs illustrate that amino acid transport into the seed does also affect seed size at maturity. In summary, the data of the amino acid analytic and the results of the seed volume show that UmamiTs have an impact on the amino acid composition of the seed and influence yield. Thiel (2014) and McCurdy and Hueros (2014) discussed the roles of transfer cells for yield improvement in crop plants. Additionally the plant hormone cytokinin was recently discussed to limit yield (Jameson and Song 2015) and also auxin seems to take indirectly control over seed size by regulating ARFs (auxin response factors) expressed in the integuments (Schruff et al. 2006). The observations are quite new, that transport proteins can indeed influence seed size too (Müller et al. 2015). In the case of sugar transporters, it could be show that SWEET-mediated transport is responsible for seed filling in maize (Sosso et al. 2015). In principle the same results were obtained for amino acid transporters in *Arabidopsis* and the challenge now is to transduce the results to other species like legumes and crop plants to contribute to the big goal to address food security in the future.

6.3.3. Integrating UmamiTs with hormonal dynamics and assimilate routes during seed development

Reproductive tissues undergo dramatic morphological changes that encompass asymmetries in the distribution of phytohormones as well as the differentiation of specialized cells for assimilate transport. One aspect that makes *UmamiTs* so unique in the unloading zone is their distinct expression pattern that appeared only after fertilization. The observation that UmamiT-positive cells are completely absent in the unfertilized state makes a trans-differentiation of parenchyma at the endpoint of the vasculature reasonable. The open question now is what are the signals that initiate this differentiation into a unique unloading zone? Looking at phytohormones, it was found that during seed development an asymmetry in the distribution of auxin and cytokinin response occurred. Cytokinin response was located solely in the developing endosperm until cellularization was seen, whereas auxin response is found in the seed coat and the unloading zone. This was in line with the observation that after fertilization auxin was absent in the endosperm and highly concentrated in the unloading zone and the integuments. One explanation for this asymmetric distribution of auxin is the spatial and temporal dynamic change in tissue specific PIN3 localization. Polar auxin transport, mediated by PIN3, can explain how an auxin accumulation in the unloading domain occurs: right after fertilization, PIN3 shows a strong expression in the funiculus and particularly in the vascular parenchyma a polar distribution in anticlinal position, indicating auxin transport towards to the fertilized ovule. At the same time, PIN3 is located in the innermost layer of the inner integument and shows - also here - a preference for polar distribution, indicating that auxin is homogenously distributed in this layer. Additionally, a polar distribution was also seen in some cells of the inner integument layer 2 close to the chalazal pole. Including the postulation that before fertilization the gametophyte harbors its own auxin pool (Panoli et al. 2015) makes the finding that auxin was absent after fertilization reasonable, looking at the localization of PIN3 in the innermost integument layer. These findings conclude that, after fertilization, auxin is exported out of the embryo sac, which explains the auxin minimum in the endosperm indicated by R2D2. At the same time, PIN3 mediates the homogenous distribution of auxin in the cell layer next to the embryo sac and the export into the following inner integument layer 2 at the proximal pole of the seed. This auxin flux is directed towards the unloading zone, where also the auxin flux coming from the funiculus is present. Cells of the unloading zone show a non-polar PIN3 localization, meaning that there is no directed auxin export out of the unloading zone. These two auxin streams (one from the funiculus, the other from the developing seed) culminate in the unloading zone and are the reason for the auxin maxima detected there and the extremely strong DR5 response. The strong auxin pulse could be the reason why UmamiTs

are specifically found in the unloading zone right after fertilization. It can be assumed that this accumulation of the hormonal signal by two auxin pools is causing the trans-differentiation of the parenchyma into functional transfer cells. An important argument for this hypothesis is the observation that *UmamiTs* are induced by auxin, indicating that auxin is a key hormone in the establishing of the unique unloading zone for the export of amino acids into seeds.
Furthermore, auxin was also present in the outer integuments, together with polarly distributed PIN3, which appeared in early stages at the proximal pole of the seed and extended during seed development to the distal parts and the micropylar end. Together with the polarized localization of D6PK it can be assumed that PIN3 is phosphorylated and in the active state. These observations lead to the conclusion that auxin is additionally exported out of the unloading zone into the outer integument and homogenously distributed there before it is transduced into the inner integument. Based on the presented results it can be concluded that auxin is using the same pathway as assimilates use in the seed. It would be possible that further UmamiTs are induced by auxin in the outer integument at early stages of seed development to export amino acids into the inner integument, where UmamiT29 shows, together with PIN3, the tendency of polar distribution in anticlinal position of the cells, indicating that amino acids and auxin are homogenously distributed along the cell file. Additionally, a localization in the membranes facing the endosperm was also observed, suggesting that the export of amino acids in direction of the developing embryo is possible.

In summary, it can be concluded that the uniqueness of the unloading zone in the seed is a result of the trans-differentiation of parenchyma cells into UmamiT-positive cells acting as functional transfer cells for amino acid export. This developmental change is initiated by the accumulation of auxin resulting by the flux of auxin which is coming from the inner integument and from the funiculus at the unloading zone. Furthermore, auxin is also streaming back into the seed at the same route assimilates are translocated from the unloading zone into the developing embryo.
This mechanism of a dual flux and recycling of auxin into the unloading zone could serve as validation signal for the mother plant that fertilization was successful and that transport processes are needed in the near future to nourish the embryo. The prolongation of the dual auxin flux into the developing seed can also serve as backup in cases when auxin flow from the vasculature is impaired due to stressful condition. In this case transport processes of amino acids would be induced furthermore by the recycling of auxin and ensure the proper translocation of amino acids into the developing embryo.

6.3.4. UmamiTs in the physiological gap of symplasmically isolated sink tissues

The analysis of the expression of *UmamiTs* in different tissues at different developmental stages highlighted their localization at positions, where a nutrient transport is crucially required. According to their physiological role they can be referred to as cells with transfer function. In literature the definition of transfer cells can be drawn either by their function (Offler et al. 2003) or their position within a tissue (Gunning and Pate, 1969, 1974). Both characteristics are true for cells which express *UmamiTs* at unloading zones, as shown in the seed (Müller et al. 2015), in anthers and in tissues around the giant cells. In the seed and anthers, the need of cells with transfer function becomes obvious by the discovery that companion cells and sieve elements do not stretch deeply into these types of sink tissues. This means that phloem tissue is physically not connected to those sinks, which includes that cells in between must overcome a transfer function of assimilates (Tegeder et al. 2000, Müller et al. 2015). Additional support of the idea to characterize UmamiT-positive cells as functionally equivalent to transfer cells is given by the observation that they are connected to the phloem by branched plasmodesmata and capable to function as a prolongation of the phloem (Werner et al. 2011). The unloading phloem cells can be interconnected by plasmodesmata too (Hoth et al. 2008) to achieve an equal distribution of compounds across the unloading zones in anthers and seeds. In contrast, in most cases the flow of assimilates from the transfer cells into the sink tissue is not that much supported by the symplasmic route (Hoth et al. 2008, Hammes et al. 2006), which is true for the nematode feeding site and the unloading zone of the seed as shown. This underlines the importance of transport processes across the plasma membrane including import and export of substrates (Hammes et al. 2005, Marella et al. 2013). Plasma membrane-associated transport processes occur in transfer cells which lead to an export of compounds into the apoplast, from where they can be taken up again by importers. This fits well in the found expression pattern of *UmamiTs* during seed development and nematode infection. For giant cells, acting as transfer cells in the nematode feeding site or during symbiotic interaction it was shown that cell wall ingrowths contribute to the nutrient exchange between the sink tissue and the transfer cell (Gunning and Pate 1974). These ingrowths lead to the increase of the membrane exchange area between the symplast-apoplast interface and can occur in juvenile phloem cells as well as in the perceiving cells like giant cells (Offler et al. 2002). In the case of UmamiT-positive cells no investigation about cell wall ingrowths was done so far but they share close physical contact to cells they support with compounds. In order to elucidate the cellular morphology of UmamiT-positive cells electron microscopy would be needed especially at the unloading domain to investigate, if there are existing cell wall ingrowths. Transfer cell differentiation can occur in many different cell types including the vascular parenchyma, pericycle or epidermal cells. In some cases the change of gene expression, which leads to the

differentiation into a transfer cell is not part of the normal developmental program but even more a result of stress response. The differentiation process is called trans-differentiation (Andriunas et al. 2013) which means that cells would first de-differentiate and subsequently re-differentiate to transfer cells. In the unloading zone of seeds, it was observed that *UmamiTs* are not expressed before fertilization, whereas after fertilization, during seed development, expression is found in the unloading zone, the seed coat and endosperm. Simultaneously, also the distribution of auxin maxima and auxin response is changing after fertilization and occurs in UmamiT-positive cells. This implies that gene expression in UmamiT-positive cells is altered during maturation and possibly regulated by auxin. Considering the cell specific expression pattern of *UmamiTs* it fits well to the findings that each seed stage has its own set of transcription factors leading to the spatio-temporal different gene expression (Le et al. 2010). Until now no unloading zone specific transcription factor was identified, which is probably a result of the discovery that most transcription factors, which were upregulated during seed development, are also involved in several contexts of the entire life cycle (Walling et al. 1986, Le et al. 2010). To find possible transcription factors involved in the regulation and differentiation process of UmamiT-positive cells at the unloading zone a tissue specific isolation of the unloading domain by laser capture or FACS would be needed.

In summary, looking at the tissue and time specific expression pattern of *UmamiTs* in cells of symplasmically isolated sink tissues and the physical connectivity of those cells to the phloem characterizes UmamiTs as key transporters of unique cells with transfer function concerning amino acid export into sink tissues.

6.3.5. UmamiTs during interaction with root-knot nematodes: supply of symplasmically isolated giant cells.

The infection with the root-knot nematode *Meloidogyne incognita* leads to the formation of a gall, a tumor like structure of the root, induced by the secretions of subpharingeal glands of the nematode (Tytgat et al. 2005). The root-knot harbors the feeding site of the nematode, which consists of the giant cells and the phloem tissue enclosed by a xylem cage (Bartlem et al. 2013). The giant cells are multinucleated and show a high metabolic rate (Jones and Northcote 1972), thus building the new sink tissue in the root (Bird, 1996, Hoth et al. 2008). Because giant cells are symplasmically isolated from the surrounding cells, the supply of this sink tissue is extremely dependent on transport processes occurring at the membranes of the adjacent phloem tissue and the giant cells (Hammes et al. 2005, Marella et al. 2013). This supply is managed by the newly formed phloem tissue around the giant cells. Phloem cells associated with the giant cells show intense auxin response also after they differentiate to sieve elements (Absmanner et al. 2013). In addition to that the cytokinin response was also monitored and the highest cytokinin response during infection was observed in the small parenchymatic cells surrounding the giant cells. This result is similar to the already published investigations of infected *Lotus* and shows that the principle mechanism of root-knot formation and the changes in the hormonal state are quite conserved in the *Meloidogyne* pathosystem (Lohar et al. 2004). The lack of auxin response and cytokinin response in the mature giant cells is surprising. Giant cells can be compared with the developing endosperm, because both tissues represent a multinucleated physiological sink tissue. In the endosperm a lack of auxin response was found, whereas a strong cytokinin response was monitored. This is a strong difference to giant cells were in the mature state no hormone response was reported anymore. In contrast to that, hormone responses can only be observed in the initial phase of giant cell formation, where auxin response reporters (Barcala et al. 2009, Absmanner et al. 2013) as well as cytokinin response reporters (Lohar et al. 2004) are clearly located in the vasculature. The same was also reported for the nitrogen-fixing symbiotic interaction in nodules of legumes, where in the initial phases hormonal responses were induced compared to mature nodules (Koltai et al. 2001). This initial induction of the hormone response in the founder giant cell is linked with cell cycle activation (Goverse et al. 2000), which leads to a reentering of mitosis and karyokinesis, thus forming a multinucleated sink tissue. After the initial phase has passed, the gene expression in the giant cells changed and hormonal response for cytokinin decreases (Barcala et al. 2009), whereas genes involved in auxin transport (*AtAUX, AtLAX3, AtPIN7*, *AtPID*) were induced (Hammes et al. 2005, Barcala et al. 2009), which makes a flow of auxin out of the giant cell reasonable. This flux of auxin into the parenchymatic tissue surrounding the giant

cells could be an explanation, why auxin response is induced in those cells and missing in giant cells, probably due to the lack of specific auxin responsive factors (ARFs) or the specific repression of auxin response in giant cells. Auxin response can be inhibited by stabilizing AUX/IAA repressor factors in the presence of the phytohormone salicylic acid (SA, Iglesias et al. 2011)). If local SA in giant cells plays a role in repressing auxin response is at the moment not investigated.

Al these results about auxin response in the root-knot stay in line with the findings that *UmamiTs* are induced by auxin and supporting the idea of a differentiation of parenchymatic tissues into UmamiT-positive juvenile phloem cells that supply the feeding site with amino acids. In combination with the cytokinin response in the same parenchymatic tissue it can help to explain the proliferation of those phloem cells and their differentiation into functional sieve elements. This phenomenon to activate cell division in non-mitotic cells is well described in lateral root formation and always seemed to be connected to the initial hormonal pulse from the auxin-cytokinin interplay (Francis and Sorrell 2001). According to the hormone level a similar situation is found in the phloem cells of the root-knot. Although the cells surrounding the giant cells are well-characterized as juvenile phloem cells (nucleated, high connectivity by plasmodesmata, APL and PD1-positive), the transport processes are so far not understood. Root-knots are symplasmically isolated (Hoth et al. 2008) but until now in parenchymatic tissues close to giant cells there were no transport proteins described with bidirectional transport function. This physiological gap could be closed by UmamiTs. It was possible to proof that they are upregulated during infection and specifically expressed in cells adjacent to the giant cells. This was independent of the age of the root-knot and true for each candidate. By immunolocalization it was shown that colocalization of UmamiT-positive cells with RS6, a sieve element marker occurred. Interestingly, the population of cells encircling the giant cells was not homogeneous. Also in very old root-knots undifferentiated parenchymatic cells that were only UmamiT-GFP positive were still found besides sieve elements which showed expression of RS6. The proportion of differentiated juvenile phloem cells increased from young to old root-knots. The mixed nature of the population of cells around the giant cells can be explained by the influence of auxin and cytokinin in the root-knot, which leads to cell proliferation of the parenchymatic cells and initiates in combination with the sink pressure of the giant cells an accumulation of differentiated phloem cells (Absmanner et al. 2013). This is also supported by the observation that APL, a transcription factor for phloem differentiation, is found in exactly those cells, which show sieve element identity close to the giant cells. Furthermore, it was also reported that the transcription factor SCR is active in giant cell associated phloem cells, even before RS6 appears. This is quite surprising, because in roots SCR is usually not associated with phloem differentiation. Its presence in the juvenile phloem tissue of root-knots underlines the tumor like constellation there, where a misregulation of developmental genes is apparent.

This misregulation is directly induced by the nematode to establish the feeding site. For example, it was discovered that a root-knot secretory peptide (encoded by the *16D10* gene) can interact with SCR-like transcription factors (Huang et al. 2006). This implicates that a bioactive parasitism peptide from the nematode can serve as ligand for a plant regulatory transcription factor and lead to a shift in cellular composition of the gall. Looking at this data the finding that SCR was present in juvenile phloem cells indicates that this tissue is not only unique by the so far described characteristics (nucleated, interconnected by branched plasmodesmata, presence of several phloem markers: APL, PD1, RS6-positive) but also in the sense of its differentiation state and gene regulation by transcription factors.

From a physiological point of view, the overlapping expression of *UmamiTs* in the phloem tissue next to giant cells makes a lot of sense. It was already reported in the seed, that candidates of different clades exhibited different substrate specificities, which can be considered to be true also in the case of roots. Nematodes are in fact depending on (essential) amino acids. A disruption of the import of amino acids into the feeding site causes a lack of nutrition of the nematodes and changes the male/female ratio of the progeny to the site of the males (Marella et al. 2013). Hammes et al. (2005) identified several AAPs that were induced during infection and highly expressed in the giant cells. Additionally, a member of the cationic amino acid transporter family (CAT6) was shown to be specifically upregulated in giant cells (Hammes et al. 2006). The data underline the importance of amino acid import into the giant cells and that the vitality of the nematode and the progeny is really depending on a high import rate of amino acids. This can only occur if at the site of the phloem tissue the export of amino acids takes place. Because giant cells were reported to be symplasmically isolated from the newly formed phloem cells (Hoth et al. 2008), all translocation processes of amino acids from the phloem into the feeding site must occur by an apoplastic step. Export of amino acids by bidirectional UmamiT transporters is discussed to happen by an electrochemical gradient or by antiport with protons (Müller et al, 2015). In a screen of induced genes during nematode infection it could be shown that in the gall H^+-ATPases are upregulated (Bird and Wilson, 1994, Bird 1996), which is also true for tissues where auxin response is found (Hager et al. 1991). This means that indeed a pool of protons is present in the apoplast of giant cells and the neighboring auxin responsive cells. These protons can furthermore be used for proton coupled transport. In this scenario the newly formed juvenile phloem cells with *UmamiT* expression would function as exporters for amino acids into the apoplast (Fig. 160), from where a reuptake by importers (AAPs, CATs) into the giant cells can occur (Hammes et al., 2006, Bartlem et al. 2013).

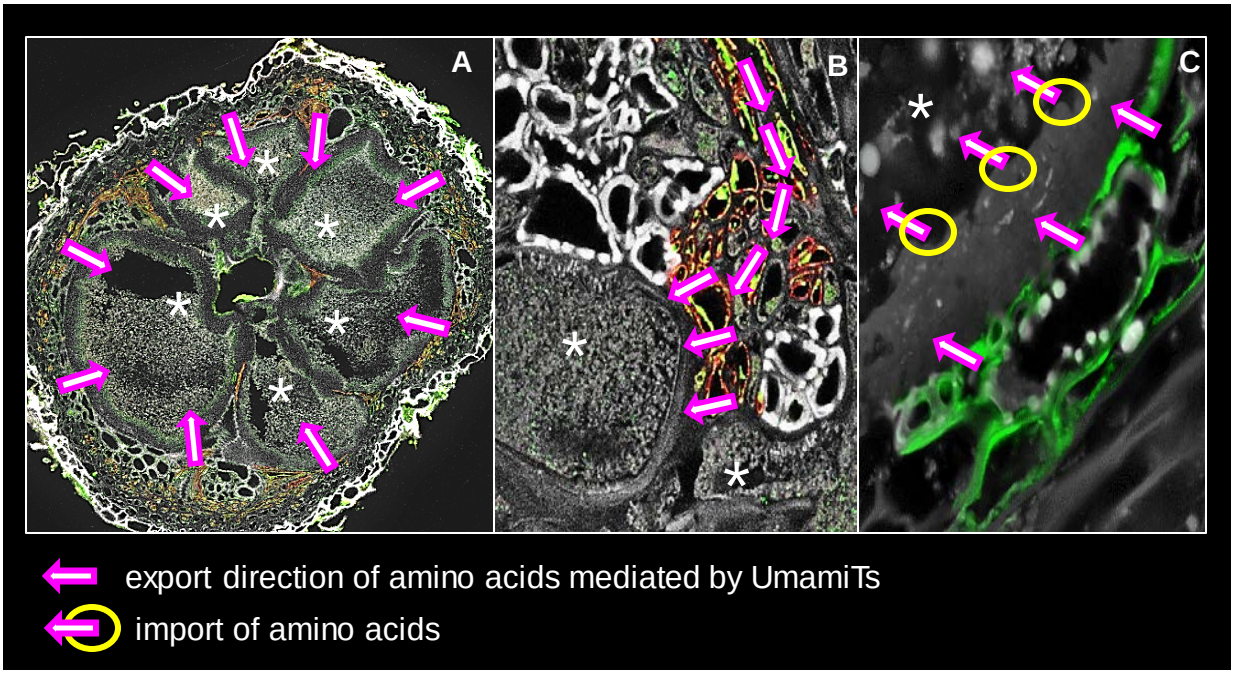

Figure 160. Model about the complex route of amino acids in the root-knot and the localization of UmamiTs in juvenile phloem cells. (A) Giant cells are embedded in vascular tissue, which delivers amino acids and exports them in direction to the sink tissue. (B) Feeding site associated vascular tissue is physically close to giant cells, UmamiT-positive and shows the sieve element specific RS6 epitope (yellowish cells), characterizing it as juvenile phloem. These cells transport amino acids from the vasculature into the feeding site. (C) To overcome the symplasmic barrier in the feeding site of root-knots amino acids are exported by UmamiT-positive juvenile phloem cells (green cells) into the apoplast and taken up from there by amino acid importers localized in giant cells. Asterisks mark giant cells.

Preliminary data of *umamit* mutant plants infected with the root-knot nematode *Meloidoyne incognita* underline the importance of UmamiTs at the feeding site, because mutants show a reduction of gall number and size, indicating that the loss-of-function influences the establishment of the nematode feeding site (Dr. Shaihd Siddique, pers. comm.). Infection studies with the cyst nematode *Heterodera schachtii* are also on the way. First results show that the syncytia size and average number of nematodes per plant is not affected by the *umamit* knock-out. This shows that UmamiTs play only a limited role in the syncytium, which is symplasmically interconnected with the surrounding vascular tissue.

From a physiological point of view, it can be concluded that UmamiTs have a role as exporters in the feeding site of root-knot nematodes, ensuring the export of amino acids towards the symplasmically isolated giant cells. By this, it is possible to make a functional characterization of UmamiT-positive cells as juvenile phloem exhibiting transfer function (Rodiuc et al. 2014) at key positions for the supply of symplasmically isolated tissues during pathogenesis.

6.3.6. UmamiTs in the root: a role in amino acid cycling

In the vegetative tissues UmamiTs were located in the vascular parenchyma and localized in sieve elements. The overlapping expression of *UmamiTs* in leaves and the shoot was already discussed under the aspect of amino acid transport specificity in the long distance transport along the vasculature. The extensive expression analyses suggested a high degree of redundancy for all *UmamiTs* of both clades in the root. All candidates were found to be expressed in the vascular tissue. Close to the root tip a transient location of UmamiTs in the protophloem and in the metaphloem was observed. The most prominent expression was found in young roots, before secondary thickening occurred, specifically in the xylem parenchyma and later on in older roots, when secondary thickening occurred, additionally in the sieve elements. This switch from cambial/parenchymatic to differentiated phloem tissue becomes very obvious in the oldest part of roots, close to the hypocotyl, where a gradual differentiation from the xylem axis towards the phloem could be observed. Here all sieve elements showed a double decoration with α-GFP and α-RS6 epitope. This switch from parenchyma to sieve elements depending on root age is quite interesting, because it implicates, that sieve elements can have different origin, as it was already proposed (Dolan, et al., 1993, Lucas et al., 2013; Furuta et al., 2014). This was further supported by the observation that the phloem-specific transcription factor APL was co-expressed in UmamiT-positive cells and that auxin response took place in exactly those parenchyma cells. The phytohormone auxin is also able to elevate the RNA levels of *UmamiTs* in roots, indicating, that an auxin pulse in parenchyma cells and the concerted activation of APL might lead to a differentiation of UmamiT-positive cells into sieve elements. The specific expression of *UmamiTs* in the xylem parenchyma of young roots is also very interesting. This tissue stays in close contact to the xylem and reaches also into the phloem poles. Several different transporters expressed in the same cell files are already described, like a sulfate transporter gene *SULTR3;5* (Kataoka et al. 2004), the nitrate transporter genes *NRT 1.5* (Lin et al. 2008) and *NRT1.8* (Li et al. 2010), a sucrose transporter gene from the walnut tree *Juglans regia JrSUT1* and hexose transporter genes *JrHT1* and *JrHT2* (Decourteix et al. 2007) and the amino acid transporter gene *AAP6* (Okumoto et al. 2002). All these findings show how important the gateway marked by the xylem parenchyma cells is. In this sense UmamiTs can also be described as important players for facilitating the retrieval and feeding of amino acids from the xylem apoplast, because they exhibit export and import activity for amino acids (Müller et al. 2015). By this mechanism, amino acids could be cycled from the phloem to the xylem. This process enables an efficient root-shoot allocation of amino acids, because UmamiTs in the conducting tissue of the root are furthermore also placed in the metaphloem and could contribute there to an efficient mechanism to mediate the amino acid cycling between xylem and phloem as described (Tegeder 2014). In the literature

only importers for amino acids were described so far and possible candidates that function as amino acid exporters were completely unknown in the root (Okumoto et Pilot 2011). UmamiTs very likely close this gap in the amino acid cycling by their capacity to take up amino acids and export them again in the surrounding tissue. Furthermore, the polar distribution of UmamiT14 in anticlinal position of the parenchymatic cells supports the idea that UmamiTs are involved in the directed translocation of amino acids along the vasculature. The same findings about the polarity of UmamiTs in the young differentiating protophloem cell layers, suggest a possible role of UmamiTs in the long distance transport of amino acids towards the root tip and phloem unloading (Fig.161).

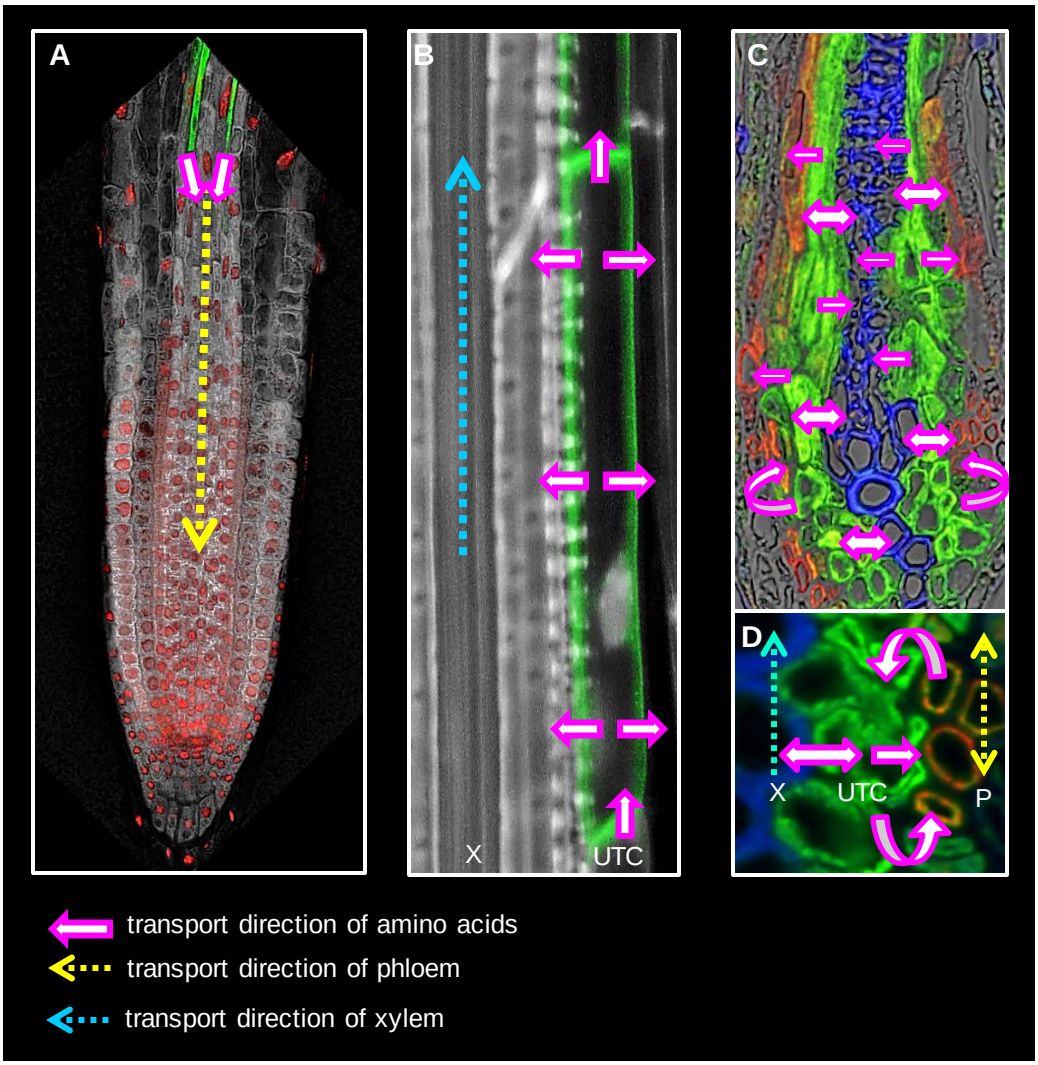

Figure 161. Model about the complex route of amino acids in the root and the localization of UmamiTs in protophloem, sieve elements and vascular parenchyma. (A) At the root tip UmamiTs are located in the protophloem and contribute to the acropetally directed transport of amino acids and phloem unloading. (B) UmamiT-positive cells are physically close to xylem and responsible for the feeding of xylem with amino acids. (C) UmamiT-positive cells (green) are associated with xylem (blue) along the root and share close vicinity to sieve elements (red), which marks the function of UmamiTs in long distance transport of amino acids and amino acid cycling. (D) Amino acids cycling between xylem and phloem is mediated by UmamiT-positive cells in between. X (xylem), p (phloem), UTC (UmamiT-positive cell).

With this knowledge it is not that surprising that *UmamiT* transcript levels were also elevated in arrays on plants infected with *Verticillium longisporum* (Christiane Gatz, pers. comm.). In infected parts, the GUS reporter lines of UmamiT14 showed a much stronger promoter activity than in uninfected GUS plants (Christiane Gatz, pers. comm.). This opens the possibility, that the fungus, residing in the xylem, indeed is manipulating the cycling system of amino acids in the root to feed itself. The regulation of UmamiTs could therefore be “used” by *Verticillium* to enhance the level of free amino acids in the xylem, a phenomenon that was long ago already reported in tomato plants (Dixon and Pegg 1972). There, the xylem exudates of susceptible and resistant cultivars were studied and it was found that, after infection, resistant tomato plants showed a reduced level of free amino acids in the xylem sap compared to susceptible cultivars. This indicates that genes for amino acid transporters are upregulated in the xylem parenchyma of susceptible plants, which leads to elevated levels of free amino acids in the xylem sap that nourishes the pathogen.

Elevated levels of free amino acids were also observed in the siliques of *umamit* knock-out plants. The seed anatomy determines that phloem and xylem are ending free in the unloading zone, meaning that amino acids cannot move backwards with the phloem stream. Similar to this, elevated amino acid levels may also occur in the root tip of the knock-outs. From there they can reenter the amino acid cycling into the xylem and move upwards with the xylem sap into the sinks. This mechanism contributes that additional free amino acids are translocated into the unloading zone of siliques, where they further accumulate due to the knock-out of an UmamiT amino acid exporter.

Altogether, the results show that UmamiTs are located in roots at strategically important position, the vascular parenchyma, that allows the amino acid cycling between phloem and xylem, which is linked with yield. This cycling enables a plant to respond to changes in the demand of amino acids of the aerial tissues and to optimize the supply of sink tissues with amino acids.

6.3.7. UmamiTs in the root: phloem-dependent impact on stem cells

Although there is an overlapping expression of *UmamiTs* in the root vasculature, a phenotype in the mutant plants could be found. In the first three weeks after sowing they exhibited shorter roots than WT plants or complementation lines but the root length was restored later on to the level of WT plants. Root elongation rate was reported to be highly dependent on the diurnal rhythm, meaning that growth activity of roots is linked with photosynthesis and energy metabolism (Yazdanbaksh and Fisahn 2011). At the moment, no study on the mutants concerning energy state of the root was done and further research is needed. Another possibility for the shorter roots might be that embryos of *umamit* mutants have a different nutritional state after germination. This might be reasonable, taking the increased level of free amino acids in siliques and the smaller seed size of mutants into consideration. Also changes in the N/C ratio of a plant are known to impact root length by influencing cell wall biogenesis and composition, which affects especially cells at the elongation zone of roots (Zheng et al. 2009). Nevertheless, the effects of shorter roots were seen only transiently, suggesting that an altered root growth rate or elongation restored mutant roots back to the length of WT plants. This is an important observation, because it implies that the root system of mature plants was not different between mutants and WT, which supports that differences in amino acid levels in siliques are dependent on transport processes rather than being due to the extension of the root system. A reduction of the length of plant organs could be a result of smaller cells or a reduction in cell number (Benfey et al. 1993, Weijschede et al. 2007). In this study the number of mitotic events in the root tip was investigated by *in situ* RNA hybridization using *CYCB1.3* probes. With exception of *umamit11* in all mutants a reduction of mRNA level, visualized by the staining intensity was observed. Scans of the whole root tip furthermore revealed that the average number of mitotic cells was significantly reduced in the mutant background, which leads to the assumption that the reduced root length is a result of a lower cell division rate in the meristematic zone of the root tip. The results indicate that the long distance transport of amino acids and the cycling of amino acids within the root do indeed impact the growth rate of meristematic cells. This is a completely new insight into the regulation of cell division and cell expansion of roots, because it explains former findings that cell production rate and elongation rate are correlated to each other (Beemster and Baskin 1998). In yeast it was shown that amino acid supply is one driving force for the cell cycle (Dudani and Prasad 1983). A common feature between singe dividing cells, such as yeast, and meristematic root cells may be the reason for the observed reduction in cell number in *umamit* mutants. This phenotype in the restricted time window recalls already published root phenotypes of phloem mutants, like for OCTOPUS (Truernit et al. 2012), BRX (Mouchel et al. 2004) and CHER (Dettmer et al.2014). All genes mentioned play a role in the differentiation process of the early protophloem. Expression data

of the investigated candidate *UmamiTs* showed at least promoter activity in the protophloem cell file for all candidates. The promoter of *UmamiT29* was unique. It was expressed near to the quiescent center in the “Octopus” cell (Truenit et al. 2012) and upwards in several cells of the vascular primordial cells. The strength of this promoter was quite weak in those cells compared to the very high signal intensity shortly before xylem differentiation takes place. Furthermore, it was noticed that expression in the protophloem was only transient and disappeared abruptly in about the same distance from the root tip, where enucleation of the protophloem was reported (Furuta et al. 2014). These findings were also true for the fusion protein of UmamiT29-GFP. Only a very weak and transient expression in the protophloem could be reported, underlining a possible role there in the amino acid supply of the meristematic zone of the root tip. Nevertheless, all candidates had their most prominent expression in about 300 µm distance from the QC in the xylem parenchymatic tissue distinct from the sieve elements. Although UmamiT-positive cells were placed in the metaphloem, too no phenotype was observed in tissues above the QC. The root morphology was indistinguishable between the single knock-outs and the WT. A closer look at the root tip beneath the QC revealed in most cases also no difference to the WT. But in very few cases (< 7%) clear differences compared to cellular composition of the WT were recognized. By mPS-PI staining of roots from *UmamiT* mutants of clade I (*UmamiT11* and *UmamiT14*) a functional columella but additionally in the columella stem cells right behind the QC an unusual accumulation of small starch granules was found that usually appeared in the second cell file behind the QC in the compared WT root (Drisch and Stahl 2015). The functional columella was also detected in single knock-outs of clade III (*UmamiT28* and *UmamiT29*), but there were observed two instead of one layer of the columella stem cell file. Although these cases were rare, they show the phenotypic plasticity in the single knock-out plants and that indeed the distribution of amino acids can have an impact on processes in the stem cells. This is an until now completely overlooked topic. Also in the animal field, where research on stem cells is much more advanced than in the plant field, only little is known about the context of stem cell maintenance and the expression of amino acid transporters. Van Winkle (2013) and Formisano (2016) showed earlier that amino acid transporters can indeed have an impact on nutrition and signaling in pluripotent stem cells. These publications showed that in the mammalian system stem cells exploit the abundance of amino acids as a signal for entering the cell cycle. Threonine and proline uptake and glutamate export by transporters was shown to trigger proliferation in mouse and human stem cells. The underlying transport mechanism was reported to be sodium dependent as usually found in the physiological context of animals but also a sodium independent transport for threonine was found. Similar research is missing in plants but it seemed to be likely that based on the findings in this thesis amino acid transport by UmamiTs in the provascular tissue of the meristematic zone does impact the amino acid supply of stem cells. Another possibility is the impact on stem

cells coming from the unloading phloem tissue above the QC. Although no morphological changes in phloem anatomy at the differentiation zone was seen, it could be possible that similar to the metabolic phenotype in seeds, not only the amino acid composition within the downward directed phloem stream is changed but also the rate of transported amino acids at the vascular endpoint. Furthermore, the preference of polar localization of UmamiTs in anticlinal position of the protophloem reveals that also the long distance transport is regulated by UmamiTs, when sieve elements are not fully mature. The presence of UmamiTs in the protophloem indicates also that the investigated candidates play a role in the unloading of amino acids, the export out of the protophloem, which makes them unique compared to the findings of the close related member *SIAR1* that is expressed in the endodermis (Ladwig et al. 2012). Unloading in root tips from the protophloem by transporters was so far only poorly investigated and mostly considered to occur *via* the symplast (Giaquinta et al. 1983). It has to be considered that there is a fine subzonation of the root tip containing cells of different size and differentiation state, which makes a general agreement of symplasmic unloading more critical. Findings of Oparka (1994) demonstrated well that symplasmic phloem unloading in root tips is only true for some cells at the elongation zone and above, which indicates that transport processes at the differentiation zone of protophloem can play a role in phloem unloading. The presented results indicate that a loss-of-function of UmamiT transporters in the protophloem would result in a change of the amino acid composition that is after unloading probably passively translocated to the meristem by the downward directed sugar flow, where it could influence the differentiation and proliferation of meristematic cells (Formisano and van Wilke 2016). Phloem contributes also to the acropetally directed long distance transport of auxin. A direct impact on the long distance transport of auxin by UmamiTs could be ruled out by oocyte experiments done by Fastner and Hammes (pers. comm) that showed that UmamiTs do not export auxin in the heterologous expression system. But *UmamiTs* do in deed respond to auxin and although the possibility of a direct impact on auxin flow was not found, it could be discussed that the distribution of this phytohormone in the root tip is somehow indirectly influenced by the presence of *UmamiTs* in the phloem and vascular parenchyma cells.

The long distance transport of auxin from the vasculature to the stem cells regulates the differentiation of distal stem cells in the root, by repressing WOX5 and thus activating PLT1 in the central root meristem (Ding and Friml 2010, Dirsch and Stahl 2015). Taking into consideration that in few root tips of *umamit11* and *umamit14* mutants the tendency to lose the columella stem cells by differentiation was monitored, it is not that surprising to see cripple plants in the double knock-out, that show no functional columella and meristematic tissue anymore. Whole mount RNA *in situ* experiments elucidated, that the mRNA of *PLT1* and *WOX5*, central marker genes for root stem cells, were furthermore not detected in the roots of the cripple plants which supported the findings, that the meristematic cells are completely

consumed in the cripple plans. The phenotype shows similarities to the *plt1* mutant (Aida et al. 2004), the *tpst1* mutant (Matsuzaki et al. 2010), the *oberon1* mutant (Saiga et al. 2008) as well as the *apl* mutant (Bonke et al. 2003). The combination of a knock-out between *UmamiT14* and *UmamiT29*, the strongest candidates of each clade was also very informative. Here the root tip was still functional and the m-RNA for *WOX5* was comparable with the WT control, but interestingly the strength of expression of *PLT1* was significantly reduced. The same observation was also made for a knock-out combination between *cat6* (Hammes et al. 2006) and respectively the strongest candidate of clade I or clade III. Both *umamit14/cat6* and *umamit29/cat6* showed a sever reduction in the signal intensity of *PLT1* in the root meristem. It can be learned from these results, that amino acid transporters do indeed influence the root meristems by the supply with amino acids, as it was already postulated in the animal field (Van Winkle 2013) and in yeast (Dudani and Prasad 1983). Malnutrition of the stem cells and/or an imbalance in the auxin flow to the QC can be responsible for the phenotype of the higher-order *umamit* mutants and the *cat6/umamit* knock-out. The loss-of-function of one amino acid exporter and one amino acid importer leads to a down regulation of *PLT1*, which was also reported to be a result of the underlying auxin gradient (Galinha et al. 2007). A reduction of the PLT1 signal can furthermore be achieved by cytokinin (Ioio et al., 2008). Cytokinin is produced in the vascular tissue of the transition zone and transported towards the root tip. Of course auxin is the master regulator in the activation of PLT1, but there are regulatory links to cytokinin. Both hormones act in a dosage dependent manner and it should not be overlooked, that the ratio between those key hormones determines which fate a cell takes (Smigocki and Owens 1989). *PLT1* expression is furthermore upregulated in cytokinin mutants (Galinha et al. 2007). This means that a higher dosage of cytokinin or a lower level of auxin leads to the same phenotype as it was observed in the double knock-out of *umamit14/29*, *umamit14/cat6* or umamit29/cat6.

At the moment the reason underlying these phenomena based on the amino acid transport by UmamiTs remains speculative. One scenario would be that auxin production or transport is affected by impacting amino acid cycling along the root. The other scenario is that the supply of the meristem with amino acids does have a direct impact on the hormonal response and gene regulation. At least also a combination of a metabolic shift between auxin and cytokinin production and/or transport due to a disruption in amino acid homeostasis can lead to a downregulation of *PLT1* and stress the root meristem, which leads to changes in the differentiation of columella stem cells.

In summary, it could be shown that UmamiTs have unique function in the amino acid cycling between phloem and xylem. Furthermore, they are involved in phloem unloading at the root tip and therefore directly linked with the nutritional state of meristematic cells. This implies that UmamiTs are integral to the long distance transport of amino acids, the cycling between

phloem and xylem and the phloem unloading at the root tip, which can regulate the growth rate and differentiation of stem cells.

Future investigations on the N/C ratio in *umamit* mutants will help to elucidate, if UmamiTs do also impact the shoot/root communication and energy balance of the plant, which could be also contribute to the observed phenotypes in stem cells. This will provide new insights into the regulation of the cell cycle of plant stem cells by amino acids as signal molecules.

6.4. UmamiTs as key transporters for amino acid cycling and the supply of symplasmically isolated sink tissues: a comprehensive summary

Amino acids are distributed within the plant by several transport processes occurring between the parenchyma tissue and the conductive tissue. Whereas the import of amino acids into tissues is well described, the export processes are less well studied. In this thesis UmamiTs were characterized as transporters for amino acid cycling in the root and the supply of endogenous sink tissues, the seed, and an exogenously induced sink tissue, the giant cell, which is formed during the pathogenic interaction with root-knot nematodes. In roots, amino acid cycling can only occur if amino acids are imported into the vascular parenchyma and exported into the phloem or xylem. UmamiTs are localized in the xylem parenchmya, which makes them perfect candidates for the supply of the xylem with amino acids (Fig. 153 A). Amino acids can also be imported by these UmamiT-positive cells and translocated into the phloem tissue, because they share close physical proximity to sieve elements and exhibit export activity. Additionally, UmamiT-positive cells were shown to differentiate into sieve elements, which makes is obvious that these transporters contribute also to phloem unloading (Fig. 162 A). Especially in the root tip, where UmamiTs are also found in the protophloem, an unloading of amino acids is essential to supply meristematic cells. Amino acids that were loaded into the xylem and sieve elements by UmamiTs enter the long distance transport to sink tissues.

A very important sink tissue in the life cycle of a plant are seeds. The switch from vegetative to generative growth induces the development of specialized tissues that ensure a high degree of protection of the offspring. After fertilization there were three different genotypes present in the seed: the diploid maternal tissues (funiculus, unloading zone and seed coat), the triploid endosperm and the diploid embryo. To separate such genetically distinct tissues and possibly to protect the germ line from viruses they are symplasmically isolated from each other. This implies that assimilates that are delivered by the vasculature of the mother plant have to be actively exported into the apoplastic space between two symplasmically separated cell layers. In *Arabidopsis,* there exist five seed coat layers, which means that there are at least five export and import steps necessary to supply the embryo with amino acids: export from the unloading zone into the outer integument, from the outer integument into the inner integument and from the inner integument into the endosperm (Fig. 153 B). *UmamiTs* were shown to have their highest expression level in siliques. They were in a spatial temporal distinct pattern located in developing seeds. UmamiT11 and UmamiT14 were both found in the unloading zone in close contact to the endpoint of phloem and xylem. The uniqueness of the unloading zone is characterized by the trans-differentiation of parenchyma into UmamiT-positive cells right after

fertilization and the lack of any phloem marker. These cells exhibit transfer cell function by exporting amino acids from the unloading zone into the outer integument. From there, amino acids were exported by UmamiT37 (outer integument layer 2) and later on by UmamiT29 (outer integument layer 1) into the inner integument. There UmamiT29 can export the amino acids into the inner integument layer1 from where a last export step into the endosperm is made. After cellularization of the endosperm UmamiT28 appeared in the endothelium and fading endosperm, implicating amino acid export there. Altogether the complex route of amino acids across and between the unloading zone, the integument layers and endosperm of the seed underlines the import key position UmamiTs have in the supply of this kind of sink tissue (Fig. 162 B).

A special form of sink tissue developed during the infection with the root-knot nematode *M. incognica*. After infection, a gall is formed harboring multinucleated giant cells that serve the nematode for nutrition. In former experiments it was shown that these giant cells are symplasmically isolated from the surrounding tissue, which underlines the importance of transport processes across the plasma membrane in the feeding site. All investigated UmamiT candidates were located in cells that were closely located to giant cells and could be

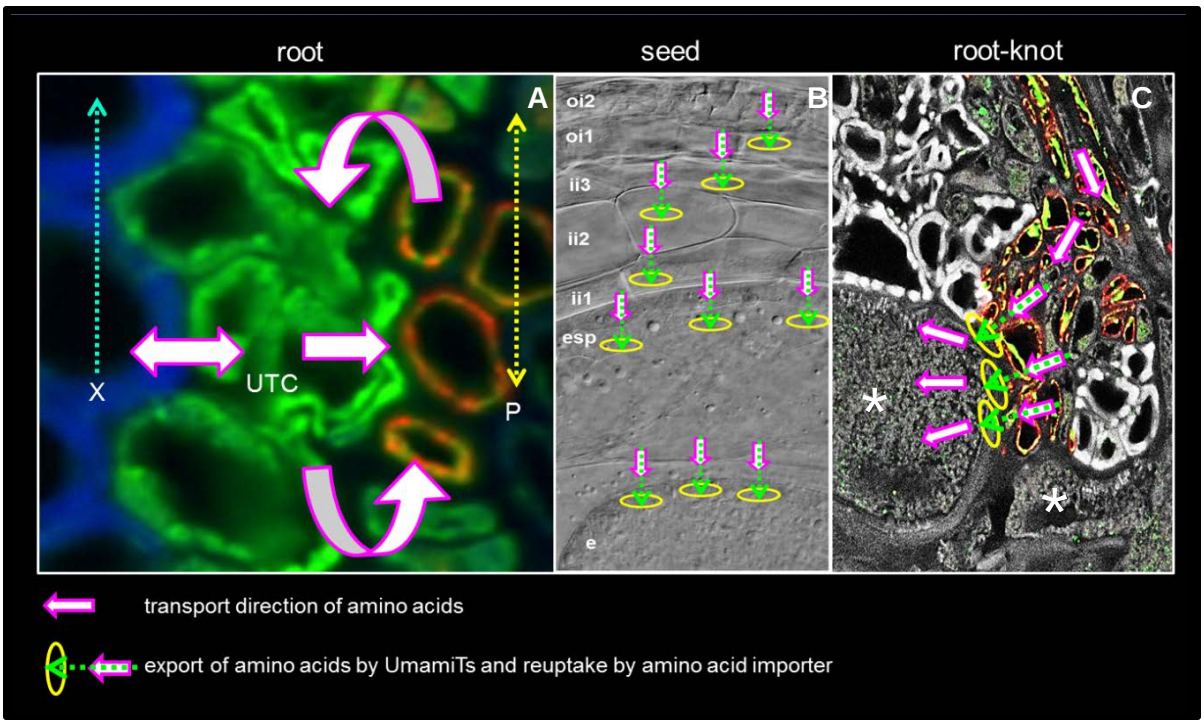

Figure 162. Similarities of UmamiT-mediated amino acid transport in the root, seed and the root-knot: Key positions for amino acid cycling and the supply of symplasmically isolated tissues. (A) UmamiT-positive cells (UTC) connect physiologically phloem (yellowish) with xylem (blue) and are responsible for amino acid cycling between different tissue types in the vasculature. (B) UmamiTs are located in symplasmically isolated tissues of the seed and (C) root-knot, where they exhibit unique transfer function in the export of amino acids to supply symplasmically isolated sink tissues. Asterisks mark giant cell. E (embryo), esp (endosperm), ii (inner integument), oi (outer integument).

characterized as juvenile phloem cells by the presence of nuclei, the phloem marker APL and PD1 and the sieve element specific RS6 epitope (Fig. 162 C).
UmamiTs export amino acids in the apoplastic space between the juvenile phloem cells and giant cells, from where giant cells can take them up by amino acid importers. By this mechanism, UmamiTs are directly involved in the nutrition of the nematode, especially with essential amino acids.
In summary, it could be shown that UmamiTs have a key position in the root to facilitate the amino acids cycling and phloem unloading. They were induced in situations where the symplasmic flow of nutrients is blocked, a situation that was found in developing seeds and the nematode feeding site. Here, they exhibit transfer cell function in cells with unique characteristics to supply symplasmically isolated sink tissues with amino acids.

The transduction of these findings to legumes and crop species will help to find mechanism for yield stability and yield safety. This will provide a chance to close the food gap especially in terms of amino acids, which would improve the quality of our diet and address the food security in the future.

7. Future aspects

. The UmamiTs investigated in this thesis are predominantly in the vascular parenchyma and sieve elements, which marks them as key transporters for the long distance transport of amino acids and amino acid cycling within the plant. Additionally a role in the supply of symplasmically isolated sink tissues like seeds or feeding sites of pathogens was shown. Although the UmamiTs investigated can explain how amino acids are transported across the integuments, there are still missing links in the story. The observed spatio-temporally distinct expression pattern of the candidates investigated shows that there are still several gaps, where none of the candidates was found. For example, it is not known which candidate UmamiTs are responsible for the export of amino acids from the outer integument into the inner integument of young seeds, which candidates are expressed in the third layer of the inner integument and in the syncytial endosperm before it breaks down or which candidates are found in the embryo to ensure the internal translocation of amino acids. Additionally, it is completely unknown, if UmamiTs can also be part of the intracellular amino acid storage and remobilization machinery including the export of amino acids out of plastids or amino acid transport across the membranes endomembrane compartments, most notably the vacuole. Especially in the late phase of seed maturation, when the outer integuments start to harden, a remobilization of nutrient compounds is reasonable. Nevertheless, the research on UmamiTs elucidated how amino acids are translocated from the vasculature into seeds. These findings are motivation to shift the focus of the UmamiT project away from *Arabidopsis* as model plant. The preferred storage compound in seeds used by *Brassiceae* is oil. This is one reason to continue the research on legumes, where proteins are the preferred form of storage compounds in the seed. In this thesis, it was shown that *UmamiTs* are induced during organismic interactions. In the case of symbiosis with nitrogen fixing bacteria or mycorrhiza fungi, *Medicago* and *Lotus* as model species can provide further insight into the role of *UmamiT* homologs during the formation of the symbiosome and the exchange of amino acids between the host plant and the symbionts. Furthermore, it would be interesting to know if UmamiTs in legumes are also associated with transfer cells in seeds and involved in the long distance transport of amino acids. In the case of crop species, homologs found in maize or barley could also be investigated not only to find a mechanism to enhance the amount of essential amino acids in seeds, but also to investigate the interaction with pathogens. Due to their special Kranz anatomy in leaves crop species also harbor the advantage to study the amino acid transport across the mesophyll and bundle sheath cells that occurs during C4 metabolism. In the mesophyll cells atmospheric carbon is pre-fixed into oxaloacetate, which can be converted to malate or aspartate. This aspartate has to be translocated from the mesophyll cells into the

bundle sheath cells to release the fixed carbon there. Afterwards the regeneration of the phosphoenolpyruvate happened by the recirculation of a 3-carbon acid represented by alanine or pyruvate. Also this step requires a transport mechanism of alanine between bundle sheath cells and the mesophyll, which considered a direct impact of amino acid transporters on photosynthesis and yield.

Altogether, the results obtained in this work open a wide field of possibilities to shift the research to agricultural important plants and to provide a possibility to find homolog *UmamiT* genes for yield stability and safety for the future.

8. Material and methods

8.1. Plants

*8.1.1. Arabidopsis **thaliana***

Al experiments on Arabidopsis were done in the Col-0 background, which was used as wildtype also for the generation of transgenic lines.
Depending on the experiment plants were kept under long day (16 hours light / 8 hours dark) or short day (8 hours light / 16 hours dark) conditions. Humidity was about 70% and growth temperature at 24 °C.

8.1.1.1. Growth on soil

Soil was made as a mixture of 65% substrate, 15% sand and 10% expanded clay. Seeds were placed on soil and stratified at 4 °C (cooling room) in the dark for two days. Afterwards they were transferred into the growth chamber with the different light periods. Watering occurred every second day.

8.1.1.2. Growth on plates

Gamborg medium ((0.3 % Gamborg medium including vitamins ((w/v), Duchefa), 1 % phytoagar ((w/v), Duchefa), pH was adjusted to 6.1 with KOH) was used for growth experiments under sterile conditions. Plates were made under the sterile hood. In the case of selection, antibiotics were added to the warm (~ 40°C not hot!) media before making plates.
Concentration of antibiotics for *Arabidopsis* was for kanamycin 50 µg/ml and for hygromycin 20µg/ml.

Seed sterilization occurred under a sterile hood. Seeds were placed in a 1.5 reaction tube and first surface sterilized for 2 min with 70% EtOH (v/v), seeds drop down to the bottom of the tube. EtOH was replaced with an aqueous solution of 1 % NaOCl (v/v) and 0.1
% Mucasol® ((v/v), Merz Consumer Care GmbH) and seeds incubated again for 2 min. Supernatant was replaced by sterile H_2O. This washing step with H_2O was repeated for three times. Afterwards the surface sterilized seeds were dispersed in 0.1 % sterile agarose (w/v) or in H_2O (for large scale selection on plates with antibiotics). Afterwards the seeds were put on plates.

8.1.2. *Lysopersicum esculentum* (tomato)

Tomato plants (cv. Moneymaker) were used as host for the root-knot nematode M. incognita, which was kept in a continuous cultivation in a separate area of the green house. Soil was the same as for *Arabidopsis*. Plants were grown for three weeks before they were inoculated. Infection with *Meloidogyne* was done by cutting the root system of infected plants into small pieces and mix them with the soil. In the next step tomato seedlings where placed in this mixture and kept for one day under humid conditions. Within two weeks infection was visible as small knots in the root system. Alternatively tomato plants were inoculated with nematode eggs or second-stage juveniles by watering the plants with a suspension containing the eggs or nematodes. For a successful infection by this method it was necessary to keep the soil wet during the first week after inoculation.

8.1.2.1. Isolation of eggs from infected roots

The root system of one infected plant was washed with water to remove most of the soil. Afterwards the roots were cut into small pieces and put into 500ml of 0.7%NaOCl (v/v). The bottle was shaken rigorously for 3min to remove the eggs from the gelatinous mass attached to the roots. At next the suspension was filtered successively through three sieves with different aperture. All the filtering steps were supported by additional H_2O. The flow through was collected in a bowl. At first a sieve with an aperture of 250µm was used to remove most of the root and remaining soil particles from the eggs. Next a 45µm sieve separated again remaining particles from the first washing step. Finally the eggs were collected with a sieve with 20µm aperture. This step was repeated two times. From there the eggs were washed off into a bottle with about 200ml tab water.
Second-stage juveniles were needed to do infection studies with *Arabidopsis* and to keep the continuous cultivation running.

8.1.2.2. Isolation of second-stage juveniles

Egg suspension containing eggs at different developmental stage was synchronized in the greenhouse for one week. This step was necessary to synchronize the hatching juveniles as much as possible. The bottle containing the egg suspension was kept in the dark in the greenhouse and additionally supplied with oxygen by an aquarium air pump (Elite). After one week the eggs were collected by the 20µm sieve and resuspended again in 100ml water. This suspension with the synchronized eggs was afterwards poured on 3 cotton wool milk filters placed in a kitchen sieve standing on a beaker. The level of water in the beaker was adjusted

in that way only to cover to bottom of the sieve. This device was placed again to the greenhouse and incubated in the dark there for one day. Hatching juveniles moved during this time through the filters and could be collected afterwards on a 20µm sieve by washing them off with water. The complete procedure could be repeated for three times. Harvested juveniles were stored at 4 °C until they were used for infection.

8.1.2.3. Infection of *Arabidopsis* with *Meloidogyne incognita*

The following steps were done in the sterile bench.

Second stage juveniles were collected on a filter placed in a small glass petri dish and washed with sterile tab water. Surface sterilization of the juveniles was done with $HgCl_2$ by placing the filter for 30 seconds into a new petri dish containing the sterilization solution. Afterwards the filters were immersed into the sterile water of another glass petri dish. Washing was repeated for three times. After the last washing step the juveniles were rinsed out from the filter into a glass petri dish with sterile water.

This surface sterilized second-stage juveniles were put on roots of at least two week old plants which were grown on plates. Pipetting of the juveniles was done near the root tips of the plants. The plates were closed again, sealed and kept horizontally for one day in the short day chamber. In the next day the plates were placed in an upright position.

Infection was also done by transferring egg mass from already infected roots on plates to fresh plates. Egg mass was removed from the donor roots by sterile tweezers and transferred to a new plate.

A third possibility for infection is to cut infected tomato roots into small pieces and mix them with the Arabidopsis soil. After piquing of several seedlings the pots were kept under humid condition in the greenhouse for one week. Plants could be cultivated further for four weeks. To isolate infected roots, the root system was washed with water and a brush. Root-knots were isolated under a binocular.

8.2. GUS staining

Plant material was put into a 1.5 ml reaction tube with GUS staining solution (0.05 M NaPO4 pH 7.2, 0.5 mM K3Fe(CN)6, 0.5 mM K4Fe(CN)6, 1 % Triton X-100 (v/v), 1.25 mM X-Gluc) and kept at 37°C in the dark. Incubation time was depending on the tissue type and staining intensity. Specimens were afterwards washed with 70% and 100% EtOH (v/v) and if necessary cleared with chloral hydrate solution (50% (w/v) chloral hydrate 10% glycerol).

8.3. Sectioning of plant tissues

For cross or longitudinal sections of plant tissue, samples were embedded in 1,5% low melting agarose in 0.05mM KPO_4 buffer (pH 7.0) in a 24 well plate. Agarose containing the samples was cooled down in a water basin standing in the cooling room. Afterwards the gel block was pulled out and fixed with instant adhesive on the cutting device and sections of 70-100µm thickness were prepared at a vibratome 1500 series sectioning system (The Vibratome Company).

8.4. Immunohistochemistry

The principle procedure was performed based on the publication of Stadler and Sauer (1996).

8.4.1. Embedding of plant tissue in methacrylate and sectioning

Tissue fixation, infiltration of methacrylate and sectioning on a microtome was done as described in Absmanner (2013).

8.4.2. Immunolocalization on sections

Removal of methacrylate, blocking and incubation with antibodies was performed as described in Absmanner (2013).
Table 2 shows the used primary and secondary antibodies.

Table 4. Primary and secondary antibodies used for immunolocalization.

name	description	dilution
anti-GFP	IgG fraction purified from rabbit polyclonal antiserum (Pineda Antikörper-Service)	1:80
anti-RS6	affinity purified from mouse monoclonal antiserum (Meyer et al. 2004; Khan et al. 2007)	1:80
anti-rabbit-Cy2	Cy2-conjugated AffiniPure goat anit-rabbit IgG (Dianova)	1:80
anti-mouse-AF594	AF594-conjugated AffiniPure goat anti-mouse IgG (Dianova)	1:80

8.4.3. Whole mount immunolocalization

The main procedure was done as described by Sauer et al.2006. Fixing solution, blocking solution and solutions for cell wall digestion and permeabilization were freshly made.
Modifications were done in the case of seeds and root tissue above the root hair zone.
After fixation the tissue was washed two times in 1xPBS and put on a microscope slide, where the boundaries of the material was marked by a PAP pen. Tissue was dried at RT. At next the sample was rehydrated with 1xPBS. Incubation with 2% Driselase occurred for 2h (seeds)/45min (roots) at 37°C in a humid chamber. After cell wall digestion the samples were washed with 1xPBS and permeabilized with IGEPAL CA-630 plus 10% DMSO for 2h (seeds)/1h (roots) at 37°C in a humid chamber. The next steps were exactly done as described in Sauer et al. 2006. In the case of older seeds the concentration of the antibodies was scaled up to 1:60. Incubation times for primary antibodies was over night at 4°C and for the secondary antibodies at least 4h at 37°C in a humid chamber.

8.5. Propidium iodid staining of plant tissues

Staining was performed as described in Müller (2015).

8.6. Whole-mount in situ RNA hybridization

Whole-mount *in-situ* hybridizations on roots and fertilized pistils were done as described in Hejatko et al. 2006.

8.7. mPS-PI staining

Staining was performed as described in Truernit et al. 2008.

8.8. Seed measurement

Length and width of dry seeds were measured using a microscope. Additionally for validation seeds were scanned. Data processing was done with the particle analysis tool of ImageJ.

8.9. Amino acid analytic

Plant material for amino acid analytic was obtained by using synchronized seeds and harvesting the siliques at the same time (form 10-12). Specimens were immediately frozen in liquid nitrogen and lyophilized. Derivatization was done using the EZ:faast™ amino acids analysis kit (Phenomenex, Torrance, California, USA). 20mg plant material was extracted with 200 µl 25% acetonitrile in 0.1 N HCl. Samples were shaken rigorously and sonicated for one minute. Incubation time was 45min. In the next step samples were centrifuged for 20min at 1350g. The liquid phase was processed further as indicated by the manufacturer.
LS-MS analysis was done with a Bruker Esquire 3000 plus mass spectrometer (Bruker, Bremen, Germany). This system was equipped with an Agilent 1100 HPLC system composed of an Agilent 1100 quaternary pump and an Agilent 1100 diodenarray detector (Agilent, Waldbronn, Germany). The column was a EZ:faast AAAMS 250x3.0 mm (Phenomenex, Torrance, California, USA). Injection volume was 5µl by a column temperature of 35°C. Three technical replicates were made. Settings for the LS-MS analysis are listed in Müller et al. 2015. Data analysis was done usinge the QuantAnalysis 2.0 software ((Bruker Daltonik, Bremen, Germany).

8.10. Statistical data processing

Blotting of data and statistical analysis was performed using the SigmaPlot 11.0 software (Systat Software Inc) with default settings.

8.11. Microscopy

Confocal microscopy was done with a confocal laser scanning microscope SP8 from Leica. Filter settings were as follows:

Excitation (nm)	Detection (nm)	Fluorescent protein
405	410-430	DAPI
488	500-530	GFP
488	500-530	Cy2
514	530-600	YFP
488	580-700	PI
561	570-630	mcherry
594	594-620	AF594

Light microscopy was carried out on a Zeiss ImagerM2 with an Axiocam 105 color camera using a Plan-Apochromat 40x/1.4 NA oil DIC objective. Imaging of large tissues was done at the Discovery V8 Zoom Stereo Microscope (Zeiss).

8.12. Molecular work

Standardized methods of molecular work were done as described in Sambrook et al. (1989) using molecular grade reagents.
Cloning was done by Gateway ® technology (Invitrogen).
Destination vector for GFP and mcherry were obtained from Bleckmann (2010).

9. Literature

9.1. References

Absmanner, B. (2013). Regulation of PIN-FORMED-mediated auxin transport and the role of auxin and cytokinin responses in plant-nematode interactions. Dissertation, Universität Regensburg.

Absmanner, B., Stadler, R., Hammes, U.Z. (2013). Phloem development in nematode-induced feeding sites: The implications of auxin and cytokinin. Front. Plant. Sci. Vol. 4: 241-255.

Andriunas, F.A., Zhang, H.M., Xia, X., Patrick, J.W., Offler, C.E. (2013). Intersection of transfer cells with phloem biology-broad evolutionary trends, functions and induction. Front. Plant. Sci., Vol. 4, 221-241.

Agre, P., Bonhivers, M., Borgnia, M.J. (1998). The aquaporins, blueprints for cellulur lumbing systems. Journal of Biological Chemistry, Vol 273: 14659-14662.

Aida, M., Beis, D., Heidstra, R., Willemsen, V., Bilou, I, Galinha, C., Nussaume, L., Noh, Y.S., Amashino, R., Scheres, B. (2004). The *PLETHORA* genes mediate patterning of the *Arabidopsis* root stem cell nichte. Cell, Vol. 119: 109-120.

Alexandatos, N., Bruinsma J. (2012). Worlds agriculutur towards 2030/2050. ESA working paper No. 12-03, Agricultural Development Economics Division.

Andrews, M. (1986). The Partitioning of Nitrate Assimilation between Root and Shoot of Higher-Plants. Plant Cell Environ. 9: 511-519.

Baluska, F., Cvrcková, F., Kendrick-Jones, J., Volkamann, D. (2001). Sink plasmodesmata as gateways for phloem unloading. Myosin VIII and calreticulin as molecular determinants of sink strenght?. Plant Physiology, Vol. 126: 39-46.

Barcala, M., García, A., Cabera, J., Casson, S., Lindsey, K., Favery, B., García-Casado, G., Solano, R., Fenoll, C., Excobar, C. (2009) Early transcriptomic events in microdisseced Arabidopsis nematode-induced giant cells. The Plant Journal, Vol. 61: 698-712.

Bartlem, D.G., Jones, M.G.K., Hammes, U.Z. (2013) Vascularization and nutrient delivery at root-knot nematode feeding sites in host roots.J. Exp. Bot. Vol. 65: 1789-98**.**

Bauby, H., Divol, F., Truenit, E., Grandjean, O., Palaqui, J.C. (2006). Protophloem differentiation in eraly Arabidopsis thaliana development. Plant Cell Physiol., Vol. 48: 97-109.

Baum, S.F., Dubrovsky, J.G., Rost, T.L. (2002). Apical organization and maturation of the cortext and vascular cylinder in *Arabidopsis thaliana* (brassicaceae) roots. Am. J. Bot. 89, 908-920.

Baroux, C., Spillane, C., Grassniklaus, U. (2002). Evolutionary origins of the endosperm in flowering plants. Genome Biology, Vol. 3: 1026.1-1026.5.

Beemster, G. T. S., Baskin, T. (1998). Analysis of cell division and elongation underlying the developmental accelaration of root growth in *Arabidopsis thaliana*.Plant Physiol, Vol. 116: 1515-1526.

Benfey, P.N., Linstead, P.L., Roberts, K., Schiefelbein, J.W., Hauser, M.T., Aeschbacher, R., A. (1993). Root development in *Arabidopsis*: four mutants wih dramatically altered root morphogenesis. Development, Vol. 119: 57-70.

Benjamins, R., Qint, A., Weijers, D., Hooykaas, P., Offringa, R. (2001). The PINOID protein kinase regulates organ development in *Arabidopsis* by enhancing polar auxin transport. Development, Vol. 128: 4057-67.

Bird, D. McK., Wilson, M. A. (1994). DNA sequence and expression analysis of root knot nematode elicited giant cell transcripts. Mol. Plant-Microbe Interact. Vol. 7: 419-424.

Bird, D. McK. 1996. Manipulation of host gene expression by root knot nematodes. J. Parasitol. Vol. 82: 881-888.

Bleckmann, A. (2010). Untersuchung zur Stammzellregulation im Apikalmeristem von *Arabidopsis thaliana*. Dissertation, Heinrich-Heine-Universtität Düsseldorf.

Bleve-Zacheo, T., Melillo, M.T. (1997). The biology of giant cells. The structure of syncytia. Cellular and Molecualr Aspects of Plant-Nematode Interatcionts. C. Fenoll, F.M.W. Grundler and S. A. Ohl. Dordrecht, The Netherlands, Kluwer Academic Publishers: 65-79.

Bonke, M., Thitamadee, S., Mähönen, A.P., Hauser , M., T., Helariutta, Y. (2003). APL regulates vascular identity in *Arabidopsis*. Nature, Vol. 13: 181-186.

Boorer, K.J., Frommer, W.B., Bush, D.R., Kreman, M., Loo, D.D., and Wright, E.M. (1996). Kinetics and specificity of a H+/amino acid transporter from *Arabidopsis thaliana*. J. Biol. Chem. 271: 2213-2220.

Borg, S., Brinch-Pedersen, H., Tauris, B., Holm, P.B. (2009). Iron transport, deposition and bioavailability in the wheat and barley grain. Plat Soil, Vol. 325: 15-24.

Bowman, J.L., Floyd, S.K., Sakakibara, K. (2007). Green genes-comparative genomic of the green branch of live.Cell 129.

Bulankova, P., Akimcheva, S., Fellner, N., Riha, K. (2013). Identification of Arabidopsis meiotic cyclins reveals functional diversification among plant cyclin genes. PLoS. Genet. Vol 9: e1003508

Bröer, S. (2008). Amino acid transport across mammalian intestinal and renal epithelia. Physiological reviews, Vol. 88: 249-286

Busov, V.B., Johannes, E., Whetten, R.W., Sederoff, R.R., Spiker S.L., Lanz-Garcia, C., Goldfarb, B. (2004). An auxin- inducible gene from loblolly pine (*Pinus taeda L.*) is differentially expressed in mature and juvenile phase shotts and encodes a putative tranmembrane protein. Planta 2004 Vol. 218: 916-627.

Cayla, T., Batailler, B., Le Hir., R., Revers, F., Anstead, J.A., Tompson, G.A., Grandjean, O., Dianant, S. (2015). Live imaging of companion cells and sieve elements in Arabidopsis leaves. PLoS. One 10 e0118122.

Chen, L. Q., Qu, X. Q., Hou, B. H., Sosso, D., Osorio, S., Fernie, A.R., Frommer, W.B. (2012). Sucrose efflux mediated by SWEET proteins as key step for phloem transport. Science, 207-11

Chen, L., Q., Lin, I., W., Qu, X., Q., Sosso, D., McFarlaune, H.E., Londono, A., Samues, A.L., Fromer, W.B. (2015). A cascade of sqeuentially expressed sucrose transporters in the seed coat and endosperm provides nutrition for the *Arabidopsis* embryo. The Plant Cell. Vol. 27: 607-619.

Cheng, Y., Dai, X., Zhao, Y. (2007). Auxin synthesized by the YUCCA flavin monooxygenase is essential for embryogenesis and leaf formation in *Arabidospis*. The Plant Cell, Vol. 19: 2430-2439.

Colon-Carmona, A., You, R., Haimovitch-Gal, T., Doerner, P. (1999). Technical advance: spatio-temporal analysis of mitotic activity with a labile cyclin-GUS fusion protein. Plant J. Vol. 24: 503-508.

Criqui, M.C., Parmetier, Y., Derevier, A., Shen, W.H., Dong, A., Genschik, P., (2000). Cell cycle-dependent proteolysis and ectopic overexpression of cyclin B1 in tobacco BY2 cells. Plant J. Vol. 24: 763-773.

Cooper, H.D., and Clarkson, D.T. (1989). Cycling of Amino-Nitrogen and Other Nutrients between Shoots and Roots in Cereals - a Possible Mechanism Integrating Shoot and Root in the Regulation of Nutrient-Uptake. J. Exp. Bot. Vol. 40: 753-762.

Cooper, H.D., Clarkson, D.T., Johnston, M.G., Whiteway, J.N., and Loughman, B.C. (1986). Cycling of amino acids between shoots and roots in wheat seedlings. Plant Soil Vol. 91: 319-322.

Cosgrove, D.J. (1999). Enzymes and other agents that enhance cell wall extensibility. Annu. Rev. Plant. Physiol. Plant. Mol. Biol. Vol 50: 245-276.

Crawford, N.M. (1995). Nitrate: nutrient and signal for plant growth. Plant Cell 7**:** 859-868.

Creff, A., Brocard, L., Ingram, G. (2014). A mechanically sensitive cell layer regulates the physical properties of the Arabidopsis seed coat. Nat. Commun. Vol. 6. 6382. doi: 10.1038/ncomms7382

Davis, E.L., Hussey, R.S., Baum, T.J., Bakker, J., Schots, A., Rosso, M.N., Abad, P. (2000). Nematode parasitism genes. Ann Rev Phytopathol Vol. 38: 365-396.

Decourteix, M., Alves, G., Bonhomme, M., Peuch, M., Baaziz, K.B., Brunel, N., Guilliot, A., Rageau, R., Améglio, T., Pétel, G., Sakr, S. (2007). Surcrose (JRSUT1) and hexose (JRHT1 and JRHT2) transporters in walnut xylem parenchyma cells: their potential role in early events of grwoth resumption. Tree Physiology, Vol. 28: 215-224.

Denance, N., Szurek, B., Noel, L.D. (2003). Emerging functions of nudulin-like proteins in non-nodulating plant species. Plant and Cell Physiology. Vol.55: 469-474.

Demura, T., Fukuda, H. (2007). Transcriptional regulation in wood formation. Trends Plant. Sci. Vol. 12: 64-70.

Dettmer, J., Ursache, R., Campilho, A., Miyashima, S., Belevich, I., O´Regan, S., Mullendore, D.L., Yadav, S.R., Lanz, C., Beverian, L., Papagni, A., Schneeberger, K., Weigel, D., Stierhof, Y. D., Morizt, T., Knoblauch, M., Jokitalo, E., Helariutta, Y. (2014) CHOLINE TRANSPORTER-LIKE1 is required for sive plate development to mediate long-distance cell-to-cell communication. Nature Communications, Vol. 5.

Diamond, J. (2002). Evolution, consequences and future of animal and plant domestication. Nature Vol. 418: 700-707.

Ding, B., Kwon, M.O., Hammond, R., Owes, R. (1997). Cell –to-cell movement of potatoe spindle tuber viroid. The plant journal, Vol. 12: 931-936.

Dixon, G., R., Pegg, G.F. (1972). Changes in amino-acid content of tomatoe xylem sap following infection with strains of Verticillum albo-atrum. Ann. Bot. Vol 36: 147-154.

Dolan, L., Janmaat, K., Willemsen, V., Linstead, P., Peothig, S., Roberts, K., Scheres, B. (1993). Cellular organization of the *Arabidopsis thaliana* root. Development, Vol. 119: 71-84.

Donoghue, M.J. (2005). Key innovations, convergence, and success:macroevolutionary lessions from plant phylogeny. Paleobiology 31(2).

Drisch, R.C., Stahl, Y. (2015). Functions and regulation of transcription factors involved in root apical meristem and stem cell maintenance. Front. Plant Sci., Vol. 6: 505.

Dudani, A.K., Prasad, R. (1983). Amino acid transport: its role in cell division and growth of Saccharomyces cerevisiae cells. Biochem. Int. Vol. 7: 15-22.

Dundar, E., and Bush, D.R. (2009). BAT1, a bidirectional amino acid transporter in Arabidopsis. Planta 229: 1047-1056.

Esau, K**.** (1969). The phloem. (Berlin, Stuttgart,: Gebr. Borntraeger).

Esau, K. (1977). Anatomy of seed plants. 2nd ed. Wiley, New York.

Eom, J.S., Chen, L Q., Sosso, D., Julius, B.T., Lin, I.W., Qu, W.W., Braun, D.M., Frommer, W.B. (2015). Sweets transporters for introcellular and intercellular sugar translocation. Curr. Poin. Plant Biol. Vol. 25: 53-62.

Flannery, K.V. 1996. Origins and ecological effects of early domestication in Iran and the Near East. In: Ucko, P.J., Dimbleby, G.W. (Eds.), The Domestication andExploitation of Plants and Animals. Duckworth, London, 73–100.

Fischer, W.N., Loo, D.D.F., Koch, W., Ludewig, U., Boorer, K.J., Tegeder, M., Rentsch, D., Wright, E.M., and Frommer, W.B. (2002). Low and high affinity amino acid H^+-cotransporters for cellular import of neutral and charged amino acids. Plant J. 29: 717-731.

Figueiredo, D.D., Köhler, C. (2016). Bridging the generation gap: communication between maternal sporophyte, female gametophyte and fertilization products. Curr. Opin. Plant Biol. Vol. 29: 16-20.

Formisano, T. M., Van Winkle, L.J. (2016). At least three transporters likely mediate threonine uptake neede for mouse embryonic stem cell proliferation. Front. Cell Dev. Biol. Vol. 4 doi: 10.3389/fcell.2016.00017

Franceschi, V.R. and Tarlyn, N.M. (2002). L- Ascorbic acid is accumulated in source leaf phloem and transported to sink tissues in plant. Plant Physiology, Vol. 130: 649-656.

Francis, D., Sorrell, D.A. (2001). The interface between the cell cycle and plant grwoth regulators: a mini review. J. Plant. Grworth Regul., Vol. 33:1-12.

Frommer, W.B., Hummel, S., Unseld, M., Ninnemann, O.(1995). Seed and vascular expression of a high affinity transporter for cationic amino acids in Arabidopsis. Proc. Natl. Acad. Sci. USA. Vol 92: 12036-12040.

Furuta, K.M., Hellmann, E., and Helariutta, Y. (2014). Molecular control of cell specification and cell differentiation during procambial development. Annu. Rev. Plant Biol. Vol. 65: 607-638.

Galinha, C., Hofhuis, H., Luijten, M., Willemsen, V., Blilou, I., Heidstra, R., Scheres, B. (2007). PLETHORA proteins are dose-dependent master regulators of Arabidopsis root development. Nature, Vol. 449: 1053-1057.

Galili, G., Avin-Wittenberg, T., Angelovici, R., Fernie, A.R. (2014). The role of photosynthesis and amino acid metabolism in the energy staty during seed development. Front. Plant. Sci. Vol. 5:447

Gamas, P., Niebel, F.C., Lescure, N., Cullimore, J.V. (1996). Use of asubttractive hybridization approach to identify new *Medicago truncatula* genes insucd during root nodule development. Mol. Plant. Microbe. Vol. 9:233-242.

Gepts, P**.** (2004). Crop domestication as a long-term selection experiment. Plant Breeding Reviews Vol. 24.

Giaquinta, R.T., Lin, W., Sadler, N.L., Franceschi, V. R. (1983). Pathway of phloem unloading of sucrose in corn roots. Plant Physiol. Vol. 72: 362-367.

Gracia, D., Saingery V., Chambrier, P., Mayer, U., Jürgens, G., Berger, F. (2003).*Arabidopsis haiku* mutants reveal new control of seed size by endosperm. Plant Phyiology, Vol. 131: 1661-1670.

Gracia, D., Fitz Gerald, J.N., Berger, F. (2004). Maternal control of integument elongation and zygotic control of endosperm growth are coordinated to determine seed size in *Arabidopsis*. The Plant Cell, Vol. 17: 52-60.

Golinowski, W., Sobczak, M., Kurek, W., Grymaszewska, G. (1997). The structure of syncytia. Cellular and Molecualr Aspects of Plant-Nematode Interatcionts. C. Fenoll, F.M.W. Grundler and S. A. Ohl. Dordrecht, The Netherlands, Kluwer Academic Publishers: 80-97.

Goverse, A., De Almeida Engler, J., Verhees, J., Van Der Krol, S., Helder, J., Gheysen, G. (2000). Cell cycle activation by plant parasitic nematodes. Plant Mol. Biol. Vol. 43: 747-761.

Gunning, B.E.S, Pate, J.S. (1969). "Transfer cells" plant cells with wall ingrwoths, specialized in relation to short distance transport of solutes-their occurrence, structure and development. Protoplasma, Vol. 68: 107-133.

Gunning, B.E.S., Pate, J.S. (1974). Transfer cells. In Dynamic Aspects of Plant Ultrastructure, ed. A. W. Robards (London: McGraw-Hill), 441-479.

Hager, A., Debus, G., Edel, G.H., Stransky, H., Serrano, R. 1991. Auxin induces exocytosis and the rapid synthesis of a high-turnover pool of plasma-membrane H^+-ATPase. Planta, Vol. 185: 527-537.

Hammes, U. Z., Schachtmann, D., P., Berg, R., H., Nielsen, E., Koch, W., McInyre, L., M.et al. (2005). Nematode induced changes of transporter gene expression in *Arabidopsis* roots. Mol. Plant – Microbe Interact. 18: 1247.1257.

Hammes, U. Z., Nielsen, E., Honaas, L. A., Taylor, C. G., and Schachtman, D.P. (2006). AtCAT6, a sink-tissue-localized transporter for essential amino acids in *Arabidopsis*. Plant J. 48: 414-426.

Hejatko, J., Bilou, I., Brewer, P.B., Friml, J., Scheres, B., and Benkova, E. (2006). In situ hybridization technique for mRNA detection in whole mount Arabidopsis samples. Nat. Protoc. Vo. 1: 1939-1946.

Hirner, A., Ladwig, F., Stransky, H., Okumoto, S., Keinath, M., Harms, A., Frommer, W.B., and Koch, W. (2006). Arabidopsis LHT1 is a high-affinity transporter for cellular amino acid uptake in both root epidermis and leaf mesophyll. Plant Cell 18: 1931-1946.

Hofius, D., Herbers, K., Melzer, M., Omid, A., Tacke, W., Wolf, S., Sonnewald, U. (2001). Evidence for expression level-dependent modulation of carbohydrate status and viral resistance by the potatoe leafroll virus movement protein in transgenic tobacco plants. Plant J. Vol. 28: 529-543.

Holdaway-Clarke, T.L., Walker, N.A., Hepler, P.H., Overall, R.L. (2000). Physiological elevations in cytoplasmic free calcium by cold or ion injection result in transient closure of higher plant plasmodesmata. Planta, Vol. 210: 329-335.

Hoth, S., Stadler, R., Sauer., N., Hammes, U.Z. (2008). Differential vascularization of nematode-induced feeding sites. Proc. Natl. Acad. Sci. U.S.A. 105:12617-12622.

Hoth, S., Schneiderit A., Lauterbach C., Scholz-Starker, J., Sauer, N. (2005). Nematode infection triggers the de novo formation of unloading phloem that allows macromolecular trafficing of green fluorescent protein into syncytia. Plant Physiol. 138: 383-392.

Huang, G., Dong, R., Allen, R., Davis, E.L., Baum, T.L., Hussey, R.S. (2006I A root-knot nematode secretory peptide functions as a ligand for a plant transcription factor.MPMI, Vol. 19: 463-470.

Iglesias, M.J., Terrile, M.C., Casalonue, C.A. (2011). Auxin and salicylic acid signalings counteract during the adaptive response to stress. Plant Signal Behav. Vol. 3: 452-454.

Ioio, R.D., Linhares, F.S., Sabatini, S. (2008) Emerging role of cytokinin as a regulator of cellular differentiation. Current Opinion in Plant Biology, Vol. 11: 23-27.

Jameson, P.E., Song, J. (2015). Cytokinin: a key driver of seed yield. J. Exp. Bot. erv461v1-erv461.

Javot, H., Maurel, C. (2002). The role of aquaporins in root water uptake. Annals of Botany, Vol. 90: 301-313.

Jones, M., G., K., Northcote, D.H. (1972). Multinucleate transfer cells induced in coleus roots by the root-knot-nematode *Meloidogyne arenaria*. Protoplasma 75, 381-395.

Imbert, E., Lefévre, F. (2003). Dispesal and gene flow of *Populus nigra* (Salicaceae) along a dynamic river system.Journal of Ecology, Vol. 91: 447-456.

Imlau, A., Truernit, E., Sauer, N. (1999). Cell-to-cell and long-distance trafficking of the green fluorescent protein in the phloem and symplastic unloading of the protin into sink tissues. The Plant Cell, Vol. 11: 309-322.

Imsande, J., and Touraine, B. (1994). N demand and the regulation of nitrate uptake. Plant Physiol. 105: 3-7.

Kataoka, T., Hayashi, N., Yamaya, T., Takashshi, H. (2004). Root-to shoot transport of sulfate in *Arabidopsis*. Evidence for the role of SULTR3; 5 as a component of low-affinity sulfate transporter system in the root vasculature. Plant Physiology, Vol. 136: 4198-4204.

Kahn, J.A., Wang, Y., Sjölund, R.D., Schulz, A., Thompson, G.A. (2007). An early nodulin-like protein accumulates in the sieve element plasma membrane of *Arabidopsis*. Plant Physiol. Vol. 143: 1576-1589.

Kim, I., Hempel, F.D., Sha, K., Pfluger, J., Zambryski, P., C. (2002). Identification of a developmental transition in plasmodesmatal function during embryogenesis in *Arabidopsis thaliana*. Development, Vol. 129: 1261-1272.

Knoblauch, M., Van Bel, A.J. (1998). Sieve Tubes in Action. The Plant Cell Vol. 10: 35-50.

Kobayashi, K., Takahashi, F., Suzuki, M., Suzuki, H. (2002). Examination of morphological changes in the first formed protoxylem in *Arabidopsis* seedlings. J. Plant. Res. Vol. 115: 107-112.

Koltai, H., Dhandaydham, M., Oppermann, C.H., Thomas, J., Bird, D. McK. (2001). Overlapping plant signal transduction pathways induced by a parasitic nematode and a rhizobioal endosymbiont. Mol. Plant-Microbe Interact., Vol. 1168-1177.

Ladwig, F., Stahl, M., Ludewig, U., Hirner, A.A., Hammes, U.Z., Stadler, R., Harter, K., and Koch, W. (2012). *Siliques are red1* from Arabidopsis acts as a bidirectional amino acid transporter that is crucial for the amino acid homeostasis of siliques. Plant Physiol. 158: 1643-1655.

Lafon-Placette, C., Köhler, C. (2014). Embryo and endosperm, patterns in seed development. Curr. Opin. Plant Biol. Vol. 17: 64-69.

Lalonde, S., Tegeder, M., Throne-Holst, M., Frommer Wolf, B., and Patrick, J.W. (2003). Phloem loading and unloading of sugars and amino acids. Plant Cell Environ. 26**:** 37-56.

Lalonde, S., Wipf, D., Frommer, W.B. (2004). Transport mechanisms for organic forms of carbon and nitrogen between source and sink. Annual Review of Plant Biology 55: 341-372.

Law, C.J., Maloney, P.C., Wang, D.N. (2008). Ins and outs of major facilitator superfamiliy antiporters. Annu. Rev. Microbiol. 62:289-305.

Le, B.H., Cheng, C., Bui, A.Q., Wagmaister, J.A., Henry, K.F., Pelletier, J., Kwong, L., Belmonte, M., Kirkbride, R., Horvath, S., Drews, G.N., Fischer, R.L., Okamuro, J.K., Harada, J.J., Goldberg, R.B. (2010). Global analysis of gene activity during *Arabidopsis* seed development and identification of seed-specific transcription factors. Proc. Natrl. CAda. Sci. Vol. 18: 8063-8070.

Leran, S., Munos, S., Brachet, C., Tillard, P., Gojon, A., Lacombe, B. (2013). Arabidopsis NRT1.1 is a bidirectional transporter invovled in root-to-shoot nitrate translocation. Front. Plant. Sci, Vol. 4.

Liao, C.Y., Smet, W., Brunoud, G., Yoshida, S., Vemoux, T., Weijers, D. (2015). Reporters for sensitve and quantitative measurment for auxin response, Nat. Methods, Vol. 3: 207-210.

Li, J.Y., Fu, Y.L., Pike, S.M., Bao, J., Tian, W., Zhang, Y., Chen, C.Z., Zhang, Y., Li, H.M., Huang, J., Li, L.G., Schroeder, J.I., Grassmann, W., Gong, J.M. (2010). The *Arabidopsis* nitrate tranporter NRT1.8 functions in nitrate removal form the xylem sap and mediates cadmium tolerance. Plant Cell 22:1633-46.

Li, J., Nie, X., Tan, J.L., Berger, (F. 2013). Integration of epigenetic and genetic controls of seed size by cytokinin i Arabidopsis. Proc. Natl. Acad. Sci. USA, Vol. 38: 15479-15484.

Lin, S.H., Kuo, H.F., Canivenc, G., Lin, C.S., Lepetit, M., Hsu, P.K., Tillard, P., Lin, H.L., Wang, Y.Y., Tsai, C.B., Gojon, A., and Tsay, Y.F. (2008). Mutation of the Arabidopsis NRT1.5 nitrate transporter causes defective root-to-shoot nitrate transport. Plant Cell 20: 2514-2528.

Livshits, V.A., Zakatacva, N.P., Aleshin, V.V., Vitushkina, M.V. (2003). Identification and characterization of the new gene *rhtA* involved in threonine and homoserine efflux in *Escherichia coli*. Re Microbiol. Vol. 154: 123-135.

Linkies, A**.**, Graeber, K., Knight, C, Leubner-Metzger, G. (2010). The evolution of seeds.New. Phytol. Vol.186:4.

Lituiev, D.S., Krohn, N.G., Müller, B., Jackson, D., Hellriegel, B., Dresselhaus, T., Grossniklaus, U. (2013). Theoretical and experimental evidence indicate that there is no detectable auxin gradient in the angiosperm female gametophyte. Development, Vol. 140: 4544-4553.

Lohaus, G., Burba, M., Heldt, H.W. (1994). Coparison of the contents of the sucrose and amino acids in the leaves, phloem sap and taproots of high and low sugar-producing hybrids of sugar beet (*Beta vulgaris* L.). J. Exp. Bot.Vol 45: 1097-1101.

Lohaus, G., Büker, M., HuBmann, M., Soave, C., Heldt, H.W. (1998). Transport of amino acids with special emphasis on the synthesis and transport or asparagin in the Illinois Low Protein and Illinois High Protein stains of maize. Planta, Vol 205: 181-188.

Lohar, D.P., Schaff, J.E., Laskey, J.G., Kieber, J.J., Bilyeu K.D., Bird, D.M. (2004). Cytokinins play opposite roles in later root formation, and nematode and Rhizobial symbioses. Plant. J. Vol. 2: 203-214.

Lucas, W.J., Ham, B. K., Kim, J. Y. (2009). Plasmodesmata-brdiging the gap between neighboring plant cells. Trens in Cell Biology, Vol 19: 495-503.

Lucas, W.J., Groover, A., Lichtenberger, R., Furuta, K., Yadav, S.R., Helariutta, Y., He, X.Q., Fukuda, H., Kang, J., Brady, S.M., Patrick, J.W., Sperry, J., Yoshida, A., Lopez-Millan, A.F., Grusak, M.A., and Kachroo, P. (2013). The plant vascular system: Evolution, development and functions. J Integr Plant Biol 55: 294-388.

Mashiguchi, K., Tanaka, K., Sakai, T., Sugawara, S., Kawaide, H., Natsume, M., Hanada, A. Yaeno, T., Shirasu, K., Yao, H., McSteen, P., Zhao, Y., Hayashi, K., Kamiya, Y., Kasahara, H. (2011). The main auxin biosynthesis pathway in Arabdiopsis. Proc. Natl. Acad. Sci. USA, Vol. 108: 18512-18517.

Maurino, V.G., Weber, P.M. (2013). Engineering photosynthesis in plants and synthetic microorganisms. J. Exp. Botany, Vol. 64: 743-751.

McCurdy, D.W., Hueros, G. (2014). Transfer cells. Front. Plant. Sci. Vol. 5: 672.

Marella, H.H., Nielsen, E., Schachtmann, D.P., Taylor C.G. (2013). The amino acid permeases AAP3 and AAP6 are invovled in root-knot nematode parasitism of *Arabidopsis*. Mol. Plant. Microbe Interact. 26: 44.54.

Matsuzaki, Y., Ogawa-Ohnishi, M., Mori, A., Matsubayashi, Y. (2010). Secreted peptide signals required for maintenance of root stem cell niche in *Arabidopsis*. Science, Vol. 329: 1065-1067.

Mitchell, P. (1962). Metabolism, transport and morphogenesis: which drives which? J. gen. Microbiol. Vol. 29: 25-37.

Mouchel, C.F., Briggs, G.C., Hardtke, C.S. (2004). Natural genetic variation in Arabidopsis identifies *BREVIS RADIX*, a nocel regulator of cell proliferation and elongation in the root. Genes and Development, Vol. 18: 700-714.

Mullendore, D.L., Windt, C.W., Van As, H., Knoblauch, M. (2010). Sieve tube geometry in relation to phloem flow. The Plant Cell, Vol. 22: 579-593.

Müller, B., Fastner, A., Karmann, J., Thomas, H., Suter-Grotemeyer, M., Rentsch, D., Truernit, E., Ladwig, F., Dresselhaus, T., Bleckmann, A., Schwab, W., and Hammes, U.Z. (2015). Amino acid export in developing Arabidopsis seeds depends on UmamiT facilitators. Curr. Biol., Vol. 25: 3126-3131.

Münch, E. (1930). Die Stoffbewegungen in der Pflanze. Gustav Fischer, Jena.

Nathan, R., Schurr, F.M., Spiegel, O., Steinlitz, O., Trakhtenbrot, A., Tsoar, A. (2008). Mechanisms of long-distance seed dispersal. Trends in Ecolog & Evolution, Vol. 23: 638-647.

Näsholm, T., Ekblad, A., Nordin, A., Giesler, R., Högberg, M., Högberg, P. (1998). Boreal forest plants take up organic nitrogen. Nature, Vol. 392: 914-916.

Nelson, B.K., Cai, X., Nebenführ, A. (2007). A multicolored set of *in vivo* organelle markers for co-localization studies in Arabidopsis and other plants. The Plant Journal, Vol. 51: 1126-1136.

Nicklin, P., Bergmann, P., Zhang, B., Treantfellow, E., Wang, H., Nyfeler, B, Yang, H., Hild, M., Kung, C., Wilson C., Myer V.E., MacKeigan, J.P., Porter, J.A., Wang, Y.K., Cantley L.C., Finan, P.M., Murphy, L.O. (2009) Bidirectional transport of amino acids regulates mTOR autophagy. Cell, Vo. 6: 521-534.

Nole-Wilson, S., Azhakanadam, S., Franks, R.G. (2010). Polar auxin transport together with AINTEGUMENTA and RVOLUTA coordinate early Arabidopsis gynoceium development. Developmental Biology, Vol. 346: 181-195.

Offler, C.E., McCurdy, D.W., Patrick, J.W., Talbot, M.J. (2002). Transfer cells: cells specialized for a special purpose. Annu. Rev. Plant Biol. Vol 54: 431-454.

Okumoto, S., Schmidt, R., Tegeder, M., Fischer, W.N., Rentsch, D., Frommer, W.B., and Koch, W. (2002). High affinity amino acid transporters specifically expressed in xylem parenchyma and developing seeds of Arabidopsis. J. Biol. Chem. 277: 45338-45346.

Okumoto, S., Pilot, G. (2011). Amino acid export in plants: a missing link in nitrogen cycling. Mol. Plant. Vol. 4: 453-463.

Oparka, K.J., Duckett, C. M., Prior, D.A.M., Fischer, D.B. (1994). Real-time imaging of phloem unloading in the root tip of Arabidopsis. The Plant Journal Vol. 6: 759-766.

Ottenschlager, I., Wolff, P., Wolverton, C., Bhalerao, R.P., Sandberg, G., Ishikawa, H., Evany, M. Palme, K. (2003). Gravity regulated differential auxin transport from columella to lateral root cap cells. Proc. Natl. ACad. Sci. USA, Vol. 100: 2987-2991.

Panoli, A., Martin, M.V., Alandete-Saez, M., Simon, M., Neff, C., Swarup, R., Bellido, A., Yan, L., Pagnussat, G.C., Sundaresan, V. (2015). Auxin import and local auxin biosynthesis are required for mitotic divisions, cell expansion and cell specification during female gametophyte development in *Arabidopsis thaliana*. PLOS one, e0126164.

Pate, J.S., Atkins, C.A., Herridge, D.F., Layzell, D.B. (1981). Synthesis, storage and utilization of amino compounds in white lupin (*Lupinus albus* L.). Plant Physiol. Vol. 67: 37-42.

Patrick, J.W., Offler, C.E. (1995). Phloem unloading: sieve element unloading and post sieve element transport. Ann Rev Plant Physiol Plant Mol Biol Vol 48: 191-222.

Patrick, J.W., Offler, C.E. (2001). Compratmentation of transport and transfer events in developing seeds. J. Exp. Bot. Vol. 52: 551-564.

Pratelli, R., Pilot, G. (2014). Regulation of amino acid metabolic enzymes and transporters ins plants. J. Exp. Bot. 65: 5535-5556and transportersinplants. J. Exp.Bot. 65, 5535–5556.

Postaire, O., Tournaire-Roux, C., Grondin, A., Boursiac, Y, Morillon, R., Schäffner, A.R., Maurel, C. (2010). A PIP1 aquaporin contributes to hydrostatic pressure-induced water transport in both the root and rosette of Arabidopsis. Plant Physiology, Vol. 152: 1418-1430.

Puthoff, D.P., Nettleton, D., Rodermel, S.R., Baum, T.J. (2003). *Arabidopsis* gene expression change during cyst nematode parasitism revealed by statistical analyses of microarray expression profiles. Plant. J. 33: 911-921.

Ranocha, P., Dima, O., Nagy, R., Felten, J., Corratgé-Faillie, C., Novák, O., Morreel, K., Lacombe, B., Martinez, Y., Pfrunder, S., Jin, X., Renou, J., P., Thibaud, J., B., Ljung, K., Fischer, U., Martinoia, E., Boerjan, W., Goffner, D. (2013). *Arabidopsis* WAT1 is a vacuolar auxin tranport facilitator required for auxin homoestasis. Nat. Commun, Vol. 4: 2625.

Rentsch, D., Schmidt, S., and Tegeder, M. (2007). Transporters for uptake and allocation of organic nitrogen compounds in plants. FEBS Lett. 581**:** 2281-2289.

Riefler, M., Novak, O., Strnad, M., Schmülling, T. (2006). *Arabidopsis* cytokinin receptor mutants reveal functions in shoot growth, leaf senescence, seed size, germination, root development and cytokinin metabolism. The Plant Cell, Vol. 18: 40-54.

Robert, H. S., Crhak Khaitova, L., Mroue, S., Benková, E. (2015). The importance of localized auxin production for morphogenesis or reproductive organs and embryos in Arabidopsis. Journal of Experimental Botany, Vol. 66: 5029-42.

Rodiuc, N., Vieira, P., Banora, M.Y., de Almeida, J. (2014). On the track of transfer cell formation by specialized plant-parasitic nematodes. Front. Plant. Sci. Vol 5, 160

Rodriguez-Ezpeleta, N., Brinkmann, H., Burey, S.C., Roure, B., Burger., G., Löffelhardt, W., Bohnert, H.J., Philippe, H., Lang B., F. (2005). Monophyly of primary phtosynthetic eukaryotes: green plants, red algeae and glaucophyts. Curr. Biol. Vol. 15: 1325-1330.

Rosnick-Shimmel, I. (1985). The influence of nitrogen nutrition on the accumulation of free amino acids in root tissue of *Urtica dioica* and their apical transport in xylem sap. Plant Cell Physiol. Vol. 26: 215-219.

Ruiz-Medrano, R., Xoconostle-Cázares, B., Kragler, F. (2004). The plasmodesmatal transport pathway for homeotic proteins, silencing signals and viruses. Current Opinion in Plant Biology Vol. 7: 641-650.

Saiga, S., Furumizu, C., Yokoyama, R., Kurata, T., Sato, S., Kato, T., Tabata, S., Suzuki, M., Komeda, Y. (2008) The *Arabidopsis OBERON1* and *OBERON2* genes encode plant homeodomain finger proteins and are required for apical meristem maintenance. Development, Vol. 135: 1751-1759.

Sallon, S., Solowey, E., Cohen, Y., Korchinxky, R., Egil, M., Woodhatch, I., Simchoni, O., Kislev, M. (2008) Germination, genetics and growth of an ancient date seed. Science 13 Vol. 320 no 5882.

Sambrook, J., Fritsch, E.F., Maniatis, T. (1989). Molecular cloning: A laboratory manual. Cold Spring Harbor, New York, Cold Srping Harbor Laboratory Press.

Sanders, A., Collier, R., Trethewy, A., Gould, G., Sieker, R., Tegeder, M. (2009). AAP1 regulates import of amino acids in to developing Arabidopsis embryos. The Plant Journal, Vol. 59: 540-552.

Sasser, J.N., Freckman, D.W. (1987). A world perspective on nematology: The role of the society. In J.A., Veech and D.W., Dickson eds. Vistas on Nematology: A commemoration of the Twenty-fifth Anniversary of the Society of Nematologists. Hysattsville, MD: Society of Nematologists, Inc. 7-14.

Sauer, M. Paciorek, T., Benková, E., Friml, J. (2006) Immnocytochemical techniques for whole-mount *in situ* protein localization in plants. Nature Protocols Vol. 1: 98-103.

Sauer, N., and Stadler, R. (1993). A sink-specific H^+/monosaccharide co-transporter from *Nicotiana tabacum*: cloning and heterologous expression in baker's yeast. Plant J. Vol. 4: 601-610.

Sauer, N. (2007). Molecular physiology of higher plant sucrose transporters. FEBS Lett. 581: 2309-2317.

Schneider, A., Schatten, T., Rennerberg, H. (1994). Exchange between phloem and xylem during long distance transport of glutathione in spruce trees (*Picea abies* (Karst.)L.). J. Exp. Bot. Vol. 45: 457-462.

Schneitz, K., Hülskamp, M., Pruitt, R. (1995). Wild type ovule development in *Arabidopsis thaliana*: a light microscope study of celared-whole mount tissue. The plant journal, Vol. 7: 731-749.

Schobert, C., Köckenberger, W., Komor, E. (1988). Uptake of amino acids by plants form the soil: a comparative study with castor bean seedlings grwon under natural and anxenic soil conditions. Plant and Soil 109:181-188.

Schobert, C., Komor, E. (1990). Transfer of amino acids and nitrate from the roots into the xylem of *Ricinus communis* seedlings. Planta, Vol. 181:85-91.

Schruff, M.C., Spielmann, M., Tiwari, S., Adams, S., Fenby, N., Scott, R.J. (2006). The *AUXIN RESPONSE FACTOR2* gene of *Arabidopsis* links auxin signalling, cell division, and the size of seeds and other organs. Development, Vol. 133: 251-261.

Schwacke, R., Scheider, A., van der Graaff, E., Fischer, K., Catoni, E, Desimone, M., Frommer, W.B., Flügge, U.I., Kunze, R. (2003) ARAMEMNON, a novel database for arabidsopsis integral membrane proteins. Plant Physiology, Vol. 131: 16-26,

Simpson, C., Thomas, C., Findlay, K., Bayer, E., Maule, A.J. (2009). An Arabidopsis GPI-anchor plasmodesmal neck protein with collose binding activity and potential ro reulate cell-to-cell trafficking. Plant Cell, Vol. 21: 581-594.

Slewinski, T.L., Zhang, C., Turgeon, R. (2013). Structural and functional heterogeneity in phloem loading and transport. Front. Plant. Sci. Vol. 4.

Smyth, D.R., Bowman, J.L., Meyerowitz, E.M. (1990) Early flower development in Arabidopsis. The Plant Cell, Vol. 2: 755-767

Smith, B., D. (2001). Documenting plant domestication: the consilience of biological and archaeological approaches. Proc. Natl Acad. Sci. USA Vol. 98: 1324-1326.

Smigocki, A.C., Owens, L.D. (1989). Cytokinin-to-auxin ratios and morphlogy of shoots are transformed by a chimeric isopentenyl transferase gene. Plant Physiol. Vol. 91: 808-811.

Sork, V. (2015). Gene flow and natural selection shape spatial patterns of genes in tree populations: implications for evolutionary processes and applications. Evolutionary Applications, Vol. 9: 291-310.

Sosso, D., Luo, D., Li, Q., B., Sasse, J., Yang, J., Gendrot, G., Suzuki, M., Koch, K.E., McCarty, D.R., Chourey, P.M., Roos-Ibarra, J., Yang, B., Frommer, W.B. (2015). Seed filling in domesticated maize and rice depends on SWEET-mediated hexose transport. Nat. Genet. Vol. 47: 1489-1483.

Stadler, R., Sauer, N. (1996). The *Arabidopsis thaliana AtSUC2* gene is specifically expressed in companion cells. Bot. Acta, Vol. 109: 299-306.

Stadler, R., Lauterbach, C., Sauer, N. (2005). Cell-to-cell movement of green fluorescence protein reveals post-phloem transport in the outer integument and identifies symplasmic domains in *Arabidopsis* seeds and ebryos. Plant Physology, Vol. 139: 701-712.

Steudle, E., Peterson C., A., (1998) How does water get through roots?J. Exp. Bot. Vol, 49: 775-788.

Sun, J., Bankston, J.R., Payandeh, J., Hinds, T.R., Zagotta, W.N., Zheng, N. (2014). Crystal structure of the plant dual-affinity nitrate transporter NRT1.1. Nature, Vol. 507: 73-77.

Svennerstam, H., Jämtgard, S., Ahmad, J., Huss-Danell, K., Näsholm, T., Ganteg, U. (2011). Transporters in *Arabidopsis* roots mediating uptake of amino acids at naturally occuring concentrations. New Phytol. 191:459-467.

Swarup, K., Bekova, E., Swarup, R., Casimiro, I., Péret, B., Yang, Y., Parry, G., Nielsen, De Smet, I., Vanneste, S., Levesque, M.P., Carrier, D., James, N., Calvo, V., Ljung, K., Kramer, E., Roberts, R., Graham, N., Marillonnet, S., Patel, K., Jones, J.D., Taylor, C.G., Schachtman, D.P., May, S., Sandberg, G., Benfey, P., Friml, J., Kerr, I., Beeckman, T., Laplaze, L., and Bennett, M.J. (2008). The auxin influx carrier LAX3 promotes lateral root emergence. Nat. Cell Biol. Vol. 10: 946-954.

Tegeder, M., Offler, C.E., Frommer, W.B., Patrick, J.W. 2000. Amino acid transporters are localized to transfer cells of developing pea seeds. Plant Physiology, Vol. 122: 319.326.

Tegeder, M. (2014). Transporters involved in source to sink partitioning of amino acids and ureids: opportunities for crop improvement. Journal of Experimental Botany, Vol. 65: 1865-1678.

Thiel, J., Müller, Ml, Weschke, W., Weber, H. (2009). Amino acid metabolism at the maternal-filial boundary of yount barley seeds: a microdissection-based-study. Planta, Vo. 230: 205-213.

Thiel, J. (2014) Development of endosperm transfer cells in barley. Front. Plant Sci. Vol. 5: 108.

Toufighi, K., Brady, S.M., Austin, R., Ly, E., Provart, N. (2005). The Botany Array Ressource: e-Northerns, Expression Angling and promoter analyses. The Plant Journal, Vol. 43: 153-163.

Truernit, E., Schmid, J., Epple, P., Illig, J., and Sauer, N. (1996). The sink-specific and stress-regulated Arabidopsis *STP4* gene: enhanced expression of a gene encoding a monosaccharide transporter by wounding, elicitors, and pathogen challenge. Plant Cell 8: 2169-2182.

Truernit, E., Bauby, H., Dubreucq, B., Grandjean, O., Runions, J. Barthélémy, J. and Palauqui, J.C. (2008). High-resolution whole-mount imaging of three dimensional tiusse organization and gene expression anbles the study of phloem development and structure in *Arabidopsis*. Plant Cell. Vol. 6: 1494.1503.

Truernit, E., Bauby, H., Belcram, K., Barthélémy, J., Palauqui, J. C. (2012). OCTOPUS, a polarly localized membrane-associated protein, regulates phloem differentiation entry in Arabidopsis thaliana. Development, Vol. 139: 1306-1315.

Tsay, Y.F., Schoeder, J.I., Feldmann, K.A., Crawfold, N.M. (1993). The herbicide sensitive gene CHL1 of Arabidopsis encodes a nitrate-inducible nitrate transporter. Cell, Vol. 75: 705-713.

Tsay, Y.F., Chiu, C.C., Tsai, C.B., Ho, C.H., and Hsu, P.K. (2007). Nitrate transporters and peptide transporters. FEBS Lett. 581: 2290-2300.

Tucker, E.B., Tucker, J.E. (1993). Cell-toce. Diffusion selectivity in staminal hais of *Setcreasea purpurea*. Protoplasma, Vol. 174, 36-45.

Turgeon, R., Medville, R., and Nixon, K.C. (2001). The evolution of minor vein phloem and phloem loading. Am. J. Bot. Vol, 88: 1331-1339.

Turgeon, R., and Wolf, S. (2009). Phloem transport: cellular pathways and molecular trafficking. Annu Rev Plant Biol Vol, 60: 207-221.

Tytgat, T., Vercauteren, I., Vanholme, B., De Meutter, J., Vanhoutte, I., Gheysen, G., Borgonie, G., Coomans, A., Gheysen, G. (2004). An SXP/RAL-2 protein produced by the subventral pharyngeal glands in the plant parasitic root-knot nematode Meloidogyne incognica. Parasitology Research, Vol. 95: 50-54.

Van Bel, A.J.E. (2003). The phloem, a miracle of ingenuity. Plant Cell Environ. 26**:** 125-149.

Van Bel, A.J.E. (1996). Interaction between sieve element and caompanion cell and the consequences for photoassimilat distribution.Two structural hardware frames with associated physiological software packages in dicotyledons. Journal of Experimental Botany 47, 1129-1140.

Van Winkle, L.J., Galat, V., Iannaccone, P.M. (2014). Threonine appears to be essential for proliferation of human as well as mouse embryonic stem cells. Front. Cell Dev. Biol., Vol. 2: 18

Walling, L., Drews, G.N., Goldberg, R.B. (1986) Transcriptional and post-transcriptional regulation of sybean seed protein mRNA levels. Proc. Natl. Acad. Sci. Vol. 83: 123-127.

Wang, X., Campbell, L. E., Miller C., M., Proud, C.G. (1998) Amino acid availability regulates p70 S6 kinase and multiple translation factors. Biochem, J. Vol. 334: 261-267.

Weijschede, J., Antonisse, K., de Calluwe, H., de Kroon, H., Huber, H. (2007). Effects of cell number and cell size on petiole length variation in a stoloinverous herb. Am. J. Bot. Vol. 95: 41-49.

Werner, D. (2011). Symplastische Kopplung in *Arabidopsis thaliana*: Untersuchungen zur Phloementladung sowie Entstehung und Verteilung von Plasmodesmata. Dissertation, Friedrich-Alexander-Universität Erlangen-Nürnberg.

Werner, D., Gerlitz, N., Stadler, R. (2011). A dual switch in phloem unloading during ovule development in Arabidopsis. Protoplasma, Vol.248: 225-235.

Weschke, W., Panitz, R., Sauer, N., Wang, Q., Neubohn, B., Weber, H., Wobus, U. (2001). Sucrose transport into barley seeds: molecular characterization of two transporters and implications for seed development and strach accumulation. Plant. J. Vol. 5: 455-467.

Wille, A.C., Lucas, W.J. (1984). Ultrastructural and histochemical studies on guard cells. Plants, Vol. 160: 129-142.

Wipf, D., Ludewig, U., Tegeder, M., Rentsch, D., Koch, W., and Frommer, W.B**.** (2002). Conservation of amino acid transporters in fungi, plants and animals. Trends Biochem. Sci. 27**:** 139-147.

Wysocka-Diller, J.W., Helariutta, Y., Fukaki, H., Malamy, J.E., Benfey, P.N. (2000). Molecular analysis of SCARECROW function reveals a radial patterning mechanism common to root and shoot. Development, Vol. 127: 595-603.

Xu, G., Fan, X., Miller, A.J.(2012) Plant nitrogen assimialtion and use efficiency. Ann. Rev. Plant Bio. Vol. 63: 153-182.

Yang, Y., Hammes, U.Z., Tayler, C.G., Schachtman, D.P., Nielsen, E. (2006). High-affinity auxin transport by the AUX1 influs carrier protein. Current biology, Vol.16: 1123-1127.

Yazdanbakhsh, N., Sulpice, R., Graf, A., Stitt, M., Fisahn, J. (2011). Cicadian control of root elongation and C partitioning in *Arabidopsis thaliana*. Plant Cell. Environ. , Vol. 34: 877-894.

Young, V.R., (1994). Adult amino acid requirements: the case for a major revision in current recommendations. J. Nutr.184.

Zádniková, P., Petrásek, J. Marhavy, P., Raz, V., Vandenbussche, F., Ding, Z., Schwarzerová, K., Morita, M.T., Tasaka, M., Hejátko, J., Van Der STraeten, D., Friml, J., Benková, E. (2010). Role of PIN-mediated auxin efflux in apical hook development of Arabidopsis thaliana. Development, Vol. 137: 607-617.

Zhang, L.Y., Peng, Y.B., Pelleschi-Travier, S., Fan, Y., Lu Y.F., Lu, Y.M., Gao, X.P., Shen, Y.Y., Delrot, S., Zhang, D.P. (2004). Evidence for apoplasmic phloem unloading in developing apple fruit. Plant Physiol. Vol. 135: 574-586.

Zheng, Z-L. (2009). Carbon and nitrogen nutrient balance signaling in plants. Plant Siganl Behav. Vol. 4: 584-591.

Zhu, X., Shaw, P.N., Pritchard, J., Newbury, J. Hunt, E. J., Barrett, D.A. (2005). Amino acid analysis by micellar electrokinetic chromatography with laser-induces fluorescence detection: application to nanolitre-volume biological samples from *Arabidopsis thaliana* and *Myzus persicae*. Electrophoresis, Vol. 26: 911-919

Zourelidou, M., Absmanner, B., Weller, B., Barbosa, I. CR., Willige, B.C., Fastner, A., Streit, V., Port, S.A., Colcombet, J., de la Fuente van Bentem, S., Hirt, H., Kuster, B., Schulze, W.X., Hammes, U.Z., Schwechheimer, C. (2014). Auxin efflus by PIN-FORMED proteins is activated by tow different protein kinases, D6 PROTEIN KINASE and PINOID. eLife 3: e02860.

Zourelidou, M., Müller, I., Willige, B.C., Nill, C., Jikumaru, Y., Li, H., Schwechheimer, C. (2009). The polarity localized D6 PROTEIN KINASE is required for efficient auxin transport in *Arabidopsis thaliana*. Development, Vol. 136: 627-636.

Zürcher, E., Tavor-Deslex, D., Lituiev, D., Enkerli, K., Tarr, P.T., Müller, B. (2013). A robust and sensitive synthetic sensor to monitor the transcriptional output of the cytokinin signaling network in planta. Plant Physiol., Vol. 13: 1066-1075.

9.2. Publications

Müller, B., Fastner, A., Karmann, J., Thomas, H., Suter Grotemeyer, M., Rentsch, D., Truernit, E., Ladwig, F., Dresselhaus, T., Bleckmann, A., Schwab, W., and Hammes, U.Z. (2015). Amino acid export in developing Arabidopsis seeds depends on UmamiT facilitators. The Plant Cell, Vol. 25: 3126-3131.

Zhou, L., Höwing, T., Müller, B., Hammes, U.Z., Gietl, C., Dresselhaus, T. (2016). Expression analysis of KDEL CysEPs programmed cell death markers during reproduction in Arabidopsis. Submitted in Plant Reproduction.

Chen, J., Mergner, J., Müller, B., Deutzmann, R., Hammes, U.Z., Schwechheimer, C., Dresselhaus, T. (2016). Grass-specific diSUMO-like DSUL interacts with substrates differing from SUMO substrates to control the first zygotic division in maize. (in preparation).

Höwing, T., Müller, B., Dann, M., Hammes, U.Z., Gietl, C. (2016). Edoplasmic reticulum KDEL-tailed cysteine endopeptidase 2 and 1 of Arabidopsis (AtCEP2 and AtCEP1) in developmental cell wall modulation of roots. (in preparation).

Müller, B., Siddique, S., Grundler, F.M.W., Weiste, C., Dröge-Laser, W., Hammes, U.Z.# UmamiT28 and 29 function in phloem to xylem transfer of amino acids and supply nematode and fungal pathogens with amino acids. (in preparation).

Müller, B., Karmann, J., Bleckmann, A., Dresselhaus, T. Weiste, C., Dröge-Laser, W. and Hammes, U.Z.# Control of root development by shoot-derived amino acids. (in preparation).

10. Appendix

10.1. Colocalization study

Statistical quantification about the colocalization score between UmamiT-GFP and a plasma membrane marker revealed for selected candidates of clade I (UmamiT11 and UmamiT14) and clade III (UmamiT28 and UmamiT29) a clear localization at the plasma membrane (Table 5)

Statistics was done without threshold; a perfect colocalization would result in values of 1, no colocalization would be 0.

Table 5: Colocalization of UmamiTs with a plasma membrane marker, validated by statistics.

	Manders M1	**Manders M2**	**Pearson´s R value**
UmamiT11	0.96	0.91	0.84
UmamiT14	0.90	0.99	0.92
UmamiT28	0.91	0.97	0.88
UmamiT29	0.95	0.91	0.86

10.2. Amino acid analytics

Single values of the amino acid analytics are shown below (Table 6).

Table 6: Content of free amino acids in fruits of wildtype, mutants and complementation lines. Values are shown in nmoles/ml. **Bold** values are significantly ($p < 0.05$) higher in mutants compared to wildtype. (One way ANOVA followed by Holm-Sidak *post hoc* test).

Amino acid	*Col-0*	*umamit11*	*umamit14*	*umamit28*	*UmamiT29*	*umamit11c*	*umamit14c*	*umamit28c*	*umamit29c*
SER	1294 ± 68	1168 ± 56	**1893 ± 116**	1306 ± 165	**1544 ± 15**	772 ± 13	1276 ± 14	1330 ± 106	1146 ± 27
ASP	953 ± 30	1063 ± 22	**1240 ± 22**	789 ± 75	969 ± 49	688 ± 6	830 ± 9	720 ± 119	680 ± 41
THR	851 ± 27	946 ± 51	**1270 ± 142**	853 ± 82	**1036 ± 38**	531 ± 26	759 ± 0,2	707 ± 53	696 ± 30
GLN	761±1	718 ± 41	**1057 ± 167**	821 ± 99	**1052 ± 44**	516 ± 25	746 ± 41	633 ± 37	540 ± 3
GLU	679 ±8	**927 ± 15**	**118 1± 42**	785 ± 113	894 ± 134	465 ± 19	725 ± 24	644 ± 23	631 ± 27
ASN	524 ±19	546 ± 22	**755 ± 61**	**759 ± 22**	588 ± 57	346 ± 3	477 ± 43	470 ± 27	511 ± 14
PRO	409 ±5	**366 ± 1**	**914 ± 3**	**650 ± 44**	**996 ± 8**	287 ± 1	204 ± 6	741 ± 25	562 ± 15
ALA	247 ±66	357 ± 19	**493 ± 7**	**705 ± 50**	**1089 ± 54**	178 ± 18	307 ± 1	373 ± 22	366 ± 85
GABA	120 ±8	139 ± 3	**300 ± 27**	**431 ± 0**	**601 ± 19**	72 ± 3	146 ± 5	150 ± 7	111 ± 6
LYS	117 ±0,3	**132 ± 3**	**260 ± 5**	116 ± 15	**179 ± 6**	51 ± 0,4	128 ± 3	113 ± 6	100 ± 6
VAL	109 ±1	**96 ± 1**	**192 ± 0**	**215 ± 42**	**235 ± 12**	63 ± 3	92 ± 4	106 ± 0.8	110 ± 5
ARG	94 ±5	102 ± 6	**150 ± 6**	**116 ± 26**	**165 ± 7**	46 ± 2	78 ± 2	50 ± 3	38 ± 19
LEU	93 ±0,8	119 ± 9	**146 ± 0**	**114 ± 9**	**143 ± 5**	54 ± 3	89 ± 7	108 ± 2	74 ± 3
ILE	84 ±9	109 ± 5	**136 ± 2**	111 ± 13	**142 ± 15**	48 ± 4	71 ± 5	40 ± 2	24 ± 2
GLY	51 ±3	82 ± 30	167 ± 70	**250 ± 26**	**306 ± 86**	23 ± 2	70 ± 11	96 ± 3	80 ± 2
MET	31 ±2	**43 ± 2**	**59 ± 7**	**13 ± 2**	**16 ± 1**	15 ± 1	42 ± 2	7 ± 0.1	6 ± 36
PHE	28 ±1	**41 ± 3**	**55 ± 5**	**14 ± 2**	**19 ± 1**	14 ± 1	34 ± 4	17 ± 3	9 ± 4
TYR	24 ±0,1	**41 ± 4**	**57 ± 2**	**40 ± 7**	**52 ± 2**	7 ± 1	23 ± 2	21 ± 4	12 ± 0.5
CIT	22 ±3,6	**5 ± 1**	38 ± 28	43 ± 3	58 ± 4	37 ± 5	16 ± 11	14 ± 2	8 ± 0.6
ORN	9.5 ±1	14 ± 1	**20 ± 0**	16 ± 0	**16 ± 1**	6 ± 1	12 ± 0,07	7 ± 0.4	6 ± 8
TRY	0.4 ±2	**11 ± 3**	**11 ± 4**	**6 ± 2**	3 ± 1	7 ± 1	n.d.	3 ± 0.1	0.5 ± 0.1
HIS	n.d.	**51 ± 1**	**26 ± 1**	**43 ± 7**	**82 ± 4**	n.d.	0 ± 0,06	38 ± 0.1	33 ± 0.1

11. Danksagung

Angekommen an diesem finalen Punkt nun ist es nur ehrlich und fair all die Personen zu erwähnen und ihnen Danke zu sagen, die einen Beitrag zum Gelingen dieser Arbeit geleistet haben.

Diesbezüglich verdient mein Supervisor **PD Dr. Ulrich Hammes** allergrößten Dank für die ausgezeichnete und vorbildlichste Betreuung meiner Doktorarbeit. Danke für die vielen wegweisenden Diskussionen unserer Daten und die facettenreiche Förderung meiner Person, die mir nachhaltig in meiner Zukunft zugutekommen wird. Du wurdest in diesem Sinne all dem, was das Amt „Doktorvater" impliziert, am meisten gerecht! Ich hab mich stets gut aufgehoben gefühlt! Hab tausendfachen Dank Uli!

Prof. Dr. Thomas Dresselhaus spreche ich meinen Dank aus für die Bereitstellung mich am Lehrstuhl aufzunehmen und meine Arbeit zu begutachten. Loben in diesem Zusammenhang möchte ich besonders die hervorragende Ausstattung am Institut bezüglich des scientific equipment, welches mir erlaubt hat so tiefe und faszinierende Einblicke in die Zellbiologie zu bekommen.

Danke auch an **Prof. Dr. Ralph Hückelhoven** für die Übernahme der 2. Mentorschaft meiner Doktorarbeit. Gerne erinnere ich mich an die sehr zielführenden progress reports zurück in denen wir im Verlauf der Diskussion meiner damaligen Daten wertvolle Vorschläge erhalten haben. Vielen Dank für Deine fachlichen Einschätzungen und Dein freundliches und interessiertes Wesen bezüglich meiner Forschung.

Ein Teil der Experimente wurde an der TUM in den Laboren des Instituts der „Biotechnologie der Naturstoffe" bei **Prof. Dr. Wilfried Schwab** durchgeführt. Hierbei unterstützten mich **Mechthild Mayershofer** und **Dr. Thomas Hoffmann** bei der Durchführung und Auswertung der Versuche und vermittelten mir stets den Eindruck willkommen zu sein. Vielen Dank an Euch alle für die Ermöglichung der Analyse der „Früchtchen" von *Arabidopsis*.

Besonderen Stellenwert für mich haben die Mitglieder des „***in situ* Kompetenzzentrum**", bestehend aus **Dr. Andrea Bleckmann** und **Angelika Rechenmacher**. Vielen herzlichen Dank Andrea für Deine Co-Betreuung meiner Arbeit, was die zahlreichen fachlichen Gespräche ebenso miteinschließt, woraus sich sehr wichtige Experimente abgeleitet haben. In diesen nachfolgenden Experimenten konnte ich stets auf die kompetente Unterstützung von Angelika zählen. Mit Deiner vielseitigen Expertise warst Du in vielen Bereichen des Labors ein wichtiger Berater, den ich auch menschlich sehr zu schätzen gelernt habe!

Insgesamt ist es mir ein wichtiges Anliegen mich ausdrücklich bei **allen** Ladies der AG Hammes inklusive Sandra Bertram für das kollegiale Miteinander zu bedanken, was für mich gesprochen einen wesentlichen Aspekt darstellt, um produktiv arbeiten zu können. Danke, war eine wirklich schöne Zeit.

Hierbei verdient insbesondere meine direkte Kollegin **Astrid Fastner** Erwähnung für Ihren wertvollen Beitrag in der biochemischen Analyse der Transporter. Danke auch für das gute Miteinander!

Besonderer Dank geht ebenfalls an **Verena Mansch** für die zuverlässige und akkurate Mitarbeit. Dein sonniges Wesen hat in unsere Reihen viel Licht und Freude gebracht! Ich danke Dir aus ganzem Herzen dafür!

Die „gute Fee“ **Julia Karmann** hat mich besonders beim Korrekturlesen der vorliegenden Arbeit unterstützt. Vielen herzlichen Dank dafür! Ich hab Dich nicht nur wegen Deiner sehr sorgfältigen Mitarbeit zu schätzen gelernt, sondern auch wegen Deines ehrlichen und freundlichen Wesens. Vielen Dank für das super Teamwork!

Bei **Jessica Neudl** und **Martina Kolb** bedanke ich mich ebenfalls für das sehr freundliche kollegiale Miteinander, sowie für die Initiierung des besten Laborvideos ever! Diese Eigeninitiative Eurerseits hat mich sehr positiv beeindruckt. Dafür meinen Respekt und mein Dank ein Teil davon geworden zu sein.

Danke möchte ich auch generell **allen Mitarbeitern** des Lehrstuhl Dresselhaus sagen für das gute Miteinander auch zwischen den Arbeitsgruppen. Auch die diversen Serviceleistungen was Verwaltungsangelegenheiten (**Veronica Mrosek**), das Bestellen von Materialien (**Angelika Rechenmacher**, **Monika Kammerer**), Autoklavieren (**Michael Schmitzberger**), sowie Instanthaltung der Sterilbänke (**Annemarie Taffner**, **Ingrid Fuchs**) betrifft sollen hier Erwähnung finden, auch wenn die vielen weiteren daran beteiligten Einzelpersonen nicht explizit einzeln genannt sind. Mir ist Euer Wirken sehr wohl aufgefallen und auch wenn es manchmal nur Kleinigkeiten waren, so trugen sie doch insgesamt zum Funktionieren des Lehrstuhls bei. Danke Euch allen!
Schließlich möchte ich unsere Gärtner **Ursula Wittmann** und **Armin Hildebrand** erwähnen, die in fachkundiger Art stets bemüht waren optimales Material für die Forschung bereitzustellen. Danke auch für die Pflege unserer Tomaten für die Nematodenzucht und dass Ihr als sehr freundliche Ansprechpartner in botanischen Angelegenheiten, die auch über Mais und *Arabidopsis* hinausgingen, stets verfügbar wart. Danke für Euer Mitwirken!

Erklärung

Hiermit bekunde ich, dass ich die zugrunde liegende Arbeit nur mit den angegebenen Hilfsmitteln angefertigt habe.

Regensburg den……. ……

(Benedikt Müller)